Physik–Department
der Technischen Universität München
Institut für Theoretische Physik T30

A Treatise on

Quantum Ballistic Motion and its Applications

from Photodetachment to Scanning Tunneling Microscopy

Christian Bracher

Vollständiger Abdruck der von der Fakultät für Physik
der Technischen Universität München
zur Erlangung des akademischen Grades eines

Doktors der Naturwissenschaften (Dr. rer. nat.)

genehmigten Dissertation.

Vorsitzender:	Univ.–Prof. Dr. G. Abstreiter
Prüfer der Dissertation:	1. Univ.–Prof. Dr. M. Kleber
	2. Univ.–Prof. Dr. H. Friedrich
	3. Univ.–Prof. Dr. W. Schleich, Universität Ulm (schriftliche Beurteilung)

Die Dissertation wurde am 23.07.1999 bei der
Technischen Universität München eingereicht und durch
die Fakultät für Physik am 06.08.1999 angenommen.

A Treatise on

Quantum Ballistic Motion and its Applications

from Photodetachment to Scanning Tunneling Microscopy

Christian Bracher

Physik–Department,
Technische Universität München

Preface

An apple falls off an apple tree,
according to the law of gravity,
that's a fact of great renown—

SO IT MAY BE SURPRISING at first to find another volume devoted to the study of ballistic motion, i. e., the dynamics of particles subjected to a homogeneous force field, some 400 years after Galilei conducted his legendary experiments on freely falling bodies. However, for several well-founded reasons, I'm convinced that the problem of uniformly accelerated motion despite its classic background still deserves attention at the brink of the third millennium A. D.: It is a little appreciated and almost unknown fact that the quantum mechanical Green function describing stationary emission of particles into a homogeneous force field environment is available as a closed-form expression. This allows to construct multipole solutions to the ballistic Schrödinger equation that in many ways resemble the spherical waves employed in the partial wave analysis familiar from the conventional treatment of scattering events. The theory of these ballistic multipole waves is developed systematically in this treatise. Apart from the formal aspect of providing a novel set of exact solutions for a problem in quantum mechanics, the theory of uniformly accelerated motion is also advantageously applied to a number of fields of active experimental research: The ballistic scattering waves are accurately realized in near-threshold photodetachment of electrons from negatively charged ions in the presence of a homogeneous electric field and have recently been employed for a demonstration of quantum interference on a macroscopic scale; an electron interferometer device based on coherent ballistic motion is under construction. The study of the quantum dynamics of free-falling objects may also become important in the gravitational decoupling of trapped ultracold atomic condensates.

The uniform force field also offers a unique opportunity to inquire into the physics of tunneling sources, i. e., particle emission into a classically forbidden sector of space. From a theoretical point of view, ballistic tunneling motion sheds some light onto the controversial topic of multidimensional tunneling phenomena. In practice, these tunneling sources to some degree are put into effect in field emission from mesoscopic

tip structures, and the peculiar characteristics of these sources find their explanation in terms of the properties of the linear barrier potential. Finally, ballistic multipole sources provide a useful starting point for a simple theoretical model of scanning tunneling microscopy (STM) that gives a good deal of insight into the imaging behavior of this device, and in particular leads to an estimate for its resolution capability.

Obviously, extensions of the theory of quantum ballistic motion and further experimental realizations of it are conceivable, but they are outside the scope of the present work which hopefully may serve as a base for these future developments. After all, as R. W. Emerson has put it,

> *It is the good reader that makes the good book.*

To contribute my part to achieve this noble objective, I have tried to prepare a complete and intelligible presentation of the subject, to state clearly any assumptions and simplifications, and to delimit their range of validity. Obviously, any mistakes and omissions are in my responsibility; nevertheless, it is the sincere hope of the author that the attentive reader may agree with the judgment once stated by a Connecticut Yankee in King Arthur's court,

> *There was things that he stretched,*
> *but mainly he told the truth.*

I owe the preceding two citations, like most of the typographical design of this volume, to D. E. Knuth, author of the TEXbook. Furthermore, I'm indebted to C. Blondel and his co-workers at LAC, Orsay (France) who generously supplied experimental data obtained with their photodetachment microscope prior to publication. Thanks are also due to M. Drexler, then at Stanford University, and H. C. Bryant at the University of New Mexico, Albuquerque, for their hospitality during a visit in the U. S. where the essential features of this treatise were first conceived. M. Riza went out of his way to provide assistance in, but not limited to, computing issues. I appreciate valuable discussions with W. Becker, C. Blondel, H. C. Bryant, B. Gottlieb, S. A. Gurvitz, M. Kleber, R. Kopold, A. Lohr, M. S. Marinov, and M. Riza, who helped shaping this project into its current form. Last but not least, since physics presents but a minor aspect of life, financial support by the Deutsche Forschungsgemeinschaft (Grant No. SFB 338) and a scholarship by the "Studienstiftung des Deutschen Volkes" are gratefully acknowledged.

Garching, Germany
July 1999 CHRISTIAN BRACHER

Table of Contents

List of Figures

Chapter 1

Introduction

ALTHOUGH a conceptually simple application of quantum theory, the dynamics of electrons in external electromagnetic fields has gained new interest during the past decade. This development has largely been stimulated by the advance of laser technology both in terms of intensity and stability, paving the way for experiments that, in most general terms, explore the interaction between atoms and laser fields. In one class of experiments, an intense laser field is employed both to strip electrons from an atom and to provide the background fields that determine their dynamics; example phenomena include high-harmonic generation (HHG) and above-threshold ionization (ATI) [1]. In a different spirit, one may separate these processes and exploit laser-atom interaction in order to operate a controlled source of electrons but apply additional external fields that subsequently govern electronic motion. Recently the latter approach has been realized experimentally; as an electron source, a beam of negatively charged ions as a carrier of electrons has been irradiated with laser photons, causing the release of surplus charges. This "photodetachment process," originally utilized in atomic physics for precision measurements of electron affinities [2, 3], is capable of providing a well-localized source of almost monoenergetic free electrons [4] that successively may be exposed to static external fields.

The present treatise is chiefly devoted to a thorough theoretical study of the quantum dynamics of particles emitted from spatially oriented pointlike sources into a three-dimensional stationary homogeneous force field, i. e., a discussion of scattering partial waves in the presence of a linear potential environment $U(\mathbf{r}) = -\mathbf{r} \cdot \mathbf{F}$. Obviously, the process under examination may be interpreted as the quantum mechanical analog to the famous problem of classical free-falling ballistic motion. In the arena of charge-field interactions, the potential corresponding to a uniform electric field presents the most elementary choice, and the subject has been issue of a number of theoretical publications [5–33]. More challenging setups involving magnetic fields [34–53] and time-dependent potentials [54–57] have been conceived and discussed. However, the simple uniform field problem exhibits two distinctive features that predestinate it for an in-depth study: From a theoretical point of view, the

problem enjoys the rare privilege to allow for a closed-form solution with no approximations required [6–9], a peculiarity that apparently has been mostly overlooked so far. Complementary, a number of experiments on the subject already have been performed [4,56–63], providing data that may serve for comparison between theory and experiment.

For these reasons, we will present a comprehensive account of the mathematical developments that lead to explicit expressions for the quantities of interest (wave functions, current distributions, and total currents generated by the sources) in the uniform field problem. The somewhat unusual starting point of our analysis will be a modified inhomogeneous Schrödinger equation. Though rarely used, the introduction of source terms into customary quantum mechanics is a simple, pictorial, yet powerful technique especially apt to the analysis of scattering phenomena. We present the basic theory of quantum sources and point out their connection to propagators and Green functions. Special emphasis is put on the notion of multipole sources, point-like oriented sources that are constructed conforming to the concept of multipoles in potential theory and advantageously applied in the analysis of scattering problems involving the exchange of angular momentum quanta. For the basic problem of scattering of asymptotically free particles, the multipole formalism simply reduces to the familiar partial wave analysis technique. However, the theory of multipole sources is easily extended to more complicated potential environments, and we will employ it to establish closed-form solutions for the multipole electronic wave functions and currents that are appropriate for the case of a surrounding homogeneous electric field. To our best knowledge, these results are new and so far have not been published.

As noted above, to a good approximation stationary multipole electron sources are realized in electron photodetachment processes at energies close to threshold. Hence, the theoretical predictions from the source model allow for comparison with experimental data on photodetachment in the presence of a homogeneous electric field. Experiments of this type have been performed by a number of groups during the past two decades. Initially, the interest was directed to a study of the photodetachment rate as a function of the excess energy of the detached electron, corresponding to the total photon absorption cross section [56–59]. This field of investigation was pioneered by the ingenious experiments performed by H. C. Bryant et al. using a relativistic H^- ion beam at Los Alamos in 1987 [60–62]. Almost a decade later, C. Blondel and his colleagues at LAC, Orsay (France) were also able to record the spatial distribution of the photodetachment current, i. e., the differential cross section for the photodetachment process [4]. In a recent paper, they present their spectacular latest experimental results [63]. Meanwhile, these authors have developed the photodetachment microscope into an extraordinarily sensitive tool for the interferometric determination of electron affinities [64]. In all these publications, the predictions from the simple multipole source model agree very well with the experimental data, thus showing

that near-threshold photodetachment phenomena are appropriately described in the framework of the source formalism.

Motion in a homogeneous field is equivalent to the textbook topic of uniform acceleration in classical mechanics, and a great deal of insight into the physics of the uniform field photodetachment process is gained by a study of ballistic motion at some fixed energy E. An advanced classical analysis of the problem [9] shows that within the sector of classically allowed motion, always two trajectories will exist that connect the particle origin with a given destination point. In a quantum mechanical description, this twofold degeneracy of classical motion will give rise to quantum interference much in the spirit of Feynman's classic double-slit gedanken experiment [65] first put into practice by Möllenstedt [66]. With a deliberate choice of parameters, the dimensions of the circular interference pattern will be macroscopic in scale. This prediction has been impressively confirmed by the experiments of Blondel et al. [4,63]. The two-path interference also leads to characteristic structures in the uniform field photodetachment total cross section. Having analytical results at hand, we are able to assess the quality of the semiclassical approximations so far used in the analysis of the photodetachment problem [10,16,33]. It turns out that, except near the boundary of the sector of classically allowed motion, the WKB approximation works surprisingly well.

Yet, an interesting picture also emerges when "tunneling" sources with negative initial kinetic energy are considered [67]. In this case, obviously no classical counterpart exists, even though the analytic continuation of the classical equations of free-falling motion into the forbidden sector is feasible, leading to "tunneling trajectories" in complex space-time whose meaning admittedly must remain obscure [9]. The ballistic multipole Green functions derived from a tunneling source are most appropriately described as scattering partial waves of simultaneously propagating and evanescent character. However, tunneling motion in a homogeneous field presents an exception with regard to the fact that the problem yields to a semiclassical description in terms of tunneling paths; for the majority of multidimensional tunneling phenomena, no simple WKB approximation is available. For this reason, we devise a description of the classically forbidden motion of particles emitted from multipole sources which is founded on elementary reasoning, yet nevertheless is able to reproduce the exact quantum solution obtained for ballistic tunneling in a surprisingly accurate fashion. This "minimum uncertainty model" is based on the insight that deviations of a tunneling trajectory from the optimum escape path in configuration as well as momentum space will be penalized by exponential suppression of the tunneling rate. On the other hand, position and momentum are complementary quantum observables and cannot be fixed simultaneously. At best, their uncertainty product may take on its minimum value familiar from Heisenberg's relation. In three spatial dimensions, this idea may be extended to accommodate angular momentum eigenstates. As an immediate result, the minimum uncertainty model predicts a simple generalized Gaussian shape of the

lateral profile of the tunneling current distribution. Supplementing an argument concerning the semiclassical tunneling time along the escape path, this model provides a comprehensive description of tunneling point sources void of free parameters which is able to explain many of the peculiar features observed in field emission from mesoscopic tip structures. These devices were experimentally designed and characterized in particular by H.-W. Fink [68–71].

The idea of point sources in a tunneling barrier environment may also be used to establish a simple quantum model for the scanning tunneling microscope (STM). This surface probe, originally introduced by Binnig and Rohrer in 1982 [72], was quickly embraced by experimentalists in the field and rapidly evolved into a standard tool for the characterization of conducting sample surfaces. The resolution capability of the STM is truly astounding; even for the arguably smoothest objects in existence, close-packed metal surfaces with interatomic separations of order $a \sim 3$ Å, atomic resolution is regularly achieved [73,74]. The operation of STM crucially depends on the presence of a sharp tip scanning the surface that terminates in a single atom protruding towards the sample surface through which almost the complete tunneling current is funneled. Naturally, within the quantum source formalism, the physical tip may be replaced by a multipole point source of electrons; the zero-temperature, zero-bias conductivity of the STM junction then is readily identified with the multipole particle current emitted by the source which in turn is related to the local density of states (LDOS) at the tip position [75,76]. This prediction matches the conclusion from the transfer Hamiltonian model put forward by Tersoff and Hamann [77,78], the most successful description of the STM proposed so far. Within the source formalism, a resolution estimate for this device is straightforwardly obtained: The position-dependent junction conductivity which renders the STM image may be decomposed into a constant background part due to the bulk-vacuum transition potential, and a superimposed corrugative contribution which stems from the surface structure. Since the tunneling current distribution at the sample surface is extended, the STM will record not the surface potential pattern itself, but rather its convolution with the current profile generated by the source. Structures on a much smaller scale than the width of this nearly Gaussian distribution will be averaged out and missed in the STM image. Finally, we point out that the strength of the tip source is limited through the Pauli exclusion principle. Its combination with the quantum source formalism offers a simple explanation for the unusual transport properties of mesoscopic conductors first explored by Landauer [79,80], thus proving the versatility of the source approach.

Let us conclude this introducing chapter and briefly outline the organization of the present work: In Chapter 2, we develop the quantum theory of sources and introduce the concept of multipole quantum sources, Green functions, and currents. In the following chapter we show that photodetachment processes near threshold are amenable to a description in terms of multipole sources; we also illustrate the source

approach by briefly considering free-particle sources. The classical mechanics of free-falling motion is revisited in Chapter 4 where we give an advanced presentation of the problem in the framework of the Hamilton-Jacobi formalism. A detailed account of the theory of pointlike electron sources in a three-dimensional homogeneous electric field, i. e., the quantum dynamics of ballistic motion, is presented in Chapter 5. There, we exhibit mathematical derivations that lead to closed-form expressions for the relevant multipole Green functions, current distributions, and total currents. In Chapter 6, the characteristic features of these solutions are motivated by a semiclassical picture of the electronic dynamics in the uniform field environment that is valid for classically allowed motion. Additionally, we compare the theoretical predictions resulting from the ballistic source model to actual data recorded in photodetachment experiments. Complementary, a tangible picture of tunneling sources is conceived in the following chapter. Starting out with a WKB approximation for the ballistic tunneling problem, we devise the minimum uncertainty model for multidimensional tunneling phenomena and apply it to motion in a linear potential barrier, utilizing the results to explain some peculiar features observed in field emission from atomically sharp tips. In Chapter 8, the findings of the preceding section are advantageously employed in surface physics for a description of scanning tunneling microscopy in terms of the source formalism which we will subsequently link to more customary theoretical approaches to the STM problem. We also provide a pictorial model for the STM imaging process and extract a simple resolution estimate from it. In combination with Pauli's exclusion principle, we additionally derive some basic transport properties of point contacts. Finally, the main developments resulting from these efforts are summarized in Chapter 9.

In order not to divert attention from the main physical content of the theory of multipole quantum sources presented in this volume, some material of a more mathematical or formal nature has been shifted into several appendices. The first of these (Appendix A) mainly deals with mathematical aspects of the Green functions playing a fundamental role within the source approach. It covers in particular the formal description of quantum sources in the framework of functional analysis, and provides some general facts concerning the analytical properties of multipole Green functions. These objects describe the emission from sources with orbital angular characteristics, hence it is not surprising that their definition refers to the corresponding functions of mathematical physics known as spherical harmonics. A number of useful theorems regarding the algebraic manipulation of spherical and solid harmonics that are not easily accessed from the generally available literature on the subject are presented in Appendix B. An analysis of the simple free-particle scattering problem in terms of the quantum source formalism is given in Appendix C. Additionally, a two-dimensional version of Heisenberg's uncertainty relation accommodating angular momentum eigenstates is proven therein. The explicit representation of the ballistic

multipole Green functions and all quantities derived from them relies heavily on the usage of Airy functions [81]. Hence, the definition of these special functions, their asymptotic properties and some useful integral relations involving them are listed in Appendix D. For convenient reference, in Appendix E we gather explicit formulae for the first few scattering partial waves and their assigned currents in the uniform field environment.

Chapter 2

Quantum Theory of Sources

THIS INTRODUCING CHAPTER presents a brief exposition of a fairly unusual approach to quantum mechanics, the quantum theory of sources. The basic idea behind this technique consists in the ad hoc addition of another term independent of the wave function, called the source term, to the common Schrödinger equation. Mathematically, the solution of the resulting inhomogeneous differential equation is naturally displayed in terms of the quantum propagator or Green function. More physically, the source term may be interpreted pictorially as a local source (or sink) of electrons. In fact, the introduction of the source term leads to a modified equation of continuity that also contains an inhomogeneous term causing localized production (or annihilation) of electrons. Their total production rate (the total current) is easily obtained from these considerations, and for pointlike sources can be established in closed form. Special attention is given to multipole sources, i. e., spatially oriented pointlike sources of definite spherical symmetry, a concept that is borrowed from electrostatics. The wave functions generated by multipole sources correspond to the familiar partial waves of common scattering theory.

It is, of course, common knowledge that in non-relativistic quantum mechanics, the total number of electrons is a conserved quantity, in contradiction to the non-unitary properties caused by the introduction of source terms into the Schrödinger equation. To resolve this dilemma, we stress here that the notion of an electron "source" always represents an approximation to the physical reality, but often a useful one: The concept of sources allows to abstract from the processes that actually "generate" the electrons under consideration, and to concentrate on their subsequent dynamics. Hence, scattering phenomena are natural candidates for a simplified description in terms of quantum source theory. The exact structure of the corresponding source term obviously depends on the nature of the scattering process, and has to be extracted from the scattering Hamiltonian. As an example, we will show that near-threshold electron photodetachment from negative ions is quite accurately modeled by a multipole electron source. We however defer this demonstration to Chapter 3.

From the aforesaid, it should have become obvious that the quantum source for-

malism merely presents a novel mathematical representation of scattering phenomena in quantum mechanics and is in its entirety compatible to the customary approaches to these problems, which are perhaps best exemplified by the transition rates obtained by Fermi's Golden Rule method (see Appendix A.6). If performed in a fairly rigorous manner, establishing the formal connection between quantum source theory, in particular its multipole variant, and the standard techniques developed for scattering problems turns out to be a rather demanding task. Therefore, we chose to discuss the technical aspects of the source approach in a separate entity (Appendix A); in the current chapter we content ourselves with a more heuristic presentation of the multipole source formalism which forms the foundation for the applications of this technique we will present later on (Chapters 3–8).

The vigilant reader may wonder whether the effort of developing an alternative formalism for scattering problems in quantum mechanics is really justified—after all, the novel method is bound to reproduce the answers provided by its approved long-standing counterparts. However, the virtues of the newly introduced approach will become apparent in Chapter 5 where we will apply source theory to quantum particles moving in a uniform force field. There, it will turn out that this problem, unlike the conventional methods, quite easily yields to the source technique, thus providing a wealth of information on quantum ballistic motion not available before.

2.1 The Origin of Sources

Let us further clarify the idea behind "sources" by considering their usage in classical field theories. As a canonical example, we take the equation of heat flow:

$$\left\{ c_H \frac{\partial}{\partial t} - \kappa_H \Delta \right\} T_\sigma(\mathbf{r}, t) = \sigma(\mathbf{r}, t) \tag{2.1}$$

Here, c_H denotes the specific heat of the substrate, κ_H represents its thermal conductivity, and $\sigma(\mathbf{r}, t)$ is easily attributed as some heat production rate per unit volume. This identification rests on the observation that $\sigma(\mathbf{r}, t)$ contributes in the same manner to heat flow as local changes in the heat reservoir $c_H \partial_t T_\sigma(\mathbf{r}, t)$. Unlike this "internal" source of heat current that manifestly acts back onto the temperature field $T_\sigma(\mathbf{r}, t)$ by cooling, the "external" heat source $\sigma(\mathbf{r}, t)$ does not depend on the temperature field and will not be influenced by its evolution. Therefore, $\sigma(\mathbf{r}, t)$ allows to include contributions from non-thermal processes (radioactive decay, electric losses, etc.); one should note, however, that these external effects are considered only as far as the production of thermal energy is concerned whereas their inner degrees of freedom are ignored. Through the use of source terms, one abstracts from the "mechanism" of the external influences on the temperature field.

2.2 Handling Sources Mathematically

As a reminder, we now present the formal solution to the heat flow equation (2.1). To do so, we first read off some elementary mathematical properties of this inhomogeneous linear differential equation (see also Appendix A.1). Obviously, two solutions $T_\sigma^{(1)}(\mathbf{r},t)$, $T_\sigma^{(2)}(\mathbf{r},t)$ will only differ by a solution of the homogeneous (source-free) problem:

$$T_\sigma^{(1)}(\mathbf{r},t) - T_\sigma^{(2)}(\mathbf{r},t) \;=\; T_{\mathrm{hom}}(\mathbf{r},t) \tag{2.2}$$

We generalize this assertion to solutions for different sources $T_{\sigma_1}(\mathbf{r},t)$ and $T_{\sigma_2}(\mathbf{r},t)$:

$$\lambda T_{\sigma_1}(\mathbf{r},t) + \mu T_{\sigma_2}(\mathbf{r},t) \;=\; T_{\lambda\sigma_1\,+\,\mu\sigma_2}(\mathbf{r},t) \tag{2.3}$$

In superposition, sources add linearly. This property allows to decompose the source term $\sigma(\mathbf{r},t)$ within an orthogonal base of functions ("eigenfunction expansion"); the solution $T_\sigma(\mathbf{r},t)$ is then available from superposition of a set of "standard" solutions.

A natural choice of the function base employs pointlike sources $D(\mathbf{r},t;\mathbf{r}',t')$ represented by Dirac delta–"functions" (Appendix A.2.1):

$$D(\mathbf{r},t;\mathbf{r}',t') \;=\; c_H\,\delta(\mathbf{r}-\mathbf{r}')\delta(t-t') \tag{2.4}$$

We now solve for a special solution $K(\mathbf{r},t;\mathbf{r}',t')$ of the heat flow equation (2.1):

$$\left\{c_H\,\frac{\partial}{\partial t} \;-\kappa_H\,\Delta\right\}\,K(\mathbf{r},t;\mathbf{r}',t') \;=\; D(\mathbf{r},t;\mathbf{r}',t') \tag{2.5}$$

From (2.2), it is obvious that the function $K(\mathbf{r},t;\mathbf{r}',t')$ is not completely fixed by equation (2.5). Rather, we have to impose boundary conditions onto $K(\mathbf{r},t;\mathbf{r}',t')$ which determine this solution uniquely. Usually, these boundary conditions follow from physical considerations. In the case of the heat flow equation, we note that heat tends to dissipate; thus, the source term $D(\mathbf{r},t;\mathbf{r}',t')$ (2.4) will cause a change in the temperature field only after the release of heat has taken place, i. e., for $t > t'$. Hence, for a physically sensible solution, $K(\mathbf{r},t;\mathbf{r}',t')$ must vanish for $t < t'$, but yields the heat contribution located at $(\mathbf{r},t)$ that stems from an unit amount of heat initially liberated at $(\mathbf{r}',t')$ for $t > t'$. The causality-preserving function $K(\mathbf{r},t;\mathbf{r}',t')$ is called the retarded propagator of the heat flow equation (2.1). (The solution of the differential equation (2.5) involves a number of quantities which are closely related yet differ distinctively in their physical meaning. For a detailed discussion of these concepts which comprise the time-evolution operator, propagator, and time-dependent Green function, in the context of quantum mechanics we refer to Appendix A.2.2.)

In the last step, the solution of the original source problem is obtained by superposition:

$$T_\sigma(\mathbf{r},t) \;=\; \frac{1}{c_H}\int d^3r'\,dt'\,K(\mathbf{r},t;\mathbf{r}',t')\,\sigma(\mathbf{r}',t') \tag{2.6}$$

We note that due to (2.2), $T_\sigma(\mathbf{r},t)$ is not uniquely given by (2.6); a solution of the homogeneous equation corresponding to (2.1) may still be added.

2.3 Quantum Sources

After these preliminaries we turn our attention to the source problem in quantum mechanics. By replacing the heat flow equation in (2.1) with its quantum mechanical analog, we obtain the inhomogeneous Schrödinger equation (for the sake of simplicity, vector potentials $\mathbf{A}(\mathbf{r},t)$ are omitted):

$$\left\{i\hbar\,\frac{\partial}{\partial t} \;+\; \frac{\hbar^2}{2M}\,\Delta \;-\; U(\mathbf{r},t)\right\}\,\Psi_\sigma(\mathbf{r},t) \;=\; \sigma(\mathbf{r},t) \tag{2.7}$$

$\sigma(\mathbf{r},t)$ now represents a "quantum source." As noted in the introduction to this chapter, this is not a customary concept in quantum mechanics. For the time being, we will however ignore the physical implications of the introduction of sources into the Schrödinger equation, but focus upon its mathematical solution.

Formally, both the heat flow and Schrödinger equations (2.1), (2.7) are parabolic (diffusion-type) differential equations. Therefore, in order to solve (2.7) we merely take over the expression (2.6) we derived in the preceding subsection:

$$\Psi_\sigma(\mathbf{r},t) \;=\; -\,\frac{i}{\hbar}\int d^3r'\,dt'\,K_F(\mathbf{r},t;\mathbf{r}',t')\,\sigma(\mathbf{r}',t') \tag{2.8}$$

Obviously, the quantum or Feynman propagator $K_F(\mathbf{r},t;\mathbf{r}',t')$ appears here [82]. As has been noted above, to select a unique solution $\Psi_\sigma(\mathbf{r},t)$ we have to impose a boundary condition upon the propagator. For reasons of causality, in this article we will consistently use the retarded propagator vanishing for $t < t'$.

2.3.1 Stationary Sources

Like in conventional quantum theory, the modified Schrödinger equation (2.7) simplifies for time-independent processes. We will call inhomogeneities $\sigma(\mathbf{r},t)$ that oscillate in time,

$$\sigma(\mathbf{r},t) \;=\; e^{-\,iEt/\hbar}\,\sigma(\mathbf{r}) \tag{2.9}$$

stationary quantum sources. When the condition (2.9) is fulfilled we may separate the time dependence of the wave function in the usual fashion [83],

$$\Psi_\sigma(\mathbf{r},t) \;=\; e^{-\,iEt/\hbar}\,\psi_\sigma(\mathbf{r};E) \tag{2.10}$$

where $\psi_\sigma(\mathbf{r};E)$ obeys the inhomogeneous stationary Schrödinger equation:

$$\left\{E + \frac{\hbar^2}{2M}\,\Delta - U(\mathbf{r})\right\}\,\psi_\sigma(\mathbf{r};E) \;=\; \sigma(\mathbf{r}) \tag{2.11}$$

To solve this differential equation, we again use the technique of Green functions. Repeating the procedure of Section 2.2, we first introduce pointlike sources $D(\mathbf{r},\mathbf{r}') = \delta(\mathbf{r}-\mathbf{r}')$ and denote the solution of:

$$\left\{E + \frac{\hbar^2}{2M}\,\Delta \;-\; U(\mathbf{r})\right\}\,G(\mathbf{r},\mathbf{r}';E) \;=\; \delta(\mathbf{r}-\mathbf{r}') \tag{2.12}$$

as the (energy) Green function $G(\mathbf{r},\mathbf{r}';E)$ of the problem. The formal properties of this quantity are examined in Appendix A.3–A.4. We note that $G(\mathbf{r},\mathbf{r}';E)$ shows more intricate behavior than the related propagator $K_F(\mathbf{r},t;\mathbf{r}',t')$ (2.8): Existence and uniqueness of the Green function depend on the eigenenergy spectrum of the Hamiltonian $H(\mathbf{r},\mathbf{p}) = p^2/2M + U(\mathbf{r})$ in (2.11). If E is contained in the point spectrum of $H(\mathbf{r},\mathbf{p})$, i. e., if a bound state with energy E is available, the Green function does not exist at all (Appendix A.3.6). Outside the spectrum of $H(\mathbf{r},\mathbf{p})$, $G(\mathbf{r},\mathbf{r}';E)$ is unique and real. In the continuous spectrum of the Hamiltonian, however, a whole family of solutions prevails. Since this case corresponds to scattering problems, we concentrate our considerations on it. In particular, we are again interested in the retarded solution $G(\mathbf{r},\mathbf{r}';E)$, which in terms of boundary conditions corresponds to an outgoing wave behavior of $G(\mathbf{r},\mathbf{r}';E)$ for large distances $|\mathbf{r}-\mathbf{r}'|$ (Appendix A.4). This nomenclature is motivated by the fact that the retarded quantum propagator $K_F(\mathbf{r},t;\mathbf{r}',t')$ (2.8) and the retarded energy Green function $G(\mathbf{r},\mathbf{r}';E)$ are interconnected by a Laplace transform:

$$G(\mathbf{r},\mathbf{r}';E) \;=\; -\,\frac{i}{\hbar}\int_0^\infty dt\, e^{iEt/\hbar}\,K_F(\mathbf{r},t;\mathbf{r}',0) \tag{2.13}$$

Using the Green function, the formal solution to the stationary quantum source problem (2.11) reads:

$$\psi_\sigma(\mathbf{r};E) \;=\; \int d^3r'\,G(\mathbf{r},\mathbf{r}';E)\,\sigma(\mathbf{r}') \tag{2.14}$$

Let us comment on the availability of the Green function. Obviously $G(\mathbf{r},\mathbf{r}';E)$ depends on the choice of potential $U(\mathbf{r})$. In one-dimensional systems, $G(z,z';E)$ is

constructed by finding appropriate eigenfunctions $\psi_<(z;E)$, $\psi_>(z;E)$ of the corresponding Schrödinger equation that behave regularly in the semi-spaces $z < z'$ and $z > z'$, respectively, and matching these at $z = z'$. (This program is carried out in Appendix A.4.) In higher-dimensional spaces, this simple concept is not applicable, and $G(\mathbf{r},\mathbf{r}';E)$ is known only for a few most elementary potentials. For the important case of physical space ($D = 3$), these include free particles ($U(\mathbf{r}) \equiv 0$) and uniform force fields ($U(\mathbf{r}) = -\mathbf{r}\cdot\mathbf{F}$). Later on, we will present a detailed analysis of the latter problem (Section 5).

2.3.2 Currents Generated By Sources

Having the solution (2.14) of the stationary quantum mechanical source problem at hand, we now derive an explicit expression for the total current J that is generated by a localized source (see also Appendix A.6). We first show that the introduction of a probability amplitude source term $\sigma(\mathbf{r},t)$ into the Schrödinger equation (2.7) leads to the formation of an electron source generating an external current. Repeating the derivation of the quantum mechanical equation of continuity [83] within the source model, we obtain:

$$\frac{\partial}{\partial t}\,|\Psi_\sigma(\mathbf{r},t)|^2 + \boldsymbol{\nabla}\cdot\mathbf{j}(\mathbf{r},t) \;=\; -\,\frac{2}{\hbar}\,\Im\left[\sigma(\mathbf{r},t)^*\Psi_\sigma(\mathbf{r},t)\right] \tag{2.15}$$

The right hand side of this modified equation of continuity manifestly displays a source term for the probability current density $\mathbf{j}(\mathbf{r},t)$ that has been defined in the conventional way,

$$\mathbf{j}(\mathbf{r},t) \;=\; \frac{\hbar}{M}\,\Im\left[\Psi_\sigma(\mathbf{r},t)^*\,\boldsymbol{\nabla}\,\Psi_\sigma(\mathbf{r},t)\right] \tag{2.16}$$

Note that this source term not only depends on $\sigma(\mathbf{r},t)$ but also on the wave function $\Psi_\sigma(\mathbf{r},t)$ and hence on the boundary condition imposed on the propagator (2.8). The character of the inhomogeneous current terms is determined by causality: Our choice of "retarded" wave functions leads to electron sources, whereas "advanced" solutions give rise to an electron drain. This non-unitary current generating behavior is limited to the source region; outside the source, $\sigma(\mathbf{r},t) \equiv 0$ holds, and the current is conserved.

For stationary sources $\sigma(\mathbf{r};E)$, the total current $J(E)$ generated by the source can be directly obtained from (2.15). Inserting the expression for the wave function $\Psi_\sigma(\mathbf{r};E)$ (2.14), the application of the divergence theorem immediately yields:

$$J(E) \;=\; -\,\frac{2}{\hbar}\,\Im\left[\int d^3r \int d^3r'\,\sigma(\mathbf{r})^*\,G(\mathbf{r},\mathbf{r}';E)\,\sigma(\mathbf{r}')\right] \tag{2.17}$$

This is a positive definite expression bilinear in the source term $\sigma(\mathbf{r})$ [75]. (We note that the current $J(E)$ may also be represented in terms of the eigenstates of the Hamiltonian $H(\mathbf{r},\mathbf{p})$ in (2.7). This expansion is listed in Appendix A.6.1.)

2.4 Multipole Sources

From (2.14) and (2.17) it is obvious that the quantum theory of sources becomes particularly simple when pointlike sources are considered. In this case, the integrations appearing in these equations become trivial. At first glance it seems that a natural choice for a pointlike quantum source is given by a Dirac delta function, $\sigma(\mathbf{r}) = C\delta(\mathbf{r}-\mathbf{r}')$; then, the wave function $\psi_\sigma(\mathbf{r};E)$ (2.14) will be proportional to the Green function $G(\mathbf{r},\mathbf{r}';E)$ itself, and the total current $J(\mathbf{r}';E)$ emitted from this pointlike source is essentially contained in the imaginary part of $G(\mathbf{r}',\mathbf{r}';E)$ (2.17). However, proceeding along this line has the drawback that the method will lead to a locally spherically symmetric current emission pattern $\mathbf{j}(\mathbf{r};E)$ (see Appendix A.5.1). This property is due to the fact that the source term $\sigma(\mathbf{r})$ is invariant with respect to rotations around $\mathbf{r}'$. Therefore, this simple-minded approach is limited to s–wave current emission patterns and is not capable to describe local electron sources with non-vanishing angular momentum. As we shall see shortly, spatially oriented emission characteristics are available in photodetachment phenomena (Section 3.1).

This shortcome will be remedied by the introduction of pointlike sources of definite angular momentum (l,m) that we denote as multipole sources. This is not a new concept; in fact, decompositions of Green functions into eigenstates of angular momentum are common in potential theory (e. g., electrostatics) where the technique is known as multipole expansion [84]. We will now develop the source picture of multipoles using electrostatics as a guide. Finally, we will transfer the concept to quantum sources.

2.4.1 Interlude: Multipole Potentials

According to this introduction, we are interested in electrostatic potentials $U_{lm}(\mathbf{r},\mathbf{r}')$ that are eigenfunctions of angular momentum (with respect to $\mathbf{r}'$). Such a function must be everywhere harmonic with the possible exceptions of the singular points, i. e., the origin $\mathbf{r}=\mathbf{r}'$ and infinity $r\to\infty$. In spherical coordinates, this leads to the condition ($\mathbf{r}\neq\mathbf{r}'$):

$$\Delta\, U_{lm}(\mathbf{r},\mathbf{r}') \;=\; \left\{\frac{1}{R}\,\frac{\partial^2}{\partial R^2}\,R \;-\; \frac{l(l+1)}{R^2}\right\} U_{lm}(\mathbf{R}) \;=\; 0 \tag{2.18}$$

Here, we denoted the relative distance vector by $\mathbf{R} = \mathbf{r} - \mathbf{r}'$. Then, a pair of solutions will be given by the harmonic polynomial $K_{lm}(\mathbf{R})$ that is regular at $\mathbf{r} = \mathbf{r}'$, and the multipole potential $\Phi_{lm}(\mathbf{R})$ which vanishes ar $r \to \infty$. In spherical coordinates, they are represented as products of spherical harmonics $Y_{lm}(\hat{R})$ with simple radial functions:

$$\begin{aligned} K_{lm}(\mathbf{R}) &= R^l \, Y_{lm}(\hat{R}) \\ \Phi_{lm}(\mathbf{R}) &= R^{-(l+1)} \, Y_{lm}(\hat{R}) \end{aligned} \tag{2.19}$$

We are mainly interested in the multipole potentials $\Phi_{lm}(\mathbf{R})$ that will correspond to "outgoing-wave" or Hankel solutions. The regular solution, however, is highly useful in this development: As an attractive feat, $K_{lm}(\mathbf{R})$ actually presents a homogeneous polynomial of order l in the vector components R_x, R_y, R_z that shows the desired (l, m) angular characteristics. (For example, $K_{20}(\mathbf{R}) = \sqrt{5/16\pi}\,(2R_z^2 - R_x^2 - R_y^2)$.)

This observation is significant because it permits to construct a differential operator of (l, m) spherical symmetry that, when acting on an arbitrary scalar function $f(R)$, will imprint its angular dependence on $f(R)$. To find this differential operator, we just replace the vector $\mathbf{R}$ in the argument of the harmonic polynomial $K_{lm}(\mathbf{R})$ by the gradient with respect to $\mathbf{r}'$ and obtain the spherical tensor gradient $K_{lm}(\partial/\partial\mathbf{r}')$ [85–87], a polynomial differential operator in $(\partial/\partial x', \partial/\partial y', \partial/\partial z')$ that manifestly exhibits (l, m) angular characteristics. (The theory of spherical tensor operators is covered in greater detail in Appendix B.3–B.5.) Note that this operator commutes with the Laplacian Δ that acts on the other variable $\mathbf{r}$. Therefore, harmonic scalar functions $h(R)$ will be transformed by application of $K_{lm}(\partial/\partial\mathbf{r}')$ into harmonic functions of angular momentum (l, m), i. e., a linear combination of $K_{lm}(\mathbf{R})$ and $\Phi_{lm}(\mathbf{R})$.

Clearly, the scalar harmonic function $h(R)$ that we have in mind here is the Green function of potential theory, $G(\mathbf{r}, \mathbf{r}') = -1/4\pi R$. In fact, one can show that the multipole potentials $\Phi_{lm}(\mathbf{R})$ are generated from $G(\mathbf{r}, \mathbf{r}')$ by the spherical tensor gradients $K_{lm}(\partial/\partial\mathbf{r}')$ [88–90]:

$$K_{lm}\left(\frac{\partial}{\partial \mathbf{r}'}\right) \left[\frac{1}{|\mathbf{r} - \mathbf{r}'|}\right] = (2l-1)!! \, \Phi_{lm}(\mathbf{r} - \mathbf{r}') \tag{2.20}$$

A proof of this assertion is presented in Appendix C.1, equation (C.20). Now, using the Green function property of $G(\mathbf{r}, \mathbf{r}')$:

$$\Delta \left[\frac{1}{|\mathbf{r} - \mathbf{r}'|}\right] = -4\pi \, \delta(\mathbf{r} - \mathbf{r}') \tag{2.21}$$

by combination of (2.20) and (2.21) we infer that the multipole potentials $\Phi_{lm}(\mathbf{R})$ are

also generated by point sources:

$$\Delta\,\Phi_{lm}(\mathbf{r}-\mathbf{r}') = \frac{1}{(2l-1)!!}\,K_{lm}\left(\frac{\partial}{\partial\mathbf{r}'}\right)\Delta\left[\frac{1}{|\mathbf{r}-\mathbf{r}'|}\right] = -\,\frac{4\pi}{(2l-1)!!}\,K_{lm}\left(\frac{\partial}{\partial\mathbf{r}'}\right)\delta(\mathbf{r}-\mathbf{r}') \tag{2.22}$$

Therefore, the sources of multipole potentials $\Phi_{lm}(\mathbf{r}-\mathbf{r}')$ are given by the spherical tensor gradients of the delta function. Obviously, the right hand side of (2.22) displays pointlike sources of definite angular momentum (l,m) that, reasonably enough, are known as multipole delta functions $\delta_{lm}(\mathbf{r}-\mathbf{r}')$ [86,87]:

$$\delta_{lm}(\mathbf{r}-\mathbf{r}') \;=\; K_{lm}\left(\frac{\partial}{\partial\mathbf{r}'}\right)\,\delta(\mathbf{r}-\mathbf{r}') \tag{2.23}$$

We note here that the s–wave multipole source $\delta_{00}(\mathbf{r}-\mathbf{r}')$ apart from a constant factor is identical to the usual point source $\delta(\mathbf{r}-\mathbf{r}')$.

2.4.2 Quantum Multipole Sources

Using these derivatives of the delta function, we adapt the theory of multipoles to quantum mechanics. Let us call the corresponding retarded solution $G_{lm}(\mathbf{r},\mathbf{r}';E)$ of the stationary Schrödinger equation:

$$\left\{E+\frac{\hbar^2}{2M}\,\Delta\;-\;U(\mathbf{r})\right\}\,G_{lm}(\mathbf{r},\mathbf{r}';E)\;=\;\delta_{lm}(\mathbf{r}-\mathbf{r}') \tag{2.24}$$

a multipole Green function or, equivalently, the (l,m) scattering partial wave in the potential $U(\mathbf{r})$. Because the Hamiltonian appearing in (2.24) commutes with the spherical tensor operator $K_{lm}(\partial/\partial r')$, we find from (2.12), (2.23) and (2.24) the following relation connecting $G_{lm}(\mathbf{r},\mathbf{r}';E)$ with the common Green function:

$$G_{lm}(\mathbf{r},\mathbf{r}';E)\;=\;K_{lm}\left(\frac{\partial}{\partial\mathbf{r}'}\right)\,G(\mathbf{r},\mathbf{r}';E) \tag{2.25}$$

The multipole Green functions are therefore obtainable from $G(\mathbf{r},\mathbf{r}';E)$ by means of differentiation. (Note that the s–wave Green function $G_{00}(\mathbf{r},\mathbf{r}';E)$ equals the ordinary Green function $G(\mathbf{r},\mathbf{r}';E)$ up to a factor $\sqrt{4\pi}$.) Clearly, this definition of $G_{lm}(\mathbf{r},\mathbf{r}';E)$ is a purely formal one. However, one may prove that (2.25) indeed leads to Green functions $G_{lm}(\mathbf{r},\mathbf{r}';E)$ that share a common behavior in the vicinity of the multipole source $\mathbf{r}\to\mathbf{r}'$ which is furthermore in agreement with the asymptotics of the multipole potential $\Phi_{lm}(\mathbf{r}-\mathbf{r}')$ (2.19), provided only that the potential function $U(\mathbf{r})$ in (2.24) is locally analytic at $\mathbf{r}=\mathbf{r}'$ (Appendix A.5.3). Thus, the functions $G_{lm}(\mathbf{r},\mathbf{r}';E)$ (2.25) are rightfully dubbed multipole Green functions.

2.4.3 Multipole Currents

Finally, we calculate the total current $J_D(\mathbf{r}';E)$ generated by a pointlike source $D(\mathbf{r}-\mathbf{r}')$ located at $\mathbf{r}'$. We shall assume that this source may be represented by a superposition of multipole contributions with relative strengths λ_{lm}:

$$D(\mathbf{r}-\mathbf{r}') \;=\; \sum_{l=0}^{\infty} \sum_{m=-l}^{l} \lambda_{lm}\, \delta_{lm}(\mathbf{r}-\mathbf{r}') \tag{2.26}$$

To calculate the current due to this source, we insert the expression for the generalized multipole source $D(\mathbf{r}-\mathbf{r}')$ (2.26) into our formula (2.17) for the total current. A series of partial integrations yields:

$$J_D(\mathbf{r}';E) \;=\; -\frac{2}{\hbar} \lim_{\mathbf{r}\to\mathbf{r}'} \Im \left[\sum_{l=0}^{\infty} \sum_{m=-l}^{l} \sum_{l'=0}^{\infty} \sum_{m'=-l'}^{l'} \lambda_{lm}^{*}\, A_{lml'm'}(\mathbf{r},\mathbf{r}';E)\, \lambda_{l'm'} \right] \tag{2.27}$$

Here, the symbol $A_{lml'm'}(\mathbf{r},\mathbf{r}';E)$ denotes the elements of an auxiliary matrix:

$$A_{lml'm'}(\mathbf{r},\mathbf{r}';E) \;=\; K_{lm}^{*}\left(\frac{\partial}{\partial \mathbf{r}}\right) K_{l'm'}\left(\frac{\partial}{\partial \mathbf{r}'}\right) G(\mathbf{r},\mathbf{r}';E) \tag{2.28}$$

Since the multiple sum in (2.27) presents a quadratic form, it immediately follows that only the anti-hermitian part of this matrix contributes to the current $J_D(\mathbf{r}';E)$. After a few transformations, we obtain the following symmetric representation (Appendix A.5.4):

$$J_D(\mathbf{r}';E) \;=\; \sum_{l=0}^{\infty} \sum_{m=-l}^{l} \sum_{l'=0}^{\infty} \sum_{m'=-l'}^{l'} \lambda_{lm}^{*}\, J_{lml'm'}(\mathbf{r}';E)\, \lambda_{l'm'} \tag{2.29}$$

where the hermitian total current matrix $J_{lml'm'}(\mathbf{r}';E)$ is given by:

$$J_{lml'm'}(\mathbf{r}';E) \;=\; \frac{i}{\hbar} \lim_{\mathbf{r}\to\mathbf{r}'} K_{lm}^{*}\left(\frac{\partial}{\partial \mathbf{r}}\right) K_{l'm'}\left(\frac{\partial}{\partial \mathbf{r}'}\right) \{G(\mathbf{r},\mathbf{r}';E) - G(\mathbf{r}',\mathbf{r};E)^{*}\} \tag{2.30}$$

This expression shows the advantage that unlike (2.28), the argument of the differential operators in (2.30) remains regular as $\mathbf{r}\to\mathbf{r}'$. We note that $G(\mathbf{r},\mathbf{r}';E) = G(\mathbf{r}',\mathbf{r};E)^{*}$ holds if E is outside the continuous spectrum of the Hamiltonian $H(\mathbf{r},\mathbf{p})$ (Appendix A.3.6). Thus, according to (2.30) current emission is restricted to scattering problems, as it must be.

The current formula (2.29) simplifies for certain symmetries of the Hamiltonian (Appendix A.5.4): If the potential function $U(\mathbf{r})$ is spherically symmetric with respect to $\mathbf{r}'$, the total current element $J_{lml'm'}(\mathbf{r}';E)$ (2.30) vanishes unless $l = l'$ and $m = m'$,

and does not depend on the magnetic quantum number m. (We will encounter this condition in Section 3.2.) If $U(\mathbf{r})$ is at least cylindrically symmetric with respect to the z axis (which is taken as the axis of angular momentum quantization), then a non-vanishing matrix element $J_{lml'm'}(\mathbf{r}';E)$ requires $m = m'$. We will exploit this property in Chapter 5 where we will deal with motion in a uniform force field ($U(\mathbf{r}) = -Fz$). There, multipole sources $\delta_l(\mathbf{r}-\mathbf{r}')$ of definite total angular momentum l will appear:

$$\delta_l(\mathbf{r}-\mathbf{r}') \;=\; \sum_{m=-l}^{l} \lambda_{lm}\, \delta_{lm}(\mathbf{r}-\mathbf{r}') \tag{2.31}$$

According to (2.29) and (2.30), this point source will generate a current $J_l(\mathbf{r}';E)$ which simply presents the weighed sum of all multipole current components $J_{lm}(\mathbf{r}';E)$:

$$J_l(\mathbf{r}';E) \;=\; \sum_{m=-l}^{l} |\lambda_{lm}|^2\, J_{lm}(\mathbf{r}';E) \tag{2.32}$$

where the partial currents may be written in the form:

$$J_{lm}(\mathbf{r}';E) \;=\; J_{lmlm}(\mathbf{r}';E) \;=\; -\frac{2}{\hbar}\lim_{\mathbf{r}\to\mathbf{r}'} \Im\left[K_{lm}^*\left(\frac{\partial}{\partial\mathbf{r}}\right) K_{lm}\left(\frac{\partial}{\partial\mathbf{r}'}\right) G(\mathbf{r},\mathbf{r}';E)\right] \tag{2.33}$$

Off-diagonal contributions are absent in this case.

We note that the total multipole currents $J_{lm}(\mathbf{r}';E)$ may be extracted from the Green function $G(\mathbf{r},\mathbf{r}';E)$ by differentiation and a limiting process; no integrations are needed for this purpose. As a special case, the s-wave current $J_{00}(\mathbf{r}';E)$ is given by:

$$J_{00}(\mathbf{r}';E) \;=\; -\frac{1}{2\pi\hbar}\,\Im\left[G(\mathbf{r}',\mathbf{r}';E)\right] \tag{2.34}$$

In passing we note that the current (2.34) may also be expressed by the local density of states (LDOS) $n(\mathbf{r}';E)$ at the location of the source $\mathbf{r}'$: $n(\mathbf{r}';E) = 2\hbar\, J_{00}(\mathbf{r}';E)$ [75,82]. (For a derivation of this formula, we refer to Appendix A.6.1.)

In conclusion, we emphasize here that if $G(\mathbf{r},\mathbf{r}';E)$ is available in analytical form, the whole series of multipole Green functions $G_{lm}(\mathbf{r},\mathbf{r}';E)$ and total multipole currents $J_{lml'm'}(\mathbf{r}';E)$ also can be calculated explicitly using (2.25), (2.30) and (2.33). We will rely on this property in Chapter 5 where we will determine comparatively compact closed-form expressions for the partial scattering waves and total multipole currents in the uniform field environment $U(\mathbf{r}) = -\mathbf{r}\cdot\mathbf{F}$.

Chapter 3

Photodetachment as a Source Process

FOLLOWING OUR MATHEMATICAL DISCUSSION of quantum source theory, we now demonstrate a specific example of a physical process that is amenable to treatment in the framework of this method. As a model system, we will consider the emission of electrons released from negatively charged ions following the absorption of a single laser photon, an event that is designated as photodetachment. (For a recent summary of negative ion spectroscopy we refer to the review by Blondel [91].) In our presentation, we point out the intimate relationship between the source theoretical description of this process and conventional perturbative scattering theory. (A formal proof of the equivalence of the quantum source method and standard perturbative approaches, represented by Fermi's Golden Rule, is the subject of Appendix A.6.2.) Furthermore, we deliver a fairly detailed account of the series of approximations implicit in the modeling of near-threshold photodetachment processes by pointlike multipole sources. (Note that several discussions of the photodetachment phenomenon can be found in the literature, see e. g. [10–12,14,15,17,19–21,23,27,31,92,93]; we will, however, direct our efforts on the source aspect of the problem.) In the second part of this chapter, as a simple and instructive example we will consider the theory of multipole sources in a field-free environment. From studies of the electron affinity of various elements, experimental data on photodetachment is readily available which provides us with the opportunity to assess the range of validity of the multipole source approximation.

3.1 Quantum Source Theory of Photodetachment

Let us first sketch a simplified picture of the electron photodetachment (or photodecomposition) phenomenon: A beam of negatively charged ions enters the interaction chamber and is irradiated by a laser beam; occasionally, an ion absorbes a photon and decays into a neutral ground-state atom which leaves the reaction site within the ion beam whereas the excess charge is detached into a continuum state (see Figure 1). The dynamics of the emitted electron is then governed by an additional external field $U_{\mathrm{ext}}(\mathbf{r})$ (if present).

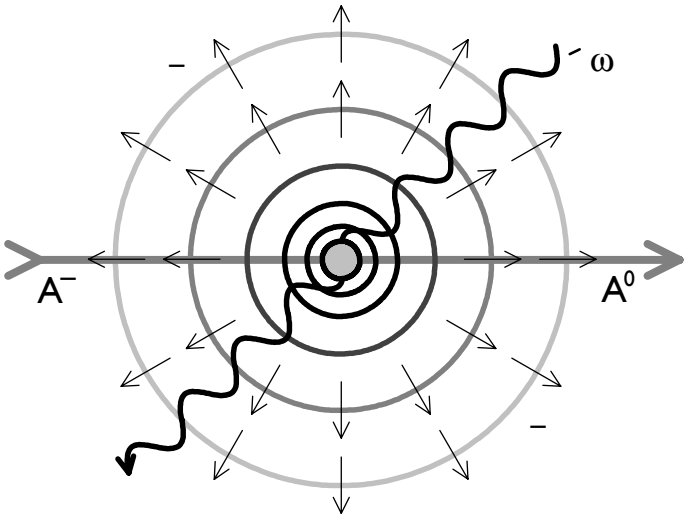

Figure 1: Theoretician's view of the photodetachment process. Negatively charged ions are irradiated with a laser beam. Occasionally, an ion absorbs a photon and releases its excess electron into an outgoing-wave continuum state.

3.1.1 Setting up the Hamiltonian

We start our theoretical analysis of this scattering process by setting up the Hamiltonian $H_L(\mathbf{r},t)$ of the ion-photon system (we use cgs units):

$$H_L(\mathbf{r},t) \;=\; \frac{1}{2M}\left[-i\hbar\boldsymbol{\nabla} + \frac{e}{c}\mathbf{A}_L(\mathbf{r},t)\right]^2 + U_{\rm at}(\mathbf{r}) + U_{\rm ext}(\mathbf{r}) \tag{3.1}$$

Here, $\mathbf{r}$ denotes the set of position vectors of the electrons in the ionic shell, $U_{\rm at}(\mathbf{r})$ represents the atomic potential, and $\mathbf{A}_L(\mathbf{r},t)$ contains the (quantized) vector potential of the laser field that reads [94]:

$$\mathbf{A}_L(\mathbf{r},t) \;=\; \sum_{\mathbf{K},\,\boldsymbol{\epsilon}} \sqrt{\frac{2\pi\hbar c^2}{\omega V}}\,\left\{e^{i\,(\mathbf{K}\cdot\mathbf{r}-\omega t)}\,\boldsymbol{\epsilon}\,\hat{a}_{\mathbf{K},\,\boldsymbol{\epsilon}} \;+\; e^{-\,i\,(\mathbf{K}\cdot\mathbf{r}-\omega t)}\,\boldsymbol{\epsilon}^*\,\hat{a}^+_{\mathbf{K},\,\boldsymbol{\epsilon}}\right\} \tag{3.2}$$

As usual, $\mathbf{K}$ is the wave vector of the photon, $\omega = Kc$ its wave number, V denotes some normalization volume, and $\boldsymbol{\epsilon}$ represents the polarisation vector of the photon. In the following we shall be content with a semiclassical model of a monochromatic laser field, i. e., a large photon density N/V is assumed. Furthermore, for the sake of simplicity we will use the dipole approximation (long wave limit) $\mathbf{K}\cdot\mathbf{r} \approx 0$. (Later on, we will formally extend the result to multipole radiation). Then, the vector potential

(3.2) reduces to:

$$\mathbf{A}_L(\mathbf{r},t) \;=\; \sqrt{\frac{2\pi\hbar c^2 N}{\omega V}}\, e^{-i\omega t}\, \boldsymbol{\epsilon} \tag{3.3}$$

(Note that we solely consider the absorption process and neglect those rare events where an electron in a continuum state is captured by a neutral atom and a photon is emitted.) Since photodetachment for photon energies $\hbar\omega$ near threshold only occasionally occurs, it is reasonable to split the Hamiltonian $H_L(\mathbf{r},t)$ (3.1) into two parts:

$$H_L(\mathbf{r},t) \;=\; H_0(\mathbf{r}) + W_L(\mathbf{r},t) \tag{3.4}$$

Here, $H_0(\mathbf{r})$ denotes the stationary atomic Hamiltonian (without laser field):

$$H_0(\mathbf{r}) \;=\; -\frac{\hbar^2}{2M}\,\Delta + U_{\text{at}}(\mathbf{r}) + U_{\text{ext}}(\mathbf{r}) \tag{3.5}$$

whereas $W_L(\mathbf{r},t)$ approximates the laser-ion interaction:

$$W_L(\mathbf{r},t) \;\approx\; -\frac{ie\hbar}{2Mc}\,\{\boldsymbol{\nabla}\cdot\mathbf{A} + \mathbf{A}\cdot\boldsymbol{\nabla}\} \;\approx\; -\frac{ie\hbar}{M}\sqrt{\frac{2\pi\hbar N}{\omega V}}\, e^{-i\omega t}\,\boldsymbol{\epsilon}\cdot\boldsymbol{\nabla} \tag{3.6}$$

3.1.2 Introducing Sources

Using this notation, the Schrödinger equation of the detachment problem can be written in the following suggestive fashion (cf. Appendix A.2.3):

$$\left\{ i\hbar\frac{\partial}{\partial t} - H_0(\mathbf{r}) \right\} \Psi(\mathbf{r},\,t) \;=\; W_L(\mathbf{r},t)\,\Psi(\mathbf{r},\,t) \tag{3.7}$$

Treating the right hand side of this equation as an inhomogeneity, source theory states that a solution is formally given by (2.8),

$$\Psi(\mathbf{r},t) \;-\; \Psi_i(\mathbf{r},t) \;=\; -\frac{i}{\hbar}\int d\mathbf{r}' \int dt'\, K_F(\mathbf{r},t;\mathbf{r}',t')\, W_L(\mathbf{r}',t')\,\Psi(\mathbf{r}',t') \tag{3.8}$$

where $\Psi_i(\mathbf{r},t)$ is the ground state of the ion without laser field, and $K_F(\mathbf{r},t;\mathbf{r}',t')$ denotes the atomic propagator representing $H_0(\mathbf{r})$. Note that we have just rewritten the Schrödinger equation in its integral form (the Lippmann-Schwinger equation); (3.8) should not be considered as a "solution" to (3.7) as the wave function $\Psi(\mathbf{r},t)$ appears on both sides of this equation. In terms of the language developed in Section 2.1, the right hand side of (3.7) presents an internal quantum source.

Clearly, in Chapter 2 we developed quantum source theory with external sources in mind. Hence, we are now faced with the problem of transforming the exact expression (3.8) by a series of approximations into some form accessible to the source approach. The necessary technique is equivalent to a well-established tool of conventional scattering theory, viz., first-order perturbation theory or, synonymous, the Born approximation. Let us recall the basic idea behind this approach: Interactions are assumed to be rare events, so for all times t the wave function $\Psi(\mathbf{r},t)$ closely resembles the initial wave function $\Psi_i(\mathbf{r},t)$:

$$\Psi_i(\mathbf{r},t) \;=\; \chi_i(\mathbf{r})\, e^{-iE_i t/\hbar} \tag{3.9}$$

Here, $\chi_i(\mathbf{r})$ denotes the ionic ground state, an eigenstate of $H_0(\mathbf{r})$ with energy E_i. Because $\Psi(\mathbf{r},t)$ and $\Psi_i(\mathbf{r},t)$ are almost equal, we may replace the actual wave function on the right hand side of (3.8) by the ionic ground state. On the other hand, neglecting multiple scattering processes, the left hand side of this equation represents the wave function of the accumulating scattering products, i. e., neutral ground-state atoms and detached electrons. For their combined wave function $\Psi_f(\mathbf{r},t)$, another eigenstate of $H_0(\mathbf{r})$ with energy E_f, we write:

$$\Psi_f(\mathbf{r},t) \;=\; \psi_f(\mathbf{r})\, e^{-iE_f t/\hbar} \tag{3.10}$$

Using these approximations, we have decoupled the scattering wave function $\Psi_f(\mathbf{r},t)$ (3.10) from the initial ionic wave function $\Psi_i(\mathbf{r},t)$ (3.10) that now serves as an external source for the reaction products. Further simplification is still possible: We remark that the photodetachment setup sketched in Figure 1 does not change in time, so a description in terms of the stationary variant of source theory should be possible. Indeed, noting that $E_f = E_i + \hbar\omega$, we infer from (3.6)–(3.10) that the source term in (3.8) oscillates with the frequency $E_f/\hbar$ and hence presents a stationary source in the sense of Section 2.3, see (2.9).

Considering (2.11)–(2.14), it is easily verified that the Born approximation to (3.8) is equivalent to the inhomogeneous stationary Schrödinger equation for the final state $\psi_f(\mathbf{r})$:

$$\{E_f \;-\; H_0(\mathbf{r})\}\;\psi_f(\mathbf{r}) \;=\; -\,\frac{ie\hbar}{M}\,\sqrt{\frac{2\pi\hbar N}{\omega V}}\;\boldsymbol{\epsilon}\cdot\boldsymbol{\nabla}\,\chi_i(\mathbf{r}) \tag{3.11}$$

Formally, an integral for this differential equation may be obtained by employing the atomic Green function $G_{\mathrm{at}}(\mathbf{r},\mathbf{r}';E)$ corresponding to $H_0(\mathbf{r})$ (2.14):

$$\psi_f(\mathbf{r}) \;=\; -\,\frac{ie\hbar}{M}\,\sqrt{\frac{2\pi\hbar N}{\omega V}}\;\int d\mathbf{r}'\, G_{\mathrm{at}}(\mathbf{r},\mathbf{r}';E_f)\;\boldsymbol{\epsilon}\cdot\boldsymbol{\nabla}'\,\chi_i(\mathbf{r}') \tag{3.12}$$

This expression is, however, of little practical use since the multi-particle atomic Green function $G_{\rm at}(\mathbf{r},\mathbf{r}';E)$ is not available. Hence, our next objective is the introduction of the one-particle Green function of the electron in the external potential $U_{\rm ext}(\mathbf{r})$.

It is reasonable to assume that the additional, weakly bound charge in the negative ion presents only a minor perturbation to the inner atomic electron shell that remains essentially unchanged when the electron is detached by the laser photon. Furthermore, following the detachment process the interaction between the escaping electron and the remaining neutral atom will be negligible. Therefore, the dynamics of the liberated electron will be governed solely by the external potential $U_{\rm ext}(\mathbf{r})$. (Note that this statement manifestly does not hold for the related photoionization process which leaves behind a charged ionic core.) These assertions allow to approximate the atomic Green function $G_{\rm at}(\mathbf{r},\mathbf{r}';E_f)$ and the final wave function $\psi_f(\mathbf{r})$ by products of independent wave functions for the remaining atomic shell $\chi_f(\mathbf{r}_s)$ and the detached electron $\psi_e(\mathbf{r}_e)$. (In a Hartree-type approximation, the set of electronic position vectors $\mathbf{r}$ has been split into a set of electrons $\mathbf{r}_s$ remaining in the emerging neutral atom, and the vector $\mathbf{r}_e$ belonging to the detached electron.)

Clearly, the final state of the neutral atomic shell $\chi_f(\mathbf{r}_s)$ obeys the atomic Schrödinger equation:

$$\left\{E_{\rm tr}+\frac{\hbar^2}{2M}\,\Delta_s-U_{\rm at}(\mathbf{r}_s)-U_{\rm ext}(\mathbf{r}_s)\right\}\,\chi_f(\mathbf{r}_s)\;=\;0 \tag{3.13}$$

Here, $E_{\rm tr}$, the threshold energy of the process, denotes the energy of the atomic ground state. Only the excess energy $E=E_f-E_{\rm tr}$ is available to the electron whose one-particle Green function in the external potential $U_{\rm ext}(\mathbf{r})$ reads:

$$\left\{E+\frac{\hbar^2}{2M}\,\Delta_e-U_{\rm ext}(\mathbf{r}_e)\right\}\,G(\mathbf{r}_e,\mathbf{r}_e';\,E)\;=\;\delta(\mathbf{r}_e-\mathbf{r}_e') \tag{3.14}$$

Then, the product approximation states that the final wave function is given by:

$$\psi_f(\mathbf{r})\;=\;\psi_e(\mathbf{r}_e)\,\chi_f(\mathbf{r}_s) \tag{3.15}$$

whereas the atomic Green function $G_{\rm at}(\mathbf{r},\mathbf{r}';E_f)$ in (3.12) is represented by:

$$G_{\rm at}(\mathbf{r},\mathbf{r}';\,E_f)\;=\;G(\mathbf{r}_e,\mathbf{r}_e';\,E)\;[\chi_f(\mathbf{r}_s)\chi_f(\mathbf{r}_s')^*] \tag{3.16}$$

Note that the atomic shell part of the multi-particle Green function (3.16) has been approximated by the projector on the atomic ground state $\chi_f(\mathbf{r}_s)$. (For spectral representations of the Green function, see Appendix A.3.6.) Inserting (3.15) and (3.16) into

(3.12) we obtain an integral equation for the wave function of the detached electron:

$$\psi_e(\mathbf{r}_e) \;=\; -\,\frac{ie\hbar}{M}\,\sqrt{\frac{2\pi\hbar N}{\omega V}}\,\int d^3r'_e\,G(\mathbf{r}_e,\mathbf{r}'_e;\,E)\int d\mathbf{r}_s\,\chi_f(\mathbf{r}'_s)^*\,\boldsymbol{\epsilon}\cdot\boldsymbol{\nabla}'\,\chi_i(\mathbf{r}') \tag{3.17}$$

3.1.3 Multipole Approximation

From (3.17) we infer that the electronic wave function $\psi_e(\mathbf{r}_e)$ is generated by a source containing the dipole matrix element of the initial and final wave functions $\chi_i(\mathbf{r})$, $\chi_f(\mathbf{r}_s)$ (3.9), (3.13) of the atomic shell. This is a fairly localized, almost energy-independent source that is basically confined to the size of the original ion. (Note, however, the appearance of the laser frequency ω in the prefactor.) In contrast, the ejected electron populates a spatially extended continuum state. Because we are interested in a macroscopic description of the electronic dynamics in the external potential, we now try to replace the source term in (3.17) by a pointlike electron source centered in the nucleus of the ion which we will set as the origin $\mathbf{r}' = \mathbf{o}$ in the following considerations. Since appreciable overlap of the wave functions only occurs for small $\mathbf{r}'_e$, the obvious way to start this enterprise is to expand the Green function $G(\mathbf{r}_e,\mathbf{r}'_e;\,E)$ into a Taylor series with respect to $\mathbf{r}'_e$. Formally,

$$G(\mathbf{r}_e,\mathbf{r}'_e;\,E) \;=\; \exp\left\{i\mathbf{r}'_e\cdot(-i\boldsymbol{\nabla}')\right\}\,G(\mathbf{r}_e,\mathbf{o};\,E) \tag{3.18}$$

Here, the momentum operator $-i\boldsymbol{\nabla}'$ is understood to act solely onto the second variable of the Green function. However, we now face the problem that the theory of quantum sources as developed in Chapter 2 builds on the notion of multipole sources $\delta_{lm}(\mathbf{r}-\mathbf{r}')$ (2.23) of fixed angular momentum, not on translations like (3.18). Therefore, we are forced to expand the exponential operator in (3.18) in terms of multipoles (B.12):

$$\exp\left\{i\mathbf{r}'_e\cdot(-i\boldsymbol{\nabla}')\right\} \;=\; 4\pi\sum_{l=0}^{\infty} Z_l(\sqrt{{r'_e}^2\Delta'})\sum_{m=-l}^{l} K^*_{lm}(\mathbf{r}'_e)\,K_{lm}(\boldsymbol{\nabla}') \tag{3.19}$$

This transformation formula can be found in Appendix B.3. Inserting this expansion first into the Taylor series (3.18) and finally into the integral representation (3.17) of the wave function $\psi_e(\mathbf{r}_e)$, we obtain an equivalent, yet fairly complicated expression:

$$\begin{aligned}\psi_e(\mathbf{r}_e) \;=\; -\,\frac{4\pi ie\hbar}{M}\,\sqrt{\frac{2\pi\hbar N}{\omega V}}\sum_{l=0}^{\infty}\sum_{m=-l}^{l}\int d^3r'_e\,K^*_{lm}(\mathbf{r}'_e)\;\times\\ \left\{\int d\mathbf{r}'_s\,\chi_f(\mathbf{r}'_s)^*\,\boldsymbol{\epsilon}\cdot\boldsymbol{\nabla}'\,\chi_i(\mathbf{r}')\right\}\,Z_l(\sqrt{{r'_e}^2\Delta'_e})\,K_{lm}(\boldsymbol{\nabla}'_e)\,G(\mathbf{r}_e,\mathbf{o};\,E)\end{aligned} \tag{3.20}$$

Note that the Green function $G(\mathbf{r}_e, \mathbf{r}'_e; E)$ no longer appears in the integrand; it has been replaced by a series of multipole Green functions $G_{lm}(\mathbf{r}_e, \mathbf{o}; E)$ in the last line of (3.20), as comparison with their definition (2.25) shows. We further simplify the expression (3.20) by neglecting "small" terms of the series. Let us remark that $K^*_{lm}(\mathbf{r}'_e)$ is a homogeneous polynomial in $\mathbf{r}'_e$ of degree l; this means that the contributions of this series will rapidly diminsh with increasing l. Hence, we will keep only the first non-vanishing term of the l series. Also, the argument ${r'_e}^2 \Delta'_e$ appearing in the function $Z_l(z)$ (B.12) is small, so we replace this operator by the value it takes on for zero argument $1/(2l+1)!!$, see (B.13).

We then find that the electronic wave function is approximately given by a superposition of multipole Green functions:

$$\psi_e(\mathbf{r}_e) \;=\; \sum_{m=-l}^{l} \lambda_{lm}\, G_{lm}(\mathbf{r}_e, \mathbf{o}; E) \tag{3.21}$$

The ion-photon interaction therefore gives rise to a pointlike electron source that may be decomposed into multipole sources $\delta_{lm}(\mathbf{r}_e)$ of order l whose relative strengths λ_{lm} are almost independent of energy and are given by:

$$\lambda_{lm} \;=\; -\,\frac{4\pi}{(2l+1)!!}\,\frac{ie\hbar}{M}\,\sqrt{\frac{2\pi\hbar N}{\omega V}}\,\int d^3 r_e\, K^*_{lm}(\mathbf{r}_e)\,\int d\mathbf{r}_s\,\chi_f(\mathbf{r}_s)^*\,\boldsymbol{\epsilon}\cdot\boldsymbol{\nabla}\,\chi_i(\mathbf{r}) \tag{3.22}$$

In general, our knowledge about the initial and final shell states $\chi_i(\mathbf{r})$, $\chi_f(\mathbf{r}_s)$ is limited. However, their total angular momenta J_i and J_f are known. (Note that here another approximation enters: The ionic (atomic) ground state shall retain spherical symmetry even when it is broken by the external potential $U_{\text{ext}}(\mathbf{r})$. For the case of electric fields we will consider later on, this means we ignore any Stark splittings of the ion and atom ground states.) It is obvious that the coefficients λ_{lm} will vanish unless the integrand in (3.22) contains a spherically scalar (rotationally invariant) contribution. This means that the angular momenta J_i, J_f and l must add up to $L = 1$. (We remark that the gradient operator $\boldsymbol{\nabla}$ behaves like a vector, i.e., is a spherical tensor of angular momentum $L = 1$. More information on spherical tensor operators is available in Appendix B.) From the addition rules for angular momenta, we find for the minimum l value the selection rule for dipole radiation:

$$l \;=\; \big|\,|J_f - J_i| \,-\, 1\,\big| \tag{3.23}$$

If we allow for general electromagnetic multipole radiation, we have to replace in (3.23) the "1" by the multipole order $j = 1, 2, 3, \ldots$. This complication will practically affect transitions with large $|J_f - J_i|$. Here, we will be content with the cases $\Delta J = 0, 1$ that are subject to dipole transitions: For $J_f = J_i$, the electron leaves in a p–wave

($l = 1$) whose orientation depends on the polarization $\boldsymbol{\epsilon}$ of the laser beam. A prime example for this type of behavior is displayed in near-threshold photodetachment of H^- that obviously involves a transition between s–states. In the case $\Delta J = 1$, the electrons are emitted isotropically ($l = 0$). Both classes of transitions have been studied experimentally [4,58–60].

3.2 Example: Free Photodetachment

Having established that photodetachment phenomena near the energy threshold allow for a description in quantum source theory by pointlike multipole electron sources $\delta_{lm}(\mathbf{r} - \mathbf{r}')$, it is instructive to present theoretical predictions for the electronic wave functions $G_{lm}^{(\mathrm{free})}(\mathbf{r}, \mathbf{r}'; E)$ and integrated photodetachment currents $J_{lm}^{(\mathrm{free})}(E)$ in the simplest case of emission without external potential, $U_{\mathrm{ext}}(\mathbf{r}) \equiv 0$. Furthermore, this is the situation most commonly found in experiments.

Clearly, in this spherically symmetric environment the electronic multipole Green functions $G_{lm}^{(\mathrm{free})}(\mathbf{r}, \mathbf{r}'; E)$ are eigenstates of angular momentum, and we expect that the free multipole source will lead to outgoing spherical electron waves, the (l, m) partial waves well-known from conventional scattering theory [83, 84].

The cornerstone of the source theoretical treatment (2.12) of the field-free emission problem is the corresponding Green function $G^{(\mathrm{free})}(\mathbf{r}, \mathbf{r}'; E)$, a solution of the Schrödinger equation:

$$\left\{ E + \frac{\hbar^2}{2M} \Delta \right\} G^{(\mathrm{free})}(\mathbf{r},\, \mathbf{r}';\, E) \;=\; \delta(\mathbf{r} - \mathbf{r}') \tag{3.24}$$

Electron emission obviously only takes place for $E > 0$. Thus, we may introduce the electronic wave number k by $E = \hbar^2 k^2 / 2M$. From Appendix C.1 we find that the retarded solution to this equation is given by (C.5):

$$G^{(\mathrm{free})}(\mathbf{r},\, \mathbf{r}';\, E) \;=\; -\frac{M}{2\pi\hbar^2} \, \frac{\exp(ik|\mathbf{r} - \mathbf{r}'|)}{|\mathbf{r} - \mathbf{r}'|} \tag{3.25}$$

Following (2.25), all multipole Green functions $G_{lm}^{(\mathrm{free})}(\mathbf{r}, \mathbf{r}'; E)$ are available from the ordinary Green function (3.25) by differentiation. As expected, the radial part of these functions is given by spherical Hankel functions (C.17):

$$G_{lm}^{(\mathrm{free})}(\mathbf{r},\, \mathbf{r}';\, E) \;=\; -\frac{M}{2\pi\hbar^2} \, k^{l+1} \, Y_{lm}(\hat{R}) \, h_l^{(+)}(kR) \tag{3.26}$$

Here, $\mathbf{R} = \mathbf{r} - \mathbf{r}'$. For reference, a mathematical derivation of this result is presented in Appendix C.1.

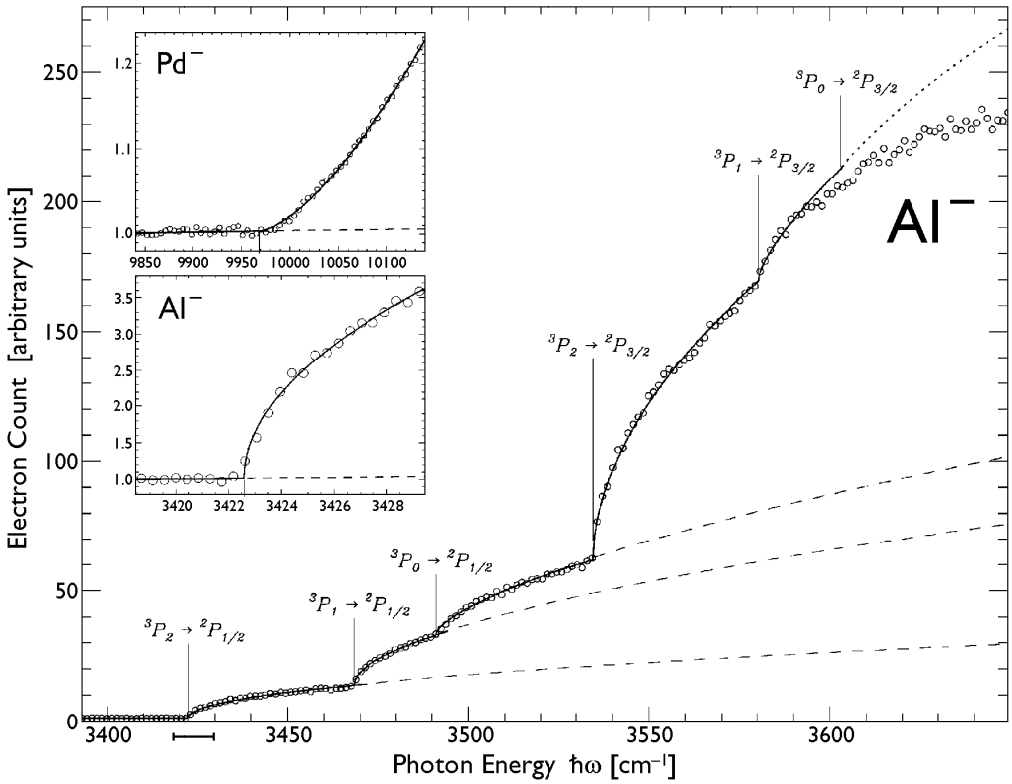

Figure 2: Experimental near-threshold photodetachment cross sections from electron affinity measurements by Scheer et al. [96, 97]. Large caption: s–wave photodetachment of Al^- ions. Due to fine structure splitting of the atomic and ionic ground states, various thresholds appear. Lower inset: Detail of the cross section for Al^- near the onset of photodetachment, fitted by the Wigner law (3.27) ($\sigma_{\rm tot}(E) \sim \sqrt{E}$). Upper inset: Photodetachment data obtained from Pd^- ions. Here, the electrons are emitted into a p–wave ($\sigma_{\rm tot}(E) \sim E^{3/2}$).

Next we discuss the total multipole current $J_{lm}^{(\rm free)}(E)$, i. e., the total photodetachment cross section in the multipole source model, as a function of energy E. The properties of this quantity are intuitively less obvious, but of higher importance since the total cross section is experimentally accessible. We have shown in Section 2.4 that $J_{lm}^{(\rm free)}(E)$ can be extracted from the Green function (3.25) by differentiation and a limiting process (2.33); in practice, this program is carried out in Appendix C.2. The calculation yields a surprisingly simple result (C.30):

$$J_{lm}^{(\rm free)}(E) \;=\; \frac{M}{4\pi^2\hbar^3}\, k^{2l+1} \tag{3.27}$$

As expected, this result does not depend on the magnetic quantum number m. This feature can be traced back to the spherical symmetry of the problem. The simple

power law dependence (3.27), known as Wigner's law [92], has long been observed for the total cross section of reactions near the energy threshold. For higher energies of the emitted electron, the approximation of a pointlike source fails, and corrections to the Wigner law (3.27) are to be expected due to the finite extension of the emitting ion. For a simple core model of the atomic electron shell such correction terms have been derived by Farley [93]. For small excess energies in the order of 10^{-2} eV (10^{3} cm^{-1}) and less that were used in the experiments discussed later in Chapter 6, the deviations from (3.27) are generally found negligibly small. This is in agreement with experimental data [95–98]. Some results from recent measurements of the electron affinity of various elements performed by Scheer and colleagues [96, 97] are displayed in Figure 2. These data confirm that in the near-threshold regime, the Wigner law (3.27) closely matches the experimental cross sections found for detachment both into electronic s– and p–waves. Thus, the multipole source approximation (3.21) provides an excellent description for the photodetachment process. (We note here that the Wigner law (3.27) is valid only for reactions not involving long-range interaction between the products. In the case of photoionization of atoms, i. e., in the presence of Coulomb interaction between the detached electron and the remaining ion core, the cross section $\sigma(E)$ exhibits steplike behavior at the energy threshold [99].)

Chapter 4

Classical Mechanics of Ballistic Motion

HAVING OUTLINED the main elements of the quantum theory of multipole sources (Chapter 2) and shown that photodetachment phenomena near threshold are aptly described in terms of pointlike multipole sources (Chapter 3), we now turn our attention to the physics of uniformly accelerated particles, i. e., their ballistic motion in a homogeneous force field $\mathbf{F}$ generated by a linear potential $U(\mathbf{r}) = -\mathbf{r} \cdot \mathbf{F}$. Apart from the special case of free particles we were considering within the preceding section, this choice of potential obviously presents the simplest problem in mechanics, and its history dates back to the days of Galilei. As we announced in the introduction, we are mainly interested in a study of quantum mechanical point sources in the homogeneous field environment, but to obtain the required quantum solutions it is advisable to examine the simpler corresponding classical problem first. Here, we largely follow a recent presentation of the subject [9].

4.1 Canonical Theory of Ballistic Motion

Integration of the classical equations of motion in a force field of constant strength and direction is one of the basic tasks of mechanics and immediately performed within the Newtonian approach, leading to the well-known pattern of ballistic parabolas. To establish the connection to quantum ballistic motion one has to make use of the canonical Hamilton–Jacobi theory. Due to the simplicity of the problem, the classical action field $S_{\mathrm{cl}}(\mathbf{r}_f, t_f; \mathbf{r}_i, t_i)$ and related quantities can be determined explicitly. It is shown that for a given energy E, at most two trajectories exist that connect the particle's initial and final positions $\mathbf{r}_i$ and $\mathbf{r}_f$. For certain combinations of these points, no classical trajectory with real time of flight exists; this case corresponds to quantum tunneling. Formally, in this case "tunneling" trajectories may be devised by analytic continuation, which populate complex space and require complex times of flight $T = t_f - t_i$. Although it is essentially impossible to visualize these paths, they provide some insight into the difficult and otherwise rather inaccessible field of multidimensional tunneling phenomena [100–110] which is plagued by a lack of analytically solvable examples. As

a major result of our study of the ballistic problem, we find that the structure of these semiclassical trajectories naturally leads to a distinction between dynamically and energetically forbidden motion. As it is absent in one-dimensional problems, the former pattern is a genuine feature of multidimensional tunneling environments.

4.1.1 The Classical Action Functional

We will start with a thorough examination of one of the simplest problems in classical mechanics, namely the motion of a particle subject to a uniform force field $\mathbf{F}$, i. e., in a potential $U(\mathbf{r}) = -\mathbf{r}\cdot\mathbf{F}$. Given its initial position $\mathbf{r}_i$ and velocity $\mathbf{v}_i$ at time $t = t_i$, the Newtonian equations of motion are immediately integrated to yield a particle's trajectory:

$$\mathbf{r}(t) \;=\; \mathbf{r}_i + \mathbf{v}_i(t-t_i) + \mathbf{F}(t-t_i)^2/2M \tag{4.1}$$

This is the common ballistic motion following parabolic paths. Here we should note in passing that since the acting force does not vary in space, the trajectory pattern is translationally invariant, i. e., is a function of $\mathbf{r}(t) - \mathbf{r}_i$ only.

The solution of the initial-value problem (4.1) is a trivial task. It is, however, well-known that the most natural links of classical and quantum mechanics rely on the use of the classical action functional $S_{\rm cl}(\mathbf{r}_f, t_f; \mathbf{r}_i, t_i)$ that is minimized by classical paths [65,83,111]. Furthermore, knowledge of this function will become indispensable when we apply the semiclassical or WKB approximation [110] to the problem of quantum ballistic motion (see Chapters 6 and 7). Therefore, we change our point of view and treat free-falling motion within the framework of Hamilton–Jacobi theory, i. e., we switch to the solution of a boundary-value problem. We will first state the principle of least action and require that:

$$S_{\rm cl}(\mathbf{r}_f, t_f; \mathbf{r}_i, t_i) \;=\; \int_{t_i}^{t_f} dt\, L(\mathbf{r}, \dot{\mathbf{r}}; t) \;=\; \min \tag{4.2}$$

Here, the terminating points of the classical path $\mathbf{r}_f = \mathbf{r}(t_f)$ and $\mathbf{r}_i = \mathbf{r}(t_i)$ are assumed fixed, and $L(\mathbf{r}, \dot{\mathbf{r}}; t)$ denotes the Lagrangian of the problem customarily given by:

$$L(\mathbf{r}, \dot{\mathbf{r}}; t) \;=\; T(\dot{\mathbf{r}}) - U(\mathbf{r}) \;=\; M\dot{\mathbf{r}}^2/2 + \mathbf{r}\cdot\mathbf{F} \tag{4.3}$$

In order to integrate the Lagrangian (4.3), let us first rewrite the particle trajectory (4.1) in terms of those quantities that remain fixed in the course of the variation of the classical action $S_{\rm cl}(\mathbf{r}_f, t_f; \mathbf{r}_i, t_i)$ (4.2). Expressing the initial velocity $\mathbf{v}_i$ as a function of the initial and final particle coordinates $\mathbf{r}_i$, $\mathbf{r}_f$ and the time of flight $T = t_f - t_i$ the

particle spends between $\mathbf{r}_i$ and $\mathbf{r}_f$, we find from (4.1):

$$\mathbf{r}(t) \;=\; \mathbf{r}_i + \left(\frac{\mathbf{r}_f - \mathbf{r}_i}{T} - \frac{\mathbf{F}T}{2M} \right) (t - t_i) + \frac{\mathbf{F}}{2M} (t - t_i)^2 \tag{4.4}$$

Here, we note that the ballistic trajectory is uniquely given by the set of global parameters $\mathbf{r}_f$, $\mathbf{r}_i$ and T. Furthermore, for $T \neq 0$ this trajectory exists for otherwise arbitrary choices of these quantities.

Introducing this trajectory into (4.2) and integrating we finally obtain the classical propagator $S_{\mathrm{cl}}(\mathbf{r}_f, t_f; \mathbf{r}_i, t_i)$ of ballistic motion:

$$S_{\mathrm{cl}}(\mathbf{r}_f, t_f; \mathbf{r}_i, t_i) \;=\; \frac{M}{2T} \, |\mathbf{r}_f - \mathbf{r}_i|^2 \;+\; \frac{1}{2} \, \mathbf{F} \cdot (\mathbf{r}_f + \mathbf{r}_i) T \;-\; \frac{1}{24M} \, F^2 T^3 \tag{4.5}$$

The action (4.5) only depends on the time of flight $T = t_f - t_i$ and hence is invariant with respect to translations in time. Unlike the trajectory pattern (4.1), however, $S_{\mathrm{cl}}(\mathbf{r}_f, \mathbf{r}_i; T)$ is not just a function of $\mathbf{r}_f - \mathbf{r}_i$, but depends also on $\mathbf{r}_f + \mathbf{r}_i$. This property becomes clearer in an energy representation of the action. Here, we note that both the Lagrangian (4.3) and the action functional (4.5) are not unique, but subject to gauge transforms. It is possible to restore the spatial translational symmetry by a suitable choice of gauge. For a detailed discussion of these topics we refer to Section 4.3. (Alternatively, the expression (4.5) for the action might have been derived by separation of variables in the Hamilton–Jacobi equation (4.7). In fact, taking the z axis as direction of force, $S_{\mathrm{cl}}(\mathbf{r}_f, \mathbf{r}_i; T)$ may be construed as sum:

$$S_{\mathrm{cl}}(\mathbf{r}_f, \mathbf{r}_i; T) \;=\; S_{\perp}(\mathbf{r}_{\perp}^f - \mathbf{r}_{\perp}^i; T) + S_{\parallel}(z_f, z_i; T) \tag{4.6}$$

Here, the "free motion" part $S_{\perp}(\mathbf{r}_{\perp}^f - \mathbf{r}_{\perp}^i; T)$ represents the directions $r_{\perp} = (x, y)^T$ perpendicular to the direction of force $\mathbf{F}$, whereas the action $S_{\parallel}(z_f, z_i; T)$ describing one-dimensional uniformly accelerated motion was given e. g. by Brown and Zhang [112]. Note that the corresponding result in the well-known book by Feynman and Hibbs [65] contains a misprint.)

4.1.2 Energy vs. Time of Flight

Since the potential $U(\mathbf{r})$ is time-independent, for a given trajectory $\mathbf{r}(t)$ the particle energy E is conserved. Here, this obvious property of our problem is reflected in the fact that the time variable t in the Hamilton–Jacobi differential equation [113]

$$\frac{\partial}{\partial t} \, S_{\mathrm{cl}}(\mathbf{r}, t; \mathbf{r}_i, t_i) + \frac{1}{2M} \, [\boldsymbol{\nabla} S_{\mathrm{cl}}(\mathbf{r}, t; \mathbf{r}_i, t_i)]^2 - \mathbf{r} \cdot \mathbf{F} \;=\; 0 \tag{4.7}$$

is separable. Hence we may simplify the expression for the classical action $S_{\mathrm{cl}}(\mathbf{r}_f, \mathbf{r}_i; T)$ by introducing Hamilton's characteristic function $W_{\mathrm{cl}}(\mathbf{r}_f, \mathbf{r}_i; E)$, which is also known as reduced classical action, via the Legendre transformation [113]:

$$S_{\mathrm{cl}}(\mathbf{r}_f, \mathbf{r}_i; T) \;=\; W_{\mathrm{cl}}(\mathbf{r}_f, \mathbf{r}_i; E) - ET \tag{4.8}$$

According to this equation, the energy E may be extracted from $S_{\mathrm{cl}}(\mathbf{r}_f, \mathbf{r}_i; T)$ by means of the simple relation:

$$E(\mathbf{r}_f,\, \mathbf{r}_i;\, T) \;=\; -\,\frac{\partial}{\partial T}\, S_{\mathrm{cl}}(\mathbf{r}_f, \mathbf{r}_i; T) \tag{4.9}$$

Thus, we obtain from (4.5) the particle energy as a function of the initial and final positions $\mathbf{r}_i, \mathbf{r}_f$ and the time of flight T:

$$E(\mathbf{r}_f, \mathbf{r}_i; T) \;=\; \frac{M}{2T^2}\, |\mathbf{r}_f - \mathbf{r}_i|^2 \;-\; \frac{1}{2}\, \mathbf{F} \cdot (\mathbf{r}_f + \mathbf{r}_i) \;+\; \frac{1}{8M}\, F^2 T^2 \tag{4.10}$$

Note that this quadratic equation in T^2 provides a relation between the time of flight T and its energy E, given fixed origin and destination $\mathbf{r}_i$, $\mathbf{r}_f$ of the ballistic trajectory. Hence, we may solve (4.10) for the time of flight $T(\mathbf{r}_f, \mathbf{r}_i; E)$. For convenience, we introduce the abbreviation:

$$\epsilon_{\pm}(\mathbf{r}_f, \mathbf{r}_i; E) \;=\; \sqrt{2E + \mathbf{F} \cdot (\mathbf{r}_f + \mathbf{r}_i) \pm F\, |\mathbf{r}_f - \mathbf{r}_i|} \tag{4.11}$$

Using this notation, the time of flight may be displayed in a symmetric fashion:

$$T_{\pm}(\mathbf{r}_f, \mathbf{r}_i; E) \;=\; \frac{\sqrt{M}}{F}\; (\epsilon_+ \pm \epsilon_-) \tag{4.12}$$

Formally, additional negative solutions $T = -T_{\pm}(\mathbf{r}_f, \mathbf{r}_i; E)$ appear that belong to particles traveling "backwards in time", or, in an alternative view, passing the opposite way from $\mathbf{r}_f$ to $\mathbf{r}_i$ in a positive time $T_{\pm}$.

Unlike the fixed-time boundary condition (4.4), using the energy-based set of parameters $\mathbf{r}_f$, $\mathbf{r}_i$ and E generally does not lead to a unique classical path. Rather, (4.10) shows the fact that for fixed particle energy E, at most two trajectories will connect the positions $\mathbf{r}_i$ and $\mathbf{r}_f$ (Figure 3) which we will denote as "slow" $(+)$ and "fast" $(-)$ paths according to their time of flight $T_{\pm}(\mathbf{r}_f, \mathbf{r}_i; E)$ (4.12). We will take up the discussion of ballistic trajectories again in Section 4.2.

4.1.3 The Reduced Action Functional

Finally, we aim at an expression for the characteristic function $W_{\mathrm{cl}}(\mathbf{r}_f, \mathbf{r}_i; E)$ which appears in the WKB approximation to stationary quantum mechanics (see Chapters 6

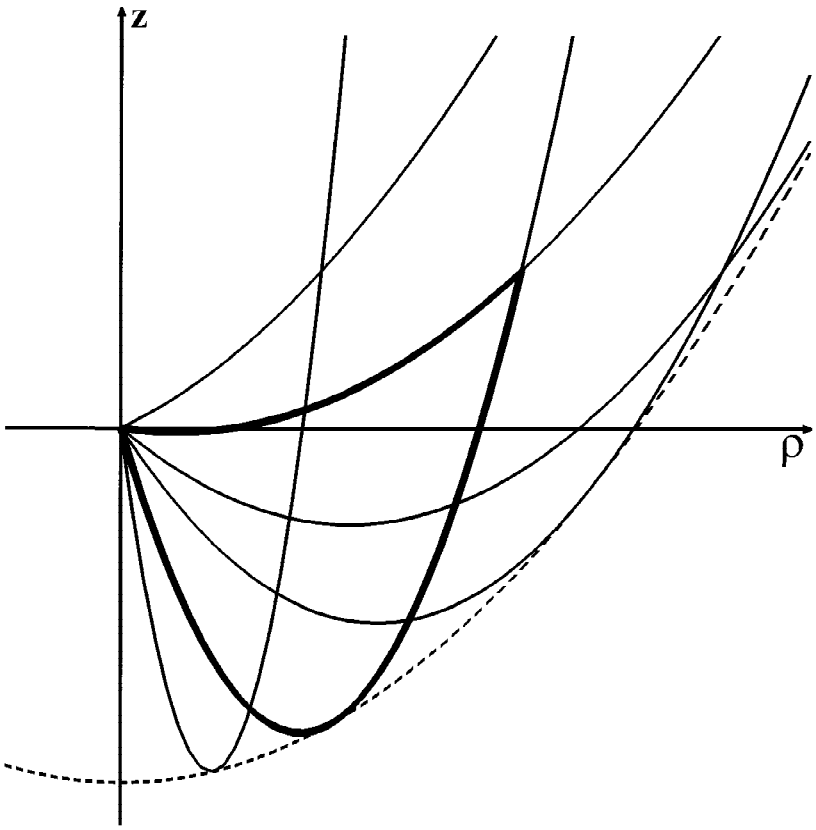

Figure 3: Ballistic motion in a uniform force field $\mathbf{F} = F\hat{e}_z$. The caption shows classical trajectories starting at the origin $\mathbf{r}_i = \mathbf{o}$ with fixed energy $E > 0$. In the sector of classically allowed motion, two parabolas will join the origin and the final point $\mathbf{r}_f$ (bold curves). These trajectories become degenerate on the turning surface $r - z = 2E/F$ (4.18), a parabola with focus $\mathbf{r}_F = \mathbf{o}$ that represents the maximum range of classical motion (dashed line). Beyond this surface, in the sector of dynamically forbidden motion, quantum tunneling prevails.

and 7). First, let us note that unlike the action functional (4.5), the reduced action $W_{\rm cl}(\mathbf{r}_f, \mathbf{r}_i; E)$ is a double-valued function whose two branches $(+)$, $(-)$ refer to the choice of trajectory in (4.12). Clearly, $W^{\pm}_{\rm cl}(\mathbf{r}_f, \mathbf{r}_i; E)$ may be obtained from the classical action functional $S_{\rm cl}(\mathbf{r}_f, \mathbf{r}_i;\, T)$ by means of the relation (4.8). To calculate the reduced action, we insert the expressions (4.5) and (4.10) into (4.8) and replace all parameters by the symbols $\epsilon_{\pm}(\mathbf{r}_f, \mathbf{r}_i; E)$ (4.11):

$$\begin{aligned} W^{\pm}_{\rm cl}(\mathbf{r}_f, \mathbf{r}_i; E) &= T_{\pm} \left\{ 2E + \mathbf{F} \cdot (\mathbf{r}_f + \mathbf{r}_i) - \frac{F^2 T_{\pm}^2}{6M} \right\} \\ &= \frac{\sqrt{M}}{F} \left(\epsilon_+ \pm \epsilon_- \right) \left\{ \frac{1}{2} \left(\epsilon_+^2 + \epsilon_-^2 \right) - \frac{1}{6} \left(\epsilon_+ \pm \epsilon_- \right)^2 \right\} \end{aligned} \tag{4.13}$$

This equation may be rearranged to obtain the compact result:

$$W_{\rm cl}^{\pm}(\mathbf{r}_f, \mathbf{r}_i; E) \;=\; \frac{\sqrt{M}}{3F}\,\left(\epsilon_+^3 \pm \epsilon_-^3\right) \tag{4.14}$$

At this point, two remarks on the structure of (4.14) are in order. First, in the one-dimensional case, $W_{\rm cl}(z_f, z_i; E)$ has a simple integral representation: Denoting the particle momentum by $p(z; E)$, the relation $W_{\rm cl}(z_f, z_i; E) = \int_{z_i}^{z_f} dz\, p(z; E)$ holds. Hence, the reduced action always can be represented as difference of a "final" and an "initial" action: $W_{\rm cl}(z_f, z_i; E) = W_{\rm cl}(z_f; E) - W_{\rm cl}(z_i; E)$. In the multi-dimensional action (4.14), the initial and final positions $\mathbf{r}_i, \mathbf{r}_f$ are no longer separated. Second, unlike the classical action $S_{\rm cl}(\mathbf{r}_f, \mathbf{r}_i; T)$ (4.5), the reduced action (4.14) apparently does not present a sum of "longitudinal" and "transverse" parts although the Hamilton–Jacobi equation (4.7) separates in the coordinates z and $\mathbf{r}_\perp$ (assuming that $\mathbf{F}$ points in the direction of the z axis). In fact,

$$W_{\rm cl}(\mathbf{r}_f, \mathbf{r}_i; E) \;=\; W_\perp(\mathbf{r}_\perp^f, \mathbf{r}_\perp^i; E_\perp) + W_\parallel(z_f, z_i; E_\parallel) \tag{4.15}$$

where $W_\parallel(z_f, z_i; E)$ and $W_\perp(\mathbf{r}_\perp^f, \mathbf{r}_\perp^i; E)$ present the Legendre transforms of $S_\parallel(z_f, z_i; T)$ and $S_\perp(\mathbf{r}_\perp^f, \mathbf{r}_\perp^i; T)$ (4.6), respectively. The "partial energies" $E_\parallel$, $E_\perp$ that are inserted as separation constants must fulfil the additional requirements:

$$\frac{\partial W_\parallel}{\partial E_\parallel} \;=\; \frac{\partial W_\perp}{\partial E_\perp}\,, \qquad E_\parallel + E_\perp \;=\; E \tag{4.16}$$

These conditions formally result from the variational principle: E is splitted between the degrees of freedom in such a way as to provide $W_{\rm cl}(\mathbf{r}_f, \mathbf{r}_i; E_\parallel, E_\perp)$ with a (local) extremum (for fixed $\mathbf{r}_f$ and $\mathbf{r}_i$). From (4.8) we observe that (4.16) just requires the time of flight T in the longitudinal and transverse directions to be equal. Like $W_{\rm cl}^{\pm}(\mathbf{r}_f, \mathbf{r}_i; E)$ (4.14), the longitudinal action $W_\parallel^{\pm}(z_f, z_i; E_\parallel)$ has two branches.

Symmetries of $W_{\rm cl}^{\pm}(\mathbf{r}_f, \mathbf{r}_i; E)$ (4.14) with regard to translations in space are discussed in Section 4.3.

4.2 Tunneling Trajectories

Let us take the classical trajectories occurring in the three-dimensional ballistic problem under somewhat closer scrutiny. As we already have noticed, for given endpoints $\mathbf{r}_f$, $\mathbf{r}_i$ and fixed energy E, the boundary problem has at most two different classically valid real solutions, the trajectories $(+)$, $(-)$ shown in Figure 3. For our semiclassical study we now assume that the equation of ballistic motion $\mathbf{r}(t)$ (4.4) and the relation between energy E and time of flight T (4.12) hold throughout the parameter space,

even though no real solution exists for certain combinations of $\mathbf{r}_f$, $\mathbf{r}_i$ and E. In this case of "classically forbidden motion," one or both arguments of the roots in (4.11) become negative, and the "times of flight" $T_\pm(\mathbf{r}_f, \mathbf{r}_i; E)$ formally take on complex values. These solutions are meaningless from a classical point of view, but correspond to quantum "tunneling" motion. Since a number of semiclassical theories of multidimensional tunneling based on trajectories in complex space-time have been construed [101–109], the analytical continuation of ballistic motion into the tunneling sector, which is readily available here, is worthy of closer examination.

To simplify the discussion, let us again assume that the particle initially starts at the origin ($\mathbf{r}_i = \mathbf{o}$) and that the force $\mathbf{F}$ is directed along the positive z axis; $\mathbf{F} = F\hat{e}_z$ with $F > 0$. Then, (4.12) reads explicitly:

$$T_\pm(\mathbf{r}_f, \mathbf{o}; E) = \frac{\sqrt{M}}{F}\left\{\sqrt{2E + F(r_f + z_f)} \pm \sqrt{2E - F(r_f - z_f)}\right\} \tag{4.17}$$

Note that this expression is naturally displayed in parabolic coordinates $\xi = r_f + z_f$, $\eta = r_f - z_f$ [81,114]. Obviously, we may distinguish between four different cases:

For positive energies $E > 0$, the first root ϵ_+ in (4.17) is always real. This property does not hold, however, necessarily for the second root ϵ_-; if its argument is also positive, two real classical trajectories joining the origin and $\mathbf{r}$ exist. This situation is depicted in Figure 3. These classical trajectories will however merge on the classical turning surface:

$$\eta = r_f - z_f = 2E/F \tag{4.18}$$

which represents the maximum range of classically allowed motion. This surface has a rotational parabolic shape, with the origin as its focal point (Figure 3).

For even larger values of η, the times of flight $T_\pm(\mathbf{r}_f, \mathbf{o}; E)$ take on conjugate complex values, i. e., the motion takes place in complex time t. We shall denote this case as dynamically forbidden motion. The corresponding trajectories show odd behavior; to see this, we may for example inspect the velocity $\mathbf{v}_\pm(t)$ of the particle. From (4.4), we find:

$$\mathbf{v}_\pm(t) = \frac{\mathbf{r}_f}{T_\pm(\mathbf{r}_f, \mathbf{o}; E)} - \frac{\mathbf{F}T_\pm(\mathbf{r}_f, \mathbf{o}; E)}{2M} + \frac{F(t - t_i)}{M} \tag{4.19}$$

Clearly, both the initial velocity at the origin $\mathbf{r}_i = \mathbf{o}$ and the final velocity are, like $T_\pm(\mathbf{r}_f, \mathbf{o}; E)$, complex quantities—no trajectory in real space will connect the origin and $\mathbf{r}_f$, although the square of the initial velocity $\mathbf{v}_i^2 = 2E/m$ is positive. It seems almost impossible to attribute any physical meaning to this complex conjugate pair of

trajectories (4.4), and there is virtually no way of displaying them. (Note that real energy tracks showing truly complex velocities are genuine features of "realistic" tunneling phenomena in several dimensions and will not appear in one-dimensional space.)

Let us consider also the case of negative initial kinetic energy, $E < 0$. Here, the argument of the second root ϵ_- in (4.17) will always be negative; classically allowed motion is obviously impossible. But the first root ϵ_+ will either be real or imaginary, depending on the value of $\xi = r_f + z_f$. In analogy to (4.18), we may define a "turning surface of tunneling motion":

$$\xi \;=\; r_f + z_f \;=\; -2E/F \tag{4.20}$$

For destinations $\mathbf{r}_f$ on this separating surface, both trajectories $(+)$, $(-)$ will again coincide. Mathematically, its shape is another rotational paraboloid centered around the origin; its aperture is however aligned along the negative z axis, i. e., opposite to the direction of force $\mathbf{F}$.

For $r_f + z_f < 2|E|/F$, both times $T_\pm(\mathbf{r}_f, \mathbf{o}; E)$ will be purely imaginary—a familiar property of the "bounce" or instanton time [115] frequently occurring in one-dimensional tunneling problems. (Formally, a semiclassical time scale of motion is obtained by analytical continuation of the corresponding classical expression into the tunneling sector $U(\mathbf{r}) > E$; in one dimension,

$$\tau_{\rm sc}(z_f, z_i; E) \;=\; \int_{z_i}^{z_f} \frac{i\sqrt{M}\, d\zeta}{\sqrt{2[U(\zeta) - E]}} \tag{4.21}$$

Its absolute value, the instanton time $\tau(z_f, z_i; E)$, is accordingly given by the time a classical particle with energy $-E$ requires to traverse the section $z_i \le \zeta \le z_f$ of the "inverted" potential $-U(\zeta)$. We shall discuss the issue of tunneling time in ballistic motion again in Chapter 7.)

Note that according to (4.19), along with $T_\pm$ and $t - t_i$, in this case the particle velocity $\mathbf{v}_\pm(t)$ also will be purely imaginary; inserting these quantities into the equation of motion (4.4), we find that the particle motion $\mathbf{r}(t)$ will however proceed completely in real space. Therefore, this case is adequately called energetically forbidden motion. Being much more mundane than the dynamically forbidden motion discussed above, apart from the imaginary clock timing the system, this case appears completely analogous to standard classical motion. Hence, we may display the corresponding semiclassical trajectory field, together with its limiting surface (4.20), in Figure 4. We note that these semiclassical trajectories point against the direction of force which should serve as an indication that they play a subordinate role in actual multi-dimensional tunneling phenomena. (In a single dimension where dynamically forbidden motion is absent, tunneling always yields to a description in terms of the instanton method [115–118]. Hence, the success of this semiclassical technique seems to

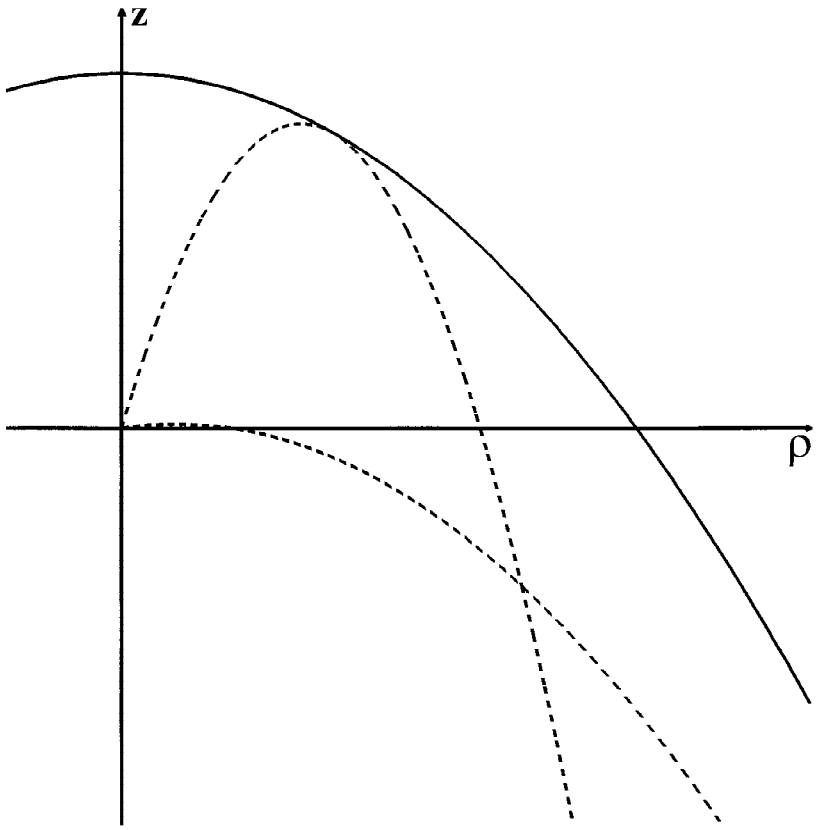

Figure 4: Same as Figure 3, but $E < 0$. In this case no trajectories of classically allowed motion exist; yet still a parabolic turning surface $r + z = -2E/F$ (4.20) remains that separates sectors of energetically forbidden and dynamically forbidden motion (solid line). In the former case a "semiclassical" trajectory scheme may be established by inverting particle energy and potential $U(\mathbf{r})$: $E \to -E, U(\mathbf{r}) \to -U(\mathbf{r})$ (dashed lines). Tunneling proceeds from the origin in the direction of force $\mathbf{F}$, i. e., into the sector of dynamically forbidden motion.

be founded largely on the premise of an artificially restricted dimensionality of space.)

Larger values of $\xi = r_f + z_f$ however will lead to positive arguments of the first root in (4.17) and consequently conjugate complex times of flight $T_\pm(\mathbf{r}_f, \mathbf{o}; E)$; here again, the usual one-dimensional treatment of tunneling problems fails, and we shall properly label this case again as dynamically forbidden motion, as it shares its properties with the related case $E > 0$, $\eta > 2E/F$ examined above. In particular, the "trajectories" $\mathbf{r}(t)$ (4.4) proceed through complex space, and the corresponding velocity $\mathbf{v}_\pm(t)$ (4.19) takes on complex values, so no intellegible trajectory picture is available. We emphasize here that dynamically forbidden motion is not merely a mathematical curiosity appearing in the ballistic problem; as a matter of fact, any realistic ballistic

tunneling process takes place in the dynamically forbidden regime where no simple semiclassical "tunneling paths" exist. Consequently, for multi-dimensional tunneling an alternative intuitive model has to be developed. We will take up this challenge in Chapter 7.

4.3 Symmetry and the Choice of Gauge

Having succeeded in a classical description of ballistic motion in the framework of Hamilton-Jacobi theory, it is worthwhile to take a detour and inquire into the manifold of classical solutions which are interconnected by gauge transformations. These classical symmetry relations, carrying a quixotic flavor yet interesting in their own right, will provide us with the clues that lead to a solution of the corresponding problem in quantum mechanics, the partial waves generated by a pointlike source in a homogeneous force field (Chapter 5).

4.3.1 Gauge Transformations

In Section 4.1, where we treated the problem of ballistic motion largely along the conventional "textbook" pathway using the customary Lagrange functional $L(\mathbf{r}, \dot{\mathbf{r}}; t)$ (4.3) we already noted that our result (4.5) for the classical action $S_{\rm cl}(\mathbf{r}_f, t_f; \mathbf{r}_i, t_i)$ is not unique. Rather, a whole class of different solutions exists which are all equivalent but based on alternative Lagrangians $L'(\mathbf{r}, \dot{\mathbf{r}}; t)$ which differ by the total time derivative of a gauge field $G(\mathbf{r}; t)$ [113]:

$$L'(\mathbf{r}, \dot{\mathbf{r}}; t) \;=\; L(\mathbf{r}, \dot{\mathbf{r}}; t) + \frac{d}{dt}\, G(\mathbf{r}; t) \tag{4.22}$$

Here, $G(\mathbf{r}; t)$ denotes an (almost) arbitrary function of the space and time coordinates. Clearly, gauge invariance on the level of the Lagrangian implies some freedom of choice for the action functional $S_{\rm cl}(\mathbf{r}_f, t_f; \mathbf{r}_i, t_i)$. In particular, equation (4.2) tells us how the classical action (4.5) is affected by the change of gauge $G(\mathbf{r}; t)$ in (4.22):

$$S'_{\rm cl}(\mathbf{r}_f, t_f; \mathbf{r}_i, t_i) \;=\; \int_{t_i}^{t_f} dt\, L'(\mathbf{r}, \dot{\mathbf{r}}; t) \;=\; S_{\rm cl}(\mathbf{r}_f, t_f; \mathbf{r}_i, t_i) + G(\mathbf{r}_f; t_f) - G(\mathbf{r}_i; t_i) \tag{4.23}$$

From (4.23), we may infer that the gauge field $G(\mathbf{r}; t)$ enters into $S_{\rm cl}(\mathbf{r}_f, t_f; \mathbf{r}_i, t_i)$ only through its values at the endpoints of the trajectory $\mathbf{r}(t)$ which itself remains unchanged.

Finally, we examine how gauge invariance manifests itself in the Hamiltonian formulation of classical mechanics [113]. This theory is built upon positions $\mathbf{r}$ and momenta $\mathbf{p}$, rather than velocities $\dot{\mathbf{r}}$ like the Lagrangian approach. Following (4.22), these

momenta depend on the choice of gauge $G(\mathbf{r};t)$ via:

$$\mathbf{p}' \;=\; \frac{\partial L'(\mathbf{r},\dot{\mathbf{r}};t)}{\partial\dot{\mathbf{r}}} \;=\; \mathbf{p} + \boldsymbol{\nabla} G(\mathbf{r};t) \tag{4.24}$$

Simultaneously, the Hamiltonian function $H(\mathbf{r},\mathbf{p};t)$ will transform under changes of the gauge field:

$$H'(\mathbf{r},\mathbf{p}';t) \;=\; \dot{\mathbf{r}}\cdot\mathbf{p}' - L'(\mathbf{r},\dot{\mathbf{r}};t) \;=\; H(\mathbf{r},\mathbf{p};t) - \frac{\partial}{\partial t}\,G(\mathbf{r};t) \tag{4.25}$$

The pair of transforms (4.24), (4.25) should be familiar from electrodynamics where it applies to the electromagnetic four-potential $(\Phi,\mathbf{A})(\mathbf{r};t)$ [84].

4.3.2 The Energy Gauge

In our derivation of the classical action $S_{\mathrm{cl}}(\mathbf{r}_f,t_f;\mathbf{r}_i,t_i)$ (4.5) in Section 4.1, we used a standard prescription for the formulation of the Lagrange functional (4.3), viz., the difference of the kinetic and potential energies [113]. The advantage of this special choice for $L(\mathbf{r},\dot{\mathbf{r}};t)$ is easily comprehended: For a conservative problem like ballistic motion, the time parameter t will not explicitly appear in the Lagrangian $L(\mathbf{r},\dot{\mathbf{r}})$. According to (4.2), this property means that the corresponding action $S_{\mathrm{cl}}(\mathbf{r}_f,t_f;\mathbf{r}_i,t_i)$ depends only on the time of flight $T = t_f - t_i$, rather than on t_f and t_i independently. We exploited this invariance with respect to translations in time by introducing the energy E of a particle as a constant of motion along a given trajectory, and this procedure finally led us to the reduced action $W^{\pm}_{\mathrm{cl}}(\mathbf{r}_f,\mathbf{r}_i;E)$ (4.14).

Apart from the translational symmetry with respect to time, the ballistic problem obviously shows another translational invariant: The force field $\mathbf{F}$ is spatially uniform, thus arbitrary translations of the trajectory field generate an equally valid pattern of paths. This property is, however, not transparent within both expressions of the action (4.5) and (4.14) as their structures will be affected by the symmetry operation. By tracing back the derivation of the reduced action $W^{\pm}_{\mathrm{cl}}(\mathbf{r}_f,\mathbf{r}_i;E)$ (4.14), we find that the introduction of the particle energy E causes this apparent incompatibility: In the course of a spatial translation $\delta\mathbf{r}$, E is subject to a shift $E' = E + U(r+\delta\mathbf{r}) - U(\mathbf{r}) = E - \delta\mathbf{r}\cdot\mathbf{F}$, i. e., the energy assigned to a particular path depends on the point of reference $\mathbf{r}_i$. As a consequence, the reduced action $W_{\mathrm{cl}}(\mathbf{r}_f,\mathbf{r}_i;E)$ obeys the combined symmetry:

$$W_{\mathrm{cl}}(\mathbf{r}_f,\mathbf{r}_i;E) \;=\; W_{\mathrm{cl}}(\mathbf{r}_f-\mathbf{r}_i,\mathbf{o};E+\mathbf{r}_i\cdot\mathbf{F}) \tag{4.26}$$

This valuable relation (which equally holds true in the quantum case) considerably simplifies the reasoning in the following section. We note here that the seven arguments of the reduced action functional $W_{\mathrm{cl}}(\mathbf{r}_f,\mathbf{r}_i;E)$ in fact boil down to only four

independent quantities, viz., the relative distance vector $\mathbf{R} = \mathbf{r}_f - \mathbf{r}_i$ and the regauged energy $E' = E + \mathbf{r}_i \cdot \mathbf{F}$. In particular, this means that without losing generality we may fix the location of the particle source at the origin ($\mathbf{r}_i = \mathbf{o}$), a condition which we shall generally assume in Chapter 5.

No such simple explanation scheme is available to interpret the feature that the time-dependent classical action functional $S_{\mathrm{cl}}(\mathbf{r}_f, \mathbf{r}_i; T)$ (4.5) apparently violates spatial translation symmetry, i. e., is not a function of $\mathbf{R} = \mathbf{r}_f - \mathbf{r}_i$ alone. This symmetry however may be restored through a different choice of gauge, as will be detailed below.

4.3.3 The Momentum Gauge

Now we are interested in a representation of the action (4.5) that explicitly contains the spatial translation symmetry imposed by the uniform force field in the ballistic problem. According to the discussion in Section 4.3.1, it should be possible to achieve this objective by choosing an appropriate Lagrange functional $L'(\mathbf{r}, \dot{\mathbf{r}}; t)$ via some gauge transformation (4.22). Repeating the argument presented in the preceding paragraphs, it should be fairly obvious that the regauged action functional $S'_{\mathrm{cl}}(\mathbf{r}_f, t_f; \mathbf{r}_i, t_i)$ (4.23) will show the desired property to depend only on the relative distance vector $\mathbf{R} = \mathbf{r}_f - \mathbf{r}_i$ provided that the Lagrangian $L'(\mathbf{r}, \dot{\mathbf{r}}; t)$ does not explicitly contain the absolute position $\mathbf{r}$, i. e., is a functional of velocity $\dot{\mathbf{r}}$ and time t only.

We immediately find that the required gauge field reads $G(\mathbf{r}; t) = -\mathbf{r} \cdot \mathbf{F}\, t$. This choice of gauge is frequently employed in the theory of radiation and there often dubbed "$\mathbf{p} \cdot \mathbf{A}$"–gauge [119]. (Correspondingly, the usual Lagrangian (4.3) is referred to as "$\mathbf{r} \cdot \mathbf{E}$"–gauge.) Note that application of $G(\mathbf{r}; t)$ in (4.22) effectively eliminates the potential term $U(\mathbf{r}) = -\mathbf{r} \cdot \mathbf{F}$:

$$L'(\mathbf{r}, \dot{\mathbf{r}}; t) \;=\; M\dot{\mathbf{r}}^2/2 - \dot{\mathbf{r}} \cdot \mathbf{F}\, t \tag{4.27}$$

As desired, the regauged Lagrangian no longer depends on the position variable $\mathbf{r}$. This means that there exists a cyclic variable, the canonical momentum $\mathbf{p}'$ (4.24):

$$\mathbf{p}' \;=\; M\dot{\mathbf{r}} - \mathbf{F}t \tag{4.28}$$

Comparison with (4.1) reveals that the conserved quantity $\mathbf{p}'$ equals the momentum at time $t = 0$, $\mathbf{p}' = M\mathbf{v}(0)$. On the other hand, the Lagrangian now explicitly contains the time variable t. This means that we now depart from the energy-based point of view we adopted in Sections 4.1 and 4.3.2.

We already have inspected how the classical action functional $S_{\mathrm{cl}}(\mathbf{r}_f, t_f; \mathbf{r}_i, t_i)$ is affected by the application of a different gauge field $G(\mathbf{r}; t)$. For the choice of gauge

(4.27), we obtain from (4.23) the regauged action field of ballistic motion:

$$S'_{\mathrm{cl}}(\mathbf{r}_f, t_f; \mathbf{r}_i, t_i) \;=\; \frac{M\,\mathbf{R}^2}{2(t_f - t_i)} \;-\; \frac{1}{2}\,\mathbf{F}\cdot\mathbf{R}(t_f + t_i) \;-\; \frac{F^2}{24M}\,(t_f - t_i)^3 \tag{4.29}$$

As required, in the new representation (4.27) the expression (4.29) for the classical action is a functional of $\mathbf{R} = \mathbf{r}_f - \mathbf{r}_i$ only. It therefore clearly shows the spatial translation symmetry of ballistic motion. Due to the appearance of the term $t_f + t_i$ in (4.29), the translational invariance with respect to time that naturally appears in the "standard" representation of the action (4.5) is however lost. In a certain sense, the action $S'_{\mathrm{cl}}(\mathbf{R}; t_f, t_i)$ (4.29) forms a counterpart of $S_{\mathrm{cl}}(\mathbf{r}_f, \mathbf{r}_i; T)$ (4.5) with interchanged roles of time and space. Hence, it turns out that both translational symmetry properties are competing in the sense that the classical action functional is just able to show plainly at most one of these symmetries whereas the other gets "hidden." By taking advantage of gauge invariance, one may, however, select the symmetry property to appear in explicit form.

The physical meaning of the choice of gauge (4.27) becomes evident by examination of the regauged Hamiltonian function $H'(\mathbf{r}, \mathbf{p}'; t)$ (4.25):

$$H'(\mathbf{r}, \mathbf{p}'; t) \;=\; \frac{1}{2M}\,(\mathbf{p}' + \mathbf{F}t)^2 \tag{4.30}$$

In contrast to the customary conservative Hamiltonian $H = \mathbf{p}^2/2M - \mathbf{r}\cdot\mathbf{F}$ underlying (4.3), the regauged Hamiltonian function (4.30) no longer contains a potential term $U(\mathbf{r})$ but becomes explicitly time-dependent. For this reason, the action field $S'_{\mathrm{cl}}(\mathbf{R}; t_f, t_i)$ (4.29) depends not only on the (relative) time of flight $T = t_f - t_i$, so one cannot employ the energy-dependent reduced Jacobi function $W_{\mathrm{cl}}(\mathbf{r}_f, \mathbf{r}_i; E)$ as we did in Section 4.1. The gauge transformation (4.27) represents the transition to a noninertial "free-falling" frame of reference.

Chapter 5

Uniform Field Green Functions

IN CHAPTER 2, we have laid out the apparatus of quantum source theory. In particular, in Section 2.4 we explained how to calculate the multipole Green functions (scattering partial waves) $G_{lm}(\mathbf{r}, \mathbf{r}'; E)$ and total multipole currents $J_{lm}(\mathbf{r}'; E)$ from the ordinary Green function $G(\mathbf{r}, \mathbf{r}'; E)$ in a given potential $U(\mathbf{r})$ (2.25), (2.33). As a demonstration, already in Section 3.2 we applied quantum source theory on the free particle scattering problem and showed how the well-established results of conventional scattering theory emerge in the source theoretical framework. Following these preliminaries, we now arrive at the heart of this treatise and present, to our best knowledge, for the first time explicit expressions for the scattering partial waves $G_{lm}(\mathbf{r}, \mathbf{r}'; E)$, current density distributions $\mathbf{j}_{lmm'}(\mathbf{r}, \mathbf{r}'; E)$ and total multipole currents $J_{lm}(\mathbf{r}'; E)$ in a three-dimensional uniform force field environment, $U(\mathbf{r}) = -\mathbf{r} \cdot \mathbf{F}$. In this section, we are mainly interested in a formal derivation of these results; it is therefore centered on the mathematics of the homogeneous field problem. The physical meaning of the solutions will be discussed subsequently in Chapters 6 and 7. There, we will compare the theoretical predictions of the present section to actual values obtained in near-threshold photodetachment experiments in the presence of an electric field, a multipole source model of which has been given in Section 3.1. Furthermore, we will use the unique opportunity to assess the quality of the semiclassical solution to this problem (which is accessible from the results of the preceding section) by means of comparison with the exact results derived in the quantum mechanical calculation below.

The mathematical apparatus required to handle the uniform field problem relies heavily on the use of Airy functions [81]. These special functions of mathematical physics are covered in some detail in Appendix D, where they are employed in the solution of the stationary quantum source problem for the motion of particles subject to a constant force in a single spatial dimension. This greatly simplified task, together with a discussion of time-dependent propagation in a linear potential which we shall start shortly, forms the basis for the developments of this section. Initially, we will proceed along the lines presented in a recent paper [9]; later on, we will apply the multipole source technique introduced in Section 2.4 onto the problem of ballistic motion.

Before we start out with our mathematical considerations, it is sensible to introduce some conventions regarding the problem of emission into a linear potential $U(\mathbf{r}) = -\mathbf{r}\cdot\mathbf{F}$. Without loss of generality, we may arbitrarily select the direction $\mathbf{F}$ of the force field; we assume here that it coincides with the direction of the z axis, so that $\mathbf{F} = F\hat{e}_z$. (The reader should be aware that in most treatments of the uniform field photodetachment problem, including the papers describing the distinguished experimental work by Blondel et al. [4,63,64], the z axis is aligned along the electric field vector $\mathbf{E}$. Since $\mathbf{F} = -e\mathbf{E}$, this convention leads to the opposite orientation of the force field $\mathbf{F}$.)

5.1 The Propagator of Ballistic Motion

Although we will deal in the following primarily with the stationary Schrödinger equation for pointlike sources (2.12), (2.24) in a homogeneous field, an important step towards its solution involves the corresponding time-dependent problem (2.7) in multidimensional space [9] (see also Appendix A.2.2):

$$\left\{ i\hbar\frac{\partial}{\partial t} + \frac{\hbar^2}{2M}\boldsymbol{\nabla}_D^2 + Fz \right\} K_D(\mathbf{r},t;\mathbf{r}',t') = i\hbar\,\delta(\mathbf{r}-\mathbf{r}')\,\delta(t-t') \tag{5.1}$$

Here, D denotes the number of spatial dimensions. Unlike its stationary counterpart $G(\mathbf{r},\mathbf{r}';E)$ (2.13), the propagator of ballistic motion in D dimensions is known almost from the beginnings of modern quantum mechanics [120], and numerous derivations for $K_D(\mathbf{r},t;\mathbf{r}',t')$ have been given [121–124]. As usual, we are mainly interested in retarded solutions vanishing for $t < t'$.

From our presentation of classical ballistic motion (Chapter 4), in particular the discussion of gauge symmetry in Section 4.3, we may devise an especially compact scheme to solve (5.1). There, we have demonstrated that the potential term $U(\mathbf{r}) = -Fz$ may be eliminated from the Hamiltonian by a suitable choice of gauge. In the momentum gauge frame of reference, translational invariance is established. Hence, in its momentum representation, the Schrödinger equation for the uniform field environment in the momentum gauge becomes an ordinary differential equation in t. Employing the regauged Hamiltonian $H'(\mathbf{p}';t)$ (4.30), we find:

$$\left\{ i\hbar\frac{\partial}{\partial t} - \frac{1}{2M}(\mathbf{p}'+\mathbf{F}t)^2 \right\} \phi'(\mathbf{p}',t) = 0 \tag{5.2}$$

The general solution to this equation is immediately found by integration:

$$\phi'(\mathbf{p}',t) = \phi'(\mathbf{p}',t')\,\exp\left\{ -\frac{i(t-t')}{2\hbar M}\left[p'^2 + p'_z F(t+t') + \frac{1}{3}F^2(t^2+tt'+t'^2) \right] \right\} \tag{5.3}$$

Rather than to the momentum wave function $\phi'(\mathbf{p}',t)$ our interest is directed to the amplitude $\psi'(\mathbf{r},t)$ in configuration space, which is obtained via the D–dimensional Fourier transform $\psi'(\mathbf{r},t) = (2\pi\hbar)^{-D/2}\int d^Dp'\, e^{i\mathbf{p}'\cdot\mathbf{r}/\hbar}\,\phi'(\mathbf{p}',t)$ [cf. (A.146), (A.147)]. In the course of this operation, the product (5.3) changes into a convolution integral:

$$\psi'(\mathbf{r},t) \;=\; \int d^Dr\, U'_D(\mathbf{r},t;\mathbf{r}',t')\,\psi'(\mathbf{r}',t') \tag{5.4}$$

where the integration kernel is Gaussian:

$$U'_D(\mathbf{r},t;\mathbf{r}',t') \;=\; \left(\frac{M}{2\pi i\hbar(t-t')}\right)^{D/2} \exp\left[\frac{i}{\hbar}\,S'_{\rm cl}(\mathbf{r}-\mathbf{r}';t,t')\right] \tag{5.5}$$

Here, $S'_{\rm cl}(\mathbf{r}-\mathbf{r}';t,t')$ is the classical action functional of ballistic motion in the momentum gauge (4.29). Finally, we switch back to the standard energy gauge, i. e., to the conservative Hamiltonian $H(\mathbf{r},\mathbf{p}) = p^2/2M - Fz$. Noting that the gauge field $G(\mathbf{r};t) = -Fzt$ enters the wave function $\psi(\mathbf{r},t)$ through [114]:

$$\psi'(\mathbf{r},t) \;=\; e^{iG(\mathbf{r};t)/\hbar}\,\psi(\mathbf{r},t) \;=\; e^{-iFzt/\hbar}\,\psi(\mathbf{r},t) \tag{5.6}$$

we obtain from (5.4) and (5.5) for the propagation of the wave function $\psi(\mathbf{r}',t')$:

$$\psi(\mathbf{r},t) \;=\; \int d^Dr\, U_D(\mathbf{r},t;\mathbf{r}',t')\,\psi(\mathbf{r}',t') \tag{5.7}$$

Here, the regauged integration kernel again involves the classical action functional $S_{\rm cl}(\mathbf{r},\mathbf{r}';t-t')$, but now in the energy gauge (4.5):

$$U_D(\mathbf{r},t;\mathbf{r}',t') \;=\; \left(\frac{M}{2\pi i\hbar(t-t')}\right)^{D/2} \exp\left[\frac{i}{\hbar}\,S_{\rm cl}(\mathbf{r},\mathbf{r}';t-t')\right] \tag{5.8}$$

By comparison with the formal theory of the time-dependent Schrödinger equation in Appendix A.2.2, we infer that the quantity $U_D(\mathbf{r},t;\mathbf{r}',t')$ displays the time evolution operator $\mathcal{U}(t,t')$ (A.12) of ballistic motion in D–dimensional configuration space representation. Therefore, $U_D(\mathbf{r},t;\mathbf{r}',t')$ is intimately related to the propagator $K_D(\mathbf{r},t;\mathbf{r}',t')$ in (5.1) that we are looking for; indeed, according to (A.20), the retarded solution to this equation is available through the restriction of $K_D(\mathbf{r},t;\mathbf{r}',t')$ to times $t > t'$:

$$K_D(\mathbf{r},\mathbf{r}';T) \;=\; \Theta(T)\,\left(\frac{M}{2\pi i\hbar T}\right)^{D/2} \exp\left[\frac{i}{\hbar}\left(\frac{M}{2T}\,|\mathbf{r}-\mathbf{r}'|^2 + \frac{FT}{2}\,(z+z') - \frac{F^2T^3}{24M}\right)\right] \tag{5.9}$$

Here, $\Theta(T)$ denotes the Heaviside step function. As expected in the energy gauge, the propagator $K_D(\mathbf{r},\mathbf{r}';T)$ depends on the time difference $T = t - t'$ rather than on t and

t' separately. In passing, we note that (5.9) coincides with the semiclassical expression for the propagator [110, 121], as is always the case when the Hamiltonian $H(\mathbf{r}, \mathbf{p}; t)$ is a polynomial of at most second degree in $\mathbf{r}$ and $\mathbf{p}$. (See also Section 7.1. For a Fourier integral representation of $K_D(\mathbf{r}, \mathbf{r}'; E)$, we refer to Appendix D.3.1.)

5.2 The Green Function of Falling Bodies

As we have shown in Section 2.4, the starting point for a determination of all multipole quantities in the uniform field problem $U(\mathbf{r}) = -Fz$ is the corresponding retarded Green function $G(\mathbf{r}, \mathbf{r}'; E)$ (2.12). To obtain this function, we may employ the integral formula (2.13) which relates $G_D(\mathbf{r}, \mathbf{r}'; E)$ to the Fourier transform of the retarded propagator $K_D(\mathbf{r}, \mathbf{r}'; T)$ (5.9). (For a formal derivation of this approach, see Appendix A.3.6.) Thus, we find that the Green function of the D–dimensional ballistic problem:

$$\left\{ E + \frac{\hbar^2}{2M} \boldsymbol{\nabla}_D^2 + Fz \right\} G_D(\mathbf{r}, \mathbf{r}'; E) \;=\; \delta(\mathbf{r} - \mathbf{r}') \tag{5.10}$$

possesses the following integral representation:

$$\begin{aligned} G_D(\mathbf{r}, \mathbf{r}'; E) \;&=\; -\frac{i}{\hbar} \int_0^\infty dT\, e^{iET/\hbar}\, K_D(\mathbf{r}, \mathbf{r}'; T) \\ &=\; -\frac{i}{\hbar} \int_0^\infty dT \left(\frac{M}{2\pi i \hbar T} \right)^{D/2} \;\times \\ &\qquad \exp\left[\frac{i}{\hbar} \left(\frac{M}{2T} \left| \mathbf{r} - \mathbf{r}' \right|^2 + \frac{T}{2} \left[2E + F(z + z') \right] - \frac{F^2 T^3}{24M} \right) \right] \end{aligned} \tag{5.11}$$

Interestingly, this expression depends on the number of spatial dimensions D only through the power of the prefactor in (5.9). This property enables us to state a formal differential relation that joins the Green functions $G_D(\mathbf{r}, \mathbf{r}'; E)$, $G_{D+2}(\mathbf{r}, \mathbf{r}'; E)$ in spaces of dimensions D and $D + 2$:

$$G_{D+2}(\mathbf{r}, \mathbf{r}'; E) \;=\; -\frac{1}{2\pi} \frac{1}{|\mathbf{r} - \mathbf{r}'|} \frac{\partial}{\partial |\mathbf{r} - \mathbf{r}'|} G_D(\mathbf{r}, \mathbf{r}'; E) \tag{5.12}$$

Therefore, once $G_D(\mathbf{r}, \mathbf{r}'; E)$ is determined explicitly, the Green functions in dimensions $D + 2, D + 4, \ldots$ are available through differentiation. In particular, the retarded Green function $G(\mathbf{r}, \mathbf{r}'; E)$ in physical space ($D = 3$) can be obtained from the one-dimensional Green function $G(z, z'; E)$. (For a closed-form expression for the uniform field Green function $G_{2k+1}(\mathbf{r}, \mathbf{r}'; E)$ in $D = 2k + 1$ spatial dimensions, we refer

to Appendix D.3.2.) For reasons of causality, this function is a solution of the one-dimensional inhomogeneous Schrödinger equation:

$$\left\{E + \frac{\hbar^2}{2M}\frac{\partial^2}{\partial z^2} + Fz\right\} G(z, z'; E) \;=\; \delta(z - z') \tag{5.13}$$

which behaves regularly in the tunneling sector $z \to -\infty$ (i. e., asymptotically vanishes there) and shows the character of an outgoing wave in the limit $z \to \infty$. (For a rigorous justification of these heuristic arguments, see Appendix A.4.) The Green function hence may be constructed by matching appropriate regular and outgoing-wave (Hankel) solutions $\psi_E(z)$, $h_E^{(+)}(z)$ of the corresponding homogeneous Schrödinger equation at $z = z'$. According to Appendix D.2, such wave functions are given by:

$$\begin{aligned} \psi_E(z) \;&=\; 2\beta\sqrt{F}\;\mathrm{Ai}\left[-2\beta(E + Fz)\right] \\ h_E^{(+)}(z) \;&=\; -2\pi\beta\sqrt{F}\;\mathrm{Ci}\left[-2\beta(E + Fz)\right] \end{aligned} \tag{5.14}$$

Here, $\mathrm{Ai}(u)$ denotes the regular Airy function (D.9) as defined by Abramowitz and Stegun [81], the Airy Hankel function $\mathrm{Ci}(u)$ (D.15):

$$\mathrm{Ci}(u) \;=\; \mathrm{Bi}(u) + i\,\mathrm{Ai}(u) \tag{5.15}$$

presents an outgoing-wave solution to the Airy differential equation (D.1), and the abbreviation β stands for an inverse energy parameter ubiquitously applied in the following:

$$\beta \;=\; \left(\frac{M}{4\hbar^2 F^2}\right)^{1/3} \tag{5.16}$$

Then, the retarded Green function $G(z, z'; E)$ of the one-dimensional ballistic problem reads in a compact notation (D.33):

$$\begin{aligned} G(z, z'; E) \;=\; -4\pi\beta^2 F\,\mathrm{Ci}\left\{-\beta\left[2E + F(z + z') + F|z - z'|\right]\right\} \;\times \\ \mathrm{Ai}\left\{-\beta\left[2E + F(z + z') - F|z - z'|\right]\right\} \end{aligned} \tag{5.17}$$

Note that the distance $|z - z'|$ in a single dimension plays the role of $|\mathbf{r} - \mathbf{r}'|$ in the differential relation (5.12). Therefore, we immediately find for the ballistic Green function $G(\mathbf{r}, \mathbf{r}'; E)$ in physical space ($D = 3$):

$$G(\mathbf{r}, \mathbf{r}'; E) \;=\; \frac{M}{2\hbar^2}\,\frac{1}{|\mathbf{r} - \mathbf{r}'|}\,\left[\mathrm{Ci}(\alpha_+)\,\mathrm{Ai}'(\alpha_-) - \mathrm{Ci}'(\alpha_+)\,\mathrm{Ai}(\alpha_-)\right] \tag{5.18}$$

Here, the arguments $\alpha_\pm$ of the Airy functions contain the expressions:

$$\alpha_\pm \;=\; -\,\beta\,[2E + F(z+z') \pm F|\mathbf{r}-\mathbf{r}'|] \tag{5.19}$$

The formula (5.18) was probably first derived by Dalidchik and Slonim [6, 7] more than 20 years ago, and independently rediscovered by Gottlieb, Kleber and Krause in 1991 [8]. (In acoustics, an equivalent problem was posed and solved by Li et al. in 1990 [125].) It should be remarked that for $\mathbf{r}' = \mathbf{o}$ the arguments $\alpha_\pm$ of the Airy functions in (5.19) are most compactly written in terms of parabolic coordinates $\xi = r + z$ and $\eta = r - z$ [89]. Hence it is not surprising that the Green function (5.18) also is accessible from a representation of the problem in parabolic coordinates [126].

We note that the Green function $G(\mathbf{r}, \mathbf{r}'; E)$ (5.18) is a function of the relative displacement vector $\mathbf{r} - \mathbf{r}'$ and the shifted energy parameter $E + Fz'$ only [9], as should be expected from the invariance relation (4.26) of the corresponding classical quantity, the reduced action $W_{\rm cl}^{\pm}(\mathbf{r}, \mathbf{r}'; E)$. This property allows further simplification: Let us identify the origin of the coordinate system with the position of the multipole source $\mathbf{r}' = \mathbf{o}$, i. e., we consider the special Green function $G(\mathbf{r}, \mathbf{o}; E)$. Then, general uniform field Green functions (5.18) due to sources at $\mathbf{r}'$ may be constructed by the parameter replacements:

$$\mathbf{r} \longrightarrow \mathbf{r} - \mathbf{r}' \;, \qquad\qquad E \longrightarrow E + Fz' \tag{5.20}$$

In the following we will always assume that $\mathbf{r}' = \mathbf{o}$.

In the study of electron dynamics in a uniform electric field, the three-dimensional Green function $G(\mathbf{r}, \mathbf{r}'; E)$ and its advantages have been largely ignored. Most investigations in the literature [13, 15, 16, 18–20, 23] start out from integral representations of (5.18) leading to cumbersome expressions that are generally evaluated numerically. Clearly, the source approach via the basic formulae (2.25) and (2.33) enables us to state all quantities of interest in an explicit fashion. However, to obtain practical expressions for the scattering waves and currents that are convenient to handle a number of mathematical transformations are still required. The purpose of the following sections is to present these developments and display the final results for the quantities under consideration.

5.3 Multipole Green Functions

Our first enterprise is to find a suitable expression for the multipole Green functions $G_{lm}(\mathbf{r}, \mathbf{o}; E)$ in the uniform field environment. In principle, these scattering partial

waves are generated from the Green function (5.18) by application of the (l, m) spherical tensor gradient (2.25):

$$G_{lm}(\mathbf{r},\, \mathbf{o};\, E) \;=\; \lim_{\mathbf{r}'\to\,\mathbf{o}}\, K_{lm}\left(\frac{\partial}{\partial \mathbf{r}'}\right)\, G(\mathbf{r},\, \mathbf{r}';\, E) \tag{5.21}$$

Direct evaluation of this formula, however, quickly leads to intricate expressions that are not easily interpreted. Therefore, we take an apparent detour that will result in a much simpler representation as a finite series.

5.3.1 Dimensionless Quantities

Before we undertake this program, we first introduce dimensionless quantities that we will use consistently in the remainder of this chapter because they provide conveniently short expressions. With the introduction of the parameter β (5.16), this task turns out to be painless. By rescaling we obtain dimensionless equivalents for the energy ϵ, time τ, position vectors $\boldsymbol{\rho} = (\xi, \upsilon, \zeta)$ and momentum vectors $\boldsymbol{\kappa}$ from their conventional counterparts E, T, $\mathbf{r} = (x, y, z)$ and $\mathbf{k}$:

$$\begin{aligned} \epsilon &= -2\beta E \qquad & \tau &= T/2\hbar\beta \\ \boldsymbol{\rho} &= \beta F \mathbf{r} \qquad & \boldsymbol{\kappa} &= \mathbf{k}/\beta F \end{aligned} \tag{5.22}$$

5.3.2 General Formula for Multipole Green Functions

Mathematically, we are now faced with the problem to get rid of the differential operator in (5.21). An obvious way to succeed is to employ a Fourier representation of $G(\mathbf{r}, \mathbf{r}'; E)$ on the right hand side of (5.21). This alternative form is available from the time-dependent propagator $K_F(\mathbf{r}, \mathbf{r}'; T)$ (5.9); for reference, its derivation is presented in Appendix D.3. Using the connection between propagator and Green function (2.13), (5.11) we find from (5.21) and (D.46):

$$\begin{aligned} G_{lm}(\boldsymbol{\rho}, \mathbf{o}; \epsilon) \;=\; & -\frac{i\beta}{4\pi^3}\,(\beta F)^{l+3} \int_0^\infty d\tau\, e^{-i\epsilon\tau - i\tau^3/12} \;\times \\ & \lim_{\boldsymbol{\rho}'\to\,\mathbf{o}}\, K_{lm}\left(\frac{\partial}{\partial \boldsymbol{\rho}'}\right) \int d^3\kappa \int d^3\kappa'\, e^{-i(\boldsymbol{\kappa}\cdot\boldsymbol{\rho} + \boldsymbol{\kappa}'\cdot\boldsymbol{\rho}')}\, e^{-i\tau(\boldsymbol{\kappa}-\boldsymbol{\kappa}')^2/16}\, \delta(\boldsymbol{\kappa} + \boldsymbol{\kappa}' + 2\tau\hat{e}_z) \end{aligned} \tag{5.23}$$

Here, formally the spherical tensor gradient $K_{lm}(\partial/\partial\boldsymbol{\rho}')$ acts upon a plane wave factor $\exp(-i\boldsymbol{\kappa}'\cdot\boldsymbol{\rho}')$ which is an eigenfunction of this polynomial operator:

$$K_{lm}\left(\frac{\partial}{\partial \boldsymbol{\rho}'}\right)\, e^{-i\boldsymbol{\kappa}'\cdot\boldsymbol{\rho}'} \;=\; i^l\, K_{lm}(-\boldsymbol{\kappa}')\, e^{-i\boldsymbol{\kappa}'\cdot\boldsymbol{\rho}'} \tag{5.24}$$

Now we may safely perform the limit $\boldsymbol{\rho}' \to \mathbf{o}$. Replacing the integration variable $\boldsymbol{\kappa}$ by $\mathbf{q} = \boldsymbol{\kappa} + \tau\hat{e}_z$ and eliminating $\boldsymbol{\kappa}'$ by means of the delta function appearing in the integrand, (5.23) simplifies to:

$$G_{lm}(\boldsymbol{\rho},\mathbf{o};\epsilon) \;=\; \frac{\beta}{4\pi^3}\,(i\beta F)^{l+3}\int_0^\infty d\tau\, e^{-i\left\{(\epsilon-\zeta)\tau+\tau^3/12\right\}}\;\times \\ \int d^3q\, e^{-i\mathbf{q}\cdot\boldsymbol{\rho}}\,K_{lm}(\mathbf{q}+\tau\hat{e}_z)\,e^{-i\tau q^2/4} \quad (5.25)$$

Using an addition theorem for harmonic polynomials (B.39) and the multipole expansion of plane waves (B.11) we may evaluate the $\mathbf{q}$–integration in the last line of (5.25). To keep the presentation compact, the actual calculation of this integral has been shifted into Appendix B.6. Here, we just insert the result (B.55) into (5.25):

$$G_{lm}(\boldsymbol{\rho},\mathbf{o};\epsilon) \;=\; -\frac{2i\beta}{\pi^{3/2}}\,(\beta F)^{l+3}\sum_{j=|m|}^{l} 2^j\,T_{jlm}\,K_{jm}(\boldsymbol{\rho})\;\times \\ \int_0^\infty \frac{d\tau}{(i\tau)^{2j-l+3/2}}\,\exp\left\{i\left[\frac{\rho^2}{\tau}+\tau(\zeta-\epsilon)-\frac{\tau^3}{12}\right]\right\} \quad (5.26)$$

The translation parameters T_{jlm} (B.40) are introduced in Appendix B.5 (see also below). Note that we were able to reduce the problem to a single integration regarding the time parameter τ. Despite the fact that the integrands remaining in (5.26) are fairly complicated rational-exponential expressions, all these integrals can be evaluated in closed form using products of Airy functions and their derivatives using some nifty mathematical technique presented in Appendix D.3.2. Using the definition (D.50) of the auxiliary functions $Q_k(\rho,\zeta;\epsilon)$ for integer k:

$$Q_k(\rho,\zeta;\epsilon) \;=\; \frac{i}{2\pi\sqrt{\pi}}\int_0^\infty \frac{d\tau}{(i\tau)^{k+1/2}}\,\exp\left\{i\left[\frac{\rho^2}{\tau}+\tau(\zeta-\epsilon)-\frac{\tau^3}{12}\right]\right\} \quad (5.27)$$

we immediately obtain the following final expression for the multipole Green functions $G_{lm}(\mathbf{r},\mathbf{o};E)$ (5.21) by replacing the original physical quantities via (5.22):

$$G_{lm}(\mathbf{r},\mathbf{o};E) \;=\; -4\beta(\beta F)^{l+3}\sum_{j=|m|}^{l}(2\beta F)^j\,T_{jlm}\,K_{jm}(\mathbf{r})\,Q_{2j-l+1}(\beta F r,\beta F z;-2\beta E) \quad (5.28)$$

Here, the coefficient T_{jlm} is given by (B.40):

$$T_{jlm} \;=\; \frac{1}{(l-j)!}\sqrt{\frac{(2l+1)\,(l+m)!\,(l-m)!}{(2j+1)\,(j+m)!\,(j-m)!}} \quad (5.29)$$

whereas according to Appendix D.3 the functions $Q_k(\rho,\zeta;\epsilon)$ explicitly read (D.54):

$$\begin{aligned} Q_k(\rho,\zeta;\epsilon) &= \left(-\frac{1}{2\rho}\frac{\partial}{\partial\rho}\right)^k \mathrm{Ci}(\epsilon-\zeta-\rho)\,\mathrm{Ai}(\epsilon-\zeta+\rho) \\ Q_{-k}(\rho,\zeta;\epsilon) &= \frac{\partial^k}{\partial\zeta^k}\,\mathrm{Ci}(\epsilon-\zeta-\rho)\,\mathrm{Ai}(\epsilon-\zeta+\rho) \end{aligned} \tag{5.30}$$

Here, $k \geq 0$ has been assumed. Not surprisingly, the arguments of the Airy functions may be represented in terms of the parameters $\alpha_\pm$ (5.19). For reference, the s– and p–waves for scattering in a uniform force field ($l = 0, 1$) are given explicitly in Appendix E.1.

5.3.3 Multipole Character of the Partial Waves

According to the results of Appendix A.5, the formal prescription (5.21) leads to multipole waves of the desired angular orientation in the vicinity of the source for the quite comprehensive class of locally analytic potentials $U(\mathbf{r})$ (Theorem LXVII). Having the final expression (5.28) at hand, it is now straightforward to verify that the behavior of $G_{lm}(\mathbf{r},\mathbf{o};E)$ predicted in Appendix A.5 indeed holds for the multipole Green functions in the homogeneous field environment $U(\mathbf{r}) = -Fz$. Using the Wronskian relation for Airy functions [81]:

$$\mathrm{Ci}'(z)\,\mathrm{Ai}(z) - \mathrm{Ci}(z)\,\mathrm{Ai}'(z) \;=\; 1/\pi \tag{5.31}$$

we infer from the differentiation representation (5.30) that the functions $Q_k(\rho,\zeta;\epsilon)$ in the limit $\rho \to 0, \zeta \to 0$ have the principal asymptotic form ($k > 0$):

$$Q_k(\rho,\zeta;\epsilon) \;\sim\; \frac{(-1)^{k+1}}{2\pi\rho}\left(\frac{\partial}{\partial\rho}\frac{1}{2\rho}\right)^{k-1} \;=\; \frac{(2k-3)!!}{2^k\pi}\frac{1}{\rho^{2k-1}} \tag{5.32}$$

Clearly, the worst divergences in the multipole Green function $G_{lm}(\mathbf{r},\mathbf{o};E)$ (5.28) in the vicinity of the source $r \to 0$ are caused by the sum term $j = l$. Then, in (5.32), we have to set $k = l + 1$, and we find for the asymptotic behavior of $G_{lm}(\mathbf{r},\mathbf{o};E)$ as $r \to 0$ using the definition of β (5.16):

$$G_{lm}(\mathbf{r},\mathbf{o};E) \;\sim\; -\frac{M}{2\pi\hbar^2}\,\frac{(2l-1)!!\,K_{lm}(\mathbf{r})}{r^{2l+1}} \tag{5.33}$$

As anticipated, we conclude that this expression is in accord with the general form of $G_{lm}(\mathbf{r},\mathbf{o};E)$ stated in Theorem LXVII. Thus, it matches the corresponding asymptotic behavior of the free particle multipole Green function $G_{lm}^{(\mathrm{free})}(\mathbf{r},\mathbf{o};E)$ (3.26) [see (C.19)] as well as the (properly normalized) multipole potential $\Phi_{lm}(\mathbf{r})$ (2.22).

Next we comment on the use of the representation (5.28) for the scattering partial waves in a uniform force field. Formally, one can interpret this formula as a series expansion in spherical coordinates. This structure is emphasized by the appearance of harmonic polynomials $K_{lm}(\mathbf{r})$ in the series, and it points towards an advantageous role of (5.28) when analyzing properties of the partial waves at locations $\mathbf{r}$ near the source where the original angular distribution pattern of the multipole source is still prevalent. (The discussion of their asymptotic behavior as $r \to 0$ (5.33) presents just an example of this.) At large distances from the source, however, the features of the multipole Green functions are completely dominated by the electron dynamics in the external field that manifestly breaks spherical symmetry and leads to a particle flux aligned towards the direction of force. Although (5.28) remains valid for all $\mathbf{r}$, application of this formula becomes impractical in the far-field sector of space. (Numerically, this inadequateness becomes apparent from the extreme values the components of (5.28) adopt there, and, worse, from the massive cancellation that takes place between different j terms in (5.28) for $|m| < l$.) Therefore, in Section 5.8 we will develop formulae for $G_{lm}(\mathbf{r}, \mathbf{o}; E)$ that, though exact only in an asymptotic sense, present simple and appropriate approximations for the far-field region.

5.3.4 Derivatives of the Multipole Green Functions

Following the derivation of a general formula for the multipole Green functions, we also want to construct a similar expression for the derivatives of $G_{lm}(\mathbf{r}, \mathbf{o}; E)$ (5.28) with respect to the direction of force z. We will require these derivatives when we calculate the distribution of the electronic current, a topic that we will take up in the following section. Fortunately, with the help of the auxiliary functions $Q_k(\rho, \zeta; \epsilon)$ these expressions may be written in a style almost as concise as the multipole Green functions themselves (5.28).

We first note that for the derivatives of $Q_k(\rho, \zeta; \epsilon)$ the recursion relations (D.52), (D.53) (see Appendix D.3) come in handy:

$$\frac{\partial}{\partial z} Q_k(\rho, \zeta; \epsilon) \;=\; \beta F \left(\frac{\zeta}{\rho} \frac{\partial}{\partial \rho} + \frac{\partial}{\partial \zeta} \right) Q_k(\rho, \zeta; \epsilon) \;=\; \beta F \left[Q_{k-1}(\rho, \zeta; \epsilon) - 2\zeta \, Q_{k+1}(\rho, \zeta; \epsilon) \right] \tag{5.34}$$

Equation (5.34), used in conjunction with the derivative rule for harmonic polynomials (B.47) stated in Appendix B.5, yields:

$$\begin{aligned} \frac{\partial}{\partial z} \left\{ K_{jm}(\boldsymbol{\rho}) \, Q_{2j-l+1}(\rho, \zeta; \epsilon) \right\} \;=\; \beta F \, \{ & \left[Q_{2j-l}(\rho, \zeta; \epsilon) - 2\zeta \, Q_{2j-l+2}(\rho, \zeta; \epsilon) \right] K_{jm}(\boldsymbol{\rho}) + \\ & T_{j-1,jm} \, K_{j-1,m}(\boldsymbol{\rho}) \, Q_{2j-l+1}(\rho, \zeta; \epsilon) \} \end{aligned} \tag{5.35}$$

Further, we find from an identity (B.48) concerning the translation coefficients T_{jlm} (5.29) the relation:

$$2^j T_{jlm} T_{j-1,jm} \;=\; 2\,[l-(j-1)]\,2^{j-1}\,T_{j-1,lm} \tag{5.36}$$

In view of (5.34)–(5.36) we observe that the derivative of the multipole Green function $\partial_z G_{lm}(\mathbf{r},\mathbf{o};E)$ may be displayed in a style similar to that of the original scattering waves (5.28):

$$\begin{aligned}\frac{\partial}{\partial z}\,G_{lm}(\mathbf{r},\mathbf{o};E) \;=\; -4\beta(\beta F)^{l+4}\sum_{j=|m|}^{l}(2\beta F)^j\,T_{jlm}\,K_{jm}(\mathbf{r})\;\times\\ \{\,Q_{2j-l}(\beta Fr,\beta Fz;-2\beta E)\;-\;2\beta Fz\,Q_{2j-l+2}(\beta Fr,\beta Fz;-2\beta E)\;+\\ 2(l-j)\,Q_{2j-l+3}(\beta Fr,\beta Fz;-2\beta E)\,\}\end{aligned} \tag{5.37}$$

This result puts us in the position to calculate the current density distributions for the partial scattering waves $G_{lm}(\mathbf{r},\mathbf{o};E)$ of the uniform force field (Section 5.4).

5.3.5 Spherical Tensor Gradient of the Green Function

Finally we remark that following the steps of the derivation of the explicit formula (5.28) for the multipole Green functions $G_{lm}(\mathbf{r},\mathbf{o};E)$, we may also establish the corresponding expression for the spherical tensor gradient of the Green function $G(\mathbf{r},\mathbf{o};E)$ with respect to the first coordinate $\mathbf{r}$:

$$\begin{aligned}K_{lm}\left(\frac{\partial}{\partial\mathbf{r}}\right)\,G(\mathbf{r},\mathbf{o};E) \;=\; -\,4\beta(\beta F)^{l+3}\sum_{j=|m|}^{l}(-2\beta F)^j\,T_{jlm}\;\times\\ K_{jm}(\mathbf{r})\,Q_{2j-l+1}(\beta Fr,\beta Fz;-2\beta E)\end{aligned} \tag{5.38}$$

Note that this result differs from the expression for the multipole waves $G_{lm}(\mathbf{r},\mathbf{o};E)$ (5.28) (which according to (5.21) represent the corresponding derivative of $G(\mathbf{r},\mathbf{r}';E)$ with respect to $\mathbf{r}'$ for $\mathbf{r}'=\mathbf{o}$) only by an additional factor $(-1)^j$ in the sum.

5.4 Current Density Distributions

As usual, we define the current density distribution $\mathbf{j}(\mathbf{r})$ (2.16) generated by some wave function $\Psi(\mathbf{r})$ by:

$$\mathbf{j}(\mathbf{r}) \;=\; -\,\frac{i\hbar}{2M}\,\{\Psi(\mathbf{r})^*\boldsymbol{\nabla}\Psi(\mathbf{r})-\Psi(\mathbf{r})\boldsymbol{\nabla}\Psi(\mathbf{r})^*\} \tag{5.39}$$

In Section 3.1, we have seen that the electron wave $\psi_e(\mathbf{r}_e)$ emitted in near-threshold photodetachment (3.21) is characterized by a unique angular momentum quantum number l, but generally consists of a superposition of different m contributions. Therefore, we aim at a general calculation scheme for the current distribution (5.39) caused by an arbitrary multipole wave $\Psi_l(\mathbf{r}, \mathbf{o}; E)$:

$$\Psi_l(\mathbf{r}, \mathbf{o}; E) \;=\; \sum_{m\,=\,-l}^{l} \lambda_{lm}\, G_{lm}(\mathbf{r}, \mathbf{o};\, E) \tag{5.40}$$

Here, we are only interested in the current density component in the direction of field $j_z(\mathbf{r}, \mathbf{o}; E)$. Introducing the finite sum (5.40) into the current density formula (5.39), we find:

$$j_z(\mathbf{r}, \mathbf{o}; E) \;=\; \sum_{m\,=\,-l}^{l} \sum_{m'\,=\,-l}^{l} \lambda^*_{lm}\, j_{lmm'}(\mathbf{r}, \mathbf{o}; E)\, \lambda_{lm'} \tag{5.41}$$

Here, $j_{lmm'}(\mathbf{r}, \mathbf{o}; E)$, the current density matrix, is a hermitian matrix whose components are given by:

$$j_{lmm'}(\mathbf{r}, \mathbf{o}; E) \;=\; -\,\frac{i\hbar}{2M}\,\Big\{ G^*_{lm}(\mathbf{r}, \mathbf{o};\, E)\,\frac{\partial}{\partial z}\, G_{lm'}(\mathbf{r}, \mathbf{o};\, E) \;-\; G_{lm'}(\mathbf{r}, \mathbf{o};\, E)\,\frac{\partial}{\partial z}\, G^*_{lm}(\mathbf{r}, \mathbf{o};\, E) \Big\} \tag{5.42}$$

Note that the diagonal elements $j_{lmm}(\mathbf{r}, \mathbf{o}; E)$ contain the current density distribution for pure (l, m) scattering partial waves.

From the expressions for the multipole Green functions and their derivatives with respect to z (5.28), (5.37) the current density matrix (5.42) for the uniform field environment is established. Since the matrix elements are generally fairly complicated, we will not display the result here. (We remark, however, that for the far-field sector, much simpler asymptotic current density distributions are at hand, see Section 5.8.) With the help of the Wronskian relation for Airy functions (5.31), more compact formulae for the diagonal elements $j_{lmm}(\mathbf{r}, \mathbf{o}; E)$ are accessible. For $l \;=\; 0, 1$, these are shown in Appendix E.2.

5.5 Multipole Currents

After having considered current density distributions, let us now examine the total multipole currents $J_{lm}(E)$ generated by a unit multipole source $\delta_{lm}(\mathbf{r})$ (2.23) located at the origin ($\mathbf{r}' \;=\; \mathbf{o}$). These quantities correspond to the partial wave scattering cross

sections $\sigma_{lm}(E)$ of conventional scattering theory. In Section 2.4, we have learned how to obtain these currents from the Green function $G(\mathbf{r},\mathbf{r}';E)$ by means of differentiation and limiting operations (2.33). There, we have found that the total current carried by the multipole wave function $\Psi_l(\mathbf{r},\mathbf{o};E)$ (5.40) of the preceding section is given by the weighed sum of its (l,m) components (2.32):

$$J_l(E) \;=\; \sum_{m\,=\,-l}^{l} |\lambda_{lm}|^2\, J_{lm}(E) \tag{5.43}$$

Unlike for the current density distribution $j_z(\mathbf{r},\mathbf{o};E)$ (5.41), no off-diagonal total current components with $m \neq m'$ will exist. Therefore, in this section it is sufficient to consider the current $J_{lm}(E)$ generated by pure (l,m) partial waves.

5.5.1 A Formula For Total Multipole Currents

For the purpose of calculation, we switch again to dimensionless coordinates (5.22):

$$J_{lm}(\epsilon) \;=\; -\,\frac{2}{\hbar}\,(\beta F)^{2l} \lim_{\boldsymbol{\rho},\boldsymbol{\rho}'\to\mathbf{o}} \Im\left[K_{lm}^*\left(\frac{\partial}{\partial\boldsymbol{\rho}}\right)\, K_{lm}\left(\frac{\partial}{\partial\boldsymbol{\rho}'}\right) G(\boldsymbol{\rho},\boldsymbol{\rho}';\epsilon)\right] \tag{5.44}$$

Since the derivative of $G(\boldsymbol{\rho},\boldsymbol{\rho}';\epsilon)$ with respect to $\boldsymbol{\rho}'$ may be expressed in terms of the multipole Green function $G_{lm}(\boldsymbol{\rho},\boldsymbol{\rho}';\epsilon)$ (5.21), we use its representation (5.25) together with the eigenfunction property of plane waves (5.24) to perform the differentiation operations and the limiting procedure. This immediately yields:

$$J_{lm}(\epsilon) \;=\; \frac{\beta}{2\pi^3\hbar}\,(\beta F)^{2l+3}\,\Im\left[\, i\int_0^\infty d\tau\, e^{-i(\epsilon\tau+\tau^3/12)}\;\times \right.$$
$$\left. \int d^3q\, K_{lm}^*(\mathbf{q}-\tau\hat{e}_z)\, K_{lm}(\mathbf{q}+\tau\hat{e}_z)\, e^{-i\tau q^2/4}\right] \tag{5.45}$$

To perform the $\mathbf{q}$ integral using spherical coordinates, we first shift the arguments in the harmonic polynomials $K_{lm}(\mathbf{q}\pm\tau\hat{e}_z)$. This leads to a radial integral related to Gaussian integrals allowing for evaluation by standard methods. This is done in Appendix B.6. Here, we just insert the result (B.60) into (5.45) to obtain another integral representation of the current $J_{lm}(\epsilon)$:

$$J_{lm}(\epsilon) \;=\; \frac{2\beta}{\pi\hbar}\,(\beta F)^{2l+3} \sum_{j\,=\,|m|}^{l} 2^j\,(2j+1)!!\; T_{jlm}^2\;\times$$
$$\Im\left[\frac{i}{2\pi\sqrt{\pi}}\int_0^\infty \frac{d\tau}{(i\tau)^{3j-2l+3/2}}\, e^{-i(\epsilon\tau+\tau^3/12)}\right] \tag{5.46}$$

Integrals of this type, however, have already been considered before. They emerge from the definition (5.27) of the auxiliary functions $Q_k(\rho,\zeta;\epsilon)$ in the limiting case $\rho \to 0, \zeta \to 0$. Hence, let us define another auxiliary quantity $\mathrm{Qi}_k(\epsilon)$:

$$\mathrm{Qi}_k(\epsilon) \;=\; \lim_{\rho\to 0}\lim_{\zeta\to 0} \Im\left\{Q_k(\rho,\zeta;\epsilon)\right\} \tag{5.47}$$

With this definition we find that the second line in (5.46) equals $\mathrm{Qi}_{3j-2l+1}(\epsilon)$.

Hence, we arrive at a closed-form expression for the total multipole current $J_{lm}(E)$ in the presence of a homogeneous force field. Inserting (5.47) into (5.46), noting that $\beta^3F^2 = M/4\hbar^2$, replacing the translation parameters T_{jlm} (B.40) from Appendix B.5, and reordering the sum in (5.46), we obtain the following final formula for $J_{lm}(E)$:

$$J_{lm}(E) \;=\; \frac{M}{4\pi\hbar^3}\,(2l+1)\,(2\beta F)^{2l+1} \;\times \sum_{\nu=0}^{l-|m|} \frac{(2l-2\nu-1)!!}{2^{l+\nu}} \binom{l+m}{\nu} \binom{l-m}{\nu} \mathrm{Qi}_{l+1-3\nu}(-2\beta E) \tag{5.48}$$

By comparison of (5.30) and (5.47) we infer that the auxiliary functions $\mathrm{Qi}_k(\epsilon)$ may be represented as derivatives of products of the regular Airy function ($k \geq 0$):

$$\mathrm{Qi}_k(\epsilon) = \lim_{z\to 0} \left(-\frac{1}{2z}\frac{\partial}{\partial z}\right)^k \mathrm{Ai}(\epsilon - z)\,\mathrm{Ai}(\epsilon + z) \tag{5.49}$$

$$\mathrm{Qi}_{-k}(\epsilon) = \lim_{z\to 0} \frac{\partial^k}{\partial z^k}\,\left\{\mathrm{Ai}(\epsilon - z)\right\}^2 \tag{5.50}$$

The functions $\mathrm{Qi}_k(\epsilon)$ can therefore be extracted from the Taylor series of the functions $\mathrm{Ai}(\epsilon - z)\,\mathrm{Ai}(\epsilon + z)$ and $\mathrm{Ai}(\epsilon - z)^2$, respectively.

We remark here that, unlike in field-free emission (Section 3.2), the total multipole current $J_{lm}(E)$ (5.48) carried by (l,m) partial waves now explicitly depends on the magnetic quantum number m. This feature stems from the symmetry-breaking linear potential environment in the uniform field problem. In Chapters 6 and 7, we will present a physical interpretation for this phenomenon. For $l = 0, 1, 2$, explicit expressions for $J_{lm}(E)$ are listed in Appendix E.3.

5.5.2 Recurrence Formulae for Total Currents

After having established a closed-form expression for $J_{lm}(E)$, it is natural to study the character of these solutions which remains concealed behind the mathematical facade of (5.48). In the following, we present an approach that is interesting also in its own right which involves recurrence formulae connecting the total currents $J_{lm}(E)$ caused

by circular ($m = \pm l$) and subcircular ($m = \pm(l-1)$) partial waves for successive angular momenta l and $l+1$. First, we note that for $m = l$ the total multipole current (5.48) adopts an especially simple form:

$$J_{ll}(E) \;=\; \frac{M}{4\pi\hbar^3}\,\frac{(2l+1)!!}{2^l}\,(2\beta F)^{2l+1}\;\mathrm{Qi}_{l+1}(-2\beta E) \tag{5.51}$$

From the definition of the functions $\mathrm{Qi}_k(\epsilon)$ (5.47) and the recurrence (D.53) in Appendix D.3 it is obvious that the following relation holds:

$$\frac{\partial}{\partial\epsilon}\,\mathrm{Qi}_{l+1}(\epsilon) \;=\; -\,\Im\left[\lim_{\rho,\zeta\to 0}\frac{\partial}{\partial\zeta}\,Q_{l+1}(\rho,\zeta;\epsilon)\right] \;=\; -\,\mathrm{Qi}_l(\epsilon) \tag{5.52}$$

We combine (5.51) and (5.52) to obtain the differentiation rule for the currents generated by circular partial waves:

$$\frac{\partial}{\partial E}\,J_{ll}(E) \;=\; (2l+1)\,\frac{M}{\hbar^2}\,J_{l-1,\,l-1}(E) \tag{5.53}$$

By a slightly more involved calculation, one arrives at the corresponding rule for subcircular ($l,\ l-1$) multipole currents:

$$\frac{\partial}{\partial E}\,J_{l,\,l-1}(E) \;=\; (2l+1)\,\frac{M}{\hbar^2}\,J_{l-1,\,l-2}(E) \tag{5.54}$$

For $l - |m| > 1$, relations analogous to (5.53) and (5.54) hold only approximately. (Not surprisingly, they are also valid for the Wigner law (3.27) describing free-particle emission that, after all, must emerge from (5.48) in the limit $F \to 0$.) From (5.53) and (5.54) we see that the (sub-)circular multipole currents are formally available by repeated integration; because this operation tends to smooth structures, these currents as a function of energy become increasingly featureless as l grows.

5.5.3 Asymptotic Behaviour of the Total Current

Finally, we want to elucidate the behavior of the total multipole current $J_{lm}(E)$ (5.48) by means of a quite different approach and try to expand the expression (5.48) into an asymptotic series with respect to $\epsilon = -2\beta E$. Since these series involve powers of the inverse of the parameter ϵ they hold good only for large values of $|\epsilon|$, and consequently here we will consider only their leading terms. As a proper starting point, we will employ the integral representation (5.46) of the current rather than the final result for $J_{lm}(E)$ in (5.48), and evaluate it by the method of steepest descents in saddle point approximation (for an introduction to these concepts, see Appendix D.1 and the monograph by Bleistein and Handelsman [127]). For the integral (5.46) of interest, application of this technique already turns out to be a rather complex task, and

the technical details have thus been shifted into Appendix D.3.3. Here, we content ourselves to cite the results of that endeavour.

Let us start out with the total multipole current $J_{lm}(E)$ in the integral representation (5.46), which reads in the notation (D.56) employed in Appendix D.3.3:

$$J_{lm}(\epsilon) \;=\; \frac{M}{4\pi^{5/2}\hbar^3}\,(\beta F)^{2l+1}\;\sum_{j\,=\,|m|}^{l}\;2^j\,(2j+1)!!\;T^2_{jlm}\,I_{jl}(\epsilon) \tag{5.55}$$

In the case of tunneling with $\epsilon = -2\beta E > 0$, for $\epsilon \gg 1$ we may approximate the integral $I_{jl}(\epsilon)$ (D.56) by the asymptotic expression (D.58):

$$I_{jl}(\epsilon) \;\sim\; \sqrt{\pi}\;(4\epsilon)^{l-1-3j/2}\;\exp\left\{-\frac{4}{3}\,\epsilon^{3/2}\right\}\left[1+\mathcal{O}(\epsilon^{-3/2})\right] \tag{5.56}$$

A somewhat more complicated behavior is observed for classically allowed motion with $\epsilon \ll -1$. In this limit, the asymptotic expansion of $I_{jl}(\epsilon)$ involves two terms of markedly differing nature (D.64):

$$\begin{aligned} I_{jl}(\epsilon) \;\sim\; & \frac{\sqrt{2\pi}\,(2|\epsilon|)^{3j-2l+1/2}}{(6j-4l+1)!!}\;\left[1+\mathcal{O}(|\epsilon|^{-3})\right] \;+ \\ & (-1)^{l+1}\,2\sqrt{\pi}\;(4|\epsilon|)^{l-1-3j/2}\;\cos\left(\frac{4}{3}\,|\epsilon|^{3/2}+\frac{j\pi}{2}\right)\left[1+\mathcal{O}(|\epsilon|^{-3/2})\right] \end{aligned} \tag{5.57}$$

We note that the first term in (5.57), the "secular contribution" to $I_{jl}(\epsilon)$, varies smoothly as a function of $|\epsilon|$, whereas the term in the second line, which obviously bears considerable resemblance to the expansion (5.56), provides oscillatory structure. Even more conspicuous, the weight of these partial expressions varies with the index j in a diametrically opposite way: Whereas the dominant secular contribution to (5.55) stems from the term of maximum index $j = l$, the asymptotic expression (5.56) and the oscillatory part in (5.57) diminish in importance with increasing j, so they are largely generated by the sum term of index $j = |m|$ in (5.55).

Inserting (5.56) and (5.57) into (5.55), we arrive at the asymptotic expansion for the current $J^{(\mathrm{as})}_{lm}(E)$ emitted by a unit source in the uniform field environment. For a concise representation, it is sensible to introduce the wave number of the electron via $k^2 = 2ME/\hbar^2$; in the case of negative energies, we employ the evanescent wave number $\kappa^2 = -2ME/\hbar^2$ for the same purpose. With this notation, we find $\kappa = 2\beta F\sqrt{\epsilon}$ and $k = 2\beta F\sqrt{|\epsilon|}$, respectively. Furthermore, let us replace the translation coefficients T_{jlm} with their explicit form (5.29). After some reordering, we finally obtain in the

limit $\epsilon \gg 1$:

$$J_{lm}^{(\mathrm{as})}(E) \sim \frac{M}{4\pi^2\hbar^3}\,\kappa^{2l+1}\,\frac{(2l+1)\,(l+|m|)!}{|m|!\,(l-|m|)!}\left(\frac{\beta F}{\kappa}\right)^{3(|m|+1)}\exp\left\{-\frac{1}{6}\left(\frac{\kappa}{\beta F}\right)^3\right\}\times \left[1+\mathcal{O}\left\{\left(\frac{\beta F}{\kappa}\right)^3\right\}\right] \quad (5.58)$$

Due to the tunneling effect, emission takes place even for $E < 0$, yet the current $J_{lm}^{(\mathrm{as})}(E)$ is exponentially suppressed. Clearly, this is a qualitatively new feature of the uniform field problem which is necessarily absent in the free-particle case (Section 3.2). We also remark that the current strength declines with increasing quantum number $|m|$. We will, however, defer a heuristic explanation for this behavior to Section 7.2.3.

In the limit of classically allowed motion, $J_{lm}^{(\mathrm{as})}(E)$ takes on a composite shape as may already be expected from (5.57). Let us first state the principal asymptotic form of the multipole current under the condition $\epsilon \ll -1$:

$$J_{lm}^{(\mathrm{as})}(E) \sim \frac{M}{4\pi^2\hbar^3}\,k^{2l+1}\left[1+\mathcal{O}\left\{\left(\frac{\beta F}{k}\right)^6\right\}\right] + \frac{M}{2\pi^2\hbar^3}\,k^{2l+1}\,\frac{(-1)^{l+1}\,(2l+1)\,(l+|m|)!}{|m|!\,(l-|m|)!}\left(\frac{\beta F}{k}\right)^{3(|m|+1)}\times \cos\left\{\frac{1}{6}\left(\frac{k}{\beta F}\right)^3+\frac{|m|\pi}{2}\right\}\left[1+\mathcal{O}\left\{\left(\frac{\beta F}{k}\right)^3\right\}\right] \quad (5.59)$$

It is seen that the secular contribution in leading order is independent of the field strength F and the magnetic quantum number m; obviously, it reproduces the Wigner law for free-particle sources (C.30). The oscillatory term becomes most apparent for linear polarization ($m = 0$); even then, it is suppressed with respect to the secular part by a factor of order $(\beta F/k)^3$. Nevertheless, due to its rapidly oscillating behavior it may imprint a conspicuous structure onto the general trend of the current $J_{lm}^{(\mathrm{as})}(E)$ given by the Wigner law. Clearly, its influence is most striking for $m = 0$, and we shall briefly investigate $J_{lm}^{(\mathrm{as})}(E)$ for this special case.

From (5.59), we find for the asymptotic form of the total current $J_{l0}^{(\mathrm{as})}(E)$, using the free particle source current $J_{l0}^{(\mathrm{free})}(E)$ (3.27) as a reference:

$$J_{l0}^{(\mathrm{as})}(E) \sim J_{l0}^{(\mathrm{free})}(E)\left\{1-(-1)^l\,\frac{2l+1}{4}\,(2\beta E)^{-3/2}\,\cos\left[\frac{4}{3}\,(2\beta E)^{3/2}\right]\right\} \quad (5.60)$$

Let us now state the derivative of (5.60). Keeping only the leading asymptotic terms, after the application of trigonometrical identities we obtain an expression in the spirit

of (5.53) and (5.54):

$$\frac{\partial}{\partial E} J_{l0}^{(\mathrm{as})}(E) \;\sim\; 2(2l+1)\,\frac{M}{\hbar^2}\, J_{l-1,0}^{(\mathrm{free})}(E)\,\sin^2\left\{\frac{2}{3}\,(2\beta E)^{3/2} + (-1)^l\,\frac{\pi}{4}\right\} \tag{5.61}$$

These formulae show that the current $J_{l0}^{(\mathrm{as})}(E)$ grows monotonically as a function of energy, yet its derivative is subject to marked oscillations. Notably, $J_{l0}^{(\mathrm{as})}(E)$ becomes stationary for a series of particular energy values $E_{\nu l}$:

$$E_{\nu l} \;=\; \frac{1}{8\beta}\,\left[3\pi(4\nu + 2l - 1)\right]^{2/3} \tag{5.62}$$

(Here, the index ν covers all integer values with $\nu > -l/2$.) Thus, we expect that plots of $J_{l0}(E)$ versus the energy E bear a staircase-like appearance. This notion will be confirmed in Section 6.3, where we will also present a physical explanation for this peculiar feature of $J_{l0}(E)$.

5.6 Momentum-Space Green Functions

Now, we will examine a set of functions $G_{lm}(\mathbf{k}_\perp, z; E)$ which describe the behavior of a multipole source in the presence of a uniform field by a mixed representation of position and momentum coordinates. We choose to keep the direction of force z as a position variable but will describe the motion along the lateral degrees of freedom $\mathbf{r}_\perp = (x, y)$ in inverse space by the momentum vector $\mathbf{k}_\perp = (k_x, k_y)$. The purpose of this split of variables is quite obvious: Propagation perpendicular to the field is free and independent from the accelerated motion in direction of $\mathbf{F}$, or, stated mathematically, the potential $U(\mathbf{r}) = -Fz$ is separable, and $\mathbf{k}_\perp$ is a constant of motion. A solution through the traditional separation approach, however, is hampered by the presence of the multipole source which is nonseparable in these coordinates. Nevertheless, the multipole Green functions (5.21) will adopt their mathematically simplest forms in the $(\mathbf{k}_\perp, z)$ representation which furthermore will present the basis for the derivation of asymptotic far-field approximations to the actual Green functions $G_{lm}(\mathbf{r}, \mathbf{o}; E)$ in position space (Section 5.8). From a physical point of view, the functions $G_{lm}(\mathbf{k}_\perp, z; E)$ are interesting since they carry information about the electronic momentum distribution $|\Psi(\mathbf{k}_\perp)|^2$, even as a function of the distance from the source z. A discussion of the physical picture behind $G_{lm}(\mathbf{k}_\perp, z; E)$ can be found in Chapter 7.

Quantum mechanics tells us that the multipole Green function in momentum space $G_{lm}(\mathbf{k}_\perp, z; E)$ is connected to the real-space Green function $G_{lm}(\mathbf{r}, \mathbf{o}; E)$ by a Fourier transform. Using the reduced momentum $\boldsymbol{\kappa}_\perp = \mathbf{k}_\perp/\beta F$ (5.22), we find from the defi-

nition of the multipole waves (5.21) in terms of dimensionless variables (5.22):

$$G_{lm}(\boldsymbol{\kappa}_\perp,\zeta;\epsilon) \;=\; \frac{(\beta F)^{l-2}}{2\pi}\int d\xi\int d\upsilon\, e^{-i\kappa_x\xi-i\kappa_y\upsilon}\;\times \\ \lim_{\boldsymbol{\rho}'\to\mathbf{o}} K_{lm}\left(\frac{\partial}{\partial\xi'}\,,\,\frac{\partial}{\partial\upsilon'}\,,\,\frac{\partial}{\partial\zeta'}\right) G(\boldsymbol{\rho},\boldsymbol{\rho}';\epsilon) \quad (5.63)$$

It is now a good idea to get rid of the primed quantities. To do so, we will use a translational symmetry of the Green function $G_{lm}(\boldsymbol{\rho},\boldsymbol{\rho}';\epsilon)$ we already mentioned in Section 5.2. There we noted that these multipole waves actually only depend on the combined parameters $\boldsymbol{\rho}-\boldsymbol{\rho}'$ and $\epsilon-2\zeta'$ (5.20). This however means that the derivatives with respect to $\boldsymbol{\rho}'$ occurring in (5.63) may be replaced by derivatives with respect to the coordinates $\boldsymbol{\rho}$ and the energy ϵ. One immediately finds:

$$\lim_{\boldsymbol{\rho}'\to\mathbf{o}} K_{lm}\left(\frac{\partial}{\partial\xi'}\,,\,\frac{\partial}{\partial\upsilon'}\,,\,\frac{\partial}{\partial\zeta'}\right) G(\boldsymbol{\rho},\boldsymbol{\rho}';\epsilon) \;=\; (-1)^l\, K_{lm}\left(\frac{\partial}{\partial\xi}\,,\,\frac{\partial}{\partial\upsilon}\,,\,\frac{\partial}{\partial\zeta}\,+\,2\,\frac{\partial}{\partial\epsilon}\right) G(\boldsymbol{\rho},\mathbf{o};\epsilon) \quad (5.64)$$

In this form, the differential operator in (5.63) may be extracted from the integral by partial integration. Furthermore, we replace the Green function $G(\boldsymbol{\rho},\mathbf{o};E)$ by its integral representation (D.47) of Appendix D.3.2. Denoting the perpendicular component of the dimensionless position vector by $\boldsymbol{\rho}_\perp=(\xi,\upsilon)$, we then obtain:

$$G_{lm}(\boldsymbol{\kappa}_\perp,\zeta;\epsilon) \;=\; \frac{2i\beta}{\pi}\,(i\beta F)^{l+1}\,K_{lm}[-\kappa_x,\,-\kappa_y,\,i\,(\partial_\zeta+2\partial_\epsilon)]\;\times \\ \left[\frac{i}{2\pi\sqrt{\pi}}\int_0^\infty\frac{d\tau}{(i\tau)^{3/2}}\;e^{i\left[\frac{\zeta^2}{\tau}+\tau(\zeta-\epsilon)-\frac{\tau^3}{12}\right]}\int d^2\rho_\perp\, e^{-i\boldsymbol{\rho}_\perp\cdot\boldsymbol{\kappa}_\perp+i\rho_\perp^2/\tau}\right] \quad (5.65)$$

The Gaussian integral appearing in the last line is easily evaluated and amounts to $i\pi\tau\exp(-i\kappa_\perp^2\tau/4)$. The remaining τ integral belongs to a type we encountered several times before; from Appendix D.3 we infer that it is just a representation of a product of Airy functions (D.49). Hence, we are led to the following form void of integrals:

$$G_{lm}(\boldsymbol{\kappa}_\perp,\zeta;\epsilon) \;=\; 2i\beta(i\beta F)^{l+1}(-1)^m\,K_{lm}[\kappa_x,\kappa_y,i(\partial_\zeta+2\partial_\epsilon)]\;\times \\ \mathrm{Ci}\left(\epsilon+\frac{\kappa_\perp^2}{4}-\zeta-|\zeta|\right)\mathrm{Ai}\left(\epsilon+\frac{\kappa_\perp^2}{4}-\zeta+|\zeta|\right) \quad (5.66)$$

Here, we additionally replaced the vector argument $-\boldsymbol{\kappa}_\perp$ in the harmonic polynomial operator by its positive counterpart $\boldsymbol{\kappa}_\perp$, and thus created the factor $(-1)^m$ as a by-product.

Equation (5.66) shows some interesting features. First of all, we note that the energy parameter ϵ has been replaced by its longitudinal counterpart $\epsilon_{\|} = \epsilon + \kappa_{\perp}^2/4$. This property arises from the fact that the lateral momentum $\boldsymbol{\kappa}_{\perp}$ orthogonal to the direction of the force field is a constant of classical motion, hence the lateral kinetic energy $\epsilon_{\perp} = -\kappa_{\perp}^2/4$ associated with it is conserved. Only the remainder $\epsilon_{\|} = \epsilon - \epsilon_{\perp}$ is available for motion in the direction of force. More intriguing, we find that the arguments of the Airy functions in (5.66) are given by $\epsilon_{\|}$ and $\epsilon_{\|} - 2\zeta$, respectively. Since the following relation holds for arbitrary functions $f(z)$,

$$\left[\frac{\partial}{\partial\zeta} \, + \, 2\,\frac{\partial}{\partial\epsilon}\right] f(\epsilon + \frac{\kappa_{\perp}^2}{4} - 2\zeta) \, = \, 0 \tag{5.67}$$

we remark that the differential operator $K_{lm}[\kappa_x, \kappa_y, i(\partial_\zeta + 2\partial_\epsilon)]$ effectively does not act on the product of Airy functions appearing in (5.66), but only on a single one of them, the selection of which depends on the sign of ζ. In the following, we shall assume that $\zeta > 0$, i. e., we consider motion in the direction of force. One then obtains for the momentum-space Green functions:

$$G_{lm}(\boldsymbol{\kappa}_{\perp}, \zeta; \epsilon) \, = \, 2i\beta(i\beta F)^{l+1}\,\mathrm{Ci}\left(\epsilon + \frac{\kappa_{\perp}^2}{4} - 2\zeta\right) \, \times \\ (-1)^m \; K_{lm}[\kappa_x, \kappa_y, 2i\partial_u]\,\mathrm{Ai}(u)\,|_{u\,=\,\epsilon+\kappa_{\perp}^2/4} \tag{5.68}$$

For motion in the sector $\zeta < 0$, the Airy function symbols $\mathrm{Ai}(\ldots)$ and $\mathrm{Ci}(\ldots)$ should be interchanged.

In order to arrive at an explicit expression for the Green function $G_{lm}(\mathbf{k}_{\perp}, z; E)$ as a finite sum of derivatives of the Airy function we represent the harmonic polynomial in (5.68) as a series in cylindrical coordinates. From Appendix B.1 we infer that this expansion reads (B.1):

$$K_{lm}[\kappa_x, \kappa_y, 2i\partial_u] \, = \, \sum_{j\,=\,|m|}^{l}{}' \, (2i)^{l-j}\, U_{jlm}\, \kappa_{\perp}^j \, e^{im\phi}\, \frac{\partial^{l-j}}{\partial u^{l-j}} \tag{5.69}$$

Here, the prime indicates that sum terms which lead to odd $j - m$ should be omitted, and ϕ denotes the polar angle assigned to $\boldsymbol{\kappa}_{\perp}$. Using the formula (B.2) for the expansion coefficients U_{jlm} and reintroducing the original set of parameters via (5.22), we finally find the following analytical result for the momentum-space multipole Green functions:

$$G_{lm}(\mathbf{k}_{\perp}, z; E) \, = \, \sqrt{\frac{(2l+1)(l+m)!(l-m)!}{4\pi}} \, \times$$

$$\beta\,(-2\beta F)^{l+1}\,(-i)^m\,e^{im\phi}\,\mathrm{Ci}\left[-2\beta\left(E-\frac{\hbar^2k_\perp^2}{2M}+Fz\right)\right]\;\times$$
$$\sum_{j=|m|}^{l}{}'\;\frac{1}{(l-j)!\,\left(\frac{j-m}{2}\right)!\,\left(\frac{j+m}{2}\right)!}\;\left(\frac{k_\perp}{4\beta F}\right)^j\;\frac{\partial^{l-j}}{\partial u^{l-j}}\;\mathrm{Ai}(u)\Big|_{u=-2\beta(E-\hbar^2k_\perp^2/2M)} \tag{5.70}$$

Again, we note that this exact result holds only for $z>0$; in the sector $z<0$, the Airy functions $\mathrm{Ai}(\dots)$ and $\mathrm{Ci}(\dots)$ in (5.70) exchange their roles.

Though the formula (5.70) at first sight may appear severely complicated, it leads to compact expressions when applied to the first few partial waves. For $l=0,1,2$, the momentum-space multipole Green functions are tabulated in Appendix E.4. We also note that the structure of $G_{lm}(\mathbf{k}_\perp,z;E)$ is conceptually simple as all partial waves share identical behavior with respect to their variation with z; this parameter exclusively occurs in the argument of the Airy wave $\mathrm{Ci}(\dots)$. Obviously, this property is due to the separability of classical ballistic motion.

5.7 Far-Field Multipole Green Functions

The momentum-space multipole Green functions (5.70) of the previous section present an ideal starting point for the establishment of asymptotic expressions for the multipole waves in physical space $G_{lm}(\mathbf{r},\mathbf{o};\,E)$ in the far-field limit where $z\to\infty$, but $r-z$ remains finite. (Note that the force field tends to align the electron trajectories along the direction of $\mathbf{F}$; according to the results of Section 5.2, motion in the "forbidden" sector $\alpha_-=\beta[F(r-z)-2E]>0$ (5.19) is exponentially suppressed.) Though only asymptotically exact, in the far-field region the expressions that we are about to derive in this section are much more convenient to handle than the exact multipole series expansions (5.28) of the multipole Green functions $G_{lm}(\mathbf{r},\mathbf{o};\,E)$ we obtained in Section 5.3.

5.7.1 Asymptotics of the Green Function

We set out with the observation that the z dependence of the momentum-space Green functions $G_{lm}(\mathbf{k}_\perp,z;E)$ (5.70) is entirely contained in a single factor, an Airy Hankel wave whose asymptotic behavior is evaluated in Appendix D.1.3 (see also [81]). Using dimensionless variables, we find (D.16):

$$\mathrm{Ci}\left(\epsilon+\frac{\kappa_\perp^2}{4}-2\zeta\right)\;\sim\;\frac{1}{\sqrt{\pi}}\left(2\zeta-\epsilon-\frac{\kappa_\perp^2}{4}\right)^{-1/4}\exp\left[\frac{2i}{3}\left(2\zeta-\epsilon-\frac{\kappa_\perp^2}{4}\right)^{3/2}+\frac{i\pi}{4}\right] \tag{5.71}$$

We may further simplify this expression by expanding it into a power series with regard to the lateral momentum $\boldsymbol{\kappa}_\perp$. In the limit $\zeta \to \infty$, (5.71) may be equivalently replaced by the Gaussian expression:

$$\mathrm{Ci}\left(\epsilon + \frac{\kappa_\perp^2}{4} - 2\zeta\right) \sim \frac{\exp\left[\frac{2i}{3}\,(2\zeta-\epsilon)^{3/2} + \frac{i\pi}{4}\right]}{\sqrt{\pi}\,(2\zeta-\epsilon)^{1/4}} \exp\left[-\frac{i\kappa_\perp^2}{4}\,(2\zeta-\epsilon)^{1/2}\right] \tag{5.72}$$

Note that with growing ζ, (5.72) as a function of $\boldsymbol{\kappa}_\perp$ will oscillate ever more rapidly. We will exploit this useful property in a moment.

According to the definition of the momentum-space Green functions (5.63), the physical-space multipole Green functions $G_{lm}(\boldsymbol{\rho}, \mathbf{o}; \epsilon)$ are available from $G_{lm}(\boldsymbol{\kappa}_\perp, \zeta; \epsilon)$ by means of a Fourier transform:

$$G_{lm}(\boldsymbol{\rho}, \mathbf{o}; \epsilon) \;=\; \frac{(\beta F)^2}{2\pi} \int d\kappa_x \int d\kappa_y\, e^{i\kappa_x \xi + i\kappa_y \upsilon}\, G_{lm}(\boldsymbol{\kappa}_\perp, \zeta; \epsilon) \tag{5.73}$$

To obtain an integral representation of the asymptotic form $G_{lm}^{(\mathrm{as})}(\boldsymbol{\rho}, \mathbf{o}; \epsilon)$ of the multipole waves, we insert the formula (5.68) for $G_{lm}(\boldsymbol{\kappa}_\perp, \zeta; \epsilon)$ into (5.73), but replace the Airy function $\mathrm{Ci}(\dots)$ by its far-field counterpart (5.72). This yields:

$$\begin{aligned} G_{lm}^{(\mathrm{as})}(\boldsymbol{\rho}, \mathbf{o}; \epsilon) \;=\; & -\frac{i\beta}{\pi\sqrt{\pi}}\,(-1)^m\,\frac{(i\beta F)^{l+3}}{(2\zeta-\epsilon)^{1/4}}\,\exp\left\{\frac{2i}{3}\,(2\zeta-\epsilon)^{3/2} + \frac{i\pi}{4}\right\} \;\times \\ & \int d\kappa_x \int d\kappa_y\, e^{i\kappa_x\xi + i\kappa_y\upsilon}\, e^{-\frac{i\kappa_\perp^2}{4}(2\zeta-\epsilon)^{1/2}}\; K_{lm}[\kappa_x, \kappa_y, 2i\partial_u]\;\mathrm{Ai}(u)\,|_{u=\epsilon+\kappa_\perp^2/4} \end{aligned} \tag{5.74}$$

Since the integrand oscillates rapidly, the momentum integration may be performed using the method of stationary phase. We note that the argument of the regular Airy function appearing in (5.74) does not depend on ζ; therefore, its variation with respect to $\boldsymbol{\kappa}_\perp$ is fixed and becomes negligible in comparison to the Gaussian contribution (5.72) for sufficiently large values of ζ, so it may be ignored in the asymptotic limit. Hence we arrive at the following condition for stationary points of the exponential phase in (5.74):

$$\frac{\partial}{\partial \boldsymbol{\kappa}_\perp}\left\{\kappa_x\xi + \kappa_y\upsilon - \frac{\kappa_\perp^2}{4}\,(2\zeta-\epsilon)^{1/2}\right\} \;=\; 0 \tag{5.75}$$

This linear equation is immediately solved for the single stationary point of the phase:

$$\kappa_x^{(s)} \;=\; \frac{2\xi}{\sqrt{2\zeta-\epsilon}}\,, \qquad \kappa_y^{(s)} \;=\; \frac{2\upsilon}{\sqrt{2\zeta-\epsilon}} \tag{5.76}$$

We now approximate the contribution of the regular Airy function expression in the integral of (5.74) by its value for the stationary point $\boldsymbol{\kappa}_\perp^{(s)}$. This leaves a Gaussian integral which is immediately integrated. This procedure finally yields:

$$\int d\kappa_x \int d\kappa_y \, e^{i\kappa_x\xi + i\kappa_y v} \, e^{-i\kappa_\perp^2 (2\zeta-\epsilon)^{1/2}/4} \, K_{lm}[\kappa_x, \kappa_y, 2i\partial_u] \, \mathrm{Ai}(u) \, |_{u=\epsilon+\kappa_\perp^2/4} \sim \frac{4\pi}{i\sqrt{2\zeta-\epsilon}} \, e^{i\boldsymbol{\kappa}_\perp^{(s)\,2} (2\zeta-\epsilon)^{1/2}/4} \, K_{lm}[\kappa_x^{(s)}, \kappa_y^{(s)}, 2i\partial_u] \, \mathrm{Ai}(u) \, \big|_{u=\epsilon+\boldsymbol{\kappa}_\perp^{(s)\,2}/4} \tag{5.77}$$

Now we inquire into the meaning of the stationary point $\boldsymbol{\kappa}_\perp^{(s)}$. Let us first expand its modulus into an asymptotic series with respect to ζ:

$$\boldsymbol{\kappa}_\perp^{(s)\,2} \;=\; \frac{4\,(\rho^2-\zeta^2)}{(\zeta+\rho)-(\epsilon+\rho-\zeta)} \;=\; 4(\rho-\zeta) + \mathcal{O}(1/\zeta) \tag{5.78}$$

(Note that we assumed $\rho-\zeta$ to be bounded.) From (5.78) we find for the asymptotical value of the argument of the Airy function in (5.77):

$$u_{(s)} \;=\; \epsilon + \boldsymbol{\kappa}_\perp^{(s)\,2}/4 \;=\; \epsilon + \rho - \zeta \tag{5.79}$$

Hence we arrive at the argument we already found in the exact expressions for the multipole Green functions $G_{lm}(\mathbf{r}, \mathbf{o}; E)$ (5.28)–(5.30).

Furthermore, most of the remaining factors in (5.74) and (5.77) may be assembled into another familiar expression. By comparison with (5.71) and (5.72) we infer that in the limit $\zeta \to \infty$, but $\rho-\zeta$ bounded, the corresponding outgoing-wave Airy function $\mathrm{Ci}(\epsilon-\rho-\zeta)$ in (5.28)–(5.30) takes the asymptotic form (D.16):

$$\mathrm{Ci}(\epsilon-\zeta-\rho) \;=\; \mathrm{Ci}\,[(\epsilon-2\zeta)-(\rho-\zeta)] \;\sim\; \frac{1}{\sqrt{\pi}\;(2\zeta-\epsilon)^{1/4}} \exp\left[\frac{2i}{3}\,(2\zeta-\epsilon)^{3/2} + i(\rho-\zeta)\,(2\zeta-\epsilon)^{1/2} + \frac{i\pi}{4}\right] \tag{5.80}$$

Noting that $\rho-\zeta \;=\; \boldsymbol{\kappa}_\perp^{(s)\,2}/4$, we find that the far-field asymptotic Green function $G_{lm}^{(\mathrm{as})}(\boldsymbol{\rho}, \mathbf{o}; \epsilon)$ (5.74) with the help of (5.80) may be rewritten in the following compact representation:

$$G_{lm}^{(\mathrm{as})}(\boldsymbol{\rho}, \mathbf{o}; \epsilon) \;=\; -4\beta(i\beta F)^{l+3} \, \frac{\mathrm{Ci}(\epsilon-\zeta-\rho)}{\sqrt{\rho+\zeta-\epsilon}} \;\times\; (-1)^m \, K_{lm}[\kappa_x^{(s)}, \kappa_y^{(s)}, 2i\partial_u] \, \mathrm{Ai}(u) \, \big|_{u=\epsilon+\rho-\zeta} \tag{5.81}$$

Finally, aiming at an explicit formula for the far-field multipole Green functions, we expand the harmonic polynomial operator appearing in (5.81) in cylindrical coordinates. To do so, we repeat the procedure presented in the preceding section (5.69)

and replace the original variables. Then, we obtain the following asymptotic expression for the asymptotic limit of the partial wave $G_{lm}^{(\mathrm{as})}(\mathbf{r},\mathbf{o};E)$ which is remarkably similar in structure to the (exact) momentum-space Green function (5.70):

$$G_{lm}^{(\mathrm{as})}(\mathbf{r},\mathbf{o};E) \;=\; i\,\sqrt{(2l+1)\,(l+m)!\,(l-m)!}\,\beta^2 F(-2\beta F)^{l+2}(-i)^m e^{im\phi}\;\times \\ \frac{\mathrm{Ci}(\alpha_+)}{\sqrt{4\pi(-\alpha_+)}}\sum_{j=|m|}^{l}{}' \frac{[\,\beta F(r-z)\,]^{j/2}}{2^j\,(l-j)!\,\left(\frac{j-m}{2}\right)!\,\left(\frac{j+m}{2}\right)!}\,\frac{\partial^{l-j}}{\partial\alpha_-^{l-j}}\,\mathrm{Ai}(\alpha_-) \quad (5.82)$$

Here, the prime again indicates that sum terms with $j-m$ odd are to be omitted. The symbols $\alpha_\pm$ (5.19) have already been defined in Section 5.2 and are given by:

$$\alpha_\pm \;=\; \epsilon-\zeta\mp\rho \;=\; -\beta\,[2E+F(z\pm r)\,] \quad (5.83)$$

To obtain explicit expressions for the first few multipole Green functions, the far-field asymptotic formula (5.82) has been evaluated for $l=0,1,2$. The results are listed in Appendix E.5.1.

5.7.2 The Far-Field Sector

Let us discuss briefly the range of validity of the asymptotic expression (5.82). In the derivation of this formula, we frequently made use of the assumption that ζ, and, therefore, $\rho+\zeta$ was large, but $\rho-\zeta$ remained finite. Hence, equation (5.82) may be interpreted as a double expansion in the (orthogonal) parabolic coordinates $\xi=\rho+\zeta$ and $\eta=\rho-\zeta$. Whereas the lateral variations of the Green function is taken care of by a finite ascending series in η which forms the sum in the last line of (5.82), in the far-field limit we are interested only in the principal term of the asymptotic series in $1/\xi$ which is given here by a simple common factor $\mathrm{Ci}(\alpha_+)/\sqrt{-\alpha_+}$. Higher-order terms in $1/\xi$ have been neglected. Thus, we may expect that the results of (5.82) are reliable only for $\zeta\gg 1$.

Note that the expression (5.82) factorizes into the ξ asymptotic term and the (lateral) η series expansion. From this observation it appears that in the far field, motion in a uniform field is most naturally described in terms of parabolic coordinates $\xi=\rho+\zeta$, $\eta=\rho-\zeta$. In contrast, we found in Section 5.3 that near the multipole source $\delta_{lm}(\mathbf{r})$, a (spherical) multipole expansion of the resulting electron wave was feasible (5.28), an expression that is quite cumbersome to use in the far-field sector. Obviously, this differing behavior may be ascribed to the fact that classical ballistic motion is separable in parabolic coordinates, yet the source emission characteristics possesses spherical symmetry. These "dynamical" and "source term" symmetries are not compatible, and the dilemma is resolved by the formation of near-field and far-field sectors where one of the symmetries "dominates." (Note that parabolic and spherical coordinates both

comprise cylindrical symmetry. Hence, the z component of angular momentum is conserved, and m is a constant of motion.)

5.7.3 Asymptotics of the Derivatives of Partial Waves

Finally we note how to construct the far-field asymptotics of the derivative of the multipole Green functions with respect to z (5.37), an expression we will require for the evaluation of the current density distributions generated by the uniform field multipole waves in the limit of large z. Noting that for large negative arguments $u \to -\infty$, the derivative of the outgoing-wave Airy function grows beyond bounds [81]:

$$|\,\mathrm{Ci}'(u)| \;\sim\; \sqrt{-u}\,|\,\mathrm{Ci}(u)| \tag{5.84}$$

we convince ourselves that the only relevant contribution to the asymptotic expression $\partial_z G_{lm}^{(\mathrm{as})}(\mathbf{r},\mathbf{o};E)$ stems from the derivative of the function $\mathrm{Ci}(\alpha_+)$. Hence, formally we obtain for the derivative of the multipole Green functions in the far-field limit:

$$\frac{\partial}{\partial z}\,G_{lm}^{(\mathrm{as})}(\mathbf{r},\mathbf{o};E) \;=\; \beta F\left(\frac{\partial}{\partial\zeta}+\frac{\rho}{\zeta}\,\frac{\partial}{\partial\rho}\right)G_{lm}^{(\mathrm{as})}(\boldsymbol{\rho},\mathbf{o};\epsilon) \;\sim\; -2\beta F\,\frac{\mathrm{Ci}'(\alpha_+)}{\mathrm{Ci}(\alpha_+)}\,G_{lm}^{(\mathrm{as})}(\mathbf{r},\mathbf{o};E) \tag{5.85}$$

This completes our study of the asymptotic Green functions, and we proceed to the calculation of the corresponding current densities.

5.8 Far-Field Current Density Distributions

In turns out that the calculation of multipole current densities in the asymptotic limit, unlike its exact counterpart in Section 5.4, is a quite simple task that is essentially completed once the far-field expressions (5.82) for the multipole waves $G_{lm}^{(\mathrm{as})}(\mathbf{r},\mathbf{o};E)$ are established. This is due to the separability of the asymptotic principal forms in parabolic coordinates discussed above. Combining (5.82) and (5.85), we may formally display the far-field asymptotics of the multipole Green functions and their derivatives in the following form:

$$G_{lm}^{(\mathrm{as})}(\mathbf{r},\mathbf{o};E) = \; i\beta^2 F(-2\beta F)^{l+2}(-i)^m e^{im\phi}\,\frac{\mathrm{Ci}(\alpha_+)}{\sqrt{-\alpha_+}}\,H_{lm}(\eta;\epsilon) \tag{5.86}$$

$$\frac{\partial}{\partial z}\,G_{lm}^{(\mathrm{as})}(\mathbf{r},\mathbf{o};E) = \; i\beta^2 F(-2\beta F)^{l+3}(-i)^m e^{im\phi}\,\frac{\mathrm{Ci}'(\alpha_+)}{\sqrt{-\alpha_+}}\,H_{lm}(\eta;\epsilon) \tag{5.87}$$

The real function $H_{lm}(\eta;\epsilon)$ contains the dependence of the asymptotic multipole Green function on the parabolic coordinate $\eta = \rho - \zeta$ and is common to both expressions:

$$H_{lm}(\eta;\epsilon) \;=\; \sqrt{\frac{(2l+1)\,(l+m)!\,(l-m)!}{4\pi}} \;\times \\ \sum_{j\,=\,|m|}^{l\,\prime} \frac{\eta^{j/2}}{2^j\,(l-j)!\,\left(\frac{j-m}{2}\right)!\,\left(\frac{j+m}{2}\right)!}\,\frac{\partial^{l-j}}{\partial\epsilon^{l-j}}\;\mathrm{Ai}(\epsilon+\eta) \quad (5.88)$$

To obtain the far-field asymptotic current matrix elements $j^{(\mathrm{as})}_{lmm'}(\mathbf{r},\mathbf{o};E)$, we repeat the calculation of Section 5.4 and insert the formulae (5.86) and (5.87) into the definition of the matrix element (5.42). The resulting expression may be considerably simplified by the Wronskian relation [81]:

$$\mathrm{Ci}(u)^*\,\mathrm{Ci}'(u) - \mathrm{Ci}(u)\,\mathrm{Ci}'(u)^* \;=\; -2i/\pi \quad (5.89)$$

which will eliminate the outgoing Airy wave expressions in (5.86) and (5.87). After a short calculation, one ends up with the following formula for the asymptotic current density matrix element:

$$j^{(\mathrm{as})}_{lmm'}(\mathbf{r},\mathbf{o};E) \;=\; -\,\frac{\beta}{4\pi\hbar\alpha_+}\,(2\beta F)^{2l+5}\,i^{m-m'}\,e^{i(m'-m)\phi}\,H_{lm}(\eta;\epsilon)\,H_{lm'}(\eta;\epsilon) \quad (5.90)$$

This expression may obviously be decomposed into a tensor product; consequently, the calculation of the current density distribution $j^{(\mathrm{as})}_z(\mathbf{r},\mathbf{o};E)$ (5.41) generated by an arbitrary multipole wave $\Psi_l(\mathbf{r},\mathbf{o};E)$ (5.40) in the far-field asymptotic limit reduces to the determination of a vector modulus:

$$j^{(\mathrm{as})}_z(\mathbf{r},\mathbf{o};E) \;=\; -\,\frac{\beta}{4\pi\hbar\alpha_+}\,(2\beta F)^{2l+5}\,\left|\sum_{m\,=\,-l}^{l}\lambda_{lm}\,(-i)^m\,e^{im\phi}\,H_{lm}(\eta;\epsilon)\right|^2 \quad (5.91)$$

Equation (5.91) constitutes the final result for the current distribution generated by a multipole source embedded in a homogeneous force field in the limit of large distances from the source.

It is possible to rewrite (5.90) in another form that emphasizes the connection of the far-field current distribution to the total current as well as the classical dynamics of ballistic motion (which will be discussed in greater detail in the following section). For our purpose, it suffices here to note that classically allowed motion is limited to a rotationally parabolic sector of space; the maximum lateral distance $R_{\mathrm{cl}}(E)$ a classical particle can travel is asymptotically given by the formula (6.1):

$$R_{\mathrm{cl}}(E)^2 \;\sim\; \frac{4Ez}{F} \;\sim\; \frac{\epsilon\alpha_+}{\beta^2F^2} \quad (5.92)$$

In the far-field limit, the parabolic coordinate $\eta = \rho - \zeta$ only depends on the radial distance R from the source,

$$\eta \;=\; \rho - \zeta \;=\; -\epsilon\, R^2 / R_{\mathrm{cl}}(E)^2 \tag{5.93}$$

Finally, we note that the energy parameter ϵ may be expressed in terms of the initial particle wave number k:

$$\epsilon \;=\; -2\beta E \;=\; \frac{k^2}{4\beta^2 F^2} \tag{5.94}$$

With these replacements, it is not difficult to show that the far-field current density matrix elements (5.90) adopt the following form:

$$\begin{aligned} j^{(\mathrm{as})}_{lmm'}(\mathbf{r},\mathbf{o};E) \;=\; & \frac{1}{\pi R_{\mathrm{cl}}(E)^2}\,\frac{M}{4\pi^2\hbar^3}\,k^{2l+1}\,i^{m-m'}\,e^{i(m'-m)\phi}\,\frac{(2l+1)\pi k}{2\beta F} \;\times \\ & \sum_{j=|m|}^{l}{}' \sum_{j'=|m'|}^{l}{}' \frac{\sqrt{(l+m)!\,(l-m)!\,(l+m')!\,(l-m')!}}{(l-j)!\,(l-j')!\,\left(\frac{j-m}{2}\right)!\,\left(\frac{j+m}{2}\right)!\,\left(\frac{j'-m'}{2}\right)!\,\left(\frac{j'+m'}{2}\right)!}\,\left(\frac{R}{2R_{\mathrm{cl}}(E)}\right)^{j+j'} \;\times \\ & \left[\left(\frac{2\beta F}{k}\,\frac{\partial}{\partial u}\right)^{l-j}\mathrm{Ai}(u)\right]\left[\left(\frac{2\beta F}{k}\,\frac{\partial}{\partial u}\right)^{l-j'}\mathrm{Ai}(u)\right] \end{aligned} \tag{5.95}$$

Here, the argument of the Airy functions u is given by:

$$u \;=\; -\,\frac{k^2}{4\beta^2 F^2}\,\left[1 - \left(\frac{R}{R_{\mathrm{cl}}(E)}\right)^2\right] \tag{5.96}$$

Though formally uniformly valid for all values of the energy E, the expression (5.95) has a simple interpretation only in the case of classically allowed motion, i. e., for real wave numbers k. Then, in the uppermost line of (5.95) we may identify the first term with the total area illuminated by the focussed electron beam, whereas the second term should be familiar from previous developments (Section 3.2)—it contains the approximate total current as calculated in the limit of field-free emission, the Wigner law (3.27). The influence of the force field manifests itself in the presence of a multiplicative factor that occupies the remaining part of formula (5.95) and modulates the differential cross section in a peculiar manner which will be explained semiclassically. This is the topic of the next section. Despite its involved appearance, actual matrix elements calculated with the help of the general formula (5.95) usually assume a compact form, and are much more convenient to handle than their exact counterparts discussed in Section 5.4. The most elementary asymptotic matrix elements ($l = 0, 1, 2$) are listed in Appendix E.5.2.

With the study of asymptotic wave functions and currents, we conclude our treatment of the mathematical aspects of the multipole source problem in a uniform field environment. In the next chapter, we will discuss the results from these derivations, explain their physical meaning in terms of classical and semiclassical mechanics, and compare the theoretical predictions of Chapter 5 with experimental data.

Chapter 6

Electrons in a Homogeneous Field

HAVING THE COMPLETE MATHEMATICAL THEORY of the quantum dynamics of electrons in a uniform force field at hand, we now proceed to display results derived from this formalism for several important, experimentally accessible quantities, namely the current density distribution $j_{lmm'}(\mathbf{r}, \mathbf{o}; E)$ (5.41), (5.42), (5.95) treated in Sections 5.4 and 5.8, and the total current $J_{lm}(E)$ (5.48) due to a pointlike multipole source $\delta_{lm}(\mathbf{r})$ (2.23) dealt with in Section 5.5. In this chapter, we will confine our considerations to the case of classically allowed motion ($E > 0$). The equally interesting behavior of particle tunneling in ballistic motion shows strikingly different characteristics and is therefore adequately discussed in a separate section of this treatise (Chapter 7). In practice, these currents are accessible in photodetachment experiments in the form of differential and total photodetachment cross sections, respectively. Plots of these quantities exhibit a number of unexpected features that are, however, naturally accounted for in terms of the semiclassical theory of ballistic motion. This is the topic of Section 6.2. In the following paragraphs, we perform a comparative study of the exact and semiclassical solutions with actual data available from recent photodetachment experiments which are found to agree mutually to a gratifying extent. The highly symmetrical, aesthetically impressive current distributions predicted by theory and confirmed in experiment suggest an interpretation as actual images of the atomic wave function, invoking the notion of a "photodetachment microscope" [4, 63]. In the concluding section of this chapter, we will present an admonishing example showing that the association of the current image with the emission characteristics of the source is not necessarily straightforward.

6.1 Mapping the Quantum Solution

Throughout Chapter 5, we restricted our treatment of the problem of quantum ballistic motion in a linear potential environment to transformations of a purely mathematical nature. In this way, we arived at closed-form expressions for the physical quantities now under consideration, the current density distribution and the corresponding total

current generated by a multipole source. This formal approach, however, is obviously of little help in explaining the physical content of these solutions which remains hidden behind the mathematical façade.

Hence, we need to visualize the results of our theoretical approach. For this purpose, we choose to display lateral cross-sections of the current density distributions $j_z^{(\mathrm{as})}(\mathbf{r}, \mathbf{o}; E)$ (5.91) generated by a variety of multipole sources $\delta_{lm}(\mathbf{r})$, thus creating a guiding map of the quantum solution that will assist us in tracking the essential features of quantum ballistic motion. The parameters used in our simulation are taken over from the actual experiment by Blondel et al. [4]. Ten lateral current profiles generated by multipole electron sources of initial energy $E = 6.08 \cdot 10^{-5}\,\mathrm{eV}$ embedded in a uniform electric field of strength $F = 116\,\mathrm{V/m}$ are assembled in Figure 5. The sections were taken at a distance $z = 0.514\,\mathrm{m}$ from the electron source. (Since these choices amount to a value of the dimensionless parabolic coordinate $\xi = \beta F(r+z) = 7.5 \cdot 10^6 \gg 1$, application of the simpler far-field asymptotic theory is fully justified. See Section 5.8.)

From this collection of current images, we may infer several general properties of uniformly accelerated quantum propagation. Most clearly, the force field tends to align electronic motion strongly along the direction of force which leads to the formation of a current filament. In the cross-sections of Figure 5, this focussing effect accounts for the circular "spot" shape of the current images. The spot size is virtually independent of the choice for the multipole indices l and m.

The emission characteristics of the source reveals itself through the presence of nodes, i. e., figures of suppressed current density, in the current patterns. Two different types of nodes exist in the images; distinct radial nodes and, less easily discernible, circular nodes. The radial nodes originate from the cylindrical emission pattern of the source. Hence, their number equals the magnetic quantum number $|m|$ of the orbital structure. With increasing $|m|$, current emission near the axis of symmetry becomes more and more suppressed, leading to a ringlet current pattern for high l circular states. Circular nodes are limited to multipole sources with $l - |m| \geq 2$; thus, they only appear in the lower right corner of Figure 5. They are caused by the projection of conical nodes in the emission pattern of the multipole sources.

The circular nodes mentioned above should not be confused with the most intriguing feature present in the current profiles, viz., a circular interference pattern that is superimposed onto the node pattern caused by the emission characteristics of the source. It consists of a structure of concentric rings that become narrower as their radius increases, giving the pattern an appearance somewhat resembling the Newtonian rings well-known from optical interference. Closer scrutiny reveals that only two different interference patterns are present in Figure 5: One is always found in connection with a bright outer fringe of the current spot; from the chequerboard pattern of its occurrence in Figure 5 we may conclude that it is associated to sources with $l - |m|$ even.

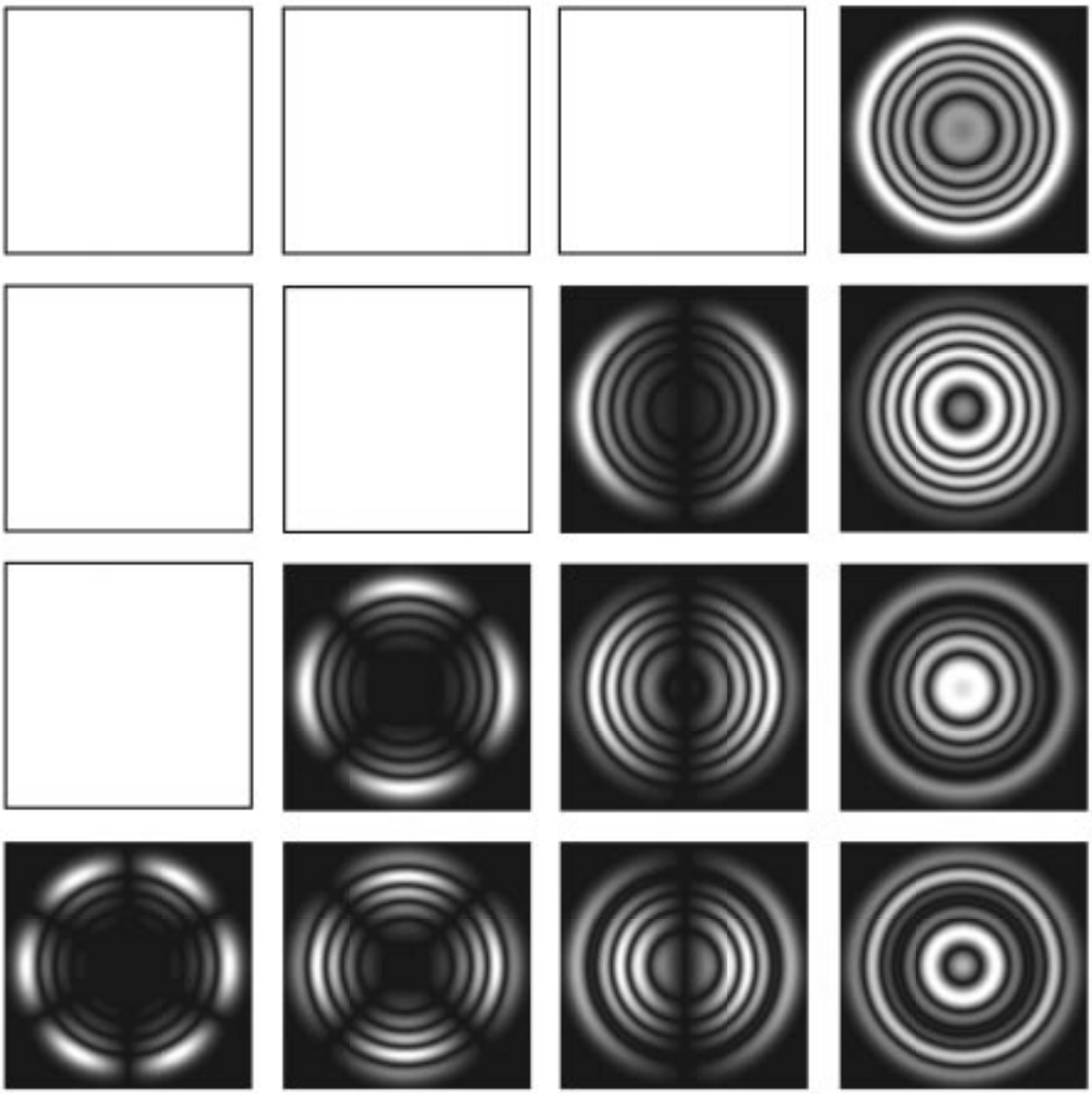

Figure 5: Lateral electronic current profiles for a monochromatic multipole electron source ($E = 6.08 \cdot 10^{-5}\,\mathrm{eV}$) in a homogeneous field environment ($F = 116\,\mathrm{V/m}$). The current distributions generated by real orbital sources $\delta_{l,|m|}(\mathbf{r}) = \delta_{lm}(\mathbf{r}) + \delta_{l,-m}(\mathbf{r})$ are plotted for $l = 0$ (top row) to $l = 3$ (bottom row) and $m = 0$ (right column) to $|m| = 3$ (left column). The sources are located at a distance $z = 0.514\,\mathrm{m}$; the area shown in each image is $(2.4\,\mathrm{mm})^2$.

The remaining case where $l-|m|$ is odd exhibits current spots with a fairly suppressed edge, and the corresponding interference pattern turns out to be the exact negative to the former structure; it features bright rings wherever dark circles are present in the case of even $l-|m|$ and vice versa. How do these observations reconcile with the classical dynamics of ballistic motion?

6.2 The Semiclassical Solution

In order to comprehend the peculiarities of quantum motion in a linear potential $U(\mathbf{r}) = -Fz$ it is reasonable to start with a discussion of the corresponding classical problem, emission of particles with energy E from a pointlike oriented source at $\mathbf{r}' = \mathbf{o}$ into a homogeneous force field [4,5,9–11,16,18,33].

At this point, we may refer to our presentation of classical ballistic motion in Chapter 4. However, the following considerations are of a slightly more modest nature as we are mainly interested in the far-field asymptotics of the motion which is assumed as $z \to \infty$. (Note that we considered exactly this limiting case in the preceding section.) Since our ambitions aim at a semiclassical description of the ballistic dynamics, this section will build upon the Hamilton-Jacobi theory of uniformly accelerated motion worked out in Section 4.1. (See also [9].)

Let us first examine how the picture of ballistic motion developed there (Figure 3) simplifies when the particle path covers a large distance r. Again, classical bodies of some fixed energy E are emitted from a point source located at the origin and travel towards a destination position $\mathbf{r}$ which we assume to be located on a distant screen perpendicular to the direction of force ($z = \text{const.}$, $z \to \infty$). As sketched already in Figure 3, the freely falling body may follow two different tracks: The "fast" trajectory, denoted by $(-)$, directly leads to the location $\mathbf{r}$, whereas the "reflected" or "slow" trajectory $(+)$ grazes at the turning surface of rotationally parabolic shape $r - z = 2E/F$ (4.18) which presents the maximum range of classically allowed motion, and afterwards also arrives at $\mathbf{r}$. In the far-field limit $z \to \infty$, we may develop the parabolic coordinate $r - z$ for $r \approx z$ into a quickly converging series with respect to the lateral distance $R = (r^2 - z^2)^{1/2}$ on the screen. Obviously, the particles there will populate a circular disc, the radius $R_{\mathrm{cl}}(E)$ of which we will label the classical radius of the current distribution. For large values of z, its limiting behavior is given by:

$$R_{\mathrm{cl}}(E)^2 \sim 4Ez/F \tag{6.1}$$

In the next step we will discuss the projection properties of the force field in the asymptotic sector, i. e., explore the relationship between the angle of emission θ (see Figure 6) and the lateral position R on the screen. Since motion perpendicular to the direction of field remains unaffected by the potential, R is wholly determined by the

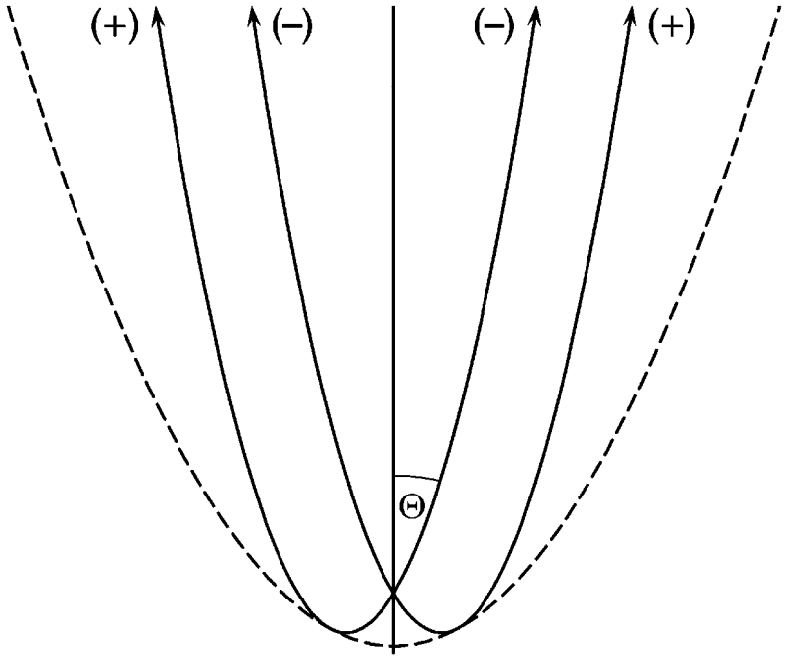

Figure 6: A schematic view of classical ballistic motion in the asymptotic limit $r \to \infty$.

lateral component of the initial particle velocity $v_i \sin\theta$ and the time of flight $T(\theta; E)$ (4.12):

$$R(\theta; E) \;=\; T(\theta; E)\, v_i \sin\theta \tag{6.2}$$

This in practice considerably involved expression dramatically simplifies in the far-field limit $z \to \infty$. Then, the time of flight $T(\theta; E)$ largely increases as $z^{1/2}$, and in leading order becomes asymptotically independent of θ and E. Under these circumstances, (6.2) is compactly expressed as:

$$R(\theta; E) \;=\; R_{\rm cl}(E) \sin\theta \tag{6.3}$$

Note that the cone $\theta = \text{const.}$ will be projected onto a circle of radius $R_{\rm cl}(E) \sin\theta$, as we already noted in the preceding section. As another important consequence of (6.3) we remark that trajectories starting under opposite angles (θ, ϕ), $(\pi - \theta, \phi)$ will asymptotically share the same destination $\mathbf{r}$ on the screen. The situation is schematically summarized in Figure 6.

From (6.3), we immediately obtain the classical differential cross section of the ballistic problem in the asymptotic limit. For both the direct and reflected path respec-

tively, we find:

$$\frac{\partial\sigma_{\mathrm{cl}}}{\partial\Omega}(R;E) \;=\; \frac{R\,dR\,d\phi}{\sin\theta\,d\theta\,d\phi} \;=\; R_{\mathrm{cl}}(E)\,\frac{dR}{d\theta} \;=\; R_{\mathrm{cl}}(E)^2\cos\theta \;=\; R_{\mathrm{cl}}(E)\,\sqrt{R_{\mathrm{cl}}(E)^2-R^2} \tag{6.4}$$

Note that the density of trajectories $\partial\Omega/\partial\sigma_{\mathrm{cl}}(R;E)$ diverges as $R \to R_{\mathrm{cl}}(E)$. This is expected near the caustic surface (4.18) [110]. In the quantum differential cross section, i. e., the actual current density distribution, this divergence will be smoothened out. Nevertheless, the bright outer fringes observed in Figure 5 can be traced back to the classical projection property (6.4). (Note that for odd $l-|m|$, the divergence in (6.4) is masked by a peripheral node circle $R = R_{\mathrm{cl}}(E)$—emission perpendicular to $\mathbf{F}$ is suppressed. Hence, the edge of the current spot appears quenched.)

Having discussed the classical projection properties of uniformly accelerated motion, we now turn our attention to the interference pattern predominant in Figure 5. Clearly, any explanation of this feature is beyond the scope of the framework of classical mechanics, so we must invoke semiclassical theory in order to deal appropriately with the phenomenon.

We have seen that within the sector of classically allowed motion, exactly two classical trajectories of fixed energy E exist that connect the origin with an arbitrarily chosen destination point $\mathbf{r}$; we denoted them in Section 4.1 as the "slow" and "fast" paths, respectively. Quantum particles generally will travel along both paths but will accumulate different phases, leading to quantum interference between the particle waves. As the phase difference depends on the location $\mathbf{r}$ on the screen—at the edge of the current spot the classical trajectories will coincide, whereas maximum phase difference is expected to occur for particles emitted (anti-)parallel to the direction of force—constructive and destructive interference will alternately take place, leading to a circular interference pattern. Conceptionally, the situation is somewhat alike the traditional double-slit setup [65,66] also leading to two-way interference. From an experimental point of view, the ballistic problem enjoys the advantage that no mechanical "slit" is involved, but the selection of paths is solely accomplished by the force field. The feasibility of this approach is aptly demonstrated by the impressive results of the experiments performed by Blondel et al. [4,63,64]. (We note, however, that the effects of uniform acceleration and the Young double-slit setup may be combined; for example, interference experiments with ultracold atoms released from an atomic trap are inevitably strongly affected by gravity. See Shimizu et al. [129].)

In order to transform this qualitative picture into a quantitative semiclassical theory, we have to calculate the quantum phases $\sigma_{\pm}(R,\phi;E)$ carried by the interfering trajectories $(+)$, $(-)$. Generally, there exist three different contributions to $\sigma_{\pm}(R,\phi;E)$: First, the trajectories will "inherit" atomic phases $\gamma(\theta,\phi)$, $\gamma(\pi-\theta,\phi)$ deriving from the angular phase distribution of the point source; second, particles traveling along

the classical paths will gather dynamical phases which in the semiclassical picture are determined by the classical reduced action $W_{\rm cl}^{(\pm)}(\mathbf{r},\mathbf{o};E)$ along the respective trajectories [9]. From Section 4.1.3, we infer that for ballistic motion, $W_{\rm cl}^{(\pm)}(\mathbf{r},\mathbf{o};E)$ may be expressed in parabolic coordinates (4.14):

$$W_{\rm cl}^{(\pm)}(\mathbf{r},\mathbf{o};E) \;=\; \frac{\sqrt{M}}{3F}\,\Big\{[2E+F(r+z)]^{3/2} \;\pm\; [2E-F(r-z)]^{3/2}\Big\} \tag{6.5}$$

Finally, an additional "phase jump" of $-\pi/2$ will occur whenever a trajectory is "reflected," i. e., grazes a caustic surface [110]. Here, only the "slow" trajectory $(+)$ will be affected, see Figure 6. (The phase jump is a pure wave phenomenon and should be familiar from electrodynamics and optics. See e. g. [84].) Hence, the semiclassical phases $\sigma_\pm(R,\phi;E)$ along the trajectories $(+)$, $(-)$ read:

$$\sigma_+(R,\phi;E) = \gamma(\pi-\theta,\phi) + \frac{1}{\hbar}\,W_{\rm cl}^{(+)}(\mathbf{r},\mathbf{o};E) - \frac{\pi}{2} \tag{6.6}$$

$$\sigma_-(R,\phi;E) = \gamma(\theta,\phi) + \frac{1}{\hbar}\,W_{\rm cl}^{(-)}(\mathbf{r},\mathbf{o};E) \tag{6.7}$$

Following these preliminaries we now may lay down the semiclassical theory of ballistic motion in the asymptotic limit $z\to\infty$. Let us denote the angular amplitude distribution at the source by $A(\theta,\phi) = |A(\theta,\phi)|\exp[i\gamma(\theta,\phi)]$; then, the semiclassical current density distribution $j_z^{(\rm sc)}(R,\phi;E)$ on the screen will be given by the classical differential cross section $\partial\sigma_{\rm cl}/\partial\Omega(R;E)$ (6.4), accounting for the projection properties of ballistic motion, modulated by an interference term representing the combined effects of source emission characteristics and quantum interference:

$$j_z^{(\rm sc)}(R,\phi;E) \;=\; \frac{\partial\Omega}{\partial\sigma_{\rm cl}}\,(R;E)\;\Big||A(\pi-\theta,\phi)|\,e^{i\,\sigma_+(R,\phi;E)} \;+\; |A(\theta,\phi)|\,e^{i\,\sigma_-(R,\phi;E)}\Big|^2 \tag{6.8}$$

Here, $\sin\theta = R/R_{\rm cl}(E)$ (6.3).

The contributions of source structure and quantum interference will disentangle if the emission pattern shows reflection symmetry with regard to the $x-y$ plane:

$$|A(\pi-\theta,\phi)|^2 \;=\; |A(\theta,\phi)|^2 \tag{6.9}$$

Then, (6.8) reduces to a product of three independent factors [16]:

$$j_z^{(\rm sc)}(R,\phi;E) \;=\; |A(\theta,\phi)|^2\,\frac{\partial\Omega}{\partial\sigma_{\rm cl}}\,(R;E)\;\Big|e^{i\,\sigma_+(R,\phi;E)} \;+\; e^{i\,\sigma_-(R,\phi;E)}\Big|^2 \tag{6.10}$$

As an illustration, we calculate the semiclassical approximation $j_{lmm}^{(\rm sc)}(\mathbf{r},\mathbf{o};E)$ to the current density distribution generated by a multipole source $\delta_{lm}(\mathbf{r})$ of pure (l,m) angular characteristics (2.23), (5.42), (5.95) that is closely related to the current images

plotted in Figure 5. Obviously, apart from an overall factor $A_0(E)$ the angular amplitude distribution of this source is given by the corresponding spherical harmonic function:

$$A(\theta,\phi) \;=\; A_0(E)\, Y_{lm}(\theta,\phi) \tag{6.11}$$

Note that we have no means to determine the total emission rate $J_{lm}(E)$ (5.48) by classical considerations; here, we pragmatically adopt the value quantum theory provides in the case of field-free emission, i. e., the Wigner law (3.27) from Section 3.2:

$$A_0(E)^2 \;=\; \frac{M}{4\pi^2\hbar^3}\, k^{2l+1} \tag{6.12}$$

Due to the parity properties of spherical harmonics under reflections [83]:

$$Y_{lm}(\pi-\theta,\phi) \;=\; (-1)^{l-m}\, Y_{lm}(\theta,\phi) \tag{6.13}$$

the simplified formula (6.10) applies. Inserting an explicit formula [128] for $Y_{lm}(\theta,\phi)$ into (6.10), eliminating the angle θ by means of (6.3) and approximating the semiclassical phase $\sigma_\pm(R,\phi;E)$ (6.5)–(6.7) by a far-field asymptotic expression in terms of the radial distance R we finally obtain after a short calculation for the semiclassical current density distribution:

$$j^{(\mathrm{sc})}_{lmm}(\mathbf{r},\mathbf{o};E) \;=\; \frac{M\,k^{2l+1}}{4\pi^3\hbar^3}\,\frac{2l+1}{R_{\mathrm{cl}}(E)\,\sqrt{R_{\mathrm{cl}}(E)^2-R^2}}\,\frac{(l-m)!}{(l+m)!}\,P_l^m\left(\sqrt{1-\frac{R^2}{R_{\mathrm{cl}}(E)^2}}\right)^2 \;\times$$
$$\sin\left\{\frac{2}{3}\left[2\beta E\left(1-\frac{R^2}{R_{\mathrm{cl}}(E)^2}\right)\right]^{3/2} \pm \frac{\pi}{4}\right\}^2 \tag{6.14}$$

Here, $P_l^m(z)$ denotes the associated Legendre polynomial [81]. The upper sign in the interference term applies for even parity in (6.13), i. e., for even $l-|m|$, whereas the lower sign is valid for odd parity ($l-|m|$ odd). Note that a change of parity is equivalent to a shift of the argument of the sine factor in (6.14) by $\pi/2$, or, stated in another way, the replacement of the sine by a cosine function. Hence, under change of parity, the interference ring pattern will reverse, thereby confirming our observations made in the preceding section. In fact, summarizing we may conclude that we have managed to explain all the features of Figure 5 we mentioned in Section 6.1 in terms of the simple semiclassical theory presented in this section.

6.3 Total Currents: Modifying Wigner's Law

With the quantum mechanical treatment of the problem of electron point sources in a surrounding homogeneous force field in Chapter 5, and its semiclassical counterpart

($E > 0$) presented in the preceding section at hand, we now may proceed to compare these results to experimental data as well as theoretical work previously done on the problem of ballistic motion, almost always in the context of negative ion photodetachment in a uniform electric field environment. We have already shown that this phenomenon may serve as a practical realization of the quantum source model (Section 3.1). We will split our enterprise into two separate parts and start out with a discussion of total currents (total cross sections). This study will be complemented by an investigation of the spatial distribution of the electronic current which we defer to the following section.

In the wake of the first observation of the modulation of a photocurrent by an externally applied static electric field announced by Bryant et al. [60] in 1987, a series of both theoretical [5, 14, 17, 19–29, 31, 32, 39, 54] and experimental [56–59, 61, 62] investigations into the problem were published and stirred renewed interest in the dynamics of electrons in external fields. However, it should be noticed that the first theoretical studies of the problem date back even further; we will mention here only the seminal papers by Fabrikant [10, 11]. (Historically, the modulation of a photocurrent due to an external electric field was first experimentally observed by Freeman et al. [130] in the photoionization of neutral Rb atoms (1978). For a comprehensive experimental investigation of near-threshold photoionization, we again refer to work performed by Blondel et al. [131]. In general, theoretical studies of the underlying LoSurdo–Stark effect follow the same lines as their counterparts devised for the photodetachment process, even though the presence of the additional long-range final-state Coulomb interaction between the photoelectron and the remaining ion extraordinarily complicates the problem. Here, we only cite a few early theoretical models [132–134] and the extensive investigation of photoionization phenomena undertaken by Kondratovich and Ostrovsky [17, 18].)

6.3.1 General Features

In order to compare our result (5.48) for the total current $J_{lm}(E)$ generated by a multipole source $\delta_{lm}(\mathbf{r})$ (2.23) with experimental data and the findings of earlier theoretical investigations, it appears reasonable to examine $J_{lm}(E)$ first, extract the main features contained in the expression (5.48), and explain them in terms of classical ballistic motion (Section 6.2), if possible. For this purpose we proceed as in Section 6.1 and establish a "multipole map" of total currents $J_{lm}(E)$ for $l = 0, 1, 2$. Figure 7 presents the multipole currents generated by a multipole source $\delta_{lm}(\mathbf{r})$ located in a uniform electric field of strength $F = 1.476 \cdot 10^5$ V/m and a field-free environment, respectively, as a function of the initial electron energy E. (The former value is taken over from the actual experiment by Gibson et al. [59].)

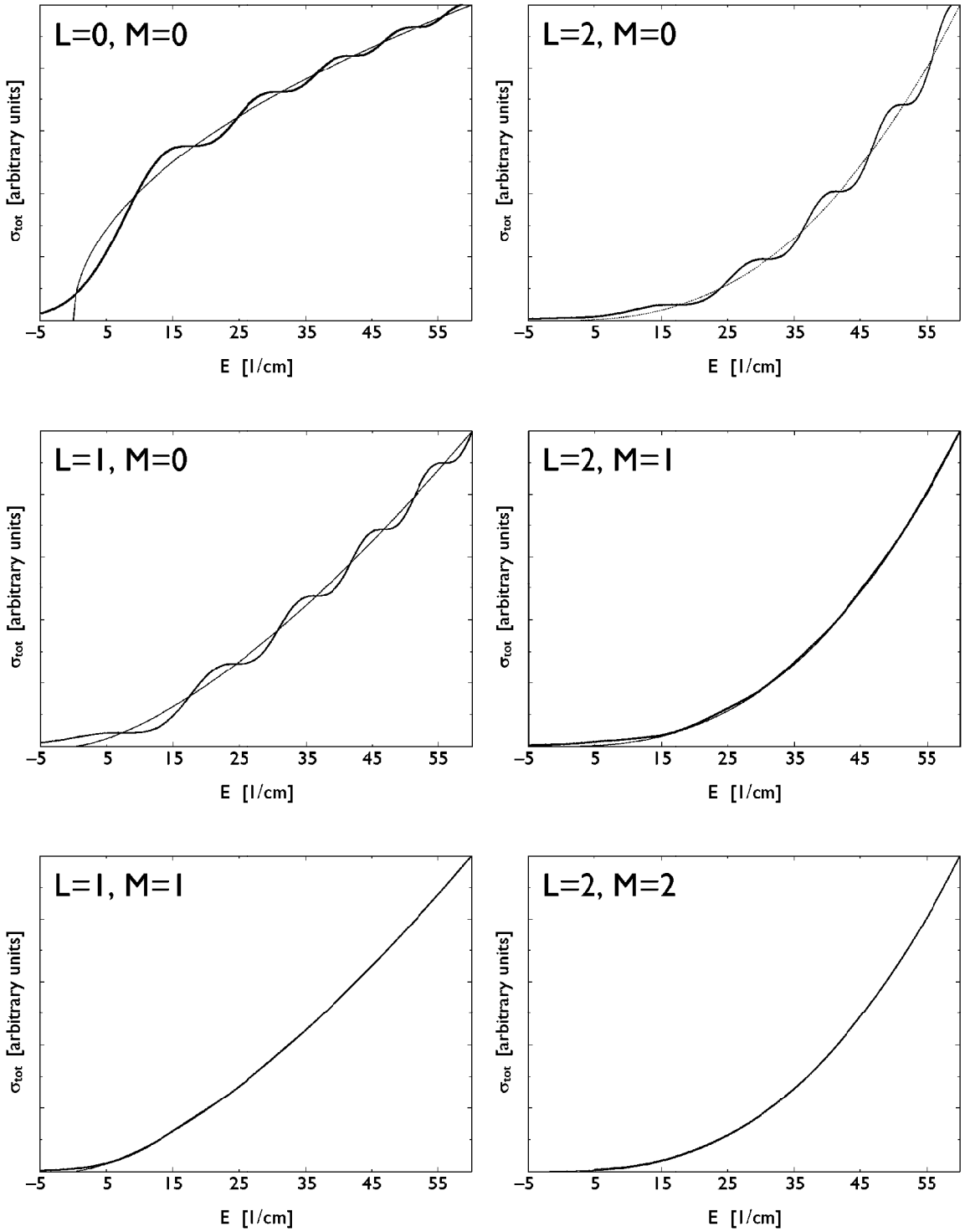

Figure 7: Predicted total multipole currents $J_{lm}(E)$ in photodetachment for angular momenta $l = 0, 1, 2$, and $0 \leq m \leq l$. Bold line: Source embedded in a uniform electric field $F = 1.476 \cdot 10^5\,\mathrm{V/m}$. Thin line: Field-free emission. (The current axes have been scaled arbitrarily.)

From Section 3.2 we infer that field-free emission leads to a simple power-law energy dependence for the multipole current, the Wigner law (3.27) $J_{lm}^{(\mathrm{free})}(E) \propto k^{2l+1}$. Effects of an additional electric field therefore manifest themselves in Figure 7 as deviations from the Wigner threshold law. In compliance with the results (5.58), (5.59) of our analysis for the multipole current $J_{lm}(E)$ in the asymptotic limit $|\beta E| \gg 1$ (Section 5.5.3), we find that the cross sections in the presence of the field $J_{lm}(E)$ generally follow their field-free counterparts, but show two additional significant structures. First, the strict threshold behavior of $J_{lm}^{(\mathrm{free})}(E)$ near $E = 0$ is softened. Due to the quantum tunneling effect, even for negative initial energy E electrons may leave the source, leading to a non-vanishing (yet exponentially suppressed) multipole current $J_{lm}(E)$ for $E < 0$. We will study these "tunneling sources" in greater detail in Chapter 7.

More conspicuously, some of the plots show an oscillatory electric-field modulation of the cross section which gives $J_{lm}(E)$ the appearance of a "staircase" built by a sequence of steep "edges" and flat "steps." As predicted in Section 5.5.3, the effect depends strongly on the magnetic quantum number m; distinctive for longitudinal polarization of the electron beam ($m = 0$), the modulation is hardly recognizable for $|m| = 1$ and for all practical means absent for $|m| = 2$. Closer scrutiny of the $m = 0$ plots reveals further details: With increasing energy E, the oscillations become smaller but more frequent, and, most interestingly, the position of the steps almost coincides for $l = 0$ and $l = 2$, but is strongly correlated to the location of the steep edges in the plot for $l = 1$. Recalling the chequerboard distribution of interference patterns in Figure 5, this alternating structure may be interpreted as a signature of the interference of classical ballistic trajectories (Sections 4.1 and 6.2).

6.3.2 Closed-Orbit Theory

Indeed, the oscillations of the total cross section may be linked to the behavior of those classical trajectories that return back to the source. The importance of this set of classical paths was first pointed out by Du and Delos [42] who developed a semiclassical theory of the cross section based on recurrent trajectories. This "closed-orbit theory" has been employed for the calculation of photodetachment spectra in external electromagnetic fields [44, 45, 47, 48, 135, 136], including the simple case of uniform electric fields here under consideration [32]. (Again, we should note that an argument very similar to the closed orbit theory sketched below was invoked to explain electric field-induced modulations in the photoionization cross section already by their discoverers [130]. Some of the complicated classical trajectories appearing in the LoSurdo–Stark problem have been depicted in Refs. [18] and [137].)

In the uniform force field problem, only a single returning classical trajectory is present. It corresponds to the emission of a particle opposite to the direction of force

F. Depending on the semiclassical phase accumulated along its free-falling orbit, the returning particle will interfere with the source, thus generating the modulation in the total current caused by the electric field. Hence, steep edges in the photocurrent are associated with constructive interference of trajectories ejected along the field direction, and should be connected to a bright interference spot in the center of the current density distribution patterns of Figure 5, whereas flat steps occur for destructive interference, i. e., dark central "holes" in the differential cross sections. Using the results obtained in Section 4.1, we may put this condition into more quantitative terms. With increasing particle energy E, the closed orbit grows in size, and the classical action $W_{\rm cl}^{(+)}(\mathbf{o},\mathbf{o};E)$ (4.14) for the recurrent path $(+)$ increases:

$$W_{\rm cl}^{(+)}(\mathbf{o},\mathbf{o};E) \;=\; \frac{2\sqrt{M}}{3F}\,(2E)^{3/2} \;=\; \frac{4}{3}\,\hbar\,(2\beta E)^{3/2} \tag{6.15}$$

A new dark interference ring in the current density pattern will spring into existence as a central "hole" whenever the relation (6.6), (6.7):

$$\sigma_+(R,\phi;E) - \sigma_-(R,\phi;E) \;=\; (2\nu+1)\pi \tag{6.16}$$

holds, where $\nu = 0, \pm 1, \pm 2, \ldots$ denotes an entire number. From (6.14) we may infer that the relation (6.16) is equivalent to the condition:

$$\sin\left\{\frac{2}{3}\,(2\beta E)^{3/2} \pm \frac{\pi}{4}\right\} \;=\; 0 \tag{6.17}$$

Here, the sign depends on the reflection parity of the source amplitude distribution (6.13), the upper sign belonging to even parity (even l for $m = 0$). Written in explicit form, the total current exhibits stationary points for the set of energies $E_{\nu l}$:

$$E_{\nu l} \;=\; \frac{1}{8\beta}\,\left[3\pi\,(4\nu + 2l - 1)\right]^{2/3} \tag{6.18}$$

This formula is in accordance with the findings of the asymptotic analysis for $J_{l0}(E)$ (5.60)–(5.62). Clearly, only two different series for even respectively odd l exist, confirming the observations extracted from Figure 7. Note that the energies $E_{\nu l}$ (6.18) approximately show scaling behavior: $E_{\nu l} \propto (\nu F)^{2/3}$. Thus, with increasing energy E the oscillations become more frequent.

So far we have exclusively considered the case of longitudinal polarization, $m = 0$. For higher $|m|$, the z axis presents a node line of the emission pattern. Hence, the single recurrent classical path in the ballistic problem is no longer populated, and semiclassical closed-orbit theory predicts that the cross section is not affected at all by the force field [32]. Although this statement is by and large correct, a closer look at

Figure 7 reveals that weak oscillations in the total current survive for $|m| > 0$. These corrections, which may be extracted from the asymptotic series of $J_{lm}(E)$ (5.59), are outside the scope of closed-orbit theory.

6.3.3 Other Theoretical Approaches

Besides closed-orbit theory and related semiclassical models [10,11,17,19], theoretical predictions for the total photodetachment cross section have been made following mainly two approaches, application of Fermi's Golden Rule [31,32,57–59] or explicit construction of the Green function $G(\mathbf{r}, \mathbf{r}'; E)$ (5.18) of the photoelectron [14,15,20,23–29].

We have already seen in Section 3.1 that the theory of quantum sources we mathematically developed in Chapter 2 is fully equivalent to first-order quantum mechanical perturbation theory. The same is obviously true for Fermi's Golden Rule, so both approaches are bound to give identical results. (Formally, this statement is proven in Appendix A.6.) This means that in the limit of pointlike multipole sources $\delta_{lm}(\mathbf{r})$ (2.23), i. e., pointlike initial ionic states $\chi_i(\mathbf{r})$ (3.9), the total current $J_{lm}(E)$ is given by the source theoretical formula (5.48), whose results are listed in Appendix E.3. Hence, the difference between both methods is entirely of methodical nature; whereas the source theoretical description immediately leads to the expression (5.48) that we derived using elementary mathematical operations (differentiation, limiting procedure) only (2.33), application of Fermi's Golden Rule requires integration over all possible final electron states, which turns out to be a tedious task—following the pioneering work of M. L. Du and Delos [31,32] in 1988, it took five years and the Green function approach for N. Y. Du et al. [15,23,24] to realize that all appearing integrations in the Golden Rule formalism can be resolved analytically. (A calculation for the total s–wave current $J_{00}(E)$ following the Golden Rule scheme is presented in Appendix A.6.1, equation (A.345). Note that this result was stated by Luc-Koenig and Bachelier as early as 1980 [134], but apparently remained unnoticed.) In fact, this article presents the first systematic theoretical study for the total multipole currents in the homogeneous field environment (Section 5.5).

The usage of Green functions, initially introduced by Rau and Wong [25–27] in 1988 under the (somewhat misleading) label "frame transformation approach," was repeatedly hampered by the fact that most authors were not aware that the three-dimensional Green function in a linear potential $U(\mathbf{r}) = -\mathbf{r} \cdot \mathbf{F}$ is available in closed form, which led them to employ integral representations of $G(\mathbf{r}, \mathbf{r}'; E)$ instead of the analytic formula (5.18) [15,19,20,23,24]. It was from these theories that explicit expressions for the multipole currents $J_{lm}(E)$ were first derived [15,23,24]. In these papers, the Green function method was extended to include effects due to the finite size of the initial ionic wave function $\chi_i(\mathbf{r})$. This topic is beyond the scope of the multipole source

approximation (3.21) to the photodetachment process in Section 3.1. According to the comments in Section 3.2, such corrections are however of little relevance for studies of near-threshold photodetachment which we are considering here.

For the sake of completeness, we mention here further theoretical approaches using more complicated assumptions. Fabrikant tried to include rescattering effects in photodetachment caused by the presence of the remaining neutral atomic core [12]. Other work was devoted to the study of multiphoton photodetachment [21,22,54].

6.3.4 Experimental Results

After having detailed the theoretical investigations into photodetachment in the uniform field environment we quote some experimental results concerning the problem. As noted above, electric field effects modulating the photocurrent near threshold were first reported by the group of Bryant et al. [60] in 1987, and later supplemented by additional work [61,62]. In their experimental setup, a relativistic beam of negatively charged hydrogen ions (H^-) was irradiated with laser light in the presence of a weak perpendicular magnetic field, which in the rest frame of the ions transforms into a giant "motional" electric field [84] of the order $F \sim 10^7\,\mathrm{V/m}$, causing large-scale oscillations in the photodetachment cross section. Because the ground states of H^- and H^0 are both spherically symmetric s–states, conservation of angular momentum (3.23) enforces that near threshold, all photoelectrons are emitted into p–waves ($l = 1$). The photocurrent $J(E)$ hence depends on the orientation of the laser beam polarization with respect to the external electric field $\mathbf{F}$: For parallel alignment of the external and laser wave electric field vectors ("π–polarization"), the photoelectrons are emitted in direction of the external field obeying a p_z angular distribution ($m = 0$). According to the discussion of Section 6.3.2, interference of direct and recurrent trajectories should lead to a ripple-like modulation overimposed to a smoothly growing cross section $\sigma(k) \propto k^{3/2}$ given by the Wigner law (3.27). After turning the laser polarization by $\pi/2$, the electric field vector of the laser beam will be orthogonal to the external field ("σ–polarization"), causing the release of electrons into an p–orbital structure orthogonal to $\mathbf{F}$, say p_x. Such a source may be construed as a superposition of $m = \pm 1$ states. Hence, the characteristic signature of the external electric field should be absent from photocurrent spectra generated by σ–polarized light, which should closely follow the zero-field Wigner law (3.27) instead. Both predictions were qualitatively confirmed, yet, probably due to the large motional fields and considerable excess energy used, the agreement was far from perfect [60–62].

These deficiencies were largely remedied through the dedicated experiments of Larson and co-workers, another group experienced and proficient in photodetachment setups [34], in 1993 [58,59]. A monoenergetic beam of negative ions was sent through an interaction chamber where a static homogeneous electric field in the range

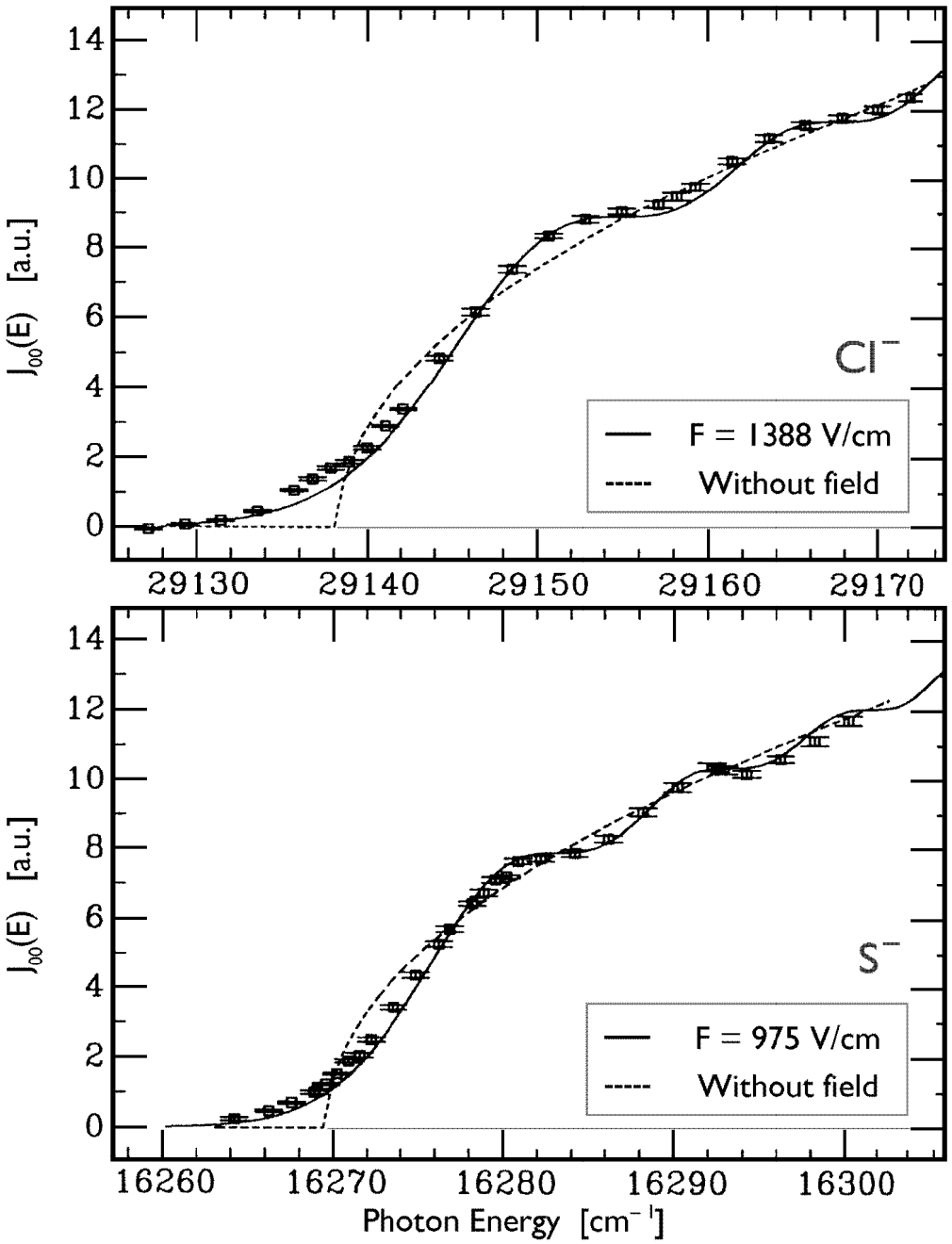

Figure 8: Experimental data on s–wave photodetachment ($l = m = 0$) in a uniform electric field. Top figure: Total photodetachment cross section $\sigma_{\rm tot}(E)$ (π polarization) for a Cl^-–beam in an electric field $F = 1.388 \cdot 10^5\,{\rm V/m}$ as a function of the laser photon energy. Bottom figure: $\sigma_{\rm tot}(E)$ (σ polarization) for a S^-–beam in an electric field $F = 9.75 \cdot 10^4\,{\rm V/m}$. Symbols denote experimental values, the bold line presents the theoretical prediction from the multipole source model (E.11). The field-free cross section (3.27) is indicated by the dotted line. The current axes have been scaled arbitrarily. (After Gibson et al. [58].)

of 10^5 V/m was applied parallel to the ion beam. In the uniform field region, an adjustable dye laser beam crosses the ion beam under right angles, causing near-threshold photodetachment. Subsequently, in the outgoing beam unaffected ions and neutral atoms produced by photodetachment were separated by a strong electric field and independently counted. The photodetachment rate was determined from these counts. By selection of different ions and laser polarizations, the photodetachment cross section for $l = 0, 1$ and $|m| = 0, 1$ was studied.

In their publications regarding these experiments [58, 59], Gibson et al. chose to compare the experimental data with a theory based on Fermi's Golden Rule, closely following the theoretical approach by Du and Delos [31,32]. Though they only arrived at integral representations for the multipole current $J_{lm}(E)$ (5.48), it is fairly easy to show that their expressions equal the explicit results of quantum source theory (E.11)–(E.13) which are listed in Appendix E.3. Hence, we may simply take over the original data analysis by Gibson et al.

The especially simple case of isotropic or s–wave photodetachment was examined using sulfur (S^-) and chlorine (Cl^-) ions [58]. Here, the results should not depend on the polarization of the laser beam, which was confirmed by acquiring S^- data in the σ mode ($m = \pm 1$), whereas the experimental values for Cl^- were recorded using π polarization ($m = 0$). No significant difference between the spectra, presented in Figure 8, could be obtained—both plots closely resemble the theoretical spectrum put onto display in Figure 7: The "staircase" modulation of the field-free (Wigner) current $J_{00}^{(\mathrm{free})}(E) \propto \sqrt{E}$ (3.27) is clearly exhibited. Also, Figure 8 shows the onset of photoelectron tunneling. In order to normalize their results, and also to emphasize the change in the photodetachment cross sections introduced by the external electric field, Gibson et al. [58, 59] often preferred not to present photocurrent spectra themselves, but plotted the ratio $H(E, F)$ between the cross sections with and without applied electric field instead (3.27), (E.11):

$$H(E,F) \;=\; \frac{\sigma_{\mathrm{tot}}(E,F)}{\sigma_{\mathrm{tot}}(E,F=0)} \;=\; \frac{J_{lm}(E)}{J_{lm}^{(\mathrm{free})}(E)} \tag{6.19}$$

This form of presentation is superior in enhancing effects of the electric field, but has the disadvantage that $H(E, F)$ diverges at the threshold. As an example, the s–wave photodetachment data shown in Figure 8 is redisplayed in terms of $H(E, F)$ in Figure 9. It is seen that the experimental data concerning s–wave photodetachment in a static electric field environment compare reasonably well with the source theoretical result (E.11).

Using the same equipment, Gibson et al. also performed studies regarding p–wave photodetachment in an external electric field [59]. As a suitable system, negatively charged gold ions (Au^-) were selected. The experimental data were compared with

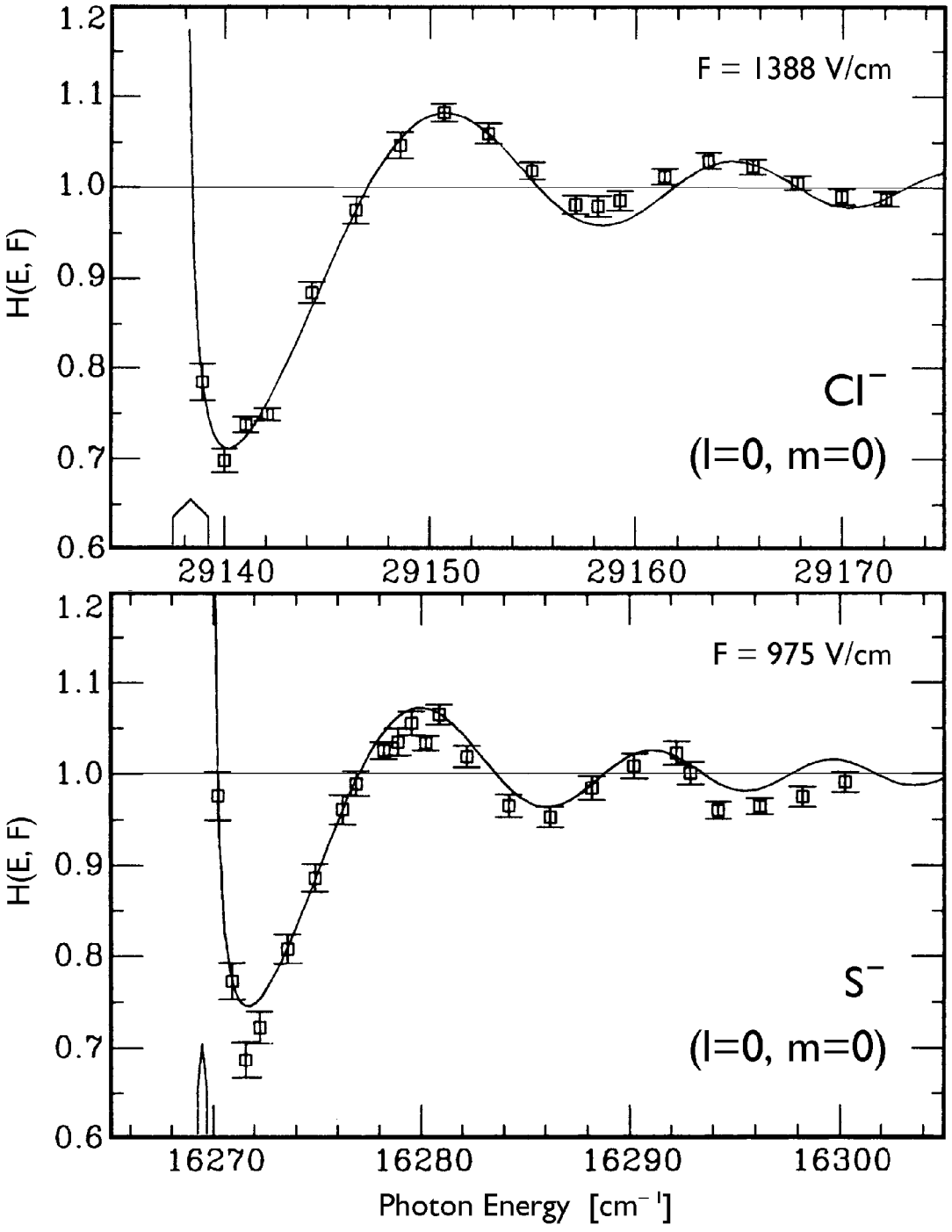

Figure 9: Electric field effects in s–wave photodetachment. Top figure: Modulation factor $H(E,F)$ (6.19) for Cl^- at field strength $F = 1.388 \cdot 10^5\,V/m$ as a function of photon energy E. Bottom figure: $H(E,F)$ for S^-, field strength $F = 9.75 \cdot 10^4\,V/m$. Symbols present experimental values, the prediction of multipole source theory is entered as a solid line. See also Figure 8. (After Gibson et al. [58].)

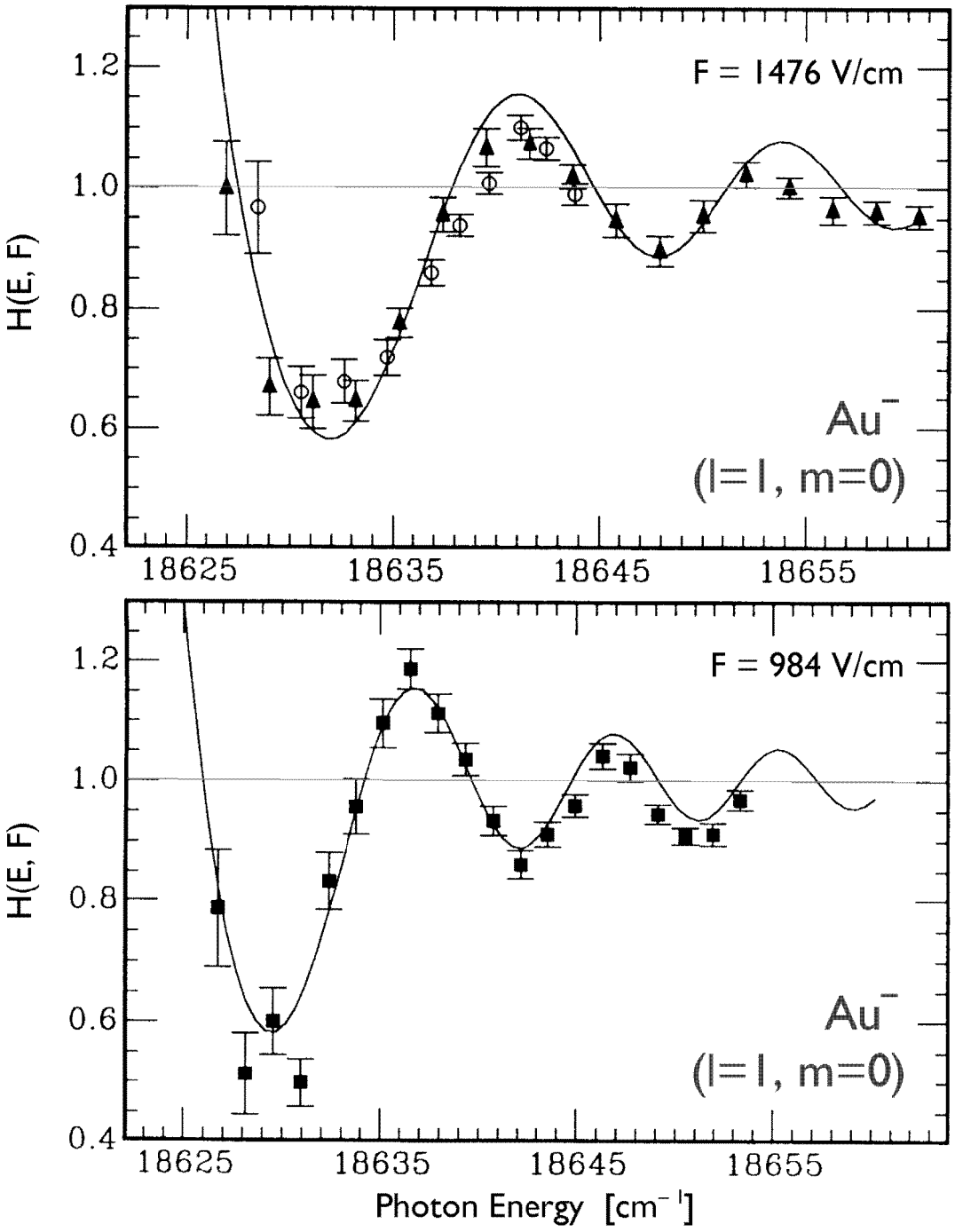

Figure 10: Electric field effects in p–wave photodetachment of Au^- ions in π laser polarization ($l = 1, m = 0$). Top figure: Modulation factor $H_\pi(E, F)$ (6.19) at field strength $F = 1.476 \cdot 10^5$ V/m as a function of photon energy E. Bottom figure: $H_\pi(E, F)$ at field strength $F = 9.84 \cdot 10^4$ V/m. Symbols present experimental values, the prediction of multipole source theory (E.12) is entered as a solid line. (After Gibson et al. [59].)

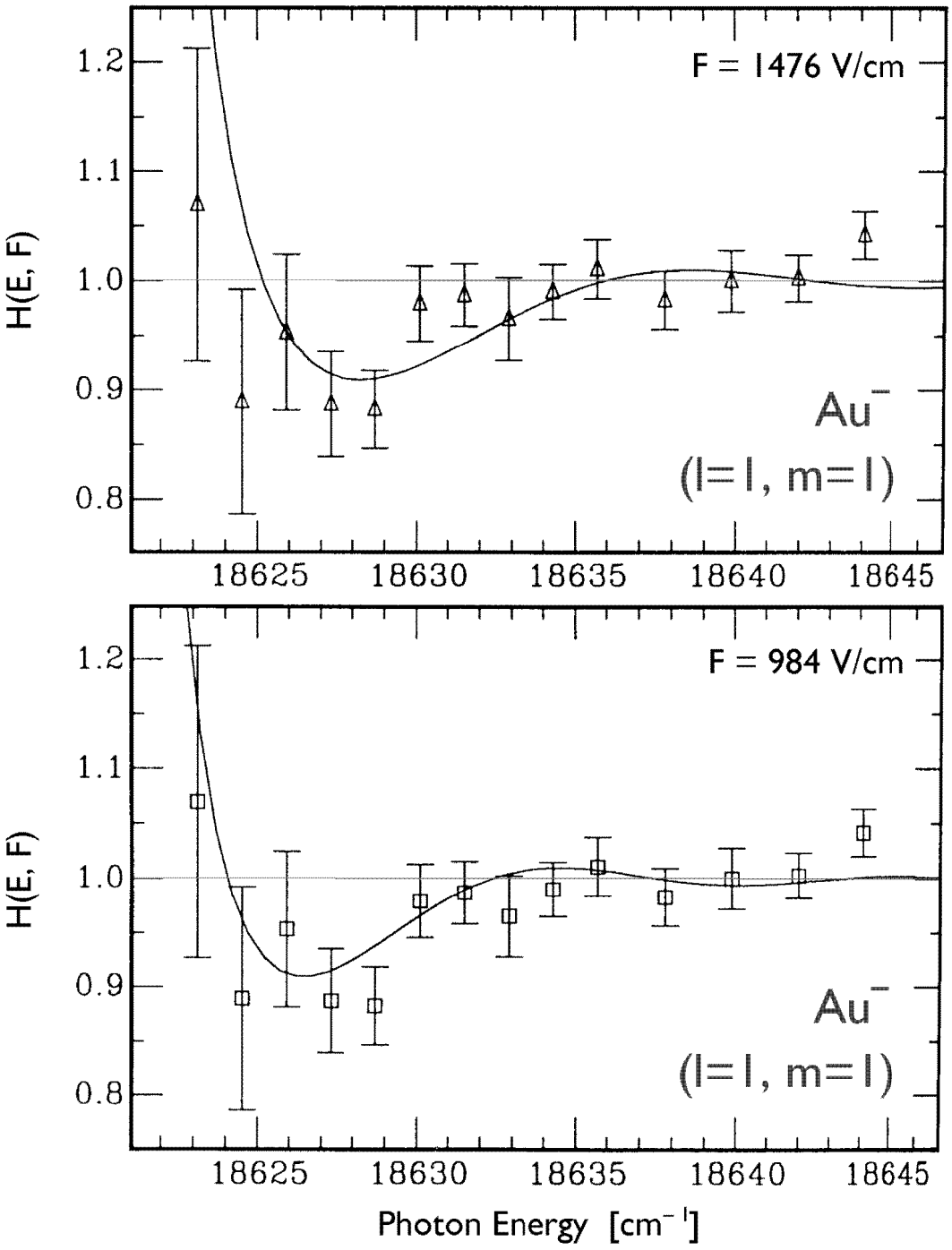

Figure 11: Electric field effects in p–wave photodetachment of Au^- ions in σ laser polarization ($l = 1, |m| = 1$). Top figure: Modulation factor $H_\sigma(E, F)$ (6.19) at field strength $F = 1.476 \cdot 10^5$ V/m as a function of photon energy E. Bottom figure: $H_\sigma(E, F)$ at field strength $F = 9.84 \cdot 10^4$ V/m. Symbols present experimental values, the prediction of multipole source theory (E.13) is entered as a solid line. See also Figure 10. (After Gibson et al. [59].)

a fairly complicated, partly numerical theory based on Fermi's Golden Rule which can be shown to boil down to the predictions of $l = 1$ multipole source theory (E.12), (E.13) after integration. Again, the authors chose to display their results in terms of the electric field modulation factor $H(E, F)$ (6.19). The results for parallel alignment of the vectors of the external and the laser electric fields (π polarization, $m = 0$) are presented in Figure 10, whereas data recorded for perpendicular alignment of both fields (σ polarization, $|m| = 1$) are displayed in Figure 11. In accordance with the closed-orbit model and the earlier experiments by Bryant et al. [60–62], the π polarization or $m = 0$ photodetachment cross section responds much more sensitively to the presence of the external field $\mathbf{F}$ than its σ or $m = \pm 1$ counterpart (note the different scaling for $H(E, F)$ in Figures 10 and 11). Therefore, it should not be surprising that the modulation factor $H(E, F)$ (6.19) appears better resolved in the case of π polarization. Nevertheless, we find that the results of the multipole source model (E.12), (E.13) are in fair agreement with the available experimental data on p–wave photodetachment in a static electric field.

6.4 Current Density Distributions

Having depicted the state of affairs regarding total cross sections in photodetachment phenomena influenced by an external electric field, we now turn our attention towards the differential cross section, i. e., the actual spatial distribution $j_z(\mathbf{r}, \mathbf{o}; E)$ (5.41), (5.42) of the photocurrent. Compared to the study of total photodetachment rates discussed in the preceding section, far less work has been devoted to the problem of determining the current density distribution. Earlier theoretical inquiries [10,11,13,16,18,20,33] were only recently complemented by the first spatially resolved recordings of a photocurrent obtained in the experiment performed by Blondel et al. [4] in 1996. In all these studies, only the far-field sector $\beta F(r + z) \gg 1$ (see Section 5.8) was explored. Hence, we will restrict our considerations to the asymptotic quantity $j^{(\mathrm{as})}_{lmm'}(\mathbf{r}, \mathbf{o}; E)$ (5.95) and its semiclassical counterpart $j^{(\mathrm{sc})}_{lmm}(\mathbf{r}, \mathbf{o}; E)$ (6.14) both valid in this region of space. (We will have to say more about the exact expressions for the current distribution $j_{lmm'}(\mathbf{r}, \mathbf{o}; E)$ (5.42) in the following chapter.)

6.4.1 Theoretical Approaches—A Survey

Probably due to the lack of experimental data, the interest in the spatial photocurrent distribution lagged behind the efforts invested into the study of the total photoabsorption cross section in the homogeneous field environment, even despite it is evident that both quantities are intimately related. The connection is illustrated by the fact that the pioneering papers of Fabrikant [10, 11] contain a semiclassical description of both the total and differential cross sections. This treatise, and its quite

complicated results, were however all but ignored. Years later, a brief surge of activity was caused by the experiments of Bryant et al. [60–62] described in the preceding section. A semiclassical model for the current profile appearing in electric-field photodetachment into a p–wave ($l = 1$) which is essentially equivalent to the theory presented in Section 6.2, equation (6.14) was presented by Du [33]. Integral representations of the corresponding quantum mechanical cross sections (5.42) were given by Fabrikant [13]. Kondratovich and Ostrovsky dealt with the analogous problem for isotropic sources ($l = 0$) [16,18]. They were able to establish a uniform approximation for the s–wave current density distribution which coincides with the asymptotic far-field result $j^{(\mathrm{as})}_{000}(\mathbf{r}, \mathbf{o}; E)$ (E.33) of the multipole source theory (Section 5.8). Recently, interest in the topic was revived by the first experimental observation of the current interference pattern (Figure 5) by Blondel et al. [4] which stimulated the publication of an article by Golovinskii [20]: Starting from an integral representation of the Green function $G(\mathbf{r}, \mathbf{r}'; E)$ (5.18), the author derives far-field asymptotic formulae for the current profiles $j^{(\mathrm{as})}_z(\mathbf{r}, \mathbf{o}; E)$ (5.91) generated in H^- photodetachment ($l = 1$) both for π ($m = 0$) and σ polarization ($|m| = 1$) of the detaching laser beam (see Section 6.3.4). These expressions agree with the results $j^{(\mathrm{as})}_{100}(\mathbf{r}, \mathbf{o}; E)$ (E.34) and $j^{(\mathrm{as})}_{111}(\mathbf{r}, \mathbf{o}; E)$ (E.35) obtained from the multipole source model in the far-field limit. The current density distributions $j^{(\mathrm{as})}_{lmm'}(\mathbf{r}, \mathbf{o}; E)$ (5.95) generated by sources embedded in a uniform force field (Section 5.8) never were systematically investigated in the literature, thus proving again the virtues of the multipole source theory presented in Section 2.4 of this paper.

6.4.2 Assessment of the Semiclassical Approximation

Because the problem of quantum ballistic motion in three-dimensional space is analytically solvable (Section 5.2), quantum dynamics in a homogeneous force field offers the rare opportunity to compare the results of a semiclassical theory (Section 6.2) with the corresponding exact quantum solution. Hence, we are able to assess the quality of this popular approximation in a multidimensional environment, where it is known to behave in a fairly complicated manner near singular surfaces, so-called caustics [110]. Along caustics, the density of classical trajectories diverges. This situation typically occurs at the classical turning surface, which confines the maximum range of classically allowed motion.

In Section 6.2, we restricted ourselves to a derivation of the semiclassical solution in the limit $z \to \infty$. Hence, we are only interested in a comparison of the semiclassical approximation $j^{(\mathrm{sc})}_{lmm}(\mathbf{r}, \mathbf{o}; E)$ (6.14) with the quantum solution in the far-field asymptotic limit $j^{(\mathrm{as})}_{lmm'}(\mathbf{r}, \mathbf{o}; E)$ (5.95). In Figure 12, the current profiles according to these theories are plotted for $l = 0, 1, 2$. In order to facilitate access to experimental data, we select the values of the parameters according to the original setup by Blondel et

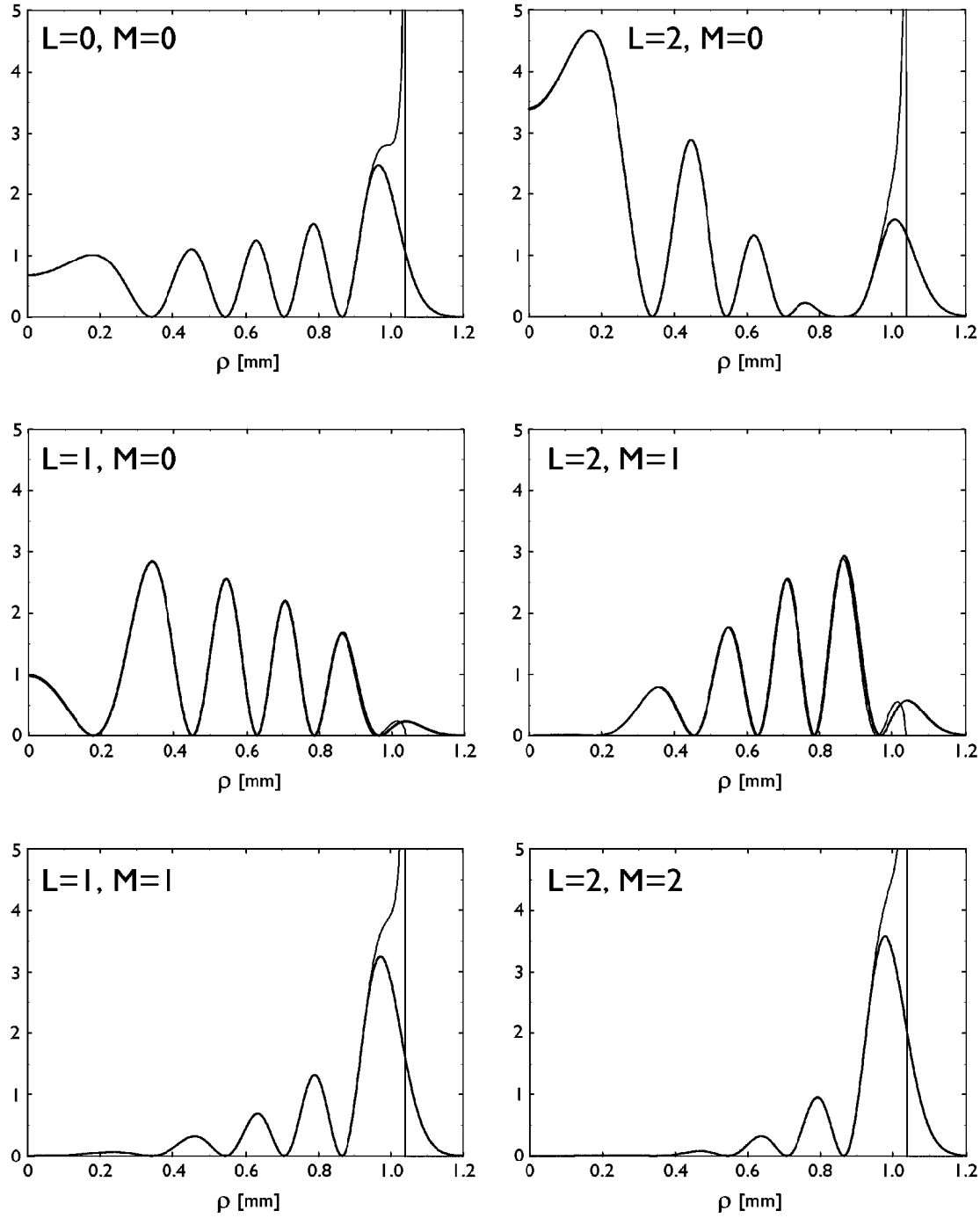

Figure 12: Radial current profiles generated by monoenergetic multipole electron sources ($E = 6.08 \cdot 10^{-5}\,\mathrm{eV}$; $0 \leq |m| \leq l \leq 2$) embedded in a uniform field of strength $F = 116\,\mathrm{V/m}$. Bold lines: Far-field asymptotic quantum result $j^{(\mathrm{as})}_{lmm}(\mathbf{r}, \mathbf{o}; E)$ (5.95). Thin lines: Semiclassical approximation $j^{(\mathrm{sc})}_{lmm}(\mathbf{r}, \mathbf{o}; E)$ (6.14). The sources are located at a distance $z = 0.514\,\mathrm{m}$. The current axes have been scaled arbitrarily. (See also Figure 5.)

al. [4] and consider multipole electron sources of energy $E = 6.08 \cdot 10^{-5}\,\mathrm{eV}$ in an electric field of strength $F = 116\,\mathrm{V/m}$. The lateral current profiles are recorded at a distance $z = 0.514\,\mathrm{m}$ from the electron source. (Since these values were employed also in Figure 5, the quantum current profiles may be interpreted as radial sections of the two-dimensional current images displayed there.)

For the case of ballistic motion, we have already seen that the caustic surface is given by a paraboloid $r - z = 2E/F$ (4.18), and we have to expect deviating behavior of the semiclassical lateral current profile in the vicinity of the classical radius $R \approx R_{\mathrm{cl}}(E)$ (6.1) of the current spot. (In Figures 5 and 12, this radius amounts to $R_{\mathrm{cl}}(E) = 1.04\,\mathrm{mm}$.) As a glance at Figure 12 shows, the semiclassical approximation indeed becomes unreliable at the edge of the current image, showing divergent behavior at $R = R_{\mathrm{cl}}(E)$. (For odd values of $l - |m|$, the divergence is masked by a node circle at $R = R_{\mathrm{cl}}(E)$ due to suppressed emission perpendicular to the direction of force; semiclassical theory nevertheless fails near the classical radius of the current distribution.) Not the failure of the semiclassical theory near $R = R_{\mathrm{cl}}(E)$ should therefore come as a surprise, but its performance within the sector of classically allowed motion: From Figure 12, we infer that the semiclassical and quantum solutions are practically indistinguishable for radii R as large as $0.95\,\mathrm{mm}$, i. e., $j^{(\mathrm{sc})}_{lmm}(\mathbf{r}, \mathbf{o}; E)$ (6.14) provides an excellent description for the electronic current in a range covering 90 percent of the sector of classically allowed motion. Hence, the semiclassical method presents a powerful and accurate approximation technique at least for the rather simple case of linear potentials $U(\mathbf{r}) = -\mathbf{r} \cdot \mathbf{F}$.

6.4.3 Comparison with Experiment

As already noted above, the first experimental observation of the spatial distribution of a photocurrent in presence of a homogeneous electric field was announced by the group of Blondel and colleagues in 1996 [4]. In their carefully devised experiment, a tunable laser beam was focussed onto a collimated monoenergetic beam of negative ions. Laser-ion interaction, resulting in the emission of a low-energy photoelectron, then is essentially limited to the size of the laser focus, and thus may effectively serve as a spatially confined incoherent electron source with a diameter of merely $50\,\mu\mathrm{m}$. Photodetached electrons are accelerated in a uniform electric field generated by a set of electrodes surrounding the interaction chamber, and, after covering a vertical distance $z = 0.514\,\mathrm{m}$, finally impinge onto a spatially sensitive detector recording the current image with a typical resolution of again $50\,\mu\mathrm{m}$. Comparison with the theoretically predicted current profiles displayed in Figures 5 and 12 which were calculated using the actual parameters of this experiment ($E = 6.08 \cdot 10^{-5}\,\mathrm{eV}$, $F = 116\,\mathrm{V/m}$) shows that under these conditions, the interference fringes should be resolvable.

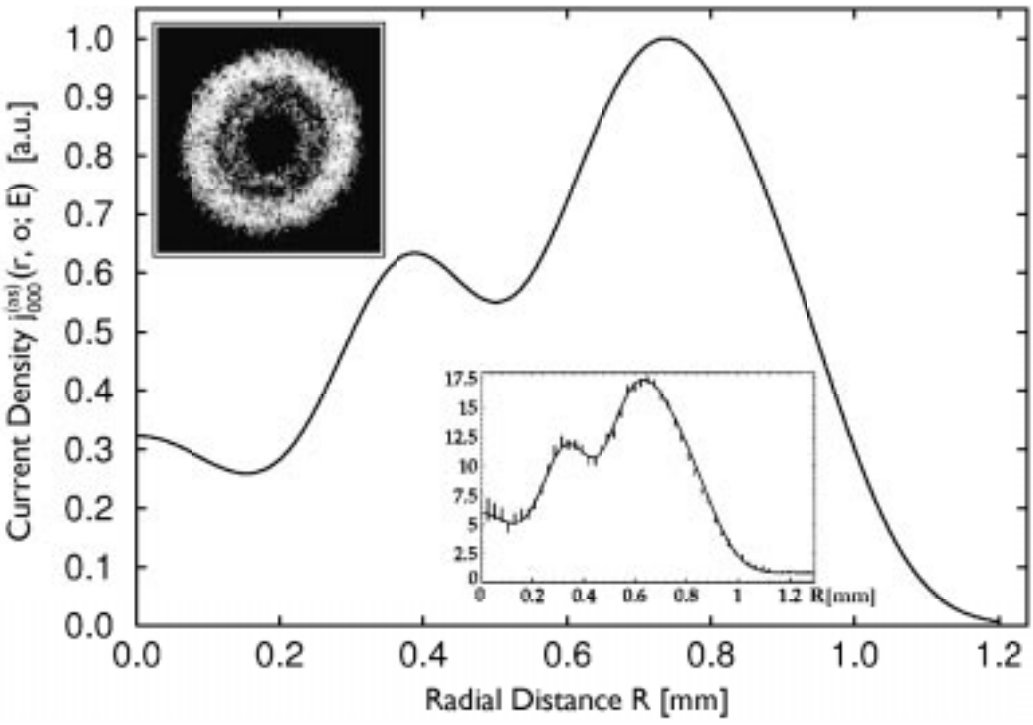

Figure 13: Experiment versus source theory in s–wave photodetachment. Electrons were detached from $^{81}\mathrm{Br}^-$ ions in presence of an electric field of strength $F = 116$ V/m and recorded after a flight of distance $z = 0.514$ m. Maximum energy of the electrons ($F = 0$) was $E = 6.08 \cdot 10^{-5}$ eV. Large plot: Current profile according to the quantum source model (E.33). Insets: Raw experimental data (top left), radial distribution function of electrons (central inset). (After Blondel et al. [4].)

Figure 13 displays the results of the experiment carried out with a $^{81}\mathrm{Br}^-$ ion beam. Near the lowest threshold, the bromine ion will undergo purely s–wave photodetachment ($l = 0$). We see that in Figure 13 one interference ring is clearly discernible, yet the structure as a whole differs quite strongly from the expected distribution, which is depicted as the top right image in Figure 5. The reason for this apparent discrepancy lies in the hyperfine interaction of the bromine nucleus with the atomic electron shell of the emerging neutral $^{81}\mathrm{Br}$ atom. In the bromine system, both the nucleus and the electron shell carry angular momentum ($I = J = 3/2$). Hence, the ground state of $^{81}\mathrm{Br}$ is split into a quadruplet of hyperfine states ($F = I + J = 0, 1, 2, 3$). All these substates, whose relative energy differences are comparable in size to the initial energy E of the detached electron [138], are actually generated in various amounts in the photodetachment experiment, thus leading to a superposition of electronic currents with four discrete energies E_F partly concealing the interference structure. (The value for E given above refers to the lowest-lying $F = 0$ hyperfine singlet state which, how-

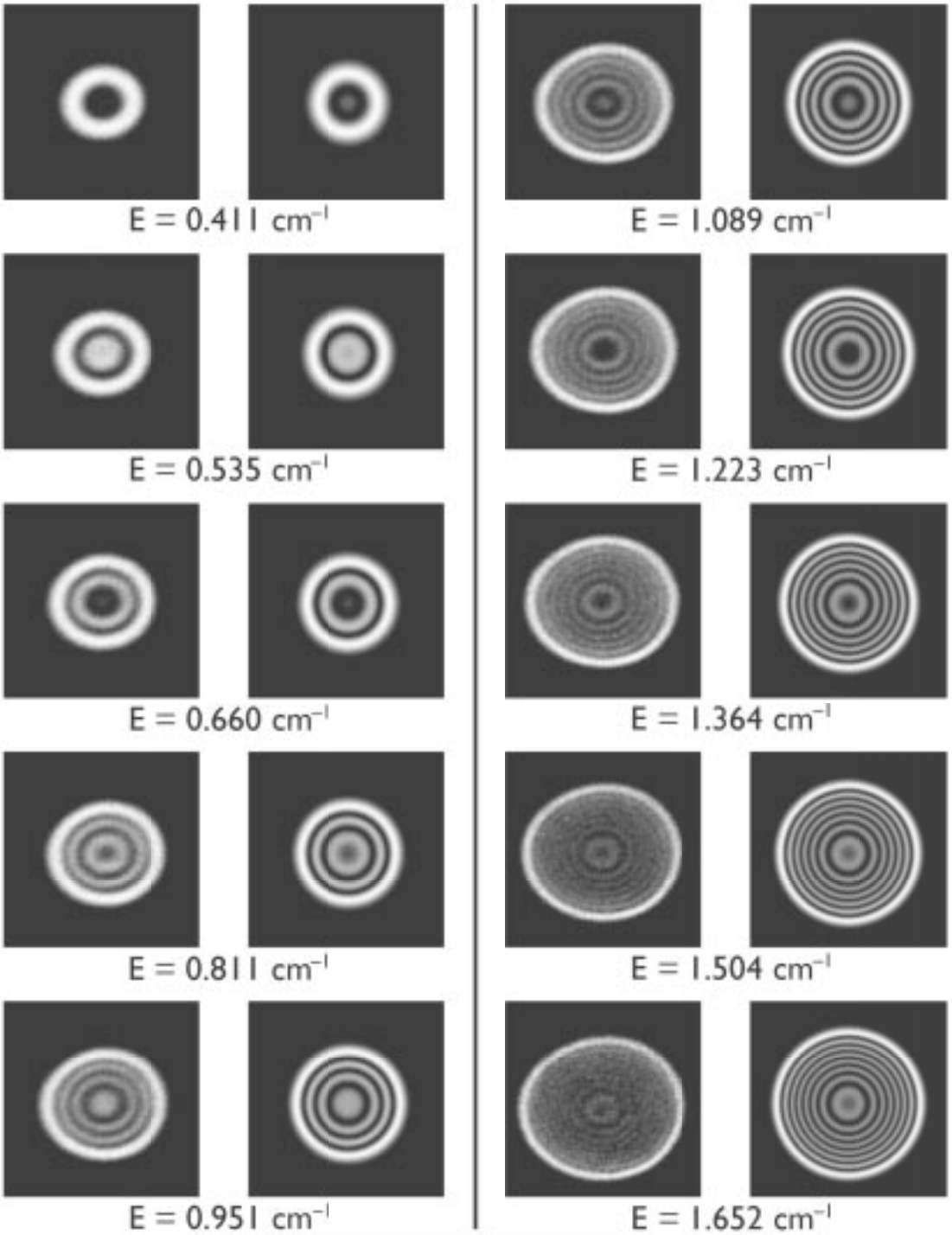

Figure 14: Interference patterns in electric-field near-threshold photodetachment of $^{16}O^-$ ions ($F = 423\,V/m$). Left columns: Experimentally recorded current images. Right columns: Predictions of multipole source theory (5.95) for isotropic sources ($l = 0$). Vertical distance between source and detector is again $z = 0.514\,m$. (After Blondel et al. [63].)

ever, contributes only about 7.5 percent to the total photocurrent.) Correcting for the effects of hyperfine splitting and finite spatial resolution, source theory (E.33) predicts a current profile (large plot in Figure 13) which agrees well with the radial section for the current distribution determined from the experimental data (small insets).

To improve this somewhat unsatisfactory situation, the experiment was recently repeated by Blondel et al. using a different choice of ion that nevertheless will show isotropic detachment ($l = 0$), negatively charged oxygen $^{16}\mathrm{O}^-$ [63]. As a nucleus with even proton and neutron numbers, $^{16}\mathrm{O}$ is a nuclear spin singlet system ($I = 0$), thus hyperfine splittings are absent. Hence, the photocurrent density distribution generated by $^{16}\mathrm{O}^-$ should directly compare to the prediction of quantum source theory (see Figure 5). That this is indeed the case is demonstrated by the spectacular results obtained in the oxygen experiment, which are shown in Figure 14: The left columns display a series of ten experimental raw current images recorded for increasing electron excess energies E which may be compared to the distributions $j^{(\mathrm{as})}_{000}(\mathbf{r}, \mathbf{o}; E)$ (E.33) generated by an idealized s–wave point source embedded in a uniform electric field of strength $F = 423\,\mathrm{V/m}$ (right-hand columns). Apart from image blurring caused by imperfect spatial resolution, theoretical predictions and experimental results coincide remarkably well, thus again confirming that the multipole source method is suitable for a theoretical description of near-threshold photodetachment phenomena.

6.5 A Photodetachment Microscope?

The current images displayed in Figures 5, 13 and 14 reveal some of the elegance disguised behind the mathematical formalism presented in Chapter 5. These pictures owe much of their aesthetic quality to the inherent symmetry of the current density distribution, and it is tempting to relate the symmetries prominent in these images with the emission characteristics of the atomic electron source. Thus, Blondel et al. put forward the idea of a "photodetachment microscope" [4]. (Indeed, the related notion of a "photoionization microscope" was originally introduced by Demkov et al. [16] in 1980. However, in their paper they actually state the current density distribution for the uniform field s–wave photodetachment process in the semiclassical limit—see Section 6.2. The photoionization microscope was put into practice by Helm and coworkers in 1993 [139–141].) Now, the main essence of a microscope obviously consists in the ability to deduce some physical properties of the examined object from its magnified "image." Below, we shall show that for the photodetachment process in a uniform field environment, such a simple connection requires a quite restrictive assumption regarding the source structure. Hence, the notion of a "photodetachment microscope" is a somewhat dubious concept.

Whether or not the emission characteristics of a pointlike source can be extracted from the current density distribution generated by it depends on a single property

of the source, viz. symmetry of the angular emission structure with respect to mirror reflections $z \to -z$ (6.9):

$$|A(\pi - \theta, \phi)|^2 \; = \; |A(\theta, \phi)|^2 \tag{6.20}$$

We have already seen in Section 6.2 that this condition means that in the asymptotic regime $z \to \infty$, the two interfering classical paths $(+)$, $(-)$ connecting the source with some destination on the screen will carry equal weight, allowing to disentangle the angular characteristics of the source $|A(\theta, \phi)|^2$ from the superimposed circular interference pattern in the semiclassical current distribution $j_z^{(\mathrm{sc})}(R, \phi; E)$ (6.10). In this case, we may read off the initial energy of the electrons E from the radius of the current spot $R_{\mathrm{cl}}(E)$ (6.1). (Alternatively, E may be extracted from the number of interference rings, i. e., the maximum phase difference $\sigma_+(0, 0; E) - \sigma_-(0, 0; E)$ (6.6), (6.7) accumulated for emission (anti-)parallel to the direction of force $\mathbf{F}$ (6.14), provided that the atomic phase function $\gamma(\theta, \phi)$ is known.) The angular emission characteristics $|A(\theta, \phi)|^2$ is available from the envelope of the current distribution $j_z(\mathbf{r}, \mathbf{o}; E)$ on the screen after correcting for classical projection effects which are summarized in the differential cross section $\partial\sigma_{\mathrm{cl}}/\partial\Omega(R; E)$ (6.4). Finally, the structure of the interference ring pattern depends on the relative phase of the classical trajectories $(+)$ and $(-)$ (6.6), (6.7); hence, the phase $\gamma(\theta, \phi)$ of the atomic wave function is implicitly encoded in the circular pattern. Thus, the current image contains comprehensive information on the source wave function.

Pure (l, m) multipole sources $\delta_{lm}(\mathbf{r})$ (2.23) may serve as especially simple and important examples for sources $A(\theta, \phi)$ exhibiting the mirror reflection symmetry (6.20). We studied them thoroughly in Sections 6.1 and 6.2 where we found that the interference pattern is determined by the parity properties of $Y_{lm}(\theta, \phi)$ (6.13), (6.14) whereas the angular emission characteristics $|Y_{lm}(\theta, \phi)|^2$ reveals itself through the presence of radial and circular node lines (Figure 5). It is instructive to examine a more intricate example of a symmetric source, the current image generated by a $l = 3$ longitudinal source ($m = 0$) rotated by $\pi/2$ around the y axis. The corresponding emission characteristics is indicated in the top-left image of Figure 15, the predicted current pattern $j_z^{(\mathrm{as})}(\mathbf{r}, \mathbf{o}; E)$ (5.91) is plotted below. (To facilitate comparison with Figures 5, 12 and 13, we again used the set of parameters which characterized the pioneering experiment by Blondel et al. [4]: $E = 6.08 \cdot 10^{-5}$ eV, $F = 116\,\mathrm{V/m}$ and $z = 0.514\,\mathrm{m}$. However, this does not imply that the source characteristics employed in this section are directly accessible in a photodetachment experiment.)

Now, let us interpret the structures prevalent in this current image. The most striking features are three parallel node lines ($x = \text{const.}$). According to (6.2), these lines are projections of trajectories with common velocity component $v_x = \text{const.}$, that, in turn, are emitted under equal angles with the x axis. Hence, the source shows two

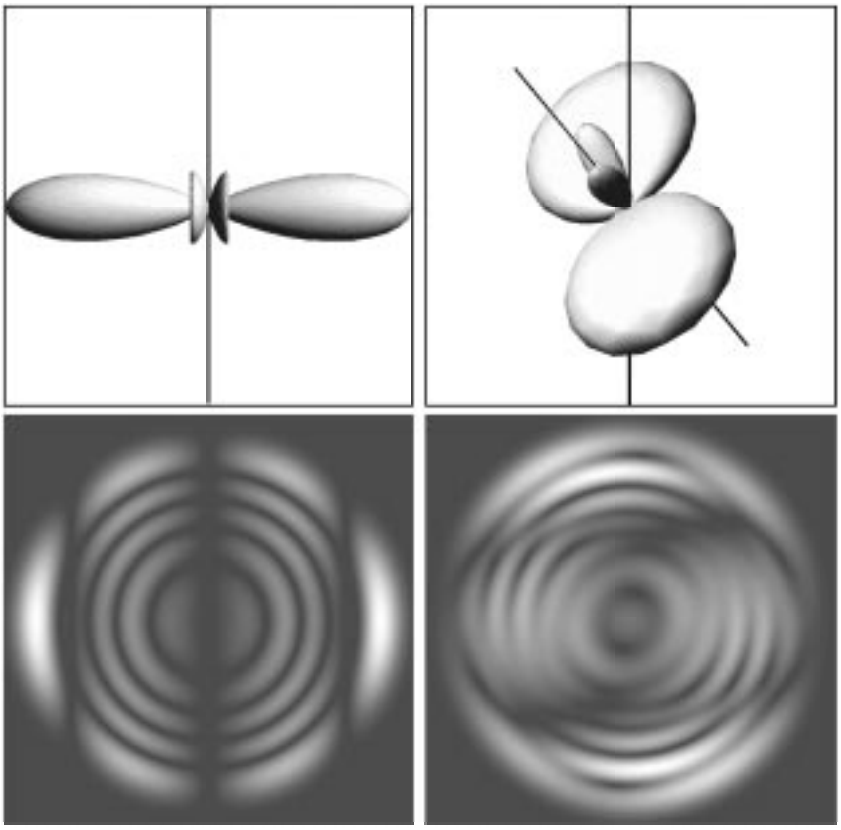

Figure 15: Emission from tilted multipole sources. Left column: $l = 3$, $m = 0$ longitudinal multipole source $\delta_{30}(\mathbf{r})$, rotated by $\pi/2$ around the y axis. Top image: Emission characteristics (projected against the x–z plane), below: Corresponding asymptotic current density distribution. Right column: Same for orbital multipole source $\delta_{31}(\mathbf{r}) + \delta_{3,-1}(\mathbf{r})$ ($l = 3$, $|m| = 1$), rotated by Euler angles $\Phi_E = \Theta_E = \Psi_E = \pi/4$. Parameters used: $E = 6.08 \cdot 10^{-5}$ eV, $F = 116\,\mathrm{V/m}$, $z = 0.514\,\mathrm{m}$. (See also Figure 5.)

node cones centered around the x axis; additionally, the y–z plane is a node plane. Furthermore, the interference pattern present in this current image is identical to that shown in Figure 5 for sources with even $l - |m|$. Therefore, $A(\theta, \phi)$ has even parity, and $\gamma(\pi - \theta, \phi) = \gamma(\theta, \phi)$ holds (6.13). (Note that the untilted source $\delta_{30}(\mathbf{r})$ possesses odd parity!) From the two bright lobes at the fringe of the current spot we may infer that emission mainly takes place in a narrow beam or "jet" along the x axis. Also, the symmetry of the emission pattern with respect to reflections $x \to -x$ and $y \to -y$ obviously follows from the corresponding properties of the current image. Gathering all this information, we are able to reconstruct a fairly accurate model of the source $A(\theta, \phi)$ from the current pattern generated by it.

In order to demonstrate that the feasibility of current image interpretation crucially

depends on the behavior of the source under mirror reflections $z \to -z$, we now study a tilted multipole source which lacks the symmetry property (6.20). For this purpose, we consider a $l = 3$, $m = \pm 1$ real orbital source $\delta_{31}(\mathbf{r}) + \delta_{3,-1}(\mathbf{r})$ (see Figure 5) which has been rotated in space by equal Euler angles [142] $\Phi_E = \Theta_E = \Psi_E = \pi/4$. The resulting emission characteristics is depicted in the top-right image of Figure 15. Using the same set of parameters as above, this tilted source generates the current density distribution plotted in the bottom right corner of this figure. Although this current image still is adequately described by the semiclassical formula (6.8), source structure and interference pattern now appear hopelessly jumbled. Distinct node curves are no longer discernible; in certain regions, the interference pattern seems to "switch" between different parities. Obviously, it would be very difficult to extract information about the source characteristics from such a current image.

With these remarks, we conclude our discussion of quantum ballistic motion in a homogeneous force field for energies $E > 0$ and turn our attention to the "tunneling" case $E < 0$. Then, interpretation in terms of classical motion is clearly impossible, yet another simple picture emerges which will be developed in the following chapter.

Chapter 7

Properties of Ballistic Tunneling

IN CONTINUATION OF OUR EFFORTS to provide physical insight into the mathematical results of the quantum source theory of ballistic motion which were presented in Chapter 5, we now examine the properties of uniformly accelerated motion in the case of tunneling sources, i. e., we are going to study the dynamics of particles whose initial kinetic energy is negative. In practice, this means that we again consider the current distributions $j_{lmm'}(\mathbf{r}, \mathbf{o}; E)$ (5.42) and total currents $J_{lm}(E)$ (5.48) generated by pointlike multipole sources for $E < 0$, since these quantities are most easily amenable to experimental verification. Hence, our investigation is organized much along the lines of the preceding chapter: We start out with a semiclassical description of ballistic tunneling that is derived from the results of our study of classical ballistic motion (Chapter 4). However, unlike in the case of classically allowed motion (Section 6.2), for tunneling sources this procedure is not easily visualized, and generalization to more complex potential environments appears difficult. Therefore, we abandon the semiclassical approach in favor of an explanation based upon a truly quantum mechanical feature, the Heisenberg uncertainty relation for position and momentum. In Section 7.2, we will put forward the minimum uncertainty model for multidimensional tunneling and elucidate its connection to the tunneling time problem, a topic that has been subject of controversial theoretical debates in recent years. Approximations for the current densities $j_{lmm}(\mathbf{r}, \mathbf{o}; E)$ and total currents $J_{lm}(E)$ in ballistic tunneling [$U(\mathbf{r}) = -Fz$] obtained in the framework of the minimum uncertainty model are discussed in the following section. There, we will compare these results not only with the source theoretical predictions stated in Chapter 5, but also shall analyze the findings of other authors on the subject in the light of the source model of ballistic motion. Unfortunately, material on ballistic tunneling is quite scarcely found in the literature; nevertheless, we may draw upon experimental data recorded in field emission from ultrasharp tips [68–71, 143–145], but likewise utilize purely numerical work concerning field emission [146–150] for comparison. To conclude this introduction, we note that the developments presented in this chapter are based upon two recent articles by the author [9, 67].

7.1 Semiclassical Ballistic Waves

Let us first attempt to develop a semiclassical model of the ballistic tunneling process. Naturally, such an asymptotic description is achieved in the framework of the WKB approximation in its multidimensional variant. This technique which is covered in depth in Schulman's monograph [110] is generally fairly cumbersome to apply, yet is feasible for the simple uniform field environment [9]. The result of the WKB calculation which corresponds to the case of dynamically forbidden motion (Section 4.2) may be interpreted as a quantum wave which is simultaneously propagating and evanescent. It may be observed in nature in the form of a narrowly confined current distribution with nearly Gaussian profile which we shall denote a "current filament." Such filaments were generated experimentally by field emission from mesoscopic tips [144]; their characteristics qualitatively match the theoretical prediction.

7.1.1 WKB Approximation to the Green Function

In the semiclassical description of quantum mechanics, for conservative problems the retarded propagator $K_F(\mathbf{r},\mathbf{r}';T)$ (2.8) is related to the action functional $S_{\rm cl}(\mathbf{r},\mathbf{r}';T)$ (4.5) of classical mechanics. Both quantities may be connected in an elegant manner by the path integral formulation of quantum mechanics [110] which founds upon classical trajectories:

$$K_F(\mathbf{r},\mathbf{r}';T) \;=\; \Theta(T) \int_{(\mathbf{r},0)}^{(\mathbf{r}';T)} \mathcal{D}\,\mathbf{x}(t)\, \exp\left\{\frac{i}{\hbar}\int_0^T dt\, L\left[\mathbf{x}(t),\dot{\mathbf{x}}(t)\right]\right\} \tag{7.1}$$

(For the origin of the Heaviside step function, see Appendix A.2.) The path integral comprises all possible paths $\mathbf{x}(t)$ which lead from $\mathbf{r}=\mathbf{x}(0)$ to $\mathbf{r}'=\mathbf{x}(T)$. Since $L(\mathbf{x},\dot{\mathbf{x}}) = T(\dot{\mathbf{x}})-U(\mathbf{x})$ (4.3) denotes the time-independent Lagrangian of the problem, the paths in the integral (7.1) are weighed by a phase factor depending on their assigned classical action.

For the WKB approximation, the path integral (7.1) is evaluated by the method of stationary phase (which is discussed in some detail in Appendix D.1). In view of (4.2), only the actual classical path(s) $\mathbf{r}_{\rm cl}(t)$ that lead to a stationary action functional $S_{\rm cl}(\mathbf{r},\mathbf{r}';T)$ and their "neighbouring" trajectories will contribute. In the ballistic problem, only a single classical path $\mathbf{r}_{\rm cl}(t)$ (4.4) exists. In this simple case, the WKB propagator reads:

$$K_{\rm sc}(\mathbf{r},\mathbf{r}';T) \;=\; \Theta(T)\,\left(\det\left[\frac{i}{2\pi\hbar}\,\frac{\partial^2 S_{\rm cl}(\mathbf{r},\mathbf{r}';T)}{\partial\mathbf{r}\,\partial\mathbf{r}'}\right]\right)^{1/2} \exp\left\{\frac{i}{\hbar}\,S_{\rm cl}(\mathbf{r},\mathbf{r}';T)\right\} \tag{7.2}$$

The prefactor, known as the Van Vleck determinant [100], takes care of the density of classical trajectories leading from $(\mathbf{r},0)$ to $(\mathbf{r}',T)$. Inserting the ballistic action functional (4.5), we obtain from (7.2) for the linear potential $U(\mathbf{r}) = -Fz$:

$$K_{\rm sc}(\mathbf{r},\mathbf{r}';T) \;=\; \Theta(T)\,\left(\frac{M}{2\pi i\hbar T}\right)^{3/2}\,\exp\left[\frac{i}{\hbar}\left(\frac{M}{2T}\,|\mathbf{r}-\mathbf{r}'|^2+\frac{FT}{2}\,(z+z')-\frac{F^2T^3}{24M}\right)\right] \tag{7.3}$$

This result is identical to the exact quantum propagator $K_F(\mathbf{r},\mathbf{r}';T)$ (5.9) that we formerly determined in Section 5.1.

Our principal interest, however, is directed to the energy Green function $G(\mathbf{r},\mathbf{r}';E)$ (5.10) rather than the quantum propagator $K_F(\mathbf{r},\mathbf{r}';T)$ of the ballistic problem. According to (2.13), these quantities are interrelated through a Laplace transform:

$$G(\mathbf{r},\mathbf{r}';E) \;=\; -\frac{i}{\hbar}\int_0^\infty dT\,e^{iET/\hbar}\,K_F(\mathbf{r},\mathbf{r}';T) \tag{7.4}$$

In Section 5.2, we used this formula in order to obtain an analytic expression for $G(\mathbf{r},\mathbf{r}';E)$ (5.18). Yet, to calculate the semiclassical approximation $G_{\rm sc}(\mathbf{r},\mathbf{r}';E)$ to the energy Green function it suffices to replace the propagator in (7.4) by its WKB counterpart $K_{\rm sc}(\mathbf{r},\mathbf{r}';E)$ and evaluate the integral again using the technique of steepest descents [127]. Then, the emerging result will present the leading asymptotic form of $G(\mathbf{r},\mathbf{r}';E)$ for large values in the exponent of the integrand in (7.4).

Introducing the WKB propagator $K_{\rm sc}(\mathbf{r},\mathbf{r}';T)$ (7.2) into (7.4), we have to identify the stationary points of the expression $ET + S_{\rm cl}(\mathbf{r},\mathbf{r}';T)$ which obviously occur for $E = -\partial S_{\rm cl}(\mathbf{r},\mathbf{r}';T)/\partial T$. According to (4.9), this condition implies that T presents a stationary value of the exponent in (7.4) whenever a classical trajectory $\mathbf{r}_{\rm cl}(t)$ (4.4) with time of flight T and particle energy E connects $\mathbf{r}$ and $\mathbf{r}'$. Not surprisingly, the phase factor of the corresponding contribution to (7.4) depends on the reduced action $W_{\rm cl}(\mathbf{r},\mathbf{r}';E)$ (4.8) for that path, which in the stationary case takes over the role of the time-dependent classical action in (7.2).

In ballistic motion, always two stationary values $T_\pm(\mathbf{r},\mathbf{r}';E)$ (which may be degenerate) are present. We already stated them in (4.12) and identified these times of flight with the direct and reflected paths in Figure 3. Naturally, to these classical trajectories, we assign a pair of reduced action functionals $W_{\rm cl}^\pm(\mathbf{r},\mathbf{r}';E)$ (4.14). However, this straightforward interpretation which we incidentally exploited in the previous chapter (Section 6.2) holds only good in the case of classically allowed motion. Nevertheless, formally a pair of complex trajectories still persists in ballistic tunneling (Section 4.2), in which case the motion is characterized by nonreal times of flight $T_\pm(\mathbf{r},\mathbf{r}';E)$ (4.12). Here, we are particularly interested in the dynamics far from the source which corresponds to dynamically forbidden motion in the sense of Section 4.2.

In this case, the times of flight $T_\pm(\mathbf{r},\mathbf{r}';E)$ form a conjugate complex pair (4.17). Likewise, the corresponding reduced action functionals $W_{\rm cl}^\pm(\mathbf{r},\mathbf{r}';E)$ (4.14) are conjugate complex. It is intuitively clear that only a single one of these conjugate "paths" will be relevant to the stationary phase evaluation of the integral (7.4): Obviously, it belongs to the choice of $T_\pm(\mathbf{r},\mathbf{r}';E)$ for which $\Im[W_{\rm cl}^\pm(\mathbf{r},\mathbf{r}';E)]$ is positive, for $G_{\rm sc}(\mathbf{r},\mathbf{r}';E)$ must be exponentially suppressed in tunneling.

To obtain the WKB approximation of (7.4), we first expand the exponent in the vicinity of the stationary points $T_\pm(\mathbf{r},\mathbf{r}';E)$:

$$ET + S_{\rm cl}(\mathbf{r},\mathbf{r}';T) \;\sim\; W_{\rm cl}^\pm(\mathbf{r},\mathbf{r}';E) + \frac{1}{2}\left.\frac{\partial^2 S_{\rm cl}(\mathbf{r},\mathbf{r}';T)}{\partial T^2}\right|_{T=T_\pm(\mathbf{r},\mathbf{r}';E)} [T - T_\pm(\mathbf{r},\mathbf{r}';E)]^2 \tag{7.5}$$

In order to determine the coefficient of the quadratic correction term, we employ the relation (4.9) and evaluate the result for the ballistic problem (4.12):

$$\left.\frac{\partial^2 S_{\rm cl}(\mathbf{r},\mathbf{r}';T)}{\partial T^2}\right|_{T=T_\pm(\mathbf{r},\mathbf{r}';E)} = \left[-\frac{\partial T_\pm(\mathbf{r},\mathbf{r}';E)}{\partial E}\right]^{-1} = \mp\frac{F}{\sqrt{M}}\,\frac{\epsilon_+\epsilon_-}{\epsilon_+ \pm \epsilon_-} \tag{7.6}$$

Here, the abbreviations $\epsilon_\pm^2 = 2E + F(z+z') \pm F|\mathbf{r}-\mathbf{r}'|$ (4.11) were used together with the obvious differentiation formula $\partial\epsilon_\pm/\partial E = 1/\epsilon_\pm$. For the action functional $W_{\rm cl}^\pm(\mathbf{r},\mathbf{r}';E)$ itself, we cite (4.14):

$$W_{\rm cl}^\pm(\mathbf{r},\mathbf{r}';E) \;=\; \frac{\sqrt{M}}{3F}\,\left(\epsilon_+^3 \pm \epsilon_-^3\right) \tag{7.7}$$

We finally have to fix the sign of the purely imaginary parameter ϵ_-; we choose $\Im[\epsilon_-] < 0$. Then, according to (7.7), $T_+(\mathbf{r},\mathbf{r}';E)$ presents the relevant stationary point in the evaluation of the integral (7.4).

Putting all pieces together (7.2)–(7.7), we find for the semiclassical approximation of $G(\mathbf{r},\mathbf{r}';E)$ in the case of dynamically forbidden motion:

$$\begin{aligned} G_{\rm sc}(\mathbf{r},\mathbf{r}';E) = &-\frac{i}{\hbar}\left(\frac{M}{2\pi i\hbar T_+(\mathbf{r},\mathbf{r}';E)}\right)^{3/2} \exp\left\{\frac{i}{\hbar}\,W_{\rm cl}^+(\mathbf{r},\mathbf{r}';E)\right\} \;\times \\ &\int d\tau\,\exp\left(-\frac{iF}{2\hbar\sqrt{M}}\,\frac{\epsilon_+\epsilon_-}{\epsilon_+ + \epsilon_-}\,\tau^2\right) \\ = &\;\frac{iMF}{2\pi\hbar^2}\,\frac{1}{\epsilon_+ + \epsilon_-}\,\frac{1}{\sqrt{\epsilon_+\epsilon_-}}\,\exp\left\{\frac{i\sqrt{M}}{3\hbar F}\,\left(\epsilon_+^3 + \epsilon_-^3\right)\right\} \end{aligned} \tag{7.8}$$

Replacing the Airy functions $\mathrm{Ai}(u)$, $\mathrm{Ci}(u)$ in the exact expression for the Green function $G(\mathbf{r},\mathbf{r}';E)$ (5.18) by their principal asymptotic forms (D.10), (D.16) which are determined in Appendix D.1, it is straightforward to show that for large arguments $\beta\epsilon_+^2 \gg 1$

and $\beta\epsilon_-^2 \ll -1$ (where $\beta^3 = M/4\hbar^2F^2$ (5.16) again denotes the inverse energy parameter of Chapter 5), the semiclassical Green function $G_{\rm sc}(\mathbf{r},\mathbf{r}';E)$ (7.8) indeed presents the leading-order approximation to the quantum mechanical Green function $G(\mathbf{r},\mathbf{r}';E)$.

7.1.2 Interpretation of the WKB Solution

Having constructed the semiclassical Green function $G_{\rm sc}(\mathbf{r},\mathbf{r}';E)$ (7.8) for ballistic tunneling problems in the far-field limit, we now provide a physical interpretation for this result. Introducing, we note that although the rather involved prefactor accompanying this exponential expression has the important duty to preserve the probability current as the Green function spreads into space, we nevertheless may conclude that all major features of $G_{\rm sc}(\mathbf{r},\mathbf{r}';E)$ are included in the exponential factor in (7.8). Thus, neglecting bookkeeping issues, we may restrict our considerations to this part of the formula. Again, it is a good idea to place the source into the origin ($\mathbf{r}' = \mathbf{o}$); then, the Green function is naturally displayed in terms of the orthogonal system of parabolic coordinates $\xi = r + z$, $\eta = r - z$ [81,114]:

$$G_{\rm sc}(\mathbf{r},\mathbf{o};E) \;\propto\; \exp\left\{-\frac{\sqrt{M}}{3\hbar F}\,[F(r-z)-2E]^{3/2}\right\}\exp\left\{\frac{i\sqrt{M}}{3\hbar F}\,[F(r+z)+2E]^{3/2}\right\} \tag{7.9}$$

Except in the vicinity of the turning surface $r + z = -2E/F$ (4.20) separating the domains of energetically and dynamically forbidden tunneling motion (Section 4.2), the formula (7.9) presents an excellent approximation to the exact quantum mechanical Green function $G(\mathbf{r},\mathbf{o};E)$ (5.18).

The expression (7.9) is conveniently interpreted in wave optical terms: $G_{\rm sc}(\mathbf{r},\mathbf{o};E)$ approximately factorizes into a product of a modulus factor solely depending on the coordinate $\eta = r - z$ with a phase factor which is a function of the orthogonal coordinate $\xi = r + z$ only. Thus, $G_{\rm sc}(\mathbf{r},\mathbf{o};E)$ represents an outgoing wave in the ξ direction where the surfaces of constant phase (wave fronts) are approximately given by the set of confocal paraboloids $\xi = r + z =$ const. In the same fashion, the exponential suppression of $G_{\rm sc}(\mathbf{r},\mathbf{o};E)$ with increasing values of the coordinate η may be visualized as the decay of an evanescent wave leaking into the η direction. which is characterized by surfaces of constant amplitude $\eta = r - z =$ const. This orthogonal set of confocal paraboloids is available from the set of wave fronts by reflection $z \to -z$. Hence, $G_{\rm sc}(\mathbf{r},\mathbf{o};E)$ simultaneously represents a propagating and an evanescent wave in the orthogonal ξ and η directions, respectively. The situation is depicted in Figure 16.

From (7.9), we may infer that the Green function in ballistic tunneling, and thus also the current distribution generated by the source, is strongly confined to the vicinity of the escape path in direction of field which is given by $\eta = 0$. This means that

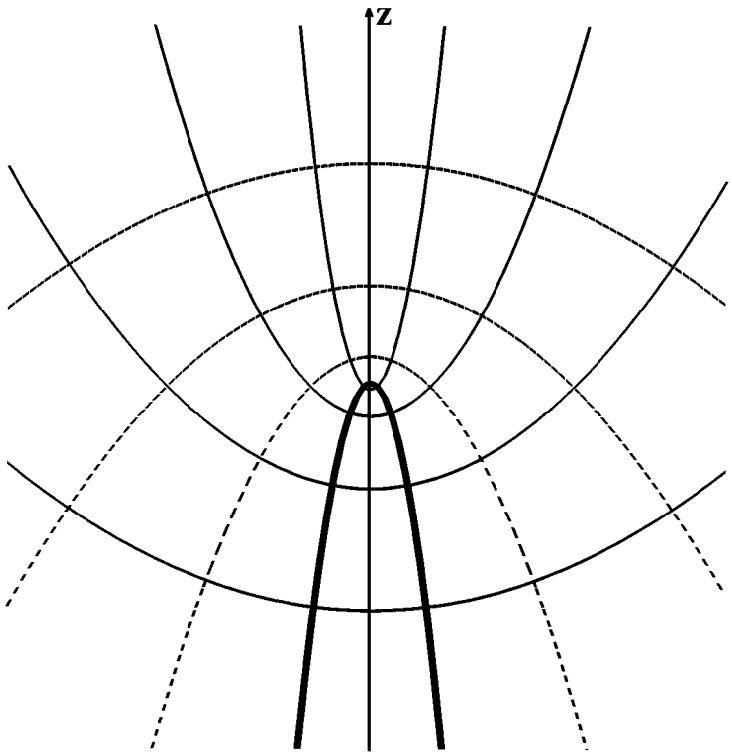

Figure 16: Interpretation of ballistic tunneling in terms of wave optics. Particles leave the source at $\mathbf{r}' = \mathbf{o}$ and travel in direction of field $\mathbf{F} = F\hat{e}_z$. The confocal set of paraboloids $\xi = r + z =$const. approximately represents wave fronts (surfaces of equal phase) of the propagating wave (dotted lines), whereas the orthogonal set of paraboloids $\eta = r - z =$const. (solid lines) denotes surfaces of constant particle density, i. e., is associated to an evanescent wave. The turning surface $r + z = -2E/F$ (4.20) separates the sectors of energetically and dynamically forbidden motion (bold line). See Section 4.2 for details.

it often suffices to consider merely the neighborhood of the positive z axis where we may approximate the particle distribution by a simple Gaussian profile. To see this, we first estimate the parabolic coordinate η for small radial distances $R = (r^2 - z^2)^{1/2}$ and obtain $R^2 = \xi\eta \approx 2\eta z$. Replacing η by $R^2/2z$ and further expanding the exponent in (7.9), it is easy to demonstrate that the particle density profile for small lateral distances R is indeed Gaussian. Denoting the Green function by $\psi(z, R; E) = G(\mathbf{r}, \mathbf{o}; E)$, we find approximately:

$$|\psi(z, R; E)|^2 \;\approx\; |\psi(z, 0; E)|^2 \, \exp\left\{-\frac{\kappa R^2}{2z}\right\} \tag{7.10}$$

Here, the inverse length scale κ is given by $\kappa^2 = -2ME/\hbar^2$. The same functional dependence holds for the current density distribution $j_z(z, R; E)$. We note that for large

lateral distances with $R/r \sim 1$, the Gaussian model tends to underestimate $|G(\mathbf{r}, \mathbf{o}; E)|^2$ as a comparison with (7.9) reveals. Naturally, this deviation is most distinct in the vicinity of the turning surface $\xi = -2E/F$ (4.20) which clearly represents the three-dimensional generalization of the "end of the tunnel" which for one-dimensional tunneling in a linear potential $U(z) = -Fz$ is located at $z = -E/F$. See also Section 4.2.

So far, our semiclassical approach to ballistic tunneling concerned only approximations to the Green function $G(\mathbf{r}, \mathbf{o}; E)$ itself. In this treatise, however, we gave special consideration to the problem of spatially oriented multipole sources $\delta_{lm}(\mathbf{r})$ (2.23) generating multipole Green functions $G_{lm}(\mathbf{r}, \mathbf{o}; E)$ (2.25). On grounds of analycity, these eigenstates of the angular momentum operator L_z must be proportional to $(x \pm iy)^{|m|} = R^{|m|} e^{im\phi}$ as is confirmed by the closed-form expression (5.28) for these functions. In view of (7.10), we hence may conjecture that the lateral multipole current profile $j_{lmm}(\mathbf{r}, \mathbf{o}; E)$ (Section 5.4) approximately takes on a universal shape that depends only on the quantum number m, but not l:

$$J^{(\mathrm{sc})}_{lmm}(\mathbf{r}, \mathbf{o}; E) \;\sim\; C_{lm}(z; E)\, R^{2|m|} \exp\left\{ -\frac{\kappa R^2}{2z} \right\} \tag{7.11}$$

At this point, a discussion of the prefactor $C_{lm}(z; E)$ which obviously adjusts the total current emitted by the multipole source must be deferred to subsequent sections. In order to assess the quality of this simple approximation, we performed a sample calculation using typical parameters for field emission phenomena ($E = -4\,\mathrm{eV}$, $F = 1\,\mathrm{eV/\AA}$). Profiles of the current distribution in a distance $z = 1\mu\mathrm{m}$ from the source for various multipole sources are displayed in Figure 17. It is seen that (7.11) provides a rough estimate for the actual current profile. However, a much better approximation may be gained if one keeps the Gaussian functional dependence, yet relaxes the restriction on the width of the Gaussian in (7.11). Least square fits to the tunneling current distribution are shown in Figure 17 from which we may conclude that the width of the distributions increases with the multipole order l. The minimum uncertainty model (Section 7.2) provides an explanation for this behavior.

Returning to the WKB result (7.11), we infer the surprising fact that the width of the current filament surrounding the escape path is essentially independent of the field strength F. Rather, the lateral spread of the particle density (7.10) which is approximately given by the average square radius $\langle R^2_{\mathrm{sq}} \rangle = 2z/\kappa$ apart from the source-detector distance z depends solely on the binding energy E of the source. We finally remark that the spatial extension of the current may also be stated in terms of the position uncertainty in (7.10):

$$\Delta x(z) \;=\; \Delta y(z) \;\approx\; \sqrt{z/\kappa} \tag{7.12}$$

We will utilize this result in a moment.

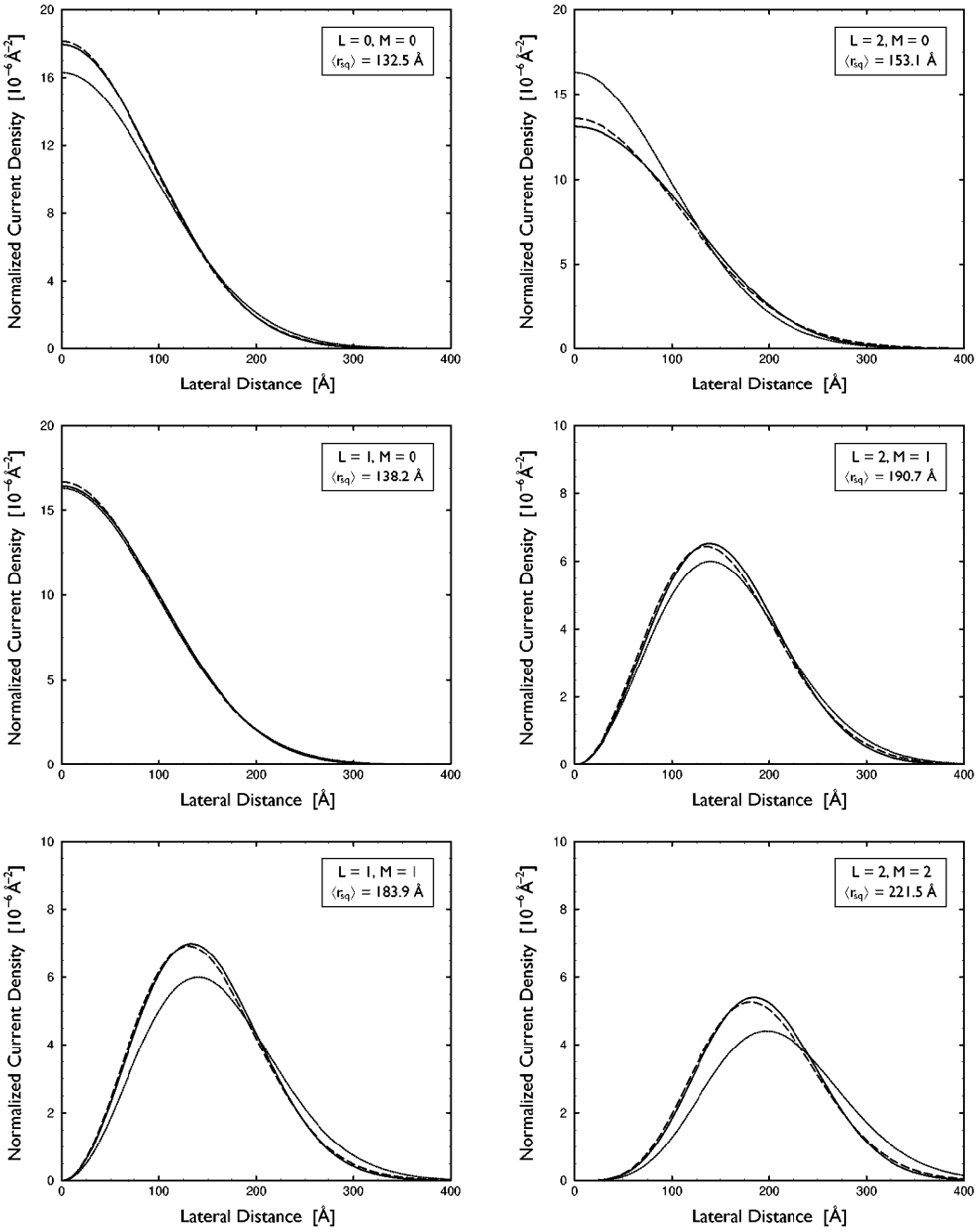

Figure 17: Theoretical predictions for the current distribution $j_{lmm}(\mathbf{r}, \mathbf{o}; E)$ in ballistic tunneling. The caption displays current profiles generated by various multipole sources ($0 \leq m \leq l \leq 2$) which are normalized to a unit total current $J_{lm}(E) = 1$. The recording distance was $z = 1\mu$m, source parameters used are $E = -4\,$eV and $F = 1\,$eV/Å. Solid lines: Exact quantum result (5.42). Dashed lines: Least square Gaussian fit; the average square width $\langle R_{\rm sq} \rangle$ of the distribution is shown in the inset. Dotted lines: WKB approximation (7.11).

7.1.3 A Wave Packet Approach

Even though the quantum source formalism is a successful and appropriate technique for the description of ballistic motion (Section 5), it bears little resemblance to the conventional scattering approaches to this class of problems. Let us therefore examine how quantum source theory reconciles with the supposedly most popular customary model of ballistic dynamics, the evolution of wave packets in a linear potential $U(\mathbf{r}) = -Fz$ governed by the time-dependent Schrödinger equation.

It should appear obvious that among the enormous variety of possible wave packets, only a very restricted subset may be used to model ballistic tunneling motion in a uniform force field. Let us see how quantum mechanics enforces the Gaussian shape (7.10) of the lateral particle distribution in the wave packet $\psi(\mathbf{r}, t)$:

Any packet $\psi(\mathbf{r}, t)$ is essentially fixed by the momenta of its probability distribution in configuration and momentum space at some instant of time, say $t = 0$. The evolution of these averages is governed by Heisenberg's relation $-i\hbar\partial_t \langle A\rangle = \langle [H; A]\rangle$. In particular, this formula comprises Ehrenfest's theorems [83] $d\langle \mathbf{r}\rangle / dt = \langle \mathbf{p}\rangle / M$ and $d\langle \mathbf{p}\rangle / dt = \langle \mathbf{F}\rangle$. For a uniform force field, these relations may be immediately integrated to obtain:

$$\begin{aligned} \langle \mathbf{r}\rangle (t) &= \langle \mathbf{r}\rangle_0 + \frac{1}{M} \langle \mathbf{p}\rangle_0 t + \frac{\mathbf{F}}{2M} t^2 \\ \langle \mathbf{p}\rangle (t) &= \langle \mathbf{p}\rangle_0 + \mathbf{F}t \end{aligned} \tag{7.13}$$

The point source $\delta(\mathbf{r})$ emits electrons in a symmetric fashion. This implies that the lateral components of $\langle \mathbf{r}\rangle (t)$ and $\langle \mathbf{p}\rangle (t)$ vanish. Additionally, we may identify the origin of time $t = 0$ with the instant of turning of the wave packet. (This notion means that $\langle z\rangle (t)$ takes on its lowest position $\langle z\rangle_0$ at $t = 0$.) Obviously, then $\langle \mathbf{p}\rangle_0 = \mathbf{o}$ holds, and for a nearly monochromatic wave packet, $\langle z\rangle_0$ should be roughly given by the classical turning point of motion $\langle z\rangle_0 \approx -E/F$. From (7.13), we then find free-falling motion of the wave packet as anticipated:

$$\langle z\rangle (t) = -\frac{E}{F} + \frac{F}{2M} t^2 \tag{7.14}$$

Here, we note that the centroid of the wave packet formally reaches the origin in an imaginary time interval $\tau_B(E) = i\hbar\kappa/F$. We will encounter this particular time scale again in Section 7.2.

For the simple linear potential environment, Heisenberg's relation permits to obtain also successively higher momenta of the position and momentum distributions in an analytic fashion [151]. In particular, the uncertainties in position and momentum

$\Delta x(t)$, $\Delta p(t)$ are available in this manner. A rather cumbersome calculation yields:

$$\begin{aligned} \Delta x(t)^2 &= \frac{(\Delta p_0)^2}{M^2}\, t^2 + \frac{1}{M}\left\{\langle xp + px\rangle_0 - 2\,\langle x\rangle_0\,\langle p\rangle_0\right\} t + (\Delta x_0)^2 \\ \Delta p(t)^2 &= (\Delta p_0)^2 \end{aligned} \tag{7.15}$$

The relations (7.15) hold for any direction in space and are independent of the actual field strength F. Here, we are interested in the lateral coordinate x. Note that Δp is a constant of motion; this behavior already follows from the fact that in a free-falling frame of reference, no external force acts on the particles (Section 4.3.3). See equations (4.30) and (5.3). We also shall insist on an evolution of the wave packet which is symmetric in time; this implies that the linear term in (7.15) should be absent, so $\langle xp + px\rangle_0 = 0$ must hold. Clearly, the uncertainty product $\Delta x(t)\Delta p(t)$ will then acquire its minimum value for $t = 0$.

Using (7.14), we may now eliminate the time parameter t in the lateral uncertainty formula (7.15) in favor of the average position coordinate $z = \langle z\rangle\,(t)$. One immediately obtains:

$$\Delta x(z)^2 = \frac{2}{MF}\,(\Delta p_0)^2\left[z + \frac{E}{F}\right] + (\Delta x_0)^2 \tag{7.16}$$

Both initial uncertainties Δx_0, Δp_0 are available from this formula if we replace the left-hand side of (7.16) by its semiclassical value $\Delta x(z)^2 = z/\kappa$ (7.12). By comparison of coefficients, it is seen that the validity of (7.16) then simultaneously requires:

$$\Delta x_0 = \Delta x\left(\langle z\rangle_0\right) = \sqrt{\frac{\hbar^2\kappa}{2MF}} \quad , \qquad \Delta p_0 = \sqrt{\frac{MF}{2\kappa}} \tag{7.17}$$

Thus, relation (7.12) fixes the initial parameters of the wave packet model of ballistic tunneling. A remarkable property of these averages is revealed through their uncertainty product:

$$\Delta x_0 \Delta p_0 = \hbar/2 \tag{7.18}$$

The uncertainty product of the lateral particle distribution of the wave packet at the turning point takes on the Heisenberg minimal value $\hbar/2$. This automatically implies that the distribution itself is necessarily of Gaussian shape [83]. (See also Section 7.2.) It is known that in a linear potential environment, the Gaussian character of a wave packet is conserved during its evolution [121]. By this peculiarity, the Gaussian nature (7.10) of the emission profile of a ballistic tunneling source is confirmed. (A rather crude version of this reasoning has been put forward in Ref. [152].)

Hence, we may conclude that the wave packet analysis of the ballistic tunneling source problem leads to results compatible to the findings of the WKB analysis, provided the proper values (7.17) for the initial wave packet parameters Δx_0, Δp_0 are chosen. These values are not implicit to the wave packet approach but must be borrowed from the source analysis (7.12). A detailed theory of the Green function $G(\mathbf{r}, \mathbf{o}; E)$ in the vicinity of the turning point of classical motion will be presented in Section 7.2.

7.1.4 Comparison to Experimental Data

Like in the case of classically allowed uniformly accelerated quantum motion, the theoretical derivations regarding the properties of ballistic tunneling presented in the previous sections should be complemented by experimental findings on the subject. Unfortunately, however, no direct counterpart to the deliberate photodetachment experiments by Blondel et al. [4,63,64] presented in Section 6.4 exists; for the tunneling sector, we have to content ourselves with data that represent by-products of applied research in electron microscopy. Measurements specifically directed to the current generated by field emission sources in a uniform field are virtually unavailable. Nevertheless, quantum source theory is able to explain the features revealed in field emission experiments in a manner better than just qualitative.

The series of experiments which we will discuss here utilizes electron emission from "ultrasharp tips." This term was coined by H.-W. Fink [68] for a pyramidal cluster of few W atoms located on top of a plane tungsten (111) surface which may be manipulated in a reproducible way by field evaporation and vapour deposition. A remarkable feature of this setup is already noted in the pioneering publication: Unlike "conventional" field emission tips, the cluster tip shows a strongly aligned emission characteristic with a beam opening of only several degrees. Instead of further examining the electron beam properties, however, subsequent publications on the subject mainly dealt with the attempt of building an electron microscope using these tips as sources, where particular attention was devoted to the development of electron holography [69–71, 143]. Apparently, these experiments have shown lack of success, and in the meantime, interest in nanoscopic cluster-type electron sources seems to have ceased altogether. Here, we will refer to the study of these tips performed by Horch and Morin in 1993 [144] which presents the most detailed investigation into the emission properties of these sources available.

From the source-theoretical point of view, the deposited cluster may be interpreted as a point source of electrons embedded in a fairly homogeneous field background provided by the W–(111) surface. Since tungsten is a typical transition metal, we may expect that electrons are extracted from the tip largely in the d–state ($l = 2$). For reasons which become clear in Section 7.2.3, only the $m = 0$ contribution needs to be considered. The energy of the electrons is determined by the work force of the tip

substrate which amounts to some $\Phi \approx 4.5\,\mathrm{eV}$. (This energy is not sharply defined as electrons populating states below the Fermi level may also leave the tip by tunneling, though at a suppressed rate; Morin and Fink [145] find a typical width of the electronic energy distribution of order $\Delta E \sim 0.25\,\mathrm{eV}$.) The actual field F obviously depends on the voltage applied to the substrate. Using the transport model (which will be presented in detail in Section 8.2) in order to adjust the strength of the pointlike d–source, the asymptotic formula (5.58) for the multipole current taken over from Section 5.5.3 delivers the following prediction regarding the total current I drawn from the tip:

$$I \sim \frac{10\,e}{\pi\hbar}\left(\frac{\kappa}{k_F}\right)^5\left(\frac{\beta F}{\kappa}\right)^3 \exp\left\{-\frac{1}{6}\left(\frac{\kappa}{\beta F}\right)^3\right\}\cdot\Delta E \tag{7.19}$$

Here, κ denotes the evanescent wave number of the emitted electrons roughly given by $\kappa \sim 1\,\mathrm{Å}^{-1}$, $k_F \sim 1.5\,\mathrm{Å}^{-1}$ is the Fermi wave number of the tungsten substrate, and we used the parameter $\beta^3 = M/4\hbar^2F^2$, as usual. The expression (7.19) may be conveniently employed to relate the field strength F to the total current I emitted by the tip. Assuming a tip-surface distance of $2\,\mathrm{Å}$, an applied field of $F = 0.25\,\mathrm{eV/Å}$ according to (7.19) draws a tunneling current of order $I \sim 2\cdot 10^{-16}\,\mathrm{A}$ which roughly corresponds to the detection threshold in [144]. Doubling the applied voltage ($F = 0.5\,\mathrm{eV/Å}$) pushes the current to $I \sim 6\cdot 10^{-11}\,\mathrm{A}$, and threefold voltage ($F = 0.75\,\mathrm{eV/Å}$) further increases I to $I \sim 5\cdot 10^{-9}\,\mathrm{A}$. (In the actual measurement, field focusing near the tip leads to an even stronger amplification of the current almost into the conduction regime ($I \sim 3\cdot 10^{-6}\,\mathrm{A}$, see also Section 8.2.3), where tip damage sets in.)

In the Horch and Morin experiment [144], little care has been taken to achieve a homogeneous field distribution. Rather, electrons emitted from the tip are accelerated towards a hollow counterelectrode and afterwards travel freely towards a detecting screen. Nevertheless, the threshold field strength $F \sim 0.25\,\mathrm{eV/Å}$ identified above together with the known minimal potential difference ($350\,\mathrm{V}$) applied in experiment allow to identify an effective extension of the field of $z_{\mathrm{eff}} = U/F \sim 1400\,\mathrm{Å}$.

What features have been observed in this experiment? Clearly, the electron distribution in the current filament is of prime interest. According to simple WKB reasoning [see formula (7.11)], the current profile should be approximately Gaussian, with a mean square width $R_{\mathrm{sq}}^2 = 2z/\kappa$ independent of F. In their article, Horch and Morin indeed reproduce an image of the current cross section which appears as a circular spot without internal structure; unfortunately, they fail to present a lateral profile of the current filament which would come in handy in verifying the Gaussian structure of the distribution. They did, however, study the aperture of the electron beam as a function of the applied potential (Figure 18). In this caption, the opening angle (the definition of which unfortunately is not disclosed) is displayed in dependence of the "reduced field strength" F^*, a fictive field which is adapted from the Fowler-Nordheim theory of

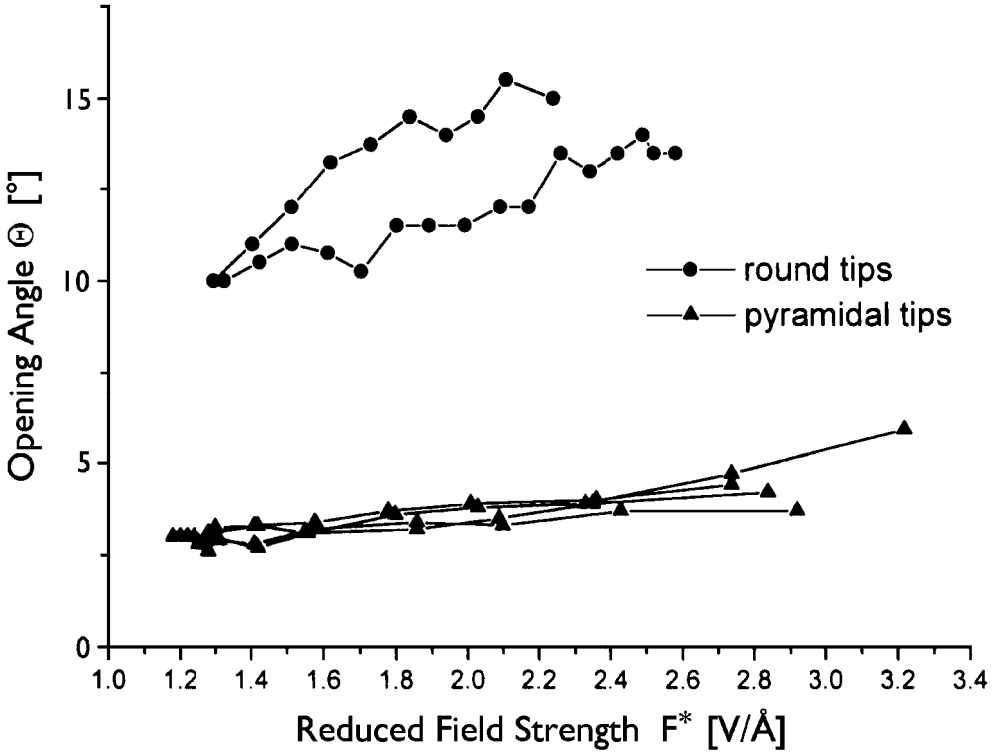

Figure 18: Opening angle Θ of the electron distribution generated from mesoscopic field emission tip sources. "Pyramidal" tips terminate in $1-3$ W atoms; they are subjected to potentials in the range $350\,\mathrm{V}$ to $950\,\mathrm{V}$. The abcissa shows fictitious field strengths F^* obtained from a Fowler-Nordheim fit; realistic values of F are smaller by a factor of about 5. (After Horch and Morin [144].)

spherical field emission [153]. Since this procedure is known to overestimate the actual field strength F by a factor of roughly five [153], the Fowler-Nordheim method (where emission onset is observed for $F^* \sim 1.2\,\mathrm{V/\AA}$) delivers field values in good agreement to our estimate derived from (7.19). It is seen that doubling of the applied voltage (which increases the tunneling current by a factor of some 10^6) causes only a slight widening of the electron beam which remains tightly compressed in a narrow tube of $3^\circ - 4^\circ$ aperture. This is in satisfactory accord with the conclusion from the semiclassical model (7.11) which predicts the emission of a current filament with Gaussian profile whose opening angle Θ is invariably given by $\Theta = R_{\mathrm{sq}}/z_{\mathrm{eff}} = \sqrt{2/\kappa z_{\mathrm{eff}}} \sim 2.2^\circ$.

7.2 The Minimum Uncertainty Model

Following our presentation of the WKB theory of ballistic tunneling, we will now set out and devise a fairly different-minded model for multidimensional tunneling phenomena which is conveniently applied also to related processes. As it is mainly

based on the Heisenberg uncertainty relation connecting position and momentum averages, we will denote it the minimum uncertainty model for tunneling problems in several dimensions. (Our wave packet description of ballistic tunneling sources already hinted at the importance of wave functions with minimum lateral uncertainty $\Delta x \cdot \Delta p$ in the uniform field setup. See Section 7.1.3.) As a quasiclassical element in our novel approach to multidimensional tunneling phenomena, the tunneling time $\tau(E)$ (4.21) enters the minimum uncertainty formalism. In fact, the dependence of the tunneling current on the potential landscape $U(\mathbf{r})$ in our model is essentially limited to the corresponding time scale $\tau_B(E)$ which we briefly introduced already in Section 4.2. Hence, let us first discuss the meaning of the tunneling time concept in the framework of tunneling in several dimensions [9,67].

7.2.1 Multidimensional Tunneling as a Quantum Clock

In Section 7.1.2, we have studied how in several dimensions the tunneling current is generally drawn along the direction of the acting force $\mathbf{F}$, but spreads out also somewhat in the orthogonal dimensions, giving rise to the formation of a "current filament" of approximately Gaussian profile (7.11). We may interpret this feature as the result of the superposition of two essentially independent dynamical patterns: Classical motion in the linear potential $U(\mathbf{r}) = -Fz$ is separable in Cartesian coordinates, so the accelerated motion in direction of $\mathbf{F}$ does not influence the transversal degrees of freedom where the particle cloud spreads freely. This property renders multidimensional tunneling phenomena attractive in a controversial field of fundamental quantum mechanics, the so-called tunneling time problem. (For recent reviews on this topic, we refer to [154–157].) Indeed, the seemingly definite and innocuous question regarding the time spent by a quantum particle traversing a sector of classically forbidden motion not only has a long-standing history; despite numerous efforts in particular during the 1980s, no unanimously accepted solution to the problem emerged, but various answers which are not necessarily compatible with each other prevail in parallel. Recently, new interest in the topic was stirred by optical experiments which were interpreted in terms of superluminal propagation of photons through evanescent "tunneling gaps" [158,159]. In the view of the author who actively partook in the search for the tunneling time [151,160–162], no unifying "clock principle" exists in the quantum realm, but every physical process which might be utilized for the determination of a traversal time carries its own proprietary set of time scales of quantum motion. Obviously, this assessment implies that the quest for a definite tunneling time is a futile exercise. On the other hand, identification of the characteristic time scales underlying some specific setup nevertheless may be an effort well worth spending.

Obviously, these deliberations throw up the question how tunneling phenomena in several dimensions give access to the tunneling time scale involved in the process.

This time interval may be read off in a very simple scheme which classifies the method among a group of related approaches known as quantum clocks [161,163–165]. Their common basic idea consists in using the evolution of an independent quantum degree of freedom in tracking particle motion through the tunneling barrier. This technique (whose interpretation turns out to be far more intricate then the humble idea might initially suggest) was originally devised with the precession of particle spin in an external magnetic field in mind, a thought experiment that is widely cited as the Larmor clock model [163–165], yet it equally works with other degrees of freedom [161]. Naturally, in multidimensional tunneling the lateral spread Δx_0 of the particle distribution near the turning point may serve as a measure for the tunneling time $\tau(E)$, provided the average transversal momentum variance Δp_0 of the particle beam is known. Then, the barrier penetration time $\tau(E)$ may be simply read off from Δx_0 via the relation $\tau(E) = M\Delta x_0/\Delta p_0$ as the particles move uniformly in directions perpendicular to $\mathbf{F}$. This is the basic idea behind the "tunneling clock."

Hence, our next task is to provide some simple model for Δp_0. In principle, the lateral momentum distribution for uniformly accelerated motion is available in closed form and may be easily determined from the multipole momentum-space Green functions $G_{lm}(\mathbf{k}_\perp, z; E)$ (5.70). For the derivation, we refer to Section 5.6. However, to illustrate the connection to the tunneling time problem, it is far more instructive to use a classical scheme based upon the developments of Chapter 4. There, we wrote down the Hamilton-Jacobi equation of ballistic motion (4.7). Separating off transversal motion in the classical action $S_{\rm cl}(\mathbf{r}, \mathbf{o}; T)$ [cf. (4.8)]:

$$W_{\rm cl}(\mathbf{p}_\perp, z; E) \;=\; S_{\rm cl}(\mathbf{r}, \mathbf{o}; T) - \mathbf{r}_\perp \cdot \mathbf{p}_\perp + ET \tag{7.20}$$

one obtains an effectively one-dimensional problem:

$$\frac{1}{2M}\left[\frac{\partial}{\partial z} W_{\rm cl}(\mathbf{p}_\perp, z; E)\right]^2 \;=\; E - \frac{p_\perp^2}{2M} + Fz \tag{7.21}$$

which is immediately integrated:

$$\begin{aligned} W_{\rm cl}^{\pm}(\mathbf{p}_\perp, z; E) &= \int_0^z d\zeta \sqrt{2M(E - p_\perp^2/2M + F\zeta)} \\ &= \pm\frac{i}{3MF}\left(2M|E| + p_\perp^2\right)^{3/2} + \frac{2\sqrt{2M}}{3F}\left(Fz + E - \frac{p_\perp^2}{2M}\right)^{3/2} \end{aligned} \tag{7.22}$$

Here, tunneling has been assumed ($E < 0$), and z should be located in the sector of dynamically forbidden tunneling (see Section 4.2), so that the right-hand side in (7.21) is positive. Like in Section 7.1.2, formula (7.9), we then may approximate the momentum-space Green function $G(\mathbf{k}_\perp, z; E)$ by a semiclassical expression which is

correct merely to exponential order ($\mathbf{p}_\perp = \hbar\mathbf{k}_\perp$):

$$G_{\rm sc}(\mathbf{k}_\perp, z; E) \sim \exp\left\{\frac{i}{\hbar} W_{\rm cl}^+(\mathbf{p}_\perp, z; E)\right\} \sim \exp\left\{-\frac{1}{3\hbar MF}\left(2M|E| + p_\perp^2\right)^{3/2}\right\} \times \exp\left\{\frac{i}{3\hbar MF}\left(2MFz + 2ME - p_\perp^2\right)^{3/2}\right\} \quad (7.23)$$

Here, the proper (decaying) solution $W_{\rm cl}^+(\mathbf{p}_\perp, z; E)$ in (7.22) has been utilized. Introducing the inverse energy parameter $\beta^3 = M/4\hbar^2F^2$ into (7.23), it is easy to show that $G_{\rm sc}(\mathbf{k}_\perp, z; E)$ indeed reproduces the asymptotic form of the exact Green function. For this purpose, the Airy functions appearing in the analytic solution (E.18) should be replaced by their estimates for large arguments (D.10), (D.16) which are derived in Appendix D.1.

Our interest is directed towards the probability distribution for the transverse momentum $\mathbf{p}_\perp$. From (7.23), we immediately may infer that this function to exponential order is given by:

$$|G_{\rm sc}(\mathbf{k}_\perp, z; E)|^2 \sim \exp\left\{-\frac{2}{\hbar}\left|W_{\rm cl}^+[\mathbf{p}_\perp, z(p_\perp); E]\right|\right\} \sim \exp\left\{-\frac{2}{3\hbar MF}\left(2M|E| + p_\perp^2\right)^{3/2}\right\} \quad (7.24)$$

Here, $z(p_\perp) = -(E - p_\perp^2/2M)/F$ denotes the classical turning point of motion. As expected, outside the "tunnel" the momentum distribution (7.24) does not depend on the actual position z where it is evaluated. Clearly, this is a consequence of the separability of the problem: Motion in the directions orthogonal to $\mathbf{F}$ is free, and the lateral momentum $\mathbf{p}_\perp$ thus conserved. We also note that this transverse momentum is connected to an "orthogonal kinetic energy" $p_\perp^2/2M$ which is not available for the accelerated motion in direction of force. Therefore, the dynamics along the z axis takes place with an effective kinetic energy $E(p_\perp) = E - p_\perp^2/2M$, or, stated otherwise, the tunneling barrier is raised by $p_\perp^2/2M$. The role of $E(p_\perp)$ is evident in (7.21)–(7.24).

From (7.24), we may conclude that tunneling trajectories with large lateral momenta $\mathbf{p}_\perp$ are exponentially suppressed, so only small values of $p_\perp$ are relevant in the distribution. For these, an expansion of the exponent in (7.24) into a Taylor series with respect to $p_\perp$ is in order. This leads to a Gaussian approximation for the momentum distribution (see also Section 7.1.3). Recalling the dependence of (7.24) on the effective kinetic energy $E(p_\perp)$, we may perform this expansion in terms of the classical sojourn time $T(E)$ between the origin and the turning point $z(0) = z(p_\perp = 0) = -E/F$:

$$W_{\rm cl}^+[\mathbf{p}_\perp, z(p_\perp); E] \sim W_{\rm cl}^+[0, z(0); E] - \frac{p_\perp^2}{2M}\left.\frac{\partial W_{\rm cl}^+[\mathbf{p}_\perp, z(p_\perp); E]}{\partial E}\right|_{\mathbf{p}_\perp = \mathbf{o}} \quad (7.25)$$

The leading order term $W_{\rm cl}^{+}[0,z(0);E]$ obviously is given by the classical reduced action for the corresponding one-dimensional tunneling motion along the escape path. Furthermore, according to (7.20), the derivative in (7.25) simply denotes the time of flight $T(E)$ which is here purely imaginary. For an explicit representation, we may make use of (7.22):

$$T(E) \;=\; -i \int_0^{-E/F} \frac{\sqrt{M}\; d\zeta}{\sqrt{2(|E| - F\zeta)}} \;=\; -i\, \frac{\hbar\kappa}{F} \tag{7.26}$$

(Again, $\kappa = \sqrt{2M|E|}\,/\hbar$ is the binding momentum of the source.) We already encountered this type of expression in Section 4.2, where we denoted its absolute value $\tau_B(E)$ as the bounce or instanton time scale of the problem (4.21). Formally, it represents the time required for a classical particle of energy $-E$ to traverse the interval $0 < \zeta < z(0)$ in the inverted potential $-U(\zeta) = F\zeta$.

Hence, the momentum distribution is approximately given by the Gaussian form:

$$|G_{\rm sc}(\mathbf{k}_\perp, z; E)|^2 \;\sim\; |G_{\rm sc}(\mathbf{o}, z; E)|^2 \;\exp\left\{ - \frac{\tau_B(E) p_\perp^2}{\hbar M} \right\} \tag{7.27}$$

From (7.27), we may read off the momentum spread Δp_0 in a given lateral direction. Together with (7.26), one quickly obtains:

$$\Delta p_0 \;=\; \sqrt{\frac{\hbar M}{2\,\tau_B(E)}} \;=\; \sqrt{\frac{MF}{2\kappa}} \tag{7.28}$$

As it must be, this result coincides with the width of the Gaussian distribution Δp_0 (7.17) we found by means of the wave packet method (Section 7.1.3).

The same semiclassical time scale $\tau(E)$ governs the reading of the multidimensional tunneling quantum clock. To see this formally, we utilize again (7.20) and (7.22):

$$\mathbf{r}_\perp \;=\; -\,\frac{\partial W_{\rm cl}(\mathbf{p}_\perp, z; E)}{\partial \mathbf{p}_\perp} \;=\; \frac{\mathbf{p}_\perp}{M}\, \frac{\partial W_{\rm cl}(\mathbf{p}_\perp, z; E)}{\partial E} \tag{7.29}$$

For motion close to the escape path, the right-hand side derivative again may be replaced by the time of flight $T(E)$. Note that as already explained in Section 4.2, classical tunneling trajectories involve complex momenta and times of flight. If one, however, is willing to discard this complication, one may replace $T(E)$ in (7.29) by its absolute value $\tau_B(E)$ at the turning point $z(0) = -E/F$. Then, the tunneling time $\tau(E)$ as measured by the multidimensional tunneling quantum clock equals the semiclassical bounce time:

$$\tau(E) \;=\; \frac{M r_\perp}{p_\perp} \;=\; \tau_B(E) \tag{7.30}$$

(Within alternative models for the quantum clock, formally fairly different quantum time scales of motion $\tau(E)$ may arise [161,165].) The same relation (7.30) should manifestly hold also for the ratio of the lateral position and momentum spreads Δx_0, Δp_0 at the end of the tunnel $z(0) = -E/F$. Thus, (7.26), (7.28), and (7.30) together predict that the width of the current filament Δx_0 at $z(0)$ is given by:

$$\Delta x_0 \;=\; \frac{\Delta p_0 \, \tau_B(E)}{M} \;=\; \sqrt{\frac{\hbar \, \tau_B(E)}{2M}} \;=\; \sqrt{\frac{\hbar^2 \kappa}{2MF}} \tag{7.31}$$

This result again agrees with the findings (7.17) obtained by the wave packet method. Therefore, the tunneling time approach is compatible with the approximation techniques presented in the first section of this chapter.

We point out that the minimum uncertainty property of the particle distribution near the turning point $z(0)$ which we first noticed in Section 7.1.3 appears very prominently within the tunneling time model. From (7.28) and (7.31), we immediately obtain:

$$\Delta x_0 \Delta p_0 \;=\; \sqrt{\frac{\hbar \, \tau_B(E)}{2M}} \cdot \sqrt{\frac{\hbar M}{2 \, \tau_B(E)}} \;=\; \frac{\hbar}{2} \tag{7.32}$$

Obviously, this fact alone would suffice to enforce the Gaussian character of the lateral position and momentum distributions which we explicitly determined in (7.10) and (7.27). The main advantage of the tunneling time model, as compared to the approaches of Section 7.1, is that we had to make very little reference to the actual structure of the potential (the uniform field environment, $U(\mathbf{r}) = -Fz$), but rather used general properties of semiclassical motion for the description of the tunneling process, in particular the bounce time $\tau_B(E)$ (7.26). In the following section, we use these favorable properties of the tunneling time approach in order to propose a simple yet powerful model for tunneling phenomena in several dimensions which is not limited to linear potentials.

7.2.2 Setting Up the Minimum Uncertainty Model

We now collect our previously gained experience with the ballistic tunneling problem into a simple set of rules describing multidimensional tunneling phenomena, the minimum uncertainty model. The basic idea behind this novel approach is the property of the tunneling wave function to approximately saturate the Heisenberg uncertainty relation (7.32) in the vicinity of the turning point of classical motion for any direction perpendicular to $\mathbf{F}$. In our former attempts at a description of tunneling in several dimensions, this property followed from the fact that the lateral position and momentum distributions show approximately Gaussian character, a peculiarity which

we deduced in Section 7.1.2 and the previous section. Let us now simply turn the argument around and present a heuristic justification of the minimum uncertainty property: Tunneling is disfavored for classical paths which deviate from the most probable trajectory, the escape path [101], because for these paths the imaginary part of the Hamilton characteristic function $W_{\mathrm{cl}}(\mathbf{r}, \mathbf{o}; E)$ is increased. (After all, the escape path is a trajectory of least action.) Since the tunneling probability in the WKB estimate decays like $\exp\{-2\,\Im[W_{\mathrm{cl}}(\mathbf{r}, \mathbf{o}; E)]/\hbar\}$ (7.5), paths which lead to a shifted lateral position $\mathbf{r}_\perp$ are exponentially suppressed. In the same way, transverse momentum components $\mathbf{p}_\perp$ occupy a part $p_\perp^2/2M$ of the available particle energy E and thus effectively raise the tunneling barrier by this "orthogonal kinetic energy" (Section 7.2.1), which again results in an exponential suppression of paths with nonvanishing perpendicular momentum. Clearly, both mechanisms tend to compress the lateral position and momentum distributions near the "end of the tunnel." However, position and momentum are complementary observables in quantum mechanics and may not be fixed simultaneously [83]. Therefore, the particle current is forced into a compromise and suppresses less favorable phase space configurations as far as quantum mechanics permits this. To put this statement into quantitative terms, we introduce the lateral uncertainties $\Delta R^2 = \langle x^2 + y^2 \rangle$ and $\Delta p^2 = \langle p_x^2 + p_y^2 \rangle$; then, the minimum uncertainty model postulates that

$$\Delta R \cdot \Delta p \stackrel{!}{=} \min . \tag{7.33}$$

near the classical turning point $z(0)$. (In the following, $R = |\mathbf{r}_\perp|$ denotes the lateral distance.) Note that we chose to avoid any specification of the meaning of "min" at this point; this allows to accommodate multipole sources (angular momentum eigenstates) into the model.

For isotropic sources $\delta(\mathbf{r})$ in a cylindrically symmetric potential environment $U(\mathbf{r})$, the current clearly will be distributed symmetrically with respect to the escape path. In this simple case, we have $\Delta R = \sqrt{2} \cdot \Delta x_0$ and $\Delta p = \sqrt{2} \cdot \Delta p_0$, where Δx_0 and Δp_0 are the corresponding uncertainties in a given lateral direction. Since Heisenberg's uncertainty relation states that $\Delta x_0 \Delta p_0 \geq \hbar/2$, the minimum uncertainty model requires that (7.33):

$$\Delta R \cdot \Delta p = \hbar \tag{7.34}$$

The minimum uncertainty property also largely determines the particle distribution in configuration and momentum space. The lateral profile of the current wave function in both representations is necessarily Gaussian:

$$\psi(R) \propto e^{-\lambda^2 R^2/2} , \qquad \tilde{\psi}(p) \propto e^{-p^2/2\hbar^2\lambda^2} \tag{7.35}$$

Here, λ^2 presents a positive real parameter. A proof of this assertion is given in virtually any textbook on quantum mechanics; see e. g. [83, 114]. We note that the corresponding uncertainties:

$$\Delta R \,=\, 1/\lambda \,, \qquad \Delta p \,=\, \hbar\lambda \tag{7.36}$$

are not fixed through the condition (7.34). Rather, there exists a trade-off between the widths ΔR and Δp: The width of the current filament ΔR may be "squeezed," but such an operation will result in an increased variance Δp of the lateral momentum distribution.

The reasoning of the previous paragraph may be conveniently extended to the multipole sources $\delta_{lm}(\mathbf{r})$ introduced in Section 2.4 of this volume. Placed in a potential relief $U(\mathbf{r})$ with cylindrical symmetry, the angular momentum quantum number m assigned to the operator L_z will be preserved in the current filament. In the resulting wave function, the additional centrifugal barrier will suppress tunneling in the vicinity of the escape path. Consequently, we may expect a larger constant than $\hbar$ (7.34) in the minimum uncertainty constraint (7.33). (In passing, we remark that the reduction of tunneling in the neighborhood of the direct path will result in a decrease of the total tunneling current since the tunneling particle is forced into trajectories characterized by larger values of the classical action $W_{\mathrm{cl}}(\mathbf{r}, \mathbf{o}; E)$. We already reached this conclusion in our asymptotic analysis of the total multipole current $J_{lm}(E)$ (5.58) in quantum ballistic motion (Section 5.5.3). A derivation of this formula in the framework of the minimum uncertainty model is presented below.)

Like in the customary one-dimensional problem, a position-momentum uncertainty relation for two-dimensional angular momentum eigenstates may be firmly established using the mathematical apparatus of functional analysis (which we extensively employ in Appendix A of this work). The argument closely resembles the traditional textbook proof of the uncertainty relation in a single dimension, but seems not to be available in the readily accessible literature on general quantum mechanics. Therefore, we provide a detailed demonstration of the following assertions in Appendix C.3. There, it is shown that for a two-dimensional angular momentum eigenstate with quantum number m, i. e., $L_z \,|\Psi\rangle \,=\, m\hbar \,|\Psi\rangle$, the uncertainty product inequality holds:

$$\Delta R \cdot \Delta p \;\geq\; (|m| + 1)\,\hbar \tag{7.37}$$

Again, minimum uncertainty is taken on for a special functional dependence of $\psi(\mathbf{r}_\perp)$ which, like (7.35), involves a Gaussian distribution. In polar coordinates (R, ϕ), the

wave functions of minimal uncertainty read:

$$\psi(R,\phi) \;=\; \alpha\lambda\,(\lambda R)^{|m|}\,\exp\left\{-\,\frac{\lambda^2 R^2}{2}\;+im\phi\right\} \tag{7.38}$$

Not surprisingly, the minimum uncertainty wave function adopts the same functional form in momentum space, as a simple Fourier transform of (7.38) reveals:

$$\tilde{\psi}(p,\phi) \;=\; \frac{\alpha}{\hbar\lambda}\,\left(\frac{p}{i\hbar\lambda}\right)^{|m|}\,\exp\left\{-\,\frac{p^2}{2\hbar^2\lambda^2}\;+im\phi\right\} \tag{7.39}$$

Here, α is a normalization coefficient, and λ denotes a positive real inverse length parameter which determines the average widths of the position and momentum distributions:

$$\Delta R \;=\; \frac{\sqrt{|m|+1}}{\lambda}\,, \qquad \Delta p \;=\; \sqrt{|m|+1}\,\cdot\hbar\lambda \tag{7.40}$$

Evidently, as a special case, these formulae comprise the results for isotropic sources (7.34)–(7.36) which arise for $m = 0$.

As we shall see later on, the minimum uncertainty constraint (7.33) is rather strictly observed in ballistic tunneling. At the classical turning point $z(0) = -E/F$, the uncertainty product $\Delta R \cdot \Delta p$ of the actual transversal particle distribution exceeds the theoretical minimum (7.37) only by a few percent. Correspondingly, the lateral curent profile may be fitted well in terms of the generalized Gaussian functions (7.38). For different multipole sources $\delta_{lm}(\mathbf{r})$, however, the optimum choice for the width parameter λ in (7.38) varies slightly. Let us finally also note that the approximate shape of the current profile (7.11) which we justified by a WKB argument is manifestly closely related to our deduction for the wave function (7.38) obtained in the framework of the minimum uncertainty model.

We have seen that the minimum uncertainty model is able to fix the wave function emitted by a tunneling multipole source, apart from a normalization constant α, in the vicinity of the classical turning point of motion up to a single parameter λ which has the dimension of an inverse length. If we are willing to confine ourselves to a semiclassical description of the tunneling current near the "end of the tunnel," we may use the results of the tunneling time approach in Section 7.2.1 in order to express the parameter λ in terms of the tunneling time $\tau(E)$ required to traverse the distance from the source to the tunnel exit along the escape path. We have seen that the relevant quantum time scale of motion is given by the bounce time $\tau_B(E)$ (7.26). By comparison with the position and momentum uncertainties Δx_0, Δp_0 (7.28), (7.31) obtained in the

tunneling time model, we find as a semiclassical estimate for the parameter λ (7.36):

$$\lambda_{\mathrm{sc}}(E) \;=\; \sqrt{\frac{M}{\hbar\,\tau_B(E)}} \tag{7.41}$$

Application of the semiclassical reasoning bears the obvious advantage that all ambiguity in the structure of the tunneling wave function (7.38) is removed; only the absolute strength of the tunneling current, expressed through the overall proportionality constant α, remains unspecified. However, the relation (7.41) is less rigourously observed in nature than the minimum uncertainty constraint (7.33): We already noted that different multipole sources in identical potential environments will lead to consistently varying values of λ in a fit of the actual tunneling wave functions to the minimum uncertainty prediction (7.38). Thus, the semiclassical supplement (7.41) to the minimum uncertainty model delivers less reliable results than the application of numerical values for the parameter λ. It should be viewed as a very simple and convenient first approximation to the tunneling process. Finally, it is instructive to note that the minimum uncertainty model in its semiclassical extension (7.41) is implicitly contained in the vastly more complicated semiclassical approaches to tunneling in several dimensions put forward by Van Horn and Salpeter [102] as well as Banks et al. [103, 104], even though the respective authors apparently have not been aware of this fact. It arises naturally from the theories presented in these papers whenever particle motion in the spatial directions perpendicular to the orientation of the force field is free.

7.2.3 Semiclassical Theory of Multipole Currents

In the previous section, we presented the minimum uncertainty model as a simple approximate theory for multidimensional tunneling processes. Within this model, we were able to show that the wave function emitted by a multipole source conforms to a generalized Gaussian structure (7.38). Together with the semiclassical extension (7.41), the particle current is fixed up to a constant of proportionality α. The objective of this section is to interrelate these constants within a multiplet of multipole sources $\delta_{lm}(\mathbf{r})$ where m may take on any integer value between $-l$ and $+l$. We will calculate the multipole current density distributions $j^{(\mathrm{sc})}_{lmm}(\mathbf{r},\mathbf{o};E)$ at the classical turning point of motion by means of a projection scheme closely related to the procedure applied in Section 6.2 for the case of classically allowed ballistic motion. By integration, also a semiclassical estimate for the total multipole current $J^{(\mathrm{sc})}_{lm}(E)$ is available.

We start out with a description of particle emission from the multipole source. We formerly argued that particle propagation along paths which lead to large elongations $\mathbf{r}_\perp$ is strongly suppressed by their large action functionals $W_{\mathrm{cl}}(\mathbf{r},\mathbf{o};E)$; only trajectories

close to the escape path are relevant in the description of tunneling phenomena. Thus, it suffices to consider the source characteristics in the vicinity of the symmetry axis where centrifugal forces become dominant. For a quantitative description, we use the representation of the spherical harmonic $Y_{lm}(\hat{r})$ in cylindrical coordinates (B.1), but keep only the leading-order term in the radial coordinate ρ:

$$Y_{lm}(\hat{r}) \;\sim\; U_{|m|lm}\,(\rho/\zeta)^{|m|}\,e^{im\phi} \tag{7.42}$$

where the expansion coefficient $U_{|m|lm}$ (B.2) is given by:

$$U_{|m|lm} \;=\; \frac{i^{m+|m|}}{2^{|m|}\,|m|!}\,\sqrt{\frac{(2l+1)\,(l+|m|)!}{4\pi\,(l-|m|)!}} \tag{7.43}$$

The axis coordinate is designated by ζ. (See also Appendix B.1.)

In the next step, we eliminate the local variables ρ and ζ in (7.42) in favor of the "macroscopic" quantities R and z (which here denotes the "end of the tunnel," i. e., $z = z(0)$ is implied). This aim may be achieved once more by virtue of the separability of lateral motion (7.30). Using the semiclassical tunneling time $\tau_B(E)$ (7.26), free propagation in directions orthogonal to z leads to the relation:

$$\mathbf{r}_\perp = \mathbf{p}_\perp \cdot \tau_B(E)/M \tag{7.44}$$

This enables us to establish a correspondence between R and the polar angle of emission Θ: We note that the particle starts from the source with a formally imaginary momentum $p_\parallel = \hbar\kappa$ in the direction of force, where κ denotes the evanescent wave number: $E = -\hbar^2\kappa^2/2M$. (For simplicity, we assume here that $U(\mathbf{o}) = 0$.) For small angles of emission Θ, we thus find:

$$\Theta \;\approx\; \sin\Theta \;\approx\; \tan\Theta \;=\; \frac{\rho}{\zeta} \;=\; \frac{p_\perp}{p_\parallel} \;=\; \frac{MR}{\hbar\kappa\,\tau_B(E)} \tag{7.45}$$

This allows to replace the expression ρ/ζ by R and $\tau_B(E)$ in (7.42).

The relation (7.45) is also useful for the description of the properties of the projection from the spherical source onto the (R, z) plane. For this purpose, we employ the differential cross section $\partial\sigma_{\rm sc}/\partial\Omega(R, z; E)$ which connects the area illuminated by the particle current to the spherical angle it is emitted from [cf. (6.4)]. According to (7.45), we obtain:

$$\frac{\partial\sigma_{\rm sc}(R, z; E)}{\partial\Omega} \;=\; \frac{R\,dR\,d\phi}{\sin\Theta\,d\Theta\,d\phi} \;=\; \left(\frac{\hbar\kappa\,\tau_B(E)}{M}\right)^2 \tag{7.46}$$

Finally, tunneling along any specific trajectory is attenuated, where the transmission amplitude in the WKB picture depends on the classical action $W_{\rm cl}(\mathbf{r},\mathbf{o};E)$ assigned to that path. In view of the Gaussian structure of (7.38), the exponential suppression factor may be separated into a product of an overall WKB prefactor describing one-dimensional tunneling along the escape path, and an additional Gaussian factor responsible for the extra decrease in the tunneling rate for paths with lateral momentum components. Combining (7.25) and (7.44), we expect that the tunneling wave function near the classical turning point $z(0)$ is proportional to:

$$G_{lm}^{(\rm sc)}(\mathbf{r},\mathbf{o};E) \;\propto\; \exp\left\{-\frac{1}{\hbar}\;|W_{\rm cl}(0,z(0);E)|\right\}\;\exp\left\{-\frac{MR^2}{2\hbar\,\tau_B(E)}\right\} \tag{7.47}$$

In order to construct our semiclassical approximation to the current density distribution, we now superpose the source characteristics (7.42), the projection term (7.46) and the attenuation factor (7.47) much in the style of Section 6.2. This procedure yields:

$$\begin{aligned} j_{lmm}^{(\rm sc)}(\mathbf{r},\mathbf{o};E) \;&=\; J_l(E)\,\frac{\partial\Omega(R,z;E)}{\partial\sigma_{\rm sc}}\;\left|U_{|m|lm}\right|^2\;\left(\frac{\rho}{\zeta}\right)^{2|m|}\;\exp\left\{-\frac{MR^2}{\hbar\,\tau_B(E)}\right\}\;\times \\ &\qquad\qquad \exp\left\{-\frac{2}{\hbar}\;|W_{\rm cl}(0,z(0);E)|\right\} \\ &=\; J_l(E)\;\;\frac{(2l+1)\,(l+|m|)!}{\pi\,(|m|!)^2(l-|m|)!}\;\left(\frac{M}{2\hbar\kappa\,\tau_B(E)}\right)^{2|m|+2}\;\times \\ &\qquad\qquad \exp\left\{-\frac{2}{\hbar}\;|W_{\rm cl}(0,z(0);E)|\right\}\;R^{2|m|}\;\exp\left\{-\frac{MR^2}{\hbar\,\tau_B(E)}\right\} \end{aligned} \tag{7.48}$$

Here, $J_l(E)$ is a prefactor with the dimension of a current which should not depend on R, $z(0)$, or m. Like in the formerly considered case of classical motion (Section 6.2), it is not accessible in the minimum uncertainty picture, but must be determined by comparison with the exact quantum solution. (We will do this in a moment.) Let us note at this point that the semiclassical current density $J_{lmm}^{(\rm sc)}(\mathbf{r},\mathbf{o};E)$ (7.48) faithfully reproduces the generalized Gaussian structure (7.38) proposed by the minimum uncertainty model.

In the final step, we may easily determine a semiclassical estimate $J_{lm}^{(\rm sc)}(E)$ for the total multipole current emitted by a source of unit strength $\delta_{lm}(\mathbf{r})$. To this end, it suffices to integrate the current density $j_{lmm}^{(\rm sc)}(\mathbf{r},\mathbf{o};E)$ (7.48) over the entire $\mathbf{r}_\perp$ plane. By means of the Gaussian integral:

$$\int d^2R\,R^{2|m|}\;\exp\left\{-\frac{MR^2}{\hbar\,\tau_B(E)}\right\}\;=\;\pi\,|m|!\;\left(\frac{\hbar\,\tau_B(E)}{M}\right)^{|m|+1} \tag{7.49}$$

we obtain for the total current $J_{lm}^{(\mathrm{sc})}(E)$:

$$J_{lm}^{(\mathrm{sc})}(E) \;=\; J_l(E)\,\frac{(2l+1)\,(l+|m|)!}{|m|!\,(l-|m|)!}\,\left(\frac{\hbar}{8\,|E|\,\tau_B(E)}\right)^{|m|+1}\,\exp\left\{-\frac{2}{\hbar}\,|W_{\mathrm{cl}}(0,z(0);E)|\right\} \tag{7.50}$$

We infer from this result that the multipole current $J_{lm}^{(\mathrm{sc})}(E)$ drops with increasing magnetic quantum number $|m|$. We already anticipated this suppression of higher $|m|$ partial currents from the raised uncertainty product threshold (7.37) of the corresponding wave functions. Unlike the overall WKB attenuation factor, the additional reduction due to centrifugal forces is polynomial in nature; it is characterized by the quantity $\hbar/8|E|\tau_B(E)$.

The only remaining task in the minimum uncertainty model consists in the determination of the current prefactor $J_l(E)$ appearing in (7.48) and (7.50). It may be performed by evaluating $J_{lm}^{(\mathrm{sc})}(E)$ (7.50) for the uniform field environment (we will tackle this problem in the following section), and comparing the result to the known asymptotic limit $J_{lm}^{(\mathrm{as})}(E)$ (5.58) of the ballistic multipole tunneling current determined in Section 5.5.3. A straightforward calculation yields:

$$J_l(E) \;=\; \frac{M}{4\pi^2\hbar^3}\,\kappa^{2l+1} \tag{7.51}$$

Strictly speaking, we may claim validity of this result only for the homogeneous field environment. However, the formula (7.51) does not contain any specifics of the uniform field problem. Rather, apart from the replacement of the wave number k by κ, it mimics the Wigner law (3.27) governing the emission from free multipole sources. These properties strongly suggest the conjecture that the form (7.51) of the current prefactor holds universally valid for unit multipole sources $\delta_{lm}(\mathbf{r})$, independent of the exact choice of potential $U(\mathbf{r})$. With this statement, we conclude our discussion of the minimum uncertainty model of multidimensional tunneling.

7.3 Currents in Ballistic Tunneling

Let us now apply the general theory of multidimensional tunneling which we devised in the course of the previous section to the central topic of this treatise, the emission of mutipole sources embedded in the uniform force field environment $U(\mathbf{r}) = -Fz$. Thus, this section serves to complement our considerations for classically allowed motion which we presented in Sections 6.3 and 6.4. We start out with a discussion of the current density distribution generated by a multipole source in the vicinity of the classical turning surface. There, we will compare the approximation (7.48) obtained in the framework of the minimum uncertainty model with the exact quantum solutions

derived in Section 5.4, the simplest of which have been tabulated in Appendix E.2. A similar analysis is performed for the total multipole currents in ballistic tunneling (Section 5.5). Finally, we will compare our developments with the studies of other authors which are, unfortunately, all numerical in nature [146–150]. Here, our interest will be centered upon the work of Lang et al. [148] who simulate field emission from atomic protrusions in a simple model which is evaluated numerically using the density functional formalism (LDA).

7.3.1 Tunneling Current Density Distributions

First, let us check the performance of the minimum uncertainty model for the analytically solvable case of ballistic tunneling motion. For this purpose, we have to insert the proper expressions for the tunneling time $\tau_B(E) = \hbar\kappa/F$ (7.26) and the imaginary part of the one-dimensional classical reduced action (7.22):

$$W_{\rm cl}(0, z(0); E) \;=\; \int_0^{z(0)} d\zeta\, \sqrt{2M(E + F\zeta)} \;=\; i\,\frac{\hbar^3\kappa^3}{3\,MF} \tag{7.52}$$

where $z(0) = -E/F$ denotes the classical turning point of motion, into the general semiclassical formula (7.48) for the current density distribution. Using the parameter $\beta^3 = M/4\hbar^2F^2$ (5.16), we obtain:

$$j^{(\rm sc)}_{lmm}(\mathbf{r}, \mathbf{o}; E) \;=\; \frac{M}{4\pi^3\hbar^3}\,\kappa^{2l+1}\,\frac{(2l+1)\,(l+|m|)!}{(|m|!)^2\,(l-|m|)!}\,\left(\frac{2\beta^3F^3}{\kappa^2}\right)^{2|m|+2} \;\times \\ \exp\left\{-\frac{1}{6}\,\left(\frac{\kappa}{\beta F}\right)^3\right\}\,R^{2|m|}\,\exp\left\{-\frac{4\,\beta^3F^3R^2}{\kappa}\right\} \tag{7.53}$$

This result may be compared to the exact current density distributions $j_{lmm}(\mathbf{r}, \mathbf{o}; E)$ which are available from the multipole Green functions $G_{lm}(\mathbf{r}, \mathbf{o}; E)$ (5.28) for ballistic motion. These functionals whose explicit expressions become rapidly more complicated with increasing multipole order l are listed for $l = 0$ and $l = 1$ in Appendix E.2. We shall use also another approximation where we keep the generalized Gaussian dependence in (7.53) but allow the width of the Gaussian envelope to vary. This approach is in the spirit of the minimum uncertainty model [see (7.38)], but does not incorporate the semiclassical element (7.41) which manifests itself through the appearance of the tunneling time $\tau_B(E)$ in (7.48). We will see that the relaxation of the width of the current spot leads to a much more accurate approximation to the actual current density profile. On the other hand, unlike (7.48), adjusting the width requires some knowledge of the quantum current distribution which is generally difficult to obtain.

A comparison of the three different approaches is performed in Figure 19. For the sample calculation, we used a set of parameters which may be viewed as typical for

field emission phenomena and scanning tunneling microscopy (STM, see Chapter 8) and furthermore allows to relate the results to our study of the tunneling current profile in the far-field limit (Figure 17 in Section 7.1.2); the values chosen are $E = -4\,\mathrm{eV}$ and $F = 1\,\mathrm{eV/\AA}$. The caption displays the radial current distributions due to several multipole sources ($0 \leq m \leq l \leq 2$), taken at the "end of the tunnel," i. e., at a distance $z = 4\,\mathrm{\AA}$ from the point source. We infer from this figure that the semiclassical estimate $j^{(\mathrm{sc})}_{lmm}(\mathbf{r}, \mathbf{o}; E)$ (7.53) may serve only as a rough guide to the actual current profile. For ballistic motion, the semiclassical width $\Delta R_{\mathrm{sc}} = \sqrt{|m|+1}\,/\lambda_{\mathrm{sc}} = \sqrt{(|m|+1)\hbar^2\kappa/MF}$ (7.40), (7.41) systematically overestimates the width of the exact quantum distributions. (For the selected parameters, one finds $\Delta R_{\mathrm{sc}} = 2.794\,\mathrm{\AA}$ in longitudinal emission with $m = 0$.) A much better fit to the quantum current profile may be achieved within the Gaussian approximation (7.53) if one allows the width parameter to float freely. In this mode, ΔR is adjusted so that the mean square deviation of the exact current distribution from its Gaussian estimate is minimized. This procedure generally leads to fairly close approximations to the actual current distribution. The quality of the estimate declines with increasing $|m|$. This property may be understood by observing that for large $|m|$, the lateral elongation of the current distribution by no means may be considered small in comparison with the source distance z. The minimum uncertainty model, however, is built upon the notion of paraxial trajectories.

For fixed $|m|$, the numerically determined widths ΔR of the Gaussian approximation show a consistent trend towards smaller values with increasing multipole order l. This behavior may be interpreted once we notice that the angular multipole emission characteristics becomes more strongly aligned towards the z axis as l grows. However, by virtue of the minimum uncertainty product requirement (7.33) and (7.37), the decrease in the position variance ΔR will be accompanied by an increase of the momentum width Δp. This quite counterintuitive property will manifest itself in the far-field current distribution for distances from the source z much larger than the classical turning point $z(0)$. Due to the separability of perpendicular motion, the average width of the far-field distribution $\langle R_{\mathrm{sq}} \rangle$ should be given by the product of Δp with the classical time of flight $T(E)$: $\langle R_{\mathrm{sq}} \rangle \sim \Delta p \cdot T(E)/M$. Thus, the momentum uncertainty model predicts that the width of the far-field current profile for fixed $|m|$ grows with increasing l. This fairly paradoxical conclusion is conveniently corroborated by comparison with the distributions put on display in Section 7.1.2 (Figure 17).

Finally, another obvious strategy to validate the minimum uncertainty model is to calculate the uncertainty product $\Delta R \cdot \Delta p$ for the lateral part of the exact multipole Green functions $G_{lm}(\mathbf{r}, \mathbf{o}; E)$ (5.28) at $z(0) = -E/F$, and compare it with the corresponding Heisenberg minimum value $\hbar\,(|m|+1)$ (7.37). The numerical results of this procedure which are shown as insets in Figure 19 indicate that the true uncertainty products exceed the lower bound (7.37) only by some five percent, thus confirming once more the suitability of the minimum uncertainty approach.

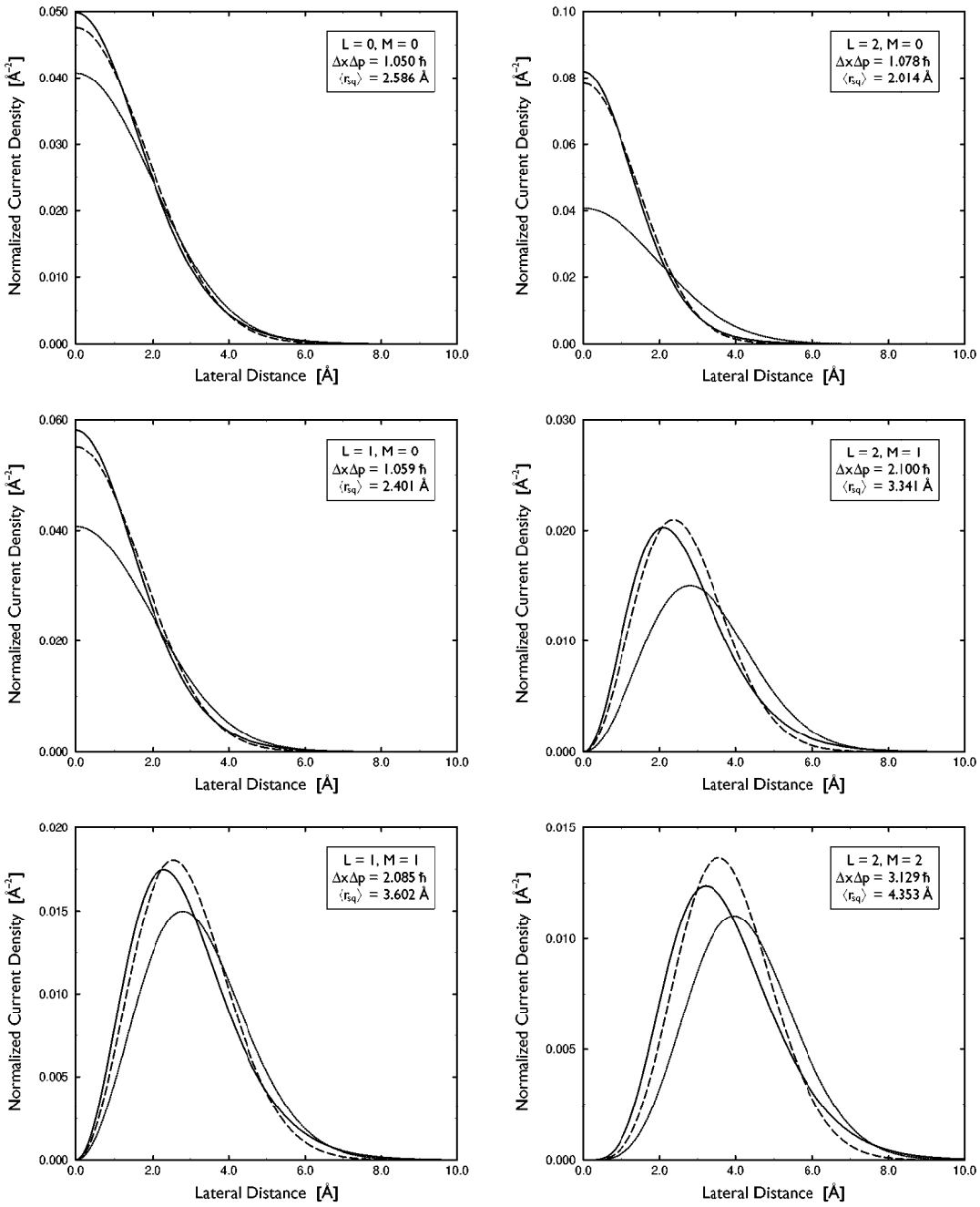

Figure 19: Comparison of exact radial current profiles $j_{lmm}(\mathbf{r}, \mathbf{o}; E)$ in ballistic tunneling with approximations from the minimum uncertainty model. Shown are multipole current distributions ($l \leq 2$) generated by sources normalized to unit total current $J_{lm}(E) = 1$. Parameters used are $E = -4\,\text{eV}$ and $F = 1\,\text{eV/Å}$; the cross sections are taken at the turning point $z(0) = 4\,\text{Å}$. Solid lines: Exact quantum result (5.42). Dotted lines: Semiclassical estimate $j^{(\text{sc})}_{lmm}(\mathbf{r}, \mathbf{o}; E)$ (7.53). Dashed lines: Generalized Gaussian approximation with widths $\Delta R = \langle r_{\text{sq}} \rangle$ adjusted by a numerical least square fit procedure. (See also Figure 17.)

7.3.2 Total Multipole Currents in Ballistic Tunneling

In the same manner as in the previous section, we now apply the result $J_{lm}^{(\mathrm{sc})}(E)$ (7.50) for the total multipole current obtained within the minimum uncertainty scheme to our standard problem of ballistic tunneling. Hence, we introduce the specific semiclassical quantities for motion in a uniform force field, the tunneling (bounce) time $\tau_B(E) = \hbar\kappa/F$ (7.26) and the Hamilton characteristic function $W_{\mathrm{cl}}(0, z(0); E)$ (7.52), into the general formula for $J_{lm}^{(\mathrm{sc})}(E)$ (7.50). This procedure yields for the semiclassical estimate of the ballistic tunneling current:

$$J_{lm}^{(\mathrm{sc})}(E) = \frac{M}{4\pi^2\hbar^3}\,\kappa^{2l+1}\,\frac{(2l+1)\,(l+|m|)!}{|m|!\,(l-|m|)!}\left(\frac{\beta F}{\kappa}\right)^{3(|m|+1)}\exp\left\{-\frac{1}{6}\left(\frac{\kappa}{\beta F}\right)^3\right\} \tag{7.54}$$

This expression identically coincides with the leading asymptotic form $J_{lm}^{(\mathrm{as})}(E)$ (5.58) of the exact quantum multipole current $J_{lm}(E)$ (5.48) obtained in Section 5.5 in the framework of the Green function technique. Manifestly, this agreement of both approaches a posteriori justifies our choice for the current prefactor $J_l(E)$ (7.51) which enters the current expressions (7.48) and (7.50) deduced from the minimum uncertainty model.

At this point, it is appropriate to examine the performance of the asymptotic (and semiclassical) current formula (5.58) or (7.54), respectively. Since the WKB prefactor in (7.54) causes an exponential decay of the tunneling current as the binding energy $|E|$ increases (a behavior one would naively expect anyway), for a meaningful comparison of the exact and approximate expression for the ballistic multipole tunneling current $J_{lm}(E)$ we choose to examine the ratio of the semiclassical and exact currents $J_{lm}^{(\mathrm{sc})}(E)/J_{lm}(E)$ (5.48), (7.54) rather than investigating $J_{lm}^{(\mathrm{sc})}(E)$ separately. Later on, we will discuss the behavior of the total current in the ballistic tunneling problem in the spirit of the multipole source idea.

For the sources of lowest multipole order ($0 \le m \le l \le 2$), these ratios are displayed in Figure 20. Since $J_{lm}^{(\mathrm{sc})}(E)$ (7.54) presents the result of a semiclassical theory, we must anticipate that the ratio $J_{lm}^{(\mathrm{sc})}(E)/J_{lm}(E)$ approaches unity as the binding energy $|E|$ increases. Obviously, no satisfactory performance of $J_{lm}^{(\mathrm{sc})}(E)$ may be expected in the vicinity of the tunneling threshold $|E| \to 0$. These general trends are confirmed by the plots in Figure 20 which depict the current ratio for a fixed field strength $F = 1\,\mathrm{eV/\AA}$. It is seen that $J_{lm}^{(\mathrm{sc})}(E)$, depending on the multipole quantum numbers l and m, may exceed as well as fall below the exact result; for typical values of the binding energy of $|E| = 4\,\mathrm{eV}$ encountered in field emission and STM, however, the relative error in $J_{lm}^{(\mathrm{sc})}(E)$ which shows conspicuous fluctuations with l and m does not go beyond $50\,\%$. In view of the exponential character of the variation of the total multipole current $J_{lm}(E)$, the quality of the semiclassical approximation nevertheless may be judged acceptable.

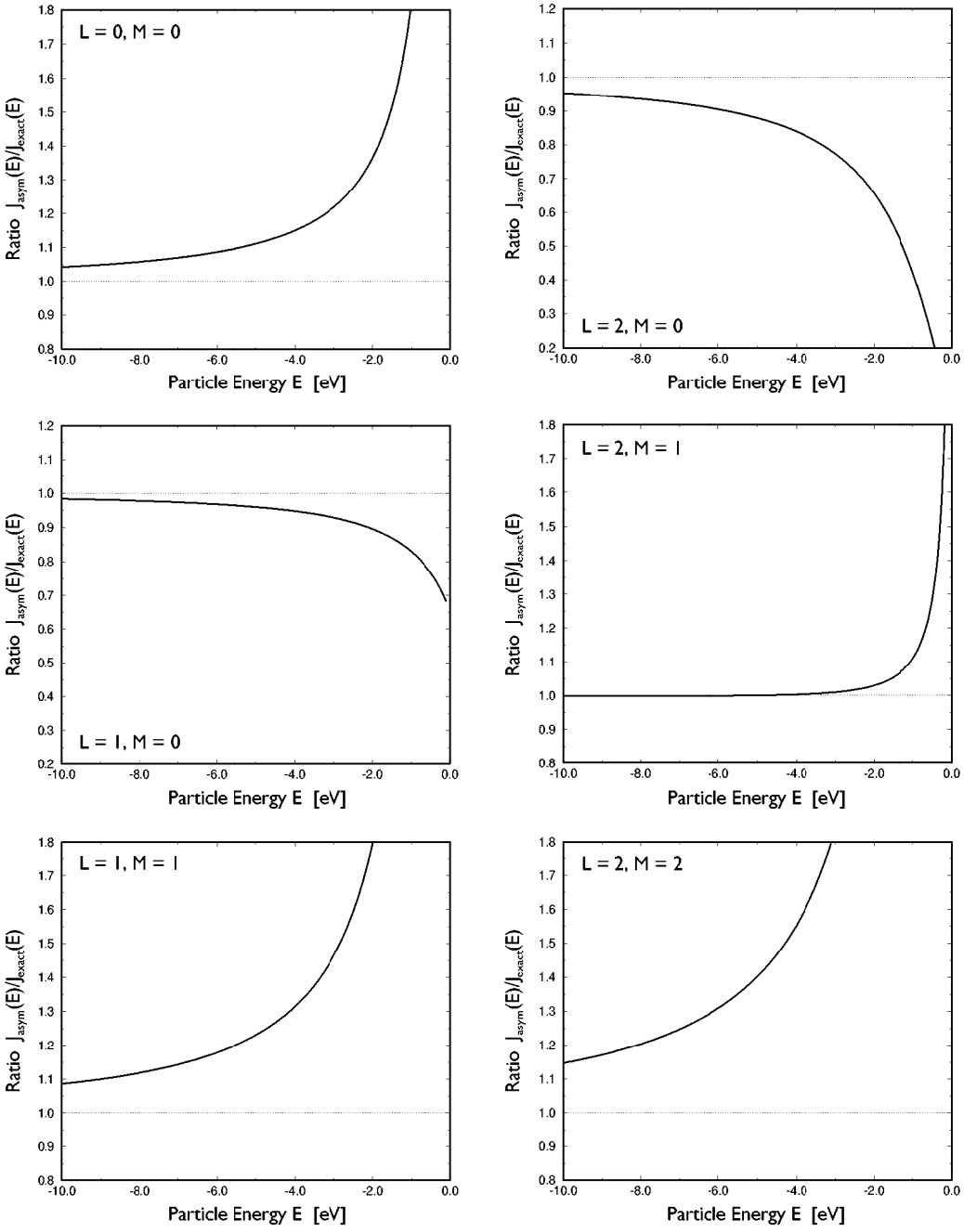

Figure 20: Assessment of the total tunneling current $J_{lm}^{(\mathrm{sc})}(E)$ (7.54) predicted by the minimum uncertainty model. The caption shows the ratio of $J_{lm}^{(\mathrm{sc})}(E)$ to the exact multipole current $J_{lm}(E)$ (5.48) obtained from the Green function approach to ballistic tunneling as a function of the binding energy $|E|$ for diverse multipole sources ($l \leq 2$). The field strength was adjusted to $F = 1\,\mathrm{eV/\AA}$.

Following our comparison of the exact and semiclassical solutions for the total multipole current in ballistic tunneling, it appears adequate to examine the current functional $J_{lm}(E)$ (5.48) for its dependence on the multipole quantum numbers l and m. Clearly, this project complements the study of the ballistic multipole current in the case of classically allowed motion which we performed in Section 6.3 of the previous chapter. There, we saw that within a multiplet of multipole sources with fixed l, for large energies $\beta E \gg 1$ all multipole total currents $J_{lm}(E)$ asymptotically share a common behavior which is given by the emission characteristics of a free-particle multipole source (Section 3.2), the Wigner law (3.27). Different $|m|$ substates only reveal themselves in the current spectra due to the presence of oscillations which we traced back to the interference of classical paths. In the tunneling case, such a process is manifestly impossible. Nevertheless, in the scheme of the minimum uncertainty model (Section 7.2.2) we identified a mechanism which leads to a differing emission behavior of the various multipole sources $\delta_{lm}(\mathbf{r})$ with constant multipole order l: The centrifugal force with growing quantum number $|m|$ increasingly forces the tunneling particles from the vicinity of the preferred escape path, thus leading to a larger bound of the Heisenberg uncertainty product $\Delta R \cdot \Delta p$ (7.37) and subsequently to a suppression of higher $|m|$ multipole currents (7.50). This effect, which may be clearly witnessed in (7.54), quite effectively quenches the current contribution of sources with large values of $|m|$, thus preferring longitudinal emission ($m = 0$). This observation bears some importance in the interpretation of the STM imaging process (Chapter 8).

As an example, we performed a calculation of the ballistic tunneling current $J_{lm}(E)$ (5.48) emitted from $l = 2$ multipole sources in the presence of a uniform force field of strength $F = 1\,\mathrm{eV/\AA}$. Figure 21 displays the current generated by sources with $|m| = 0, 1, 2$. The most obvious common property of all these current characteristics consists in the exponential decay of the tunneling current which may be conveniently explained by the WKB penetration factor present in (7.54). However, it is seen that with increasing $|m|$, tunneling is additionally impeded; the extra suppression, which grows with the binding energy $|E|$ of the source and the quantum number $|m|$, may easily amount to several orders of magnitude. (The current modulations, however, which are observed for $E > 0$ cannot be traced beyond the tunneling threshold.)

7.3.3 Comparison to Numerical Studies

Following our assessment of the minimum uncertainty model for ballistic tunneling phenomena, it would be desirable to corroborate the results of our semiclassical approach by comparison with experimental data. Unfortunately, unlike the case of classically allowed free-falling motion (Sections 6.3 and 6.4), no experimental information on the tunneling current distribution in the vicinity of the source is available; only the far-field properties of the current generated by nanoscopic field emission tips have

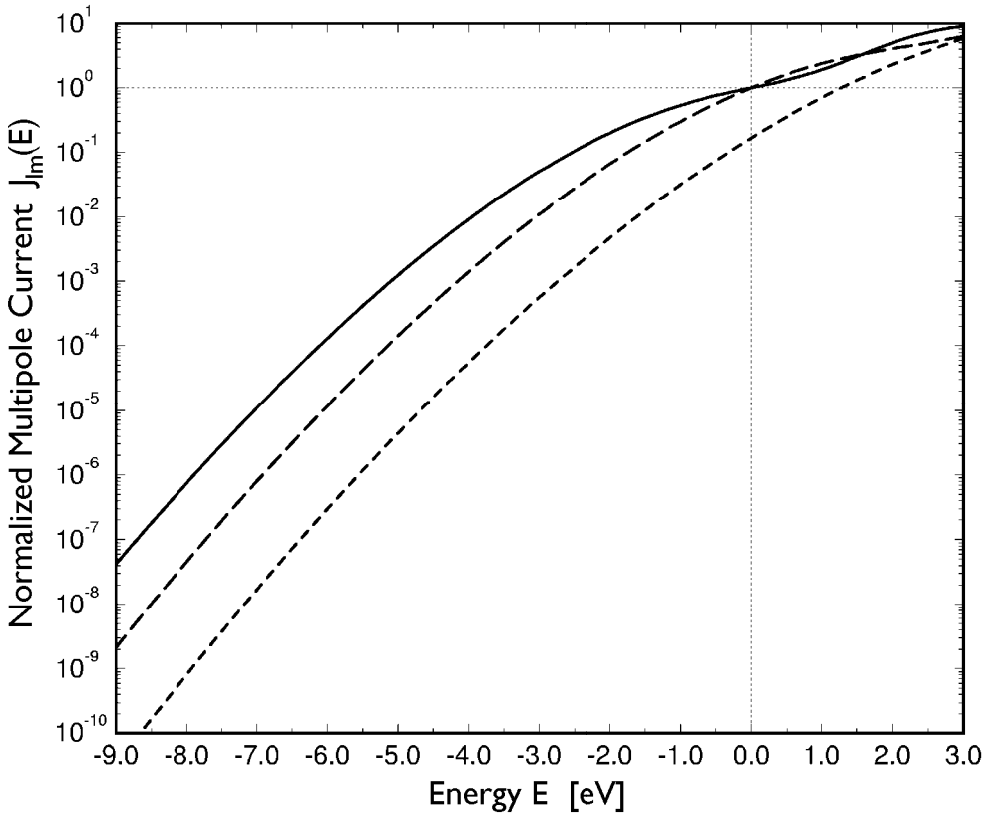

Figure 21: Total multipole currents $J_{lm}(E)$ (5.48) generated by d–wave multipole sources ($l = 2$) in a uniform field environment ($F = 1\,\mathrm{eV/\AA}$) as a function of the electron energy E. The current multiplet has been normalized to $J_{20}(0) = 1$. Solid line: $J_{20}(E)$ (E.14). Long dashed line: $J_{21}(E)$ (E.15). Short dashed line: $J_{22}(E)$ (E.16).

been practically explored. We already summarized the findings of these studies in Section 7.1.4. Hence, for a critical examination of the performance of our simple model, we must rely for comparison on further theoretical research regarding the ballistic tunneling problem. A number of articles on the subject appeared in the literature during the late 80s in the wake of the first announcement of field emission from single-atom tips by H.-W. Fink [68] (see Section 7.1.4). All these publications were devoted to a purely numerical analysis of the problem, though the methods used by different authors varied: Lucas et al. put forward a Green function approach [146], whereas Garcia et al. [147,149] examined the emission properties of a narrow constriction connected to a free electron reservoir terminated by a tunneling barrier by solving the corresponding Schrödinger equation. Finally, the ultrasharp tip setup used in Fink's experiment was simulated by Lang, Yacobi, and Imry [148] who used the density functional formalism (LDA) in order to determine details of the current generated in field emission. This model, which was also considered by Tekman et al. [150], perhaps presents the

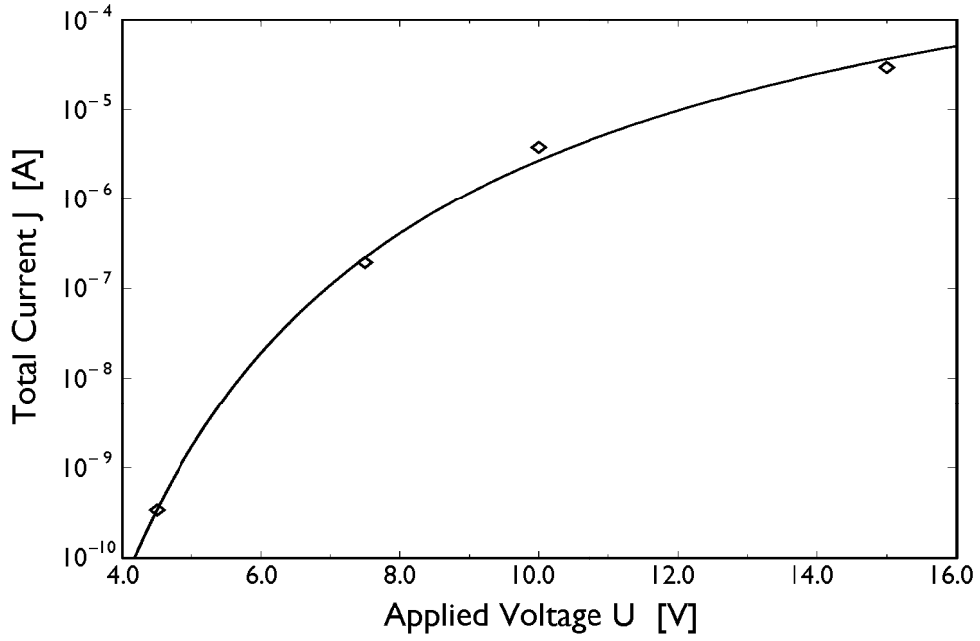

Figure 22: Field emission current as a function of bias in the model by Lang, Yacobi, and Imry [148]. Diamonds: Results of the LDA calculation by Lang et al. Solid line: Total s–wave current $\Delta E \cdot |\lambda_{00}(E)|^2 J_{00}(E)$ (E.11) in the source model of ballistic tunneling for $E = -3.38$ eV. The strength parameter $|\lambda_{00}(E)|^2$ was treated as a free parameter.

most realistic study of the field emission process, and we will use it for comparison with our analytic description of quantum ballistic dynamics provided in Chapter 5.

In the simulation by Lang et al., the monatomic tip was modeled by a sodium atom located 3 Bohr (1 Bohr $= 0.529$ Å) in front of a plane "electrode" made up of a jellium electron gas (where the density parameter r_s was chosen as $r_s = 2$ Bohr, a typical value for a transition metal like tungsten [166]). A parallel identical jellium surface located in 30 Bohr distance served as a counterelectrode. A "field emission" current from the Na tip atom was stimulated by applying a bias voltage between the jellium substrates which provided the uniform field background. The total current drawn from the tip was calculated within the density functional approach for four values of the bias voltage (Figure 22). Additionally, for a particular choice of bias ($U = 10$ V), also the current density distribution in the gap between the jellium surfaces was determined (Figure 23).

From Figure 22, we quickly infer that for voltages of order $U \sim 10$ V, corresponding to a field strength $F = 0.63$ eV/Å, the total current slowly saturates in the μA regime. (This observation is in agreement with the experimental results obtained later by Horch and Morin [144]. See Section 7.1.4.) Obviously, these large currents require a very small value of the differential resistivity $\partial U/\partial I$ of the tip junction in the order

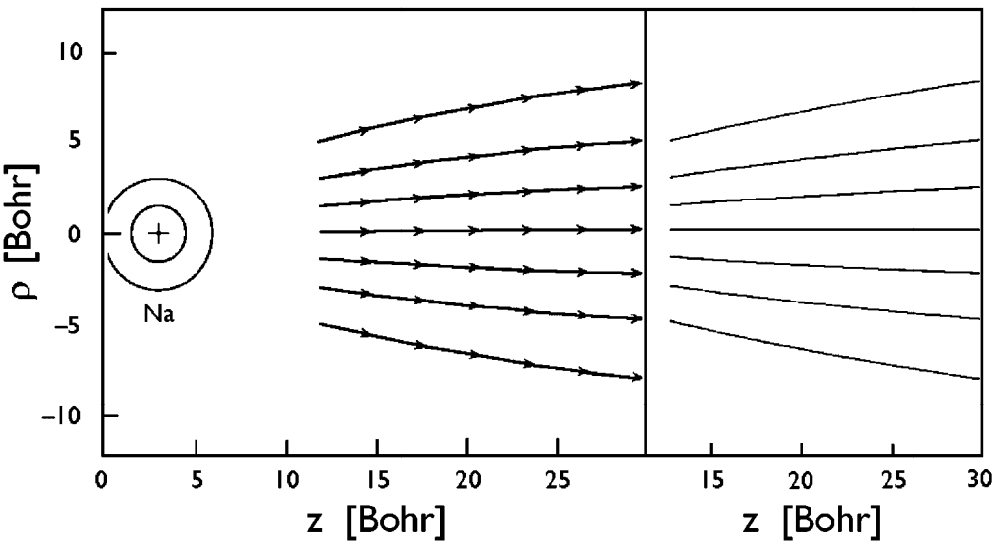

Figure 23: Current density distribution in field emission. The left part of the figure depicts the streamline pattern obtained by Lang, Yacobi, and Imry [148] for $10\,\mathrm{V}$ bias voltage. On the right side, the corresponding result (E.8) for an s–wave electron source of energy $E = -3.38$ eV embedded in a uniform field of strength $F = 0.63\,\mathrm{eV/Å}$ is shown. Successive pairs of streamlines enclose $1/18$, $2/9$, and $1/2$ of the total current, respectively. (1 Bohr $= 0.529$ Å.)

of the quantized Landauer point contact resistance $R = \pi\hbar/e^2 \approx 12.9\,\mathrm{k\Omega}$ which means that the "tunneling gap" hardly obstructs electronic transmission at all. (A detailed discussion of conductivity quantization in the framework of the quantum source approach is deferred to Section 8.2 where a simple model for the source strength $\lambda_{lm}(E)$ of a metallic tip will be proposed.) In their LDA calculation, Lang et al. find that the presence of the Na atom for a strong electric field distorts the potential distribution in the junction sufficiently as to remove the tunneling barrier completely in front of the tip. Electrons are transmitted classically through the emerging hornlike "opening" in the barrier. Lang et al. furthermore claim that this transmission mechanism apart from the large current flow is also responsible for the beam focusing observed in experiment (see Figure 18).

How do the results of Lang et al. [148] reconcile with the quantum source approach put forward in this work? In a very simple approximation, the sodium tip atom may be replaced by an s–wave point source embedded in a uniform electric field environment maintained by the jellium surfaces. The energy of the emitted electrons is roughly given by the work function of the jellium surface which for the density parameter $r_s = 2$ Bohr used in the LDA estimate amounts to $\Phi = 3.89$ eV [167]. However, we chose to determine the binding energy $|E|$ by a numerical fit of the s–wave ballistic total current $I = |\lambda_{00}(E)|^2 J_{00}(E) \cdot \Delta E$ (E.11) generated by a point source $\lambda_{00}(E) \cdot \delta_{00}(\mathbf{r})$

of adjustable strength $\lambda_{00}(E)$ to the set of data points provided by Lang et al. (ΔE presents a factor accounting for the width of the electronic energy distribution and is of order $\Delta E \sim 200\,\mathrm{meV}$.) This procedure yielded an empirical value $E = -3.38\,\mathrm{eV}$ for the electron energy which is reasonably close to the work functions of the jellium surface as well as sodium metal ($\Phi \approx 2.75\,\mathrm{eV}$). The resulting $U - I$ characteristic is shown in Figure 22. Although overall agreement with the calculation by Lang et al. is satisfactory, the source model is faced with the serious problem that the source strength $\lambda_{00}(E)$ required to achieve currents in the μA range is excessively large: Inserting the expression $|\lambda_{00}(E)|^2 = 8\pi\hbar^2/Mk_F$ which is suggested by the transport model of the STM tunneling process (Section 8.2.2) for the strength of the s–wave source (where $k_F \approx 1.82\,\mathrm{\AA}^{-1}$ is the Fermi wave number of the jellium electron gas [166]), the current formula stated above for $10\,\mathrm{V}$ bias delivers a total current of some $10^{-9}\,\mathrm{A}$, three orders of magnitude below the result of Lang et al. We must attribute this discrepancy to the fact that our assumption of a uniform force field cannot account for field focusing near the tip atom. We had to admit earlier a similar shortcoming in our discussion of the experimental findings on field emission by Horch and Morin [144] in Section 7.1.4.

Having the binding energy $|E|$ of the field emission tip at hand, we may proceed and calculate the current streamline pattern generated by the source in the homogeneous field environment provided by the charged electrode surfaces for a bias voltage $U = 10\,\mathrm{V}$. This allows for comparison with the LDA calculation performed by Lang et al. whose results are displayed in Figure 23. If we endorse the reasonable assumption that within the width ΔE of the electronic energy distribution of the tunneling current, the current density profile $\mathbf{j}(\mathbf{r}; E)$ only slightly varies with E, the current pattern may be calculated along the lines of Section 5.4 [67, 168]. The s–wave current distribution $j_{000}(\mathbf{r}, \mathbf{o}; E)$ (E.8) has been used to obtain a plot of the streamline pattern in the simple point source model of ballistic tunneling (right part in Figure 23). It is seen that it delivers an almost perfect match to the results of the involved calculation carried out by Lang et al. We thus find as an empirical rule that although the source model of ballistic tunneling performs rather poorly in the determination of the total tunneling current, which is probably due to the sensitivity of this quantity to details of the potential relief $U(\mathbf{r})$ in the vicinity of the tip, it is able to reproduce the current distribution generated by the source in a quantitative manner. This property renders the multipole source model attractive for the theoretical description of an imaging device capable of atomic resolution of surfaces, the scanning tunneling microscope (STM). This is the topic of the following chapter.

Chapter 8

A Source Model of STM

SINCE THE FIRST REPORT regarding the successful implementation of a scanning tunneling microscope (STM) was published by Binnig et al. [72] in 1982, scanning probe techniques have revolutionized the study of material surface properties. The basic idea behind the novel instrument to step some physical sensor of mesoscopic size over the sample surface and thus record a spatially resolved response pattern was quickly embraced by the experimental community, and a multitude of "microscopes" founded upon different physical principles has been developed since. Here, we mention only two of the most popular scanning devices, the atomic force microscope (AFM) [169] measuring changes of the cantilever resonance oscillation near the sample surface, and the optical near-field microscope (SNOM) [170, 171] sensitive to evanescent light transmission into the probe. The number of applications of these instruments are nowadays innumerable, as is amply illustrated by the proceedings of a recent major conference [172]. However, these spin-off developments are far outside the scope of this treatise; therefore, we refer the interested reader to a number of articles, compilations and monographs on the subject [173–179]. Here, we shall content ourselves with a greatly simplified "toy model" of the original STM setup that is based upon the quantum source model of ballistic motion, but nevertheless is able to reproduce the outstanding properties of this surface probe, in particular its spectacular ability to resolve single atoms even in close-packed metal surfaces, arguably the smoothest objects in existence [73, 74]. This is the topic of the current chapter.

Let us briefly recapitulate the essentials of Binnig's innovative apparatus. A specifically prepared metal tip, guided by piezoelectric elements, is scanned over the surface of a conducting sample; the tip itself is moved towards or withdrawn from the sample surface as to maintain a constant tunneling conductivity σ_0 for a fixed bias voltage V applied between tip and sample (constant current mode of STM). The measured vertical deflection $\Delta z'(x', y'; \sigma_0)$ of the tip, the so-called corrugation amplitude, is thought to reflect the topography of the examined surface. (In another, less popular operation mode of the STM, the vertical tip position is fixed and the current $I(x', y', z')$ is recorded instead; it is known as the constant height mode.) We note that unlike in

optical microscopy or transmission electron microscopy (TEM), the image in STM is built by stepping the sensitive part of the instrument over the probe; a single "measurement" does not yield spatially resolved data.

Due to the strong dependence of the electronic transmission rate on the width of the tunneling gap, current emission is essentially limited to one (or few) atoms protruding from the tip towards the sample. In our theoretical approach, a primer of which already has been published [75, 180], the physical tip is replaced by some electronic source term $\sigma(\mathbf{r})$ mimicking its emission properties, thus allowing to employ the source formalism introduced in Chapter 2. Clearly, this concept in the spirit of Section 2.1 radically simplifies the theoretical description of STM as the tip is no longer explicitly considered. As we already know from Section 7.3 that the current distribution generated by a pointlike source even in nanoscopic distances extends over several Å and thus distinctly exceeds the size of individual atoms, we may restrict our tip model to pointlike multipole sources $\delta_{lm}(\mathbf{r})$ (Section 2.4) which nevertheless allow to incorporate the orbital character of the atomic tip states involved. Despite its simplicity, using the functional analytic formalism presented in Appendix A one may prove the equivalence of the source description of STM with the standard perturbative scattering approach by Tersoff and Hamann [77, 78, 181] and its refinements proposed by Chen [182–184] who concluded that the topography of STM images reproduces collective properties of the set of sample electronic wave functions at the tip location $\mathbf{r}'$, in the most basic case the local density of states (LDOS) $n(\mathbf{r}'; E)$ (Appendix A.6).

Like in our description of photodetachment phenomena (Chapters 3 and 6), the properties of the physical electron source are summarized in a single parameter, the source strength $\lambda_{lm}(E)$ which depends on the details of the emission process. Although of no special importance in explaining the features observed in STM images, a complete source theory of STM obviously requires a determination of $\lambda_{lm}(E)$ founded upon a microscopic model of electronic transport in the tip body. In Section 8.2, we will offer a simple theory for this quantity that links the quantum source approach to the modern description of conduction through mesoscopic structures, in particular the quantized Landauer resistance [79, 80, 185, 186].

The final sections of this chapter are devoted to the problem of approximating the Green function $G(\mathbf{r}, \mathbf{r}'; E)$ underlying the tunneling process in the STM junction. Clearly, exact solutions for $G(\mathbf{r}, \mathbf{r}'; E)$ in the presence of the combined tip-sample potential relief $U(\mathbf{r})$ are generally not available. We propose two techniques for constructing estimates to $G(\mathbf{r}, \mathbf{r}'; E)$: The first one is founded upon a customary perturbation expansion of the Green function (Appendix A.3.6), while the second method utilizes the exact solution of the inhomogeneous Schrödinger equation for an approximate sample potential $U(\mathbf{r})$ which is arranged as an ensemble of pointlike scatterers that reflects the atomic structure of the sample surface. Both approaches are illustrated by example calculations.

8.1 Source-Theoretical Description of the STM

As already indicated in the introduction to this chapter, we now will present a theoretical model for STM which ignores the technical complexities connected with a real-world scanning tunneling microscope. Rather than trying to incorporate the actual structure of the probing tip and the electrical circuitry required to control STM operation, our study concentrates upon a "bare" model which has been simplified to the utmost, the interaction of an electron source at position $\mathbf{r}'$ replacing the STM tip with the sample surface which is characterized by an effective potential $U(\mathbf{r})$. According to the discussion in Chapter 2 of this volume, the multipole Green function formalism presents a natural framework for the description of the properties of this arrangement which we will pursue in Section 8.1.1. Using a formal expansion of the Green function which we take over from Appendix A.3.6, it requires but a simple calculation in order to extract the experimentally observable quantities in STM from our setup, viz., the corrugation conductivity $\Delta\sigma(x', y', z')$ or the corrugation amplitude $\Delta z'(x', y'; \sigma_0)$, respectively (Section 8.1.2). The astonishing resolution capabilities of the STM will be the topic of the following section, where we will employ the results of the minimum uncertainty model (Section 7.2) in order to gain a resolution estimate for this type of microscope. Finally, in Section 8.1.4, we will discuss the relationship of the source formalism put forward in this work to various other theoretical models of STM, in particular the theory proposed by Tersoff and Hamann [77,78] which has become the benchmark against which any novel approach to the STM problem needs to be tested. Indeed, using the functional analytic methods presented in Appendix A.6, it may be shown that the source theory of STM includes the transfer Hamiltonian model (that the Tersoff–Hamann formalism is founded upon) as a special case.

8.1.1 Green Function Formalism

Let us now transform our idea into a mathematical approach using the Green function technique of Chapter 2. Introducing, we note that electronic tunneling through the STM junction is governed by the semiclassical bounce time $\tau_B(E)$ (7.26) which we identified in Section 7.2 as the relevant time scale of motion. Since, in order to achieve an appreciable flow of electrons, probe and sample are only distances of several Å apart, the tunneling process of a single electron is completed within femtoseconds, whereas the stepping motion and tip readjustment in the STM setup take place on much larger, macroscopic time scales. Hence, we may consider the variation of the STM current as an adiabatic process which is properly discussed in the framework of stationary quantum mechanics. In another, perhaps drastic, simplification of the real tunneling process, we adopt the independent electron approximation: Electrons of a given energy E are scattered elastically across the junction, either moving towards the sample represented through an effective potential $U(\mathbf{r})$ (which additonally will

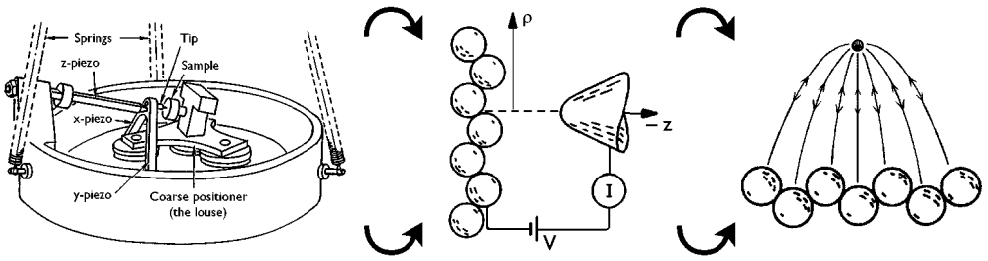

Figure 24: The source model of STM (right) is obtained from a real-world setup (left) by a series of abstractions.

comprise contributions from the tip potential and the externally applied field), or approaching the tip. Many-particle effects are covered only through the assumption of electron reservoirs in the tip and sample sectors which are in thermodynamic equilibrium as a consequence of our quasistationary model; however, their respective Fermi levels are shifted by the bias voltage V which is externally applied to the STM junction. In a last step of idealization, we will omit any effects caused by magnetic fields and set $\mathbf{A} = \mathbf{o}$ for the electrodynamic vector potential.

Replacing the tip reservoir by a stationary source $\sigma(\mathbf{r}; E)$ of electrons with energy E in an approach spirited by the deliberations of Section 2.1, our model describes the transfer of electrons of this particular energy through the tunneling gap into the sample in terms of the inhomogeneous stationary Schrödinger equation (2.11):

$$\left\{ E + \frac{\hbar^2}{2M} \Delta - U(\mathbf{r}) \right\} \psi_\sigma(\mathbf{r}; E) \; = \; \sigma(\mathbf{r}; E) \tag{8.1}$$

We studied the formal properties of this equation in Section 2.3. In practice, we may further simplify (8.1) and replace the spatially extended electron source $\sigma(\mathbf{r}; E)$ by a point source localized at the tip position $\mathbf{r}'$ (Figure 24). This approach is justified by the fact that the current emitted from different parts of the source strongly depends on the distance to the sample surface; only the topmost tip atom will deliver an appreciable contribution to the tunneling current. Furthermore, the current distribution generated by a point source several Å distant from the sample surface will already spread over an area ~ 5 Å across, as illustrated by Figure 19 (Section 7.3.1). Thus, only a negligible error is introduced by ignoring the spatial extension of the emitting tip atom, which justifies our point source approach. (This simple picture obviously breaks down if several atoms of the tip protrude to comparable distances from the sample surface. Then, however, the interpretation of STM images is severely impeded by quantum interference between the partial wave functions picked up by these atoms [187], and it is unlikely that such tips are employed to record experimental data.) Then, we obtain the point source model of STM that was formerly studied by the author for simple s–wave tips with isotropic emission characteristic [75, 172]. Here, our considerations

are extended to spatially oriented multipole point sources $\delta_{lm}(\mathbf{r}-\mathbf{r}')$ (2.23) which were originally introduced in Section 2.4 of this treatise. Equation (8.1) then simplifies to:

$$\left\{E + \frac{\hbar^2}{2M}\,\Delta - U(\mathbf{r})\right\}\,\psi_{lm}(\mathbf{r},\mathbf{r}';E) \;=\; \lambda_{lm}(E)\,\delta_{lm}(\mathbf{r}-\mathbf{r}') \tag{8.2}$$

(For the sake of clarity, we will only deal with sources of purely (l,m) orbital characteristics. In general, the angular spectrum of a realistic tip will involve a linear superposition of various spherical partial waves. The theory presented in the following may be extended to the case of mixed multipole sources by means of the more general formulae derived in Section 2.4.3.)

In (8.2), apart from the multipole structure, all properties of the STM tip have been condensed into a single parameter, the source strength $\lambda_{lm}(E)$. Though convenient for calculational purposes, the source model itself provides no clue which values to insert for $\lambda_{lm}(E)$; the transfer process in the STM junction must be analyzed in detail in order to obtain the proper choice for this parameter. (We made a quite similar observation in Chapter 3 where we had to examine laser-ion interaction for the determination of the source strength prefactor λ_{lm} (3.22) occurring in the source model of negative ion photodetachment.) Obviously, a reasonably complete source theory of STM requires a means to calculate $\lambda_{lm}(E)$ in (8.2), and we will present a simple ansatz based on fundamental properties of nanoscopic low-dimensional transport phenomena in Section 8.2. It should be noted, however, that the interpretation of STM images does not depend on a detailed understanding of the emission process. This is explained in the following section.

Let us now turn our attention back to the study of (8.2). Clearly, among the set of solutions to this equation, those describing the emission or absorption of electrons at the point source deserve special attention. In the sample bulk, far from the source region, these wave functions take on the character of an outgoing or incoming wave; in Appendix A.4, it is formally demonstrated that these solutions coincide (apart from a constant of proportionality) with the retarded and advanced multipole Green functions $G_{lm}(\mathbf{r},\mathbf{r}';E)$ (2.24) assigned to the potential relief $U(\mathbf{r})$:

$$\psi_{lm}^{(\mathrm{in/out})}(\mathbf{r},\mathbf{r}';E) \;=\; \lambda_{lm}(E)\,G_{lm}^{(\mathrm{adv/ret})}(\mathbf{r},\mathbf{r}';E) \tag{8.3}$$

We note at this point that the absorption of electrons at the source (then more aptly called a "sink") may be viewed as the time-reversed counterpart to the emission process. In the Green function formalism, this property is reflected by the symmetry relation $G_{\mathrm{ret}}(\mathbf{r},\mathbf{r}';E) = G_{\mathrm{adv}}(\mathbf{r}',\mathbf{r};E)^*$ (see Appendix A.5.2). This formula comes in handy when calculating the partial currents $J_{lm}^{(\mathrm{in/out})}(\mathbf{r}';E)$ carried by the wave functions $\psi_{lm}^{(\mathrm{in/out})}(\mathbf{r},\mathbf{r}';E)$ (8.3) which will finally add up to the total current $J_{lm}(\mathbf{r}')$, the experimentally accessible quantity in scanning tunneling microscopy.

The outgoing partial multipole particle current $J_{lm}^{(\mathrm{out})}(\mathbf{r}';E)$ generated by the Green function $G_{lm}(\mathbf{r},\mathbf{r}';E)$ with retarded character which we generally implicitly assume in this work was already derived in the course of Section 2.4.3 and reads (2.32):

$$J_{lm}^{(\mathrm{out})}(\mathbf{r}';E) \;=\; -\,\frac{2}{\hbar}\,|\lambda_{lm}(E)|^2 \lim_{\mathbf{r}\to\mathbf{r}'} \Im\left[K_{lm}^{*}\left(\frac{\partial}{\partial\mathbf{r}}\right) K_{lm}\left(\frac{\partial}{\partial\mathbf{r}'}\right) G_{\mathrm{ret}}(\mathbf{r},\mathbf{r}';E)\right] \tag{8.4}$$

Hence, the "intrinsic" current $J_{lm}^{(\mathrm{out})}(\mathbf{r}';E)$ is available as the spherical tensor gradient of the multipole Green function $G_{lm}(\mathbf{r},\mathbf{r}';E) = K_{lm}[\partial/\partial\mathbf{r}']\,G_{\mathrm{ret}}(\mathbf{r},\mathbf{r}';E)$, evaluated at the tip position $\mathbf{r} = \mathbf{r}'$. Taking advantage of the symmetry relation $G_{\mathrm{ret}}(\mathbf{r},\mathbf{r}';E) = G_{\mathrm{adv}}(\mathbf{r}',\mathbf{r};E)^*$ cited above, from expression (8.4) the reciprocity relation

$$J_{lm}^{(\mathrm{in})}(\mathbf{r}';E) \;=\; -\,J_{lm}^{(\mathrm{out})}(\mathbf{r}';E) \tag{8.5}$$

is straightforwardly verified. Obviously, the time-reversal symmetry of our quasistationary STM model manifests itself in (8.5).

So far, our analysis only covered the process of transmission of a single electron through the STM junction in a specified direction. Whether such a transfer of charge actually takes place however depends on the properties of the electron reservoirs located on both sides of the junction. For an emission process, obviously the corresponding tip state must be occupied, whereas the proper sample state at energy E should be empty; the argument holds vice versa also for electron absorption from the sample. Assuming thermodynamic equilibrium within both reservoirs, the intrinsic currents $J_{lm}^{(\mathrm{in/out})}(\mathbf{r}';E)$ (8.4), (8.5) therefore must be weighed by appropriate occupation probability factors:

$$\begin{aligned}
\left\langle J_{lm}^{(\mathrm{out})}(\mathbf{r}';E)\right\rangle &= f(\mu_{\mathrm{tip}};E)\,[1-f(\mu_{\mathrm{sample}};E)]\,J_{lm}^{(\mathrm{out})}(\mathbf{r}';E)\\
\left\langle J_{lm}^{(\mathrm{in})}(\mathbf{r}';E)\right\rangle &= f(\mu_{\mathrm{sample}};E)\,[1-f(\mu_{\mathrm{tip}};E)]\,J_{lm}^{(\mathrm{in})}(\mathbf{r}';E)
\end{aligned} \tag{8.6}$$

In these relations of detailed balance, μ_{tip} and μ_{sample} denote the electronic chemical potentials of the tip and sample reservoirs, respectively, and $f(\mu;E)$ presents the usual fermionic Fermi–Dirac occupation factor:

$$f(\mu;E) \;=\; f(E-\mu) \;=\; \left[1+\exp\left(\frac{E-\mu}{k_B T}\right)\right]^{-1} \tag{8.7}$$

We may identify μ_{sample} with the Fermi level E_F in the specimen bulk; then, the tip chemical potential μ_{tip} will be shifted with respect to E_F by $-eV$, where V represents the STM bias voltage applied between tip and sample: $\mu_{\mathrm{tip}} = E_F - eV$. According to (8.6), this shift gives rise to a net current $\langle J_{lm}(\mathbf{r}';E)\rangle$ from tip to sample in the spectral

energy range $[E; E + dE]$:

$$\langle J_{lm}(\mathbf{r}'; E)\rangle \, dE \;=\; [f(E - E_F + eV) - f(E - E_F)] \, J_{lm}^{(\mathrm{out})}(\mathbf{r}'; E) \, dE \tag{8.8}$$

Finally, the total particle current $J_{lm}(\mathbf{r}')$ flowing from the tip at $\mathbf{r}'$ into the sample bulk arises from (8.8) by integration over the entire range of electron energies:

$$J_{lm}(\mathbf{r}') \;=\; \int dE \; [f(E - E_F + eV) - f(E - E_F)] \, J_{lm}^{(\mathrm{out})}(\mathbf{r}'; E) \tag{8.9}$$

In practice, during an STM scan the electric current $I_{lm}(\mathbf{r}') = -eJ_{lm}(\mathbf{r}')$ is recorded. For an interpretation of (8.9), it is best to consider the low-bias limit at zero temperature ($T \to 0$) which appears particularly suited to the application of the STM probe to metal surfaces (where we may expect the most favorable results from our simple analysis). In this limiting case, the Fermi–Dirac distribution (8.7) degenerates to a step function, and from (8.8) we immediately find:

$$\lim_{T \to 0} \lim_{V \to 0} \frac{I_{lm}(\mathbf{r}')}{V} \;=\; e^2 \, J_{lm}^{(\mathrm{out})}(\mathbf{r}'; E_F) \tag{8.10}$$

Thus, the intrinsic current $J_{lm}^{(\mathrm{out})}(\mathbf{r}'; E_F)$ is available in experiment as the zero-bias, zero-temperature conductivity of the STM junction $\sigma_{lm}(\mathbf{r}')$. Together with (8.4), we obtain an expression for $\sigma_{lm}(\mathbf{r}')$ in terms of the (retarded) Green function $G(\mathbf{r}, \mathbf{r}'; E_F)$ for the local potential environment $U(\mathbf{r})$ due to tip and sample:

$$\sigma_{lm}(\mathbf{r}') \;=\; \lim_{T \to 0} \left. \frac{\partial I_{lm}(\mathbf{r}')}{\partial V} \right|_{V=0} \;=\; -\frac{2e^2}{\hbar} \, |\lambda_{lm}(E_F)|^2 \;\times \lim_{\mathbf{r} \to \mathbf{r}'} \Im \left[K_{lm}^* \left(\frac{\partial}{\partial \mathbf{r}} \right) \, K_{lm} \left(\frac{\partial}{\partial \mathbf{r}'} \right) G(\mathbf{r}, \mathbf{r}'; E_F) \right] \tag{8.11}$$

We see that the zero-bias conductivity $\sigma_{lm}(\mathbf{r}')$ is related to the imaginary part of the system one-particle Green function, evaluated for $E = E_F$ at the tip position $\mathbf{r}'$.

Using a formal representation of the Green function in terms of energy eigenfunctions $\psi_E(\mathbf{r})$ for the potential relief $U(\mathbf{r})$, one may establish a connection between $\sigma_{lm}(\mathbf{r}')$ (8.11) and the sample electron density of states at the location of the tip. Let us assume that the base of eigenfunctions $\psi_{\mu_1, \mu_2, \ldots, \mu_n}(\mathbf{r})$ forms a complete orthogonal set in physical space, where the wave functions (apart from an overall phase factor) are uniquely determined by their quantum numbers $\{\mu_1, \mu_2, \ldots, \mu_n\}$. (These notions are by no means trivial; for details of their mathematical definition, see Appendix A.3.4 and A.3.5.) Then, the intrinsic multipole current $J_{lm}^{(\mathrm{out})}(\mathbf{r}'; E)$ (8.4) may be expressed in terms of the corresponding spherical tensor gradients of this set of wave functions. We omit the intermediate steps of the calculation which are listed in Appendix A.6.1;

here, we shall content ourselves with a slightly simplified version of the exact functional analytic result (A.343):

$$\sigma_{lm}(\mathbf{r}') \;=\; \frac{2\pi e^2}{\hbar}\,|\lambda_{lm}(E_F)|^2 \int d\mu_1 \int d\mu_2 \cdots \int d\mu_n\, \delta\left[E_F - E(\mu_1,\mu_2,\ldots,\mu_n)\right] \;\times \\ \left| K_{lm}\left(\frac{\partial}{\partial \mathbf{r}'}\right)\, \psi_{\mu_1,\mu_2,\ldots,\mu_n}(\mathbf{r}') \right|^2 \qquad (8.12)$$

In this formula, the parameters $\mu_1, \mu_2, \ldots, \mu_n$ denote continuous quantum numbers, and $E(\mu_1, \mu_2, \ldots, \mu_n)$ is the eigenenergy of the corresponding state $\psi_{\mu_1,\mu_2,\ldots,\mu_n}(\mathbf{r})$. (For an extension which additionally covers discrete spectra, we refer to Appendix A.3.4. There, also some examples are presented, including the ballistic problem of Chapter 5.) From (8.12), we infer that the zero-bias conductivity $\sigma_{lm}(\mathbf{r}')$ is governed by the local density of the spherical tensor gradient of the eigenstates $\psi_{\mu_1,\mu_2,\ldots,\mu_n}(\mathbf{r})$ in the STM potential environment of the combined tip-sample system, which must be evaluated at the tip position $\mathbf{r}'$ for the Fermi level E_F. In particular, for an isotropic s–wave source, we have $l = m = 0$, and (8.12) simplifies to the expression:

$$\sigma_{00}(\mathbf{r}') \;=\; \frac{e^2}{2\hbar}\,|\lambda_{00}(E_F)|^2\, n(\mathbf{r}';E_F) \qquad (8.13)$$

where $n(\mathbf{r}';E)$ denotes the local density of states (LDOS):

$$n(\mathbf{r}';E) \;=\; \int d\mu_1 \int d\mu_2 \cdots \int d\mu_n\, \delta\left[E - E(\mu_1,\mu_2,\ldots,\mu_n)\right]\, |\psi_{\mu_1,\mu_2,\ldots,\mu_n}(\mathbf{r}')|^2 \qquad (8.14)$$

The representation for the conductivity (8.11) of the source-theoretical approach to STM is especially suited for comparison with alternative proposals (Section 8.1.4). We finally note that the derivation presented in the course of this section assumes a particularly elegant appearance if performed in the functional analytic framework provided in Appendix A.3 and A.6. There, the STM particle current $J(\mathbf{r}')$ (8.9) is formally obtained in a generalized Stieltjes integral representation (A.364).

8.1.2 The Corrugation Amplitude

Apart from the determination of the source strength prefactor $|\lambda_{lm}(E_F)|^2$ (Section 8.2), the zero-bias conductivity $\sigma_{lm}(\mathbf{r}')$ (8.11), (8.12) in principle already presents the final result of source theory for the STM problem. However, these expressions are hardly useful for the practical evaluation of data obtained during an STM scan: In general, the absolute position $\mathbf{r}'$ of the tip is not available; rather the piezoelectric stepping mechanism only delivers information on the lateral components x' and y' of this vector, as a function of which the tunneling current $I(x', y', z_0)$ is recorded at fixed vertical distance

(constant height mode). Alternatively, and more commonly, the tip-sample distance is readjusted by withdrawing the tip from the surface some distance $\Delta z'$ as to maintain a constant tunneling current I_0 in the STM junction (constant current mode). In STM images, the so-called corrugation amplitude $\Delta z'(x', y'; I_0)$ is usually interpreted as the topography of the scanned surface.

Hence, the STM apparatus operating in constant height mode records deviations of $I(x', y', z_0)$ from an average background current I_0, and similarly relative displacements $\Delta z'(x', y'; I_0)$ from a mean position z_0 in constant current mode. Let us first focus upon the constant height case because it is more intimately related to the discussion in the preceding section. For ease of notation, we restrict our considerations to the zero-bias, zero-temperature limit; with the help of relation (8.9), the extension to more general external conditions is straightforward. Then, we may equally replace the current $I(x', y', z_0)$ by the intrinsic conductivity $\sigma_{lm}(\mathbf{r}')$ (8.11), (8.12), for which the following decomposition is suggested by the experimental circumstances:

$$\sigma_{lm}(x', y', z_0) \;=\; \sigma_{lm}^{(0)}(z_0) + \Delta\sigma_{lm}(x', y', z_0) \tag{8.15}$$

Obviously, $\sigma_{lm}^{(0)}(z_0)$ represents the background conductivity which is modulated by the corrugative part $\Delta\sigma_{lm}(x', y', z_0)$. Since $\sigma_{lm}^{(0)}(z_0)$ does not change under lateral translations, it appears natural to assign the background conductivity to a uniform background potential $U_0(z)$ which is equally invariant with respect to shifts parallel to the surface and thus characterizes the overall properties of the bulk-vacuum transition barrier near the sample surface. The remaining corrugative potential $W(\mathbf{r})$ describes the surface structure and gives rise to the current variations observed in STM:

$$U(\mathbf{r}) \;=\; U_0(z) + W(\mathbf{r}) \tag{8.16}$$

Therefore, the conductivity decomposition (8.15) just reflects the corresponding separation of the potential into background and corrugative parts.

The validity of this idea is easily verified within the multipole source approach of Section 8.1.1 which yields simple explicit expressions for both partial conductivities $\sigma_{lm}^{(0)}(z_0)$, $\Delta\sigma_{lm}(x', y', z_0)$ in terms of Green functions. To this end, we insert the decomposition of the potential $U(\mathbf{r})$ (8.16) into the inhomogeneous stationary Schrödinger equation (8.2):

$$\left\{E + \frac{\hbar^2}{2M}\,\Delta - U_0(z)\right\}\,\psi_{lm}^{(\mathrm{out})}(\mathbf{r}, \mathbf{r}'; E) \;=\; \lambda_{lm}(E)\,\delta_{lm}(\mathbf{r} - \mathbf{r}') + W(\mathbf{r})\,\psi_{lm}^{(\mathrm{out})}(\mathbf{r}, \mathbf{r}'; E) \tag{8.17}$$

According to (2.14), this equation may formally be solved in terms of the Green func-

tion $G^{(0)}(\mathbf{r},\mathbf{r}';E)$ of the background potential $U_0(z)$:

$$\left\{E + \frac{\hbar^2}{2M}\Delta - U_0(z)\right\} G^{(0)}(\mathbf{r},\mathbf{r}';E) \;=\; \delta(\mathbf{r}-\mathbf{r}') \tag{8.18}$$

We note that $G^{(0)}(\mathbf{r},\mathbf{r}';E)$ inherits the translational symmetry property of its parent "background" Hamiltonian $H_0(z,\mathbf{p})$ (for a formal proof of this reasonable assertion, we refer to Appendix A.5.4). From a calculational point of view, the invariance of $G^{(0)}(\mathbf{r},\mathbf{r}';E)$ with respect to lateral shifts $\mathbf{r}_\perp$ allows for a rather simple determination of the Green function; indeed, it is easy to infer from (8.18) that $G^{(0)}(\mathbf{r},\mathbf{r}';E)$ represents the Fourier transform of the retarded Green function $G^{(0)}(z,z';E-p_\perp^2/2M)$ of the corresponding one-dimensional problem with respect to $\mathbf{r}_\perp$ [9]:

$$\begin{aligned} G^{(0)}(\mathbf{r},\mathbf{r}';E) \;&=\; \frac{1}{(2\pi\hbar)^2}\int d^2p_\perp\, e^{i(\mathbf{r}_\perp-\mathbf{r}'_\perp)\cdot\mathbf{p}_\perp/\hbar}\, G^{(0)}(z,z';E-p_\perp^2/2M) \\ &=\; \frac{1}{2\pi\hbar^2}\int_0^\infty p_\perp\, dp_\perp\, J_0(R_\perp p_\perp/\hbar)\, G^{(0)}(z,z';E-p_\perp^2/2M) \end{aligned} \tag{8.19}$$

Here, $R_\perp = |\mathbf{r}_\perp - \mathbf{r}'_\perp|$ denotes the projection of the distance on the $x-y$ plane, and $J_0(z)$ presents the regular Bessel function of order zero [81]. Noting that the one-dimensional Green function appearing in (8.19) may be constructed by matching properly selected eigenfunctions of the background potential $U_0(z)$ at the source position $z = z'$ (this procedure is laid out in detail in Appendix A.4), we conclude that the "background" Green function $G^{(0)}(\mathbf{r},\mathbf{r}';E)$ is available from these eigenfunctions by means of a single quadrature. Nevertheless, explicit expressions are known only for two most basic potentials, both of which are considered in this volume, viz., the free-particle Green function $G^{(\mathrm{free})}(\mathbf{r}-\mathbf{r}';E)$ (Appendix C.1), and the ballistic Green function $G(\mathbf{r},\mathbf{r}';E)$ of the uniform force field problem $U(\mathbf{r}) = -Fz$ which we extensively studied in Chapter 5. We will use the latter solution as a crude approximation to the Green function belonging to the actual bulk-vacuum transition potential $U_0(z)$ in our example STM simulations (Section 8.3).

Following this interlude, we again take up the discussion of equation (8.17). Recognizing that $\psi_{lm}^{(\mathrm{out})}(\mathbf{r},\mathbf{r}';E) = \lambda_{lm}(E)\, G_{lm}(\mathbf{r},\mathbf{r}';E)$ is just a multiple of the multipole Green function to the full potential $U(\mathbf{r})$ (8.3), application of (2.14) to (8.17) yields:

$$\psi_{lm}^{(\mathrm{out})}(\mathbf{r},\mathbf{r}';E) \;=\; \lambda_{lm}(E)\left\{G_{lm}^{(0)}(\mathbf{r},\mathbf{r}';E) \;+\; \int d^3r''\, G^{(0)}(\mathbf{r},\mathbf{r}'';E)\, W(\mathbf{r}'')\, G_{lm}(\mathbf{r}'',\mathbf{r}';E)\right\} \tag{8.20}$$

We note that (8.20) does not present a true solution to (8.17) as the Green function $G_{lm}(\mathbf{r},\mathbf{r}';E)$ appears on both sides of this equation. (A formal derivation of (8.20) in the framework of functional analysis is presented in Appendix A.3.6.)

From (8.20), it is easy to assign the partial conductivities $\sigma^{(0)}_{lm}(z_0)$, $\Delta\sigma_{lm}(x', y', z_0)$ introduced in (8.15). For this purpose, we first calculate the intrinsic current $J^{(\mathrm{out})}_{lm}(\mathbf{r}'; E)$ carried by the wave function $\psi^{(\mathrm{out})}_{lm}(\mathbf{r}, \mathbf{r}'; E)$. Following the prescription specified in Section 2.4, we end up with a decomposition of the current (8.4):

$$J^{(\mathrm{out})}_{lm}(\mathbf{r}'; E) \;=\; -\frac{2}{\hbar}\,|\lambda_{lm}(E)|^2 \lim_{\mathbf{r}\to\mathbf{r}'} \Im\left[K^*_{lm}\left(\frac{\partial}{\partial\mathbf{r}}\right) K_{lm}\left(\frac{\partial}{\partial\mathbf{r}'}\right) G^{(0)}(\mathbf{r}, \mathbf{r}'; E) + (-1)^m \int d^3r''\, \mathfrak{G}^{(0)}_{l,\,-m}(\mathbf{r}, \mathbf{r}''; E)\, W(\mathbf{r}'')\, G_{lm}(\mathbf{r}'', \mathbf{r}'; E)\right] \tag{8.21}$$

In this formula, $\mathfrak{G}^{(0)}_{lm}(\mathbf{r}, \mathbf{r}''; E)$ denotes the spherical tensor gradient of the retarded Green function $G^{(0)}(\mathbf{r}, \mathbf{r}''; E)$ with respect to the first variable $\mathbf{r}$:

$$\mathfrak{G}^{(0)}_{lm}(\mathbf{r}, \mathbf{r}''; E) \;=\; K_{lm}\left(\frac{\partial}{\partial\mathbf{r}}\right) G^{(0)}(\mathbf{r}, \mathbf{r}''; E) \tag{8.22}$$

In contrast to the conceptionally related multipole Green functions $G_{lm}(\mathbf{r}, \mathbf{r}'; E)$ (2.24), $\mathfrak{G}^{(0)}_{lm}(\mathbf{r}, \mathbf{r}'; E)$ generally is not a solution to a simple inhomogeneous Schrödinger equation. For the ballistic problem $U(\mathbf{r}) = -Fz$, the spherical tensor gradients (8.22) have been displayed in closed form (5.38) in Section 5.3.5. In passing, we note that in (8.21) we utilized the mathematical identity $K_{lm}(z)^* = (-1)^m K_{l,\,-m}(z)$ (see e. g. the textbook by Messiah [83], p. 495).

Let us now analyze (8.21) in terms of the conductivities defined in (8.15). Equation (8.11) shows that $\sigma_{lm}(\mathbf{r}'; E_F)$ differs from the intrinsic current (8.21) only by an additional factor e^2. By comparison, the first term in (8.21) is seen to represent the conductivity that would arise in the sole presence of the bulk-vacuum transition potential $U_0(z)$. Hence, it provides the featureless background conductivity $\sigma^{(0)}_{lm}(z_0)$ in the decomposition (8.15):

$$\sigma^{(0)}_{lm}(z_0) \;=\; -\frac{2e^2}{\hbar}\,|\lambda_{lm}(E_F)|^2 \lim_{\mathbf{r}\to\mathbf{r}'} \Im\left[K^*_{lm}\left(\frac{\partial}{\partial\mathbf{r}}\right) K_{lm}\left(\frac{\partial}{\partial\mathbf{r}'}\right) G^{(0)}(\mathbf{r}, \mathbf{r}'; E_F)\right] \tag{8.23}$$

Thus, the remaining part of (8.21) forms the corrugative contribution $\Delta\sigma_{lm}(x', y', z_0)$ to the zero-bias conductivity:

$$\Delta\sigma_{lm}(x', y', z_0) \;=\; -\frac{2e^2}{\hbar}\,|\lambda_{lm}(E_F)|^2\,(-1)^m \;\times \Im\left[\int d^3r''\, \mathfrak{G}^{(0)}_{l,\,-m}(\mathbf{r}', \mathbf{r}''; E_F)\, W(\mathbf{r}'')\, G_{lm}(\mathbf{r}'', \mathbf{r}'; E_F)\right] \tag{8.24}$$

Both expressions (8.23) and (8.24) still contain the source strength parameter $|\lambda_{lm}(E_F)|^2$ which is not supplied by the simple source model of STM presented previously. We

remark, however, that this unknown quantity drops out from the relative conductivity corrugation $\Delta\sigma_{lm}(x', y', z_0)/\sigma^{(0)}_{lm}(z_0)$. A more serious problem is posed by the presence of the multipole Green function $G_{lm}(\mathbf{r}'', \mathbf{r}'; E_F)$ belonging to the full potential $U(\mathbf{r})$ in the integrand of (8.24). In general, this expression, in contrast to $G^{(0)}(\mathbf{r}, \mathbf{r}'; E_F)$ (8.19), will not be accessible in a computationally inexpensive manner. Thus, the use of approximation schemes which express $G_{lm}(\mathbf{r}, \mathbf{r}'; E)$ in terms of the background Green function $G^{(0)}(\mathbf{r}, \mathbf{r}'; E)$ is advisable here. We will present two different approaches in Section 8.3.

Finally, we turn our attention to the constant current mode of STM. We have seen that in this operation mode, the tunneling current I_0, and thus the conductivity σ_0, is kept fixed. This is achieved by readjusting the tip-sample distance; the required interval, the corrugation amplitude $\Delta z'(x', y'; \sigma_0)$, provides a topographic image of the scanned surface. Obviously, the relation of the corrugation amplitude to the partial conductivities $\sigma^{(0)}_{lm}(z')$, $\Delta\sigma_{lm}(x', y', z')$ (8.23), (8.24) gained in the source description of the constant height mode of STM is of considerable interest. Inserting $\Delta z'(x', y'; \sigma_0)$ into the decomposition (8.15), we obtain the implicit relation:

$$\sigma_0 \;=\; \sigma_{lm}\left[x', y', z_0 + \Delta z'(x', y')\right] \;=\; \sigma^{(0)}_{lm}\left[z_0 + \Delta z'(x', y')\right] + \Delta\sigma_{lm}\left[x', y', z_0 + \Delta z'(x', y')\right] \tag{8.25}$$

which in general must be solved numerically for $\Delta z'(x', y'; \sigma_0)$. However, equation (8.25) finds a quite simple interpretation in the limit of small corrugation amplitudes, $\Delta z'(x', y'; \sigma_0) \to 0$. Then, also $\Delta\sigma_{lm}(x', y'; z_0)$ must become small, and linearization of (8.25) is in order. Since for vanishing corrugation, $\sigma_0 = \sigma^{(0)}_{lm}(z_0) = \text{const.}$ holds, we may replace (8.25) by the expression:

$$\sigma_0 \;=\; \sigma_0 + \left.\frac{\partial\sigma^{(0)}_{lm}(z')}{\partial z'}\right|_{z' = z_0} \Delta z'(x', y'; \sigma_0) + \Delta\sigma_{lm}(x', y', z_0) + \mathcal{O}(\Delta z'^2) \tag{8.26}$$

In the next step, we note that the background conductivity $\sigma^{(0)}_{lm}(z')$ decays exponentially with increasing tip-surface distance. Indeed, we already performed a semiclassical calculation for the corresponding intrinsic multipole current $J^{(0)}_{lm}(z'; E)$ in the framework of the minimum uncertainty model before (Section 7.2.3). Formula (7.50) shows that $\sigma^{(0)}_{lm}(z')$ is essentially governed by the WKB penetrability factor due to the bulk-vacuum transition potential $U_0(z')$. Hence, we find:

$$\left.\frac{\partial\sigma^{(0)}_{lm}(z')}{\partial z'}\right|_{z' = z_0} \approx\; -\frac{2}{\hbar}\left.\frac{\partial W_{\mathrm{cl}}(0, z'; E)}{\partial z'}\right|_{z' = z_0} \sigma^{(0)}_{lm}(z_0) \;=\; -\,2\kappa(z_0)\,\sigma^{(0)}_{lm}(z_0) \tag{8.27}$$

where $\kappa(z_0)^2 = 2M[U_0(z_0) - E]/\hbar^2$ is the binding wave number at the tip position and typically of order $\kappa(z_0) \sim 1\,\text{Å}^{-1}$. (In their pioneering study of Au surfaces, Wintterlin

et al. [74] experimentally obtained $\kappa(z') \sim 0.95\,\text{Å}^{-1}$ throughout their scanning range.) Solving (8.26) for the corrugation amplitude $\Delta z'(x', y'; \sigma_0)$, we arrive at the simple relation:

$$\Delta z'(x', y'; \sigma_0) \approx \frac{1}{2\kappa(z_0)} \frac{\Delta\sigma_{lm}(x', y', z_0)}{\sigma_0} \tag{8.28}$$

where $\sigma_0 = \sigma_{lm}^{(0)}(z_0)$. It is noteworthy that $\Delta z'(x', y'; \sigma_0)$ in the small-corrugation limit does not depend on the source strength $|\lambda_{lm}(E)|^2$, i. e., the free parameter of the STM source model. The range of validity of the approximation (8.28) is limited by the exponential character of the background conductivity $\sigma_{lm}^{(0)}(z')$: The corrugation amplitude $\Delta z'(x', y', z_0)$ should be much smaller than the decay length governing $\sigma_{lm}^{(0)}(z')$, which leads to the condition $2\kappa(z_0)\,\Delta z'(x', y', z_0) \ll 1$. Thus, the corrugation amplitude should not exceed $\Delta z' \sim 0.2\,\text{Å}$. These small corrugations are typical of smooth metal surfaces and have been regularly resolved experimentally during the past decade [73,74].

8.1.3 Resolution Estimate for the STM

Apart from the practical problem of determining the Green function $G_{lm}(\mathbf{r}, \mathbf{r}'; E_F)$ for the STM junction environment potential $U(\mathbf{r})$, a complete mathematical description of the source theory of STM is contained in (8.23), (8.24), and (8.28). (A simple model for the source strength parameter $|\lambda_{lm}(E_F)|^2$ which remains unspecified within the source approach will be presented in Section 8.2.) However, these formal results are not easily grasped and thus offer little assistance in understanding the imaging mechanism in STM. Therefore, within this section we want to develop a pictorial representation of the scattering process underlying STM which is founded upon the minimum uncertainty model for multidimensional tunneling phenomena outlined in Chapter 7 of this treatise.

There, we have seen that the exponential suppression of tunneling trajectories deviating from the escape path leads to the formation of a narrow current filament emitted by the point source which, in the STM setup, is intersected by the sample surface near the "end of the tunnel." Thus, we may imagine the sample being "illuminated" by an electronic "spotlight," i. e., a current density distribution $j_z(\mathbf{r}, \mathbf{r}'; E)$ which approximately is of generalized Gaussian shape (7.48). Locally, this overall current density whose characteristic parameters are entirely determined by the background potential $U_0(z)$ describing the bulk-vacuum transition is modulated by the details of the sample surface structure which are summarized in the corrugative part $W(\mathbf{r})$ of the potential. The situation is depicted in Figure 25. During the scanning process, different parts of the surface are irradiated by the current filament. Depending on the tip position, the surface-modulated current density in the "spot" will add up to a slightly

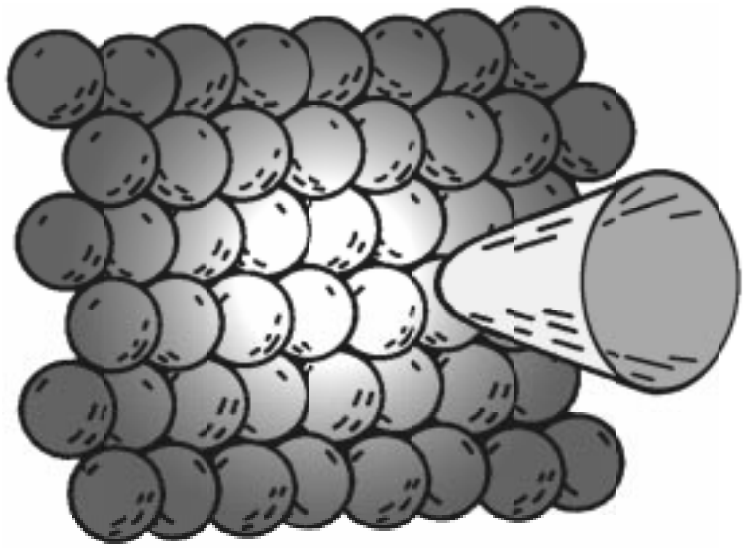

Figure 25: The "spotlight" model of STM. Electrons emitted by the tip impinge on a tightly confined surface section centered below the tip; the electron density distribution is approximately Gaussian.

varying total integrated current $I(\mathbf{r}')$, and this variation in turn renders the STM image. It is seen that the image formation in STM results from an averaging process; details in the surface potential structure whose characteristic length scale falls much below the width ΔR of the Gaussian current profile are averaged out and will not appear in the data. Naturally, this effect limits the resolving power of the STM to structures whose size is of order ΔR, and a successful attempt to reduce the value of this quantity will enhance the corrugation observed on any given probe surface.

We will now become more specific and transform these considerations into a simple mathematical model. Ahead, let us note that multipole current contributions originating from $|m| > 0$ orbitals are additionally suppressed through the centrifugal contribution to the tunneling barrier $U_0(z)$ (see Section 7.2.3), and thus usually play but a minor role in the formation of the STM image. (This assertion will be confirmed in Section 8.2.3 where we will study the multipole dependence of the background conductivities $\sigma_{lm}^{(0)}(z)$ for two different model potentials $U_0(z)$.) Therefore, we will limit our presentation to longitudinal ($m = 0$) multipole point sources. According to the minimum uncertainty model (Section 7.2), the current density distribution $j_{l00}(\mathbf{r}, \mathbf{r}'; E)$ due to a multipole point source of orbital quantum number l is approximately given by a simple Gaussian:

$$j_{l00}(\mathbf{r}, \mathbf{r}'; E) \approx \alpha^2 \lambda^2 \exp(-\lambda^2 R^2) \tag{8.29}$$

where $\mathbf{R} = \mathbf{r}'_\perp - \mathbf{r}_\perp$ denotes the lateral displacement vector from the center of the distribution (i. e., R is the distance of the position $\mathbf{r}$ from the escape path in tunneling),

and $\lambda = 1/\Delta R$ is the inverse width of the Gaussian which to a certain degree depends on the source orbital character (see Section 7.3).

In our model, the "spotlight" (8.29) scans a periodically structured crystal surface whose corrugative potential $W(\mathbf{r})$ may be expanded into a discrete Fourier series in the lateral directions:

$$W(\mathbf{r}) \;=\; \sum_{j,\,k}{}' \; u_{jk}(z)\; \exp(i\,\mathbf{G}_{jk}\cdot\mathbf{r}_\perp) \tag{8.30}$$

Here, the symbols $u_{jk}(z)$ denote the Fourier components of the potential; the prime indicates that the summation should exclude the index pair $(0,0)$, and

$$\mathbf{G}_{jk} \;=\; j\mathbf{G}_1 + k\mathbf{G}_2 \tag{8.31}$$

presents a reciprocal lattice vector of the surface. The primitive vectors $\mathbf{G}_1$, $\mathbf{G}_2$ span the unit cell in momentum space and may be related to a set of surface basis vectors $\mathbf{a}_1$, $\mathbf{a}_2$ via the condition $\mathbf{G}_m \cdot \mathbf{a}_n \;=\; 2\pi\,\delta_{mn}$ for $m,n \;=\; 1,2$ [166]. In particular, for a rectangular unit cell, $G_m \;=\; 2\pi/a_m$ holds. (The more realistic case of surfaces whose point symmetry group is hexagonal will be extensively discussed in Section 8.3.1.) In passing, we note that the Fourier component $u_{00}(z)$ omitted in (8.30) presents a translationally invariant contribution to the potential $U(\mathbf{r})$ and thus is properly enclosed within the background potential $U_0(z)$ in (8.16).

The Gaussian estimate. For simplicity, let us assume a linear dependence of the corrugative part $\Delta j_{l00}(\mathbf{r},\mathbf{r}';E)$ of the current density distribution on the potential $W(\mathbf{r})$ (see also Section 8.3.2):

$$\Delta j_{l00}(\mathbf{r},\mathbf{r}';E) \;\propto\; W(\mathbf{r})\, j^{(0)}_{l00}(\mathbf{r},\mathbf{r}';E) \tag{8.32}$$

As we have seen, the STM is sensitive only to the total zero-bias conductivity variation $\Delta\sigma_{l0}(\mathbf{r}')$ (8.24) recorded by the multipole tip which is available from (8.32) by integration. (Here, we consider the constant height operation mode of STM.) Assuming that the corrugative potential $W(\mathbf{r})$ is essentially limited to the uppermost surface layer $z \;=\; z_0$, we may exploit the invariance of $G^{(0)}_{l0}(\mathbf{r},\mathbf{r}';E_F)$ with respect to lateral shifts $\mathbf{R}_\perp$ and represent the change of conductivity in the form of a two-dimensional convolution integral:

$$\Delta\sigma_{l0}(\mathbf{r}') \;\propto\; \int d^2r_\perp\, W(\mathbf{r}_\perp, z_0)\, j^{(0)}_{l00}(\mathbf{r}'_\perp - \mathbf{r}_\perp; z_0, z'; E_F) \tag{8.33}$$

Since z_0 will be located close to the classical turning surface for the background barrier potential $U_0(z)$, we may adopt the Gaussian profile (8.29) for the current density

due to $U_0(z)$ predicted by the minimum uncertainty model of tunneling. Then, it is straightforward to evaluate (8.33), and we obtain the simple result:

$$\Delta\sigma_{l0}(\mathbf{r}') \;\propto\; \pi\alpha^2 \sum_{j,\,k}{}' \; u_{jk}(z_0)\; \exp(-\,G_{jk}^2/4\lambda^2)\; \exp(i\,\mathbf{G}_{jk}\cdot\mathbf{r}'_{\perp}) \tag{8.34}$$

It is seen that the current variation in the $x-y$ scan faithfully reproduces the periodicity of the surface potential $W(\mathbf{r})$ (8.30). Due to averaging, however, Fourier components of the potential $u_{jk}(z)$ with small periodicity (large G_{jk}) fade away; they are exponentially suppressed in the STM image. We infer that details of the surface structure are easily resolved if the condition $G_{jk} \lesssim 2\lambda$ holds; otherwise, $u_{jk}(z_0)$ will deliver rapidly diminishing contributions (which may nevertheless be detected if the background noise is kept at a sufficiently low level). Clearly, in this regime the STM resolving capability depends in a particularly sensitive manner on the spot width parameter λ. In physical space, we may define a characteristic resolution estimate a by:

$$a \;\sim\; 2\pi/G \;\sim\; \pi/\lambda \tag{8.35}$$

Let us now provide a typical numerical value for a that is valid for common experimental conditions.

According to the semiclassical minimum uncertainty model, λ is determined by the instanton (or bounce) tunneling time $\tau_B(E)$ between tip and sample surface (7.41):

$$a_{\rm sc}(E) \;\sim\; \pi\,\sqrt{\frac{\hbar\,\tau_B(E)}{M}} \tag{8.36}$$

Note that this theory (Chapter 7.2) predicts a spotwidth $1/\lambda$, and thus a resolution estimate $a_{\rm sc}(E)$, which are independent of the orbital quantum number l. We may now use this formula to calculate $a_{\rm sc}(E)$ for two limiting cases of the background potential distribution $U_0(z)$. In ballistic tunneling, we found $\tau_B(E) = \hbar\kappa/F$ (7.26), where $E = -\hbar^2\kappa^2/2M$. Let us set $z' = 0$; if one chooses to place the corrugative potential at the turning surface, then $F = -E/z_0$, and (8.36) becomes:

$$a_{\rm ball}(E) \;\sim\; \pi\,\sqrt{2z_0/\kappa} \tag{8.37}$$

The linear potential presents a fairly shallow tunneling barrier. It is obviously of interest to study also the opposite extreme which is taken on for an abrupt bulk-vacuum transition potential $U_0(z)$ at $z = z_0$, i. e., a rectangular step barrier of height $\Phi = \hbar^2\kappa^2/2M$. Here, $\tau_B(E) = Mz_0/\hbar\kappa$, and according to (8.36), it follows that:

$$a_{\rm step}(E) \;\sim\; \pi\,\sqrt{z_0/\kappa} \tag{8.38}$$

(For simplicity, we again assume that $z' = 0$.) Compared to (8.37), the resolution estimate only improves by a factor of $\sqrt{2}$. Even this reduction appears somewhat exaggerated in view of the fact that the rectangular step barrier suppresses tunneling more efficiently than the triangular one does. In the minimum uncertainty model, the total current (7.50), and therefore also the background conductivity $\sigma_{l0}^{(0)}(z_0)$, is essentially controlled by the one-dimensional classical action $W_{\rm cl}(0, z_0; E)$ (7.22) along the tunneling escape path via the WKB penetrability of the barrier $U_0(z)$; for ballistic tunneling (7.52), we find $W_{\rm cl}^{(\rm ball)}(0, z_0; E) = \hbar^3\kappa^3/3MF = 2\hbar\kappa z_0/3$, whereas $W_{\rm cl}^{(\rm step)}(0, z_0; E) = \hbar\kappa z_0$ holds in the rectangular barrier case. To achieve roughly equal total currents at fixed distance z_0, it appears sensible to replace κ by $\kappa' = 2\kappa/3$ in (8.38). Then, the results (8.37) and (8.38) differ only by a factor $2/\sqrt{3}$. As realistic bulk-vacuum transition potentials will fall somewhere between the extreme model barriers examined here, it is seen that the predicted resolution in STM will depend only weakly on the detailed shape of the background potential $U_0(z)$, and we may give a general prediction for the value of a. For energies of order $E \approx -4\,$eV (a typical work function for many metals), we obtain a resolution estimate for the STM of roughly $a \sim 4\sqrt{z_0}$ Å, where z_0 is the tip-sample separation in Angstrom. This is consistent with the observation that surface steps and surface reconstructions are routinely recorded from the very beginnings of STM [72].

According to the expression (8.34), the resolution of objects of smaller scale than a in STM strongly depends on the size of the electron "spotlight" ΔR. Even a small reduction of the size of the electron distribution will result in a drastic enhancement of the contrast in the STM image. In Section 7.3, we have seen that at least in the case of ballistic tunneling, the spot radius will diminish with increasing orbital quantum number l. Thus, these multipole sources should offer better resolution properties. This expectation is empirically corroborated by the common usage of transition metals, in particular tungsten and iridium, as base materials for tips; at their respective Fermi energies, the electronic structure of these metals is dominated by d–bands ($l = 2$) [166].

But the simple formula (8.34) manifestly cannot account for the atomic resolution observed on smooth low-index metal surfaces [73,74] for which the suppression factor $\exp(-G_{jk}^2/4\lambda^2)$ even for narrowly emitting d–wave sources ($1/\lambda = \Delta R \sim 2\,$Å) (Figure 19) and the lowest reciprocal lattice vectors $\mathbf{G}_{jk}$ falls below 0.01 (for the determination of $\mathbf{G}_{jk}$ in these surfaces, see Section 8.3.1). In this exponential regime, the Gaussian model (8.29) is inadequate, and we must take refuge to a more sophisticated representation of the tunneling current distribution.

Corrugation in the exponential regime. To obtain a realistic description of the STM imaging behavior for surface details that vary on a scale smaller than (8.35), we have to abandon the convenient Gaussian current density approximation (8.29) and replace it by a more accurate estimate: In the course of the averaging process, the conductivity

variation $\Delta\sigma_{l0}(\mathbf{r}')$ (8.24) becomes small with respect to the average background conductivity $\sigma_{l0}^{(0)}(z_0)$ (8.23), so even minute deviations of the minimum uncertainty model from the actual current distribution may cause large relative errors in $\Delta\sigma_{l0}(\mathbf{r}')$. In particular, this condition affects the tails of the current density distribution $j_{l00}(\mathbf{r},\mathbf{r}';E)$ for large lateral distances $R_\perp$ where the paraxial Gaussian approximation increasingly fails. Let us now show how an improved estimate for the ballistic current distribution leads to a resolution suppression factor in (8.34) which behaves more moderate than the Gaussian model with its spuriously high efficience in averaging.

For this purpose, we employ the exact current distribution $j_{000}(\mathbf{r},\mathbf{o};E)$ (E.8) generated by an isotropic s–wave source in the uniform field environment. Since we are interested in an analytic estimate for the resolution behavior, we replace the Airy functions appearing in this rather complicated formula by their asymptotic limit (Appendix D.1). This procedure results in a simplified form for $j_{000}(\mathbf{r},\mathbf{o};E)$ that could have been obtained also from the semiclassical WKB theory of multidimensional ballistic tunneling put forward in Section 7.1.1:

$$j_{000}(\mathbf{r},\mathbf{o};E) \;\sim\; \frac{M\sqrt{M}F}{64\,\pi^3\hbar^4}\,\frac{r+z}{r^2}\,\frac{\exp\left\{-\frac{2\sqrt{M}}{3\,\hbar F}\,[F(r-z)-2E]^{3/2}\right\}}{\sqrt{F(r-z)-2E}} \tag{8.39}$$

The kinship of this expression to the semiclassical Green function $G_{\rm sc}(\mathbf{r},\mathbf{o};E)$ (7.9) is obvious. Nevertheless, (8.39) is still too complicated to be suitable for the analytic evaluation of the convolution integral (8.33). Hence, we expand the powers in (8.39) and neglect higher orders in $r-z$, assuming that $r-z \ll |E|/F$. Unlike in the Gaussian model, however, we do not further replace this parabolic coordinate itself:

$$j_{000}(\mathbf{r},\mathbf{o};E) \;\sim\; \frac{M^2F}{32\,\pi^3\hbar^5}\,\exp\left\{-\frac{2}{3}\,\frac{\hbar^2\kappa^3}{MF}\right\}\,\frac{\exp\{-\kappa(r-z)\}}{\kappa r} \tag{8.40}$$

This surprisingly simple expression shares with its Gaussian counterpart (7.10) the notable feature that the lateral profile of the current distribution is independent of the field strength F, yet it presents a far more accurate representation of the actual Green function for large distances $R_\perp$ from the escape path. For the following considerations, we neglect the prefactor in (8.40) as it is irrelevant in the determination of the resolving power of the STM. Following (8.33) and (8.40), the conductivity variation $\Delta\sigma_{00}(\mathbf{r}')$ due to the periodic surface (8.30) in the ballistic model in linear approximation is given by:

$$\Delta\sigma_{00}^{(\rm ball)}(\mathbf{r}') \;\propto\; {\sum_{j,\,k}}' \; u_{jk}(z_0)\,\exp(i\,\mathbf{G}_{jk}\cdot\mathbf{r}'_\perp)\int d^2R_\perp\, e^{-\,i\,\mathbf{G}_{jk}\cdot\mathbf{R}_\perp}\,\frac{e^{-\,\kappa\left(\sqrt{R_\perp^2+z_0^2}-z_0\right)}}{\kappa\,\sqrt{R_\perp^2+z_0^2}} \tag{8.41}$$

(Here, we inserted $(\mathbf{r}-\mathbf{r}')^2 = R_\perp^2 + z_0^2$, and kept $z'=0$ as usual.) This integral may be evaluated in polar coordinates [180]. The angular integration delivers a Bessel func-

tion via $\int_0^{2\pi} d\phi\, e^{i\,\mathbf{G}\cdot\mathbf{r}} = 2\pi\, J_0(Gr)$ [81]. Upon the substitution $\rho = (1 + R_\perp^2/z_0^2)^{1/2}$, the remaining radial integral adopts a form which has been tabulated (No. 6.646.1 in the table by Gradshteyn and Ryzhik [188]). Here, we merely state the final result:

$$\int d^2R_\perp\, e^{-i\,\mathbf{G}_{jk}\cdot\mathbf{R}_\perp}\, \frac{e^{-\kappa\left(\sqrt{R_\perp^2+z_0^2}-z_0\right)}}{\kappa\,\sqrt{R_\perp^2+z_0^2}} \;=\; 2\pi\,\frac{e^{-\,z_0\left(\sqrt{\kappa^2+G_{jk}^2}-\kappa\right)}}{\kappa\,\sqrt{\kappa^2+G_{jk}^2}} \tag{8.42}$$

The suppression factor (8.42) clearly improves the simple estimate $\exp(-G_{jk}^2 z_0/2\kappa)$ which follows in view of (8.37) from the Gaussian model (8.34). As expected, for large-scale features ($G_{jk} \ll \kappa$ or $a \gg 2\pi/\kappa$), both expressions agree; in the exponential regime, however, the corrugation decays much slower than predicted by (8.34): For $G_{jk} \gg \kappa$ or $a \ll 2\pi/\kappa$, the decay constant is essentially linear in G_{jk}, replacing the quadratic dependence of the Gaussian theory. We note that in agreement with the Gaussian estimate, the corrugative part of the conductivity $\Delta\sigma_{00}(\mathbf{r}')$ drops exponentially with the tip-surface distance z_0. (We will examine the performance of the approximation formula (8.42) later in Section 8.3.2.)

A consideration of the local density of states (LDOS) due to the surface Bloch wave functions in a periodic potential (see Section 8.1.4) leads to a formally very similar estimate for the resolution capability of the STM in the opposite case of a rectangular step background potential $U_0(z)$ [78]:

$$\Delta\sigma_{00}^{(\mathrm{step})}(\mathbf{r}') \;\propto\; {\sum_{j,k}}' \; u_{jk}(z_0)\, \exp(i\,\mathbf{G}_{jk}\cdot\mathbf{r}'_\perp)\, \exp\left\{-2z_0\left(\sqrt{\kappa^2+G_{jk}^2/4}\,-\kappa\right)\right\} \tag{8.43}$$

(We again set $z' = 0$.) The abrupt potential step tends to confine the current filament more strongly than the shallower linear potential barrier in (8.42), thus improved resolution (as compared to the case of ballistic tunneling) is consistently found. However, if the reduced transmissivity of the rectangular barrier is properly taken into account (see above), the effect is not marked. We finally mention that in the large structure limit $a \gg \pi/\kappa$, the minimum uncertainty model result (8.38) is recovered from (8.43) since the attenuation factor is again approximately Gaussian: $\Delta\sigma_{00}^{(\mathrm{step})}(\mathbf{r}') \propto \exp(-G_{jk}^2 z_0/4\kappa)$.

8.1.4 Relation to Other Theoretical Approaches

Having derived an expression for the zero-bias conductivity $\sigma_{lm}(\mathbf{r}')$ (8.11) and its decomposition into background and corrugative parts $\sigma_{lm}^{(0)}(z')$, $\Delta\sigma_{lm}(\mathbf{r}')$ (8.23), (8.24), our formal representation of the multipole source theory of scanning tunneling microscopy is complete apart from the determination of the proper source strength prefactor $|\lambda_{lm}(E_F)|^2$, a problem we will take up in Section 8.2. We illustrated the physical imaging mechanism behind the source model by means of a simple "spotlight" picture

which nevertheless is able to provide sensible resolution estimates for periodically corrugated surfaces. At this point, it seems advisable to examine the relation of the source approach to STM to its contenders based on various other theoretical models, a number of which have been proposed since the first announcement of a STM experiment in 1982.

For the purpose of a brief review, these theories may be subdivided in various classes with differing approaches to the STM problem. Among the first attempts at a theoretical description were wave scattering models which inquired into the electron distribution found in a vacuum barrier bounded by two "surfaces" with sinelike corrugation, representing the sample and a tip array, respectively (Garcia et al., 1983 [189]; Stoll et al., 1984 [190]). The conventional analysis of this scattering problem using perturbation theory is surprisingly difficult; Stoll et al., however, found that their numerical data on the tip corrugation $\Delta z'$ was fitted well by the Gaussian expression $\Delta z'(z_0) \propto \exp(-G^2 z_0/4\kappa)$ where G presents the wave number of the surface profile, a result that coincides with our prediction obtained from the minimum uncertainty model of tunneling for steplike barriers $U_0(z)$ (8.34), (8.38). Huang et al. [191] proposed to use a multidimensional extension of WKB theory to tackle electron tunneling in the STM junction which is based on complex semiclassical trajectories, a topic we briefly touched upon in Section 4.2 of this work; in practice, however, implementation of this program failed due to insurmountable numerical difficulties [168]. As another formal attempt in this direction we note the very complicated Green function method suggested by Noguera [192].

A quite different theoretical approach to STM whose origins also date back to the time of invention of this device has proven much more fertile, and today is considered the reliable standard in STM theories by most experts in the field. These models are summarizingly labeled "transfer Hamiltonian theories," and their common ancestor is a brief seminal paper published by Tersoff and Hamann in 1983 [77]. In this contribution, these authors adapted a perturbation theory for the tunneling current, the "transfer Hamiltonian" approach which was originally devised by Bardeen [193] to describe electron transport through a planar tunneling junction (the superconducting SIS diodes first examined by Giaever [194]), to the peculiar geometry of the STM setup. (For a detailed discussion of the transfer Hamiltonian formalism, we refer to an article by Duke [195].) Assuming an isotropic s–wave current distribution in the vicinity of the tip, Tersoff and Hamann found that the zero-bias conductivity of the STM junction should be proportional to the local density (LDOS) of sample surface states $n(\mathbf{r}'; E_F)$ (8.14), (A.152) at the center of curvature $\mathbf{r}'$ of the (extended) tip. Clearly, this result is in agreement with the source-theoretical prediction (8.13) if $\mathbf{r}'$ is identified with the position of the isotropic point source $\delta_{00}(\mathbf{r} - \mathbf{r}')$, and the tip contribution to the total STM junction potential $U(\mathbf{r})$ is ignored. Indeed, the theory of Tersoff and Hamann implicitly contains many elements of the quantum source formalism presented in Section 2.3,

so it should not come as a surprise that the equivalence of both methods may be formally proven using the mathematical apparatus of functional analysis. This program is carried out in Appendix A.6.3.

Using their result that the junction conductivity $\sigma_{00}(\mathbf{r}')$ for an s–wave tip is proportional to the LDOS $n(\mathbf{r}';E_F)$, Tersoff and Hamann further concluded that the corrugation amplitude $\Delta z'(x',y';\sigma_0)$ (8.28) for a sinelike surface structure (wave vector $\mathbf{G}$) should exponentially decay like (8.43) [78]. The transfer Hamiltonian formalism was considerably extended by Chen [182–184] who pioneered in the investigation of tip states with nonspherical symmetry, i. e., p– and d–orbitals. Using a quite complicated scheme, Chen was able to show that in the transfer Hamiltonian model, a tip state with (l,m) orbital symmetry will collect a STM current which is proportional to the density of the corresponding spherical tensor gradients $K_{lm}(\partial/\partial\mathbf{r}')\,\psi_{\mu_1,\mu_2,\ldots,\mu_n}(\mathbf{r}')$ of the unperturbed eigenstates of the sample with energy E_F, evaluated at the center of curvature $\mathbf{r}'$ of the tip. Obviously, this result again agrees with the prediction of multipole source theory for $\sigma_{lm}(\mathbf{r}')$ (8.12) if $U(\mathbf{r})$ is identified with the sample potential. From his model, Chen concluded that the resolution of the STM will drastically improve with increasing orbital angular momentum quantum number l of the tip state for small objects (i. e., in the exponential regime $a \ll a_{\mathrm{sc}}(E)$ (8.36) considered in the preceding section), and explained the atomic resolution achieved on densely packed metal surfaces [73,74] with the d–wave character of the tips used in these experiments. From our analysis of ballistic tunneling (Chapter 7), we know that the width of the electronic "spotlight" in uniformly accelerated motion shrinks with increasing l (Figure 19), and we will see in the example section (Section 8.3) that this mechanism indeed results in a remarkable enhancement of the calculated corrugation. It was furthermore noted by Chen that tunneling from orbital states with $|m| > 0$ is suppressed and thus usually may be neglected in the simulation of STM images; we performed a detailed study of the consequences of an additional centrifugal barrier in multidimensional tunneling in the course of our analysis of the minimum uncertainty model which confirms Chen's qualitative assessment (see (7.50) and Figure 20). The monograph by Chen [176] presents a comprehensive source of information on the Tersoff-Hamann approach to STM and its further extensions.

Let us note several applications of the transfer Hamiltonian model which are of interest in the context of the multipole source theory of STM. We start out with an insightful examination of the resolution capability of the STM conducted by Sacks et al. [196]. The authors studied the changes of the electronic LDOS occurring when deforming a free electron gas surface adjacent to a steplike tunneling barrier; they found that the LDOS obeys a decay law $n(z_0;E) \propto \exp(-2\kappa z_0)/z_0$ in accordance with our findings (7.50) from the minimum uncertainty model (Section 7.2). A sinelike surface corrugation will be faithfully reproduced in the STM image, but the recorded corrugation will be subject to exponential attenuation: $\Delta z'(z_0) \propto \exp(-G^2 z_0/4\kappa)$. In

contrast, an abrupt surface step of fixed height will cause the tip to withdraw an equal distance, yet the transition is blurred and takes place on a length scale $a \sim \sqrt{8z_0/\kappa}$. Both observations are compatible with our simple spotlight model for the resolution of a STM, as comparison with (8.34) and (8.38) shows. Lawunmi and Payne [197] have pointed out the importance of multipole current contributions in the explanation of so-called "giant corrugations," which have been observed on layered materials, in particular graphite.

The transfer Hamiltonian formalism was further validated in a series of spectacular experiments performed by Don Eigler and his colleagues. Having succeeded in the controlled manipulation of adsorbed atoms using the STM in 1990 [198], the group used this experimental technique to construct "quantum corrals," closed chains of Fe atoms formed as an adsorbate on top of a *fcc*–(111) Cu surface (for the geometry of these surfaces, see Section 8.3.1). These atoms are able to couple the surface states of the Cu surface (these states are localized in a thin surface layer and evanescent in both the bulk and vacuum directions, see the textbook by Zangwill [199], p. 72) to the ordinary bulk states of the Cu crystal, which makes these surface states visible in STM (note that a pure surface state carries no current in the z direction and thus does not contribute to the STM current). According to Tersoff-Hamann theory, the tip records the density of current-carrying states at E_F, which leaves out those surface states that do not couple to the Fe adsorbate atoms, i. e., states whose wave function vanishes along the Fe chain and thus are eigenstates of the corresponding hard-wall quantum corral. Hence, the STM image presents a "negative" exposure of the quantum corral eigenstates whose energy may be selected through the choice of STM bias voltage V. The impressive images of these states have aroused much interest, also outside the scientific community [200–203]. As a recent example of the application of the Tersoff-Hamann model in interpreting STM images we briefly mention the both experimental and theoretical work performed by Sacks et al. [204] on the electronic structure of transition metal dichalcogenides. These peculiar composites which form distinctively layered substrates (the well-known lubricant molybdenum disulfide MoS_2 presents an example) may undergo a transition at low temperatures whereby the hexagonal unit cell of the high-temperature phase (lattice constant a) reorders into a superstructure (hexagonal unit cell, lattice constant $3a$). This conversion which is mediated by electron-lattice interactions serves to reduce the density of electronic states near E_F, but also causes a characteristic oscillatory LDOS component with wavelength $3a$, known as the charge density wave (CDW). In accordance with Tersoff-Hamann theory, in the STM image the CDW is seen as a corrugation wave superimposing the periodic pattern generated by the surface structure of the former unit cell. This example demonstrates that STM corrugation profiles do not necessarily reflect the geometry of the scanned surface.

Let us now turn our attention to approaches to the STM problem which do not

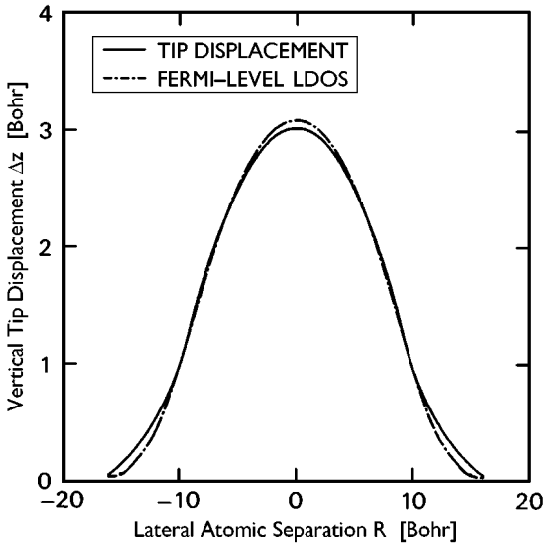

Figure 26: Corrugation amplitude vs. LDOS contour in the STM model devised by Lang [206]. The figure displays the vertical deflection $\Delta z'(R)$ while scanning a plane jellium surface ($r_s = 2$ Bohr) with an adsorbed Na atom past an identical counterelectrode where the tunneling current is kept fixed. The original intersurface separation is $z_0 = 16$ Bohr. (1 Bohr $= 0.529$ Å.)

aim at a general description of the tunneling current under varying circumstances but concentrate onto specific setups. Among the earliest studies in this direction were the LDA calculations performed by Lang [205–207]. Starting out with a scheme very similar to his simulations of the field emission problem (which we extensively quoted in Section 7.3.3), Lang devised a STM model consisting of a sodium atom adsorbed to a plane jellium gas surface ($r_s = 2$ Bohr, which amounts to a work function $\Phi = 3.89$ eV [167]) acting as the "tip," which faces another plane jellium surface oriented in parallel. To this surface, a further adsorbate atom is attached (the "sample"). In a "scan," these surfaces are shifted laterally with respect to each other; their distance is varied as to maintain a constant tunneling current (constant current mode of STM). Initially, for large lateral separation of the atoms, the intersurface distance is fixed at $z_0 = 16$ Bohr (8.46 Å). Eigenfunctions of both hemispheres are calculated using the density functional method (LDA); the corresponding tunneling current is determined in the Bardeen approximation [193,195].

Figure 26 displays the corrugation $\Delta z'(x', y', z_0)$ obtained in Lang's model as a function of the lateral atomic distance if both adsorbed atoms are chosen as sodium. (Other tip/adsorbate atomic combinations yield curves of very similar shape although the absolute corrugation amplitude differs. The pattern may even be inverted.) It is found that the tip deflection fairly closely follows the LDOS contour in this system which corroborates the validity of the Tersoff-Hamann approximation. We also note

that both curves may be roughly fitted by a Gaussian of width $\Delta R \sim 5.5\,\text{Å}$. This is quite large compared to the naive prediction of the minimum uncertainty model $\Delta R \sim \sqrt{z_0/\kappa} \sim 2.9\,\text{Å}$ (8.38). This discrepancy indicates that the tunneling barrier $U_0(z)$ for the selected separation z_0 already deviates massively from its far-field vacuum value Φ. (Another possible explanation involves the fact that the amplitude $\Delta z'(x', y', z_0)$ cannot be considered small in the sense of (8.28).) A calculation of the effective tunneling barrier height as a function of the surface separation is performed in Ref. [207]. In a certain sense, the simulation by Lang was put into practice by Crommie et al. [208] who performed spatially resolved tunneling spectroscopy of Fe atoms adsorbed on a *fcc*–(111) Pt surface, thereby extracting the induced changes of the LDOS by measuring the conductivity $\sigma(\mathbf{r}')$ of the STM junction as a function of the bias voltage V.

As an even more specialized approach at a theory of STM, we may mention the "quantum chemistry" techniques which start out by modeling tip and surface as clusters of atoms and try to determine the STM current from first principles (where the term "ab initio calculation" should be taken cum grano salis). These methods may provide detailed insight into the current density distribution for a specifically designed setup; apart from their numerical complexity, a troublesome aspect of them is that they fail to deliver useful information on general aspects of the STM problem. Doyen et al. [209] examine the imaging mechanism on the *fcc*–(111) surface of aluminum and note possibly important effects caused by the elastic deformation of the tip in scanning (i. e., those forces responsible for resolution in atomic force microscopy (AFM) [169]), though no further explanation is given. Variations of a standard experiment, STM on graphite surfaces, are the topic of an extensive paper by Tsukada et al. [187] who model the tip as a cluster of tungsten atoms, and vary size and shape of the cluster. They find that clusters with a well-defined topmost tip atom record the surface LDOS, in agreement with Tersoff-Hamann theory; "flattened" clusters containing several emitting atoms generally give rise to abnormal STM images which are difficult to interpret and sensitively depend on the orientation of the cluster, due to interference between the various emitters. Yet it appears unlikely that these "blunt" tips are applied in experiments requiring high resolution. Finally, we mention the technique developed by Joachim et al. [210, 211] who model the junction as a scattering center in a crystalline environment and extract its conductivity from Landauer's formula for low-dimensional conductors (see Section 8.2.2). In their work, the influence of adsorbate electronic states on the imaging behavior of the STM is particularly emphasized. The chemical identification of adsorbate atoms on smooth noble metal *fcc*–(111) surfaces (see Section 8.3) has also been the topic of a recent study by Tilinin et al. [212]; in their article, experimental results obtained for Pd–(111) surfaces are compared to numerical calculations based on a tight-binding Hamiltonian formalism. The authors claim good agreement between experiment and simulation.

Finally, we shall discuss a formalism that appears closely related to the multipole source theory of STM proposed in this treatise, the Green function description devised by Sacks and Noguera in 1991 [213]. In their model, the environment of the STM junction is subdivided into four distinct parts: The surface is separated from the tip by a vacuum barrier, whereas within the tip, a spherical emission region is specially considered. Within this spherical well, the surface wave function may be expanded into spherical electron waves, where the remainder of the tip is treated as a perturbation. Application of the Lippmann-Schwinger equation naturally leads to the (implicit) introduction of multipole Green functions whose strength however is modified (renormalized) due to the finite extension of the source region, an effect we will later achieve through the introduction of regularized pointlike scattering operators (zero-range potentials, see Section 8.3.3). Apart from this modification, the model proposed by Sacks and Noguera confirms the validity of Tersoff-Hamann theory as well as its multipole extension derived by Chen, and emphasizes their connection to the quantum source theory of STM.

8.2 Sources in the Transport Limit

In our presentation of the multipole source theory of STM, we covered all relevant theoretical aspects of the source approach in the preceding section, with a single yet important exception: The effective strength $|\lambda_{lm}(E_F)|^2$ of the multipole source in the final formulae (8.11), (8.23), and (8.24) so far remained undefined. Recalling the idea underlying the introduction of source terms into field theories which we illustrated in Section 2.1 of this work, this apparent shortcoming should not be surprising; it is exactly the inhomogeneous contribution that allows to abstract from the actual physical processes taking place at the tip, modeling electron "generation" instead. Although the parameter $|\lambda_{lm}(E_F)|^2$ plays but a subordinate role in the interpretation of STM images (as is illustrated by the fact that the amplitude corrugation $\Delta z'(x', y'; \sigma_0)$ (8.28) in leading order does not depend on its value), the source description of STM obviously is incomplete without a theory that specifies the source characteristics. We therefore have to set up and examine a microscopic model of the electron transport through the STM tunneling junction which will permit us to extract a numerical value for the source strength coefficient $|\lambda_{lm}(E_F)|^2$. (In a quite similar fashion, we obtained in Section 3.1 the proper intensity of the source λ_{lm} (3.22) for the photodetachment problem by a detailed analysis of photon-ion interaction.)

Thus, let us present a considerably simple line of arguments that leads to an instructive picture of the events taking place at the STM junction, and allows to derive a reasonable estimate for $|\lambda_{lm}(E_F)|^2$. It is based on an unusual concept of mesoscopic conduction which was originally proposed by Landauer some forty years ago [185] but found widespread acceptance only in recent years [186]. We will put forward

the basic idea behind Landauer's approach for the simple model of an idealized one-dimensional conductor in the following section; for a formal derivation of Landauer's formula and a detailed discussion of its extensions, we refer to the monographs written by Datta [79] and Imry [80]. We will show that Landauer's idea may be expressed within the Green function formalism as a simple natural limit that arises through the fermionic nature of the particles emitted from the source: The transfer rate is limited through the Pauli exclusion principle. Mathematically, this condition may be put into a simple statement that shows that the conductivity of the system has a universal upper bound $\sigma_{\rm tr} = 4e^2/h$ (which is exactly four times the quantized conductance standard seen in the integer quantum Hall effect [214]).

In Section 8.2.2, we will extend this result to multipole sources in three spatial dimensions and prove that for each multipole orbital channel, the same upper conductivity bound $\sigma_{\rm tr}$ applies, and derive the corresponding maximum source strength $|\lambda_{lm}(E_F)|^2$ permitted by the Pauli principle. In particular, we will present explicit expressions for free-particle multipole sources (Section 3.2). Finally, in Section 8.2.3 we will exploit these insights to supplement our concept of the STM and consider the tip as an electron "valve" which extracts electrons from the tip body and thus acts as a transport-limited electron sink which in a second step emits these electrons towards the sample surface (or vice versa). This idea, which completes our source model of STM, includes the theory of ideal point contacts as a special case.

8.2.1 Source Theory of One-Dimensional Conductors

We start out our considerations with a brief recapitulation of the conductivity properties of an ideal one-dimensional conductor of length L. Clearly, assuming open boundary conditions, the electronic eigenfunctions within this conductor are given by ($p^2 = 2ME$):

$$\psi_p^{(\pm)}(x) \;=\; \frac{1}{\sqrt{L}} \exp\left(\pm ipx/\hbar\right) \tag{8.44}$$

These eigenfunctions have been normalized as to contain one electron per state. In the next step, we calculate the density of these states $N(E)$ per energy interval $[E; E+dE]$:

$$N(E) \;=\; \frac{2}{2\pi\hbar}\, L \int dp\; \delta[E - E(p)] \;=\; \frac{2ML}{\pi\hbar p} \tag{8.45}$$

In (8.45), we allowed for spin degeneracy. Taking into account that only half of these states will carry current to the right side, the maximum conductivity $\sigma(E)$ of the ideal wire is given with $dE = -e\,dU$, $I^{(+)}(E) = e\,j^{(+)}(E)\,N^{(+)}(E)\,dE$ from (8.44) and (8.45):

$$\sigma(E) \;=\; \frac{\partial I^{(+)}(E)}{\partial U} \;=\; \frac{e^2}{\pi\hbar} \;=\; \sigma_q \;=\; 7.748 \cdot 10^{-5}\,\Omega^{-1} \tag{8.46}$$

Remarkably, σ_q is independent of the electronic energy E and the length L of the conductor. Indeed, (8.46) rather provides information on the process of coupling electrons from the leads into an ideal wire. The inverse of the conductivity σ_q is known as Landauer's quantized resistance [185].

How does this simple theory of conduction reconcile with the theory of quantum sources in the transport limit? Let us recall from the introduction to this section that the Pauli exclusion principle effectively serves to restrict the current emission from a point source, as any state cannot contain more than a single electron. The same property should hold valid for the outgoing-wave states generated by a pointlike source $\delta(z - z')$. In one dimension, these wave functions are simply proportional to the retarded Green function $G(z, z'; E)$:

$$\psi(z; E) \;=\; \lambda(E)\, G(z, z'; E) \tag{8.47}$$

Here, the constant of proportionality is given by the source strength $\lambda(E)$. Mathematically, the Pauli principle now may be expressed through the normalization condition for the continuous spectrum of wave functions (8.47):

$$\int dz\, \psi(z; E)^* \psi(z; E') \;=\; \lambda(E)^* \lambda(E') \int dz\, G(z, z'; E)^* G(z, z'; E') \;\sim\; \delta(E - E') \tag{8.48}$$

Here, orthogonality of Green functions with differing energies $E \neq E'$ has been assumed. (This proposition is reasonable as the Green functions for $z \neq z'$ are themselves eigenfunctions of the one-dimensional Hamiltonian. See also Appendix A.4.)

Let us now again specialize to the case of ideal wires considered above. Inserting a point source $\lambda(E)\, \delta(z - z')$ into the one-dimensional wire, the electrons will move freely to both directions. A symmetric solution to the retarded Green function problem for a free particle in a single dimension may be easily constructed according to the prescriptions laid out in Appendix A.4.3. Here, we just cite the simple result:

$$G^{(\mathrm{free})}(z, z'; E) \;=\; -\frac{iM}{\hbar^2 k}\, \exp\left(ik|z - z'|\right) \tag{8.49}$$

where $k^2 = 2ME/\hbar^2$ as usual ($k > 0$). For the evaluation of (8.48), we have to multiply (8.49) with a converging factor $\exp\left(-\eta|z - z'|\right)$, where $\eta \to 0^+$ is an infinitesimal positive auxiliary quantity. (We repeatedly used this procedure in Appendix A.3.6.) Then, the integration becomes trivial:

$$\begin{aligned} \int dz\, G^{(\mathrm{free})}(z, z'; E)^* G^{(\mathrm{free})}(z, z'; E') \;&=\; \frac{2M^2}{\hbar^4 k^2} \lim_{\eta \to 0^+} \frac{i}{k' - k + i\eta} \\ &=\; \frac{2M^2}{\hbar^4 k^2} \left\{ \pi\, \delta(k' - k) \;+\; i\, \mathrm{PP}\left(\frac{1}{k' - k}\right) \right\} \end{aligned} \tag{8.50}$$

Here, we used a well-known formula (A.192) from distribution theory; $\mathrm{PP}(\dots)$ indicates that an integration of the argument should be carried out as a Cauchy principal value integral. (For a more rigorous justification of (8.50), we refer to Appendix A.3.6, and recommend to consult the booklet by Halperin and Schwartz [215].) For the comparison in (8.48), we shall keep only the singular part in (8.50):

$$\int dz\, G^{(\mathrm{free})}(z,z';E)^* G^{(\mathrm{free})}(z,z';E') \;\sim\; \frac{2\pi M^2}{\hbar^4 k^2}\,\delta(k-k') \;=\; \frac{2\pi M}{\hbar^2 k}\,\delta(E-E') \qquad (8.51)$$

Clearly, this means that an upper bound for the source strength $\lambda(E)$ is given by $|\lambda(E)|^2 = \hbar^2 k/2\pi M$. However, we still have to correct for spin degeneracy in (8.51), hence we obtain:

$$|\lambda_{\mathrm{tr}}(E)|^2 \;=\; \frac{\hbar^2 k}{\pi M} \qquad (8.52)$$

To determine the current $J(E)$ delivered by the source $\lambda_{\mathrm{tr}}(E)\,\delta(z-z')$, we may exploit the general formula (2.17) of Section 2.3.2; recalling that the ensuing conductivity $\sigma_{\mathrm{tr}}(E)$ differs from the outgoing current only by a factor e^2 (8.10), we finally find for the conductivity caused by the point source:

$$\sigma_{\mathrm{tr}}(E) \;=\; -\,\frac{2e^2}{\hbar}\,|\lambda_{\mathrm{tr}}(E)|^2\,\Im\left[G^{(\mathrm{free})}(z',z';E)\right] \;=\; \frac{2e^2}{\pi\hbar} \qquad (8.53)$$

From (8.46), we find that the Pauli exclusion principle limits the flow of electrons from an one-dimensional pointlike source to a maximum rate $\sigma_{\mathrm{tr}} = 2\sigma_q$. Obviously, the additional factor 2 in comparison to (8.46) stems from the bidirectional emission pattern of the source and thus is entirely geometrical in nature. Otherwise, both approaches agree in their results.

8.2.2 The Transport Limit for Multipole Sources

We have seen how the source model in combination with Pauli's exclusion principle recovers Landauer's result regarding the conductivity of ideal one-dimensional conductors. However, in reality all scattering processes take place in three-dimensional configuration space; in particular, the geometry of the STM setup leaves little scope for a description in terms of a one-dimensional approximation. Thus, we shall extend our analysis of the transport limit onto the source strength to the multipole point sources introduced in Section 2.4, and we start out this pursuit with the particularly simple and important case of free-particle multipole sources (Section 3.2; Appendix C).

Let us first deal with the isotropic case $l = m = 0$. Then, the free-particle multipole

Green function $G_{lm}^{(\mathrm{free})}(\mathbf{r},\mathbf{o};E)$ (3.26), (C.17) which we state here again for convenience,

$$G_{lm}^{(\mathrm{free})}(\mathbf{r},\mathbf{o};E) \;=\; -\,\frac{M}{2\pi\hbar^2}\,k^{l+1}\,Y_{lm}(\hat{r})\,h_l^{(+)}(kr) \tag{8.54}$$

with $h_0^{(+)}(z) = e^{iz}/z$ [81] reduces to a simple outgoing spherical wave, and we immediately find for the normalization integral (8.48),

$$\int d^3r\,G_{00}^{(\mathrm{free})}(\mathbf{r},\mathbf{o};E)^*G_{00}^{(\mathrm{free})}(\mathbf{r},\mathbf{o};E') \;=\; \left(\frac{M}{2\pi\hbar^2}\right)^2\,\int_0^\infty dr\,e^{i(k'-k)r} \;\sim\; \frac{M^2}{4\pi\hbar^4}\,\delta(k-k') \tag{8.55}$$

which by comparison with (8.48) leads to a maximum source strength $|\lambda_{00}^{(\mathrm{free})}(E)_{\mathrm{tr}}|^2 = 8\pi\hbar^2/Mk$. (This result already accounts for spin degeneracy.) Interestingly, in comparison to its one-dimensional counterpart (8.52), the wave number k is shifted from the numerator into the denominator of this fraction.

Expanding this result to general multipole sources (2.23) of (l,m) spherical symmetry turns out to be a straightforward exercise. We note that the singular part in the normalization integrals (8.48), (8.55) obviously depends only on the asymptotic behavior of the multipole Green function $G_{lm}^{(\mathrm{free})}(\mathbf{r},\mathbf{o};E)$ (8.54) as $r\to\infty$; hence, for our purposes, we may replace the spherical Hankel function $h_l^{(+)}(kr)$ in (8.54) by its principal asymptotic form $h_l^{(+)}(z) \sim \exp\left[i(z-l\pi/2)\right]/z$ (C.14) which allows to evaluate the integral (8.55) immediately for the general multipole case:

$$\int d^3r\,G_{lm}^{(\mathrm{free})}(\mathbf{r},\mathbf{o};E)^*G_{lm}^{(\mathrm{free})}(\mathbf{r},\mathbf{o};E') \;\sim\; \frac{Mk^{2l+1}}{4\pi\hbar^2}\,\delta(E-E') \tag{8.56}$$

Correcting for spin degeneracy, from (8.48) we thus obtain the following bound for the source strength of a free-particle multipole source:

$$\left|\lambda_{lm}^{(\mathrm{free})}(E)_{\mathrm{tr}}\right|^2 \;=\; \frac{8\pi\hbar^2}{M}\,k^{-\,(2l+1)} \tag{8.57}$$

We see that the source strength $\lambda_{lm}^{(\mathrm{free})}(E)_{\mathrm{tr}}$ decays with increasing wave number k and orbital quantum number l; however, this behavior is compensated by the source efficiency, which for a unit strength multipole source is given by the Wigner law $J_{lm}^{(\mathrm{free})}(E) = Mk^{2l+1}/4\pi^2\hbar^3$ (3.27), (C.30). Combining this result with (8.57), we finally find for the maximum quantum yield of a free-particle multipole source permitted by the exclusion principle, expressed as a conductivity $\sigma_{lm}^{(\mathrm{free})}(E)_{\mathrm{tr}}$:

$$\sigma_{lm}^{(\mathrm{free})}(E)_{\mathrm{tr}} \;=\; e^2\left|\lambda_{lm}^{(\mathrm{free})}(E)_{\mathrm{tr}}\right|^2 J_{lm}^{(\mathrm{free})}(E) \;=\; \frac{2e^2}{\pi\hbar} \tag{8.58}$$

Hence, we recover the result (8.53) from the corresponding one-dimensional theory. We may restate (8.58) and note that the maximum conductivity contribution of a free point source is twice Landauer's quantized conductivity $\sigma_q = e^2/\pi\hbar$ (8.46) per orbital multipole channel. Notably, $\sigma_{lm}^{(\mathrm{free})}(E)_{\mathrm{tr}}$ is independent of l, m, and E, but a product of natural constants only.

Digressing from the discussion of the source theory of STM, we will show in the following that the result (8.58) is not a peculiarity of the free-particle emission problem, but generally applies to multipole point sources in three dimensions for arbitrary potential environments $U(\mathbf{r})$. Let us briefly sketch a (slightly heuristic) proof for this statement. Consider the defining equation for the multipole Green function $G_{lm}(\mathbf{r},\mathbf{r}';E)$ (2.24). By multiplication, we find the set of equations:

$$\begin{aligned} G_{lm}(\mathbf{r},\mathbf{r}';E'+i\eta)^* \left\{ E + \frac{\hbar^2}{2M}\Delta - U(\mathbf{r}) \right\} G_{lm}(\mathbf{r},\mathbf{r}';E) \;&=\; \delta_{lm}(\mathbf{r}-\mathbf{r}')\, G_{lm}(\mathbf{r},\mathbf{r}';E'+i\eta)^* \\ G_{lm}(\mathbf{r},\mathbf{r}';E) \left\{ E' - i\eta + \frac{\hbar^2}{2M}\Delta - U(\mathbf{r}) \right\} G_{lm}(\mathbf{r},\mathbf{r}';E'+i\eta)^* \;&=\; \delta_{lm}(\mathbf{r}-\mathbf{r}')^*\, G_{lm}(\mathbf{r},\mathbf{r}';E) \end{aligned} \tag{8.59}$$

Again, $\eta \to 0^+$ denotes an infinitesimal positive auxiliary quantity. Now subtract these equations and integrate the result over a sphere $\mathbb{S}$ centered around $\mathbf{r}'$:

$$\begin{aligned} (E - E' + i\eta) \int_{\mathbb{S}} d^3r\, G_{lm}(\mathbf{r},\mathbf{r}';E'+i\eta)^* G_{lm}(\mathbf{r},\mathbf{r}';E) \;+\; & \\ \frac{\hbar^2}{2M} \oint_{\partial\mathbb{S}} \{ G_{lm}(\mathbf{r},\mathbf{r}';E'+i\eta)^* \boldsymbol{\nabla} G_{lm}(\mathbf{r},\mathbf{r}';E) \;-\; & \\ G_{lm}(\mathbf{r},\mathbf{r}';E)\, \boldsymbol{\nabla}\, G_{lm}(\mathbf{r},\mathbf{r}';E'+i\eta)^* \} \cdot d\mathbf{n}(\mathbf{r}) \;=\; & \\ \lim_{\mathbf{r}\to\mathbf{r}'} \left\{ K_{lm}\left(\frac{\partial}{\partial\mathbf{r}}\right) G_{lm}(\mathbf{r},\mathbf{r}';E'+i\eta)^* \;-\; K_{lm}^*\left(\frac{\partial}{\partial\mathbf{r}}\right) G_{lm}(\mathbf{r},\mathbf{r}';E) \right\} & \end{aligned} \tag{8.60}$$

The last line in (8.60) follows from (2.23) by partial integration, and the second line has been transformed into a surface integral using the divergence theorem. Now let the radius of the sphere $\mathbb{S}$ diverge; then, the first line in (8.60) will contain the normalization integral for the Green function (8.48) that this theory of the source strength parameter relies upon. As an outgoing wave, $G_{lm}(\mathbf{r},\mathbf{r}';E'+i\eta)$ vanishes for $r \to \infty$ for any $\eta > 0$ due to the causality of the retarded Green function. (See Appendix A.3.6; implicitly, we employed this technique already in (8.50).) Thus, the surface term must also vanish as the radius of the sphere $\mathbb{S}$ approaches infinity. Replacing the multipole Green functions on the r. h. s. of (8.60) by their definition (2.25), we obtain from (8.60):

$$\lim_{\eta\to 0^+} \int d^3r\, G_{lm}(\mathbf{r},\mathbf{r}';E'+i\eta)^* G_{lm}(\mathbf{r},\mathbf{r}';E) \;=$$

$$\lim_{\mathbf{r}\to\mathbf{r}'}\lim_{\eta\to 0^+}\frac{K_{lm}\left(\frac{\partial}{\partial\mathbf{r}}\right)K^*_{lm}\left(\frac{\partial}{\partial\mathbf{r}'}\right)G(\mathbf{r},\mathbf{r}';E'+i\eta)^* \;-\; K^*_{lm}\left(\frac{\partial}{\partial\mathbf{r}}\right)K_{lm}\left(\frac{\partial}{\partial\mathbf{r}'}\right)G(\mathbf{r},\mathbf{r}';E)}{E-E'+i\eta}\;\sim$$
$$-\,2\pi\,\delta(E-E')\lim_{\mathbf{r}\to\mathbf{r}'}\Im\left[K^*_{lm}\left(\frac{\partial}{\partial\mathbf{r}}\right)K_{lm}\left(\frac{\partial}{\partial\mathbf{r}'}\right)G(\mathbf{r},\mathbf{r}';E)\right] \quad (8.61)$$

Here, we used again the distribution relation (A.192) to extract the singular part in (8.61). Comparing with the general expression for the unit total multipole current $J_{lm}(\mathbf{r}';E)$ (2.33), we find for the normalization integral (8.48):

$$\int d^3r\,G_{lm}(\mathbf{r},\mathbf{r}';E')^*G_{lm}(\mathbf{r},\mathbf{r}';E)\;\sim\;\pi\hbar\,J_{lm}(\mathbf{r}';E)\,\delta(E-E') \quad (8.62)$$

Therefore, the source strength limit $\lambda_{lm}(\mathbf{r}';E)_{\rm tr}$ imposed by the Pauli principle onto multipole sources reads in terms of the total current (corrected for spin multiplicity):

$$\left|\lambda_{lm}(\mathbf{r}';E)_{\rm tr}\right|^2\;=\;\frac{2}{\pi\hbar J_{lm}(\mathbf{r}';E)} \quad (8.63)$$

Obviously, this expression directly leads back to the universal conductivity limit (8.58) we already found for free-particle multipole sources:

$$\sigma_{lm}(\mathbf{r}';E)_{\rm tr}\;=\;e^2\left|\lambda_{lm}(\mathbf{r}';E)_{\rm tr}\right|^2J_{lm}(\mathbf{r}';E)\;=\;\frac{2e^2}{\pi\hbar} \quad (8.64)$$

Hence, the maximum conductance of an electron source per multipole channel is given by the quantized value $2\sigma_q = 2e^2/\pi\hbar = 1.55\cdot 10^{-4}\,\Omega^{-1}$. Clearly, the actual strength of a physical multipole source will usually fall below the upper bound (8.64), a remark that should hold in particular for the tunneling sources specific to STM.

8.2.3 A Source-Sink Model of STM

Having the results (8.57) and (8.63) detailing the maximum strength of a multipole point source compatible with Pauli's exclusion principle at hand, we are now in a position to complete the multipole source model of STM introduced in Section 8.1. There, we originally considered the STM tip as an electron source (or sink) able to maintain a constant rate of electron generation (or annihilation); yet we did not care about conservation of the total number of electrons, and temporarily accepted that shortcoming to exploit the advantages of the source approach (Section 2.1). Employing the transport model in order to fix the source strength, we are now able to overcome this deficiency and present an improved theory of STM which no longer contains the source strength as an unspecified parameter.

The source-sink model of STM. Basically, the idea behind the new development is to supplement the picture of the tip as a quantum source emitting electrons towards the sample by simultaneously interpreting the tip as a multipole sink of electrons of the same orbital structure (i. e., identical quantum numbers l and m) which absorbs electrons from the tip body. (Here, we restrict ourselves to the study of electrons moving from the tip into the sample; the inverse event may be considered the time-reversed counterpart to the process analyzed here (Section 8.1.1), so the extension to the general case is straightforward.) Thus, within the extended model the tip may be considered as a pointlike electron "valve" which passes the current from the tip material into the sample bulk.

Let us enter a more detailed description of this idea. Electron transfer across the STM tunneling junction basically presents a two-step process. In the first step, the outermost atom of the tip collects electrons from the surrounding tip body. As we are interested only in an intelligible pictorial model, in a crude approximation we will replace the actual electronic structure of the tip material by a plain free-electron gas which is completely characterized by a single parameter, the Fermi wave number k_F of the tip. Since the electrons within the metallic tip move almost uninhibited, it appears reasonable to assume that the electron transport into the tip is limited only through the availability of phase space; in other words, the source strength for this process should be given by the maximum bound for free-electron multipole sources $|\lambda_{lm}^{(\mathrm{free})}(E_F)|^2_{\mathrm{tr}}$ (8.57). Most of the electrons approaching the tip point source will simply be reflected back into the tip body; only a fraction of them will be emitted towards the sample surface in a second step, an event aptly described by the multipole Green function $G_{lm}(\mathbf{r},\mathbf{r}';E)$ for the STM junction potential barrier, and extensively discussed already in Section 8.1. Hence, in the source-sink model of STM, the current characteristics (and thus the scanned image) is determined by the local surface potential relief $U(\mathbf{r})$ via its associated multipole Green function $G_{lm}(\mathbf{r},\mathbf{r}';E)$ whereas the absolute magnitude of the tunneling current is a function of the electronic tip structure only, and in our simple free-electron approximation merely depends on the electron density in the tip material. From (8.11) and (8.57), we obtain the source-sink model prediction for the zero-bias, zero-temperature conductivity $\sigma_{lm}(\mathbf{r}')$ of the STM junction due to a pointlike tip state of pure (l,m) orbital symmetry:

$$\sigma_{lm}(\mathbf{r}') \;=\; \frac{8\pi e^2\hbar^2}{M}\,k_F^{-(2l+1)}\,J_{lm}(\mathbf{r}';E_F) \tag{8.65}$$

Here, $J_{lm}(\mathbf{r}';E_F)$ denotes the total multipole current carried by $G_{lm}(\mathbf{r},\mathbf{r}';E_F)$ (2.33) which we calculated first in Section 2.4, E_F is the Fermi level of the tip-sample system, and k_F represents the Fermi wave vector of the electron gas within the tip body. As a general rule, the source-sink extension of the source model of STM in practice requires the replacement of the unspecified source strength $|\lambda_{lm}(E_F)|^2$ by its free-particle value

in the transport limit (8.57), $|\lambda_{lm}(E_F)|^2 = 8\pi\hbar^2/Mk_F^{2l+1}$.

Point contacts and the Landauer formula. Despite its quite different formal appearance, our prediction (8.65) for the zero-bias conductivity $\sigma_{lm}(\mathbf{r}')$ of a multipole point source bears a certain resemblance to Landauer's formula for the conductivity of a non-ideal mesoscopic conductor [186]:

$$\sigma_L(E) = \frac{e^2}{\pi\hbar}|T(E)|^2 \tag{8.66}$$

This result, also known as the Engquist-Anderson-Imry conductivity, is supposed to hold valid for an effectively one-dimensional connection between two extended electron reservoirs. $|T(E)|^2$ denotes the transmission coefficient for this channel. (Generalizations of this theory have been given in particular by Büttiker. See the monographs by Datta and Imry [79, 80].)

What we want to point out here is that the quantity $T(E)$ which provides information with regard to a scattering process is implicitly contained in the total multipole current $J_{lm}(\mathbf{r}'; E_F)$ in (8.65). This fact is clearly revealed by comparison of (8.66) with our semiclassical estimate (7.50) for this current derived in the framework of the minimum uncertainty model (Section 8.2). This kinship becomes particularly conspicuous when considering a symmetric junction between two identical free-electron gas "metals." In this case, $|T(E)|^2 = 1$ should nearly hold, and (8.66) reduces to the quantized conductivity $\sigma_q = e^2/\pi\hbar$ we first obtained in (8.46). But, under these circumstances, the multipole current in (8.65) is given by its free-particle value, i. e., the Wigner law $J_{lm}^{(\mathrm{free})}(E_F) = Mk_F^{2l+1}/4\pi^2\hbar^3$ (3.27), and the ensuing conductivity takes on its maximum amount $\sigma_{lm}(\mathbf{r}') = 2\sigma_q = 2e^2/\pi\hbar$ (8.64). We already noted that the remaining discrepancy between both results may be explained by the different geometrical assumptions behind these approaches (8.53).

The saturation of the conductivity of a STM junction in the contact regime probably has been pointed out first by Lang [207] who noticed the formation of a "plateau" in the close proximity limit when numerically studying the resistance for his simple model for the STM as a function of the interatomic separation using the density functional approach (for details on the simulations performed by Lang, we refer to Sections 7.3.3 and 8.1.4). Following a quite different line of reasoning based on the tight-binding Hamiltonian formalism, Ferrer et al. [216] arrived at the conclusion that the conductivity of a STM point contact should be given by Landauer's value σ_q (8.46). Subsequent to the discovery that the STM may be used as a tool for the manipulation of surfaces on an atomic scale [198], the study of point contacts has evolved into an active field of experimental research. Here, we shall only cite the result obtained by Yazdani et al. [217] who measured the conductivity profile of plane metallic electrodes connected via atomic adsorbates, thus putting Lang's simple model into prac-

tice. These authors found that the conductivity of a metallic Ni/W atomic contact indeed saturates at a value close to $e^2/\pi\hbar$. Upon inserting Xe atoms into the contact, i. e., forming an insulating xenon "wire," the residual conductivity drops steeply, indicating small values of the transmissivity $|T(E)|^2$ in (8.66).

Zero-bias conductivities of multipole sources. Once the Fermi wave vector k_F in the source strength prefactor of (8.65) is fixed, the source-sink model of STM provides a unique relation between the STM potential environment $U(\mathbf{r})$ and the ensuing zero-bias conductivity $\sigma_{lm}(\mathbf{r}')$ of the STM junction. According to the current decomposition presented in Section 8.1.2, the distance dependence of the STM current is basically determined by the background conductivity $\sigma_{lm}^{(0)}(z')$ (8.23) due to the averaged bulk-vacuum transition potential $U_0(z)$ which is invariant with respect to lateral shifts of the tip; only the remaining corrugative potential $W(\mathbf{r})$ will lead to deviations $\Delta\sigma_{lm}(\mathbf{r}')$ (8.24) of the conductivity from the mean value $\sigma_{lm}^{(0)}(z')$ which in turn render the STM image. Hence, it appears appropriate to study first the distance dependence of $\sigma_{lm}^{(0)}(z')$ for various background potentials $U_0(z)$ and choices of multipole sources (i. e., combinations of the quantum numbers l and m) before turning to actual simulations of STM images (Section 8.3).

For the purpose of this inquiry, two simple model background potentials $U_0(z)$ present natural candidates: The ballistic potential $U_0(z) = -Fz$ extensively discussed in Chapter 5 of this volume, and the step potential $U_0(z) = \Phi \cdot \Theta(z)$ that describes an abrupt potential increase at the sample surface. Indeed, we already employed these potentials for our estimate of the STM resolution capability (Section 8.1.3). Despite the fact that these model barriers in a sense present opposite extremes, with the actual potential distribution $U_0(z)$ in a realistic STM junction positioned in between, we nevertheless found that the resolutions obtained for both models (8.37), (8.38) and (8.42), (8.43) do not differ dramatically. We shall show in the following that this finding also holds true for the background conductivities $\sigma_{lm}^{(0)}(z')$ obtained for both example barriers. Hence, we must conclude that the current density distribution within the STM junction does not depend in a particularly sensitive manner on the choice of combination for tip and sample materials. (We should however note that even small differences in the electron distribution may cause large changes in the observed corrugation since the tip deflection is an exponential function of the resolution estimate, see (8.34).)

For our case study, we shall fix the value of the Fermi wave vector k_F in (8.65) at $k_F = 1.5\,\text{Å}^{-1}$. This choice corresponds to a Fermi energy $E_F = 8.6\,\text{eV}$ of the assumed free-electron gas in the tip, a typical value for many transition metals [166]. Now let us turn our attention to the linear potential environment $U_0(z) = -Fz$ (Chapter 5). In this case, the total ballistic multipole currents $J_{lm}(\mathbf{r}'; E)$ due to a source of unit strength are available in closed form (5.48) and conveniently tabulated in Appendix E.3, so the evaluation of the STM background conductivity $\sigma_{lm}^{(0)}(z')$ (8.65) within the source-sink

model introduced above is straightforward. To facilitate comparison with the results obtained for the field-emission problem in Chapter 7 (Figures 17 and 19), we take over the value for the initial electronic kinetic energy E at the source location employed there and set $E = -4\,\mathrm{eV}$, and choose to adjust the field strength F instead: $F = E/z_0$, where z_0, the "tip-sample separation," denotes the distance of the point source to the classical turning surface (Chapter 4). The results of this calculation for the simplest multipole sources ($0 \leq l \leq 2$) are plotted in the top caption of Figure 27 in terms of the background resistance $\sigma_{lm}^{(0)}(z_0)^{-1}$ of the STM junction.

We infer that the distance dependence of $\sigma_{lm}^{(0)}(z_0)$ for all three "longitudinal" multipole sources with $m = 0$ roughly coincides, whereas the conductivity for sources with additional angular momentum $|m| > 0$ is markedly lower, thus illustrating the importance of the centrifugal barrier in the suppression of the tunneling current, a mechanism that we discussed in detail during our presentation of the semiclassical minimum uncertainty model of multidimensional tunneling phenomena (Section 7.2). Hence, we may conclude that orbital tip states with $m \neq 0$ will contribute but a negligible part to the total tunneling current in STM, and in a first approximation may be ignored altogether, thus confirming the verdict formerly stated by Chen [183] and Lang [205]. For this reason, we will confine our STM simulations to multipole sources with $m = 0$. In a second observation, we note that $\sigma_{l0}^{(0)}(z_0)$ rather closely follows an exponential decay law and decreases approximately to $1/4$ of its initial value for each additional Å that the tip is withdrawn from the "surface." This value is rather close to the prediction from the semiclassical formula (7.50) which is dominated by the one-dimensional WKB transmission factor $\exp(-2|W_{\mathrm{cl}}(0, z_0; E)|/\hbar) = \exp(-4\,\kappa z_0/3)$ (see (7.52) and the discussion in Section 8.1.2) that amounts here to $e^{-1.37\,z_0}$ (where z_0 is given in Å), although this agreement appears fortituously good. In comparison to the results of the experiment conducted by Wintterlin et al. [74] who found a 6.6–fold increase of the STM junction resistivity per Å on the close-packed *fcc*–(111) surface of Al (see Section 8.3.1), the ballistic model at least for the parameters chosen here delivers a conductivity-distance characteristic $\sigma_{lm}^{(0)}(z_0)$ which is rather shallow.

We corrected for this inadequacy by means of our choice of parameters for the second model background potential $U_0(z)$, the rectangular step barrier. Unlike the ballistic problem, no closed-form expressions for the total multipole tunneling current $J_{lm}(\mathbf{r}'; E)$ generated by sources embedded in this potential environment are known; hence, we are forced to replace the current factor in the conductivity formula (8.65) valid in the source-sink model of STM by its semiclassical counterpart (7.50) obtained in Section 7.2. This yields the approximation:

$$\sigma_{lm}^{(0)}(z_0) \;\approx\; \frac{2e^2}{\pi\hbar}\,\left(\frac{\kappa}{k_F}\right)^{2l+1}\,\frac{(2l+1)\,(l+|m|)!}{|m|!\,(l-|m|)!}\,\frac{\exp(-2\,\kappa z_0)}{(4\,\kappa z_0)^{|m|+1}} \tag{8.67}$$

Here, $\kappa^2 = 2M\Phi/\hbar^2$ denotes the evanescent particle momentum in the barrier, and Φ

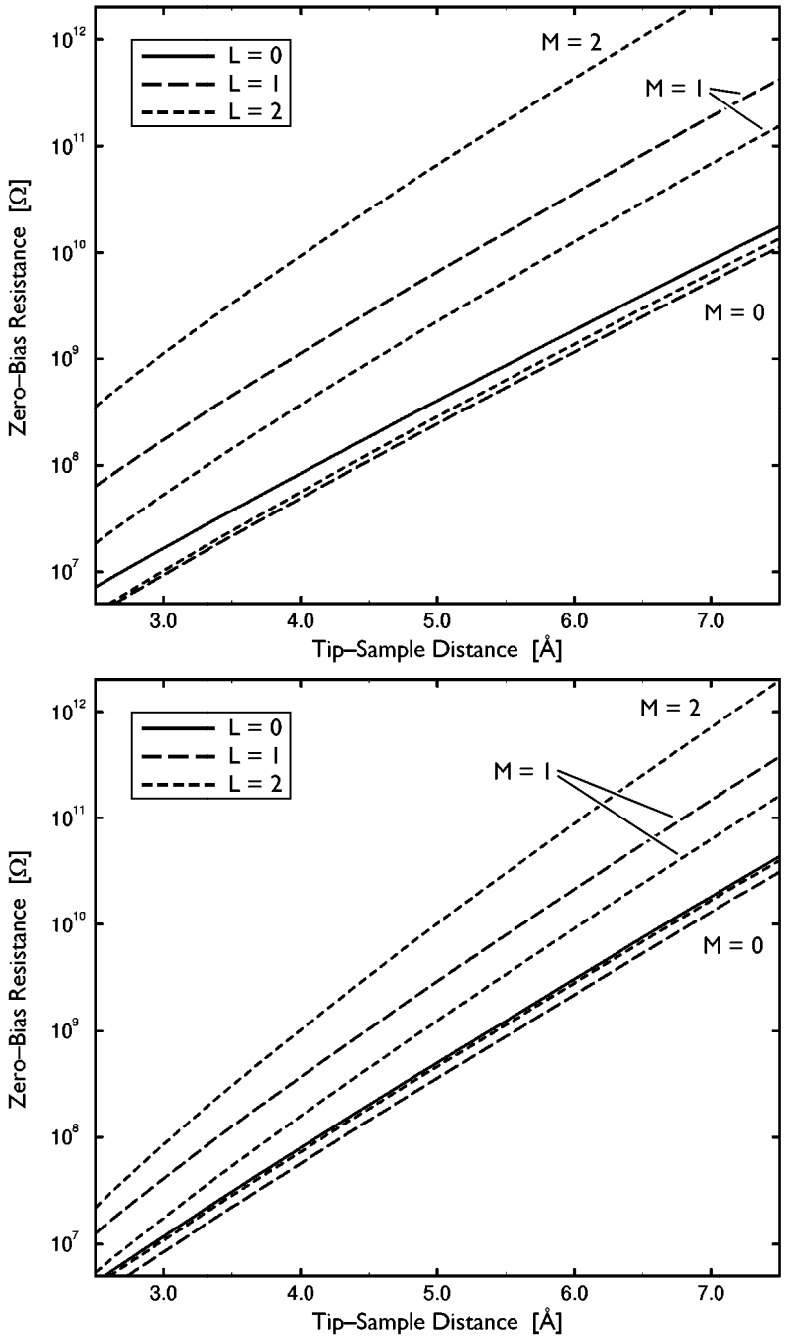

Figure 27: Distance dependence of the zero-bias, zero-temperature resistivity $\sigma_{lm}^{(0)}(z_0)^{-1}$ (8.65) for various multipole sources ($0 \leq |m| \leq l \leq 2$) according to the source-sink model of STM. Top: Ballistic environment potential $U_0(z) = -Fz$, where $F = E/z_0$, $E = -4\,\mathrm{eV}$ (cf. Figures 17 and 19). Bottom: Rectangular step potential with barrier height $\Phi = 2.5\,\mathrm{eV}$. In both cases, the Fermi wave vector of the tip electron gas has been chosen as $k_F = 1.5\,\mathrm{Å}^{-1}$.

may be identified with the work function of the surface. We note, however, that Φ will generally fall below its vacuum level due to image forces between tip and sample. (The effective barrier height has been calculated as a function of the tip-surface separation by Lang [207].) Agreement with Wintterlin's result may now be enforced by setting $\Phi = 2.5\,\mathrm{eV}$, which for longitudinally emitting sources ($m = 0$) leads to an average decay factor for the conductivity $6.6\,\text{Å}^{-1}$ in the distance regime of interest $3\,\text{Å} < z_0 < 5\,\text{Å}$. (In passing, we note that the exponential factor $e^{-2\kappa z_0}$ only in part accounts for this decay rate; close to the source, the prefactor due to the centrifugal potential may not be neglected.) The resulting relation between resistance of the junction and tip-sample separation has been plotted in the lower part of Figure 27 for multipole sources with $0 \leq l \leq 2$. Though both graphs differ in detail, the conductivity profiles for both the ballistic and step potential bear the same general features: Sources with longitudinal orientation ($m = 0$) for $l = 0, 1, 2$ show very similar current characteristics, whereas sources that generate electrons carrying angular momentum ($|m| > 0$) are significantly suppressed (an effect that is more pronounced in the ballistic case). Thus, we may be confident that an analogous situation prevails for the bulk-vacuum transition potential present in an actual STM junction. With this reasonable assumption, we turn to simulations of the corrugation observed in STM scans, the topic of the following section.

8.3 Example Calculations

Within the previous two sections of this chapter, we presented and discussed a complete multipole source theory of scanning tunneling microscopy whose final formal results are summarized in the expressions for the zero-bias conductivity $\sigma_{lm}(\mathbf{r}')$ (8.11), (8.65) of the STM tunneling junction. In order to illustrate the results of this simple theoretical STM model, and to show that the corrugation amplitude $\Delta z'(x', y'; \sigma_0)$ (8.28) obtained in our simulated STM surface profiles (following the majority of experiments, we also choose to conduct our calculations for the constant current operation mode of STM) indeed is comparable to the tip deflections observed in actual experiments, we set up a surface model potential $W(\mathbf{r})$ that is sufficiently simple as to warrant an analytic solution to the STM source problem. For this purpose, we employ an array of pointlike isotropic regularized scatterers ("zero-range potentials" or ZRPs for short) which mimics a surface plane within a densely packed lattice of ionic cores, an appropriate model for many simple metals, including the noble metals [166]. The ingredients of this surface potential approximation are discussed in detail in Section 8.3.1. Having introduced our simple model of a smooth metal surface, we proceed to perform STM image simulations within the multipole source-sink model, which according to the theory of Section 8.1.2 depend on the evaluation of the corrugative part of the conductivity $\Delta\sigma_{lm}(\mathbf{r}')$ (8.24). As noted in this section, in order to determine the

conductivity by this formula, knowledge of the Green function $G(\mathbf{r},\mathbf{r}';E_F)$ belonging to the full tip-surface potential $U(\mathbf{r}) = U_0(z) + W(\mathbf{r})$ (8.16) is required. Usually, this function is not available in any computationally inexpensive manner, so we are forced to retreat to an approximative scheme, and a natural choice for that is to employ the Born approximation for the surface scattering process. This program is carried out in Section 8.3.2 for our metal surface imitation. Fortunately, the ZRP lattice from a mathematical point of view is sufficiently simple as to allow also for a direct determination of the Green function $G(\mathbf{r},\mathbf{r}';E_F)$ assigned to our surface model potential $W(\mathbf{r})$. This, in turn, permits us to obtain the exact conductivity profile $\sigma_{lm}(\mathbf{r}')$ (8.24), and from that we may finally solve for the corrugation amplitude $\Delta z'(x',y';\sigma_0)$ (8.28) as our quantity of interest. The ZRP approach will be presented in greater detail in Section 8.3.3.

8.3.1 Setting Up the Model

Hence, let us start out and construct the model potential $U(\mathbf{r})$ for our STM simulations within the source-sink theory (Section 8.2). As we are interested in an analytically solvable problem, our choice for the background potential $U_0(z)$ describing the average tunneling barrier for the electron transfer from tip to sample is essentially limited to the uniform force field environment $U_0(z) = -Fz$, for which we stated the solution to the multipole Green function problem in Chapter 5. The triangular barrier admittedly presents a rather crude approximation to the actual potential relief in the STM junction; however, we have already seen in Sections 8.1.3 and 8.2.3 that neither the resolution estimate $a_{\mathrm{sc}}(E)$ (8.36) nor the background conductivity $\sigma^{(0)}_{lm}(z')$ (8.23) (see Figure 27) depend in a particularly sensitive way on the choice of the bulk-vacuum transition potential. Thus, it appears justified to simulate the metal surface as a periodic lattice built from ZRPs which is superimposed to the homogeneous field background potential $U_0(z)$. For consistency, we will take over the prescription already used for the calculation shown in Figure 27 and fix the kinetic energy E of the particles emitted by the mutlipole source at an initial value $E = -4\,\mathrm{eV}$, regardless of its position $\mathbf{r}'$; at the same time, we will identify the turning surface of classical motion in the potential $U_0(z)$ with the topmost layer of surface "atoms." This requires to adjust the field strength F in dependence of the tip-surface separation z_0: $F = -E/z_0$. We now turn our attention to the arrangement of "atoms" within the ZRP lattice.

Characterization of *fcc*–(111) surfaces. A number of simple metals, among them the noble metals (with the exception of Re, Ru, and Os, which form hexagonally close packed (*hcp*) structures) under standard conditions crystallize into a face-centered cubic (*fcc*) primitive lattice [218]. This structure may be interpreted as one stable configuration of densely packed spheres which may be identified with the ionic cores forming the positive background for the delocalized electron gas present in these metals [166];

the less symmetric *hcp* structure presents another densely packed configuration. The left part of Figure 28 illustrates the cubic *fcc* lattice; due to its octahedral symmetry, the space diagonal of the cubic cell, i. e., the [111] direction within the *fcc* crystal, presents a threefold rotation axis. Cutting the crystal structure perpendicular to the [111] axis discloses the *fcc*–(111) surface which correspondingly shows threefold rotational symmetry with respect to each atomic position in the surface layer; its plane point symmetry group or ornamental group is denoted by the symbol *p3m1* [219]. As Figure 28 illustrates, the surface generated in this way apparently shows an even higher degree of symmetry, indeed the maximally allowed number of symmetry elements compatible with the discrete translational symmetry of a plane tiling, which is designated as the hexagonal ornamental group *p6mm* [219] with a sixfold rotational axis. This symmetry is, however, broken by the sub-surface atomic layers in which the atoms alternatingly occupy the interstitial positions of the topmost layer. (In passing, we note that the *hcp*–(0001) surface of the hexagonally close packed metals has a very similar structure and differs from the *fcc*–(111) surface model only in the second sub-surface atomic layer. Thus, the following considerations apply as well to metals which order into *hcp* lattices.)

Due to its sixfold coordination, the *fcc*–(111) close-packed surface is extraordinarily smooth and not prone to complicated surface reconstructions (however, the *fcc*–(111) Au surface presents an exception from this rule [176]), and for simple metals, where the interatomic distance is merely of order $a = 2.9\,\text{Å}$, form the smoothest surfaces available at all for standard ambient conditions. Nevertheless, atomic resolution of these surfaces has been achieved in STM [74]. For these samples, the STM clearly operates in the exponential resolution regime (8.42) of Section 8.1.3, where the observed corrugation $\Delta z'(x', y'; \sigma_0)$ depends sensitively on the width of the tunneling electron distribution. We may therefore expect that sub-surface atomic layers will leave only a negligible imprint on the STM image which basically renders the hexagonal symmetry of the topmost atomic layer.

For the same reason, the lowest Fourier components $u_{jk}(z)$ (8.30) of the periodic surface potential $W(\mathbf{r})$ will dominate the STM image. (We will examine this assertion in Section 8.3.3.) To determine them, let us take a closer look at the geometry of the densely packed surface [75, 176]. A set of basis vectors $\mathbf{a}_1$, $\mathbf{a}_2$ which spans the surface unit cell has been indicated in the right caption of Figure 28:

$$\mathbf{a}_{1,\,2} = \frac{a}{2} \begin{pmatrix} 1 \\ \pm\sqrt{3} \end{pmatrix} \tag{8.68}$$

Here, a denotes the next-neighbour distance in the *fcc* lattice; it is connected to the conventional lattice constant A of the cubic cell by $a = A/\sqrt{2}$ [219]. For our simulations, we will use the appropriate value for silver, $a = 2.89\,\text{Å}$ [218]. From the discussion in Section 8.1.3 we may infer that the STM resolution behavior depends

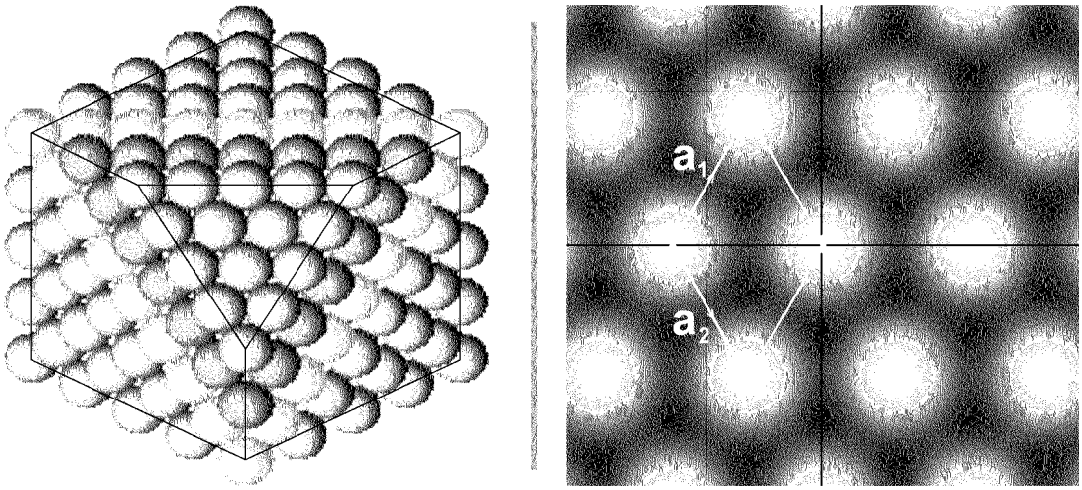

Figure 28: Schematic view of the *fcc*–(111) densely packed surface. Left: Cutting an *fcc* arrangement of spheres perpendicular to the space diagonal of the cubic cell reveals a lattice plane of hexagonal symmetry, the *fcc*–(111) surface. Spheres of the first and second sub-surface layers occupy the interstitial positions of the topmost layer in an alternating pattern. In the right figure, elements of the *p6mm* ornamental symmetry group are illustrated. The basis vectors $\mathbf{a}_1$ and $\mathbf{a}_2$ span a unit cell of the plane lattice (tiling). Atomic positions are centers of sixfold rotational symmetry; the two principal axes of mirror symmetry are indicated as black lines. They either connect atomic locations directly or run through interstitial positions ("hollows"). In the background, the simplest potential $W(\mathbf{r})$ (8.70) compatible with the ornamental symmetry group is shown as a grayscale plot.

on the surface structure in reciprocal space rather than real space (8.30). Therefore, we determine a set of reciprocal basis vectors $\mathbf{G}_1$, $\mathbf{G}_2$ via the orthonormality relation $\mathbf{a}_j \cdot \mathbf{G}_k = 2\pi\,\delta_{jk}$ [166]. Furthermore, it is sensible to introduce another reciprocal lattice vector $\mathbf{G}_3$ via $\mathbf{G}_3 = \mathbf{G}_1 - \mathbf{G}_2$:

$$\mathbf{G}_{1,2} \;=\; \frac{2\pi}{\sqrt{3}\,a}\begin{pmatrix}\sqrt{3}\\ \pm 1\end{pmatrix}\;, \qquad \mathbf{G}_3 \;=\; \frac{4\pi}{\sqrt{3}\,a}\begin{pmatrix}0\\ 1\end{pmatrix} \tag{8.69}$$

These three vectors share a common wave number $G = 4\pi/\sqrt{3}\,a$; for the case of silver, we find $G = 2.51\,\text{Å}^{-1}$. The median lines to the six basic reciprocal lattice vectors $\pm\mathbf{G}_1, \pm\mathbf{G}_2, \pm\mathbf{G}_3$ enclose a regular hexagon in momentum space, the two-dimensional Brillouin zone of the reciprocal lattice which (unlike the reciprocal lattice of the *fcc* structure in three dimensions) shares the point symmetry of the real space surface grid. Since the corrugative potential $W(\mathbf{r})$ besides the sixfold rotational symmetry additionally contains mirror symmetries (e. g., the mirror axes indicated as black lines

in Figure 28), it is not difficult to conclude that the Fourier components of the potential $W(\mathbf{r})$ assigned to the six basic reciprocal lattice vectors mentioned above must be all equal and real, so a proper approximation to the decomposition (8.30) reads:

$$W(\mathbf{r}) \sim u(z) \sum_{k=1}^{3} \cos \mathbf{G}_k \cdot \mathbf{r}_\perp \tag{8.70}$$

where the factor $u(z)$ may be determined by integration over the surface unit cell:

$$u(z) = \frac{4}{\sqrt{3}\, a^2} \int_{\text{U.C.}} d^2 r_\perp \, e^{i\, \mathbf{G}_k \cdot \mathbf{r}_\perp} \, W(\mathbf{r}_\perp, z) \tag{8.71}$$

Here, $\mathbf{G}_k$ presents one of the six reciprocal lattice vectors of wave number G, and the area of the Brillouin zone is encoded in the prefactor.

The superposition of wavelike potential contributions (8.70) generates a characteristic pattern which is shown as a grayscale plot in the right part of Figure 28. The potential function (8.70) oscillates between extremal values of $3\, u(z)$ (at the atomic locations, i. e., $\mathbf{r}_\perp = \mathbf{o}$ and equivalent positions) and $-1.5\, u(z)$ (at the interstitial positions of the lattice, which within the unit cell are formally found at the locations $\frac{2}{3}\, \mathbf{a}_1 + \frac{1}{3}\, \mathbf{a}_2$ and $\frac{1}{3}\, \mathbf{a}_1 + \frac{2}{3}\, \mathbf{a}_2$). The apparent discrepancy between these extremal values is explained by the fact that each unit cell contains only one lattice point, but two interstitials or "hollows." Since Fourier components of the potential $W(\mathbf{r})$ at least within a linear approximation are mapped onto corresponding Fourier components of the corrugation amplitude $\Delta z'(x', y'; \sigma_0)$ (see the following section), the right caption in Figure 28 also gives an impression of the corrugation profiles that we have to expect from our simulations (Section 8.3.3).

The zero-range potential model. Having discussed the atomic arrangement of our model for a smooth metal surface, we now specify the properties of the ionic cores represented by simple spheres in Figure 28. Clearly, we are interested in a description which allows for the complete solution of the Green function problem (2.12) as the knowledge of the Green function $G(\mathbf{r}, \mathbf{r}'; E_F)$ assigned to the full STM environment potential $U(\mathbf{r})$ enables us to calculate the corrugative part $\Delta\sigma_{lm}(\mathbf{r}')$ (8.24) of the zero-bias conductivity of the STM junction directly (Section 8.3.3). We have inferred already in Section 2.3 that the set of potentials $U(\mathbf{r})$ for which the Green function is available as a closed-form expression all but vanishes. Fortunately, there exists an established method of constructing new solutions to the Green function problem from given ones by adding special pointlike scattering centers to the original potential $U_0(z)$. The technique in principle dates back to the 1930s where it was developed by Fermi in an attempt to describe the scattering of slow neutrons off nuclei; it is known as the contact potential or Fermi pseudopotential. In its application to the Green function prob-

lem, a more rigorous mathematical description is required; for a detailed presentation, we refer to the monograph by Demkov and Ostrovskii [220]. Basically, the pointlike isotropic interaction which from the discussion of multipole sources in Section 2.4 may be naively expected to be proportional to a simple Dirac δ–function must be modified by adding a differential operator. For a single isotropic scattering center at $\mathbf{r} = \mathbf{r}_j$, this so-called zero-range potential (ZRP) reads:

$$W_j(\mathbf{r}) \;=\; W_j\,\delta(\mathbf{r}-\mathbf{r}_j)\,\frac{\partial}{\partial|\mathbf{r}-\mathbf{r}_j|}\;|\mathbf{r}-\mathbf{r}_j| \tag{8.72}$$

Clearly, when applied to a function which is analytic in a neighbourhood of $\mathbf{r}_j$, the action of (8.72) is indistinguishable from that of a simple δ–spike potential $\tilde{W}_j(\mathbf{r}) = W_j\delta(\mathbf{r}-\mathbf{r}_j)$. Unlike its naive counterpart, however, the operator (8.72) still returns a meaningful result when acting on a function with a simple pole at $\mathbf{r} = \mathbf{r}_j$, in which case the singular part of this function is effectively ignored. This property affects in particular the action of $W_j(\mathbf{r})$ on the local Green function $G(\mathbf{r},\mathbf{r}_j;E)$ which according to the theory presented in Appendix A.5 in three dimensions always exhibits this simple pole structure (see Theorem LXVI). Thus, the zero-range potential (8.72) is able to lift the singular nature of the Green function $G(\mathbf{r},\mathbf{r}_j;E)$ in the limit $\mathbf{r}\to\mathbf{r}_j$; the ZRP is therefore also known as the tempered or regularized delta distribution in three-dimensional space. For its (fairly involved) construction in spaces of arbitrary dimension D, we refer to the article by Wódkiewicz [221].

Let us briefly discuss the scattering properties of the pointlike ZRP potential (8.72). For this purpose, it is obviously useful to shift the scattering center to the origin $\mathbf{r} = \mathbf{o}$. Then, the imaginary part of the scattering wave function $\psi_{lm}(\mathbf{r};E)$ is a regular solution of the Schrödinger equation:

$$\left\{E + \frac{\hbar^2}{2M}\,\frac{1}{r}\,\frac{\partial^2}{\partial r^2}\,r - \frac{\hbar^2 l(l+1)}{2Mr^2} - W_j\delta(\mathbf{r})\,\frac{\partial}{\partial r}\,r\right\}\psi_{lm}(\mathbf{r};E) \;=\; 0 \tag{8.73}$$

Outside the origin, i. e., for $r > 0$, the radial part of any solution to this equation must be given by a superposition of regular and irregular spherical Bessel functions, $\psi_l(r;E) = \alpha_l(E)j_l(kr) + \beta_l(E)n_l(kr)$ (see also Appendix C.1). For $l > 0$, $\psi_l(r;E)$ will vanish at the origin $r = 0$, hence the ZRP potential (8.72) has no effect on the wave function. In s–wave scattering, we may express this linear combination in terms of the scattering phase $\delta_0(k)$ and set $\psi_0(r;E) = \sin[kr+\delta_0(k)]/kr$ (where $k^2 = 2ME/\hbar^2$ as usual); then, by comparison with the free-particle Green function (3.25), it is straightforward to prove that the phase angle is given by $\delta_0(k) = -\arctan(k/\kappa_j)$, which in turn gives rise to a total s–wave scattering cross section $\sigma_{00}(k)$ [83]:

$$\sigma_{00}(k) \;=\; \frac{4\pi}{k^2}\,\sin^2\,\delta_0(k) \;=\; \frac{4\pi}{k^2+\kappa_j^2} \tag{8.74}$$

Here, we used the abbreviation $\kappa_j = 2\pi\hbar^2/MW_j$. We note that $\sigma_{00}(k)$ diverges for $E_j = -\hbar^2\kappa_j^2/2M$ [221]. For proper choice of sign for the interaction strength W_j (which is of dimension [energy]×[volume]), E_j presents the single discrete eigenenergy of the attractive ZRP problem, where the bound state is given by a Yukawa function: $\psi_0(r) \propto \exp(-\kappa_j r)/r$.

Our main interest is directed towards the scattering properties of (8.72), however. Keeping in mind that the electrons in STM impinge on the sample surface with nearly zero momentum, we may ignore the k dependence in (8.74), and conclude that a ZRP (8.72) of strength W_j acts as an isotropic scatterer with total cross section $\sigma_j = \pi b_j^2$, where b_j is the scattering length of the ZRP:

$$b_j = \frac{2}{\kappa_j} = \frac{MW_j}{\pi\hbar^2} \tag{8.75}$$

(Note that our definition of b_j as the radius of a disk differs from the conventional one by a factor of two.) For a first approximation, we may adapt the scattering length b_j to the ionic radius of the corresponding metallic kation that is available from the structure determination of salt compounds, as this number should be fairly similar to the radius of the impenetrable ionic cores forming the backbone of the metallic lattice. Indeed, these values fall only slightly below half the interatomic distance a within the metallic *fcc* crystal, so the approximation of a densely packed spheres lattice invoked above appears justified. For our example of Ag, we find as an estimate for the ionic radius of Ag^+ in sixfold coordination $b_j = 1.15\,\text{Å}$, corresponding to a strength of the ZRP potential (8.75) $W_j = -27.6\,\text{eV}\cdot\text{Å}^3$ [218]. (We will employ this value despite the fact that the coordination number of a *fcc* lattice is actually 12.) In passing, we note that "defects" may easily be accommodated within our model by varying the scattering length b_j of one of the atomic ZRP's within the array; we will make use of this opportunity in Section 8.3.3. There, we will also show how to obtain the full Green function $G(\mathbf{r}, \mathbf{r}'; E)$ for the combined potential of the ballistic background $U_0(z)$ and the ZRP surface imitation $W(\mathbf{r})$. But first, we shall tackle the much simpler task of obtaining the Born approximation for the STM imaging problem.

8.3.2 The Born Approximation

Hence, we turn our attention to the formal description of the corrugative part of the zero-bias conductivity in STM $\Delta\sigma_{lm}(\mathbf{r}')$ (8.24) which we obtained in Section 8.1.2. According to this formula, $\Delta\sigma_{lm}(\mathbf{r}')$ depends on the corrugative surface potential $W(\mathbf{r}'')$ in form of an integral equation which contains the product of the spherical tensor gradient of the multipole Green function $\mathfrak{G}^{(0)}_{l,-m}(\mathbf{r}', \mathbf{r}''; E_F)$ due to the background potential $U_0(z)$ with the actual multipole Green function $G_{lm}(\mathbf{r}'', \mathbf{r}'; E_F)$ assigned to the full potential $U_0(z) + W(\mathbf{r})$ as an integral kernel. This expression is exact and will present the

basis of the developments of Section 8.3.3; here, however, we will content ourselves with an approximation of this equation which is linear in the corrugative potential $W(\mathbf{r}'')$. To achieve this objective, we obviously have to eliminate the implicit dependence of $G_{lm}(\mathbf{r}'', \mathbf{r}'; E_F)$ on $W(\mathbf{r}'')$ which in practice is equivalent to the replacement of $G_{lm}(\mathbf{r}'', \mathbf{r}'; E_F)$ by the background Green function $G^{(0)}_{lm}(\mathbf{r}'', \mathbf{r}'; E_F)$ belonging to $U_0(z)$. Inserting the source strength $|\lambda_{lm}(E_F)|^2 = 8\pi\hbar^2/Mk_F^{2l+1}$ (8.57) found in the source-sink model of STM into (8.24), we obtain the following estimate:

$$\Delta\sigma^{(\mathrm{Born})}_{lm}(\mathbf{r}') \;=\; -\,\frac{16\pi e^2\hbar}{Mk_F^{2l+1}}\,(-1)^m\,\Im\left[\int d^3r''\,\mathfrak{G}^{(0)}_{l,\,-m}(\mathbf{r}', \mathbf{r}''; E_F)\,W(\mathbf{r}'')\,G^{(0)}_{lm}(\mathbf{r}'', \mathbf{r}'; E_F)\right] \tag{8.76}$$

Within the source model of quantum mechanics (Section 2.3), the approximation (8.76) plays essentially the same role that the Born approximation takes on in conventional scattering theory [238], thus we will take over this designation for the expression (8.76). Like its counterpart in scattering theory, we may expect best performance of (8.76) for "weak" corrugative potentials $W(\mathbf{r}'')$ which hardly affect the Green function $G(\mathbf{r}, \mathbf{r}'; E)$.

Images of the ZRP lattice in Born approximation. Following this general explanation, we now apply the Born approximation (8.76) to the ZRP potential model of a metal *fcc*–(111) surface we laid out in Section 8.3.1. For practical reasons, we perform our numerical simulations of the STM image only for a finite slab representing the entire surface. (Clearly, this replacement is permissible as long as the slab area remains much larger than the size of the electron "spotlight" emitted by the point source towards the sample surface; see Section 8.1.3.) For the following simulations, a single-layered array of 14×14 ZRP "silver atoms" ($a = 2.89$ Å, $W_0 = -27.6\,\mathrm{eV}\cdot\mathrm{Å}^3$) was employed; for slabs of this extension, no finite-size effects were discernible. For our imitated *fcc*–(111) surface of Ag, we thus use in this section the model corrugative ZRP lattice potential (8.72):

$$W(\mathbf{r}) \;=\; W_0 \sum_{j\,=\,0}^{13}\sum_{k\,=\,0}^{13} \delta(\mathbf{r} - \mathbf{r}_{jk})\,\frac{\partial}{\partial|\mathbf{r} - \mathbf{r}_{jk}|}\,|\mathbf{r} - \mathbf{r}_{jk}| \tag{8.77}$$

where $\mathbf{r}_{jk} = j\mathbf{a}_1 + k\mathbf{a}_2$, and $\mathbf{a}_{1,\,2}$ are the unit cell basis vectors stated in (8.68). All calculations were performed for the central unit cell within the slab.

Inserting (8.77) into (8.76), it is obvious that the integral in the formula for the zero-bias conductivity variation in Born approximation (8.76) reduces to a simple sum. Since all Green function expressions appearing in this formula contain the tip position $\mathbf{r}'$ as one center, the regularization operator in (8.77) has no effect and may be ignored.

We finally note that the tunneling currents for source contributions with additional angular momentum $m \neq 0$ are generally overshadowed by the dominant longitudinal ($m = 0$) multipole sources (see Section 8.2.3, especially Figure 27) and hence are only of academic interest; we will not examine them in the following. Thus, we are left with this expression for $\Delta\sigma_{l0}^{(\mathrm{Born})}(\mathbf{r}')$:

$$\Delta\sigma_{l0}^{(\mathrm{Born})}(\mathbf{r}') \;=\; -\,\frac{16\pi e^2\hbar W_0}{M k_F^{2l+1}} \sum_{j\,=\,0}^{13}\sum_{k\,=\,0}^{13} \Im\left[\mathfrak{G}_{l0}^{(0)}(\mathbf{r}', \mathbf{r}_{jk}; E)\, G_{l0}^{(0)}(\mathbf{r}_{jk}, \mathbf{r}'; E)\right] \tag{8.78}$$

Instead of presenting the corrugative part of the conductivity at fixed tip-sample separation z_0 (constant current mode of STM), we chose to solve numerically for z_0 for given values of the zero-bias conductivity σ_0. Therefore, all figures show topographical contour lines and simulate the popular constant current operation mode of STM. Throughout this section, the source is held at an emission (Fermi) energy of $E = -4$ eV (cf. Figures 17, 19, and 27), whereas the ZRP array (8.77) is located on the classical turning surface of the ballistic potential $U_0(z)$. Thus, the ballistic field strength F is adapted to z_0 via $F = -E/z_0$. For the Fermi wave vector k_F of the tip material, we selected the value $k_F = 1.5\,\text{Å}^{-1}$ (see Section 8.2.3).

Figure 29 shows a series of simulated STM profiles for our model potential (8.77), performed for longitudinal s–, p–, and d–wave multipole tips, respectively. The left column provides information about the distance dependence of the equiconductivity lines. Here, the tip scans along the long diagonal of the *p6mm* unit cell (vertical black line in the right caption of Figure 28), starts at an atomic position and crosses the interstitials of the densely packed array. These may be discerned as two shallow minima symmetrically located at 1/3 and 2/3 of the total scanning range ($\sqrt{3}\,a \sim 5.01\,\text{Å}$). The right column presents a more detailed view of the corrugation profiles obtained for $\sigma_0 = 2\,\text{M}\Omega$. In addition to the simulated scan data for the long unit cell diagonal, also results for the direct interatomic connection (short unit cell diagonal, horizontal black line in Figure 28) have been displayed. As a result, we infer that all three tip models deliver a very similar dependence of the average tip-surface separation z_0 on the zero-bias conductivity σ_0 in accordance with the results from Section 8.2.3; however, the observed corrugation amplitude $\Delta z'(x', y'; \sigma_0)$ (8.28) grows drastically with increasing angular momentum quantum number l of the multipole tip source, in particular when viewed as a function of the average distance z_0 (Figure 30). The right column in Figure 29 shows that this variation only affects the total corrugation $\Delta z'(\sigma_0)$, but not the shape of the simulated STM profiles; no resolution beyond the fundamental Fourier components of the potential distribution $W(\mathbf{r})$ (8.70) has been achieved. In fact, all six profiles plotted in this part of the figure almost perfectly match the "hexagonal cosine function" $\sum_{k\,=\,1}^{3} \cos \mathbf{G}_k \cdot \mathbf{r}_\perp$ prominent in (8.70) [176].

The tendency of higher angular momentum tunneling sources to emit electrons

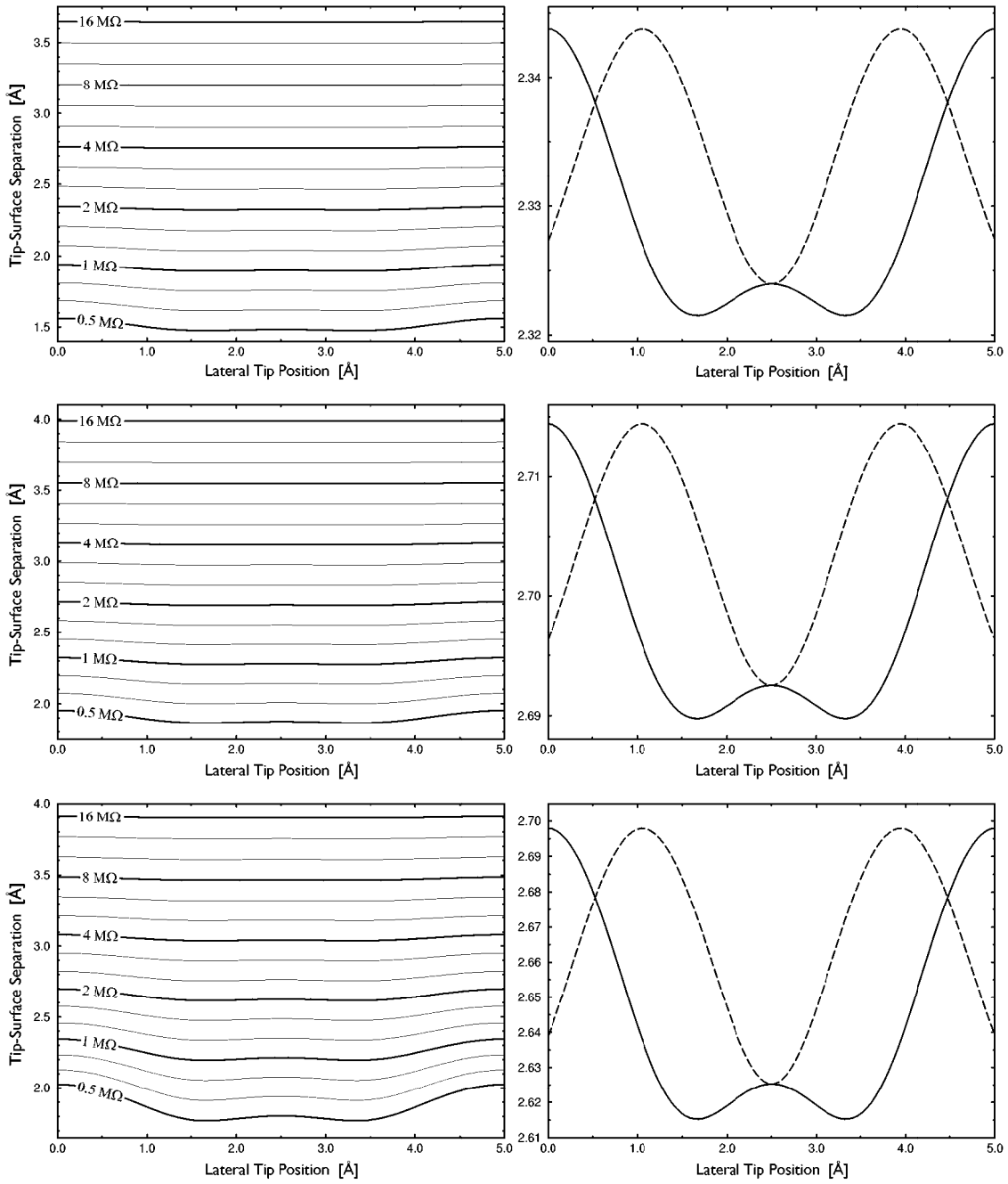

Figure 29: Simulated STM profiles (8.78) for the *fcc*–(111) Ag surface in Born approximation using different multipole source tips (top row: $l = m = 0$, central row: $l = 1$, $m = 0$, bottom row: $l = 2$, $m = 0$). Left column: Constant zero-bias conductivity scans performed across the long diagonal of the surface unit cell (Figure 28). Right column: Detailed view of the corrugation profile obtained for scans along the short (dashed line) and long (full line) diagonal of the unit cell, for a conductivity $\sigma_0 = 2\,\mathrm{M\Omega}$. (Parameters used: $E = -4\,\mathrm{eV}$, $k_F = 1.5\,\mathrm{\AA}^{-1}$, $a = 2.89\,\mathrm{\AA}$, $W_0 = -27.6\,\mathrm{eV{\cdot}\AA}^3$, $14 \times 14 \times 1$ ZRP array surface model.)

into more strongly confined current filaments (cf. Section 7.3.1, in particular Figure 19) is of considerable importance in STM because the corrugation amplitude in the exponential resolution regime of Section 8.1.3 depends sensitively on the size of the electronic "spotlight" on the sample surface. Therefore, in Figure 30, we plotted the total corrugation amplitude $\Delta z'(\sigma_0)$ extracted from our calculations for the Ag model surface as a function of the average tip-sample separation z_0. It is seen that in Born approximation, $\Delta z'(z_0)$ depends very nearly exponentially on the distance z_0, in agreement with the predictions from the pictorial model put forward in Section 8.1.3. There, we provided an estimate for the resolution of small-scale structures embedded in a ballistic background potential (8.42) which for the values of G (8.69) and E assumed here amounts to an exponential decay law $\Delta z'(z_0) \propto \exp(-\alpha z_0)$ where the decay constant α is given by $\alpha \sim 1.69\,\text{Å}^{-1}$. Indeed, for the numerical results plotted in Figure 30, regression analysis delivers very similar values for α_l ($\alpha_{l=0} \sim 1.74\,\text{Å}^{-1}$, $\alpha_{l=1} \sim 1.72\,\text{Å}^{-1}$, $\alpha_{l=2} \sim 1.68\,\text{Å}^{-1}$), so formula (8.42) presents a surprisingly accurate approximation to our numerical results. However, the multipole sources differ considerably in their offset values for this exponential decay, as Figure 30 illustrates; realistically, within the Born approximation, atomic resolution of the *fcc*–(111) surface of silver is feasible only with d–wave tip states. In this context, we already mentioned the preferred usage of transition metals (W, Ir) as tip materials in STM.

Imaging of wavelike corrugative potentials. Let us now turn our attention to a slightly more complicated application for the source-sink model of STM, its imaging behavior for wavelike corrugative potential structures which for simplicity we shall confine to the turning surface of classical motion, $W(\mathbf{r}) = W_0 \exp(i\,\mathbf{G}\cdot\mathbf{r}_\perp)\,\delta(z)$. This problem is of considerable interest because within the Born approximation (8.76), the corrugative part of the zero-bias conductivity $\Delta\sigma_{lm}^{(\text{Born})}(\mathbf{r}')$ depends linearly on the surface potential $W(\mathbf{r})$; whenever the latter is a periodic function (like our model potential for the *fcc*–(111) metal surface introduced in Section 8.3.1), the potential $W(\mathbf{r})$ may be expanded into a discrete Fourier series with respect to the lateral coordinates $\mathbf{r}_\perp$ (8.30), and the resulting image in Born approximation will simply represent the superposition of the partial images due to the Fourier components of $W(\mathbf{r})$. Formally, the Fourier decomposition procedure involves an infinite number of contributions. However, we have already inferred from the pictorial "spotlight" model of STM (Section 8.1.3) that the observed conductivity corrugation $\Delta\sigma_{lm}(\mathbf{r}')$ (8.24) drops exponentially for wavelike surface structures whose period is much smaller than the spotlight size a (8.35), so in practice we may apply some cut-off wave number $G_{\max}$ and thus limit the number of relevant Fourier components of $W(\mathbf{r})$ involved in the formation of the image. In the following, the properties of STM for sheet-like periodic potentials $W(\mathbf{r})$ according to the source model in Born approximation are summarized; for isotropic s–wave tips, an article published by the author provides further information [75].

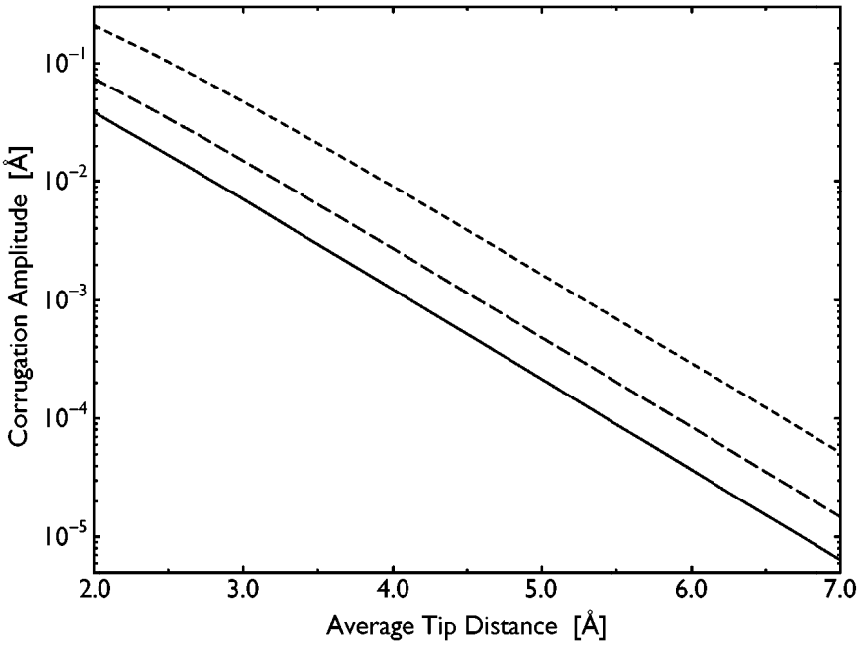

Figure 30: Dependence of the total corrugation amplitude $\Delta z'(z_0)$ on the average tip-sample separation z_0 in Born approximation for the *fcc*–(111) silver model surface (8.77). Full line: s–wave tip state, dashed line: p–wave source ($l = 1$, $m = 0$), dotted line: d–wave tip state ($l = 2$, $m = 0$). (Parameters used: $E = -4\,\mathrm{eV}$, $k_F = 1.5\,\mathrm{\AA}^{-1}$, $a = 2.89\,\mathrm{\AA}$, $W_0 = -27.6\,\mathrm{eV{\cdot}\AA}^3$. The simulation was performed for a $14 \times 14 \times 1$ ZRP array surface model.)

As already indicated above, in the framework of the Born approximation, Fourier components of $W(\mathbf{r})$ are mapped onto corresponding Fourier components of the conductivity $\Delta\sigma_{lm}^{(\mathrm{Born})}(\mathbf{r}')$. Using its definition (8.76), the proof of this assertion is indeed simple. We note ahead that the background Green function $G^{(0)}(\mathbf{r}, \mathbf{r}'; E_F)$ is based on a potential $U_0(z)$ which is invariant with respect to shifts parallel to the surface, and it is shown in Appendix A.5.4 that $G^{(0)}(\mathbf{r}, \mathbf{r}'; E_F)$ inherits this symmetry property from its generating potential $U_0(z)$. (Obviously, the same translational symmetry also persists for the multipole Green functions $G_{l0}^{(0)}(\mathbf{r}, \mathbf{r}'; E_F)$ and the spherical tensor gradients $\mathfrak{G}_{l0}^{(0)}(\mathbf{r}, \mathbf{r}'; E_F)$ derived from this Green function.) Inserting the definition of a sheet-like potential with wave vector $\mathbf{G}$, $W_{\mathbf{G}}(\mathbf{r}) = w_{\mathbf{G}} \exp(i\,\mathbf{G}\cdot\mathbf{r}_\perp)\delta(z)$, into (8.76), we obtain with $\mathbf{R} = \mathbf{r}_\perp - \mathbf{r}'_\perp$:

$$\Delta\sigma_{l0}^{(\mathrm{Born})}(\mathbf{r}') \;=\; -\,\frac{16\pi e^2\hbar}{M k_F^{2l+1}}\,\Im\left[w_{\mathbf{G}}\, e^{\,i\,\mathbf{G}\cdot\mathbf{r}'_\perp} \int d^2R\, \mathfrak{G}_{l0}^{(0)}(z', \mathbf{R}; E_F)\, e^{\,i\,\mathbf{G}\cdot\mathbf{R}}\, G_{l0}^{(0)}(\mathbf{R}, z'; E_F)\right] \tag{8.79}$$

Since the Green function derivatives appearing in (8.79) like $U_0(z)$ are additionally invariant with respect to rotations around the z axis, according to the results of Ap-

pendix A.5.4 these expressions are functions of the lateral distance $R = |\mathbf{r}_\perp - \mathbf{r}'_\perp|$ only, and an angular integration may be carried out analytically in (8.79). Therefore, in reciprocal space, the relation holds:

$$\Delta\sigma_{l0}^{(\mathrm{Born})}(\mathbf{G}) \;=\; R_{l0}(G, z'; E_F)\, W(\mathbf{G}) \tag{8.80}$$

where the response function $R_{l0}(G, z'; E_F)$ reads:

$$R_{l0}(G, z'; E_F) \;=\; -\frac{32\pi^2 e^2 \hbar}{M k_F^{2l+1}} \int_0^\infty dR\, R\, J_0(GR)\, \Im\left[\mathfrak{G}_{l0}^{(0)}(z', R; E_F)\, G_{l0}^{(0)}(R, z'; E_F)\right] \tag{8.81}$$

In (8.80), $\Delta\sigma_{l0}^{(\mathrm{Born})}(\mathbf{G})$ and $W(\mathbf{G})$ denote the Fourier transform of the corrugative part of the conductivity and of the surface potential with respect to the lateral coordinates $\mathbf{r}'_\perp$ and $\mathbf{r}_\perp$, respectively. We emphasize that the relation (8.80) implies that for a sheet-like potential $W(\mathbf{r}) = W_\perp(\mathbf{r}_\perp)\delta(z)$ and fixed tip-surface separation z_0, there exists a one-to-one correspondence between the surface potential $W_\perp(\mathbf{r}_\perp)$ and the conductivity profile $\Delta\sigma_{l0}^{(\mathrm{Born})}(\mathbf{r}')$. In reciprocal space, this relation is easily inverted. Therefore, in the constant height operation mode of STM, a sheet-like surface potential $W_\perp(\mathbf{r}_\perp)$ is uniquely assigned to each conductivity profile $\sigma_{l0}(x', y'; z_0)$. For weak corrugations, thanks to the approximately valid formula (8.28) the same reasoning applies also to the more common real-space corrugation profiles $\Delta z'(x', y'; \sigma_0)$ obtained in the constant current mode of STM. Thus, the Born approximation shows the attractive feature of connecting experimental data to the surface potential distribution in a quite direct manner.

Clearly, it is exactly the response function $R_{l0}(G, z'; E_F)$ (8.81) that we implicitly referred to in our intuitive analysis of the resolution in STM performed in Section 8.1.3. There, we presented a rather complicated formula (8.42) for the prefactor in (8.80) which we derived from a semiclassical analysis of ballistic tunneling (Section 7.1). Using the expression (8.81) valid in Born approximation, we now may inquire into the reliability of this semiclassical estimate. For a connection to the *fcc*–(111) metal surface model presented in Section 8.3.1, we will calculate the total corrugation amplitude $\Delta z'(\sigma_0)$ in constant current mode not for a simple potential Fourier component $w_{\mathbf{G}} \exp(i\,\mathbf{G}\cdot\mathbf{r}_\perp)\delta(z)$, but for the "hexagonal cosine function" $W\,\delta(z)\sum_{k=1}^{3}\cos\mathbf{G}_k\cdot\mathbf{r}_\perp$ (8.70) compatible to the *p6mm* ornamental symmetry of this crystalline surface which may be viewed as a superposition of six plane waves that share a common wave number $G = 4\pi/\sqrt{3}\,a$ (8.69). (This choice also facilitates comparison to the distance dependence of the total corrugation $\Delta z'(z_0)$ displayed in Figure 30.) Being merely a factor of proportionality, for simplicity we fix the strength of the surface potential Fourier components at $W = 1\,\mathrm{eV}\cdot\mathrm{Å}$; for the average tip-surface separation z_0, the value $z_0 = 3\,\mathrm{Å}$ has been selected, which for an electron emission energy $E = -4\,\mathrm{eV}$ amounts to a

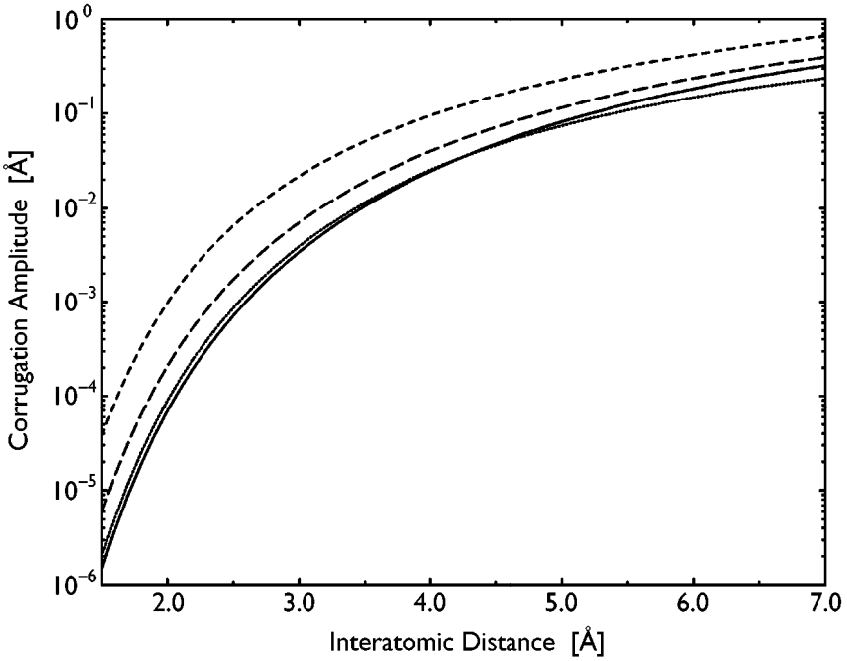

Figure 31: Dependence of the total corrugation amplitude $\Delta z'$ in ballistic tunneling on the lattice constant a of the *p6mm* ornamental grid in Born approximation. A sheet-like potential $W(\mathbf{r}) = W\delta(z)\sum_{k=1}^{3}\cos\mathbf{G}_k\cdot\mathbf{r}_\perp$ (8.69), (8.70) was assumed in the calculation. Full line: s–wave source, long dashed line: p_z–tip state, short dashed line: d_{z^2}–wave source. The semiclassical estimate for $\Delta z'(a)$ (8.42) is also plotted (dotted line; total displacement adapted to s–wave result). (Parameters used: $E = -4\,\text{eV}$, $k_F = 1.5\,\text{Å}^{-1}$, $z_0 = 3\,\text{Å}$, $W = 1\,\text{eV}\cdot\text{Å}$.)

mean field strength $F = 1.33\,\text{eV/Å}$. In Figure 31, the resulting total corrugation amplitude in Born approximation $\Delta z'$ has been displayed as a function of the interatomic distance a for s–, p–, and d–wave tip states. It is seen that all three multipole sources lead to a corrugation characteristic $\Delta z'(a)$ of closely related shape; as already inferred from Figure 30, the resolving capability improves with increasing orbital quantum number l of the source. For an assessment of the performance of the semiclassical resolution estimate (8.42) which was originally devised for isotropic sources, we additionally plotted a graph of this function in Figure 31 (where the absolute value of the corrugation was adapted to the results obtained from (8.81) for the case $l = 0$). It is seen that (8.42) indeed presents a useful first approximation to the surface periodicity dependence $\Delta z'(a)$ for all three multipole tip states considered in Figure 31.

8.3.3 Results for Zero-Range Potential Lattices

Finally, we turn our attention towards an exact solution of the Green function problem (and thus, an example surface potential $W(\mathbf{r})$ analytically solvable in the framework

of the source-sink model of STM) which is available for arrays of zero-range potential (ZRP) isotropic scattering centers (8.72), as noted already in Section 8.3.1. There, we discussed the scattering properties of a single regularized point interaction potential $W_j(\mathbf{r})$ (8.72), in particular its cross section for elastic scattering processes $\sigma_{00}(E)$ (8.74). Obviously, it is now our task to extend this analysis to sets of ZRP potentials; the solution of the scattering problem for several point centers requires proper handling of multiple scattering events, in particular those that involve the repeated return of an electron to the same point scatterer. (Here, the regularization operator in (8.72) plays a decisive role.) Clearly, the Green function $G(\mathbf{r}, \mathbf{r}'; E)$ assigned to the combination of background potential $U_0(z)$ and the ZRP array $W(\mathbf{r})$ provides all available information on the propagation of electrons within this system, and we must first explore its derivation before we again take up STM simulations for the ZRP lattice mimicking the *fcc*–(111) surface of silver that we introduced in Section 8.3.1.

Construction of the Green function. Therefore, let us first state the corrugative potential $W(\mathbf{r})$ due to N pointlike ZRP scatterers (8.72):

$$W(\mathbf{r}) \;=\; \sum_{j=1}^{N} W_j(\mathbf{r}) \;=\; \sum_{j=1}^{N} W_j\, \delta(\mathbf{r}-\mathbf{r}_j)\, \frac{\partial}{\partial|\mathbf{r}-\mathbf{r}_j|}\, |\mathbf{r}-\mathbf{r}_j| \tag{8.82}$$

Here, the coefficents W_j are related to the scattering lengths b_j of the various scattering centers by $W_j = \pi\hbar^2 b_j/M$ (8.75). In the next step, we shall express the background Green function $G^{(0)}(\mathbf{r}, \mathbf{r}'; E)$ in terms of the Green function $G(\mathbf{r}, \mathbf{r}'; E)$ for the combined potential $U(\mathbf{r}) = U_0(z) + W(\mathbf{r})$ that we are interested in. For this purpose, we interpret $G^{(0)}(\mathbf{r}, \mathbf{r}'; E)$ as the "perturbed" Green function that arises from $G(\mathbf{r}, \mathbf{r}'; E)$ by adding $-W(\mathbf{r})$ to the potential $U(\mathbf{r})$. According to (8.20), or more formally, (A.200) in Appendix A.3.6, we may expand $G^{(0)}(\mathbf{r}, \mathbf{r}'; E)$:

$$G^{(0)}(\mathbf{r}, \mathbf{r}'; E) \;=\; G(\mathbf{r}, \mathbf{r}'; E) \;-\; \int d^3r''\, G(\mathbf{r}, \mathbf{r}''; E)\, W(\mathbf{r}'')\, G^{(0)}(\mathbf{r}'', \mathbf{r}'; E) \tag{8.83}$$

In the STM problem, we will finally consider the case where neither $\mathbf{r}$ nor $\mathbf{r}'$ will be located at the position of some scattering center $\mathbf{r}_j$ in (8.82). Then, the integral in (8.83) reduces to a simple sum:

$$G(\mathbf{r}, \mathbf{r}'; E) \;=\; G^{(0)}(\mathbf{r}, \mathbf{r}'; E) \;+\; \sum_{j=1}^{N} W_j\, G(\mathbf{r}, \mathbf{r}_j; E)\, G^{(0)}(\mathbf{r}_j, \mathbf{r}'; E) \tag{8.84}$$

Thus, we infer that the full Green function $G(\mathbf{r}, \mathbf{r}'; E)$ is available once the special values $G(\mathbf{r}, \mathbf{r}_j; E)$ for $j = 1, 2, \ldots, N$ are known. To calculate these, we set $\mathbf{r}' = \mathbf{r}_j$ in (8.83)

and obtain:

$$G(\mathbf{r},\mathbf{r}_j;E) \;=\; G^{(0)}(\mathbf{r},\mathbf{r}_j;E) \;+\; \sum_{k\,=\,1}^{N} G(\mathbf{r},\mathbf{r}_k;E)\,A_{jk}(E) \tag{8.85}$$

Here, the matrix elements $A_{jk}(E)$ are obviously given by:

$$A_{jk}(E) \;=\; \begin{cases} W_k\,G^{(0)}(\mathbf{r}_k,\mathbf{r}_j;E) & (j\neq k) \\ W_k \lim\limits_{\mathbf{R}\,\to\,\mathbf{r}_k} \dfrac{\partial}{\partial|\mathbf{R}-\mathbf{r}_k|}\left\{|\mathbf{R}-\mathbf{r}_k|\,G^{(0)}(\mathbf{R},\mathbf{r}_k;E)\right\} & (j=k) \end{cases} \tag{8.86}$$

and may be calculated from the background Green function $G^{(0)}(\mathbf{r},\mathbf{r}';E)$ which we assume to be known analytically. We note that the regularization operator in (8.72), (8.82) prevents the diagonal matrix element $A_{kk}(E)$ from diverging; according to the mathematical theory of Green functions in three spatial dimensions (Appendix A.5), $G^{(0)}(\mathbf{r},\mathbf{r}';E)$ possesses a simple pole at $\mathbf{r}=\mathbf{r}'$ (Theorem LXVI) which is removed by the operator part in (8.72), leaving the constant term of the Laurent series expansion of $G^{(0)}(\mathbf{r},\mathbf{r}';E)$ around $\mathbf{r}=\mathbf{r}'$ as a finite result. Thus, the tempered zero-range distribution (8.72) renders the point scattering problem renormalizable [220,221].

We note that the coefficients $A_{kj}(E)$ (8.86) represent the propagation of electrons in the background potential $U_0(z)$ from the scattering center $\mathbf{r}_j$ to a second point scatterer at $\mathbf{r}_k$; the diagonal terms $A_{kk}(E)$ describe the self-propagating amplitude, which we now shall state for the potentials $U_0(z)$ discussed in this work, free-particle propagation (Appendix C) and the uniform force field potential $U_0(z)=-Fz$ (Chapter 5). The functions $A_{kk}(E)$ are most easily extracted from the series expansions (A.261), (A.262) of the corresponding Green functions that are provided in Appendix A.5.2. For free particles, we find:

$$A_{kk}^{(\mathrm{free})}(E) \;=\; -\,\frac{iMk}{2\pi\hbar^2}\,W_k \tag{8.87}$$

(where $k^2 = 2ME/\hbar^2$ denotes the wave number in the prefactor), whereas the ballistic problem yields a more involved result that may be presented in terms of Airy functions (Appendix D.1):

$$A_{kk}(E) \;=\; -\,W_k\,\frac{M\beta F}{\hbar^2}\,\left[\mathrm{Ai}'(\alpha)\,\mathrm{Ci}'(\alpha)-\alpha\,\mathrm{Ai}(\alpha)\,\mathrm{Ci}(\alpha)\right] \tag{8.88}$$

Here, β is given as usual (5.16) by $\beta^3 = M/4\hbar^2F^2$, and the argument of the Airy functions in (8.88) reads $\alpha=-2\beta(E+Fz')$ (5.19).

Having established the propagation matrix $A_{jk}(E)$ (8.86), we return to the determination of the set of Green functions $G(\mathbf{r},\mathbf{r}_j;E)$. To this end, we note that (8.85) presents

a finite linear system for these functions:

$$\sum_{k=1}^{N} [\delta_{jk} - A_{jk}(E)]\, G(\mathbf{r}, \mathbf{r}_k; E) \;=\; G^{(0)}(\mathbf{r}, \mathbf{r}_j; E) \tag{8.89}$$

which may be solved by introducing the scattering T matrix of the system [238] related to the inverse of the matrix $I - A(E)$:

$$T_{jk}(E) \;=\; W_j\; [I - A(E)]^{-1}_{kj} \tag{8.90}$$

(This step is equivalent to the summation of a formal geometrical series for the resolvent operator $\mathcal{R}_\lambda(E)$ (A.201) that we obtained in Appendix A.3.6.) Finally, by replacing the Green functions $G(\mathbf{r}, \mathbf{r}_j; E)$ in (8.84) with the help of (8.89) and (8.90), we express the Green function $G(\mathbf{r}, \mathbf{r}'; E)$ of the combined system of background potential $U_0(z)$ and ZRP array $W(\mathbf{r})$ (8.82) as a functional of the background Green function $G^{(0)}(\mathbf{r}, \mathbf{r}'; E)$ alone:

$$G(\mathbf{r}, \mathbf{r}'; E) \;=\; G^{(0)}(\mathbf{r}, \mathbf{r}'; E) \;+\; \sum_{j=1}^{N} \sum_{k=1}^{N} G^{(0)}(\mathbf{r}, \mathbf{r}_k; E)\, T_{kj}(E)\, G^{(0)}(\mathbf{r}_j, \mathbf{r}'; E) \tag{8.91}$$

In our model for the STM, we are principially interested in the probability current $J_{lm}(\mathbf{r}'; E_F)$ (2.33) emitted by a multipole point source $\delta_{lm}(\mathbf{r} - \mathbf{r}')$ (2.23) located at the tip position $\mathbf{r}'$. Using the definitions for the multipole Green function $G^{(0)}_{lm}(\mathbf{r}, \mathbf{r}'; E_F)$ (2.25) and the spherical tensor gradient $\mathfrak{G}^{(0)}_{lm}(\mathbf{r}, \mathbf{r}'; E_F)$ (8.22) of the Green function, we find from (8.91) for the total multipole current:

$$\begin{aligned} J_{lm}(\mathbf{r}'; E_F) \;=\; J^{(0)}_{lm}(\mathbf{r}'; E_F) - \frac{2}{\hbar}\,(-1)^m \;\times \\ \sum_{j=1}^{N} \sum_{k=1}^{N} \Im\left[\mathfrak{G}^{(0)}_{l,-m}(\mathbf{r}', \mathbf{r}_k; E_F)\, T_{kj}(E_F)\, G^{(0)}_{lm}(\mathbf{r}_j, \mathbf{r}'; E_F)\right] \end{aligned} \tag{8.92}$$

(Note that the particle "loss" of the source is connected to the imaginary part of the sum of all propagators describing closed paths in the ZRP lattice. This property is akin to the "optical theorem" or Bohr–Peierls–Placzek relation of conventional scattering theory [238]. The Born approximation (8.78) is recovered from (8.92) by replacing the T matrix with a diagonal matrix $T^{(\mathrm{Born})}_{kj}(E_F) \;=\; W_j\, \delta_{kj}$. See also (A.202) in Appendix A.3.6.)

Finally, we invoke the connection of the particle current (8.92) to the zero-bias conductivity in STM (8.10), its decomposition into background and corrugative parts (8.15), and insert the source strength $|\lambda_{lm}(E_F)|^2$ (8.57) found in the source-sink model

of STM (Section 8.2.3) to obtain the corrugative part of the zero-bias conductivity $\Delta\sigma_{lm}(\mathbf{r}')$ (8.65) for the ZRP array (8.82):

$$\Delta\sigma_{lm}(\mathbf{r}') \;=\; -\,\frac{16\pi e^2\hbar}{Mk_F^{2l+1}}\,(-1)^m \sum_{j\,=\,1}^{N}\sum_{k\,=\,1}^{N} \Im\left[\mathfrak{G}^{(0)}_{l,\,-m}(\mathbf{r}',\mathbf{r}_k;E_F)\,T_{kj}(E_F)\,G^{(0)}_{lm}(\mathbf{r}_j,\mathbf{r}';E_F)\right] \tag{8.93}$$

Within our source model of STM, this result is exact, and we shall apply it in the following for simulations of the *fcc*–(111) ZRP surface model (Section 8.3.1). (In passing, we note that a quite similar formalism has been employed by Heller et al. [201–203, 222] in order to interpret their STM images of the "quantum corrals" described briefly in Section 8.1.4.)

STM simulations for the *fcc*–(111) surface model. Before we actually start out with the calculation of STM scanning profiles using a ZRP surface model amenable to a discussion in terms of (8.93), we briefly explain two possible modifications of this formula when employing the uniform field environment $U_0(z) = -Fz$ for the background potential barrier as we shall generally do in the following. First, we note that the Green function $G(\mathbf{r},\mathbf{r}';E)$ in its original form (8.91) indiscriminately couples to all scattering point centers $W_j(\mathbf{r})$ (8.72) independent of their relative vertical distance to the tip; this approximation does not appear justified for sub-surface atoms because of their location in the sample bulk where the linear surface vacuum transition potential $U_0(z)$ is absent. Also, it seems unlikely that the topmost layer of ionic cores which covers a large fraction of the surface (after all, we modeled the metallic crystal as a lattice of densely packed spheres in Section 8.3.1) allows the source to couple unimpeded to atomic centers below the surface. As a simple remedy, we confine the summations in (8.93) to ZRPs which are members of the surface layer. For the same reason, the usage of the ballistic Green function $G^{(0)}(\mathbf{r}_j,\mathbf{r}_k;E_F)$ for the determination of the scattering T matrix (8.90) appears inappropriate; rather, we choose to model the propagation between scattering centers in the sample by the free-particle Green function $G^{(\mathrm{free})}(\mathbf{r}_j,\mathbf{r}_k;\tilde{E}_F)$ (3.25), where $\tilde{E}_F$ is the Fermi energy of electrons in the sample bulk.

Before we actually set out with our simulations, we have to define the specific ZRP model for the *fcc*–(111) surface slab potential $W(\mathbf{r})$ (8.82) that we will base our calculations of the zero-bias conductivity $\Delta\sigma_{l0}(\mathbf{r}')$ (8.93) upon. (Like in the preceding section, we will consider only longitudinal multipole tip states with $m = 0$.) Since the ZRP model is more flexible than the Born approximation for which our simulations have been confined to sheet-like potentials compressed into a single surface plane (8.79)–(8.81), we will employ a potential model that includes the first sub-surface layer. For this purpose, we supplement the pair of basis vectors $\mathbf{a}_{1,\,2}$ (8.68) of the *p6mm* ornament

with a third basis vector $\mathbf{a}_3$ connecting adjacent layers, thus providing a primitive basis for the *fcc* Bravais lattice:

$$\mathbf{a}_{1,2} = \frac{a}{2}\begin{pmatrix} 1 \\ \pm\sqrt{3} \\ 0 \end{pmatrix}, \qquad \mathbf{a}_3 = \frac{a}{\sqrt{3}}\begin{pmatrix} 1 \\ 0 \\ \sqrt{2} \end{pmatrix} \tag{8.94}$$

This implies that adjacent layers in the *fcc*–(111) surface structure are separated by a distance $\sqrt{2/3}\,a$ which for an Ag crystal amounts to 2.36 Å. For a finite ZRP array, we cut out a rectangular slab from an *fcc* lattice where the grid positions calculated from the basis set (8.94) are populated by identical attractive ZRPs (8.72) with a strength $W_0 = -27.6\,\mathrm{eV}\cdot\mathrm{Å}^3$, adapted to the ionic radius of Ag^+ (8.75) (see Section 8.3.1). We selected a rectangular surface section containing two layers which is large enough to render finite-size effects negligible ($|x| < 17.6$ Å, $|y| < 16.5$ Å, 0 Å $\leq z \leq 4$ Å); it was centered around a surface unit cell (Figure 28) and contained 311 ZRP point scatterers. Simulations were performed on the central unit cell.

In this first study of our ZRP model of the *fcc*–(111) Ag surface, we basically repeated the calculations made already in Born approximation for the slightly different potential $W(\mathbf{r})$ stated in (8.77), so quantitative agreement between both simulations should not be expected. Figure 32 shows sets of corrugation profiles $\Delta z'(x', y'; \sigma_0)$ for fixed conductivity σ_0 of the STM junction (i. e., in the constant current mode of STM), numerically obtained from (8.93) for multipole tip states with quantum numbers $m = 0$ and $l = 0, 1, 2$. For convenient comparison to the corresponding results of the Born approximation (Figure 29), we took over the ordering scheme from there and placed the results delivered by the source model of STM for each multipole tip in a separate row (top: s–wave source, center: p–wave tip state, bottom: d–wave source). The left column displays sets of equiconductivity profiles for scans guided along the long diagonal of the surface unit cell spanned by $\mathbf{a}_1$ and $\mathbf{a}_2$ (8.68) (vertical line in Figure 28), whereas the right column in Figure 32 presents close-ups for the corrugation amplitude $\Delta z'(x', y'; \sigma_0)$ observed in STM for scans along both unit cell diagonals performed for $\sigma_0 = 2\,\mathrm{M}\Omega$. A comparison with Figure 29 shows that the profiles gained by the use of the complete Green function in the calculation (8.93) render the surface more distinctly than the simpler Born approximation (8.78) predicts, and thus provide an enlarged tip displacement amplitude; however, virtually no resolution beyond the principal Fourier components of the *p6mm* ornamental pattern, i. e., the "hexagonal cosine function" $\sum_{k=1}^{3} \cos \mathbf{G}_k \cdot \mathbf{r}_\perp$ (8.70), has been achieved, as the graphs in the right column of Figure 32 illustrate. In particular, the sub-surface layer of ZRP's which breaks the hexagonal symmetry of the topmost surface layer by occupying just a single of the two interstitial positions in each surface unit cell cannot be traced in the corrugation profiles of Figure 32 which still appear symmetric.

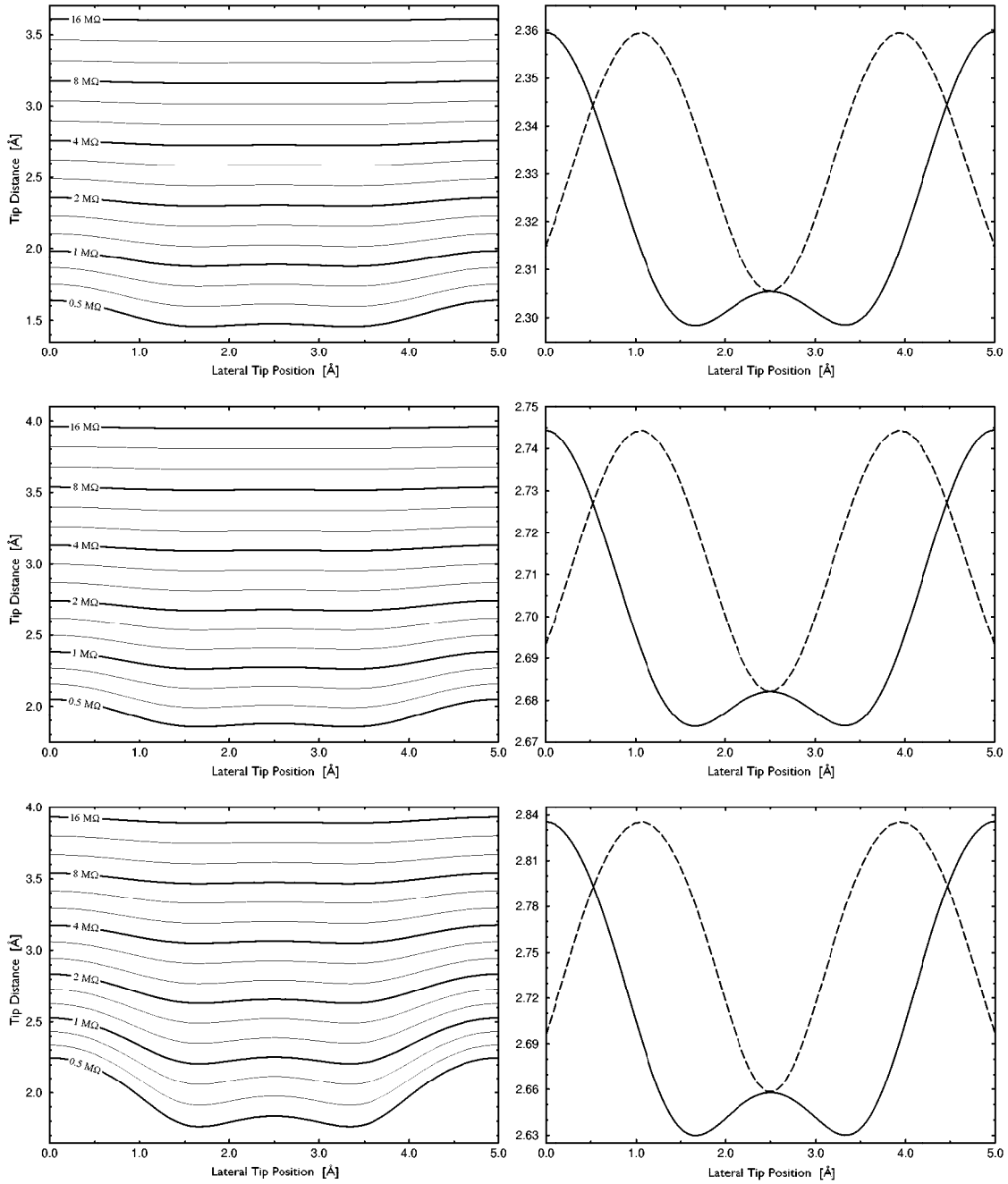

Figure 32: Simulation of STM corrugation profiles for a ZRP *fcc*–(111) silver surface model. Top row: Isotropic source ($l = m = 0$), center row: p–wave tip state ($l = 1$, $m = 0$), bottom row: d–wave source ($l = 2$, $m = 0$). Left column: Constant current profiles for scans following the long diagonal of the surface unit cell (Figure 28). Right column: Profiles for $\sigma_0 = 2\,\mathrm{M\Omega}$ scans along the short (dashed line) and long (full line) unit cell diagonal. See also Figure 29. (Parameters used: $E = -4\,\mathrm{eV}$, $k_F = \tilde{k}_F = 1.5\,\mathrm{\AA}^{-1}$, $a = 2.89\,\mathrm{\AA}$, $W_0 = -27.6\,\mathrm{eV{\cdot}\AA}^3$, 311 center two-layer ZRP array.)

Like in the preceding section, we may extract the dependence of the total corrugation amplitude $\Delta z'$ on the average tip-surface separation z_0 from the numerical data. (Again, we assume that the surface, i. e., the topmost ZRP layer, coincides with the turning surface of classical motion, whereas the emission energy E of electrons generated by the tip state is fixed at $E = -4\,\mathrm{eV}$.) In Born approximation, the observed $\Delta z'(z_0)$ characteristic shows exponential dependence (Figure 30) and is quite accurately described by the semiclassical formula (8.42) derived in the framework of the spotlight model (Figure 31). Let us now inquire into the corresponding results for the complete solution (8.93) of the STM source problem for the ZRP *fcc*–(111) lattice model which have been plotted in Figure 33. As already noted above, it is seen that the absolute tip displacement $\Delta z'(z_0)$ is enlarged in comparison with the results in Born approximation (Figure 30); this effect may be at least partly due to the differing surface potential models $W(\mathbf{r})$ used in these simulations. Also, as expected, the corrugation amplitude grows with increasing orbital quantum number l of the multipole source. From Figure 33, we infer that the exponential law $\Delta z'(z_0) \propto \exp(-\alpha z_0)$ still presents a good approximation to the actual characteristic also for the full ZRP lattice calculation; deviations from the exponential dependence are most easily recognized in the proximity regime $z_0 < 3.5\,\text{Å}$ where the curves slightly flatten out. Excluding this part of the caption, numerical estimates for the decay constants α_l have been determined by regression analysis for the various multipole tip states ($\alpha_{l=0} = 1.56\,\text{Å}^{-1}$, $\alpha_{l=1} = 1.54\,\text{Å}^{-1}$, $\alpha_{l=2} = 1.50\,\text{Å}^{-1}$). Thus, all three multipole sources share a common distance dependence of the corrugation amplitude which, however, deviates noticeably from the decay law derived within the semiclassical spotlight model (Section 8.1.3), $\Delta z'(z_0) \propto \exp(-\alpha z_0)$ where $\alpha = (\kappa^2 + G^2)^{1/2} - \kappa \sim 1.69\,\text{Å}^{-1}$ (8.42). While the reason for this discrepancy is not obvious, we remark here that the resolution estimate obtained from the spotlight model implicitly assumes a linear mapping of the corrugative surface potential $W(\mathbf{r})$ onto the conductivity variation $\Delta\sigma_{lm}(\mathbf{r}')$, so it is not surprising that the Born approximation (Figure 30) delivers results closer to (8.42).

STM images of a point defect. In our final example, we shall examine the imaging behavior of our STM source model for a *fcc*–(111) simple metal surface that contains a "point defect." Within the exactly solvable ZRP array model (8.82) for the surface potential $W(\mathbf{r})$, such a defect is easily inserted by the replacement of one regular scattering center within the ZRP lattice by a point scatterer (8.72) of different strength W_j, and we shall use this model to study the resolution mechanism in STM. To be concise, let us initially state the potential distribution $W(\mathbf{r})$ within the ZRP surface slab:

$$W(\mathbf{r}) = \sum_{i=-7}^{7} \sum_{j=-7}^{7} \sum_{k=0}^{1} W_{ijk}\, \delta(\mathbf{r} - \mathbf{r}_{ijk})\, \frac{\partial}{\partial |\mathbf{r} - \mathbf{r}_{ijk}|}\, |\mathbf{r} - \mathbf{r}_{ijk}| \tag{8.95}$$

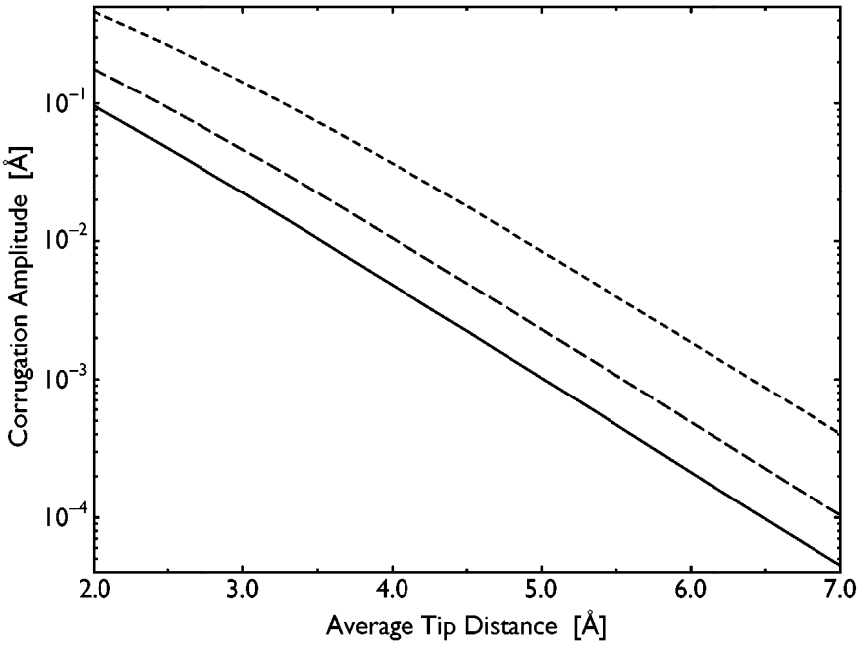

Figure 33: Dependence of the total corrugation amplitude $\Delta z'$ on the average tip-sample separation z_0 within the source model of STM for a ZRP model of the *fcc*–(111) Ag surface. Full line: s–wave source result, dashed line: p–wave tip state ($l = 1, m = 0$), dotted line: d–wave multipole source ($l = 2, m = 0$). See also Figure 30. (Parameters used: $E = -4\,\text{eV}$, $k_F = \tilde{k}_F = 1.5\,\text{Å}^{-1}$, $a = 2.89\,\text{Å}$, $W_0 = -27.6\,\text{eV}\cdot\text{Å}^3$. The simulation was performed for a two-layer *fcc* ZRP lattice slab containing 311 scattering centers.)

[cf. (8.82)]. Here, $\mathbf{r}_{ijk} = i\mathbf{a}_1 + j\mathbf{a}_2 + k\mathbf{a}_3$, where $\mathbf{a}_1, \mathbf{a}_2, \mathbf{a}_3$ denotes the set of primitive basis vectors for the *fcc* Bravais lattice (8.94). For the 450 ZRPs representing the ionic cores in this two-layered surface slab, we selected the parameters familiar from the silver surface model and chose the interatomic distance at $a = 2.89\,\text{Å}$ and the ZRP interaction strength as $W_{ijk} = -27.6\,\text{eV}\cdot\text{Å}^3$. In this form, (8.95) again describes a clean *fcc*-(111) Ag surface; by replacing the central ZRP in the topmost surface layer with a point scatterer $W_{000}(\mathbf{r})$ of different strength $W_{000} = -23.0\,\text{eV}\cdot\text{Å}^3$ (our simple approximation of a "copper atom"), we obtain a model of a disturbed Ag surface with a point defect in it. For the purpose of comparison, simulations were performed for both ZRP arrays. As usual, the corrugative surface potential $W(\mathbf{r})$ (8.95) was placed in a constant force field environment $U_0(z) = -Fz$ which coupled the various multipole tip states employed ($l = 0, 1, 2; m = 0$) to both layers of the ZRP surface slab; however, propagation within the ZRP array was assumed to proceed freely (8.87) with an electronic wave number $\tilde{k}_F = 1.5\,\text{Å}^{-1}$. (In technical terms, this means that the scattering T matrix in (8.93) was calculated using the free-particle Green function $G^{(\text{free})}(\mathbf{r}, \mathbf{r}'; \tilde{E}_F)$ (3.25).) The following three figures show corrugation profiles $\Delta z'(x', y'; \sigma_0)$ obtained in constant current

mode, where the zero-bias conductivity σ_0 has been adapted so that the average scanning distance z_0 for the unperturbed Ag model surface (8.95) was fixed at $z_0 = 2.5\,\text{Å}$. (For the s–wave source, this is equivalent to $\sigma_0 = 2.68\,\text{M}\Omega$; the corresponding numbers for the oriented tip states are $\sigma_0 = 1.39\,\text{M}\Omega$ ($l = 1$, $m = 0$), and $\sigma_0 = 1.30\,\text{M}\Omega$ ($l = 2$, $m = 0$), respectively.) Like in the other examples shown, the emission energy of the electrons at the tip position was chosen as $E = -4\,\text{eV}$, whereas the topmost ZRP layer in (8.95) was placed at the plane of zero kinetic energy. The model is uniquely fixed by providing a value for the Fermi wave vector k_F for the tip material in (8.93), which we selected as $k_F = 1.5\,\text{Å}^{-1}$.

Figure 34 displays the corrugation profiles $\Delta z'(x', y'; z_0)$ obtained from the source-sink model of STM for the surface potential $W(\mathbf{r})$ (8.95) including the point defect for the three longitudinal multipole tip sources with $l \leq 2$ (top caption: s–wave source, center: p–tip state ($l = 1$, $m = 0$), bottom: d–wave source ($l = 2$, $m = 0$)). From the figure, it is plain that the resolution of the surface drastically improves with increasing l, as must have been expected from the spotlight model of STM (Section 8.1.3) in connection with the observation that the electronic current filament width in ballistic tunneling narrows as l grows (Figure 19). (In fact, Figure 34 may serve as an illustration to the $\Delta z'(z_0)$ curves plotted in Figure 33.) The point defect causes a shallow depression in the STM images which is somewhat wider than the interatomic distance a; its diameter only slightly reduces as the orbital quantum number l of the multipole source increases. Clearly, in the exponential resolution regime of Section 8.1.3 which here obviously applies, the point defect itself is not resolved. Rather, the lattice defct serves to scan an inverse image of the lateral density profile of the tunneling current filament at the surface which is superimposed to the "hexagonal cosine" pattern (8.70) caused by the *p6mm* ornamental symmetry of the unperturbed *fcc*–(111) topmost surface layer (Section 8.3.1).

Once we have this simulation at hand, we may analyze the numerical data to inquire further into the mapping properties of our source-sink STM model. In the following figure, we shall examine exclusively those contributions to the corrugation amplitude $\Delta z'(x', y'; z_0)$ that are not due to the simple "hexagonal cosine" pattern $\sum_{k=1}^{3} \cos \mathbf{G}_k \cdot \mathbf{r}_\perp$ (8.70) characteristic of the *p6mm* point symmetry group of the clean *fcc*–(111) surface layer. In the point defect model surface, such contributions may arise from two different mechanisms: First, the point defect connected to $W_{000}(\mathbf{r})$ (8.95) itself breaks the discrete translational symmetry of the surface layer, thus the central depression arising as an image of the lateral current profile emitted from the source should be accentuated. Second, higher Fourier components of the periodic surface potential $W(\mathbf{r})$ (8.95) may periodically render the entire STM corrugation image; we expect that the remaining periodic image is dominated by the six equivalent reciprocal lattice vectors of second-lowest modulus which are e. g. represented by $\mathbf{G}_1 + \mathbf{G}_3$ (8.69) and share a common wave number $\tilde{G} = \sqrt{3}\,G = 4\pi/a$ (Figure 28; for the Ag

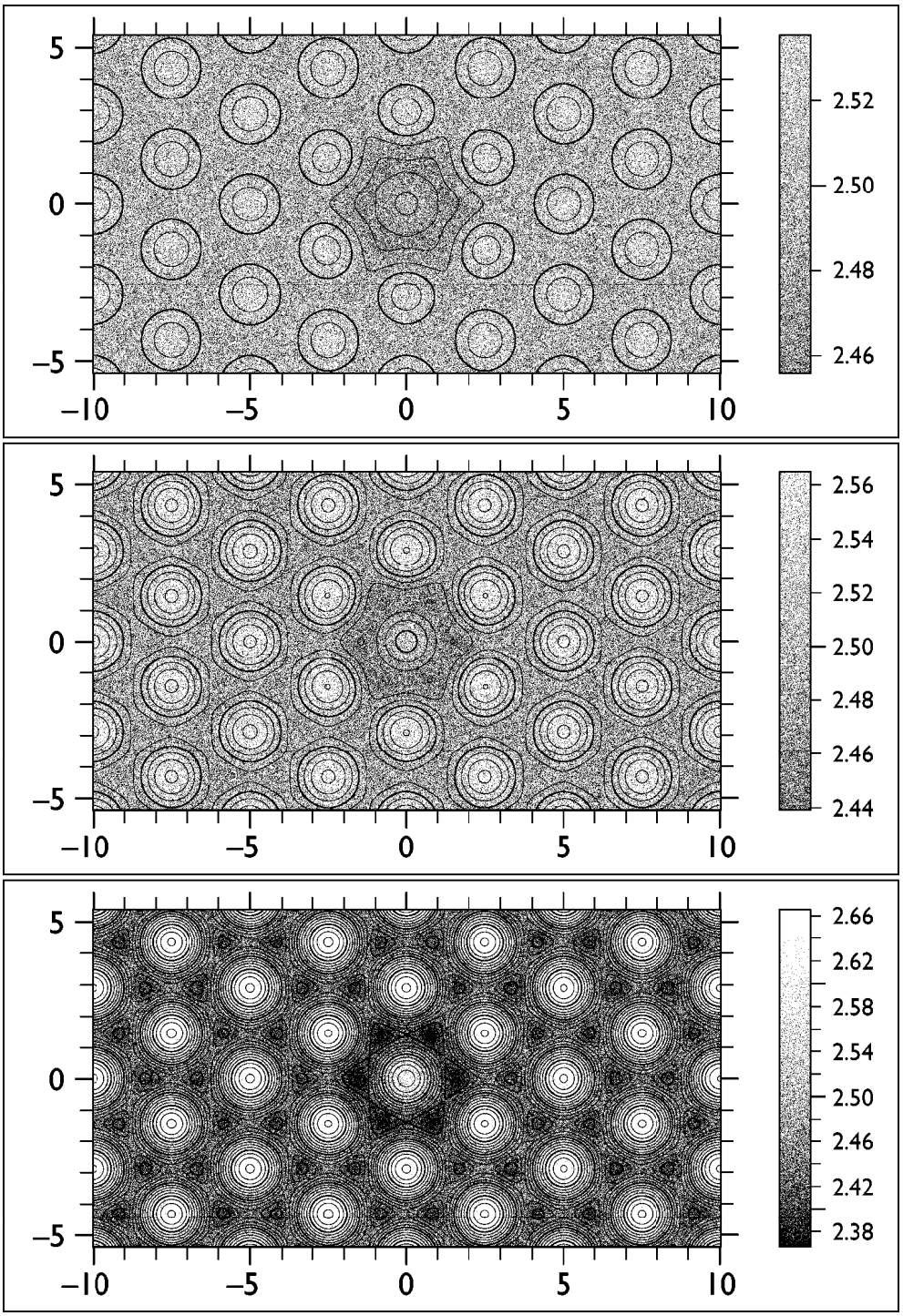

Figure 34: STM image simulations for a *fcc*–(111) ZRP Ag surface model (8.95) including a point defect. Top: s–wave image, center: p_z–tip profile, bottom: d_{z^2}–wave source. The average tip-surface separation is $z_0 = 2.5$ Å. (Parameters used: $E = -4$ eV, $k_F = \tilde{k}_F = 1.5\,\text{Å}^{-1}$, $a = 2.89$ Å, $W_0 = -27.6\,\text{eV}\cdot\text{Å}^3$, $W_{\text{Defect}} = -23.0\,\text{eV}\cdot\text{Å}^3$, two-layer ZRP array containing 450 "atoms.")

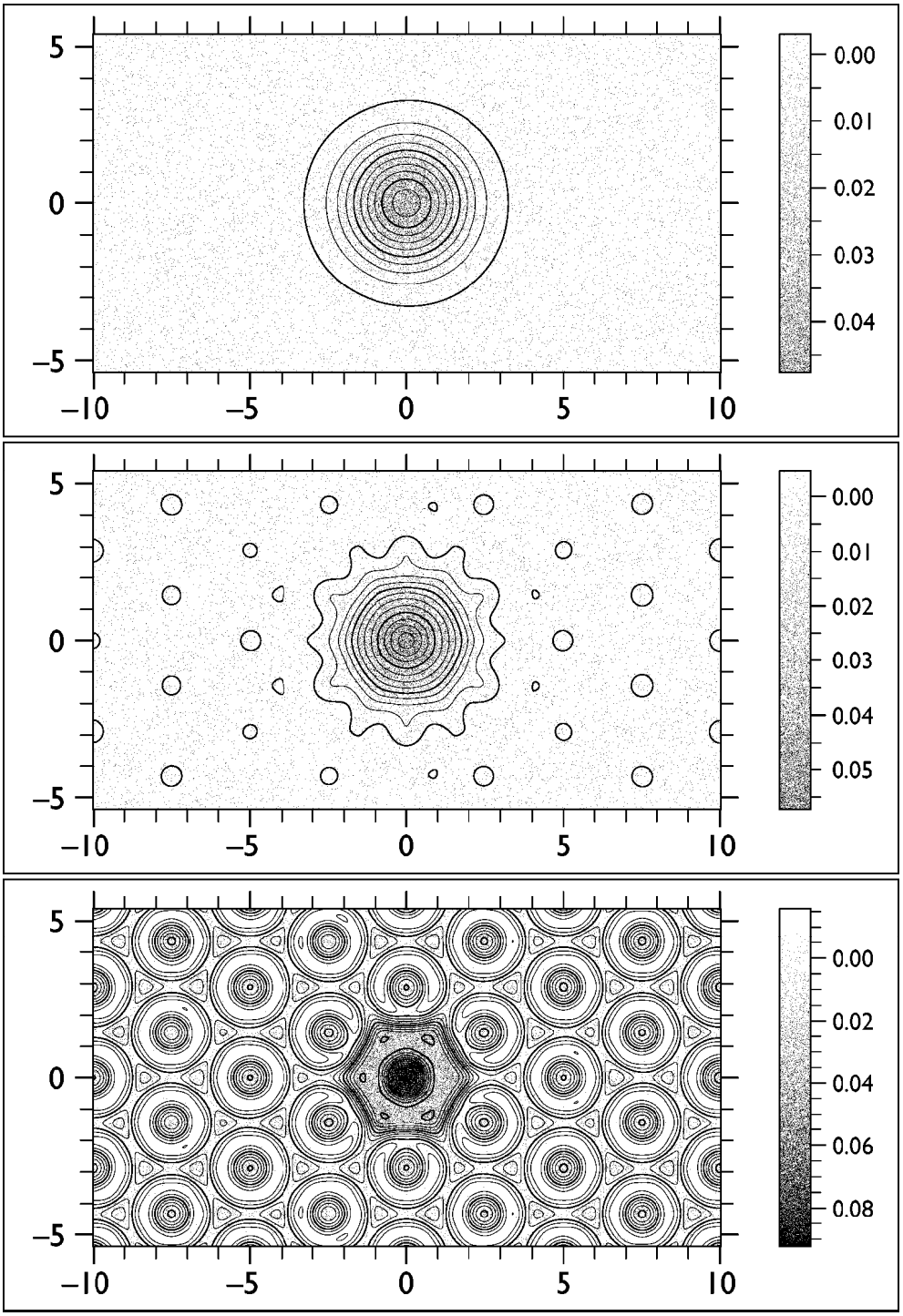

Figure 35: STM image simulations for a model of the Ag–(111) surface containing a point defect (8.95), processed to remove the contributions due to the basic reciprocal lattice vectors $\mathbf{o}$, $\pm\mathbf{G}_{1,2,3}$ (8.69) of the periodic surface pattern. Top: s–wave source, center: p_z–tip state, bottom: d_{z^2}–wave source. (Simulation parameters as in Figure 34.)

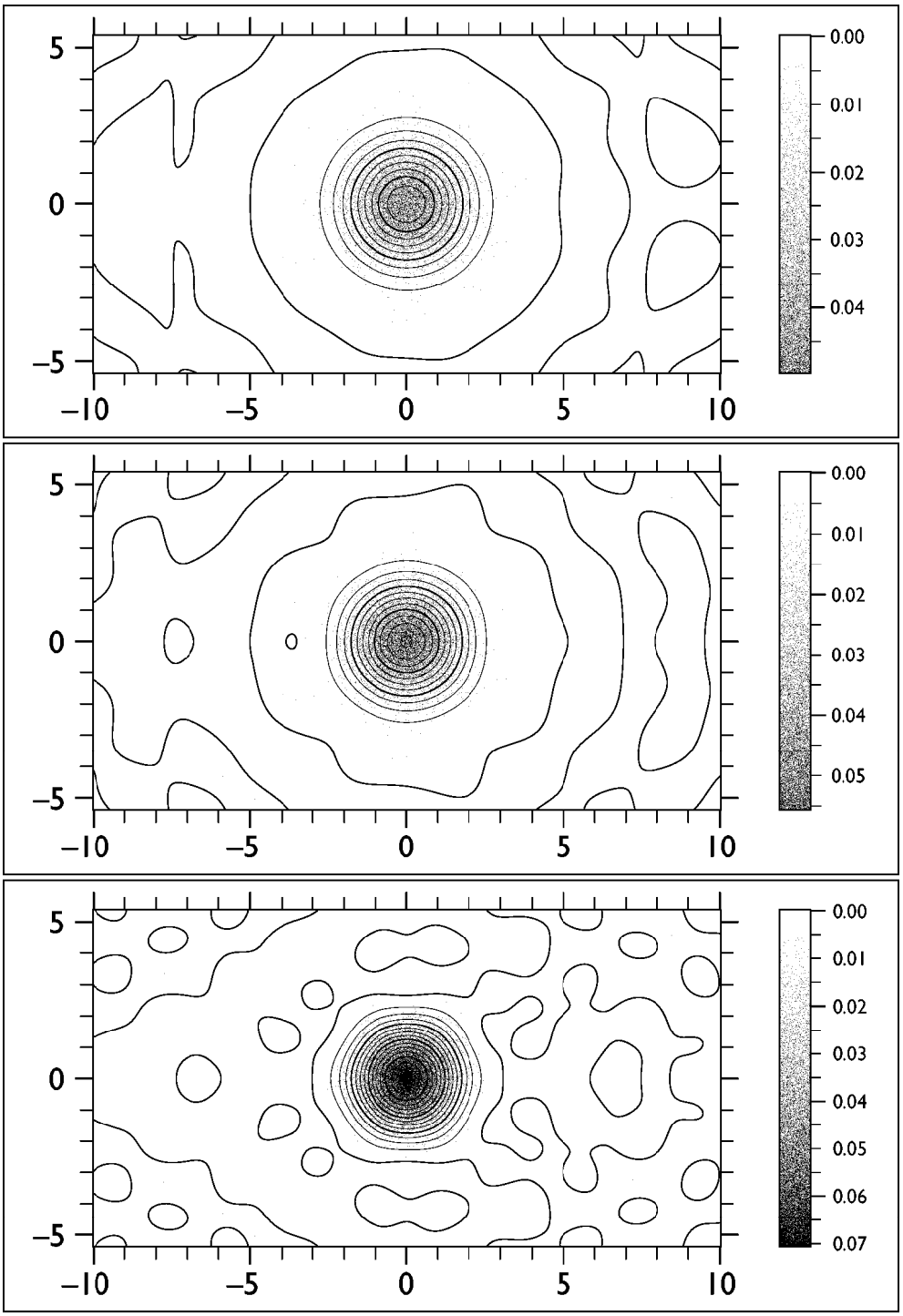

Figure 36: Difference images of a surface point defect, obtained from subtraction of STM corrugation simulations for a ZRP *fcc*–(111) surface imitating Ag (8.95) with and without the perturbing point defect. Top caption: s–wave source, center: p_z–tip state, bottom: d_{z^2}–wave source. (Parameters as in Figures 34 and 35.)

surface, $\tilde{G} \sim 4.35\,\text{Å}^{-1}$). Figure 35 shows the reconstruction of the STM images displayed in Figure 34 after removing the discrete Fourier components of $\Delta z'(x', y'; z_0)$ connected to the fundamental reciprocal lattice vectors $\mathbf{o}$, $\pm\mathbf{G}_1$, $\pm\mathbf{G}_2$, $\pm\mathbf{G}_3$ (8.69) of the *fcc*–(111) periodic surface. No trace of the periodic tiling is visible for the s–wave tip image, only a neat circular projection of the s–wave "spotlight" remains (top caption). The p–tip state ($l = 1$, $m = 0$) image of the current profile appears slightly deformed, and the *fcc*–(111) surface pattern is barely visible for this tip (center). Only the d–wave source ($l = 2$, $m = 0$) shows a distinct periodic corrugation structure superimposing the central spot image (bottom). It is seen that the Fourier components of wave number $\tilde{G} = \sqrt{3}\,G$ form a screwnut-like pattern with a central and outer depression in the *p6mm* Wigner–Seitz cell [166], separated by an elevated ringlike structure. Nevertheless, the total corrugation amplitude does not exceed 0.04 Å.

Finally, another obvious technique to isolate the effects due to the point defect $W_{000}(\mathbf{r})$ in (8.95) is to record STM image simulations for both the perturbed and unperturbed ZRP surface slab (8.95) and study the difference scan formed by subtraction of the STM corrugation amplitudes $\Delta z'(x', y'; z_0)$ obtained in both cases. The results are displayed in Figure 36. We infer that the difference method is very effective in eliminating the contributions due to the periodic *fcc*–(111) surface ZRP lattice background. As expected from the spotlight model of STM (Section 8.1.3), the point defect renders the lateral current density profile of the tunneling current filament emitted by the multipole sources, easily recognized in the difference images as depressions of circular shape. In accordance with the increased resolution capability (Figures 33 and 34), the radius of these "spots" slightly decreases with growing orbital quantum number l. (The oddly shaped patterns conspicuous in Figure 36 may be considered as numerical artifacts which arise from inexact cancellation of both STM images.)

Chapter 9

Summary and Outlook

NOW THAT WE HAVE COMPLETED our systematic study of quantum ballistic motion that we first outlined in the introduction to this treatise (Chapter 1), it appears advisable to pause for a moment and recapitulate our findings as well as to indicate where further progress might be achieved. Thus, let us present a brief survey of multipole sources in quantum mechanics, explicit representations of the multipole partial waves in the uniform field environment, and the practical application of the ballistic source formalism towards photodetachment phenomena, the field emission process, and scanning tunneling microscopy (STM).

We shall start out with a concise summary of quantum source theory that was covered in detail in Chapter 2 and Appendix A of this volume. We motivated the introduction of source terms into the Schrödinger equation by comparison to other field theories and inferred that the source inhomogeneity term provides a straightforward way to include "external" influences onto the evolution of a quantum system. Naturally, the actual shape of the source term is only available from an analysis of the scattering process providing the probability amplitude fed into the quantum system under consideration by the source. Mathematically, the source problem yields to a description in terms of Green functions, special solutions for pointlike inhomogeneities (Dirac δ–functions). For the time-dependent Schrödinger equation, the Green function is known as the propagator and intimately related to the time evolution operator of the system (Appendix A.2). For time-independent potentials, a Laplace transform of the propagator (2.13) results in the Green function $G(\mathbf{r}, \mathbf{r}'; E)$ for the stationary inhomogeneous Schrödinger equation (2.12). This quantity, which presents the central concept in the quantum source formalism developed in this treatise, allows for an interpretation as the spatial representation of the resolvent operator $\mathcal{R}(E) = (E\mathcal{E} - \mathcal{H})^{-1}$ of the system (Appendix A.3) and thus may be expanded within a complete set of eigenfunctions of the Hamiltonian operator $\mathcal{H}$. The inhomogeneous Schrödinger equation gives rise to a modified equation of continuity that contains a particle current source which depends on the imaginary part of the Green function. Therefore, the total current emitted by an isotropic point source at the position $\mathbf{r}'$ is simply proportional to

$\Im[G(\mathbf{r}', \mathbf{r}'; E)]$ (2.34). Alternatively, the eigenfunction expansion of $G(\mathbf{r}', \mathbf{r}'; E)$ shows that the current may also be expressed through the local density of states (LDOS) $n(\mathbf{r}'; E)$ at the source location $\mathbf{r}'$ (Appendix A.6).

Point sources are convenient to handle mathematically, but their conventional form of a Dirac δ–distribution $\delta(\mathbf{r}-\mathbf{r}')$ is unfortunately rather inflexible—close to the source, the emission pattern implicit in $G(\mathbf{r}, \mathbf{r}'; E)$ will invariably show spherical symmetry. This property renders the simple δ–source inappropriate whenever the source mechanism enforces the generation of particles carrying angular momentum. (Processes of this type occur in photodetachment, field emission, and STM. See Chapter 3 and 6–8.) Borrowing the idea from potential theory (Section 2.4), we introduce pointlike multipole sources $\delta_{lm}(\mathbf{r} - \mathbf{r}')$ (2.23) that emerge from the conventional inhomogeneity $\delta(\mathbf{r} - \mathbf{r}')$ by application of a differential operator acting on $\mathbf{r}'$. Obviously, the solution $G_{lm}(\mathbf{r}, \mathbf{r}'; E)$ to the modified inhomogeneous Schrödinger equation (2.24) is generated by the same spherical tensor gradient $K_{lm}(\partial/\partial\mathbf{r}')$ acting on the Green function $G(\mathbf{r}, \mathbf{r}'; E)$ (2.25). Since $K_{lm}(\partial/\partial\mathbf{r}')$ presents an operator of orbital (l, m) spherical symmetry, this angular characteristic should be transferred to the multipole Green function $G_{lm}(\mathbf{r}, \mathbf{r}'; E)$. As expected, for free-particle sources this procedure simply reproduces the spherical wave solutions familiar from partial wave analysis (Appendix C.1). However, a lengthy proof (Appendix A.5) shows that in the vicinity of the source $\mathbf{r} \to \mathbf{r}'$, all multipole Green functions share a common asymptotic form dependent only on the angular momentum quantum numbers l and m, but not on the potential relief $U(\mathbf{r})$ or the energy E, thus confirming the multipole property of $G_{lm}(\mathbf{r}, \mathbf{r}'; E)$. Again, the total current $J_{lm}(\mathbf{r}'; E)$ (2.33) generated by the multipole source $\delta_{lm}(\mathbf{r}-\mathbf{r}')$ is available from the Green function $G(\mathbf{r}, \mathbf{r}'; E)$, but its calculation additionally involves differentiation operations and a limiting process. Alternatively, the multipole current $J_{lm}(\mathbf{r}'; E)$ also may be represented in terms of spherical derivatives of the eigenfunctions of the Hamiltonian $\mathcal{H}$ (Appendix A.6). These concepts were conceived and verified for scalar potentials $U(\mathbf{r})$ only which excludes magnetic fields $\mathbf{B} = \boldsymbol{\nabla} \times \mathbf{A}$ from the following considerations. The extension to general electromagnetic potentials is left as a future task.

We illustrated the implementation of quantum multipole sources employing near-threshold photodetachment processes as an instructive example which is furthermore relevant in practice (Chapter 3). Emphasizing its connection to Fermi's golden rule in conventional perturbation theory (Appendix A.6), we detailed how a series of approximations leads from the analysis of photon-ion interaction to the pictorial model of a monochromatic multipole point source of electrons. Depending on the parities of the parent ionic and daughter atomic states involved, in this way isotropic s–wave sources as well as outgoing electronic p–waves (whose orientation naturally depends on the polarization of the absorbed photon) may be realized experimentally. Best performance of the multipole source formalism is expected in the long wavelength limit,

i. e., for small initial kinetic energies of the detached electron. This corresponds to photon wave numbers close to the electron affinity of the examined ion. An analysis of the free-particle source model (Appendix C.2) shows that in the vicinity of the detachment threshold, the total electronic current generated by the source should obey a simple power law, the Wigner law $J_{lm}^{(\mathrm{free})}(E) \propto E^{l+1/2}$ (3.27), leading to a characteristic distinction between the threshold behavior of s– and p–wave sources. Indeed, the photodetachment cross sections observed in experiment very closely follow the predictions from the multipole source model (Section 3.2).

Yet, multipole source theory could be rightfully called a superfluous exercise in mathematics, were its applicability limited to the analysis of free-particle scattering events. Fortunately, there is another long-range potential $U(\mathbf{r})$ that allows for a solution of the stationary source problem in terms of closed-form expressions, the linear potential $U(\mathbf{r}) = -\mathbf{r} \cdot \mathbf{F}$ corresponding to the uniform force field environment. Although this fact has been known for more than two decades, it remained virtually unnoticed, which initiated the comprehensive mathematical study of the ballistic multipole source problem that presents a major aspect of this treatise. In order to be able to grasp the full physical meaning of these solutions, it is instructive to revisit first the classical mechanics of free-falling motion (Chapter 4) and examine the ballistic trajectories connecting the source and destination locations $\mathbf{r}$ and $\mathbf{r}'$ for fixed particle energy E. To ease connection to the quantum domain, this inquiry is best performed in the framework of Hamilton-Jacobi theory. A surprisingly involved calculation yields the classical ballistic paths $\mathbf{r}(t)$, the time of flight T (4.12), and the reduced action functional W_{cl} (4.14), all as a function of $\mathbf{r}$, $\mathbf{r}'$, and E (Section 4.1). Depending on the choice of these parameters, three different regimes of ballistic motion, delimited by a parabolic turning surface, may be discerned. Besides classically allowed motion which may generally take part along two different trajectories, the sector of classically forbidden motion may further be subdivided into energetically and dynamically forbidden motion: Whereas the former pattern may be fitted into a semiclassical trajectory scheme (motion of particles with energy $-E$ in the inverted potential landscape $-U(\mathbf{r})$), it is yet of merely academic interest; the latter cannot be visualized as it formally takes place in complex spacetime. A genuine feature of tunneling phenomena in several dimensions, it is essential to achieve some understanding of dynamical tunneling as this type of forbidden motion prevails in ballistic tunneling processes (field emission, STM).

Next, we turned our attention towards the multipole quantum source formalism for the uniform force field environment $U(\mathbf{r}) = -\mathbf{r} \cdot \mathbf{F}$. First, we derived the time-dependent propagator $K(\mathbf{r}, t; \mathbf{r}', t')$ (5.9) for this problem. This quantity has been accessed in a number of different ways; we presented an elegant approach based upon gauge transformations for the classical ballistic problem (Section 4.3). The simple structure of the propagator permits to state a differential relation (5.12) which relates

the stationary ballistic Green function $G(\mathbf{r},\mathbf{r}';E)$ in configuration space to the one-dimensional Green function $G(z,z';E)$ assigned to the linear potential $U(z)=-Fz$ that may be constructed rather easily by properly matching eigenfunctions of the uniform field problem at $z=z'$. (The mathematical foundation for this prescription is discussed in Appendix A.4.) The ballistic Green function $G(\mathbf{r},\mathbf{r}';E)$ (5.18) mainly consists of a linear combination of products of Airy functions whose arguments depend on parabolic coordinates $r\pm z$ (5.19). The definition of these special functions, their asymptotic properties and some integral relations involving them are the topic of Appendix D.

The remainder of Chapter 5 deals with the multipole Green functions and the corresponding currents generated by sources embedded within a homogeneous force field. Although this pursuit appears as a simple application of the mathematical apparatus already laid out in Chapter 2 of this treatise, in practice a fairly sophisticated approach is required to obtain an analytical representation for these quantities. (This reasoning often involves mathematical identities concerning the transformation of spherical harmonics and related functions that are not easily accessed from the literature on the subject. Thus, they are covered in Appendix B of this volume.) The ballistic multipole Green functions $G_{lm}(\mathbf{r},\mathbf{o};E)$ (5.28) are derived in Section 5.3, and the current density distributions $j_{lmm'}(\mathbf{r},\mathbf{o};E)$ (5.41) pertaining to them are briefly examined in Section 5.4. A rather exhaustive study of the total currents $J_{lm}(E)$ generated by multipole sources located in the origin $\mathbf{r}=\mathbf{o}$ of the linear potential $U(\mathbf{r})=-\mathbf{r}\cdot\mathbf{F}$ is performed in Section 5.5; in addition to the exact quantum result (5.48), also an asymptotic analysis for $J_{lm}(E)$ in the limit of large energies has been carried out (5.58), (5.59). All these expressions tend to become lengthy and difficult to handle when written in full, in particular for large values of the quantum numbers l and m. In many applications, however, usage of the exact formulae is unnecessary, but their principal asymptotic forms for large distance r between source and destination suffice completely. As a proper vehicle to attain them, we constructed the lateral momentum representation $G_{lm}(\mathbf{k}_\perp,z;E)$ (5.70) of the ballistic multipole Green function (Section 5.6). Explicit representations for the far-field asymptotics of the Green functions $G_{lm}^{(\mathrm{as})}(\mathbf{r},\mathbf{o};E)$ (5.82) and the current density distributions $j_{lmm'}^{(\mathrm{as})}(\mathbf{r},\mathbf{o};E)$ (5.95) derived from them in the limit $r\to\infty$ are presented in Sections 5.7 and 5.8. For convenient reference, full expressions for all these quantities have been listed for the lowest multipole orders l in Appendix E.

We displayed the results of the theory of ballistic multipole sources for the case of classically allowed motion (emission of particles with positive kinetic energy) in the course of Chapter 6. There, we also made use of the opportunity to interpret the peculiar features observed in the current density pattern generated by ballistic sources in terms of the classical dynamics of freely falling bodies (Chapter 4). Furthermore, we compared experimental data obtained from photodetachment processes taking place

in a uniform electric field environment to the theoretical predictions derived in the preceding chapter. In Section 6.1, we started out by plotting a "map" of the lateral current profiles generated by ballistic multipole sources representing various orbital emission characteristics. Apart from providing some information on the geometrical source structure, the current "spot" images of Figure 5 show a common conspicuous pattern of concentric dark and bright rings. The nature of this circular texture, as well as all other features discernible within this figure, are fully explained by a semiclassical analysis of motion in a uniform force field that is carried out in Section 6.2. In particular, the circular structure could be traced back to quantum interference due to the twofold degeneracy of classical ballistic paths connecting the source with a given destination on the screen. Thus, the homogeneous force field acts in a similar way as the conventional double slit setup in Feynman's famous gedankenversuch. In an ingenious experiment, C. Blondel and his colleagues were able to record this interference pattern which choosing proper values for the emission energy E and the field strength F may attain macroscopic sizes in the mm range (Section 6.4). Within experimental accuracy, no deviations from the simple ballistic source picture were found (Figure 14). Meanwhile, these authors have further developed their "photodetachment microscope" into an electron interferometer device designed to measure electron affinities with high precision.

Interference of classical trajectories also affects the total current emission by a multipole source embedded in a uniform force field (Section 6.3). Figure 7 depicts the results from a quantum calculation; we inferred that $J_{lm}(E)$ overall shares the character of the current emitted by a corresponding free-particle source $J_{lm}^{(\mathrm{free})}(E)$, i. e., roughly follows Wigner's power law. However, the graphs displayed in this figure additionally show an exponentially decaying sub-threshold tail due to ballistic tunneling, and for $E > 0$, the multipole currents generated by longitudinal sources ($m = 0$) are shaped into a characteristic "staircase" pattern, whereas $J_{lm}(E)$ for $|m| > 0$ hardly deviates from the Wigner law. Within the semiclassical "closed-orbit" theory, the modulation of the photocurrent is explained by the interference of the single returning classical path starting out from the source opposite to the direction of force with the trajectory emitted along the escape path. The presence of the centrifugal barrier forestalls the emission of particles parallel to $\mathbf{F}$ for sources with $|m| > 0$; hence, their assigned currents remain unaffected by the interference mechanism. Comparison of the theoretically predicted ballistic currents with the best available data from photodetachment experiments performed by D. J. Larson and his co-workers (Figures 8–11) indicates acceptable agreement.

Besides representing the quantum analog of classical free-falling motion, the ballistic source problem offers the unique opportunity to study tunneling phenomena in several spatial dimensions guided by an analytically solvable model (Chapter 7). Clearly, in the tunneling case, the complex "trajectories" $\mathbf{r}(t)$ formally obtained from

the classical dynamics of uniformly accelerated motion are of little help in the interpretation of the ballistic partial waves $G_{lm}(\mathbf{r}, \mathbf{o}; E)$. Nevertheless, we established a WKB model of ballistic tunneling motion by analytical continuation of Hamilton's characteristic function $W_{\mathrm{cl}}(\mathbf{r}, \mathbf{o}; E)$ (4.14) into the complex plane. The emerging semiclassical wave function presents simultaneously a propagating and an evanescent wave, where the respective wave fronts are approximately given by the orthogonal sets of confocal paraboloids $r \pm z = \mathrm{const}$. This structure essentially confines the tunneling particle distribution to a narrow "current filament" centered around the escape path in direction of the force field. Close to this axis, the lateral profile of the tunneling current is approximately of Gaussian shape. Interestingly, the width of this Gaussian profile does not depend on the force strength F. The predictions from the semiclassical model of ballistic tunneling, in particular the shape invariance of the current density distribution, are largely confirmed in experiments dealing with field emission from mesoscopic cluster tips containing few tungsten atoms. However, the simple ballistic theory fails to explain the magnitude of the tunneling currents observed by H.-W. Fink et al. This shortcoming probably results from the omission of field enhancement effects in the tip neighborhood which break the lateral symmetry of the uniform field approximation.

Another noteworthy inference from the ballistic WKB model involves the structure of the lateral particle distribution in the vicinity of the tunnel exit: According to semiclassical reasoning, there the product of the uncertainties ΔR and Δp in configuration and momentum space with regard to the directions perpendicular to $\mathbf{F}$ saturates Heisenberg's famous inequality. This observation served as the motivation to devise a novel approximation scheme for multidimensional tunneling whose range of validity far exceeds the special case of ballistic tunneling, the minimum uncertainty model. It is based on the insight that within the classically forbidden sector, deviations of the tunneling trajectory from the escape path will be penalized since the action functional $W_{\mathrm{cl}}(\mathbf{r}, \mathbf{r}'; E)$ then no longer presents a local minimum; any increase of its imaginary part will lead to an exponentially suppressed probability amplitude in WKB approximation. In the same way, perpendicular momentum components will reduce the effective energy available for propagation along the escape path and are equally discouraged in tunneling. This mechanism tends to confine the tunneling current to the escape path. However, lateral position and momentum present complementary observables in quantum mechanics and cannot be fixed simultaneously; at best, their uncertainty product $\Delta R \cdot \Delta p$ may take on the minimum value allowed by the Heisenberg uncertainty principle. This is the fundamental assumption behind the minimum uncertainty model of multidimensional tunneling. Extending the uncertainty relation to accommodate angular momentum eigenstates of quantum number $|m| > 0$ (Appendix C.3), we were able to show that the minimum uncertainty relation (7.37) enforces a "generalized Gaussian" lateral profile of the tunneling wave function

both in configuration and momentum space (7.38), (7.39) which pertains to the ground state of a two-dimensional harmonic oscillator in the $L_z = m\hbar$ subspace. The model entirely fixes the shape of the multipole tunneling wave apart from a single parameter, the width of the Gaussian distribution. To estimate this quantity, the minimum uncertainty model was supplemented by a semiclassical argument which relates the variances ΔR and Δp through the bounce or instanton tunneling time (4.21) required to pass along the escape path.

We elaborated the predictions of the minimum uncertainty model into a semiclassical theory of the multipole tunneling current (Section 7.2). Although asymptotically exact for the uniform force field problem, comparison with the actual current density distributions in ballistic tunneling shows that the generalized Gaussian shape is quite strictly realized, whereas the semiclassical width estimate (7.41) should be viewed only as a rough approximation to the true diameter of the current filament (Section 7.3). As a general trend, we found that the radius ΔR of the tunneling current profile shrinks with increasing multipole order l (Figure 19). Obviously, this narrowing of the current filament is accompanied by a widening of the lateral momentum distribution, and thus also by an enlarged opening angle of the field emission current in the far-field sector $r \to \infty$ (Figure 17).

The conception of a tunneling current filament generated by some pointlike multipole source provided the basis for a pictorial yet successful theoretical model of scanning tunneling microscopy (Chapter 8). As is generally known, the operation of the STM device relies on the presence of an atomically sharp tip that emits electrons towards (or absorbs electrons from) the surface of the examined sample. In a good approximation, the entire tunneling current measured in STM is funneled through the outermost atom of the tip which we replaced in the source model of STM by a multipole tunneling source of suitable orbital character. It is straightforward to relate the intrinsic multipole current $J_{lm}(\mathbf{r}'; E_F)$ generated by the pointlike "tip" located at $\mathbf{r}'$ to the zero-bias, zero-temperature conductivity $\sigma_{lm}(\mathbf{r}')$ (8.11) of the STM junction. Alternatively, $\sigma_{lm}(\mathbf{r}')$ may be linked to the eigenfunction representation of the multipole current (Appendix A.6), thus regaining the reliable result of the standard Tersoff-Hamann theory of STM that the tunneling current is proportional to the local density of states (LDOS) $n(\mathbf{r}'; E_F)$ (8.13) at the tip position for isotropic s–wave sources. (In general, the topography of STM images displays constant-density surfaces for the spherical tensor gradients of the sample wave functions (8.12).)

It proved sensible to decompose the zero-bias conductivity $\sigma_{lm}(\mathbf{r}')$ of the STM junction for constant scanning height z_0 into two parts: The average conductivity $\sigma^{(0)}_{lm}(z_0)$ pertains to some background potential $U_0(z)$ which is invariant with respect to translations parallel to the surface and describes the overall properties of the bulk-vacuum transition, whereas the remaining corrugative conductivity $\Delta\sigma_{lm}(\mathbf{r}')$ provides information about the surface structure encoded in the corrugative potential contribution

$W(\mathbf{r})$ and is responsible for rendering the STM image. This separation is also naturally reflected in the series expansion of the multipole Green function $G_{lm}(\mathbf{r},\mathbf{r}';E_F)$ with respect to the background Green function $G^{(0)}_{lm}(\mathbf{r},\mathbf{r}';E_F)$ assigned to $U_0(z)$ which shares the shift invariance of this potential (8.20). Obviously, the properties of the mapping of the surface structure potential $W(\mathbf{r})$ onto the corrugative conductivity $\Delta\sigma_{lm}(\mathbf{r}')$ are of central importance in STM and determine in particular the resolution capability of this device. To gain an estimate for this quantity, we devised a pictorial concept, the "spotlight model": Assuming that the conductivity variation depends linearly on the corrugative potential, we approximated $\Delta\sigma_{lm}(\mathbf{r}')$ by the convolution integral of the unperturbed current density distribution due to $G^{(0)}_{lm}(\mathbf{r},\mathbf{r}';E_F)$ with $W(\mathbf{r})$ (8.33). In reciprocal space, this relation simplifies to a product; replacing the current profile by a Gaussian "spot" as proposed by the minimum uncertainty model of multidimensional tunneling, the transfer function in the conductivity-potential relation also adopts Gaussian shape (8.34), allowing to identify an estimate $a_{\mathrm{sc}}(E)$ for the resolution capability of STM (8.36). It turns out that the current distribution within the STM gap is rather insensitive to the actual barrier potential $U_0(z)$ which leads to a typical resolution estimate of order $a \sim 4\sqrt{z_0}$ Å (where z_0 is also given in Å). For smaller structures, resolution loss caused by averaging sets in, and the observed corrugation drops exponentially, as a more sophisticated analysis of the spotlight model based upon the WKB wave function in ballistic tunneling shows (8.42). In this regime, the corrugation depends sensitively upon the width of the lateral current profile near the surface. From our study of ballistic tunneling from multipole sources, we inferred that d–wave tip states with their narrow emission cone present preferred electron sources in STM. Indeed, in practice STM tips are mostly fabricated from transition metals (W, Ir) with dominant d–bands near their respective Fermi energies.

As noted above, the quantum source formalism itself fails to predict the absolute magnitude of the current generated by the source; this task is left to an examination of the scattering event which actually supplies the source with particles. Hence, a supplement to the simple source theory of STM stating the tip efficiency is in order. (However, it should be noted that a detailed understanding of the emission process is not required for the interpretation of STM images.) The somewhat unusual starting point for our theory of the source strength of a metallic tip was the Pauli exclusion principle which naturally limits the phase space density of electrons in the tip body (Section 8.2). From the Pauli principle, a global maximum bound for the particle current emitted by a multipole point source of pure (l,m) orbital symmetry was found; in terms of the zero-bias conductivity in STM, it reads $\sigma_{lm}(\mathbf{r}') \leq 2e^2/\pi\hbar$ (8.64). This universal value is closely related to the quantized resistance $\pi\hbar/e^2$ observed in the quantum Hall effect and plays an important role in the description of the electric properties of one-dimensional mesoscopic conductors. In fact, we inferred that Landauer's theory for the resistance of point contacts may be deduced from the point

source formalism. To implement this transport bound into the source model of STM, we represented the tip as a free-electron gas with an embedded multipole scattering center which absorbs electrons at the maximum rate permitted by the Pauli principle (8.57). In a second step, some of the electrons are emitted towards the sample, a process described by the multipole Green function $G_{lm}(\mathbf{r}, \mathbf{r}'; E_F)$ for the junction environment, while most are simply reflected back into the tip body. This enhanced source-sink model of STM leads to an unambiguous prediction for the junction conductivity (8.65). As a first application, we used it to show that tip states with $|m| > 0$ due to their lower conductance caused by the additional centrifugal tunneling barrier are irrelevant for the STM imaging process (Figure 27).

Finally, we presented a surface model potential which allows for a closed-form solution in the framework of the source model of STM (Section 8.3). It is composed of an array of zero-range potentials (ZRPs) embedded into a uniform force field background and simulates the densely packed *fcc*–(111) surface of a silver crystal. ZRPs describe pointlike isotropic scattering centers (8.72) with renormalizable self-interaction; in the context of STM source theory, they show the favorable property that the Green function $G(\mathbf{r}, \mathbf{r}'; E)$ assigned to the combined system of barrier potential $U_0(z)$ and ZRP array $W(\mathbf{r})$ may be expressed in terms of the background Green function $G^{(0)}(\mathbf{r}, \mathbf{r}'; E)$ belonging to $U_0(z)$ (8.91). For the ballistic model, this quantity is known, so the corrugative conductivity $\Delta\sigma_{lm}(\mathbf{r}')$ is available as an analytical expression (8.93). We employed the ZRP surface model to study the imaging behavior of STM for a periodically tiled pattern (Figures 29 and 32); the numerical simulation confirmed the resolution estimate obtained from the pictorial "spotlight model" of STM (Figures 30, 31, and 33). Furthermore, we examined a surface model with a built-in point defect (Figures 34–36). The image simulations for this sample are illuminatingly interpreted in terms of the source theory of STM which clearly opens up a variety of different options for future research.

Appendix A

Aspects of Quantum Source Theory

IN THIS FIRST APPENDIX, we develop a number of formal properties of Green functions and propagators, emphasizing the mathematical aspects of the subject of sources in quantum mechanics. In a sense, the presentation delivered in this chapter appears complementary to the rather informal introduction to quantum source theory given in Chapter 2, and we will establish results that are advantageously applied in the main body of this treatise. For more information on the use of the Green function technique for the solution of partial differential equations we refer to the monographs written by Rauch and Roach [223, 224].

Let us first summarize the contents of this appendix: Following a brief formal definition of the Green function technique for the solution of inhomogeneous linear partial differential equations (Section A.1), we specialize to the time-dependent Schrödinger equation in Section A.2. There, we present the idea of the time evolution operator and propagators of a quantum system, and introduce the notion of advanced and retarded solutions. Subsequently, in Section A.3 we give a rather detailed discussion of the formal functional analytic approach to quantum theory, in particular to its stationary variant. The purpose of this section is to provide some firm mathematical complement to the heuristic presentation of the theory of quantum sources (Section 2.3). This fairly comprehensive study illustrates features and problems of the common eigenfunction expansion of the Hamiltonian and related operators for the simple case of finite-dimensional spaces, and then turns to Hilbert spaces of infinite dimension. Proceeding step by step, we introduce the spectral representation of self-adjoint operators, provide a no-nonsense definition for the in a strict sense non-normalizable eigenfunctions of the Hamiltonian in its continuous spectrum, give criteria for the completeness of sets of eigenfunctions and show that they are fulfilled for a number of important problems in quantum theory, including the uniform field problem of Section 5. Finally, we state conditions for the existence and uniqueness of the resolvent operator the spatial representation of which are the Green functions of source theory, and we establish the spectral representation of the retarded solution employed in Section 2.3. In Section A.4, we show how to apply these formal developments to the simple case

of one-dimensional quantum motion. Here, our interest is primarily directed to the dynamics in unbounded potentials $U(x)$ like the field emission potential $U(x) = -Fx$. The simple multipole source theory presented in the main body of this volume finds its mathematical justification in Section A.5 of this appendix where we will strictly prove that for a wide class of potentials $U(\mathbf{r})$, the differentiation technique of Section 2.4 indeed leads to the desired angular characteristics of the multipole wave function in the vicinity of the source. Finally, we show how to arrive at some well-known results of conventional perturbation theory, including the eigenfunction representation of the current, Fermi's Golden Rule and the transfer Hamiltonian method originally devised by Bardeen, in the framework of the quantum source approach (Section A.6).

A.1 Inhomogeneous Linear Systems and Green Functions

We will start out with the formal definition of the time-dependent Green function $G(\mathbf{r}, t; \mathbf{r}', t')$ and its application to the solution of inhomogeneous linear differential equations. In order to obtain a formal variant of this technique already presented in Section 2.2 using the heat flow equation as an example, we introduce the notation $D(\mathbf{r}, \mathbf{p}; t)$ for a general linear differential operator. Following the customs of quantum mechanics, $\mathbf{p} = -i\hbar\boldsymbol{\nabla}$ here denotes the hermitian momentum operator as a replacement for the gradient $\boldsymbol{\nabla}$ (where the differential operator is understood to act on the unprimed variable $\mathbf{r}$). By definition, every solution of the special inhomogeneous linear differential equation (2.5):

$$D(\mathbf{r}, \mathbf{p}; t)\, G(\mathbf{r}, t; \mathbf{r}', t') \;=\; \delta(\mathbf{r} - \mathbf{r}')\, \delta(t - t') \tag{A.1}$$

is called a time-dependent Green function $G(\mathbf{r}, t; \mathbf{r}', t')$ of the linear operator $D(\mathbf{r}, \mathbf{p}; t)$. (Note that the definition (A.1) differs from the defining equation of the propagator $K(\mathbf{r}, t; \mathbf{r}', t')$ (2.5) by some prefactor c_H. Hence, we assign slightly different meanings to these terms. The origin of this discrepancy will become clear in the following section.)

In a sense, $G(\mathbf{r}, t; \mathbf{r}', t')$ presents the inverse to $D(\mathbf{r}, \mathbf{p}; t)$. As is well-known from the analogous, yet finite-dimensional theory of systems of linear equations [225], such a solution need not necessarily exist for all $D(\mathbf{r}, \mathbf{p}; t)$, nor will it be generally unique. Later on, we will establish that in the case of time-dependent quantum mechanics, $G(\mathbf{r}, t; \mathbf{r}', t')$ always exists, but is never unique (see Section A.2.2). Once its existence is established, we may however exploit the linearity of $D(\mathbf{r}, \mathbf{p}; t)$ in order to obtain the general solution for the inhomogeneous differential equation (2.1):

$$D(\mathbf{r}, \mathbf{p}; t)\, \Psi(\mathbf{r}, t) \;=\; \sigma(\mathbf{r}, t) \tag{A.2}$$

where $\sigma(\mathbf{r}, t)$ denotes some inhomogeneity ("source"). Its quadrature may be displayed as an integral containing the Green function $G(\mathbf{r}, t; \mathbf{r}', t')$ as a kernel (2.6):

$$\Psi(\mathbf{r}, t) \;=\; \Psi_0(\mathbf{r}, t) + \int d^3r' \int dt'\, G(\mathbf{r}, t; \mathbf{r}', t')\, \sigma(\mathbf{r}', t') \tag{A.3}$$

Here, $\Psi_0(\mathbf{r}, t)$ represents an arbitrary eigenfunction of $D(\mathbf{r}, \mathbf{p}; t)$ with eigenvalue $\Lambda = 0$, i. e., a solution of the corresponding homogeneous differential equation:

$$D(\mathbf{r}, \mathbf{p}; t)\, \Psi_0(\mathbf{r}, t) \;=\; 0 \tag{A.4}$$

Again employing the linearity property of the differential operator, we find that any two Green functions $G(\mathbf{r}, t; \mathbf{r}', t')$ and $G'(\mathbf{r}, t; \mathbf{r}', t')$ belonging to $D(\mathbf{r}, \mathbf{p}; t)$ differ only by a solution of the homogeneous problem (2.2):

$$D(\mathbf{r}, \mathbf{p}; t)\, [G(\mathbf{r}, t; \mathbf{r}', t') - G'(\mathbf{r}, t; \mathbf{r}', t')] \;=\; 0 \tag{A.5}$$

As a consequence, the Green function $G(\mathbf{r}, t; \mathbf{r}', t')$ will be unique if the homogeneous problem $D(\mathbf{r}, \mathbf{p}; t)\, \Psi_0(\mathbf{r}, t) = 0$ (A.4) possesses only the trivial solution $\Psi_0(\mathbf{r}, t) \equiv 0$.

A.2 The Time-Dependent Schrödinger Equation

Let us now specialize to our first case of interest, the time-dependent inhomogeneous Schrödinger equation of quantum mechanics (Section 2.3). In this parabolic partial differential equation, the linear operator $D(\mathbf{r}, \mathbf{p}; t)$ shows the general structure:

$$D(\mathbf{r}, \mathbf{p}; t)\, \Psi(\mathbf{r}, t) \;=\; [i\hbar\partial_t - H(\mathbf{r}, \mathbf{p}; t)]\, \Psi(\mathbf{r}, t) \;=\; \sigma(\mathbf{r}, t) \tag{A.6}$$

where $H(\mathbf{r}, \mathbf{p}; t)$ denotes the hermitian Hamilton operator of the physical model under consideration. In order to deal with this equation, it is a good idea to get rid of the spatial dependence in (A.6) first.

A.2.1 Dirac Representation Theory

For systems involving self-adjoint linear operators $\mathcal{A} = \mathcal{A}^+$ acting in a complex vector space an elaborate theory called functional analysis is available which connects the solution of these systems to the eigenvalues (the spectrum) and corresponding eigenfunctions of $\mathcal{A}$. We will develop the fundamental results of this formalism in Section A.3 of this appendix. Since quantum mechanics is presumably the most important practical application of functional analysis, it should not be surprising that quantum theory has adopted a special notation that dwells upon the advantages of

this mathematical technique. It is known as representation theory and was first proposed by Dirac [226].

In representation theory, the wave function $\Psi(\mathbf{r},t)$ is just the coordinate space appearance of a more fundamental object, the state (or ket vector) $|\Psi(t)\rangle$. We also may call $\Psi(\mathbf{r},t)$ the projection of the state $|\Psi(t)\rangle$ onto the position vector $|\mathbf{r}\rangle$ and write formally $\Psi(\mathbf{r},t) = \langle\mathbf{r}|\Psi(t)\rangle$. (In analogy to the scalar product in complex vector spaces, $\langle\mathbf{r}|$ is known as the adjoint state to $|\mathbf{r}\rangle$, or simply as the bra vector.) In the same fashion, a linear operator $\mathcal{A}(t,t')$ transforms a state $|\Psi(t')\rangle$ into another state $|\Phi(t)\rangle$. The projection of $\mathcal{A}(t,t')\,|\mathbf{r}'\rangle$ onto the position vector $|\mathbf{r}\rangle$ is called the coordinate representation $A(\mathbf{r},t;\mathbf{r}',t') = \langle\mathbf{r}\,|\mathcal{A}(t,t')|\,\mathbf{r}'\rangle$ of the operator. We denote the continuous set of states $|\mathbf{r}\rangle$ as the base states of coordinate space; they form an orthonormal base system:

$$\langle\mathbf{r}|\mathbf{r}'\rangle \;=\; \delta(\mathbf{r}-\mathbf{r}') \tag{A.7}$$

Furthermore, the orthonormal base $|\mathbf{r}\rangle$ is complete. This statement means that the sum over all possible projections is equal to the identity operator $\mathcal{E}$:

$$\int d^3r\;|\mathbf{r}\rangle\,\langle\mathbf{r}| \;=\; \mathcal{E} \tag{A.8}$$

Our main interest is directed towards stationary problems in quantum mechanics, i. e., self-adjoint operators $\mathcal{H}$ that do not depend on the time variable t. The linear operator $\mathcal{H}$ is called hermitian or self-adjoint, if for any two states $|\Psi\rangle$, $|\Phi\rangle$ the following relation holds:

$$\langle\Phi\,|\mathcal{H}|\,\Psi\rangle \;=\; (\langle\Psi\,|\mathcal{H}|\,\Phi\rangle)^* \tag{A.9}$$

Any non-vanishing state $|\Psi\rangle$ which fulfils the relation $\mathcal{H}\,|\Psi\rangle = E\,|\Psi\rangle$ is called eigenstate of the operator $\mathcal{H}$ with eigenvalue E. The set of all eigenvalues is called the point spectrum of $\mathcal{H}$. (In this brief form, the definitions above hold strictly only for systems in finite-dimensional spaces (Section A.3.1). For the most important spaces of infinite dimension, these statements must be considerably refined. See Section A.3.)

Later on in Section A.3, we will give some insight behind the definitions (A.7)–(A.9) and work out the outstanding role of the eigenstates in the theory of linear systems. Before we take a closer look onto the Schrödinger equation in the framework of representation theory, we will however state two important general properties of the eigenstates of the Hamiltonian $\mathcal{H}$ which immediately follow from the property (A.9). First, we note that $\mathcal{H}$ shows only real eigenvalues E; the spectrum of $\mathcal{H}$ is therefore constrained to the real axis. Second, if $|\Psi\rangle$ and $|\Phi\rangle$ are any two eigenstates of $\mathcal{H}$ with different eigenvalues E, E', then $|\Psi\rangle$, $|\Phi\rangle$ will be orthogonal:

$$\mathcal{H}\,|\Psi\rangle = E\,|\Psi\rangle \;\;\wedge\;\; \mathcal{H}\,|\Phi\rangle = E'\,|\Phi\rangle \quad\Longrightarrow\quad \langle\Phi|\Psi\rangle = 0 \tag{A.10}$$

These two simple statements form the basis for the developments of Section A.3.

A.2.2 Advanced and Retarded Solutions

Let us now restate the inhomogeneous time-dependent Schrödinger equation of non-relativistic quantum mechanics (A.6) in the notation of representation theory:

$$[i\hbar\partial_t - \mathcal{H}(t)]\,|\Psi(t)\rangle \;=\; |\sigma(t)\rangle \tag{A.11}$$

Here, $\sigma(\mathbf{r},t) = \langle\mathbf{r}|\sigma(t)\rangle$, and $\mathcal{H}(t)$ is the Hamilton operator of the physical setup under consideration, which is related to the usual coordinate space representation $H(\mathbf{r},\mathbf{p};t)$ by $\langle\mathbf{r}\,|\mathcal{H}(t)|\,\mathbf{r}'\rangle = \delta(\mathbf{r}-\mathbf{r}')H(\mathbf{r},\mathbf{p};t)$. (Note that the Hamiltonian $H(\mathbf{r},\mathbf{p};t)$ is diagonal in $\mathbf{r}$ and vanishes for $\mathbf{r}\neq\mathbf{r}'$.)

In this section, we are going to define special advanced and retarded propagators $K_{\mathrm{ret/adv}}(\mathbf{r},t;\mathbf{r}',t') = \big\langle\mathbf{r}\,\big|\mathcal{K}_{\mathrm{ret/adv}}(t,t')\big|\,\mathbf{r}'\big\rangle$ closely related to the time-dependent Green function $G(\mathbf{r},t;\mathbf{r}',t')$ (A.2), and present them in terms of the time evolution operator $\mathcal{U}(t,t')$ of the system. (For further investigations on the application of Green functions to the Schrödinger equation, we refer to the work of Economou [82].)

We note that the Schrödinger equation (A.11) is a first-order differential equation with regard to the time variable t. Let us first assume that the equation is homogeneous, i. e., the source term in (A.11) vanishes: $|\sigma(t)\rangle = 0$. Then, any superposition of solutions $|\Psi(t)\rangle$ again presents a solution to (A.11). Hence, the solution $|\Psi(t)\rangle$ at time t depends linearly on the same solution $|\Psi(t')\rangle$ at some other time t'. This mapping, in turn, defines a linear operator $\mathcal{U}(t,t')$, the time evolution operator of the system, which by definition translates a homogeneous solution $|\Psi(t')\rangle$ from time t' to time t. Using the generic Dirac bra-ket notation, we may formally write:

$$|\Psi(t)\rangle \;=\; \mathcal{U}(t,t')\;|\Psi(t')\rangle \tag{A.12}$$

Since the total particle number is conserved, $\langle\Psi(t)|\Psi(t)\rangle = \text{const.}$, $\mathcal{U}(t,t')$ must be a unitary operator, $\mathcal{U}(t,t')\mathcal{U}(t,t')^{+} = \mathcal{E}$, where $\mathcal{E}$ denotes the representation of the identity (A.8). Note that $|\Psi(t)\rangle$ is uniquely fixed through its initial value at some moment t'. Equation (A.12) is also known as the solution to the Cauchy problem for (A.11).

Inserting (A.12) into (A.11), we find that with $|\Psi(t)\rangle$ also the evolution operator $\mathcal{U}(t,t')$ itself presents a solution of the source-free Schrödinger equation (A.11):

$$[i\hbar\partial_t - \mathcal{H}(t)]\,\mathcal{U}(t,t') \;=\; 0 \tag{A.13}$$

We note that since $\mathcal{U}(t',t') = \mathcal{E}$, the evolution operator in configuration space obeys the special initial condition (A.7):

$$\lim_{t\to t'} U(\mathbf{r},t;\mathbf{r}',t') \;=\; \langle\mathbf{r}\,|\mathcal{U}(t',t')|\,\mathbf{r}'\rangle \;=\; \langle\mathbf{r}|\mathbf{r}'\rangle \;=\; \delta(\mathbf{r}-\mathbf{r}') \tag{A.14}$$

Consequently, $U(\mathbf{r},t;\mathbf{r}',t')$ represents the quantum evolution of a particle that was localized at $\mathbf{r}'$ at time $t = t'$. Note that this wave function is unique and symmetric in time: $U(\mathbf{r},t;\mathbf{r}',t') = U(\mathbf{r}',t';\mathbf{r},t)^*$.

Let us for the moment assume that the Hamiltonian $H(\mathbf{r},\mathbf{p})$ appearing in the Schrödinger equation (A.6) does not explicitly depend on the time variable t, i. e., we restrict ourselves to the analysis of the quantum dynamics of conservative systems. In this case, the first-order differential equation of the time evolution operator $\mathcal{U}(t,t')$ (A.13) is immediately integrated. Exploiting the unitarity requirement $\mathcal{U}(t',t') = \mathcal{E}$, we find that the evolution operator may be formally displayed as the exponential of the Hamiltonian:

$$\mathcal{U}(t,t') \;=\; \exp\left\{-\frac{i}{\hbar}\,\mathcal{H}\,(t-t')\right\} \tag{A.15}$$

Since the system is invariant with respect to translations in time $t \to t+\tau$, $t' \to t'+\tau$, the evolution operator $\mathcal{U}(T)$ obviously is a function of the relative time difference $T = t-t'$ only (see also Section 4.3.2).

Returning to general Hamiltonians $\mathcal{H}(t)$, we may infer from (A.13) that the time evolution operator is closely connected to the Green function $\mathcal{G}(t,t')$ which within the Dirac formalism presents a solution to the inhomogeneous equation (A.1):

$$[i\hbar\partial_t - \mathcal{H}(t)]\,\mathcal{G}(t,t') \;=\; \mathcal{E}\,\delta(t-t') \tag{A.16}$$

For $t \neq t'$, (A.13) and (A.16) become identical, and apart from a scaling factor λ, $\mathcal{G}(t,t')$ must equal $\mathcal{U}(t,t')$. However, the coefficient λ may assume different values for $t > t'$ and $t < t'$. To construct the Green function $\mathcal{G}(t,t')$, we therefore pursue the obvious matching ansatz:

$$\mathcal{G}(t,t') \;=\; \begin{cases} \lambda_-\,\mathcal{U}(t,t') & (t<t') \\ \lambda_+\,\mathcal{U}(t,t') & (t>t') \end{cases} \tag{A.17}$$

Note that the Green function $\mathcal{G}(t,t')$ is discontinuous at $t = t'$. To calculate the coefficients $\lambda_\pm$, we integrate the defining equation (A.16) over an infinitesimally small interval $t'-\epsilon < t < t'+\epsilon$, $\epsilon \to 0^+$ which yields the condition:

$$\lim_{\epsilon\,\to\,0^+}\; i\hbar\,[\mathcal{G}(t'+\epsilon,t') - \mathcal{G}(t'-\epsilon,t')] \;=\; i\hbar\,(\lambda_+ - \lambda_-)\,\mathcal{U}(t',t') \;=\; \mathcal{E} \tag{A.18}$$

Hence, the jump at $t = t'$ is fixed to $\lambda_+ - \lambda_- = -i/\hbar$. As expected, the Green function $\mathcal{G}(t,t')$ is not unique, but the condition (A.18) ensures that any two Green functions $\mathcal{G}(t,t')$, $\mathcal{G}'(t,t')$ differ only by a multiple of the homogeneous solution $\mathcal{U}(t,t')$ (A.5).

Obviously, particularly simple members of the set of Green functions are obtained if one selects the pairs of parameters $\lambda_+ = -i/\hbar$, $\lambda_- = 0$ or $\lambda_+ = 0$, $\lambda_- = i/\hbar$ in

(A.17). The latter choice is called the advanced Green function $\mathcal{G}_{\rm adv}(t,t')$, whereas the former model is commonly labeled as retarded Green function $\mathcal{G}_{\rm ret}(t,t')$. They are most easily displayed as multiples of the corresponding advanced and retarded propagators $\mathcal{K}_{\rm adv}(t,t')$ and $\mathcal{K}_{\rm ret}(t,t')$ which are defined via the time evolution operator $\mathcal{U}(t,t')$ by:

$$\mathcal{K}_{\rm adv}(t,t') = \Theta(t'-t)\,\mathcal{U}(t,t') \tag{A.19}$$

$$\mathcal{K}_{\rm ret}(t,t') = \Theta(t-t')\,\mathcal{U}(t,t') \tag{A.20}$$

Here, $\Theta(t)$ denotes as usual the Heaviside step function which assumes the value $\Theta(t)=1$ for $t>0$, and $\Theta(t)=0$ otherwise. Note that unlike the evolution operator $\mathcal{U}(t,t')$ (A.13) itself, the propagators (A.19) and (A.20) are neither solutions of the homogeneous Schrödinger equation (A.11), nor are they Green functions of the system in the sense of the definition (A.16). They do, however, share the property of $U(\mathbf{r},t;\mathbf{r}',t')$ to represent a localized particle at $\mathbf{r}'$ for $t \to t'$ (A.14). Since $\mathcal{K}_{\rm adv}(t,t')$ vanishes for $t>t'$, the advanced propagator in physical space $K_{\rm adv}(\mathbf{r},t;\mathbf{r}',t') = \langle \mathbf{r}\,|\mathcal{K}_{\rm adv}(t,t')|\,\mathbf{r}'\rangle$ describes the dynamics of a particle which is annihilated at the position $\mathbf{r}=\mathbf{r}'$ at the moment $t=t'$. In the same fashion, $K_{\rm ret}(\mathbf{r},t;\mathbf{r}',t')$ generates a quantum particle at $\mathbf{r}=\mathbf{r}'$, $t=t'$, and propagates it into the "future" $t>t'$, which explains the designation of this mathematical object.

According to (A.17), the advanced and retarded Green functions are obtained from the corresponding quantum (or Feynman) propagators (A.19), (A.20) by a scaling operation:

$$\mathcal{G}_{\rm adv}(t,t') = \frac{i}{\hbar}\,\mathcal{K}_{\rm adv}(t,t') \tag{A.21}$$

$$\mathcal{G}_{\rm ret}(t,t') = -\frac{i}{\hbar}\,\mathcal{K}_{\rm ret}(t,t') \tag{A.22}$$

Hence, a special solution $|\Psi_{\rm ret}(t)\rangle$ to the Schrödinger equation with inhomogeneous part $|\sigma(t)\rangle$ (A.11) is obtained by integration of the retarded propagator $\mathcal{K}_{\rm ret}(t,t')$ (A.3):

$$|\Psi_{\rm ret}(t)\rangle = -\frac{i}{\hbar}\int dt'\,\mathcal{K}_{\rm ret}(t,t')\;|\sigma(t')\rangle \tag{A.23}$$

In coordinate space, this state translates into the wave function $\Psi_{\rm ret}(\mathbf{r},t)$ solving the Schrödinger equation with inhomogeneous part $\sigma(\mathbf{r},t)$ (2.7). Following (A.8), $\Psi_{\rm ret}(\mathbf{r},t)$ may be displayed as integral containing the $K_{\rm ret}(\mathbf{r},t;\mathbf{r}',t')$ as a kernel (2.8):

$$\Psi_{\rm ret}(\mathbf{r},t) = -\frac{i}{\hbar}\int d^3r' \int dt'\,K_{\rm ret}(\mathbf{r},t;\mathbf{r}',t')\,\sigma(\mathbf{r}',t') \tag{A.24}$$

As the integral kernel $K_{\rm ret}(\mathbf{r},t;\mathbf{r}',t')$ vanishes for $t<t'$ (A.20), this special wave function $\Psi_{\rm ret}(\mathbf{r},t)$ exclusively depends on the structure of the source term $\sigma(\mathbf{r}',t')$ for $t'<t$,

i. e., on the "history" of the source. In particular, $\Psi_{\rm ret}(\mathbf{r},t)$ will vanish for inhomogeneities which are "switched on" only at some time $t' > t$. Thus, the solution $|\Psi_{\rm ret}(t)\rangle$ obtained by employing the retarded propagator $\mathcal{K}_{\rm ret}(t,t')$ preserves the chronological order of cause (the source $|\sigma(t')\rangle$) and effect (the wave function $|\Psi_{\rm ret}(t)\rangle$). Since this behavior is generally observed in nature (for example, in electrodynamics the choice of the retarded Maxwell propagator analogous to (A.24) is known as the Sommerfeld radiation condition [84]), in the following we will generally deal with the retarded quantum propagator, unless otherwise stated, and denote it as the Feynman propagator $K_F(\mathbf{r},t;\mathbf{r}',t')$ [227].

A.2.3 Time-Dependent Perturbations

Quantum systems, i. e., Hamiltonians $\mathcal{H}(t)$ only rarely allow for a closed solution in terms of the time evolution operator $\mathcal{U}(t,t')$. However, one often has to deal with systems whose Hamiltonians $\mathcal{H}(t)$ may be interpreted as the sum of a "simple" Hamiltonian $\mathcal{H}_0(t)$ and a distortion caused by a "perturbative" potential $\mathcal{V}(t)$: $\mathcal{H}(t,\lambda) = \mathcal{H}_0(t) + \lambda\mathcal{V}(t)$. Formally, λ describes the strength of the perturbation.

Let us now assume that the time evolution operator $\mathcal{U}_0(t,t')$ due to the unperturbed Hamiltonian $\mathcal{H}_0(t)$ ($\lambda = 0$) is available. Then, the time evolution operator $\mathcal{U}_\lambda(t,t')$ of the complete Hamiltonian $\mathcal{H}(t,\lambda)$ may be formally expressed in a power series in λ. To obtain this series, we first note that according to (A.13), $\mathcal{U}_\lambda(t,t')$ is the single solution of the operator equation:

$$[i\hbar\partial_t - \mathcal{H}_0(t)]\,\mathcal{U}_\lambda(t,t') \;=\; \lambda\mathcal{V}(t)\,\mathcal{U}_\lambda(t,t') \tag{A.25}$$

which simplifies to the identity for $t = t'$: $U_\lambda(t,t) = \mathcal{E}$. This expression takes the form of an inhomogeneous operator equation, and ignoring the unitarity constraint, one obtains a special solution $\tilde{\mathcal{U}}_\lambda(t,t')$ for (A.25) by means of the propagator formalism presented above (A.23):

$$\tilde{\mathcal{U}}_\lambda(t,t') \;=\; -\frac{i\lambda}{\hbar}\int d\tau\,\mathcal{K}^{(0)}_{\rm ret}(t,\tau)\,\mathcal{V}(\tau)\,\mathcal{U}_\lambda(\tau,t') \tag{A.26}$$

Here, $\mathcal{K}^{(0)}_{\rm ret}(t,t')$ denotes the retarded propagator assigned to $\mathcal{H}_0(t)$. To this special solution $\tilde{\mathcal{U}}_\lambda(t,t')$ we now have to add a solution $\hat{\mathcal{U}}_\lambda(t,t')$ of the unperturbed equation $[i\hbar\partial_t - \mathcal{H}_0(t)]\hat{\mathcal{U}}_\lambda(t,t') = 0$ chosen in such a way as to restore the unitarity of $\mathcal{U}_\lambda(t,t')$. Noting that for $t = t'$ we have $\mathcal{E} = \mathcal{U}_0(t',t') = \mathcal{U}_\lambda(t',t')$, we immediately infer that the proper combination reads:

$$\mathcal{U}_\lambda(t,t') \;=\; \mathcal{U}_0(t,t') - \frac{i\lambda}{\hbar}\int_{t'}^{t} d\tau\,\mathcal{U}_0(t,\tau)\,\mathcal{V}(\tau)\,\mathcal{U}_\lambda(\tau,t') \tag{A.27}$$

From this integral equation for $\mathcal{U}_\lambda(t,t')$, the series expansion in λ is obtained by repeatedly replacing the time evolution operator in the integrand by the complete expression itself. (Here, we do not discuss the convergence radius of the series.)

Assuming that the perturbation $\lambda\mathcal{V}(t)$ is "weak," we content ourselves with the linear correction term in that series. In practice, the linear approximation amounts to the replacement of $\mathcal{U}_\lambda(t,t')$ by the known operator $\mathcal{U}_0(t,t')$ on the right-hand side of (A.27). Applying the equation onto some state $|\Psi(t')\rangle$, we obtain the Born approximation for the evolution of that state:

$$|\Psi(t)\rangle - |\Psi(t)\rangle_0 \;\approx\; -\frac{i\lambda}{\hbar}\int_{t'}^{t} d\tau\, \mathcal{U}_0(t,\tau)\,\mathcal{V}(\tau)\;|\Psi(\tau)\rangle_0 \tag{A.28}$$

Here, $|\Psi(t)\rangle_0$ denotes the evolution of the (given) state $|\Psi(t')\rangle = |\Psi(t')\rangle_0$ due to the unperturbed Hamiltonian $\mathcal{H}_0(t)$.

A.3 A Crash Course in Operator Theory

Having defined the notions of the time evolution operator $\mathcal{U}(t,t')$ (A.12) and the quantum propagator $\mathcal{K}_{\rm ret}(t,t')$ (A.20), we will now show that these operators are intimately connected to the properties of the Hamiltonian $\mathcal{H}$. (In the following sections, we confine our considerations to conservative systems with time-independent Hamiltonian.) Indeed, under fairly general circumstances all these operators may be expressed as functionals of the eigenvalues E and eigenstates $|\Phi\rangle$ of the Hamiltonian $\mathcal{H}$. This procedure turns out to be particularly simple in Hilbert spaces (state spaces) $\mathbb{H}_N$ of finite dimension, as demonstrated in the following section. There, the theory of hermitian operators is equivalent to the treatment of symmetric matrices in linear algebra [225], and the representations in terms of eigenvalues and -states are analogous to the principal axis transformation of a hermitian matrix.

Unfortunately, the simple theory of finite state spaces is insufficient to explain the characteristics of sources as encountered in the main body of this treatise—the equivalents of sources in $\mathbb{H}_N$ are incapable of generating any current. As we shall show, this property is invariably tied to the presence of a continuous spectrum of the Hamiltonian, which in turn requires a Hilbert space $\mathbb{H}$ of infinite dimension. Not only is it hard to conceive any pictorial model of such types of space; the theory of operators in $\mathbb{H}$, especially unbounded ones, relies on quite subtle properties, and one has to take considerable care in manipulating states and operators in these spaces. Therefore, we will first summarize some of the well-known properties of wave functions in quantum mechanics, in particular those of the continuous spectrum, before we start with a step-by-step mathematical treatment: Beginning with the spectral theorem, the equivalent of the principal axis transformation in $\mathbb{H}$, we proceed to the useful yet ill-defined notion of "eigenfunctions of the continuous spectrum," which we will first develop for

non-degenerate spectra and later generalize to some important "separable" Hamiltonians showing degenerate spectra. Finally, we analyze under which circumstances the resolvent $\mathcal{R}(E)$, an inverse operator to $E\mathcal{E} - \mathcal{H}$, exists, and whether it is unique. The Green function approach presented in Chapter 2 is mathematically founded on the theory of resolvents.

A.3.1 Finite-Dimensional Systems

In the beginning of this mathematical tour-de-force, as an instructive example we are going to prove that $\mathcal{H}$, the evolution operator $\mathcal{U}(t-t')$, and hence also the Green function $\mathcal{G}_{\rm ret}(t,t')$, of a quantum system acting in a finite-dimensional space of states $|\Psi(t)\rangle$ are completely determined by the set of eigenstates and eigenvalues (energies) of $\mathcal{H}$ in this space, and expand these quantities into series of eigenstates of $\mathcal{H}$. (These restricted problems are not only of mathematical interest. Rather, they turn up whenever one deals with subgroups of finite dimension in state space, like the $(2j+1)$–dimensional space of spin states with fixed angular momentum j. Another prominent example are Hamiltonians that act only on a (finite) lattice rather than in continuous physical space. In this work, we exploit the favorable properties of these finite systems in an exactly solvable model for the STM, the zero-range potential crystal lattice. See Section 8.3.3.)

To begin with, from (A.15) we immediately may conclude that the evolution of a state $|\Psi(t')\rangle$ becomes trivial if it is an eigenstate of the Hamiltonian operator:

$$\mathcal{H}\,|\Psi(t')\rangle \;=\; E\;|\Psi(t')\rangle \qquad \Longrightarrow \qquad |\Psi(t)\rangle \;=\; e^{-\,iE(t-t')/\hbar}\;|\Psi(t')\rangle \;=\; e^{-\,iEt/\hbar}\;|\Psi\rangle \quad \text{(A.29)}$$

Therefore, the eigenstates of $\mathcal{H}$ play a major role in the determination of $\mathcal{U}(t-t')$, and the time dependence of the eigenstates $|\Psi(t)\rangle$ may be split off into a unitary prefactor: $|\Psi(t)\rangle = \exp(-iEt/\hbar)\,|\Psi\rangle$. Hence, $|\Psi\rangle$ is also known as stationary state.

We already have gathered some fundamental properties of these eigenstates. By definition, the Hamiltonian operator $\mathcal{H}$ is a self-adjoint operator. Therefore, its spectrum contains real eigenvalues only. Furthermore, eigenstates $|\Psi\rangle$ and $|\Phi\rangle$ to different eigenvalues $E \neq E'$ will be orthogonal (A.10): $\langle \Psi_E | \Phi_{E'} \rangle = 0$.

The eigenstate expansion. We will now demonstrate how all relevant operators are expanded into eigenstates in a N–dimensional state space $\mathbb{H}_N$, where $N < \infty$. Let $\mathcal{H}_0$ be a self-adjoint linear operator acting in this Hilbert space which is positively definite and bounded from above, i. e., we require that in the space of base states $|\Phi\rangle$, the inequality holds:

$$0 \;<\; E_{\rm min} \;=\; \min_{\langle\Phi|\Phi\rangle\,=\,1} \langle \Phi\,|\mathcal{H}_0|\,\Phi\rangle \;\leq\; \max_{\langle\Phi|\Phi\rangle\,=\,1} \langle \Phi\,|\mathcal{H}_0|\,\Phi\rangle \;=\; E_1 \qquad \text{(A.30)}$$

(Note that the restriction $E_{\min} > 0$ may always be fulfilled by shifting the eigenvalue spectrum: $\mathcal{H}_0 \longrightarrow \mathcal{H}_0 + \lambda\mathcal{E}$.)

The first step of our development consists in showing that the maximum value E_1 of $\mathcal{H}_0$ in the space of normalized states $\langle\Phi|\Phi\rangle = 1$ presents an eigenvalue of $\mathcal{H}_0$. This theorem is known as the principle of Rayleigh–Ritz and indeed the foundation of all variational approaches to stationary quantum mechanics:

■ THEOREM I (RAYLEIGH-RITZ PRINCIPLE)
Every normalized state $|\Phi\rangle$, $\langle\Phi|\Phi\rangle = 1$, which leads to a stationary value of the functional $\langle\Phi\,|\mathcal{H}_0|\,\Phi\rangle$ presents an eigenstate of $\mathcal{H}_0$: $\mathcal{H}_0\,|\Phi\rangle = \mu\,|\Phi\rangle$.

Proof. We employ the method of Lagrange multipliers for the variation under constraints and find for the normalized state $|\Phi_1\rangle$ which maximizes the functional (A.30):

$$\frac{\partial}{\partial\,\langle\Phi_1|}\,\{\langle\Phi_1\,|\mathcal{H}_0|\,\Phi_1\rangle - \mu\,\langle\Phi_1|\Phi_1\rangle\} \;=\; \mathcal{H}_0\,|\Phi_1\rangle - \mu\,|\Phi_1\rangle \;=\; 0 \tag{A.31}$$

Therefore, $|\Phi_1\rangle$ is eigenstate of $\mathcal{H}_0$ with eigenvalue $\mu = E_1$. ■

To proceed, we introduce the projection operator $\mathcal{P}_1 = |\Phi_1\rangle\,\langle\Phi_1|$ assigned to the eigenstate $|\Phi_1\rangle$. Obviously, $\mathcal{P}_1 = \mathcal{P}_1^+$ is a hermitian operator. We also note that $\mathcal{P}_1^2 = \mathcal{P}_1$ holds, and in the same manner $f(z\mathcal{P}_1)\mathcal{P}_1 = f(z)\mathcal{P}_1$ for any analytic function $f(z)$.

Clearly, we may construct another bounded self-adjoint operator from $\mathcal{H}_0$ by subtracting the weighed projector $\mathcal{P}_1$ and set:

$$\mathcal{H}_1 \;=\; \mathcal{H}_0 - E_1\,\mathcal{P}_1 \tag{A.32}$$

For this operator, we clearly have $\mathcal{H}_1\,|\Phi_1\rangle = 0$, so $|\Phi_1\rangle$ is eigenstate of $\mathcal{H}_1$ with eigenvalue 0. On the other hand, from the Rayleigh-Ritz principle (A.31) we know that $\mathcal{H}_1$ assumes its maximum value E_2 in the space of normalized states for an eigenstate $|\Phi_2\rangle$:

$$\max_{\langle\Phi|\Phi\rangle\,=\,1}\,\langle\Phi\,|\mathcal{H}_1|\,\Phi\rangle \;=\; E_2 \qquad\Longrightarrow\qquad \mathcal{H}_1\,|\Phi_2\rangle - E_2\;|\Phi_2\rangle \;=\; 0 \tag{A.33}$$

Now, we note that $E_2 > 0$ holds, because the functional (A.33) will be positive for all states $|\Phi\rangle$ orthogonal to the eigenstate $|\Phi_1\rangle$, $\langle\Phi_1|\Phi\rangle = 0$. For those states, we obtain

$$\langle\Phi\,|\mathcal{H}_1|\,\Phi\rangle \;=\; \langle\Phi\,|\mathcal{H}_0|\,\Phi\rangle \;>\; 0 \tag{A.34}$$

by our assumptions (A.30), (A.32). We conclude that $|\Phi_1\rangle$ and $|\Phi_2\rangle$ are both eigenstates of the self-adjoint operator $\mathcal{H}_1$, but for different eigenvalues 0 and $E_2 > 0$! Consequently, these eigenstates must be orthogonal: $\langle\Phi_1|\Phi_2\rangle = 0$. But following (A.34), we find that $|\Phi_2\rangle$ is also eigenstate with respect to the original operator $\mathcal{H}_0$:

$$\mathcal{H}_0\,|\Phi_2\rangle - E_2\;|\Phi_2\rangle \;=\; 0 \tag{A.35}$$

Comparing with (A.30), we see that $E_2 \leq E_1$. In this manner, we have found the second-largest eigenstate $|\Phi_2\rangle$ of $\mathcal{H}_0$. Since $\langle\Phi_1|\Phi_2\rangle = 0$ holds, these eigenstates are linearly independent.

We now may repeat this procedure, define in the next step the projection operator $\mathcal{P}_2 = |\Phi_2\rangle\langle\Phi_2|$ and introduce the hermitian operator $\mathcal{H}_2 = \mathcal{H}_1 - E_2\,\mathcal{P}_2$ instead of (A.32). Following through the steps (A.33)–(A.35), we obtain another eigenstate $|\Phi_3\rangle$ with eigenvalue $E_3 \leq E_2 \leq E_1$ which is orthonormalized, $\langle\Phi_j|\Phi_k\rangle = \delta_{jk}$, thus guaranteeing linear independence of the eigenstates $|\Phi_j\rangle$ for $j = 1, 2, 3$, and so on.

The argument loop finally breaks down with the operator $\mathcal{H}_N$:

$$\mathcal{H}_N \;=\; \mathcal{H}_0 - \sum_{k=1}^{N} E_k\,\mathcal{P}_k \tag{A.36}$$

Because the linear independent set of N pairwise orthogonal states $\{|\Phi_1\rangle, \ldots, |\Phi_N\rangle\}$ forms a complete base in the space of states, every state $|\Psi\rangle$ may be decomposed into a linear combination of the eigenstates of $\mathcal{H}_0$—we have exhausted the N–dimensional state space. Consequently, we find:

$$\mathcal{H}_N\;|\Psi\rangle \;=\; \mathcal{H}_N \sum_{k=1}^{N} \alpha_k\,|\Phi_k\rangle \;=\; \sum_{k=1}^{N} \alpha_k\,\mathcal{H}_N\,|\Phi_k\rangle \;\equiv\; 0 \tag{A.37}$$

Therefore, $\mathcal{H}_N$ is equal to the null operator: $\mathcal{H}_N = 0$. Hence, from (A.36) we obtain the following decomposition of $\mathcal{H}_0$:

■ THEOREM II (SPECTRAL THEOREM)
In N–dimensional space $\mathbb{H}_N$, every bounded hermitian operator $\mathcal{H}_0$ may be expanded into its normalized eigenstates $|\Phi_k\rangle$ and eigenvalues E_k:

$$\mathcal{H}_0 \;=\; \sum_{k=1}^{N} E_k\,\mathcal{P}_k \;=\; \sum_{k=1}^{N} E_k\;|\Phi_k\rangle\langle\Phi_k| \tag{A.38}$$

Moreover, from (A.38) follows the completeness theorem:

■ THEOREM III (RESOLUTION OF THE IDENTITY)
The set of eigenstates $|\Phi_k\rangle$ of a hermitian operator $\mathcal{H}_0$ acting in $\mathbb{H}_N$ generates a resolution of the identity $\mathcal{E}$ ("decomposition of unity"):

$$\mathcal{E} \;=\; \sum_{k=1}^{N} \mathcal{P}_k \;=\; \sum_{k=1}^{N} |\Phi_k\rangle\langle\Phi_k| \tag{A.39}$$

Proof. The eigenstates $|\Phi_k\rangle$ of $\mathcal{H}_0$ obviously are also eigenstates of the identity operator $\mathcal{E}$ with eigenvalue $\mu_k \equiv 1$. Since $\mathcal{E}$ is self-adjoint, the spectral theorem (A.38) applies. ■

A notable consequence of completeness is the generalized Fourier theorem:

■ THEOREM IV (FOURIER DECOMPOSITION)
In $\mathbb{H}_N$, the self-adjoint operator $\mathcal{H}_0$ generates a base of exactly N mutually orthonormal eigenstates $|\Phi_k\rangle$, $k = 1, \ldots, N$. Any state vector $|\Psi\rangle$ may be decomposed into this base:

$$|\Psi\rangle \;=\; \sum_{k=1}^{N} \alpha_k \, |\Phi_k\rangle \;, \qquad \alpha_k \;=\; \langle \Phi_k | \Psi \rangle \tag{A.40}$$

Evolution of states. Finally, we derive the eigenstate expansion of the time evolution operator $\mathcal{U}(t-t')$ for the "finite-dimensional Schrödinger equation." Denoting the N–dimensional Hamiltonian by $\mathcal{H}$, the evolution operator $\mathcal{U}(t-t')$ for the conservative system may be expressed by $\mathcal{H}$ via (A.15):

$$\mathcal{U}(t-t') \;=\; \exp\left\{ -\frac{i}{\hbar} \mathcal{H}\,(t-t') \right\} \mathcal{E} \tag{A.41}$$

Using the completeness theorem for $\mathcal{E}$ with respect to the eigenstates of $\mathcal{H}$ (A.39), and the eigenstate property (A.29), we immediately find from (A.41) the eigenstate decomposition of $\mathcal{U}(t-t')$:

$$\mathcal{U}(t-t') \;=\; \sum_{k=1}^{N} e^{-\,i\,E_k\,(t-t')/\hbar} \; |\Phi_k\rangle \, \langle \Phi_k| \tag{A.42}$$

We may use these decompositions to represent the "causal" solution $|\Psi_{\rm ret}(t)\rangle$ (A.23) to the inhomogeneous Schrödinger equation (A.11) in terms of the eigenstates $|\Phi_k\rangle$ of the Hamiltonian $\mathcal{H}$. First, we perform the decomposition of the source state $|\sigma(t)\rangle$ according to the generalized Fourier theorem (A.40):

$$|\sigma(t)\rangle \;=\; \sum_{k=1}^{N} \sigma_k(t) \, |\Phi_k\rangle \;, \qquad \sigma_k(t) \;=\; \langle \Phi_k | \sigma(t) \rangle \tag{A.43}$$

Expressing the Green function $\mathcal{G}_{\rm ret}(t,t')$ in terms of the time evolution operator (A.20), (A.22), application of its eigenstate decomposition (A.42) yields:

$$\begin{aligned} |\Psi_{\rm ret}(t)\rangle \;&=\; -\frac{i}{\hbar} \int dt'\, \Theta(t-t')\, \mathcal{U}(t,t') \, |\sigma(t')\rangle \\ &=\; -\frac{i}{\hbar} \sum_{k=1}^{N} \left\{ \int_{-\infty}^{t} dt'\, e^{-\,i\,E_k\,(t-t')/\hbar}\, \sigma_k(t') \right\} |\Phi_k\rangle \end{aligned} \tag{A.44}$$

We note that this solution exists at least if the functions $\sigma_k(t)$ are absolutely integrable.

The complete solution $|\Psi(t)\rangle$ to the inhomogeneous Schrödinger problem (A.11) is finally obtained by adding the general solution $|\Psi_{\rm hom}(t)\rangle$ of the corresponding homogeneous equation to the special state $|\Psi_{\rm ret}(t)\rangle$ (A.44). In the preceding section, we have found that for any arbitrarily given initial state $|\Psi(t')\rangle$ of the system, there exists a unique solution $|\Psi_{\rm hom}(t)\rangle$ of the homogeneous equation which is propagated from $|\Psi(t')\rangle$ by the evolution operator $\mathcal{U}(t,t')$ (A.12). Let us verify this property here. Performing generalized Fourier analysis on $|\Psi(t')\rangle$ (A.40) and decomposing $\mathcal{U}(t,t')$ (A.42), we find at last for the complete solution:

$$|\Psi(t)\rangle \;=\; \sum_{k\,=\,1}^{N} \left\{ \alpha_k \;-\; \frac{i}{\hbar} \int_{-\infty}^{t} dt'\, e^{\,i\,E_k\,t'/\hbar}\, \sigma_k(t') \right\} e^{-\,i\,E_k\,t/\hbar}\, |\Phi_k\rangle \tag{A.45}$$

Here, $\{\alpha_1, \ldots, \alpha_N\}$ denotes a set of arbitrary complex constants of integration. It is a notable fact that the time-dependent inhomogeneous Schrödinger equation (A.11) can be solved under very general circumstances. The solution space $|\Psi(t)\rangle$ is always N–fold degenerate; as may be inferred from (A.45), for any given initial state $|\Psi(t')\rangle$ of the inhomogeneous system, exactly one continuation $|\Psi(t)\rangle$ for all t exists. Hence, the initial value (Cauchy) problem for the time-dependent inhomogeneous Schrödinger equation has a unique solution.

The resolvent operator. As we are generally interested in inhomogeneous problems, we next deal with the time-independent equation $(E\mathcal{E} - \mathcal{H}_0)\,|\Psi\rangle \;=\; |\sigma\rangle$. Using the spatial representation (Section A.2.1), this formal expression translates into the inhomogeneous stationary Schrödinger equation (2.11). Denoting the wave function by $\psi_\sigma(\mathbf{r};E) = \langle \mathbf{r}|\Psi\rangle$ and the (stationary) source by $\sigma(\mathbf{r}) = \langle \mathbf{r}|\sigma\rangle$, we obtain:

$$\{E - H_0(\mathbf{r},\mathbf{p})\}\; \psi_\sigma(\mathbf{r};E) \;=\; \sigma(\mathbf{r}) \tag{A.46}$$

Clearly, in state space its formal solution is given by $|\Psi\rangle = \mathcal{R}(E)\,|\sigma\rangle$, where the resolvent operator $\mathcal{R}(E)$ obeys:

$$\mathcal{R}(E)\,(E\mathcal{E} - \mathcal{H}_0) \;=\; (E\mathcal{E} - \mathcal{H}_0)\,\mathcal{R}(E) \;=\; \mathcal{E} \tag{A.47}$$

Now assume that both $|\Psi\rangle$, $|\Psi'\rangle$ are solutions to the inhomogeneous equation. Then, $(E\mathcal{E} - \mathcal{H}_0)(|\Psi\rangle - |\Psi'\rangle) = 0$, which implies that unless E presents an eigenvalue of $\mathcal{H}_0$, $|\Psi\rangle$ is uniquely given by $|\sigma\rangle$, provided the solution exists at all. On the other hand, if E is not a member of the point spectrum of $\mathcal{H}_0$, a solution $|\Psi\rangle$ always exists. To see that, we note that the well-defined variational problem:

$$[\langle\Psi|\,(E\mathcal{E} - \mathcal{H}_0) - \langle\sigma|]\;[(E\mathcal{E} - \mathcal{H}_0)\,|\Psi\rangle - |\sigma\rangle] \;=\; \min \tag{A.48}$$

according to the Ritz principle (Theorem I) is equivalent to the eigenvalue equation:

$$(E\mathcal{E} - \mathcal{H}_0)\,[(E\mathcal{E} - \mathcal{H}_0)\,|\Psi\rangle - |\sigma\rangle] \;=\; 0 \tag{A.49}$$

So if the inhomogeneous equation $(E\mathcal{E} - \mathcal{H}_0)\,|\Psi\rangle = |\sigma\rangle$ has no solution, the "best approximation" in state space $|\Psi\rangle$ generates an eigenstate $(E\mathcal{E} - \mathcal{H}_0)\,|\Psi\rangle - |\sigma\rangle$ of $\mathcal{H}_0$ with eigenvalue E, which is impossible if $E \neq E_k$ for all $k = 1, \ldots, N$. Thus, for $E \neq E_k$ the resolvent $\mathcal{R}(E)$ is a unique operator on the entire state space $\mathbb{H}_N$.

It is obvious from (A.47) that the operator $E\mathcal{E} - \mathcal{H}_0$ and its inverse $\mathcal{R}(E)$ share their eigenstates $|\Phi_k\rangle$. This means that $\mathcal{R}(E)$ may be expanded into this set of eigenstates if E is in the resolvent set (not a member of the spectrum) of $\mathcal{H}_0$. Indeed, its structure is easily inferred from (A.38), (A.39). We may summarize these properties of $\mathcal{R}(E)$ into the following statement:

■ THEOREM V

In the finite-dimensional space $\mathbb{H}_N$, the hermitian operator $E\mathcal{E} - \mathcal{H}_0$ has an inverse, the resolvent $\mathcal{R}(E)$, if and only if E is not contained in the spectrum $\{E_1, \ldots, E_N\}$ of $\mathcal{H}_0$. In terms of the eigenstates $|\Phi_k\rangle$ of $\mathcal{H}_0$, the resolvent operator $\mathcal{R}(E)$ reads:

$$\mathcal{R}(E) \;=\; \sum_{k=1}^{N} \frac{\mathcal{P}_k}{E - E_k} \;=\; \sum_{k=1}^{N} \frac{|\Phi_k\rangle\,\langle\Phi_k|}{E - E_k} \tag{A.50}$$

As a function of E, $\mathcal{R}(E)$ diverges as E approaches the eigenvalues E_k of $\mathcal{H}_0$.

Employing again the spatial representation of the states (A.46), we find from $|\Psi\rangle = \mathcal{R}(E)\,|\sigma\rangle$ following Section A.2.1,

$$\psi_\sigma(\mathbf{r}; E) \;=\; \int d^3r'\; \langle \mathbf{r}\,|\mathcal{R}(E)|\,\mathbf{r}'\rangle\; \sigma(\mathbf{r}') \tag{A.51}$$

By comparison with (2.14), this means that the spatial representation of $\mathcal{R}(E)$ is just the energy Green function of the system:

$$G(\mathbf{r}, \mathbf{r}'; E) \;=\; \langle \mathbf{r}\,|\mathcal{R}(E)|\,\mathbf{r}'\rangle \;=\; \sum_{k=1}^{N} \frac{\phi_k(\mathbf{r})\,\phi_k^*(\mathbf{r}')}{E - E_k} \tag{A.52}$$

Here, the symbols $\phi_k(\mathbf{r}) = \langle \mathbf{r}|\Phi_k\rangle$ denote the eigenfunctions of $H_0(\mathbf{r}, \mathbf{p})$.

A noteworthy consequence of (A.52) consists in the fact that the diagonal elements $G(\mathbf{r}, \mathbf{r}; E)$ as well as the expression in brackets in (2.17) deliver only real values, which according to (2.17), (2.34) implies that sources $\sigma(\mathbf{r})$ in finite-dimensional state space cannot generate any current; $J \equiv 0$. To remedy this serious shortcoming, we have to consider Hilbert spaces $\mathbb{H}$ of infinite dimension. This complex task will be the topic of the following sections.

Degeneracy of the spectrum. Finally, we drop a few remarks regarding the point spectrum $\{E_1, \ldots, E_N\}$ of the N–dimensional Hamiltonian operator $\mathcal{H}_0$. Obviously, this set can contain at most N different discrete real values. In the non-degenerate case, all eigenvalues of $\mathcal{H}_0$ are distinct, and the set of eigenstates $\{|\Phi_1\rangle, \ldots, |\Phi_N\rangle\}$ is, apart from prefactors, completely fixed by the Hamiltonian $\mathcal{H}_0$. In the degenerate case, subsets of identical eigenvalues $\{E_m, \ldots, E_{m+p(E_k)-1}\}$ within the point spectrum of $\mathcal{H}_0$ exist. The corresponding eigenstates form a degeneracy subspace $|\Phi_m\rangle \otimes \cdots \otimes |\Phi_{m+p(E_k)-1}\rangle$ of dimension $p(E_k)$ within state space. Within that subspace, the set of eigenstates is not unique, but may be changed by unitary base transformations. Both cases may be summarized into the following notation. In general, the spectrum consists of $1 \leq q \leq N$ different eigenvalues $\{E_1, \ldots, E_q\}$ with degeneracies $p_1, \ldots, p_q$, where $p_1 + \ldots + p_q = N$. Next, we define a unique projector $\mathcal{P}(E_k)$ onto the degeneracy subspace belonging to the eigenvalue E_k of $\mathcal{H}_0$ simply by adding up the corresponding projectors on a complete base of eigenstates $\{|\Phi_m\rangle, \ldots, |\Phi_{m+p(E_k)-1}\rangle\}$ in that space. Then, the spectral theorem (Theorem II) takes the unambiguous form:

$$\mathcal{H}_0 = \sum_{k=1}^{q} E_k \, \mathcal{P}(E_k) \quad \text{, where} \qquad \mathcal{P}(E_k) = \sum_{j=0}^{p_k-1} |\Phi_{m+j}\rangle \langle \Phi_{m+j}| \tag{A.53}$$

A.3.2 Quantum Mechanics: A Heuristic View

After having dealt with the pedagogical example of quantum mechanics in finite-dimensional state space, we have to deliver the corresponding results for the customary time-dependent Schrödinger equation in physical space (A.6). There, the Hamiltonian $H(\mathbf{r}, \mathbf{p})$ that we still assume to be conservative obviously presents an operator acting in the continuous space of square-integrable wave functions $\langle \mathbf{r}|\Psi\rangle = \psi(\mathbf{r}, t) \in \mathbb{L}^2$, where the natural norm of $|\Psi\rangle$ is given by the integral of $|\psi(\mathbf{r}, t)|^2$ over all space [83]. We already introduced an orthonormal base of states in configuration space, the position states $|\mathbf{r}\rangle$ of Section A.2.1. Clearly, the dimension of this base is not only infinite, the set even is not countable. Therefore, our inductive proof that the Hermitian operator $\mathcal{H}$ generates a complete orthonormal base of eigenstates in state space (A.38)–(A.40) is not viable for the conventional Hamiltonian $H(\mathbf{r}, \mathbf{p})$, and we have to resort to more subtle methods in the development of a theory of operators. In this introducing section, we first gather obvious properties of well-known operators in quantum mechanics which are necessarily absent in Hilbert spaces $\mathbb{H}_N$ of finite dimension.

We start with the observation that the Hamiltonian operator $\mathcal{H}$ supports normalized states $|\Psi\rangle$ whose average particle energy $E_{\text{av}} = \langle \Psi \, |\mathcal{H}| \, \Psi \rangle$ may take on arbitrarily large values. For example, the simple free-particle Hamiltonian $H_{\text{free}}(\mathbf{p}) = p^2/2M$ sustains wave packets with mean energies in the continuous range $0 < E_{\text{av}} < \infty$. It is intuitively clear that the Hamiltonian for the uniform field $H(\mathbf{r}, \mathbf{p}) = H_{\text{free}}(\mathbf{p}) - \mathbf{r} \cdot \mathbf{F}$

that this treatise is centered upon even supports states $|\Psi\rangle$ with arbitrary average energies $-\infty < E_{\rm av} < \infty$. Thus, the operators we are going to deal with are generally unbounded, a property which turns out to present a major source of trouble.

The simplest case to be considered obviously are bounded operators $\mathcal{A}$ with discrete spectrum. Even then, it is impossible to give a complete expansion into eigenstates as was done in the finite space $\mathbb{H}_N$ (A.38), as the degeneracy subspaces will generally be of infinite dimension. As an example, consider the parity operator $\mathcal{Q}$ which transforms a wave function $\psi(\mathbf{r},t)$ into its mirror image $\psi(-\mathbf{r},t)$. Clearly, in configuration space the parity operator is represented by $Q(\mathbf{r},\mathbf{r}') = \langle \mathbf{r}\,|\mathcal{Q}|\,\mathbf{r}'\rangle = \delta(\mathbf{r}+\mathbf{r}')$; unlike the operator $H(\mathbf{r},\mathbf{p})$, $\mathcal{Q}$ is a nonlocal operator. As $\mathcal{Q}$ is a self-adjoint operator, and $\mathcal{Q}^2 = \mathcal{E}$, the eigenvalues must be $q = \pm 1$, and the spectrum contains just two entries. As any normalizable function $\psi(\mathbf{r})$ of even ($q = 1$) or odd ($q = -1$) parity belongs to the corresponding eigenspaces, these are clearly of infinite dimension.

Next, we note that there may appear "eigenfunctions" $\phi(\mathbf{r})$ of the Hamiltonian $H(\mathbf{r},\mathbf{p})$ that are not normalizable, and hence strictly spoken do not represent any state in the Hilbert space $\mathbb{H}$. Let's again take the free-particle Hamiltonian $H_{\rm free}(\mathbf{p}) = p^2/2M$ as an example. Clearly, any plane wave function $\phi_{\mathbf{q}}(\mathbf{r}) = \exp(i\mathbf{q}\cdot\mathbf{r})$ fulfils $H_{\rm free}(\mathbf{p})\phi_{\mathbf{q}}(\mathbf{r}) = E(\mathbf{q})\phi_{\mathbf{q}}(\mathbf{r})$ with $E(\mathbf{q}) = \hbar^2 q^2/2M$, so $\phi_{\mathbf{q}}(\mathbf{r})$ is an eigenfunction of $H_{\rm free}(\mathbf{p})$. But for any infinitely extended sector Ω in physical space, the integral of $|\phi_{\mathbf{q}}(\mathbf{r})|^2$ diverges, hence $\phi_{\mathbf{q}}(\mathbf{r})$ is not normalizable. We have encountered another example of these pseudo-eigenstates already in Section A.2.1: The "position states" $|\mathbf{r}\rangle$ obey the orthonormality relation (A.7) $\langle\mathbf{r}|\mathbf{r}'\rangle = \delta(\mathbf{r}-\mathbf{r}')$ which implies that they are not normalizable in the classical sense.

Another implication of the model free-particle Hamiltonian $H_{\rm free}(\mathbf{p})$ discussed in the previous paragraph lies in the existence of a continuous range of eigenvalues $0 < E < \infty$ which, however, only appears if one is willing to account for the non-normalizable "eigenfunctions" $\phi_{\mathbf{q}}(\mathbf{r})$ introduced above. These continuous parts of the spectrum of $\mathcal{H}$, which may appear alongside a conventional discrete point spectrum $\{E_k\}$ with corresponding normalized eigenstates $|\Phi_k\rangle$ (the best known example being the ubiquitous hydrogen problem, see e. g. [83]), surely deserves special attention in any mathematical theory of linear operators in infinite-dimensional spaces.

From the foregoing notes, it should appear self-evident that operators in $\mathbb{H}$ may feature properties distinctly different from those in finite-dimensional spaces. In order to provide a solid background to the heuristic arguments presented in the main body of this volume, it is our objective to deliver an intellegible, no-nonsense description of the theory of operators in infinite-dimensional space, in particular configuration space that closely follows a naive approach rather than plunge deep into the recesses of elaborate mathematical formalism.

Functional analysis is the topic of numerous books, and we will point out only a few authors. Some of the following developments are based on the extensive and

fairly readable monograph by Kato [228]. A detailed presentation of the measure theoretical approach to the continuous spectrum can be found in the book by Reed and Simon [229]. A rather short introduction to a number of concepts presented below is contained in the textbook by Newton [230]. Occasionally, we refer to the convenient formalism of generalized Dirac "delta functions" [226]. A concise introduction to the theory of distributions is provided e. g. by the booklet of Halperin and Schwartz [215].

A.3.3 Spectral Decomposition of Self-Adjoint Operators

The first step in our development of a theory of unbounded operators $\mathcal{A}$ consists in establishing an analogue to the spectral theorem (A.38) we found for operators in finite-dimensional spaces. Clearly, the inductive approach we pursued in $\mathbb{H}_N$ (A.32)–(A.36) is not feasible in infinite-dimensional Hilbert space, so we have to resort to a different method which is developed below. However, first we have to state some assumptions concerning "well-behaved" operators $\mathcal{A}$.

Remarks on closed operators. One of the subtle points in dealing with unbounded operators $\mathcal{A}$ in infinite-dimensional space $\mathbb{H}$ consists in the fact that the action of $\mathcal{A}$ onto a valid normalizable state $|\Psi\rangle$, i. e., $\mathcal{A}\,|\Psi\rangle$ by no means must exist. For example, $H_{\text{free}}(\mathbf{p})\psi(\mathbf{r})$ is undefined if $\psi(\mathbf{r})$ is not continuous, yet this property obviously does not prevent $\psi(\mathbf{r})$ from being $\mathbb{L}^2-$integrable. Thus, it is sensible to single out the set of states $|\Psi\rangle$ for which $\mathcal{A}\,|\Psi\rangle$ is defined; it is called the domain $\mathbb{D}$ of $\mathcal{A}$ in the Hilbert space $\mathbb{H}$. Now, there is a class of linear operators which admit rather detailed treatment despite the fact that they are not bounded. These operators are called closed (see Kato [228], p. 165). For our purpose, the following definition is completely sufficient:

■ DEFINITION VI
An operator $\mathcal{A}$ in $\mathbb{H}$ is called closed if for every sequence of states $|\Psi_n\rangle$ in the domain $\mathbb{D}$ of $\mathcal{A}$ in $\mathbb{H}$ that converges towards zero, $|\Psi_n\rangle \to 0$ as $n \to \infty$, the corresponding image series $\mathcal{A}\,|\Psi_n\rangle$ is convergent and has the limit $\mathcal{A}\,|\Psi_n\rangle \to 0$ as $n \to \infty$.

In the following we shall assume that the operators under consideration are all closed. One may be tempted to restrict oneself to operators $\mathcal{A}$ which are defined in $\mathbb{H}$ rather than in a subset $\mathbb{D} \subset \mathbb{H}$; unfortunately, the closed graph theorem (Kato [228], p. 166) states that $\mathcal{A}$ in this case is bounded. Hence, the best thing we may assume with regard to the domain of $\mathcal{A}$ is that $\mathcal{A}$ is densely defined, i. e., its domain $\mathbb{D}$ is dense in $\mathbb{H}$, and any state $|\Psi\rangle \in \mathbb{H}$ may be arbitrarily closely approximated by a state $|\Phi\rangle$ in $\mathbb{D}$, i. e., the distance $\|\Psi - \Phi\|$ may be chosen as small as desired.

Finally, the issue of domains also causes trouble in the definition of a self-adjoint operator (Kato [228], p. 269). We have to require that the domains of $\mathcal{A}$ and its adjoint

$\mathcal{A}^+$ are identical, $\mathbb{D}(\mathcal{A}) = \mathbb{D}(\mathcal{A}^+)$ in order to state the condition for self-adjointness (A.9): $\langle \Phi \,|\mathcal{A}|\, \Psi \rangle = (\langle \Psi \,|\mathcal{A}|\, \Phi \rangle)^*$ for every pair of states $|\Phi\rangle$, $|\Psi\rangle$ in the domain of $\mathcal{A}$.

The square root theorem. This is the fundamental property of self-adjoint operators for the following developments.

■ THEOREM VII
Let $\mathcal{A}$ be a self-adjoint operator which is additionally non-negative, $\langle \Psi \,|\mathcal{A}|\, \Psi \rangle \geq 0$ for all $|\Psi\rangle$ in $\mathbb{D}(\mathcal{A})$. Then, there exists a unique square root operator $\sqrt{\mathcal{A}}$ with these properties:

(i). $\sqrt{\mathcal{A}}$ is self-adjoint and non-negative

(ii). The domain $\mathbb{D}(\mathcal{A})$ is dense in the domain $\mathbb{D}(\sqrt{\mathcal{A}})$ of $\sqrt{\mathcal{A}}$

(iii). Let $\mathcal{B}$ be a bounded operator that commutes with $\mathcal{A}$. Then, $\mathcal{B}$ also commutes with $\sqrt{\mathcal{A}}$:

$$\mathcal{A}\mathcal{B} = \mathcal{B}\mathcal{A} \qquad \Longrightarrow \qquad \sqrt{\mathcal{A}}\mathcal{B} = \mathcal{B}\sqrt{\mathcal{A}} \tag{A.54}$$

Proof. See Kato [228], p. 281. ■

Polar decomposition of an operator. For any self-adjoint operator $\mathcal{A}$, it square $\mathcal{A}^2$ fulfils the conditions of the square root theorem (Theorem VII), so a unique modulus $|\mathcal{A}| = |\mathcal{A}|^+ = \sqrt{\mathcal{A}^2}$ of the operator $\mathcal{A}$ exists. Since $\langle \mathcal{A}\Psi | \mathcal{A}\Psi \rangle = \langle |\mathcal{A}|\Psi | |\mathcal{A}|\Psi \rangle = \langle \Psi \,|\mathcal{A}^2|\, \Psi \rangle$, the domains of $\mathcal{A}$ and $|\mathcal{A}|$ in $\mathbb{H}$ are identical, which implies that there is a linear functional $\mathcal{U}$, i. e., an operator $\mathcal{U}$ which maps the states $|\mathcal{A}|\,|\Psi\rangle$ onto the states $\mathcal{A}\,|\Psi\rangle$. We write:

$$\mathcal{A}\,|\Psi\rangle = \mathcal{U}|\mathcal{A}|\,|\Psi\rangle \tag{A.55}$$

As it stands, $\mathcal{U}$ is only defined in the image space $\mathbb{R} \subseteq \mathbb{H}$ of the domain $\mathbb{D}(\mathcal{A})$ under $|\mathcal{A}|$. We may extend $\mathcal{U}$ into the entire Hilbert space $\mathbb{H}$ by defining $\mathcal{U}\,|\Phi\rangle = 0$ for the subspace of all states $|\Phi\rangle \in \mathbb{R}^\perp$ orthogonal to the image space $\mathbb{R}$:

$$\langle \Phi \,||\mathcal{A}||\, \Psi \rangle = 0 \quad \text{for all } |\Psi\rangle \in \mathbb{D}(\mathcal{A}) \quad \Longrightarrow \quad \mathcal{U}\,|\Phi\rangle = 0 \tag{A.56}$$

With this extension we may write (Kato [228], p. 334) $\mathcal{A} = \mathcal{U}|\mathcal{A}|$. This form resembles the decomposition of a complex number $z = |z| \exp(i\varphi)$ into modulus and phase and is therefore called the polar decomposition of the self-adjoint operator $\mathcal{A}$. (A more general version for arbitrary linear operators is available.) We now collect some properties of the polar decomposition and presented them as the following theorem:

■ THEOREM VIII

The polar decomposition has the following properties:

(i). $\mathcal{U}\,|\Phi\rangle = 0$ if, and only if, $\mathcal{A}\,|\Phi\rangle = 0$

(ii). $\mathcal{U}$ is partially isometric:

$$\mathcal{U}^{+}\mathcal{U}\,|\Phi\rangle \;=\; \begin{cases} |\Phi\rangle & \text{for } |\Phi\rangle \in \mathbb{R} \\ 0 & \text{for } \mathcal{A}\,|\Phi\rangle = 0 \end{cases} \tag{A.57}$$

(iii). $\mathcal{U}$, $|\mathcal{A}|$ and $\mathcal{A}$ commute

(iv). $\mathcal{U}$ is hermitian: $\mathcal{U}^{+} = \mathcal{U}$

(v). For any $|\Psi\rangle \in \mathbb{H}$, $\mathcal{U}^{2}(\mathcal{U}\,|\Psi\rangle) = \mathcal{U}\,|\Psi\rangle$

(vi). If $\mathcal{B}$ is bounded and commutes with $\mathcal{A}$, then $|\mathcal{A}|\mathcal{B} = \mathcal{B}|\mathcal{A}|$ and $\mathcal{U}\mathcal{B} = \mathcal{B}\mathcal{U}$

Proof. For (i), let first $\mathcal{U}\,|\Phi\rangle = 0$, i. e., $|\Phi\rangle \in \mathbb{R}^{\perp}$. Then, according to (A.56) $\langle\Phi\,||\mathcal{A}||\,\Psi\rangle = 0$ for all $|\Psi\rangle \in \mathbb{H}$. Set $|\Psi\rangle = |\mathcal{A}|\,|\Phi\rangle$; then, $\langle|\mathcal{A}|\Phi||\mathcal{A}|\Phi\rangle = \langle\Phi\,|\mathcal{A}^{2}|\,\Phi\rangle = \|\mathcal{A}\,|\Phi\rangle\|^{2} = 0$. Hence, $\mathcal{A}\,|\Phi\rangle = 0$. On the other hand, if $\mathcal{A}\,|\Phi\rangle = 0$, then also $|\mathcal{A}|\,|\Phi\rangle = 0$, so $\langle\Psi\,||\mathcal{A}||\,\Phi\rangle^{*} = \langle\Phi\,||\mathcal{A}||\,\Psi\rangle = 0$ for all $|\Psi\rangle \in \mathbb{H}$. Hence, $|\Phi\rangle \in \mathbb{R}^{\perp}$, and following (A.56), $\mathcal{U}\,|\Phi\rangle = 0$.

To prove (ii), assume that $|\Phi\rangle$, $|\Psi\rangle$ are states in the domain of $\mathcal{A}$. Then, $\langle\Phi\,|\mathcal{A}^{2}|\,\Psi\rangle = \langle\Phi\,|\mathcal{A}^{+}\mathcal{A}|\,\Psi\rangle = \langle|\mathcal{A}|\Phi\,|\mathcal{U}^{+}\mathcal{U}|\,|\mathcal{A}|\Psi\rangle$. But also, $\langle\Phi\,|\mathcal{A}^{2}|\,\Psi\rangle = \langle\Phi\,||\mathcal{A}|^{2}|\,\Psi\rangle = \langle|\mathcal{A}|\Phi|\mathcal{A}|\Psi\rangle$. Hence, we find $\langle|\mathcal{A}|\Phi\,|\mathcal{U}^{+}\mathcal{U} - \mathcal{E}|\,|\mathcal{A}|\Psi\rangle = 0$. Since, $|\mathcal{A}|\,|\Phi\rangle$, $|\mathcal{A}|\,|\Psi\rangle$ cover the subspace $\mathbb{R}$ densely, for all states $|\Phi\rangle \in \mathbb{R}$ the relation $\mathcal{U}^{+}\mathcal{U}\,|\Phi\rangle = |\Phi\rangle$ holds. In $\mathbb{R}^{\perp}$, $\mathcal{U}\,|\Phi\rangle = 0$ by definition.

To show (iii), we first prove that $|\mathcal{A}| = \mathcal{U}|\mathcal{A}|\mathcal{U}^{+}$. Because the operator on the right-hand side is manifestly hermitian and non-negative, according to the uniqueness of the square root (Theorem VII) it is sufficient to show that its square equals $\mathcal{A}^{2}$. Indeed, as $\mathcal{A} = \mathcal{U}|\mathcal{A}| = |\mathcal{A}|\mathcal{U}^{+}$, we find using property (ii) of the polar decomposition that $(\mathcal{U}|\mathcal{A}|\mathcal{U}^{+})^{2} = \mathcal{A}\mathcal{U}^{+}\mathcal{U}\mathcal{A} = \mathcal{A}^{2}$. Multiplying this relation by $\mathcal{U}$ from the right, we obtain $|\mathcal{A}|\mathcal{U} = \mathcal{U}|\mathcal{A}|\mathcal{U}^{+}\mathcal{U} = \mathcal{U}|\mathcal{A}|$, thus $\mathcal{U}$ and $|\mathcal{A}|$ commute. By multiplication of this commutator with $\mathcal{U}$ from the left we finally obtain $\mathcal{A}\mathcal{U} = \mathcal{U}\mathcal{A}$.

Using this commutation relation, we note that $\mathcal{U}^{+}|\mathcal{A}| = (|\mathcal{A}|\mathcal{U})^{+} = (\mathcal{U}|\mathcal{A}|)^{+} = \mathcal{A}^{+} = \mathcal{A} = \mathcal{U}|\mathcal{A}|$, and therefore $(\mathcal{U}^{+} - \mathcal{U})|\mathcal{A}| = 0$. For all $|\Phi\rangle \in \mathbb{R}$, this implies $\mathcal{U}^{+}\,|\Phi\rangle = \mathcal{U}\,|\Phi\rangle$. If $|\Phi\rangle \in \mathbb{R}^{\perp}$, then $\mathcal{U}\,|\Phi\rangle = \mathcal{U}^{+}\,|\Phi\rangle = 0$. This means that $\mathcal{U}^{+} = \mathcal{U}$, as stated in (iv).

To prove (v), we remark that from the definition of $\mathcal{U}$ it is obvious that $\mathcal{U}\,|\Psi\rangle \in \mathbb{R}$. Statement (v) then immediately follows from (ii) and (iv).

The first part of (vi) follows from the square root theorem [Theorem VII, part (iii)]. With $\mathcal{A}\mathcal{B} = \mathcal{B}\mathcal{A}$, we also have $\mathcal{A}^{2}\mathcal{B} = \mathcal{B}\mathcal{A}^{2}$, and with $|\mathcal{A}| = \sqrt{\mathcal{A}^{2}}$, we find $|\mathcal{A}|\mathcal{B} = \mathcal{B}|\mathcal{A}|$. Therefore, we obtain $\mathcal{A}\mathcal{B} = \mathcal{U}|\mathcal{A}|\mathcal{B} = \mathcal{U}\mathcal{B}|\mathcal{A}|$ and $\mathcal{B}\mathcal{A} = \mathcal{B}\mathcal{U}|\mathcal{A}|$, so $(\mathcal{U}\mathcal{B} - \mathcal{B}\mathcal{U})|\mathcal{A}| = 0$. This implies $\mathcal{U}\mathcal{B}\,|\Phi\rangle = \mathcal{B}\mathcal{U}\,|\Phi\rangle$ for all $|\Phi\rangle \in \mathbb{R}$. For $|\Phi\rangle \in \mathbb{R}^{\perp}$, we note that also $\mathcal{B}\,|\Phi\rangle \in \mathbb{R}^{\perp}$, because $\mathcal{A}\mathcal{B}\,|\Phi\rangle = \mathcal{B}\mathcal{A}\,|\Phi\rangle = 0$, see (i). Thus, $\mathcal{U}\mathcal{B}\,|\Phi\rangle = \mathcal{B}\mathcal{U}\,|\Phi\rangle = 0$ in this case. In summary, this yields $\mathcal{U}\mathcal{B} = \mathcal{B}\mathcal{U}$. ■

Decomposing Hilbert space. The operator $\mathcal{U}$ associated with the self-adjoint operator $\mathcal{A}$ provides a very convenient means to decompose state space $\mathbb{H}$ into "positive" and "negative" parts, as well as the $\lambda = 0$ eigenspace (defect space). Indeed, from the properties (ii) and (iv) of the polar decomposition of the operator $\mathcal{A}$ (Theorem VIII), we immediately conclude that $(\mathcal{U}^2)^2 = \mathcal{U}^2$ which means that $\mathcal{U}^2$ presents a projection operator with possible eigenvalues $\tilde{\lambda} = 0, 1$, from which we instantaneously infer that $\mathcal{U}$ has at most three eigenvalues $\lambda = 0, \lambda = \pm 1$. The valuable property of the eigenspaces of $\mathcal{U}$ is stated in the decomposition theorem:

■ THEOREM IX

(i). The (disjunct) eigenspaces $\mathbb{M}_\pm$ $(\lambda = \pm 1)$ and $\mathbb{M}_0 = \mathbb{R}^\perp$ $(\lambda = 0)$ of $\mathcal{U}$ span the entire Hilbert space: $\mathbb{H} = \mathbb{M}_+ \oplus \mathbb{M}_- \oplus \mathbb{M}_0$

(ii). The projectors $\mathcal{P}_\pm, \mathcal{P}_0$ on the spaces $\mathbb{M}_\pm, \mathbb{M}_0$ are quadratic functions of $\mathcal{U}$:

$$\mathcal{P}_\pm = \frac{1}{2}\left(\mathcal{U}^2 \pm \mathcal{U}\right) \quad , \qquad \mathcal{P}_0 = \mathcal{E} - \mathcal{U}^2 \tag{A.58}$$

Proof. Using Theorem VIII, (v) one immediately finds from (A.58) that $\mathcal{P}_\pm^2 = \mathcal{P}_\pm$, $\mathcal{P}_0^2 = \mathcal{P}_0$. All mixed products $\mathcal{P}_0\mathcal{P}_+$ etc. vanish. In the same manner one checks that $\mathcal{U}\mathcal{P}_+ = \mathcal{P}_+, \mathcal{U}\mathcal{P}_- = -\mathcal{P}_-, \mathcal{U}\mathcal{P}_0 = 0$. Thus, for all $|\Psi\rangle$ in the domain of $\mathcal{A}$, $\mathcal{P}_\pm|\Psi\rangle \in \mathbb{M}_\pm$ and $\mathcal{P}_0|\Psi\rangle \in \mathbb{M}_0$ are eigenstates of $\mathcal{U}$ with eigenvalues $\lambda = \pm 1$ and $\lambda = 0$, respectively.

By adding up (A.58), we obtain $\mathcal{E} = \mathcal{P}_+ + \mathcal{P}_- + \mathcal{P}_0$. Hence, the decomposition of $|\Psi\rangle$ is complete: $|\Psi\rangle = \mathcal{P}_+|\Psi\rangle + \mathcal{P}_-|\Psi\rangle + \mathcal{P}_0|\Psi\rangle$ for every $|\Psi\rangle \in \mathbb{D}(\mathcal{A})$, which covers the Hilbert space $\mathbb{H}$ densely. This implies that $\mathbb{M}_\pm$ and $\mathbb{M}_0$ span the entire state space. ■

We note that as polynomials of $\mathcal{U}$, the projectors $\mathcal{P}_\pm$ and $\mathcal{P}_0$ commute with $\mathcal{A}$, $|\mathcal{A}|$, $\mathcal{U}$, and any bounded operator $\mathcal{B}$ which commutes with $\mathcal{A}$. This follows directly from Theorem VIII, parts (iii) and (vi). Thus, with $|\Psi\rangle \in \mathbb{M}_\pm$, also $\mathcal{A}|\Psi\rangle \in \mathbb{M}_\pm$, and the same property holds for $\mathbb{M}_0$. The spaces $\mathbb{M}_\pm, \mathbb{M}_0$ are invariant subspaces of $\mathbb{H}$ under the action of $\mathcal{A}$.

One would naively expect that $\mathcal{P}_\pm$ single out "positive" and "negative" subspaces of $\mathbb{H}$ where $\mathcal{A}$ acts like $\pm|\mathcal{A}|$. This is indeed confirmed by the following theorem:

■ THEOREM X

Let $|\Psi\rangle \in \mathbb{M}_+$. Then, $\langle\Psi|\mathcal{A}|\Psi\rangle \geq 0$. If $|\Psi\rangle \neq 0$, then the matrix element is strictly positive: $\langle\Psi|\mathcal{A}|\Psi\rangle > 0$. (An analogous statement holds for $\mathbb{M}_-$.)

Proof. Since $\mathcal{P}_+|\Psi\rangle = |\Psi\rangle$, we have $\langle\Psi|\mathcal{A}|\Psi\rangle = \langle\Psi|\mathcal{P}_+\mathcal{U}|\mathcal{A}|\mathcal{P}_+|\Psi\rangle = \langle\Psi|\mathcal{P}_+|\mathcal{A}|\mathcal{P}_+|\Psi\rangle = \langle\Psi||\mathcal{A}||\Psi\rangle \geq 0$, thanks to the square root theorem (Theorem VII), part (i).

Let now $\langle\Psi|\mathcal{A}|\Psi\rangle = 0$. Then, also $\langle\Psi||\mathcal{A}||\Psi\rangle = 0$. By the square root theorem, the non-negative operator $|\mathcal{A}|$ has a root; thus $\langle\Psi||\mathcal{A}||\Psi\rangle = \langle\sqrt{|\mathcal{A}|}\Psi|\sqrt{|\mathcal{A}|}\Psi\rangle = 0$. This implies $\sqrt{|\mathcal{A}|}|\Psi\rangle = 0$. Multiplying by $\mathcal{U}\sqrt{|\mathcal{A}|}$, we obtain $\mathcal{U}|\mathcal{A}||\Psi\rangle = \mathcal{A}|\Psi\rangle = 0$. According to Theorem

VIII, part (i), this however means that also $\mathcal{U}|\Psi\rangle = 0$, or $|\Psi\rangle = \mathcal{P}_0|\Psi\rangle = \mathcal{P}_0\mathcal{P}_+|\Psi\rangle = 0$, as $\mathcal{P}_0\mathcal{P}_+ = 0$. ■

In a sense, the subspaces $\mathbb{M}_\pm$ present the most comprehensive negative and positive parts of $\mathbb{H}$, as the following theorem shows:

■ THEOREM XI
If, and only if, for every state $|\Psi\rangle \in \mathbb{S}$ in an invariant subspace $\mathbb{S} \subseteq \mathbb{H}$ under $\mathcal{A}$ (i. e., $\mathcal{A}|\Psi\rangle \in \mathbb{S}$ if $|\Psi\rangle \in \mathbb{S}$) the relation $\langle\Psi|\mathcal{A}|\Psi\rangle \leq 0$ holds, then $|\Psi\rangle \in \mathbb{M}_- \oplus \mathbb{M}_0$, i. e., $\mathbb{S} \subseteq \mathbb{M}_- \oplus \mathbb{M}_0$.

Proof. Let first $\mathbb{S} \subseteq \mathbb{M}_- \oplus \mathbb{M}_0$. Then, by decomposition, for every $|\Psi\rangle \in \mathbb{S}$ we have $|\Psi\rangle = \mathcal{P}_-|\Psi\rangle + \mathcal{P}_0|\Psi\rangle$, and, as $\mathcal{A}\mathcal{P}_0|\Psi\rangle = 0$ [see Theorem VIII, part (i)], with $\mathcal{U}\mathcal{P}_- = -\mathcal{P}_-$ we find $\langle\Psi|\mathcal{A}|\Psi\rangle = \langle\Psi|\mathcal{P}_-\mathcal{U}|\mathcal{A}|\mathcal{P}_-|\Psi\rangle = -\langle\mathcal{P}_-\Psi||\mathcal{A}||\mathcal{P}_-\Psi\rangle \leq 0$ according to the square root theorem (Theorem VII), part (i).

Now, let for every $|\Psi\rangle \in \mathbb{S}$, $\mathcal{A}|\Psi\rangle \in \mathbb{S}$, and $\langle\Psi|\mathcal{A}|\Psi\rangle \leq 0$ shall hold. First, we prove that from $|\Psi\rangle \in \mathbb{S}^\perp$, i. e., $|\Psi\rangle$ in the orthogonal complement of $\mathbb{S}$, $\mathcal{A}|\Psi\rangle \in \mathbb{S}^\perp$ follows. Let us denote the projection of $\mathcal{A}|\Psi\rangle$ onto $\mathbb{S}$ by $|\Phi\rangle = \mathcal{P}_S\mathcal{A}|\Psi\rangle = \mathcal{P}_S^2\mathcal{A}|\Psi\rangle$, where $\mathcal{P}_S|\chi\rangle = |\chi\rangle$ for all $|\chi\rangle \in \mathbb{S}$, and $\mathcal{P}_S|\chi\rangle = 0$ for all $|\chi\rangle \in \mathbb{S}^\perp$. Since $|\Phi\rangle \in \mathbb{S}$, also $\mathcal{A}|\Phi\rangle \in \mathbb{S}$. Yet $|\Psi\rangle \in \mathbb{S}^\perp$ is orthogonal to all states in $\mathbb{S}$, so we have: $\langle\Psi|\mathcal{A}|\Phi\rangle = \langle\Psi|\mathcal{A}\mathcal{P}_S^2\mathcal{A}|\Psi\rangle = \|\mathcal{P}_S\mathcal{A}|\Psi\rangle\|^2 = 0$. Therefore, $\mathcal{P}_S\mathcal{A}|\Psi\rangle = 0$ and $\mathcal{A}|\Psi\rangle \in \mathbb{S}^\perp$.

This implies that $\mathcal{A}\mathcal{P}_S = \mathcal{P}_S\mathcal{A}$ holds, for any state $|\Psi\rangle \in \mathbb{H}$ is decomposed by $\mathcal{P}_S$ into states $|\Phi\rangle \in \mathbb{S}$ and $|\chi\rangle \in \mathbb{S}^\perp$, and $(\mathcal{A}\mathcal{P}_S - \mathcal{P}_S\mathcal{A})|\Phi\rangle = \mathcal{A}|\Phi\rangle - \mathcal{A}|\Phi\rangle = 0$ as well as $(\mathcal{A}\mathcal{P}_S - \mathcal{P}_S\mathcal{A})|\chi\rangle = 0$.

Since $\mathcal{P}_S$ is a bounded self-adjoint operator, Theorem VIII, part (vi) states that $\mathcal{P}_S$ commutes with $\mathcal{U}$, and, as $\mathcal{P}_+$ is a functional of $\mathcal{U}$ (Theorem IX), this implies also $\mathcal{P}_S\mathcal{P}_+ = \mathcal{P}_+\mathcal{P}_S$. Therefore, $\mathcal{P}_S\mathcal{P}_+|\Psi\rangle = \mathcal{P}_+|\Psi\rangle$ for all $|\Psi\rangle \in \mathbb{S}$, so by supposition we have $\langle\mathcal{P}_+\Psi|\mathcal{A}|\mathcal{P}_+\Psi\rangle \leq 0$. But $\mathcal{P}_+|\Psi\rangle \in \mathbb{M}_+$, so according to Theorem X, simultaneously $\langle\mathcal{P}_+\Psi|\mathcal{A}|\mathcal{P}_+\Psi\rangle \geq 0$ must hold. Thus, this matrix element identically vanishes. But Theorem X also states that this can only happen if $\mathcal{P}_+|\Psi\rangle = 0$ itself vanishes, implying $|\Psi\rangle \in \mathbb{M}_- \oplus \mathbb{M}_0$. ■

(Note: The same argument evidently holds for $\langle\Psi|\mathcal{A}|\Psi\rangle \geq 0$ for all $|\Psi\rangle \in \mathbb{S}$; then, $|\Psi\rangle \in \mathbb{M}_+ \oplus \mathbb{M}_0$.)

The spectral family. As we have seen (Theorem IX), the operator $\mathcal{U}$ imposes an decomposition of the Hilbert space $\mathbb{H}$ into positive, negative and defect parts $\mathbb{M}_\pm$, $\mathbb{M}_0$ with regard to the self-adjoint operator $\mathcal{A}$. Since with $\mathcal{A}$ also the "shifted" operator $\mathcal{A} - \lambda\mathcal{E}$ for real λ is self-adjoint, we may indeed define a continuous family of polar decompositions via $\mathcal{A} - \lambda\mathcal{E} = \mathcal{U}(\lambda)|\mathcal{A} - \lambda\mathcal{E}|$. Now the idea is fairly obvious that with increasing λ, the corresponding negative subspace $\mathbb{M}_-(\lambda)$ "grows" on expense of the positive subspace $\mathbb{M}_+(\lambda)$ since eigenstates $\mathcal{A}|\Psi\rangle = \alpha|\Psi\rangle$ will be contained in $\mathbb{M}_-(\lambda)$ for $\alpha < \lambda$. In the same manner, $\mathbb{M}_0(\lambda)$ scans through the eigenspaces of the eigenstates of $\mathcal{A}$. Therefore, we may expect that every self-adjoint operator $\mathcal{A}$ via its corresponding operator family $\mathcal{U}(\lambda)$ generates an "ordering" within Hilbert space $\mathbb{H}$.

For this purpose, we introduce a more versatile vehicle than $\mathcal{U}(\lambda)$ (Kato [228], p. 353) and summarize its principal properties:

■ DEFINITION XII
The projector function

$$\Pi(\lambda) \;=\; \mathcal{P}_{-}(\lambda) + \mathcal{P}_{0}(\lambda) \;=\; \mathcal{E} - \frac{1}{2}\left[\mathcal{U}(\lambda) + \mathcal{U}(\lambda)^{2}\right] \tag{A.59}$$

is called the spectral family $\Pi(\lambda)$ generated by the self-adjoint operator $\mathcal{A}$. It projects onto the subspace $\mathbb{M}(\lambda) = \mathbb{M}_{-}(\lambda) + \mathbb{M}_{0}(\lambda)$.

■ THEOREM XIII
The spectral family $\Pi(\lambda)$ has the following properties:

(i). $\Pi(\lambda)$ commutes with $\mathcal{A}$ and with itself: $\Pi(\lambda)\mathcal{A} = \mathcal{A}\Pi(\lambda)$, $\Pi(\lambda)\Pi(\mu) = \Pi(\mu)\Pi(\lambda)$

(ii). $\Pi(\lambda)$ is monotonic: For $\mu > \lambda$, $\Pi(\lambda)\Pi(\mu) = \Pi(\lambda)$

(iii). $\Pi(\lambda)$ is complete: $\lim\limits_{\lambda\to-\infty} \Pi(\lambda) = 0$, $\lim\limits_{\lambda\to\infty} \Pi(\lambda) = \mathcal{E}$

(iv). $\Pi(\lambda)$ is right continuous: $\lim\limits_{\eta\to 0^{+}} \Pi(\lambda+\eta) = \Pi(\lambda)$

Proof. Property (i) clearly follows from the fact that $\mathcal{U}(\lambda)$ commutes with $\mathcal{A} - \lambda\mathcal{E}$ and hence with $\mathcal{A} - \mu\mathcal{E}$ for any μ, in particular also with $\mathcal{A}$ [Theorem VIII, part (iii)]. Furthermore, $\mathcal{U}(\lambda)$ commutes with any bounded operator that commutes with $\mathcal{A} - \lambda\mathcal{E}$ [Theorem VIII, part (vi)], including $\mathcal{U}(\mu)$. Since the spectral family $\Pi(\lambda)$ is a quadratic function of $\mathcal{U}(\lambda)$, both statements follow immediately.

To prove (ii), let $\lambda < \mu$. For every state $|\Phi\rangle \in \mathbb{M}(\lambda)$ in the subspace $\mathbb{M}(\lambda)$, we have by Theorem XI $\langle\Phi\,|\mathcal{A} - \lambda\mathcal{E}|\,\Phi\rangle \leq 0$, or $\langle\Phi\,|\mathcal{A}|\,\Phi\rangle \leq \lambda\langle\Phi|\Phi\rangle < \mu\langle\Phi|\Phi\rangle$. This implies for every state $|\Phi\rangle$ in the invariant subspace $\mathbb{M}(\lambda)$ that $\langle\Phi\,|\mathcal{A} - \mu\mathcal{E}|\,\Phi\rangle \leq 0$. Following Theorem XI and Definition XII, this means that $|\Phi\rangle \in \mathbb{M}(\mu)$, or, in projector form, $\Pi(\mu)\,|\Phi\rangle = |\Phi\rangle$. Therefore, the subspace $\mathbb{M}(\lambda)$ is contained in $\mathbb{M}(\mu)$: $\mathbb{M}(\lambda) \subseteq \mathbb{M}(\mu)$. Finally, for every $|\Psi\rangle \in \mathbb{H}$, we find by definition $\Pi(\lambda)\,|\Psi\rangle \in \mathbb{M}(\lambda)$. Using the commutation relation (i), this means that $\Pi(\lambda)\Pi(\mu)\,|\Psi\rangle = \Pi(\mu)\Pi(\lambda)\,|\Psi\rangle = \Pi(\lambda)\,|\Psi\rangle$ for every $|\Psi\rangle \in \mathbb{H}$, so (ii) follows.

If $|\Phi\rangle \in \mathbb{M}(-\infty)$, then $|\Phi\rangle \in \mathbb{M}(\lambda)$ for all $\lambda < 0$ according to (ii). Theorem X then states that $\langle\Phi|\Phi\rangle \leq \lambda^{-1}\,|\langle\Phi\,|\mathcal{A}|\,\Phi\rangle|$ for all $\lambda > 0$. For any state $|\Phi\rangle$ in the domain of $\mathcal{A}$ in $\mathbb{H}$, the matrix element on the right-hand side is necessarily bounded, so $\langle\Phi|\Phi\rangle = 0$, which implies $|\Phi\rangle = 0$. Thus, $\mathbb{M}(-\infty)$ only contains the trivial zero state, which implies $\Pi(-\infty) = 0$. The same reasoning applies for the relation $\mathcal{E} - \Pi(\infty) = 0$.

To show (iv), we assume that the statement is invalid, i. e., $\mathbb{M}(\lambda+\eta) \supset \mathbb{M}(\lambda)$ for all $\eta \to 0^{+}$. Then, there must exist a state $|\Phi\rangle \neq 0$ so that $\langle\Phi\,|\mathcal{A} - \lambda\mathcal{E}|\,\Phi\rangle \leq \eta\,\langle\Phi|\Phi\rangle$ for all $\eta > 0$ (Theorem XI). Simultaneously, $|\Phi\rangle \perp \mathbb{M}(\lambda)$ which by Definition XII implies $|\Phi\rangle \in \mathbb{M}_{+}(\lambda)$. Following Theorem X, we find $\langle\Phi\,|\mathcal{A} - \lambda\mathcal{E}|\,\Phi\rangle = \delta$ with some fixed $\delta > 0$. Hence, we are led into the contradiction that $\eta\,\langle\Phi|\Phi\rangle \geq \delta$ for all $\eta > 0$, which means that property (iv) must hold. ■

We note that there may exist values of λ so that $\mathbb{M}(\lambda - \eta) \subset \mathbb{M}(\lambda)$ for all $\eta \to 0^+$. This obviously occurs whenever there are states $|\Phi\rangle$ in $\mathbb{M}_0(\lambda)$, i. e., $\mathcal{A}\,|\Phi\rangle = \lambda\,|\Phi\rangle$. λ is then a member of the spectrum of $\mathcal{A}$. (See also below.)

Interval projectors. Up to now, we only considered decompositions of the Hilbert space into "positive" and "negative" parts $\mathbb{H} = \mathbb{M}(\lambda) \oplus \mathbb{M}_+(\lambda)$ imposed by the action of the self-adjoint operator $\mathcal{A} - \lambda\mathcal{E}$. We have seen that increasing λ to $\mu > \lambda$ shifts parts of $\mathbb{M}_+(\lambda)$ into $\mathbb{M}(\mu)$, so λ presents a kind of ordering parameter in $\mathbb{H}$. Next, we want to show that the set of transferred states $\mathbb{M}(\lambda, \mu) = \mathbb{M}_+(\lambda) \cap \mathbb{M}(\mu)$ indeed presents an subspace of $\mathbb{H}$ invariant under $\mathcal{A}$. The projector $\mathcal{I}(\lambda, \mu)$ onto the subspace $\mathbb{M}(\lambda, \mu)$ is called an interval projector. Clearly, interval projectors refine the decomposition of $\mathbb{H}$, as $\mathbb{M}(\mu) = \mathbb{M}(\lambda) \oplus \mathbb{M}(\lambda, \mu)$. The interval projectors $\mathcal{I}(\lambda, \mu)$ have the following rather obvious properties:

■ THEOREM XIV
For $\lambda < \mu$, the interval projector $\mathcal{I}(\lambda, \mu)$ onto the subspace $\mathbb{M}(\lambda, \mu) = \mathbb{M}_+(\lambda) \cap \mathbb{M}(\mu)$ is given by:

$$\mathcal{I}(\lambda, \mu) \;=\; [\mathcal{E} - \Pi(\lambda)]\,\Pi(\mu) \;=\; \Pi(\mu) - \Pi(\lambda) \tag{A.60}$$

The basic properties of the projectors $\mathcal{I}(\lambda, \mu)$ are:

(i). Commutativity: $\mathcal{A}\mathcal{I}(\lambda, \mu) = \mathcal{I}(\lambda, \mu)\mathcal{A}$
(This implies that $\mathbb{M}(\lambda, \mu)$ is an invariant subspace under $\mathcal{A}$.)

(ii). Idempotency: $\mathcal{I}(\lambda, \mu)^2 = \mathcal{I}(\lambda, \mu)$

(iii). Additivity: For $\lambda < \nu < \mu$, $\mathcal{I}(\lambda, \mu) = \mathcal{I}(\lambda, \nu) + \mathcal{I}(\nu, \mu)$

(iv). Orthogonality: For $\mu \leq \lambda'$, $\mathcal{I}(\lambda, \mu)\mathcal{I}(\lambda', \mu') = 0$

(v). Boundedness: If $|\Phi\rangle \in \mathbb{M}(\lambda, \mu)$ is an element of the interval subspace $\mathbb{M}(\lambda, \mu)$, the relation follows:

$$\lambda\,\langle\Phi|\Phi\rangle \;\leq\; \langle\Phi\,|\mathcal{A}|\,\Phi\rangle \;\leq\; \mu\,\langle\Phi|\Phi\rangle \tag{A.61}$$

Conversely, if the condition (A.61) holds for all state vectors $|\Psi\rangle \in \mathbb{S}$ of an invariant subspace $\mathbb{S} \subseteq \mathbb{H}$, then $\mathbb{S} \subseteq \mathbb{M}(\lambda, \mu) \oplus \mathbb{M}_0(\lambda)$.

(vi). Boundedness of the norm: For every $|\Phi\rangle \in \mathbb{M}(\lambda, \mu)$ we have:

$$0 \;\leq\; \|(\mathcal{A} - \lambda\mathcal{E})\,|\Phi\rangle\|^2 \;\leq\; (\mu - \lambda)^2\,\langle\Phi|\Phi\rangle \tag{A.62}$$

Proof. This theorem hardly requires any comment. It is straightforward to check that $\mathcal{I}(\lambda,\mu)$ as defined in (A.60) indeed projects on states in $\mathbb{M}_+(\lambda)\cap\mathbb{M}(\mu)$. The second form follows from Theorem XIII, part (ii), which may also be used to prove property (iv). For (i) and (ii), we note that $\Pi(\lambda)$ commutes with $\mathcal{A}$ and $\Pi(\mu)$ [see Theorem XIII, part (i)]. Part (iii) is a direct consequence of (A.60), whereas (v) is obtained by applying Theorem XI consecutively on $\mathcal{A}-\lambda\mathcal{E}$ and $\mathcal{A}-\mu\mathcal{E}$. Finally, to prove (vi), we note that $\mathcal{A}-\lambda\mathcal{E}$ is a non-negative operator in the restricted domain $\mathbb{M}(\lambda,\mu)$. Thus, $\sqrt{\mathcal{A}-\lambda\mathcal{E}}$ exists there (Theorem VII), and we may use (A.61) to estimate $\|(\mathcal{A}-\lambda\mathcal{E})\,|\Phi\rangle\|^2 = \langle\sqrt{\mathcal{A}-\lambda\mathcal{E}}\,\Phi\,|\mathcal{A}-\lambda\mathcal{E}|\,\sqrt{\mathcal{A}-\lambda\mathcal{E}}\,\Phi\rangle \le (\mu-\lambda)\langle\sqrt{\mathcal{A}-\lambda\mathcal{E}}\,\Phi|\sqrt{\mathcal{A}-\lambda\mathcal{E}}\,\Phi\rangle = (\mu-\lambda)\,\langle\Phi\,|\mathcal{A}-\lambda\mathcal{E}|\,\Phi\rangle \le (\mu-\lambda)^2\,\langle\Phi|\Phi\rangle$ for states $|\Phi\rangle\in\mathbb{M}(\lambda,\mu)$. ■

The point and continuous spectra. In the finite-dimensional model of Hilbert spaces $\mathbb{H}_N$ we took under consideration in Section A.3.1 we introduced projectors $\mathcal{P}(E)$ onto eigenspaces of the operator $\mathcal{H}_0$ (A.53). In the present theory of operators in $\mathbb{H}$, a corresponding role is taken over by the projector $\mathcal{P}_0(\lambda)$ on the subspace $\mathbb{M}_0(\lambda)$ [see Theorem VIII, part (i), and Theorem IX, part (ii)]. But whereas in $\mathbb{H}_N$ the projectors $\mathcal{P}(E)$ were sufficient to build a complete decomposition of the Hilbert space, as shown by the Fourier decomposition (Theorem IV) of arbitrary vectors (A.40), in $\mathbb{H}$ we have to retreat to the quite different concept of an interval projector $\mathcal{I}(\lambda,\mu)$. It now appears reasonable to assume that the ordinary projectors $\mathcal{P}_0(\mu)$ are obtained from their interval counterparts $\mathcal{I}(\lambda,\mu)$ in the limit $\lambda\to\mu$. As Theorem XIII, part (iv) tells us we have to take some caution in the limiting procedure. We first define the projector $\mathcal{P}(\lambda)$ as limit of an interval projector and proceed to show that indeed $\mathcal{P}(\lambda)=\mathcal{P}_0(\lambda)$.

■ DEFINITION XV

The projector $\mathcal{P}(\lambda)$ assigned to a self-adjoint operator $\mathcal{A}$ is defined as the left limiting value of an interval projector:

$$\mathcal{P}(\lambda) \;=\; \lim_{\eta\to 0^+}\;\Pi(\lambda)-\Pi(\lambda-\eta) \tag{A.63}$$

If $\mathcal{P}(\mu)=0$, then the spectral family $\Pi(\lambda)$ is denoted as continuous at $\mu=\lambda$, otherwise discontinuous.

■ THEOREM XVI

If, and only if, $\Pi(\lambda)$ is discontinuous at $\lambda=\mu$, then μ is an eigenvalue of $\mathcal{A}$ with eigenspace $\mathbb{M}_0$. μ is said to belong to the point spectrum of $\mathcal{A}$.

Proof. Let us first assume that $|\Phi\rangle\in\mathbb{M}_0(\mu)$ is a (non-vanishing) eigenstate of $\mathcal{A}$, $\mathcal{A}\,|\Phi\rangle=\mu\,|\Phi\rangle$. Then, for all $\eta\to 0^+$, $|\Phi\rangle\in\mathbb{M}_+(\mu-\eta)$ (Theorem XI). Thus, we have $\langle\Phi\,|\mathcal{P}(\mu)|\,\Phi\rangle=\langle\Phi\,|\Pi(\mu)|\,\Phi\rangle=\langle\Phi|\Phi\rangle>0$, as $\mathbb{M}_0(\mu)\subseteq\mathbb{M}(\mu)$, but simultaneously $\langle\Phi\,|\Pi(\mu-\eta)|\,\Phi\rangle=0$. This means $\mathcal{P}(\mu)\neq 0$, and $\Pi(\lambda)$ is discontinuous.

On the other hand, from the orthogonality of the projectors we have $\Pi(\mu)\mathcal{P}_0(\mu)=[\mathcal{P}_0(\mu)+\mathcal{P}_-(\mu)]\mathcal{P}_0(\mu)=\mathcal{P}_0(\mu)$ and, as the eigenspace $\mathbb{M}_0(\mu)$ for all $\eta>0$ is contained in the positive

space of $\mathcal{A}-(\mu-\eta)\mathcal{E}$, $\mathbb{M}_0(\mu) \subseteq \mathbb{M}_+(\mu-\eta)$, it follows $\Pi(\mu-\eta)\mathcal{P}_0(\mu) = 0$. According to Definition XV, this means that $\mathcal{P}(\mu)\mathcal{P}_0(\mu) = \mathcal{P}_0(\mu)$, which shows that every eigenstate $|\Phi\rangle$ of $\mathcal{A}$ with eigenvalue μ, i. e., the subspace $\mathbb{M}_0(\mu)$ remains invariant under the projection $\mathcal{P}(\mu)$. Therefore, the image space of $\mathcal{P}(\mu)$ at least comprises the space of eigenstates $\mathbb{M}_0(\mu)$. In order to show that there are no additional states, we assume for the moment that there exists some state $|\Psi\rangle$ with $\mathcal{P}(\mu)|\Psi\rangle = |\Psi\rangle$ which is not contained in the μ eigenspace of $\mathcal{A}$, i. e., $(\mathcal{A}-\mu\mathcal{E})|\Psi\rangle = |\Phi\rangle \neq 0$. But then we have by Theorem XIV, part (vi) that $\langle\Phi|\Phi\rangle = \|(\mu\mathcal{E}-\mathcal{A})|\Psi\rangle\|^2 \leq \eta^2\langle\Psi|\Psi\rangle$ for every $\eta > 0$, which implies $|\Phi\rangle = 0$ in contradiction to our assumption. Thus, the image space of $\mathcal{P}(\mu)$ is exactly the eigenspace $\mathbb{M}_0(\mu)$ of eigenstates of $\mathcal{A}$ with eigenvalue μ. ■

Therefore, the set of eigenvalues $\{\mu\}$ of $\mathcal{A}$ which we denote as the point spectrum of $\mathcal{A}$, and the set of discontinuities of the spectral family $\Pi(\lambda)$ coincide. Unlike the finite-dimensional case where from (A.53) the spectral family $\Pi(E)$ is seen to be constant between consecutive eigenvalues $E_k \leq E < E_{k+1}$, in $\mathbb{H}$ there is more to the spectral family than just its discontinuities. In fact, $\Pi(\nu)$ may grow in a continuous way, i. e., for certain values of $\nu = \mu$ the expectation value $\langle\Psi|\Pi(\mu)|\Psi\rangle$ of the spectral family may be strictly monotonic for some state $|\Psi\rangle \in \mathbb{H}$. Then, for any finite-size interval $\lambda < \nu \leq \mu$ the projector $\mathcal{I}(\lambda,\mu)$ cannot vanish. This condition is connected to the existence of a continuous spectrum of $\mathcal{A}$. The properties of interval projectors outside the point spectrum are summarized in the following theorem.

■ THEOREM XVII
Let $\mathcal{I}(\lambda,\mu)$ be an projector for an interval $\lambda \leq \nu \leq \mu$ that does not contain an eigenvalue of $\mathcal{A}$. Then, one of these alternatives holds:

(i). The spectral family $\Pi(\nu)$ is constant in the interval: $\Pi(\lambda) = \Pi(\mu)$, i. e., $\mathcal{I}(\lambda,\mu) = 0$ vanishes, and $\mathcal{I}(\lambda,\mu)|\Phi\rangle = 0$ for all $|\Phi\rangle \in \mathbb{H}$.

(ii). The image space $\mathbb{M}(\lambda,\mu)$ of $\mathcal{I}(\lambda,\mu)$ is of infinite dimension.

Proof. We just have to exclude the possibility that the image space $\mathbb{M}(\lambda,\mu)$ of $\mathcal{I}(\lambda,\mu)$ is of finite dimension, say N. If this would be true, then we would be able to create a base of N normalized eigenstates $|\Phi_k\rangle$ of $\mathcal{A}$ in $\mathbb{M}(\lambda,\mu)$ by the inductive process presented in Section A.3.1. Since according to theorem XIV, part (v) for all states $|\Phi\rangle$ in the invariant subspace $\mathbb{M}(\lambda,\mu)$, $\lambda\langle\Phi|\Phi\rangle \leq \langle\Phi|\mathcal{A}|\Phi\rangle \leq \mu\langle\Phi|\Phi\rangle$ holds, the interval $\lambda \leq \nu \leq \mu$ contains N eigenvalues of $\mathcal{A}$, in contradiction to our assumption. ■

Clearly, Theorem XVII holds as well for any sub-interval $\lambda' \leq \nu \leq \mu'$ entirely contained in the original interval $\lambda \leq \nu \leq \mu$. Therefore, a sensible definition of the points of constancy and growth of $\Pi(\nu)$ is given by:

■ DEFINITION XVIII
Let $\lambda < \nu < \mu$ be an interval that is disjunct to the point spectrum of $\mathcal{A}$, i. e., contains no eigenvalue of $\mathcal{A}$.

(i). If for any sub-interval $\lambda < \lambda' < \nu < \mu' < \mu$ the interval projector $\mathcal{I}(\lambda', \mu')$ vanishes ($\mathbb{M}(\lambda', \mu')$ contains only the zero state), then the interval $\lambda < \nu < \mu$ is said to belong to the resolvent set of $\mathcal{A}$.

(ii). If no sub-interval $\lambda < \lambda' < \nu < \mu' < \mu$ belongs to the resolvent set, then the interval $\lambda < \nu < \mu$ is called part of the continuous spectrum of $\mathcal{A}$.

(iii). The continuous spectrum of $\mathcal{A}$ is defined as the union of all intervals $\lambda < \nu < \mu$ belonging to the continuous spectrum of $\mathcal{A}$ according to (ii).

We once again note that according to this definition, there exist no eigenstates of $\mathcal{A}$ with eigenvalues in the continuous spectrum!

The spectral theorem. Using the notion of interval projectors we now may proceed to construct the infinite-dimensional equivalent of the spectral theorem (Theorem II) and the resolution of the identity (Theorem III). It is clear from the preceding chapter that the spectral representations of $\mathcal{A}$ and $\mathcal{E}$ will be built upon interval projectors $\mathcal{I}(\lambda, \mu)$ rather than the projectors $\mathcal{P}(\lambda)$ onto eigenstates of $\mathcal{A}$ that we utilized in (A.38) and (A.39).

Thus, we introduce the notion of a partitioning of the real axis into intervals. For this purpose we employ a countable ordered set $\{\lambda_k\}$, $-\infty < k < \infty$ with $\lambda_k < \lambda_{k+1}$, $\lim_{k\to\pm\infty} \lambda_k \to \pm\infty$ in order to resolve the real axis into finite intervals $\lambda_k \leq \lambda < \lambda_{k+1}$. The partitioning may always be refined by introducing a new point λ' with $\lambda_k < \lambda' < \lambda_{k+1}$ for some value of the index k. Clearly, in this manner we may arrange partitionings $\{\lambda_k\}$ in a way that the maximum size of the intervals does not exceed a given upper limit $\eta > 0$. Hence, the parameter η presents a measure for the coarseness of the partitioning.

We may use arbitrary partitionings of the real axis to achieve decompositions of the identity operator $\mathcal{E}$ into a sum of interval operators. Indeed, from the completeness of the spectral family $\Pi(\lambda)$ of any self-adjoint operator $\mathcal{A}$ [Theorem XIII, part (iii)] and the very definition of the interval projector $\mathcal{I}(\lambda_k, \lambda_{k+1})$ (A.60) we obtain using some given partitioning $\{\lambda_k\}$:

$$\mathcal{E} = \Pi(\infty) - \Pi(-\infty) = \sum_k \Pi(\lambda_{k+1}) - \Pi(\lambda_k) = \sum_k \mathcal{I}(\lambda_k, \lambda_{k+1}) \tag{A.64}$$

We may use this result to show a property of the spectral family $\Pi(\lambda)$ that is essential for the proof of the spectral theorem:

■ COROLLARY XIX

The spectral family $\Pi(\lambda)$ is of bounded variation. (This means that for any two states $|\Phi\rangle$, $|\Psi\rangle$ in the Hilbert space $\mathbb{H}$, $\langle\Phi\,|\Pi(\lambda)|\,\Psi\rangle$ is of bounded variation in $-\infty < \lambda < \infty$.)

Proof. The corollary asserts that for any partitioning $\{\lambda_k\}$ of the real axis, the variation V of the matrix element is finite:

$$\begin{aligned} V &= \sum_k \left| \langle \Phi \left| \Pi(\lambda_{k+1}) \right| \Psi \rangle - \langle \Phi \left| \Pi(\lambda_k) \right| \Psi \rangle \right| \\ &= \sum_k \left| \langle \Phi \left| \mathcal{I}(\lambda_k, \lambda_{k+1}) \right| \Psi \rangle \right| \;\leq\; \sum_k \sqrt{\langle \Phi \left| \mathcal{I}(\lambda_k, \lambda_{k+1}) \right| \Phi \rangle \, \langle \Psi \left| \mathcal{I}(\lambda_k, \lambda_{k+1}) \right| \Psi \rangle} \end{aligned} \tag{A.65}$$

In the last line, we used the projector property $\mathcal{I}(\lambda_k, \lambda_{k+1})^2 = \mathcal{I}(\lambda_k, \lambda_{k+1})$ [Theorem XIV, part (ii)] and the Cauchy-Schwarz inequality for states in $\mathbb{H}$. To proceed, we denote the diagonal elements appearing in (A.65) by $\alpha_k^2 = \langle \Phi \left| \mathcal{I}(\lambda_k, \lambda_{k+1}) \right| \Phi \rangle$, $\beta_k^2 = \langle \Psi \left| \mathcal{I}(\lambda_k, \lambda_{k+1}) \right| \Psi \rangle$ (note that the interval projector $\mathcal{I}(\lambda_k, \lambda_{k+1})$ is non-negative), where we may choose $\alpha_k, \beta_k \geq 0$. Clearly, the interval decomposition of the identity $\mathcal{E}$ (A.64) implies that $\sum_k \alpha_k^2 = \langle \Phi | \Phi \rangle$, $\sum_k \beta_k^2 = \langle \Psi | \Psi \rangle$. Therefore, we have from (A.65):

$$V \;\leq\; \sum_k \alpha_k \beta_k \;\leq\; \sqrt{(\sum_k \alpha_k^2)(\sum_k \beta_k^2)} \;=\; \sqrt{\langle \Phi | \Phi \rangle \, \langle \Psi | \Psi \rangle} \tag{A.66}$$

Here, we used again the Cauchy-Schwarz inequality in its vector component form [81]. We see that V is bounded by the norm of the states $|\Phi\rangle$ and $|\Psi\rangle$. ■

The valuable property shown in Corollary XIX is that boundedness of the variation of $\Pi(\lambda)$ ensures that for any continuous function $f(\lambda)$, the operator $\mathcal{B}[f, \{\lambda_k\}]$:

$$\mathcal{B}[f, \{\lambda_k\}] \;=\; \sum_k f(\lambda_k) \left\{ \Pi(\lambda_{k+1}) - \Pi(\lambda_k) \right\} \tag{A.67}$$

converges towards a unique limiting operator $\mathcal{B}[f]$ as the partitioning of the real axis $\{\lambda_k\}$ is increasingly refined: $\eta \to 0$, with $\eta = \max_k (\lambda_{k+1} - \lambda_k)$ (see above). In fact, the matrix element $\langle \Phi \left| \mathcal{B}[f] \right| \Psi \rangle$ is just the Stieltjes integral of $f(\lambda)$ over the spectral function $\langle \Phi \left| \Pi(\lambda) \right| \Psi \rangle$. (For a comprehensive discussion of Stieltjes integrals, see e. g. the textbook by Taylor [231], p. 392.). Thus, we may write $\mathcal{B}[f]$ formally as an operator Stieltjes integral:

$$\mathcal{B}[f] \;=\; \int f(\lambda) \, \mathrm{d}\Pi(\lambda) \tag{A.68}$$

As $\Pi(\lambda)$ is constant in the resolvent set (Definition XVIII), and discontinuities, given by the projector $\mathcal{P}(\lambda)$, occur only if $\lambda = \mu_k$ is a member of the point spectrum (Theorem XVI), i. e., if μ_k presents an eigenvalue of $\mathcal{A}$, we may rewrite the operator Stieltjes integral (A.68) in the following symbolic form:

$$\mathcal{B}[f] \;=\; \sum_k f(\mu_k) \mathcal{P}(\mu_k) \;+\; \int_{\text{c.s.}} f(\mu) \, \mathrm{d}\Pi(\mu) \tag{A.69}$$

where the sum index k is a counter in the set of eigenvalues of $\mathcal{A}$, and the subscript "c.s." denotes the continuous spectrum of $\mathcal{A}$. In the case of finite-dimensional Hilbert spaces $\mathbb{H}_N$, (A.69) reduces to the sum over projectors familiar from Section A.3.1, as then no continuous spectrum exists.

We already encountered an important representant of this class of operator integrals. Indeed, if we set $f \equiv 1$, from (A.67) we obtain again (A.64), hence $\mathcal{E} = \mathcal{B}[1]$. Obviously, this integral presents the extension of the resolution of the identity (Theorem III) to the infinite-dimensional space $\mathbb{H}$:

■ THEOREM XX (RESOLUTION OF THE IDENTITY)
The spectral family $\Pi(\mu)$ of every self-adjoint operator $\mathcal{A}$ generates a resolution of the identity $\mathcal{E}$ in the Hilbert space $\mathbb{H}$:

$$\mathcal{E} = \int \mathrm{d}\Pi(\mu) = \sum_k \mathcal{P}(\mu_k) + \int_{\text{c.s.}} \mathrm{d}\Pi(\mu) \tag{A.70}$$

For the interpretation of $\mathcal{B}[f]$ for more complicated functions $f(\lambda)$, we may advantageously use the results obtained for spaces $\mathbb{H}_N$ (Section A.3.1) as a guideline. By comparison of the spectral theorem (Theorem II) in the form (A.53) with the representation (A.69) of the operator Stieltjes integrals, we conspicuously find that in the finite-dimensional case, any self-adjoint operator $\mathcal{H}_0$ acting in $\mathbb{H}_N$ may be represented by $\mathcal{B}(E)$: $\mathcal{H}_0 = \mathcal{B}(E) = \sum_k E_k \mathcal{P}(E_k)$. Thus, we may expect that in the Hilbert space, $\mathcal{A} = \mathcal{B}(\lambda)$ holds generally. This is indeed true (see Kato [228], p. 360):

■ THEOREM XXI (SPECTRAL THEOREM)
In $\mathbb{H}$, every self-adjoint operator $\mathcal{A}$ admits an expansion into its spectral family $\Pi(\lambda)$:

$$\mathcal{A} = \int \mu \, \mathrm{d}\Pi(\mu) = \sum_k \mu_k \mathcal{P}(\mu_k) + \int_{\text{c.s.}} \mu \, \mathrm{d}\Pi(\mu) \tag{A.71}$$

Proof. Let $|\Psi\rangle \in \mathbb{D}(\mathcal{A})$ be an arbitrary state in the domain of the operator $\mathcal{A}$ in $\mathbb{H}$. Using a partition $\{\lambda_k\}$ of the real axis with maximum interval size η, we may decompose $|\Psi\rangle$ into a sum of vectors $|\Psi\rangle = \sum_k |\Psi_k\rangle$ by projecting $|\Psi_k\rangle = \mathcal{I}(\lambda_k, \lambda_{k+1}) |\Psi\rangle$ [this is just the decomposition according to the resolution of identity (A.64)]. Clearly, we have $\langle\Psi|\Psi\rangle = \sum_k \langle\Psi_k|\Psi_k\rangle$.

Now, as $|\Psi_k\rangle \in \mathbb{M}(\lambda_k, \lambda_{k+1})$, according to Theorem XIV, part (vi) we have the inequality $\|(\mathcal{A} - \lambda_k \mathcal{E}) |\Psi_k\rangle\|^2 \leq \eta^2 \langle\Psi_k|\Psi_k\rangle$. Using the decomposition of the identity (A.64) again, we find successively by the orthonormality of the interval projection operators [Theorem XIV, parts (i),

(ii) and (iv)]:

$$\left\| \mathcal{A} - \sum_k \lambda_k \mathcal{I}(\lambda_k, \lambda_{k+1}) \, |\Psi\rangle \right\|^2 = \sum_{j,\,k} \langle \Psi \, | \mathcal{I}(\lambda_j, \lambda_{j+1}) \, (\mathcal{A} - \lambda_j \mathcal{E}) \, (\mathcal{A} - \lambda_k \mathcal{E}) \, \mathcal{I}(\lambda_k, \lambda_{k+1}) | \, \Psi \rangle$$
$$= \sum_k \left\langle \Psi_k \left| (\mathcal{A} - \lambda_k \mathcal{E})^2 \right| \Psi_k \right\rangle \leq \sum_k \eta^2 \, \langle \Psi_k | \Psi_k \rangle = \eta^2 \, \langle \Psi | \Psi \rangle \tag{A.72}$$

As $\eta \to 0$, the operator sum $\sum_k \lambda_k \mathcal{I}(\lambda_k, \lambda_{k+1})$ turns into the operator Stieltjes integral $\mathcal{B}[\lambda]$ (A.67), (A.68). But as the right-hand side in (A.72) then vanishes, $\mathcal{A} = \mathcal{B}[\lambda]$ must hold. ■

From this result, we may be confident that also the more general type of operators $\mathcal{B}[f(\lambda)]$ defined in (A.68), (A.69) is amenable to a description in terms of the self-adjoint operator $\mathcal{A}$. We will assume that $f(\lambda) = \sum_\nu a_\nu \lambda^\nu$ is an analytic function of λ; then, we obtain successively from the projector property of $\mathcal{I}(\lambda_k, \lambda_{k+1})$ [Theorem XIV, parts (ii) and (iv)] for the operator functional $\mathcal{B}[f(\lambda), \{\lambda_k\}]$ (A.67) based on a partitioning $\{\lambda_k\}$:

$$\mathcal{B}[f(\lambda), \{\lambda_k\}] = \mathcal{B}\left[\sum_{\nu=0}^{\infty} a_\nu \lambda^\nu, \{\lambda_k\} \right] = \sum_{\nu=0}^{\infty} a_\nu \left\{ \sum_k \lambda_k^\nu \, \mathcal{I}(\lambda_k, \lambda_{k+1}) \right\}$$
$$= \sum_{\nu=0}^{\infty} a_\nu \left\{ \sum_k \lambda_k \, \mathcal{I}(\lambda_k, \lambda_{k+1}) \right\}^\nu = \sum_{\nu=0}^{\infty} a_\nu \mathcal{B}[\lambda, \{\lambda_k\}]^\nu = f(\mathcal{B}[\lambda, \{\lambda_k\}]) \tag{A.73}$$

Here, we obviously set $\mathcal{B}[\lambda, \{\lambda_k\}]^0 = \mathcal{E}$.

Therefore, we may exchange the sequence of operator $\mathcal{B}$ and analytic function $f(\lambda)$: $\mathcal{B}[f(\lambda), \{\lambda_k\}] = f(\mathcal{B}[\lambda, \{\lambda_k\}])$. Indeed, this property holds even in the limit of a densely spaced partitioning of the real axis ($\eta \to 0$). The spectral theorem (Theorem XXI) then immediately yields:

■ THEOREM XXII

If $f(\lambda)$ is an analytic function, then the operator functional $f[\mathcal{A}]$ may be expanded into the spectral family $\Pi(\lambda)$ assigned to the self-adjoint operator $\mathcal{A}$ in $\mathbb{H}$:

$$f[\mathcal{A}] = \int f(\lambda) \, \mathrm{d}\Pi(\lambda) = \sum_k f(\mu_k) \mathcal{P}(\mu_k) + \int_{\text{c.s.}} f(\mu) \, \mathrm{d}\Pi(\mu) \tag{A.74}$$

Proof. We just have to show that in the limit of dense partitionings $\{\lambda_k\}$, where $\eta = \max_k(\lambda_{k+1} - \lambda_k) \to 0$, in the last line of (A.73) the argument of the functional f may be replaced by its limiting operator $\mathcal{A}$ (Theorem XXI). The proof is very similar to that of the spectral theorem, so we take over the notation we employed there (see above). We first note that due to

the fact that $\mathbb{M}(\lambda_k\,,\,\lambda_{k+1})$ is an invariant subspace under $\mathcal{A}$, we may use Theorem XIV to show that:

$$\sum_k \left\langle \Psi_k \left| (\mathcal{A}-\lambda_k\mathcal{E})^{2\nu+2} \right| \Psi_k \right\rangle \;\leq\; \sum_k \eta^2 \left\langle \Psi_k \left| (\mathcal{A}-\lambda_k\mathcal{E})^{2\nu} \right| \Psi_k \right\rangle \;\leq\; \cdots \;\leq\; \eta^{2\nu+2} \left\langle \Psi | \Psi \right\rangle \quad \text{(A.75)}$$

Using (A.75), the resolution of the identity (A.64) and the triangle inequality for the norm, we find with $f(z) = \sum_\nu a_\nu z^\nu$ that for every $|\Psi\rangle \in \mathbb{D}(\mathcal{A})$ the difference between $f[\mathcal{A}]$ and the approximation $\mathcal{B}[f(\lambda),\{\lambda_k\}]$ vanishes as $\eta \to 0$:

$$\begin{aligned} \left\| \left(f[\mathcal{A}] - \mathcal{B}[f(\lambda),\{\lambda_k\}] \right) |\Psi\rangle \right\| &= \left\| \sum_{\nu\,=\,1}^{\infty} a_\nu \left(\mathcal{A} - \sum_k \lambda_k\, \mathcal{I}(\lambda_k,\lambda_{k+1}) \right)^\nu |\Psi\rangle \right\| \\ &\leq \sum_{\nu\,=\,1}^{\infty} |a_\nu| \left\| \sum_k (\mathcal{A}-\lambda_k\mathcal{E})^\nu\, |\Psi_k\rangle \right\| \;\leq\; \|\Psi\| \sum_{\nu\,=\,1}^{\infty} |a_\nu|\, \eta^\nu \end{aligned} \quad \text{(A.76)}$$

For locally analytic $f(z)$, the right-hand sum clearly converges towards zero. ■

As an important example for such a derived operator that we already dealt with in the finite-dimensional space $\mathbb{H}_N$, we re-examine the time evolution operator $\mathcal{U}(t,t') = \exp[-i\mathcal{H}(t-t')/\hbar]$ (A.15) assigned to a stationary Hamiltonian operator $\mathcal{H} = \mathcal{A}$. Clearly, its expansion reads:

$$\mathcal{U}(t,t') \;=\; \exp(-i\mathcal{H}(t-t')/\hbar) \;=\; \sum_k e^{-\,iE_k(t-t')/\hbar}\, \mathcal{P}(E_k) \;+\; \int_{\text{c.s.}} e^{-\,iE(t-t')/\hbar}\, \mathrm{d}\Pi(E) \quad \text{(A.77)}$$

This obviously includes the eigenstate decomposition (A.42) of $\mathcal{U}(t,t')$ in $\mathbb{H}_N$.

A.3.4 The Eigenfunctions of the Continuous Spectrum

We have seen that in the continuous spectrum of the self-adjoint operator $\mathcal{A}$, no eigenvalues and proper normalizable eigenstates exist. On the other hand, the non-normalizable eigenfunctions $\psi_E(\mathbf{r})$ in the continuous spectrum of the Hamiltonian operator $H(\mathbf{r},\mathbf{p})$ of Section A.3.2 are a common and useful tool in the analysis of problems in quantum mechanics (see e. g. the textbooks by Messiah [83,238]). Clearly, it is of interest to infer how the notion of "eigenfunctions in the continuous spectrum" emerges in the context of functional analysis. The common mathematical approach to the continuous spectrum is based on Borel sets and the Lebesgue measure (see Kato, p. 514 [228]. The topic is treated more extensively by Reed and Simon [229].), and therefore not particularly apt for the development of a theory of monoenergetic "eigenfunctions." Here, we present another approach that leads directly to the eigenfunctions of the continuous spectrum and related concepts.

"Almost eigenstates." We have already seen [Theorem XVII, part (ii)] that to any finite-size interval projector $\mathcal{I}(\lambda, \mu)$ that projects onto the continuous spectrum, there is an invariant subspace $\mathbb{M}(\lambda, \mu)$ of infinite dimension that remains unchanged in the course of the projection. We already have shown that for any such state $|\chi\rangle \in \mathbb{M}(\lambda, \mu)$, the inequality holds [Theorem XIV, part (vi)]:

$$\| [\mathcal{A} - \lambda \mathcal{I}(\lambda, \mu)] \, |\chi\rangle \|^2 \leq (\lambda - \mu)^2 \, \langle \chi | \chi \rangle \tag{A.78}$$

Hence, as $\mu \to \lambda$, the states $|\chi\rangle$ become "almost eigenstates" of $\mathcal{A}$ with "almost eigenvalue" λ. But, by Definition XVIII, no true eigenstate of $\mathcal{A}$ exists in the interval $\lambda < \nu < \mu$.

On the other hand, we were able to show that for arbitrary states $|\Psi\rangle$, $|\Phi\rangle \in \mathbb{H}$, the matrix element $\langle \Phi \, |\Pi(\nu)| \, \Psi \rangle$ is of bounded variation (Corollary XIX). This property implies that $\langle \Phi \, |\Pi(\nu)| \, \Psi \rangle$ is differentiable almost everywhere, i. e., with the possible exception of a set of values $\{\nu\}$ that is of vanishing measure (see e. g. Taylor [231], p. 409). As a consequence, the interval eigenstates considered in (A.78) are rather special; in the common case, $\langle \Phi \, |\mathcal{I}(\lambda, \mu)| \, \Psi \rangle$ grows linearly with the size of the interval $\mu - \lambda$ and vanishes as $\mu \to \lambda$. This behavior makes it plausible that the eigenfunctions of the continuous spectrum are connected to the derivative of the spectral family rather than to the spectral family $\Pi(\nu)$ itself.

The density of states "operator." To develop further the idea of continuous eigenfunctions, we now make the assumption that the matrix element function $\langle \Phi \, |\Pi(\nu)| \, \Psi \rangle$ is indeed continuously differentiable everywhere in the continuous spectrum. This represents not a very demanding requirement since this matrix element a priori is differentiable almost everywhere as we have stated above. (In the lingo of the set theoretical approach, our assumption is equivalent to the request that the spectrum be absolutely continuous, and the invariant subspace of singularly continuous states vanishes.) For some simple cases, including the free-particle Hamiltonian $H_{\text{free}}(\mathbf{p}) = p^2/2M$, it may be directly verified that this property actually holds true (see Kato [228], p. 518). However, we will often reverse the line of argument and use the properties of the eigenfunctions of the continuous spectrum in order to infer information on the operator $\mathcal{A}$ and its spectrum. Anyway, under the conditions stated above it is reasonable to define:

■ DEFINITION XXIII

For any two states $|\Psi\rangle$, $|\Phi\rangle \in \mathbb{H}$ and every self-adjoint operator $\mathcal{A}$ with continuously differentiable spectral family $\Pi(\nu)$ in the continuous spectrum, the functional:

$$\left\langle \Phi \left| \frac{\partial \Pi(\nu)}{\partial \nu} \right| \Psi \right\rangle = \lim_{\eta \to 0^+} \frac{1}{\eta} \, \langle \Phi \, |\mathcal{I}(\nu - \eta, \nu)| \, \Psi \rangle \tag{A.79}$$

is denoted as the matrix element of the density of states "operator" $\partial\Pi(\nu)/\partial\nu$ belonging to $\mathcal{A}$.

It is obviously tempting to strip off the states $|\Phi\rangle$ and $|\Psi\rangle$ in this definition and deal with the "operator" $\partial\Pi(\nu)/\partial\nu$ rather than the unwieldy matrix element. This, however, does not work—the naive expectation that any sesquilinear form may be interpreted as the expectation value of some operator is an invalid notion in spaces $\mathbb{H}$ of infinite dimension (though it obviously holds in $\mathbb{H}_N$). In fact, if a state $|\Psi\rangle \in \mathbb{H}$ has support in every interval containing μ, i. e., $\langle\Psi\,|\Pi(\nu)|\,\Psi\rangle$ is actually a growing function in the vicinity of $\nu = \mu$ which is obviously a necessary condition for a non-vanishing matrix element in (A.79), then $|\Psi\rangle$ does not belong to the domain of $\partial\Pi(\mu)/\partial\mu$. It is easy to show that there is no normalizable state $\partial\Pi(\nu)/\partial\nu\,|\Psi\rangle$:

$$\left\|\frac{\partial\Pi(\mu)}{\partial\mu}\,|\Psi\rangle\right\|^2 \;=\; \lim_{\eta\to 0^+}\left\langle\Psi\left|\left(\frac{\mathcal{I}(\mu-\eta,\mu)}{\eta}\right)^2\right|\Psi\right\rangle \;=\; \lim_{\eta\to 0^+}\frac{1}{\eta}\left\langle\Psi\left|\frac{\partial\Pi(\mu)}{\partial\mu}\right|\Psi\right\rangle \;\longrightarrow\; \infty \tag{A.80}$$

Here, the contribution of the "almost eigenstates" $\mathcal{I}(\mu-\eta,\mu)\,|\Psi\rangle$ to the state $|\Psi\rangle$ (A.78) manifests itself. Keeping in mind the difference between the matrix element and the "operator" it is based upon, we will keep the handy notation $\partial\Pi(\mu)/\partial\mu$ and the term operator (without quotation marks).

Formally, the operator $\partial\Pi(\mu)/\partial\mu$ may be written in a representation as an operator Stieltjes integral involving the Dirac delta "function." Indeed, reducing the size of the interval $\eta = \mu - \lambda$, we find using the Heaviside step function $\Theta(x)$ and the definition of the density of states operator:

$$\frac{\partial\Pi(\mu)}{\partial\mu} \;=\; \lim_{\eta\to 0^+}\int\frac{1}{\eta}\left[\Theta(\nu-\mu+\eta)-\Theta(\mu-\nu)\right]\mathrm{d}\Pi(\nu) \;=\; \int\delta(\mu-\nu)\,\mathrm{d}\Pi(\nu) \tag{A.81}$$

As a consequence, we may rewrite the operator Stieltjes integral describing the resolution of the identity (Theorem XX) in the form of a conventional Riemann integral taking advantage of $\partial\Pi(\mu)/\partial\mu$:

$$\mathcal{E} \;=\; \sum_k \mathcal{P}(\mu_k) \;+\; \int_{\text{c.s.}}\frac{\partial\Pi(\mu)}{\partial\mu}\,d\mu \tag{A.82}$$

Analogous expressions are available for the spectral theorem (Theorem XXI) and for derived operators (Theorem XXII). Here, we obviously have to keep in mind the rather peculiar properties of the "operator" $\partial\Pi(\mu)/\partial\mu$.

Finally, we want to state in the form of a corollary a useful inequality for the matrix elements of the density of states operator. As a direct consequence, the existence of

the diagonal matrix elements of the $\partial\Pi(\mu)/\partial\mu$ guarantees the boundedness of the off-diagonal element $\langle\Phi\,|\partial\Pi(\mu)/\partial\mu|\,\Psi\rangle$:

■ COROLLARY XXIV
For any two states $|\Phi\rangle, |\Psi\rangle \in \mathbb{H}$, the inequality holds:

$$\left|\left\langle \Phi \left| \frac{\partial\Pi(\mu)}{\partial\mu} \right| \Psi \right\rangle\right|^2 \leq \left\langle \Phi \left| \frac{\partial\Pi(\mu)}{\partial\mu} \right| \Phi \right\rangle \left\langle \Psi \left| \frac{\partial\Pi(\mu)}{\partial\mu} \right| \Psi \right\rangle \tag{A.83}$$

Proof. For any fixed $\eta > 0$, according to the projector property $\mathcal{I}(\mu-\eta,\mu)^2 = \mathcal{I}(\mu-\eta,\mu)$, the Cauchy-Schwarz inequality for the projections on $\mathbb{M}(\mu-\eta,\mu)$ reads in slightly rewritten form:

$$\frac{1}{\eta^2}\,|\langle\Phi\,|\mathcal{I}(\mu-\eta,\mu)|\,\Psi\rangle|^2 \leq \frac{1}{\eta}\,\langle\Phi\,|\mathcal{I}(\mu-\eta,\mu)|\,\Phi\rangle\,\frac{1}{\eta}\,\langle\Psi\,|\mathcal{I}(\mu-\eta,\mu)|\,\Psi\rangle \tag{A.84}$$

In the limit $\eta \to 0^+$, (A.83) emerges. ■

The orthonormal family of "operators" assigned to a state. In the preceding paragraph, we introduced the matrix elements of some "operator" $\partial\Pi(\mu)/\partial\mu$ (Definition XXIII), gathered some of its peculiar properties and already hinted upon the fact that the action of this operator might be connected to the existence of non-normalizable eigenfunctions of the continuous spectrum of $\mathcal{A}$ well-known from quantum mechanics (Section A.3.2). However, the actual connection between eigenfunction and density of states operator so far remains utterly unclear.

To establish the step from operator theory to the conventional eigenfunction approach, we introduce in this section a whole family of "operators" $\mathcal{C}_\Psi(\mu)$ which is generated by a (normalizable) state $|\Psi\rangle$ in Hilbert space $\mathbb{H}$ and is closely related to the density of states operator $\partial\Pi(\mu)/\partial\mu$. In preparation, we note that for every state $|\Psi\rangle \in \mathbb{H}$ whose spectral decomposition has support at some value $\nu = \mu$ in the continuous spectrum of $\mathcal{A}$, i. e., $\langle\Psi\,|\partial\Pi(\mu)/\partial\mu|\,\Psi\rangle > 0$, we may rewrite the inequality of Corollary XXIV in the following form. For all $|\Phi\rangle \in \mathbb{H}$, we have:

$$\lim_{\eta\to 0^+} \frac{1}{\eta}\frac{\langle\Phi\,|\mathcal{I}(\mu-\eta,\mu)|\,\Psi\rangle\,\langle\Psi\,|\mathcal{I}(\mu-\eta,\mu)|\,\Phi\rangle}{\langle\Psi\,|\mathcal{I}(\mu-\eta,\mu)|\,\Psi\rangle} = \frac{\left|\left\langle \Phi \left| \frac{\partial\Pi(\mu)}{\partial\mu} \right| \Psi \right\rangle\right|^2}{\left\langle \Psi \left| \frac{\partial\Pi(\mu)}{\partial\mu} \right| \Psi \right\rangle} \leq \left\langle \Phi \left| \frac{\partial\Pi(\mu)}{\partial\mu} \right| \Phi \right\rangle \tag{A.85}$$

Thus, the left-hand side of this equation exists; we may interpret it as the diagonal matrix element of an "operator" $\mathcal{C}_\Psi(\mu)$. It turns out that this projection of state space (the generating state $|\Psi\rangle$) onto an operator family $\mathcal{C}_\Psi(\mu)$ provides the key to a viable treatment of the continuous spectrum of the self-adjoint operator $\mathcal{A}$. The following definition logically extends (A.85) to all real values of μ, including the point spectrum and the resolvent set.

■ DEFINITION XXV
The orthonormal family of operators $\mathcal{C}_\Psi(\mu)$ assigned to a given state $|\Psi\rangle \in \mathbb{H}$ for a self-adjoint operator $\mathcal{A}$ with differentiable continuous spectrum is defined by:

(i). If μ is a member of the continuous spectrum of $\mathcal{A}$ and $\langle\Psi\,|\partial\Pi(\mu)/\partial\mu|\,\Psi\rangle > 0$, then

$$\mathcal{C}_\Psi(\mu) \;=\; \lim_{\eta\to 0^+} \frac{\mathcal{I}(\mu-\eta,\mu)\,|\Psi\rangle\,\langle\Psi|\,\mathcal{I}(\mu-\eta,\mu)}{\eta\;\langle\Psi\,|\mathcal{I}(\mu-\eta,\mu)|\,\Psi\rangle} \tag{A.86}$$

(ii). If μ is a member of the point spectrum of $\mathcal{A}$, i. e., μ is an eigenvalue of $\mathcal{A}$ and $\langle\Psi\,|\mathcal{P}(\mu)|\,\Psi\rangle > 0$, then

$$\mathcal{C}_\Psi(\mu) \;=\; \frac{\mathcal{P}(\mu)\,|\Psi\rangle\,\langle\Psi|\,\mathcal{P}(\mu)}{\langle\Psi\,|\mathcal{P}(\mu)|\,\Psi\rangle} \tag{A.87}$$

(iii). For all other real values μ, we set $\mathcal{C}_\Psi(\mu) = 0$.

Like its counterpart $\partial\Pi(\mu)/\partial\mu$ (A.80), $\mathcal{C}_\Psi(\mu)$ is not an operator in the strict sense, as the tentative "states" $\mathcal{C}_\Psi(\mu)\,|\Phi\rangle$ are generally non-normalizable. We emphasize here that $\mathcal{C}_\Psi(\mu)$ is not a linear functional of the state $|\Psi\rangle$. The mapping of $\mathbb{H}$ onto $\mathcal{C}_\Psi(\mu)$ is not even injective; e. g., $\mathcal{C}_\Psi(\mu)$ is invariant with respect to scalings of the state $|\Psi\rangle \to \lambda\,|\Psi\rangle$ ($\lambda \neq 0$). Rather, the dimension of the resulting image space of orthonormal families is closely connected to the notion of degeneracy (see Section A.3.1). Later on, we will dwell on this property of the orthonormal families. But first we will collect a number of important properties of $\mathcal{C}_\Psi(\mu)$ into the following theorem:

■ THEOREM XXVI
The orthonormal family of operators $\mathcal{C}_\Psi(\mu)$ assigned to a state $|\Psi\rangle \in \mathbb{H}$ and a self-adjoint operator $\mathcal{A}$ possesses the following fundamental properties:

(i). $\mathcal{C}_\Psi(\mu)$ is non-negative and hermitian

(ii). $\mathcal{C}_\Psi(\mu)$ is bounded by $\partial\Pi(\mu)/\partial\mu$:

$$\langle\Phi\,|\mathcal{C}_\Psi(\mu)|\,\Phi\rangle \;\leq\; \begin{cases} \langle\Phi\,|\mathcal{P}(\mu)|\,\Phi\rangle & (\mu \in \text{p.s.}) \\ \langle\Phi\,|\partial\Pi(\mu)/\partial\mu|\,\Phi\rangle & (\mu \in \text{c.s.}) \end{cases} \tag{A.88}$$

(iii). Boundedness of the family $\mathcal{C}_\Psi(\mu)$:

$$\left\{\sum_{\text{p.s.}} + \int_{\text{c.s.}} d\mu\right\} \langle\Phi\,|\mathcal{C}_\Psi(\mu)|\,\Phi\rangle \;\leq\; \langle\Phi|\Phi\rangle \tag{A.89}$$

(iv). Action of $\mathcal{C}_\Psi(\mu)$ on its parent state $|\Psi\rangle$:

$$\langle\Phi\,|\mathcal{C}_\Psi(\mu)|\,\Psi\rangle \;=\; \begin{cases}\langle\Phi\,|\mathcal{P}(\mu)|\,\Psi\rangle & (\mu\in\text{p.s.})\\ \langle\Phi\,|\partial\Pi(\mu)/\partial\mu|\,\Psi\rangle & (\mu\in\text{c.s.})\end{cases} \tag{A.90}$$

(v). Spectral decomposition of $|\Psi\rangle$:

$$\left\{\sum_{\text{p.s.}}+\int_{\text{c.s.}}d\mu\right\}\mathcal{C}_\Psi(\mu)\,|\Psi\rangle \;=\; |\Psi\rangle \tag{A.91}$$

(vi). Expansion of non-diagonal matrix elements:

$$|\langle\Phi\,|\mathcal{C}_\Psi(\mu)|\,\chi\rangle|^2 \;=\; \langle\Phi\,|\mathcal{C}_\Psi(\mu)|\,\Phi\rangle\,\langle\chi\,|\mathcal{C}_\Psi(\mu)|\,\chi\rangle \tag{A.92}$$

(vii). Explicit representation of diagonal matrix elements:

$$\langle\Phi\,|\mathcal{C}_\Psi(\mu)|\,\Phi\rangle \;=\; \begin{cases}\frac{|\langle\Phi|\mathcal{P}(\mu)|\Psi\rangle|^2}{\langle\Psi|\mathcal{P}(\mu)|\Psi\rangle} & (\mu\in\text{p.s.})\\ \frac{|\langle\Phi|\partial\Pi(\mu)/\partial\mu|\Psi\rangle|^2}{\langle\Psi|\partial\Pi(\mu)/\partial\mu|\Psi\rangle} & (\mu\in\text{c.s.})\end{cases} \tag{A.93}$$

(viii). Orthogonality of families: For $\lambda\neq\mu$ and arbitrary parent states $|\Phi\rangle$, $|\Psi\rangle\in\mathbb{H}$:

$$\mathcal{C}_\Phi(\lambda)\,\mathcal{C}_\Psi(\mu) \;=\; 0 \tag{A.94}$$

(ix). Orthonormality relations for $\mathcal{C}_\Psi(\mu)$:

$$\mathcal{C}_\Psi(\lambda)\,\mathcal{C}_\Psi(\mu) \;=\; \begin{cases}\delta_{\lambda\mu}\,\mathcal{C}_\Psi(\mu) & (\mu\in\text{p.s.})\\ \delta(\lambda-\mu)\,\mathcal{C}_\Psi(\mu) & (\mu\in\text{c.s.})\end{cases} \tag{A.95}$$

(x). $\mathcal{C}_\Psi(\mu)$ is "eigenoperator" of $\mathcal{A}$ with eigenvalue μ. If $\phi(z)$ is a regular function, then:

$$\mathcal{A}\mathcal{C}_\Psi(\mu) = \;\mu\,\mathcal{C}_\Psi(\mu) \tag{A.96}$$

$$\phi[\mathcal{A}]\mathcal{C}_\Psi(\mu) = \;\phi(\mu)\,\mathcal{C}_\Psi(\mu) \tag{A.97}$$

(xi). The orthonormal family $\mathcal{C}_\Psi(\mu)$ commutes with its parent operator $\mathcal{A}$:

$$\mathcal{C}_\Psi(\mu)\mathcal{A} \;=\; \mathcal{A}\mathcal{C}_\Psi(\mu) \;=\; \mu\,\mathcal{C}_\Psi(\mu) \tag{A.98}$$

Proof. Most of these statements, like (i), follow quite obviously from the definition of $\mathcal{C}_\Psi(\mu)$. In (ii) and (vii), we have rewritten the inequality (A.85). Property (iii) follows from (ii) by summing over all μ, using the completeness relation (A.82). Performing the matrix elements of (A.90), we are led back to the original definition of the density of states operator (Definition XXIII), which proves (iv). Summing (iv) again over all μ, we may discard of the bra state $\langle\Phi|$ and end up with (v). Part (vi) is immediately obtained by inserting the definition of the orthonormal family (Definition XXV) and reordering matrix elements. According to Theorem XIV, part (iv) interval projectors $\mathcal{I}(\lambda,\mu)$ over disjunct intervals are orthogonal; this immediately proves proposition (viii).

It remains to show the validity of (ix)–(xi). The statement in (ix) is obviously correct if μ is a member of the point spectrum of $\mathcal{A}$. In the case of the continuous spectrum we have to verify that for any continuous test function $\phi(\mu)$, the relation:

$$\int d\mu\,\phi(\mu)\,\mathcal{C}_\Psi(\lambda)\,\mathcal{C}_\Psi(\mu) \;=\; \phi(\lambda)\,\mathcal{C}_\Psi(\lambda) \tag{A.99}$$

holds. For this purpose, we use a partitioning $\{\mu_k\}$ of the real axis and approximate (A.99). Here, it is advisable to fix $\mu_0 = \lambda - \eta$, $\mu_1 = \lambda$, since then only the $k = 0$ term in the summation of the integral will survive:

$$\begin{aligned}\mathcal{C}_\Psi(\lambda)\int d\mu\,\phi(\mu)\,\mathcal{C}_\Psi(\mu) \;&=\; \lim_{\eta\to 0^+}\frac{\mathcal{I}(\lambda-\eta,\lambda)\,|\Psi\rangle}{\eta\,\langle\Psi\,|\mathcal{I}(\lambda-\eta,\lambda)|\,\Psi\rangle}\\
&\times\lim_{\mu_{k+1}-\mu_k\to 0}\sum_k \phi(\mu_k)(\mu_{k+1}-\mu_k)\,\frac{\langle\Psi\,|\mathcal{I}(\lambda-\eta,\lambda)\mathcal{I}(\mu_k,\mu_{k+1})|\,\Psi\rangle\,\langle\Psi|\,\mathcal{I}(\mu_k,\mu_{k+1})}{(\mu_{k+1}-\mu_k)\,\langle\Psi\,|\mathcal{I}(\mu_k,\mu_{k+1})|\,\Psi\rangle}\\
&=\lim_{\eta\to 0^+}\frac{\mathcal{I}(\lambda-\eta,\lambda)\,|\Psi\rangle\,\langle\Psi|\,\mathcal{I}(\lambda-\eta,\lambda)}{\eta\,\langle\Psi\,|\mathcal{I}(\lambda-\eta,\lambda)|\,\Psi\rangle}\,\phi(\lambda) \;=\; \phi(\lambda)\,\mathcal{C}_\Psi(\lambda)\end{aligned} \tag{A.100}$$

Thus, (ix) is proven. To show (x), we note that for sufficiently small $\eta > 0$, by orthogonality the interval projector $\mathcal{I}(\mu-\eta,\mu)$ annihilates the orthonormal family operator $\mathcal{C}_\Psi(\lambda)$ unless $\lambda = \mu$. However, for $\lambda = \mu$ we find $\mathcal{I}(\mu-\eta,\mu)\mathcal{C}_\Psi(\mu) = \mathcal{C}_\Psi(\mu)$ for all $\eta > 0$. Applying the spectral theorem (Theorem XXI), we may exploit this orthogonality property: Using a partitioning of the real axis with $\mu_1 = \lambda$, we immediately obtain an expression in which only the $k = 0$ term does not vanish:

$$\mathcal{A}\mathcal{C}_\Psi(\lambda) \;=\; \lim_{\mu_{k+1}-\mu_k\to 0}\sum_k \mu_k\,\mathcal{I}(\mu_k,\mu_{k+1})\,\mathcal{C}_\Psi(\lambda) \;=\; \lim_{\eta\to 0^+}\lambda\mathcal{I}(\lambda-\eta,\lambda)\,\mathcal{C}_\Psi(\lambda) \;=\; \lambda\,\mathcal{C}_\Psi(\lambda) \tag{A.101}$$

The same argument applies for $\mathcal{C}_\Psi(\lambda)\mathcal{A} = \lambda\mathcal{C}_\Psi(\lambda)$, so additionally (xi) is confirmed. The extension of this technique onto the point spectrum of $\mathcal{A}$ and regular functionals $\phi[\mathcal{A}]$ (Theorem XXII) is straightforward. ■

Eigenfunction representation. The orthonormality relation for the orthonormal operator family $\mathcal{C}_\Psi(\mu)$ stated in Theorem XXVI, part (ix) is clearly very similar to the corresponding property of "normalized" eigenfunctions $\psi_E(\mathbf{r})$ of the Hamiltonian $H(\mathbf{r},\mathbf{p})$

in quantum mechanics. Therefore, we may expect that both concepts are intimately connected, and this is indeed true: In order to obtain these eigenfunctions, we simply form the spatial representation of the orthonormal family and define:

$$\langle \mathbf{r} \,|\mathcal{C}_\Psi(\mu)|\, \mathbf{r}' \rangle \;=\; \psi_\mu(\mathbf{r})\, \psi_\mu(\mathbf{r}')^* \tag{A.102}$$

Here, the newly introduced function $\psi_\mu(\mathbf{r})$ according to Definition XXV is obviously given by:

$$\psi_\mu(\mathbf{r}) \;=\; \lim_{\eta \to 0^+} \frac{e^{i\gamma(\mu)}\, \langle \mathbf{r} \,|\mathcal{I}(\mu-\eta,\mu)|\, \Psi \rangle}{\sqrt{\eta\, \langle \Psi \,|\mathcal{I}(\mu-\eta,\mu)|\, \Psi \rangle}} \qquad \text{and} \qquad \psi_\mu(\mathbf{r}) \;=\; \frac{e^{i\gamma(\mu)}\, \langle \mathbf{r} \,|\mathcal{P}(\mu)|\, \Psi \rangle}{\sqrt{\langle \Psi \,|\mathcal{P}(\mu)|\, \Psi \rangle}} \tag{A.103}$$

for the continuous and point spectrum of $\mathcal{A}$, respectively. Unlike the operator family $\mathcal{C}_\Psi(\mu)$, the functions $\psi_\mu(\mathbf{r})$ are only fixed up to a unitary phase $\gamma(\mu)$. This type of gauge invariance is familiar from quantum mechanics.

We show next that the family of functions $\psi_\mu(\mathbf{r})$ indeed presents a normalized set of eigenfunctions in the discrete and continuous spectrum of the operator $A(\mathbf{r},\mathbf{r}') = \langle \mathbf{r} \,|\mathcal{A}|\, \mathbf{r}' \rangle$ in its spatial representation (see Section A.2.1). To see this, we employ the eigenoperator property of $\mathcal{C}_\Psi(\mu)$ [Theorem XXVI, part (x)] in its spatial form. Using the resolution of the identity (A.8), one immediately finds:

$$\int d^3r'\; \langle \mathbf{r} \,|\mathcal{A}|\, \mathbf{r}' \rangle\, \langle \mathbf{r}' \,|\mathcal{C}_\Psi(\mu)|\, \mathbf{r}'' \rangle \;=\; \mu\, \langle \mathbf{r} \,|\mathcal{C}_\Psi(\mu)|\, \mathbf{r}'' \rangle \tag{A.104}$$

which reads expanded in eigenfunctions $\psi_\mu(\mathbf{r})$ (A.102):

$$\int d^3r'\, A(\mathbf{r},\mathbf{r}')\, \psi_\mu(\mathbf{r}') \;=\; \mu\, \psi_\mu(\mathbf{r}) \tag{A.105}$$

Hence, $\psi_\mu(\mathbf{r})$ is an eigenfunction of the integral kernel $A(\mathbf{r},\mathbf{r}')$ with eigenvalue μ. In quantum mechanics, (A.105) adopts an even simpler form. We have already seen that commonly used Hamiltonians are diagonal: $\langle \mathbf{r} \,|\mathcal{H}|\, \mathbf{r}' \rangle = \delta(\mathbf{r}-\mathbf{r}')H(\mathbf{r},\mathbf{p})$. Thus, we obtain the usual expression $H(\mathbf{r},\mathbf{p})\psi_E(\mathbf{r}) = E\,\psi_E(\mathbf{r})$. We realize that the functions $\psi_E(\mathbf{r})$ represent normalized eigenstates of the Hamiltonian $\mathcal{H}$ both in its discrete and continuous spectrum [83].

Furthermore, we may easily check that the family of eigenfunctions $\psi_\lambda(\mathbf{r})$ is properly normalized. Using the orthonormality relation of the operator family $\mathcal{C}_\Psi(\mu)$ [The-

orem XXVI, part (ix)] and (A.8), we successively obtain:

$$\int d^3r\, \psi_\mu(\mathbf{r})^* \psi_\lambda(\mathbf{r}) = \frac{\int d^3r\ \langle \mathbf{r}' | \mathcal{C}_\Psi(\mu) | \mathbf{r} \rangle \langle \mathbf{r} | \mathcal{C}_\Psi(\lambda) | \mathbf{r}' \rangle}{\psi_\mu(\mathbf{r}') \psi_\lambda(\mathbf{r}')^*}$$
$$= \frac{\langle \mathbf{r}' | \mathcal{C}_\Psi(\mu) \mathcal{C}_\Psi(\lambda) | \mathbf{r}' \rangle}{\psi_\mu(\mathbf{r}') \psi_\lambda(\mathbf{r}')^*} = \begin{cases} \delta_{\mu\lambda} & \text{(p.s.)} \\ \delta(\lambda - \mu) & \text{(c.s.)} \end{cases} \tag{A.106}$$

Non-degeneracy and the resolution of the identity. In the preceding paragraph we have established the close connection between the orthonormal family of operators $\mathcal{C}_\Psi(\mu)$ and the eigenfunctions $\psi_\mu(\mathbf{r})$ in particular of the continuous spectrum of the self-adjoint operator $\mathcal{A}$ which arise from the spatial representation of $\mathcal{C}_\Psi(\mu)$ (A.102). We already checked that $\psi_\mu(\mathbf{r})$ indeed presents a family of eigenfunctions of the operator $\mathcal{A}$ in its spatial form $A(\mathbf{r}, \mathbf{r}')$ (A.105), and is furthermore properly normalized (A.106). However, we remained silent about the third property that is usually tacitly assumed to hold for eigenfunction systems of self-adjoint operators $A(\mathbf{r}, \mathbf{r}')$ [83], their completeness which we so far were only able to prove in the case of finite-dimensional spaces $\mathbb{H}_N$ (Theorems III, IV).

In fact, the functions $\psi_\mu(\mathbf{r})$ in general do not form a complete base of functions which allows for the expansion of arbitrary functions $\phi(\mathbf{r}) = \langle \mathbf{r} | \Phi \rangle$. This can be seen quickly if one recalls that the family of functions $\psi_\mu(\mathbf{r})$ derives from the orthonormal family $\mathcal{C}_\Psi(\mu)$ which is explicitly based on some specific state $|\Psi\rangle \in \mathbb{H}$. From the orthogonality relation of orthonormal families [Theorem XXVI, part (viii)] it is clear that the expansion of another eigenfunction of $\mathcal{A}$, say $\chi_\lambda(\mathbf{r})$ generated by some different state $|\chi\rangle \in \mathbb{H}$ via $\chi_\mu(\mathbf{r}) \chi_\mu(\mathbf{r}')^* = \langle \mathbf{r} | \mathcal{C}_\chi(\mu) | \mathbf{r}' \rangle$ (A.102), can only involve the function $\psi_\lambda(\mathbf{r})$. Obviously, this "expansion" is only feasible if $\chi_\lambda(\mathbf{r})$ and $\psi_\lambda(\mathbf{r})$ are linearly dependent which means either $\mathcal{C}_\chi(\lambda) = 0$ (the trivial case) or $\mathcal{C}_\chi(\lambda) = \mathcal{C}_\psi(\lambda)$.

We may summarize the discussion above and state that as a necessary condition for completeness of the system of functions $\psi_\mu(\mathbf{r})$ we must require that for every value of μ, as $|\chi\rangle$ scans through the Hilbert space $\mathbb{H}$ the orthonormal families $\mathcal{C}_\chi(\mu)$ either vanish or take on an unique value $\mathcal{C}(\mu)$. This leads to the definition:

■ DEFINITION XXVII

Let $\{\Psi\}$ be the set of all states in $\mathbb{H}$ that has support at μ, i. e., $\langle \Psi | \mathcal{P}(\mu) | \Psi \rangle > 0$ if μ is an element of the point spectrum of $\mathcal{A}$, or $\langle \Psi | \partial\Pi(\mu)/\partial\mu | \Psi \rangle > 0$ if μ is in the continuous spectrum of $\mathcal{A}$. If for any two states $|\Phi\rangle$, $|\Psi\rangle$ within this set the relation $\mathcal{C}(\mu) = \mathcal{C}_\Phi(\mu) = \mathcal{C}_\Psi(\mu)$ holds, then μ is called a non-degenerate eigenvalue of $\mathcal{A}$ in the (discrete or continuous) spectrum.

Indeed, this definition of non-degeneracy covers the original notion developed for operators $\mathcal{H}_0$ in the finite-dimensional space $\mathbb{H}_N$ (Section A.3.1). There, we have seen

that the projector $\mathcal{P}(E_k)$ on the non-degenerate subspace of eigenstates of $\mathcal{H}_0$ with eigenvalue $E = E_k$ may always be expressed through the normalized eigenstate $|\Phi_k\rangle$ (A.53): $\mathcal{P}(E_k) = |\Phi_k\rangle\langle\Phi_k|$. Then, following Definition XXV, part (ii), we find for the orthonormal family assigned to some state $|\Psi\rangle \in \mathbb{H}_N$:

$$\mathcal{C}_\Psi(E_k) \;=\; \frac{|\Phi_k\rangle\langle\Phi_k|\Psi\rangle\langle\Psi|\Phi_k\rangle\langle\Phi_k|}{\langle\Psi|\Phi_k\rangle\langle\Phi_k|\Psi\rangle} \;=\; |\Phi_k\rangle\langle\Phi_k| \;=\; \mathcal{P}(E_k) \tag{A.107}$$

Therefore, $\mathcal{C}_\Psi(E_k) = \mathcal{P}(E_k)$, independent of the choice of $|\Psi\rangle$ (provided $|\Psi\rangle$ has support at E_k, i. e., $|\langle\Psi|\Phi_k\rangle|^2 > 0$). In the same way, it is easy to verify that the orthonormal family $\mathcal{C}_\Psi(E_j)$ actually depends on the parent state $|\Psi\rangle$ if E_j is a degenerate eigenvalue of $\mathcal{A}$ with $\mathcal{P}(E_j) = \sum_\nu |\Phi_{j,\nu}\rangle\langle\Phi_{j,\nu}|$. An analogous property holds for the infinite-dimensional case:

■ THEOREM XXVIII
If μ is a non-degenerate eigenvalue of $\mathcal{A}$, then $\mathcal{C}(\mu) = \mathcal{P}(\mu)$ (point spectrum), or $\mathcal{C}(\mu) = \partial\Pi(\mu)/\partial\mu$ (continuous spectrum), respectively.

Proof. For the continuous spectrum, we have to show that for any two states $|\Phi\rangle, |\Psi\rangle \in \mathbb{H}$, the relation $\langle\Phi\,|\mathcal{C}(\mu)|\,\Psi\rangle = \langle\Phi\,|\partial\Pi(\mu)/\partial\mu|\,\Psi\rangle$ holds. We may distinguish between two cases: First, the state $|\Psi\rangle$ may have no support at μ in the spectrum of $\mathcal{A}$; then, by Definition XXIII, $\langle\Phi\,|\partial\Pi(\mu)/\partial\mu|\,\Psi\rangle = 0$. But this means that the matrix element of $\mathcal{C}(\mu)$ also vanishes, see Definition XXV.

In the other case, $\mathcal{C}_\Psi(\mu)$ exists. But then, $\mathcal{C}(\mu) = \mathcal{C}_\Psi(\mu)$. Using Theorem XXVI, part (iv), we immediately infer that $\langle\Phi\,|\mathcal{C}(\mu)|\,\Psi\rangle = \langle\Phi\,|\mathcal{C}_\Psi(\mu)|\,\Psi\rangle = \langle\Phi\,|\partial\Pi(\mu)/\partial\mu|\,\Psi\rangle$. Thus, we have proven our initial assertion. The same technique works also for the point spectrum of $\mathcal{A}$. ■

Consequently, for an entirely non-degenerate spectrum of the operator $\mathcal{A}$, we may expand $\mathcal{A}$ and regular operator functionals $\phi[\mathcal{A}]$ derived from it, including the identity operator $\mathcal{E} = \mathcal{A}^0$, into the unique orthonormal family $\mathcal{C}(\mu)$ generated by $\mathcal{A}$:

■ THEOREM XXIX
Every self-adjoint operator $\mathcal{A}$ with non-degenerate, continuously differentiable spectrum allows for an expansion into its orthonormal family of operators $\mathcal{C}(\mu)$. The same is true for the identity operator $\mathcal{E}$ and operators $\phi[\mathcal{A}]$ derived from $\mathcal{A}$ by a regular function $\phi(z)$:

$$\mathcal{E} \;=\; \left\{\sum_{\text{p.s.}} + \int_{\text{c.s.}} d\mu\right\} \mathcal{C}(\mu) \tag{A.108}$$

$$\mathcal{A} \;=\; \left\{\sum_{\text{p.s.}} + \int_{\text{c.s.}} d\mu\right\} \mu\,\mathcal{C}(\mu) \tag{A.109}$$

$$\phi[\mathcal{A}] \;=\; \left\{\sum_{\text{p.s.}} + \int_{\text{c.s.}} d\mu\right\} \phi(\mu)\,\mathcal{C}(\mu) \tag{A.110}$$

Proof. The relation (A.108) follows from the corresponding decomposition for the density of states operator $\partial\Pi(\mu)/\partial\mu$ (A.82) by Theorem XXVIII. By application of $\mathcal{A}$ onto (A.108), we may employ the eigenoperator property of $\mathcal{C}(\mu)$ [Theorem XXVI, part (x)] to obtain both (A.109) and (A.110). ■

Non-degeneracy of the spectrum of $\mathcal{A}$ implies that there exists also a non-degenerate set of eigenfunctions $\psi_\mu(\mathbf{r})$ which is defined via $\psi_\mu(\mathbf{r})\psi_\mu(\mathbf{r}')^* = \langle \mathbf{r} \,|\mathcal{C}(\mu)|\, \mathbf{r}' \rangle$ (A.102) and, apart from unitary scaling operations, unique. Using (A.108), it is now easy to show that the functions $\psi_\mu(\mathbf{r})$ form a complete base set. Indeed, upon expanding $\chi(\mathbf{r}) = \langle \mathbf{r}|\chi\rangle = \langle \mathbf{r} \,|\mathcal{E}|\, \chi\rangle$ in the spatial representation, we are immediately led to:

■ THEOREM XXX (FOURIER DECOMPOSITION)
Let $\psi_\mu(\mathbf{r})$ denote the set of eigenfunctions of the operator $\mathcal{A}$ with non-degenerate spectrum. Then, the function $\chi(\mathbf{r}) = \langle \mathbf{r}|\chi\rangle$ may be expanded into these eigenfunctions:

$$\chi(\mathbf{r}) \;=\; \left\{ \sum_{\text{p.s.}} + \int_{\text{c.s.}} d\mu \right\} \beta(\mu)\, \psi_\mu(\mathbf{r}) \qquad \text{with} \qquad \beta(\mu) \;=\; \int d^3r\, \psi_\mu(\mathbf{r})^* \chi(\mathbf{r}) \quad \text{(A.111)}$$

(Note: Strictly spoken, (A.111) implies only that the "initial" and "final" functions $\chi(\mathbf{r})$ are equal except on a set of points $\{\mathbf{r}\}$ of measure zero. In this case the difference of both functions $\Delta(\mathbf{r})$ has support only on a set of measure zero. Since our theory is founded upon the $\mathbb{L}^2$ norm, $\|\Delta\|^2 = \int d^3r\, |\Delta(\mathbf{r})|^2 = 0$ implies that the state Δ is the zero state, despite $\Delta(\mathbf{r}) = 0$ need not hold for every $\mathbf{r}$. In a sense, the $\mathbb{L}^2$ norm acts on equivalence classes of functions that are equal almost everywhere rather than functions itself. The expansion (A.111) is sometimes said to converge in the mean, i. e., almost everywhere to $\chi(\mathbf{r})$. This peculiar behavior may be studied in the classical Fourier analysis of discontinuous functions. See, e. g., the monograph by Sansone [232].)

As an important example which is connected to the main subject of this treatise, we refer to the quantum mechanics of uniform acceleration in a single dimension. Here, the Hamiltonian reads in spatial representation $H(x,p) = \hbar^2 p^2/2M - Fx$. As we shall establish later on (Section A.4, in particular Theorem LIV), for every energy E in the entire range $-\infty < E < \infty$ there exists exactly one linearly independent eigenfunction $\psi_E(x)$ (whose explicit form (D.26) is separately treated in Appendix D, Section D.2.1). Hence, the corresponding operator $\mathcal{H}$ possesses a non-degenerate continuous differentiable spectrum of eigenfunctions, and no normalizable eigenstates are present, as the point spectrum of $\mathcal{H}$ is empty. Thus, according to Theorem XXX every square-integrable function $\phi(x)$ allows for an expansion into the continuous set of eigenfunctions $\psi_E(x)$ of the uniform field problem which converges almost everywhere. (Another proof of this statement is given in Appendix D.2.3.)

Representation of arbitrary operators and uniqueness. Finally, we want to demonstrate some important properties of the orthonormal family of operators $\mathcal{C}(\lambda)$ generated by a non-degenerate self-adjoint operator $\mathcal{A}$. They are all based on the following "projector" representation of $\mathcal{C}(\lambda)$:

■ COROLLARY XXXI
Let $|\chi\rangle \in \mathbb{H}$ be some state in the Hilbert space which has support in the spectrum at λ, i. e., $\langle\chi\,|\mathcal{C}(\lambda)|\,\chi\rangle > 0$. Then, we have:

$$\mathcal{C}(\lambda) \;=\; \frac{\mathcal{C}(\lambda)\,|\chi\rangle\,\langle\chi|\,\mathcal{C}(\lambda)}{\langle\chi\,|\mathcal{C}(\lambda)|\,\chi\rangle} \tag{A.112}$$

Proof. If λ is in the point spectrum of $\mathcal{A}$, then according to Theorem XXVIII we may replace $\mathcal{C}(\lambda)$ by $\mathcal{P}(\lambda)$ in the right-hand side of (A.112). But this procedure yields exactly the definition of $\mathcal{C}_\chi(\lambda)$ [see Definition XXV, part (ii)]. Since $\mathcal{C}(\lambda) = \mathcal{C}_\chi(\lambda)$ is unique, (A.112) is verified.

For the case of λ in the continuous spectrum of $\mathcal{A}$, we may introduce the projector family $\mathcal{C}_\eta(\lambda)$ on a finite interval of size η via:

$$\mathcal{C}_\eta(\lambda) \;=\; \frac{1}{\eta}\,\frac{\mathcal{I}(\lambda-\eta,\lambda)\,|\chi\rangle\,\langle\chi|\,\mathcal{I}(\lambda-\eta,\lambda)}{\langle\chi\,|\mathcal{I}(\lambda-\eta,\lambda)|\,\chi\rangle} \tag{A.113}$$

This (bounded) operator family clearly fulfils relation (A.112) if we replace all occurrences of $\mathcal{C}(\lambda)$ by $\mathcal{C}_\eta(\lambda)$. Now consider the limit $\eta \to 0^+$; then, $\mathcal{C}_\eta(\lambda) \to \mathcal{C}(\lambda)$ (Definition XXV) due to non-degeneracy, and (A.112) emerges. This concludes our proof of Corollary XXXI. ■

Corollary XXXI provides a convenient means to represent arbitrary operators $\mathcal{H}$ in terms of the orthonormal operator family $\mathcal{C}(\lambda)$ related to the operator $\mathcal{A}$ and thus gain a "spectral representation" of $\mathcal{H}$. To this end, we employ "matrix elements" of $\mathcal{H}$ involving the generally non-normalizable "states" $\mathcal{C}(\lambda)\,|\chi\rangle$. Using the resolution of the identity into the family $\mathcal{C}(\lambda)$ (Theorem XXIX), we find for the expectation value of $\mathcal{H}$ involving two arbitrary states $|\Phi\rangle, |\Psi\rangle \in \mathbb{H}$:

$$\begin{aligned}
\langle\Phi\,|\mathcal{H}|\,\Psi\rangle \;&=\; \langle\Phi\,|\mathcal{E}\mathcal{H}\mathcal{E}|\,\Psi\rangle \\
&=\; \left\{\sum_{\text{p.s.}} + \int_{\text{c.s.}} d\lambda\right\}\left\{\sum_{\text{p.s.}} + \int_{\text{c.s.}} d\mu\right\}\langle\Phi\,|\mathcal{C}(\lambda)\mathcal{H}\mathcal{C}(\mu)|\,\Psi\rangle \\
&=\; \left\{\sum_{\text{p.s.}} + \int_{\text{c.s.}} d\lambda\right\}\left\{\sum_{\text{p.s.}} + \int_{\text{c.s.}} d\mu\right\} \\
&\qquad\qquad \times\,\frac{\langle\Phi\,|\mathcal{C}(\lambda)|\,\chi\rangle\,\langle\chi\,|\mathcal{C}(\lambda)\mathcal{H}\mathcal{C}(\mu)|\,\chi\rangle\,\langle\chi\,|\mathcal{C}(\mu)|\,\Psi\rangle}{\langle\chi\,|\mathcal{C}(\lambda)|\,\chi\rangle\,\langle\chi\,|\mathcal{C}(\mu)|\,\chi\rangle}
\end{aligned} \tag{A.114}$$

As usual, by the "operator" $\mathcal{C}(\lambda)\mathcal{H}\mathcal{C}(\mu)$ we denote the kernel of the sesquilinear form $\langle\Phi\,|\mathcal{C}(\lambda)\mathcal{H}\mathcal{C}(\mu)|\,\Psi\rangle$ that emerges from the operator matrix element $\langle\Phi\,|\mathcal{C}_\eta(\lambda)\mathcal{H}\mathcal{C}_\eta(\mu)|\,\Psi\rangle$ (A.113) in the limit $\eta \to 0^+$. See also (A.80).

Note that the operator $\mathcal{H}$ now solely acts onto the state $|\chi\rangle$. It has been effectively "isolated" from the bra and ket states $\langle\Phi|$ and $|\Psi\rangle$. Therefore, we obtain the following representation of $\mathcal{H}$ within the spectrum of $\mathcal{A}$:

■ THEOREM XXXII
Let $|\Phi\rangle$, $|\Psi\rangle \in \mathbb{H}$ be states in the Hilbert space, and $\mathcal{H}$ some operator. If $\mathcal{A}$ is a non-degenerate self-adjoint operator with orthonormal family $\mathcal{C}(\lambda)$ and $|\chi\rangle \in \mathbb{H}$ a test state in $\mathbb{H}$ chosen in such a way that $\langle\chi\,|\mathcal{C}(\lambda)|\,\chi\rangle > 0$ throughout the spectrum of $\mathcal{A}$, then the expectation value $\langle\Phi\,|\mathcal{H}|\,\Psi\rangle$ admits an expansion into the sesquilinear form:

$$\langle\Phi\,|\mathcal{H}|\,\Psi\rangle \;=\; \left\{\sum_{\text{p.s.}} + \int_{\text{c.s.}} d\lambda\right\}\left\{\sum_{\text{p.s.}} + \int_{\text{c.s.}} d\mu\right\}\langle\Phi\,|\mathcal{C}(\lambda)|\,\chi\rangle\, H_\chi(\lambda,\mu)\,\langle\chi\,|\mathcal{C}(\mu)|\,\Psi\rangle \tag{A.115}$$

whereby the "matrix element" $H_\chi(\lambda,\mu)$ of $\mathcal{H}$ is given by:

$$H_\chi(\lambda,\mu) \;=\; \frac{\langle\chi\,|\mathcal{C}(\lambda)\mathcal{H}\mathcal{C}(\mu)|\,\chi\rangle}{\langle\chi\,|\mathcal{C}(\lambda)|\,\chi\rangle\,\langle\chi\,|\mathcal{C}(\mu)|\,\chi\rangle} \tag{A.116}$$

We note that due to the orthonormality property of the operator family $\mathcal{C}(\lambda)$ [Theorem XXVI, part (ix)], the matrix element $H_\chi(\lambda,\mu)$ may involve Dirac delta functions. For example, the identity operator $\mathcal{E}$ obviously leads to a representation $E_\chi(\lambda,\mu) = \delta(\lambda-\mu)/\langle\chi\,|\mathcal{C}(\lambda)|\,\chi\rangle$. The appearance of these pointlike singularities is connected to the fact that $\mathcal{C}(\lambda)$ is not a proper operator, and the objects $\mathcal{C}(\lambda)\,|\chi\rangle$ cannot be regarded as states in Hilbert space in a strict sense as they are not normalizable. Nevertheless, such "states" may be advantageously applied; in fact, we have used them routinely in form of the position states $|\mathbf{r}\rangle$ of Section A.2.1 which obey an analogous orthonormality relation (A.7).

As a most important application, we now prove the uniqueness theorem. We have already noted [Theorem XXVI, part (x)] that the orthonormal family $\mathcal{C}(\lambda)$ presents a set of eigenoperators to its non-degenerate parent operator $\mathcal{A}$: $\mathcal{A}\mathcal{C}(\lambda) = \mathcal{C}(\lambda)\mathcal{A} = \lambda\mathcal{C}(\lambda)$. The uniqueness theorem now asserts that if the spectrum of $\mathcal{A}$ is non-degenerate, the orthonormal family operator $\mathcal{C}(\lambda)$ is essentially the only eigenoperator available:

■ THEOREM XXXIII
Let $\mathcal{C}(\lambda)$ denote the orthonormal family generated by a self-adjoint operator $\mathcal{A}$ with non-degenerate spectrum. If the operator $\mathcal{B}$ commutes with $\mathcal{A}$ and is an eigenoperator to $\mathcal{A}$: $\mathcal{A}\mathcal{B} = \mathcal{B}\mathcal{A} = \lambda\mathcal{B}$, then $\mathcal{B}$ is a multiple of $\mathcal{C}(\lambda)$: $\mathcal{B} = \mu\mathcal{C}(\lambda)$.

Proof. We first show that $\mathcal{B}$ annihilates any member of the orthonormal family $\mathcal{C}(\nu)$ with the possible exception of $\mathcal{C}(\lambda)$. Due to the eigenoperator property of $\mathcal{B}$ and $\mathcal{C}(\nu)$, we have $\lambda\mathcal{B}\mathcal{C}(\nu) = (\lambda\mathcal{B})\mathcal{C}(\nu) = \mathcal{A}\mathcal{B}\mathcal{C}(\nu)$, but also $\nu\mathcal{B}\mathcal{C}(\nu) = \mathcal{B}[\nu\mathcal{C}(\nu)] = \mathcal{B}\mathcal{A}\mathcal{C}(\nu)$. Subtracting both

expressions, we obtain: $(\lambda - \nu)\mathcal{B}\mathcal{C}(\nu) = (\mathcal{A}\mathcal{B} - \mathcal{B}\mathcal{A})\mathcal{C}(\nu) = 0$, as we assumed $\mathcal{A}\mathcal{B} = \mathcal{B}\mathcal{A}$. Consequently, $\mathcal{B}\mathcal{C}(\nu) = 0$ for $\lambda \neq \nu$.

This means that the representation of $\mathcal{B}$ in terms of the orthonormal family $\mathcal{C}(\nu)$ must be very simple. Let us first note that $\mathcal{B}$ will vanish if λ belongs to the resolvent set of $\mathcal{A}$, because then $\mathcal{C}(\nu)\mathcal{B}\mathcal{C}(\mu) = 0$ for all values of ν and μ, which according to Theorem XXXII means that $\langle \Phi \,|\mathcal{B}|\, \Psi \rangle = 0$ for arbitrary states $|\Phi\rangle, |\Psi\rangle \in \mathbb{H}$. This implies $\mathcal{B} = 0$.

If λ is an element of the point spectrum of $\mathcal{A}$, then we may use the spectral representation of $\mathcal{B}$ (Theorem XXXII) together with the orthogonality property noted above to show that:

$$\langle \Phi \,|\mathcal{B}|\, \Psi \rangle = \frac{\langle \Phi \,|\mathcal{C}(\lambda)|\, \chi \rangle \langle \chi \,|\mathcal{C}(\lambda)\mathcal{B}\mathcal{C}(\lambda)|\, \chi \rangle \langle \chi \,|\mathcal{C}(\lambda)|\, \Psi \rangle}{\langle \chi \,|\mathcal{C}(\lambda)|\, \chi \rangle \langle \chi \,|\mathcal{C}(\lambda)|\, \chi \rangle} \tag{A.117}$$

whereas for $\mathcal{C}(\lambda)$ we obtain from Corollary XXXI:

$$\langle \Phi \,|\mathcal{C}(\lambda)|\, \Psi \rangle = \frac{\langle \Phi \,|\mathcal{C}(\lambda)|\, \chi \rangle \langle \chi \,|\mathcal{C}(\lambda)|\, \Psi \rangle}{\langle \chi \,|\mathcal{C}(\lambda)|\, \chi \rangle} \tag{A.118}$$

By comparison of (A.117) and (A.118) we conclude that:

$$\mathcal{B} = \frac{\langle \chi \,|\mathcal{C}(\lambda)\mathcal{B}\mathcal{C}(\lambda)|\, \chi \rangle}{\langle \chi \,|\mathcal{C}(\lambda)|\, \chi \rangle}\, \mathcal{C}(\lambda) \tag{A.119}$$

as both operators possess equal matrix elements. Therefore, $\mathcal{B}$ is a multiple of $\mathcal{C}(\lambda)$.

To complete the proof, we now assume that λ belongs to the continuous spectrum of $\mathcal{A}$. Then, we may restate $\langle \Phi \,|\mathcal{B}|\, \Psi \rangle$, very much along the previous line of argument,

$$\begin{aligned}
\langle \Phi \,|\mathcal{B}|\, \Psi \rangle &= \lim_{\eta \to 0^+} \int_{\lambda-\eta}^{\lambda+\eta} d\mu \int_{\lambda-\eta}^{\lambda+\eta} d\nu\, \frac{\langle \Phi \,|\mathcal{C}(\mu)|\, \chi \rangle \langle \chi \,|\mathcal{C}(\mu)\mathcal{B}\mathcal{C}(\nu)|\, \chi \rangle \langle \chi \,|\mathcal{C}(\nu)|\, \Psi \rangle}{\langle \chi \,|\mathcal{C}(\mu)|\, \chi \rangle \langle \chi \,|\mathcal{C}(\nu)|\, \chi \rangle} \\
&= \frac{\langle \Phi \,|\mathcal{C}(\lambda)|\, \chi \rangle \langle \chi \,|\mathcal{C}(\lambda)|\, \Psi \rangle}{\langle \chi \,|\mathcal{C}(\lambda)|\, \chi \rangle} \lim_{\eta \to 0^+} \int_{\lambda-\eta}^{\lambda+\eta} d\mu \int_{\lambda-\eta}^{\lambda+\eta} d\nu\, \frac{\langle \chi \,|\mathcal{C}(\mu)\mathcal{B}\mathcal{C}(\nu)|\, \chi \rangle}{\langle \chi \,|\mathcal{C}(\lambda)|\, \chi \rangle} \\
&= \langle \Phi \,|\mathcal{C}(\lambda)|\, \Psi \rangle \lim_{\eta \to 0^+} \int_{\lambda-\eta}^{\lambda+\eta} d\mu \int_{\lambda-\eta}^{\lambda+\eta} d\nu\, \frac{\langle \chi \,|\mathcal{C}(\mu)\mathcal{B}\mathcal{C}(\nu)|\, \chi \rangle}{\langle \chi \,|\mathcal{C}(\lambda)|\, \chi \rangle}
\end{aligned} \tag{A.120}$$

Again, we find that the matrix elements of $\mathcal{B}$ and $\mathcal{C}(\lambda)$ are in constant proportion, thus $\mathcal{B} = \alpha\, \mathcal{C}(\lambda)$. (Note that the replacement of the operators $\mathcal{C}(\mu)$, $\mathcal{C}(\nu)$ by $\mathcal{C}(\lambda)$ in the second line of (A.120) is permitted because matrix elements of the type $\langle \Phi \,|\mathcal{C}(\mu)|\, \chi \rangle$ are continuous functions by proposition—$\mathcal{C}(\mu) = \partial\Pi(\mu)/\partial\mu$ (Theorem XXVIII) is continuous, as the spectral family $\Pi(\mu)$ is assumed continuously differentiable. We have kept the integrals in the last line of (A.120) since the matrix element occurring in the integrand generally will involve Dirac delta functions, as discussed above.) ■

Let us remark here that Theorem XXXIII implies that the (differentiable) spectrum of a self-adjoint operator $\mathcal{A}$ is non-degenerate if, and only if, any two eigenfunctions $\psi_\lambda(\mathbf{r})$, $\phi_\lambda(\mathbf{r})$ of $A(\mathbf{r}, \mathbf{r}') = \langle \mathbf{r} \,|\mathcal{A}|\, \mathbf{r}' \rangle$ (A.105) with common eigenvalue λ are linearly dependent: $\psi_\lambda(\mathbf{r}) = \mu\phi_\lambda(\mathbf{r})$. Hence, we may infer information about the operator $\mathcal{A}$ from its behavior in the spatial representation $A(\mathbf{r}, \mathbf{r}')$.

Finally, we now apply the uniqueness theorem to prove the fairly surprising fact that every closed operator $\mathcal{H}$ that commutes with a self-adjoint operator $\mathcal{A}$ with non-degenerate differentiable spectrum $\Pi(\lambda)$ is, in a sense, just a functional of $\mathcal{A}$. (In principle, one may even drop the assertion that $\mathcal{A}$ shows a non-degenerate spectrum. See Riesz and Sz.–Nagy [233].)

■ THEOREM XXXIV

Let $\mathcal{A}$ be a self-adjoint operator with non-degenerate spectrum, and $\mathcal{C}(\lambda)$ its assigned orthonormal family of operators. If the closed operator $\mathcal{H}$ commutes with $\mathcal{A}$, $\mathcal{H}\mathcal{A} = \mathcal{A}\mathcal{H}$, then:

(i). $\mathcal{C}(\lambda)$ is eigenoperator of $\mathcal{H}$: $\mathcal{H}\mathcal{C}(\lambda) = \mathcal{C}(\lambda)\mathcal{H} = E(\lambda)\mathcal{C}(\lambda)$

(ii). $\mathcal{H}$ is a functional of $\mathcal{A}$: $\mathcal{H} = E[\mathcal{A}] = \left\{\sum_{\text{p.s.}} + \int_{\text{c.s.}} d\lambda\right\} E(\lambda)\,\mathcal{C}(\lambda)$

Proof. We first show that $\mathcal{H}\mathcal{C}(\lambda)$ and $\mathcal{C}(\lambda)\mathcal{H}$ are eigenoperators of $\mathcal{A}$:

$$\begin{aligned} \mathcal{A}[\mathcal{H}\mathcal{C}(\lambda)] &= \mathcal{H}[\mathcal{A}\mathcal{C}(\lambda)] = \lambda\,\mathcal{H}\mathcal{C}(\lambda) \\ [\mathcal{C}(\lambda)\mathcal{H}]\mathcal{A} &= [\mathcal{C}(\lambda)\mathcal{A}]\mathcal{H} = \lambda\,\mathcal{C}(\lambda)\mathcal{H} \end{aligned} \tag{A.121}$$

Furthermore, as $\mathcal{A}$ commutes with $\mathcal{H}$ and $\mathcal{C}(\lambda)$ [Theorem XXVI, part (xi)], we additionally have $\mathcal{A}[\mathcal{H}\mathcal{C}(\lambda)] = [\mathcal{H}\mathcal{C}(\lambda)]\mathcal{A}$ and $\mathcal{A}[\mathcal{C}(\lambda)\mathcal{H}] = [\mathcal{C}(\lambda)\mathcal{H}]\mathcal{A}$, so the assumptions of the uniqueness theorem (Theorem XXXIII) are met, and the eigenoperator property (A.121) implies that $\mathcal{H}\mathcal{C}(\lambda)$, $\mathcal{C}(\lambda)\mathcal{H}$ are just multiples of the orthonormal family operator $\mathcal{C}(\lambda)$: $\mathcal{H}\mathcal{C}(\lambda) = E(\lambda)\mathcal{C}(\lambda)$, $\mathcal{C}(\lambda)\mathcal{H} = E'(\lambda)\mathcal{C}(\lambda)$. To prove that the functions $E(\lambda)$ and $E'(\lambda)$ actually coincide, we note that $\mathcal{C}(\mu)\mathcal{H}\mathcal{C}(\lambda) = E(\lambda)\mathcal{C}(\mu)\mathcal{C}(\lambda) = E'(\mu)\mathcal{C}(\mu)\mathcal{C}(\lambda)$, and therefore $[E(\lambda) - E'(\mu)]\mathcal{C}(\mu)\mathcal{C}(\lambda) = 0$. Considering the orthonormality relation of the operators $\mathcal{C}(\lambda)$ [Theorem XXVI, part (ix)], this implies that $E(\lambda) = E'(\lambda)$. Thus, part (i) of the theorem is proven.

For the second statement, we note that according to Theorem XXIX, we successively obtain:

$$\mathcal{H} = \mathcal{H}\mathcal{E} = \left\{\sum_{\text{p.s.}} + \int_{\text{c.s.}} d\lambda\right\} \mathcal{H}\mathcal{C}(\lambda) = \left\{\sum_{\text{p.s.}} + \int_{\text{c.s.}} d\lambda\right\} E(\lambda)\,\mathcal{C}(\lambda) = E[\mathcal{A}] \tag{A.122}$$

which completes the proof. ■

As an interesting consequence of the functional property of commuting operators [Theorem XXXIV, part (ii)], we may expand any operator $\mathcal{H}$ that commutes with $\mathcal{A}$ into the set of eigenfunctions $\psi_\lambda(\mathbf{r})$ generated by the orthonormal family $\mathcal{C}(\lambda)$, even if $\mathcal{H}$ itself does not show a non-degenerate spectrum $\Pi(E)$. (This case will obviously occur if $E(\lambda) = E(\mu)$ for some $\lambda \neq \mu$.) For example, the spectral density $\partial\Pi(E)/\partial E$ due to $\mathcal{H}$ which is given by (A.81) (if it exists at all):

$$\delta(E - \mathcal{H}) = \int \delta(E - \mu)\,\mathrm{d}\Pi(\mu) \tag{A.123}$$

may be expressed in terms of the orthonormal family $\mathcal{C}(\lambda)$ assigned to $\mathcal{A}$:

$$\begin{aligned}\frac{\partial\Pi(E)}{\partial E} &= \delta(E-\mathcal{H}) = \delta(E-E[\mathcal{A}]) \\ &= \left\{\sum_{\text{p.s.}} + \int_{\text{c.s.}} d\lambda\right\}\delta(E-E(\lambda))\,\mathcal{C}(\lambda) = \sum_{E(\lambda)=E}\left|\frac{\partial\lambda(E)}{\partial E}\right|\mathcal{C}[\lambda(E)] \qquad \text{(A.124)}\end{aligned}$$

A.3.5 Total Decompositions of Hilbert Space

We have seen in the course of the preceding section how the familiar picture of a complete set of eigenfunctions $\psi_E(\mathbf{r})$ generated by a self-adjoint operator $\mathcal{H}$ emerges from the abstract notions of functional analysis. However, our developments so far rely upon the important restriction that the spectrum of $\mathcal{H}$ be non-degenerate, a condition that is rarely fulfilled by the operators occurring in quantum physics, in particular if they operate in multidimensional physical space like the Hamiltonian of uniformly accelerated motion in three dimensions that this work is centered upon. Therefore, the eigenfunction formalism developed in Section A.3.4 does not apply in its present form. We may, however, extend this formalism to several important problems by means of a technique that relates to the separability of the Schrödinger equation. We will first give a general description in terms of the spectral family $\Pi(\lambda)$.

Commuting operators and their spectrum space. Let us first state the basic idea behind the following approach. Let $\mathcal{A}_1$ be some self-adjoint operator whose spectrum is degenerate, i. e., for some real values λ in the discrete or continuous spectrum there exists more than one linearly independent eigenfunction. This ambiguity may be resolved by application of another self-adjoint operator $\mathcal{A}_2$ which decomposes the degenerate eigenspaces of $\mathcal{A}_1$ into a set of non-degenerate eigenstates of $\mathcal{A}_2$, thus refining the "one-dimensional" spectrum $\{\lambda_1\}$ of $\mathcal{A}_1$ into a non-degenerate "product spectrum" $\{\lambda_1,\lambda_2\}$ of the pair of operators $\mathcal{A}_1$, $\mathcal{A}_2$. This implies that to each pair of numbers $\{\lambda_1,\lambda_2\}$ apart from scaling there is assigned at most one simultaneous eigenfunction $\psi_{\lambda_1,\lambda_2}(\mathbf{r})$ of $\mathcal{A}_1$ and $\mathcal{A}_2$.

Clearly this procedure requires that both operators $\mathcal{A}_1$, $\mathcal{A}_2$ share their eigenfunctions, or stated in a more general form, that the subspace $\mathbb{M}_1(\lambda_1)$ that the spectral family $\Pi_1(\lambda_1)$ generated by $\mathcal{A}_1$ projects upon (Definition XII) remains invariant under the action of $\mathcal{A}_2$, and vice versa. According to the following theorem, the assumption that both operators commute is a sufficient condition for this invariance:

■ THEOREM XXXV
Let $\mathcal{A}_1$, $\mathcal{A}_2$ be bounded self-adjoint operators that commute: $\mathcal{A}_1\mathcal{A}_2 = \mathcal{A}_2\mathcal{A}_1$. Then, also the spectral families $\Pi_1(\lambda_1)$ and $\Pi_2(\lambda_2)$ commute with $\mathcal{A}_1$, $\mathcal{A}_2$ and with each other.

Proof. With $\mathcal{A}_1$, $\mathcal{A}_2$, also $\mathcal{A}_1 - \lambda_1\mathcal{E}$, $\mathcal{A}_2 - \lambda_2\mathcal{E}$ commute. From the polar decomposition theorem [Theorem VIII, part (vi)], we know that this means that also $\mathcal{U}_1(\lambda_1)\mathcal{A}_2 = \mathcal{A}_2\mathcal{U}_1(\lambda_1)$ holds. Since the spectral family $\Pi(\lambda_1)$ is a quadratic function of $\mathcal{U}_1(\lambda_1)$ (see Definition XII), we find: $\Pi_1(\lambda_1)\mathcal{A}_2 = \mathcal{A}_2\Pi_1(\lambda_1)$, and in the same way, $\Pi_2(\lambda_2)\mathcal{A}_1 = \mathcal{A}_1\Pi_2(\lambda_2)$. As $\Pi_2(\lambda_2)$ commutes with $\mathcal{A}_1 - \lambda_1\mathcal{E}$, so it does with $\mathcal{U}_1(\lambda_1)$, which leads to $\Pi_1(\lambda_1)\Pi_2(\lambda_2) = \Pi_2(\lambda_2)\Pi_1(\lambda_1)$. ■

In the following, we will assume that Theorem XXXV holds even for pairs of operators $\mathcal{A}_1$, $\mathcal{A}_2$ that are not bounded. (After all, Theorem XXXV holds at least for any restriction of $\mathcal{A}_1$, $\mathcal{A}_2$ onto a finite spectrum.)

Obviously, Theorem XXXV implies the existence of combined interval projectors $\mathcal{I}(\lambda_1 - \eta_1, \lambda_1; \lambda_2 - \eta_2, \lambda_2)$ onto the product spectrum of both operators $\mathcal{A}_1$, $\mathcal{A}_2$:

$$\begin{aligned}\mathcal{I}(\lambda_1 - \eta_1, \lambda_1; \lambda_2 - \eta_2, \lambda_2) &= \mathcal{I}_1(\lambda_1 - \eta_1, \lambda_1)\mathcal{I}_2(\lambda_2 - \eta_2, \lambda_2) \\ &= \mathcal{I}_2(\lambda_2 - \eta_2, \lambda_2)\mathcal{I}_1(\lambda_1 - \eta_1, \lambda_1)\end{aligned} \tag{A.125}$$

which commute with $\mathcal{A}_1$, $\mathcal{A}_2$, $\Pi_1(\lambda_1)$, and $\Pi_2(\lambda_2)$. From Hilbert space $\mathbb{H}$, the interval projector $\mathcal{I}(\lambda_1 - \eta_1, \lambda_1; \lambda_2 - \eta_2, \lambda_2)$ singles out the maximum subspace $\mathbb{M}(\lambda_1 - \eta_1, \lambda_1; \lambda_2 - \eta_2, \lambda_2)$ invariant under $\mathcal{A}_1$, $\mathcal{A}_2$ whose state vectors fulfil simultaneously [Theorem XIV, part (v)]:

$$\begin{aligned}(\lambda_1 - \eta_1)\langle\Psi|\Psi\rangle &< \langle\Psi|\mathcal{A}_1|\Psi\rangle \leq \lambda_1\langle\Psi|\Psi\rangle \\ (\lambda_2 - \eta_2)\langle\Psi|\Psi\rangle &< \langle\Psi|\mathcal{A}_2|\Psi\rangle \leq \lambda_2\langle\Psi|\Psi\rangle\end{aligned} \tag{A.126}$$

These interval projectors project a rectangle from the two-dimensional spectrum space $\{\lambda_1, \lambda_2\}$. They obviously present a refinement to their one-dimensional counterparts $\mathcal{I}_1(\lambda_1 - \eta_1)$ and $\mathcal{I}_2(\lambda_2 - \eta_2)$.

For the decomposition of the identity $\mathcal{E}$, we obtain with partitionings of the λ_1– and λ_2–axes $\{\lambda_j^{(1)}\}$, $\{\lambda_k^{(2)}\}$ using (A.64):

$$\mathcal{E} = \mathcal{E}\mathcal{E} = \sum_j \mathcal{I}_1(\lambda_j^{(1)}, \lambda_{j+1}^{(1)}) \sum_k \mathcal{I}_2(\lambda_k^{(2)}, \lambda_{k+1}^{(2)}) = \sum_{jk} \mathcal{I}(\lambda_j^{(1)}, \lambda_{j+1}^{(1)}; \lambda_k^{(2)}, \lambda_{k+1}^{(2)}) \tag{A.127}$$

This is a partitioning of the (λ_1, λ_2) space into rectangles. As $\lambda_{k+1}^{(1,2)} - \lambda_k^{(1,2)} \to 0$, we obtain the following double Stieltjes integral for the resolution of the identity (Theorem XX):

$$\mathcal{I} = \lim_{\lambda_{j+1}^{(1)} - \lambda_j^{(1)} \to 0} \lim_{\lambda_{k+1}^{(2)} - \lambda_k^{(2)} \to 0} \sum_{jk} \mathcal{I}(\lambda_j^{(1)}, \lambda_{j+1}^{(1)}; \lambda_k^{(2)}, \lambda_{k+1}^{(2)}) = \int \mathrm{d}^2\Pi(\lambda_1, \lambda_2) \tag{A.128}$$

In the same way, one obtains the analogue to the spectral theorem (Theorem XXI):

$$\mathcal{A}_{1,2} = \int \lambda_{1,2}\, \mathrm{d}^2\Pi(\lambda_1, \lambda_2) \tag{A.129}$$

and for any regular function $\phi[\mathcal{A}_1, \mathcal{A}_2]$ of the operators $\mathcal{A}_1$, $\mathcal{A}_2$ (Theorem XXII):

$$\phi[\mathcal{A}_1, \mathcal{A}_2] \;=\; \int \phi(\lambda_1, \lambda_2)\, \mathrm{d}^2\Pi(\lambda_1, \lambda_2) \tag{A.130}$$

Obviously, this theory may be extended to sets of n pairwise commuting self-adjoint operators $\{\mathcal{A}_1, \mathcal{A}_2, \ldots, \mathcal{A}_n\}$. The spectrum $\{\lambda_1, \lambda_2, \ldots, \lambda_n\}$ of this set comprises at most the product of the spectra $\{\lambda_k\}$ of the operators $\mathcal{A}_k$. We note here that the product of interval projectors $\mathcal{I}_j(\lambda_j - \eta_j, \lambda_j)\mathcal{I}_k(\lambda_k - \eta_k, \lambda_k)$ may vanish even as the factors are non-zero, as the interval operators may be orthogonal; thus, the spectrum of the set generally is smaller than the product of the spectra of all constituting operators $\mathcal{A}_k$.

Orthonormal families. Let us now assume that the spectra of the operators $\mathcal{A}_k$ consist only of a point spectrum $\{\lambda_{k,j}\}$ and a differentiable continuous spectrum $\{\lambda_k\}$, i. e., the density of states operators $\partial\Pi_k(\lambda_k)/\partial\lambda_k$ shall exist (Definition XXIII). Then, the decomposition of the identity may be rewritten in the form (A.82):

$$\mathcal{E} \;=\; \int \mathrm{d}^n\Pi(\lambda_1, \ldots, \lambda_n) \;=\; \prod_{k=1}^{n} \left\{ \sum_{\text{p.s.}} \mathcal{P}(\lambda_{k,j}) \;+\; \int_{\text{c.s.}} \frac{\partial\Pi_k(\lambda_k)}{\partial\lambda_k}\, d\lambda_k \right\} \tag{A.131}$$

as the limiting case of the interval decomposition (A.128) above. In the same way, we obtain from (A.130):

$$\phi[\mathcal{A}_1, \ldots, \mathcal{A}_n] \;=\; \prod_{k=1}^{n} \left\{ \sum_{\text{p.s.}} \mathcal{P}(\lambda_{k,j}) \;+\; \int_{\text{c.s.}} \frac{\partial\Pi_k(\lambda_k)}{\partial\lambda_k}\, d_k \right\} \phi(\lambda_1, \ldots, \lambda_n) \tag{A.132}$$

Now suppose that $(\lambda_1, \lambda_2, \ldots, \lambda_n)$ is a member of the spectrum of $\{\mathcal{A}_1, \mathcal{A}_2, \ldots, \mathcal{A}_n\}$, i. e., there exist eigenstates $|\Phi\rangle$ of the interval operator $\mathcal{I}(\lambda_1 - \eta_1, \lambda_1; \ldots; \lambda_n - \eta_n, \lambda_n)$ for arbitrarily small positive values $\eta_1, \ldots, \eta_n \to 0^+$. Also let $|\Psi\rangle \in \mathbb{H}$ be a state with support in that interval, i. e., $\langle\Psi\,|\mathcal{I}(\lambda_1 - \eta_1, \lambda_1; \ldots; \lambda_n - \eta_n, \lambda_n)|\,\Psi\rangle > 0$ for all $\eta_1, \ldots, \eta_n > 0$. We further assume that $\lambda_1, \ldots, \lambda_m$ are eigenvalues of the operators $\mathcal{A}_1, \ldots, \mathcal{A}_m$ with projectors $\mathcal{P}_1(\lambda_1), \ldots, \mathcal{P}_m(\lambda_m)$, whereas $\lambda_{m+1}, \ldots, \lambda_n$ are members of the continuous spectra of $\mathcal{A}_{m+1}, \ldots, \mathcal{A}_n$ (this ordering can always be achieved by rearranging the set of operators $\{\mathcal{A}_1, \ldots, \mathcal{A}_n\}$). Then, the notion of the orthonormal family $\mathcal{C}_\Psi(\lambda_1, \ldots, \lambda_n)$ is most naturally adapted from the single-operator case (Definition XXV) by defining:

$$\mathcal{C}_\Psi(\lambda_1, \ldots, \lambda_n) \;=\; \lim_{\eta_{m+1}\to 0^+} \cdots \lim_{\eta_n \to 0^+} \frac{\mathcal{P}^{\lambda_1,\ldots,\lambda_n}_{\eta_{m+1},\ldots,\eta_n}\, |\Psi\rangle\,\langle\Psi|\, \mathcal{P}^{\lambda_1,\ldots,\lambda_n}_{\eta_{m+1},\ldots,\eta_n}}{\eta_{m+1} \cdot \ldots \cdot \eta_n \left\langle \Psi \left| \mathcal{P}^{\lambda_1,\ldots,\lambda_n}_{\eta_{m+1},\ldots,\eta_n} \right| \Psi \right\rangle} \tag{A.133}$$

In (A.133), for convenience we have introduced the abbreviation $\mathcal{P}^{\lambda_1,\ldots,\lambda_n}_{\eta_{m+1},\ldots,\eta_n} = \mathcal{P}_1(\lambda_1)\cdot \ldots \cdot \mathcal{P}_m(\lambda_m)\mathcal{I}_{m+1}(\lambda_{m+1}-\eta_{m+1},\lambda_{m+1})\cdot\ldots\cdot\mathcal{I}_n(\lambda_n-\eta_n,\lambda_n)$.

All properties of $\mathcal{C}_\Psi(\lambda_1,\ldots,\lambda_n)$ essentially translate from the single-operator case. In particular, we obtain [Theorem XXVI, part (iv)]:

$$\langle\Phi\,|\mathcal{C}_\Psi(\lambda_1,\ldots,\lambda_n)|\,\Psi\rangle \;=\; \left\langle \Phi \left| \mathcal{P}_1(\lambda_1)\cdot\ldots\cdot\mathcal{P}_m(\lambda_m)\,\frac{\partial\Pi_{m+1}(\lambda_{m+1})}{\partial\lambda_{m+1}}\;\cdot\ldots\cdot\,\frac{\partial\Pi_n(\lambda_n)}{\partial\lambda_n}\right|\Psi\right\rangle \tag{A.134}$$

Furthermore, the orthogonality relation $\mathcal{C}_\Phi(\mu_1,\ldots,\mu_n)\mathcal{C}_\Psi(\lambda_1,\ldots,\lambda_n) = 0$ for all $|\Phi\rangle$, $|\Psi\rangle \in \mathbb{H}$ if $(\mu_1,\ldots,\mu_n) \neq (\lambda_1,\ldots,\lambda_n)$ [Theorem XXVI, part (viii)] keeps its validity, as well as the orthonormality relation [Theorem XXVI, part (ix)]

$$\begin{aligned}\mathcal{C}_\Psi(\mu_1,\ldots,\mu_n)\mathcal{C}_\Psi(\lambda_1,\ldots,\lambda_n) \;=\; \delta_{\mu_1,\lambda_1}\cdot\ldots\cdot\delta_{\mu_m,\lambda_m}\;\times \\ \delta(\mu_{m+1}-\lambda_{m+1})\cdot\ldots\cdot\delta(\mu_n-\lambda_n)\,\mathcal{C}_\Psi(\lambda_1,\ldots,\lambda_n)\end{aligned} \tag{A.135}$$

and the eigenoperator property [Theorem XXVI, parts (x), (xi)]:

$$\mathcal{A}_k\mathcal{C}_\Psi(\lambda_1,\ldots,\lambda_n) \;=\; \mathcal{C}_\Psi(\lambda_1,\ldots,\lambda_n)\mathcal{A}_k \;=\; \lambda_k\,\mathcal{C}_\Psi(\lambda_1,\ldots,\lambda_n) \tag{A.136}$$

for all $k = 1,\ldots,n$.

The spatial representation of $\mathcal{C}_\Psi(\lambda_1,\ldots,\lambda_n)$ provides the eigenfunctions $\psi_{\lambda_1,\ldots,\lambda_n}(\mathbf{r})$ of the set of operators $\{\mathcal{A}_1,\ldots,\mathcal{A}_n\}$ (A.102):

$$\langle\mathbf{r}\,|\mathcal{C}_\Psi(\lambda_1,\ldots,\lambda_n)|\,\mathbf{r}'\rangle \;=\; \psi_{\lambda_1,\ldots,\lambda_n}(\mathbf{r}')^*\psi_{\lambda_1,\ldots,\lambda_n}(\mathbf{r}) \tag{A.137}$$

Like its single-operator counterpart, $\psi_{\lambda_1,\ldots,\lambda_n}(\mathbf{r})$ is a simultaneous eigenfunction of the n integral equations ($k = 1,\ldots,n$) (A.105):

$$\int d^3r'\,A_k(\mathbf{r},\mathbf{r}')\,\psi_{\lambda_1,\ldots,\lambda_n}(\mathbf{r}') \;=\; \lambda_k\,\psi_{\lambda_1,\ldots,\lambda_n}(\mathbf{r}) \tag{A.138}$$

where $A_K(\mathbf{r},\mathbf{r}') = \langle\mathbf{r}\,|\mathcal{A}_k|\,\mathbf{r}'\rangle$ denotes the spatial representation of the operators $\mathcal{A}_k$. These eigenfunctions are orthonormal (A.106):

$$\begin{aligned}\int d^3r\,\psi_{\mu_1,\ldots,\mu_n}(\mathbf{r})^*\psi_{\lambda_1,\ldots,\lambda_n}(\mathbf{r}) \;=\; \delta_{\mu_1,\lambda_1}\cdot\ldots\cdot\delta_{\mu_m,\lambda_m}\;\times \\ \delta(\mu_{m+1}-\lambda_{m+1})\cdot\ldots\cdot\delta(\mu_n-\lambda_n)\end{aligned} \tag{A.139}$$

Unless all λ_k are in the point spectra of the $\mathcal{A}_k$, i. e., $m = n$, the functions $\psi_{\lambda_1,\ldots,\lambda_n}(\mathbf{r})$ are not normalizable in the strict sense. The set $\{\lambda_1,\ldots,\lambda_n\}$ may be denoted as the "quantum numbers" of the function $\psi_{\lambda_1,\ldots,\lambda_n}(\mathbf{r})$.

Decomposition of $\mathbb{H}$ into non-degenerate families. We define non-degeneracy of some point $(\lambda_1, \ldots, \lambda_n)$ contained in the spectral space of a set of commuting operators $\{\mathcal{A}_1, \ldots, \mathcal{A}_n\}$ in the same manner as for single operators (Definition XXVII):

■ DEFINITION XXXVI
Let $\{|\Psi\rangle\}$ be the set of states in $\mathbb{H}$ for which the orthonormal family $\mathcal{C}_\Psi(\lambda_1, \ldots, \lambda_n)$ does not vanish. If for any pair of such states $|\Phi\rangle$, $|\Psi\rangle$ the relation $\mathcal{C}_\Phi(\lambda_1, \ldots, \lambda_n) = \mathcal{C}_\Psi(\lambda_1, \ldots, \lambda_n)$ holds, then $(\lambda_1, \ldots, \lambda_n)$ is called a non-degenerate eigenvalue of the commuting set $\{\mathcal{A}_1, \ldots, \mathcal{A}_n\}$, and we write $\mathcal{C}_\Psi(\lambda_1, \ldots, \lambda_n) = \mathcal{C}(\lambda_1, \ldots, \lambda_n)$.

Again, we have for non-degenerate $(\lambda_1, \ldots, \lambda_n)$ (Theorem XXVIII):

$$\mathcal{C}(\lambda_1, \ldots, \lambda_n) \;=\; \mathcal{P}_1(\lambda_1) \cdot \ldots \cdot \mathcal{P}_m(\lambda_m) \frac{\partial \Pi_{m+1}(\lambda_{m+1})}{\partial \lambda_{m+1}} \cdot \ldots \cdot \frac{\partial \Pi_n(\lambda_n)}{\partial \lambda_n} \tag{A.140}$$

For a completely non-degenerate spectrum space, we obtain following Theorem XXIX:

$$\mathcal{E} \;=\; \prod_{k=1}^{n} \left\{ \sum_{\text{p.s.}} + \int_{\text{c.s.}} d\lambda_k \right\} \mathcal{C}(\lambda_1, \ldots, \lambda_n) \tag{A.141}$$

$$\phi[\mathcal{A}_1, \ldots, \mathcal{A}_n] \;=\; \prod_{k=1}^{n} \left\{ \sum_{\text{p.s.}} + \int_{\text{c.s.}} d\lambda_k \right\} \phi(\lambda_1, \ldots, \lambda_n)\, \mathcal{C}(\lambda_1, \ldots, \lambda_n) \tag{A.142}$$

In particular, the generalized Fourier theorem (Theorem XXX) continues to hold: For every state $|\chi\rangle \in \mathbb{H}$, its spatial representation $\langle \mathbf{r}|\chi\rangle = \chi(\mathbf{r})$ may be expanded into eigenfunctions $\psi_{\lambda_1, \ldots, \lambda_n}(\mathbf{r})$:

$$\chi(\mathbf{r}) \;=\; \prod_{k=1}^{n} \left\{ \sum_{\text{p.s.}} + \int_{\text{c.s.}} d\lambda_k \right\} \beta(\lambda_1, \ldots, \lambda_n)\, \psi_{\lambda_1, \ldots, \lambda_n}(\mathbf{r}) \tag{A.143}$$

where the coefficient function $\beta(\lambda_1, \ldots, \lambda_n)$ is given by:

$$\beta(\lambda_1, \ldots, \lambda_n) \;=\; \int d^3 r\, \psi_{\lambda_1, \ldots, \lambda_n}(\mathbf{r})^* \chi(\mathbf{r}) \tag{A.144}$$

The integral representation (A.143) converges to $\chi(\mathbf{r})$ in the mean, i. e., everywhere except at most on a set of points $\{\mathbf{r}\}$ of measure zero [232]. (See also the notes following Theorem XXX.)

As an example, we consider the Fourier decomposition in the $x - y$ plane, which is equivalent to the quantum mechanical theory of momentum in two-dimensional space [83]. Let $A_1(\mathbf{r}, \mathbf{r}') = \mathrm{p}_x = -i\hbar\delta(x - x')\partial/\partial x$ and $A_2(\mathbf{r}, \mathbf{r}') = \mathrm{p}_y = -i\hbar\delta(y - y')\partial/\partial y$ be the x– and y–components of momentum. $\mathcal{A}_1$ and $\mathcal{A}_2$ manifestly commute; their

combined spectrum (p_x, p_y) covers the whole space $\mathbb{R}^2$ and is differentiably continuous and non-degenerate, since, apart from irrelevant scaling operations, unique eigenfunctions $\psi_{p_x,p_y}(x,y)$ are given by:

$$\psi_{p_x,p_y}(x,y) \;=\; \frac{1}{2\pi\hbar}\,\exp\left(\frac{i}{\hbar}\,(p_x x + p_y y)\right) \tag{A.145}$$

Following (A.143) and (A.144), the pair of related Fourier transforms is given by:

$$\Phi(x,y) \;=\; \frac{1}{2\pi\hbar}\int dp_x \int dp_y\, e^{i(p_x x + p_y y)/\hbar}\,\phi(p_x,p_y) \tag{A.146}$$

$$\phi(p_x,p_y) \;=\; \frac{1}{2\pi\hbar}\int dx \int dy\, e^{-i(p_x x + p_y y)/\hbar}\,\Phi(x,y) \tag{A.147}$$

For square-integrable $\Phi(\mathbf{r}) = \langle \mathbf{r}|\Phi\rangle$, (A.146) converges almost everywhere to the original function.

Separable Operators. We have already noted that several important operators in quantum mechanics feature degenerate spectra, and therefore cannot be decomposed into eigenfunctions in a straightforward manner. However, we may achieve this objective for an important class of operators $\mathcal{H}$ which we will denote separable operators by means of sets of commuting operators $\{\mathcal{A}_1, \ldots, \mathcal{A}_n\}$. To this end, we define:

■ DEFINITION XXXVII
An operator $\mathcal{H}$ is called separable within a set of self-adjoint operators $\{\mathcal{A}_1, \ldots, \mathcal{A}_n\}$ if:

(i). $\mathcal{H}$ commutes with the operators $\mathcal{A}_k$: For all $k = 1, \ldots, n$, $\mathcal{H}\mathcal{A}_k = \mathcal{A}_k\mathcal{H}$

(ii). The operators $\mathcal{A}_k$ form a commuting set: For all $j, k = 1, \ldots, n$, $\mathcal{A}_j\mathcal{A}_k = \mathcal{A}_k\mathcal{A}_j$

(iii). The spectrum space $(\lambda_1, \ldots, \lambda_n)$ of the set of operators $\{\mathcal{A}_1, \ldots, \mathcal{A}_n\}$ is non-degenerate.

Let us deliver some prominent examples from quantum mechanics. Despite its simplicity, the one-dimensional Schrödinger equation for a bounded potential $U(x)$ features a degenerate spectrum as there exist two linearly independent eigenfunctions $\psi_E(x)$, $\phi_E(x)$ for sufficiently large values of the eigenenergy E. However, if the potential $U(x)$ is symmetric, $U(x) = U(-x)$, then the self-adjoint parity operator $\mathcal{Q}$ that we first considered in Section A.3.2 may be used to separate these solutions into odd and even functions. Hence, the Hamiltonian $\mathcal{H}$ then is separable within the set $\mathcal{A}_1 = \mathcal{H}$, $\mathcal{A}_2 = \mathcal{Q}$.

As a second example, we quote the Schrödinger equation in three dimensions with radially symmetric potential $U(r)$. This problem has been extensively studied and is often referred to simply as "scattering theory," thus expelling the more challenging problem of interaction with non-isotropic potentials. (For a comprehensive discussion, see the monograph by Newton [230].) Here, the Hamiltonian $\mathcal{H}$ is separable within the set $\mathcal{A}_1 = \mathcal{H}$, $\mathcal{A}_2 = \mathcal{L}^2$, $\mathcal{A}_3 = \mathcal{L}_z$, where $\mathcal{L}^2$, $\mathcal{L}_z$ denote the familiar operators of angular momentum. (Note that the pure point spectrum of $\mathcal{L}^2$ comprises all values $\lambda_2 = l(l+1)$ with $l = 0, 1, 2, \ldots$, whereas $\mathcal{A}_3 = \mathcal{L}_z$ allows for eigenvalues $\lambda_3 = m = 0, \pm 1, \pm 2, \ldots$. But the combined projector $\mathcal{P}_2(\lambda_2)\mathcal{P}_3(\lambda_3)$ vanishes for $l < |m|$, so the spectrum of the pair $\mathcal{A}_2$, $\mathcal{A}_3$ is not simply the product of the spectra of both operators.)

Finally, the Hamiltonian $\mathcal{H}$ of motion in a three-dimensional uniform force field which is of central interest in this treatise is also separable. Indeed, if we set $\mathcal{A}_1 = \mathrm{p}_x$, $\mathcal{A}_2 = \mathrm{p}_y$, and $A_3(z, p_z) = \langle z\,|\mathcal{A}_3|\,z'\rangle = \delta(z - z')[\,p_z^2/2M - Fz]$, we find that the lateral momentum operators $\mathcal{A}_1$, $\mathcal{A}_2$ and the Hamiltonian $\mathcal{A}_3$ of one-dimensional uniformly accelerated motion mutually commute and provide non-degenerate, entirely continuous spectra of eigenfunctions for their respective coordinate x, y, and z (see Appendix D.2). Thus, the normalized eigenfunctions $\psi_{\lambda_1,\lambda_2,\lambda_3}(\mathbf{r})$ of the set $\{\mathcal{A}_1, \mathcal{A}_2, \mathcal{A}_3\}$ with quantum numbers $(\lambda_1, \lambda_2, \lambda_3)$ are uniquely given by the product of the corresponding one-dimensional eigenfunctions $\psi_{\lambda_k}^{(k)}(x_k)$ of $\mathcal{A}_1$, $\mathcal{A}_2$, and $\mathcal{A}_3$, which means that $\{\mathcal{A}_1, \mathcal{A}_2, \mathcal{A}_3\}$ forms a non-degenerate set of operators. Using the results of the Fourier decomposition derived above (A.145) and the explicit form of the normalized eigenfunctions of the one-dimensional uniform field problem (D.26), the eigenfunctions $\psi_{\lambda_1,\lambda_2,\lambda_3}(\mathbf{r})$ read (we use the physical notation $p_x = \lambda_1$, $p_y = \lambda_2$, $E_\parallel = \lambda_3$):

$$\psi_{p_x,p_y,E_\parallel}(\mathbf{r}) \;=\; \frac{1}{2\pi\hbar}\,\exp\left(\frac{i}{\hbar}\,(p_x x + p_y y)\right)\; 2\beta\sqrt{F}\;\mathrm{Ai}\left[-2\beta(E_\parallel + Fz)\right] \tag{A.148}$$

(Here, $\beta^3 = M/4\hbar^2F^2$ denotes the ubiquitous inverse energy parameter of the uniform field problem first introduced in Section 5.2.) The Hamiltonian $\mathcal{H}$ of field emission in three dimensions is separable within the set $\{\mathcal{A}_1, \mathcal{A}_2, \mathcal{A}_3\}$ as it may be represented as a polynomial in the $\mathcal{A}_k$: $\mathcal{H} = (\mathcal{A}_1^2 + \mathcal{A}_2^2)/2M + \mathcal{A}_3$.

The existence of a separating set $\{\mathcal{A}_1, \ldots, \mathcal{A}_n\}$ has wide-ranging consequences for the spectrum of $\mathcal{H}$, as the following extension of Theorem XXXIV to commuting sets of operators shows:

■ THEOREM XXXVIII

Let $\mathcal{H}$ be separable in the set $\{\mathcal{A}_1, \ldots, \mathcal{A}_n\}$. Then the orthonormal family $\mathcal{C}(\lambda_1, \ldots, \lambda_n)$ generated by this set is an eigenoperator of $\mathcal{H}$, and $\mathcal{H}$ is a functional of that set:

(i). $\mathcal{H}\mathcal{C}(\lambda_1, \ldots, \lambda_n) = \mathcal{C}(\lambda_1, \ldots, \lambda_n)\mathcal{H} = E(\lambda_1, \ldots, \lambda_n)\,\mathcal{C}(\lambda_1, \ldots, \lambda_n)$

(ii). $\mathcal{H} = E[\mathcal{A}_1, \ldots, \mathcal{A}_n]$

Proof. The proof is completely analogous to that of Theorem XXXIV, so we will just cite the major steps. Like in the simpler case of a single operator $\mathcal{A}$ with non-degenerate spectrum (Theorem XXXIII), there is a uniqueness theorem which states that any operator $\mathcal{B}$ (in the generalized sense) which is a simultaneous eigenoperator of all $\mathcal{A}_k$, $(k = 1, \ldots, n)$ of the set, and commutes with all $\mathcal{A}_k$, is just a multiple of the member of the orthonormal family $\mathcal{C}(\lambda_1, \ldots, \lambda_n)$ with the corresponding eigenvalues of $\mathcal{B}$: If $\mathcal{A}_k\mathcal{B} = \mathcal{B}\mathcal{A}_k = \lambda_k\mathcal{A}_k$ for $k = 1, \ldots, n$, then $\mathcal{B} = \mu\,\mathcal{C}(\lambda_1, \ldots, \lambda_n)$.

Now, for every $\mathcal{A}_k$, $k = 1, \ldots, n$, we have $\mathcal{A}_k[\mathcal{H}\mathcal{C}(\lambda_1, \ldots, \lambda_n)] = \mathcal{H}[\mathcal{A}_k\mathcal{C}(\lambda_1, \ldots, \lambda_n)] = \lambda_k\,\mathcal{H}\mathcal{C}(\lambda_1, \ldots, \lambda_n)$, and also $\mathcal{A}_k\mathcal{H}\mathcal{C}(\lambda_1, \ldots, \lambda_n) = \mathcal{H}\mathcal{C}(\lambda_1, \ldots, \lambda_n)\mathcal{A}_k$ [as $\mathcal{A}_k$ commutes with $\mathcal{H}$ and the orthonormal family (A.136)], so by uniqueness $\mathcal{H}\mathcal{C}(\lambda_1, \ldots, \lambda_n)$ must be a multiple of $\mathcal{C}(\lambda_1, \ldots, \lambda_n)$. Hence, the family $\mathcal{C}(\lambda_1, \ldots, \lambda_n)$ is an eigenoperator of $\mathcal{H}$:

$$\mathcal{H}\mathcal{C}(\lambda_1, \ldots, \lambda_n) \;=\; E(\lambda_1, \ldots, \lambda_n)\,\mathcal{C}(\lambda_1, \ldots, \lambda_n) \tag{A.149}$$

The same reasoning holds for $\mathcal{C}(\lambda_1, \ldots, \lambda_n)\mathcal{H}$, and it may be shown as in Theorem XXXIV that $\mathcal{H}$ and $\mathcal{C}(\lambda_1, \ldots, \lambda_n)$ indeed commute. Thus, part (i) is proven.

To verify the second part, we use the resolution of the identity $\mathcal{E}$ into the spectral family $\mathcal{C}(\lambda_1, \ldots, \lambda_n)$ and obtain using (i) and the expansion (A.142):

$$\begin{aligned}\mathcal{H}\mathcal{E} \;&=\; \prod_{k=1}^{n}\left\{\sum_{\text{p.s.}} + \int_{\text{c.s.}} d\lambda_k\right\}\,\mathcal{H}\mathcal{C}(\lambda_1, \ldots, \lambda_n) \\ &=\; \prod_{k=1}^{n}\left\{\sum_{\text{p.s.}} + \int_{\text{c.s.}} d\lambda_k\right\}\,E(\lambda_1, \ldots, \lambda_n)\,\mathcal{C}(\lambda_1, \ldots, \lambda_n) \;=\; E[\mathcal{A}_1, \ldots, \mathcal{A}_n]\end{aligned} \tag{A.150}$$

Thus, $\mathcal{H} = E[\mathcal{A}_1, \ldots, \mathcal{A}_n]$, as was to be shown. ■

We note that this theorem implies that any self-adjoint operator commuting with a set of operators which forms a non-degenerate spectrum is actually a functional of this set—in a certain sense, the class of separable operators is therefore "closed."

Because the decomposition of $E[\mathcal{A}_1, \ldots, \mathcal{A}_n]$ into the orthonormal family of operators $\mathcal{C}(\lambda_1, \ldots, \lambda_n)$ (A.142), (A.150) and thus into non-degenerate eigenfunctions $\psi_{\lambda_1,\ldots,\lambda_n}(\mathbf{r})$ (A.137) is established, any operator $\mathcal{H}$ separable in the set $\{\mathcal{A}_1, \ldots, \mathcal{A}_n\}$ allows for an eigenfunction expansion even though the spectrum of $\mathcal{H}$ is generally degenerate. The same property obviously holds for regular functionals $\phi[\mathcal{H}]$ of $\mathcal{H}$. For example, we find for the spatial representation $H(\mathbf{r}, \mathbf{r}') = \langle \mathbf{r}\,|\mathcal{H}|\,\mathbf{r}'\rangle$ of the operator $\mathcal{H}$:

$$H(\mathbf{r}, \mathbf{r}') \;=\; \prod_{k=1}^{n}\left\{\sum_{\text{p.s.}} + \int_{\text{c.s.}} d\lambda_k\right\}\,E(\lambda_1, \ldots, \lambda_n)\,\psi_{\lambda_1,\ldots,\lambda_n}(\mathbf{r}')^*\psi_{\lambda_1,\ldots,\lambda_n}(\mathbf{r}) \tag{A.151}$$

and, according to (A.124), for the density of states operator $\partial\Pi_{\mathcal{H}}(E)/\partial E$ assigned to $\mathcal{H}$, provided it exists at all:

$$\left\langle \mathbf{r} \left| \frac{\partial\Pi_{\mathcal{H}}(E)}{\partial E} \right| \mathbf{r}' \right\rangle = \prod_{k=1}^{n} \left\{ \sum_{\text{p.s.}} + \int_{\text{c.s.}} d\lambda_k \right\} \times \delta[E - E(\lambda_1, \ldots, \lambda_n)]\, \psi_{\lambda_1,\ldots,\lambda_n}(\mathbf{r}')^* \psi_{\lambda_1,\ldots,\lambda_n}(\mathbf{r}) \quad \text{(A.152)}$$

since $\partial\Pi_{\mathcal{H}}(E)/\partial E = \delta(E - \mathcal{H})$.

As an example, we calculate the local density of states (LDOS) $n(\mathbf{o}; E)$ for the uniform field problem in three-dimensional configuration space. (By the local density of states we mean the diagonal element of the density of states operator in spatial representation: $n(\mathbf{r}; E) = \langle \mathbf{r} \,|\partial\Pi(E)/\partial E|\, \mathbf{r} \rangle$. From symmetry considerations in the uniform force field scheme (Section 4.3.2), the calculation of $n(\mathbf{r}; E)$ for one special position $\mathbf{r}_0$ suffices to determine $n(\mathbf{r}; E)$ in general; for simplicity, we choose $\mathbf{r}_0 = \mathbf{o}$.) We have seen above that the Hamiltonian of free-falling motion $H(\mathbf{r}, \mathbf{p}) = H_{\text{free}}(\mathbf{p}) - Fz$ is separable in the set of operators p_x, p_y, and $H_{1\text{d}}(z, \mathrm{p}_z) = \mathrm{p}_z^2/2M - Fz$. Thus, we may expand $n(\mathbf{o}; E)$ into the eigenfunctions $\psi_{p_x,p_y,E_\parallel}(\mathbf{r})$ (A.148) of this set. Following (A.152), this procedure yields:

$$n(\mathbf{o}; E) = \frac{\beta^2 F}{\pi^2\hbar^2} \int dp_x \int dp_y \int dE_\parallel\, \delta[E - E_\parallel - (p_x^2 + p_y^2)/2M]\ \mathrm{Ai}(-2\beta E_\parallel)^2 \quad \text{(A.153)}$$

Here, again $\beta^3 = M/4\hbar^2F^2$ (5.16). Introducing cylindrical coordinates, we may eliminate the delta function in (A.153). Let $E_\perp = (p_x^2 + p_y^2)/2M$); then,

$$\int dp_x \int dp_y\, \delta(E - E_\parallel - E_\perp) = 2\pi M \int_0^\infty dE_\perp \delta(E - E_\parallel - E_\perp) = 2\pi M \Theta(E - E_\parallel) \quad \text{(A.154)}$$

Here $\Theta(z)$ denotes the Heaviside step function. Thus,

$$n(\mathbf{o}; E) = \frac{2M\beta^2 F}{\pi\hbar^2} \int_{-\infty}^{E} dE_\parallel\ \mathrm{Ai}(-2\beta E_\parallel)^2 = \frac{M\beta F}{\pi\hbar^2} \left\{ \mathrm{Ai}'(\epsilon)^2 - \epsilon\, \mathrm{Ai}(\epsilon)^2 \right\} \quad \text{(A.155)}$$

where $\epsilon = -2\beta E$ (for the dimensionless variables in the uniform field problem, see Section 5.3.1). The integral appearing in (A.155) which is strangely missing in the commonly used tables [81, 188] may be resolved by partial integration [151, 234]. (See also (D.34) in Appendix D.2.3.)

The result (A.155) directly relates to the retarded Green function $G(\mathbf{r}, \mathbf{r}'; E)$ (2.12) as will be demonstrated in the following section. Therefore, the local density of states $n(\mathbf{r}; E)$ is intimately tied to the current $J_{00}(\mathbf{r}; E)$ generated by a s–wave pointlike

source (2.34). For sources embedded in a homogeneous field, this is confirmed by a comparison of (A.155) with the result (E.11) in Appendix E.3.

A.3.6 The Resolvent Operator

In the main body of this volume, our interest was directed not so much to the eigenvalue spectrum of the Hamiltonian $\mathcal{H}$ and the related time evolution operator of the system $\mathcal{U}(t-t') = \exp[-i\mathcal{H}(t-t')/\hbar]$ (A.15), but rather onto the time-independent energy Green function $G(\mathbf{r},\mathbf{r}';E)$ of the system (Section 2.3), which is defined as the special solution of (2.12):

$$\{E - H(\mathbf{r},\mathbf{p})\}\; G(\mathbf{r},\mathbf{r}';E) \;=\; \delta(\mathbf{r}-\mathbf{r}') \tag{A.156}$$

and is related to the retarded propagator $K_F(\mathbf{r},t;\mathbf{r}',t') = \langle \mathbf{r}\,|\mathcal{K}_{\rm ret}(t,t')|\,\mathbf{r}'\rangle$ (A.20) via the integral transform (2.13). In order to return to the formal operator theory we developed so far, we note that (A.156) just presents the spatial representation (Section A.2.1) of the operator equation:

$$(E\mathcal{E} - \mathcal{H})\,\mathcal{R}(E) \;=\; \mathcal{E} \tag{A.157}$$

where the Green function $G(\mathbf{r},\mathbf{r}';E) = \langle \mathbf{r}\,|\mathcal{R}(E)|\,\mathbf{r}'\rangle$ is given as the spatial representation of some operator family $\mathcal{R}(E)$, which is generally known as the resolvent operator belonging to $\mathcal{H}$ (see Kato [228], p. 272). We now proceed to establish the properties of $\mathcal{R}(E)$, and elucidate its connection to the spectrum of $\mathcal{H}$.

Definition of the resolvent. We first give a general definition of the resolvent operator, which in a sense represents the inverse of a given operator, following (A.157):

■ DEFINITION XXXIX
The family of operators $\mathcal{R}(\lambda)$ assigned to the self-adjoint operator $\mathcal{A}$ by the relation:

$$\mathcal{R}(\lambda)(\mathcal{A} - \lambda\,\mathcal{E}) \;=\; (\mathcal{A} - \lambda\,\mathcal{E})\mathcal{R}(\lambda) \;=\; \mathcal{E} \tag{A.158}$$

is denoted as the resolvent operator belonging to $\mathcal{A}$.

Uniqueness theorems. We next examine the scope of the operator family $\mathcal{R}(\lambda)$. Obviously, for particular values of λ, $\mathcal{R}(\lambda)$ will not exist at all, as is well-known from the theory of finite-dimensional linear systems (where $\mathcal{R}(\lambda)$ is not available if λ presents an eigenvalue of $\mathcal{A}$); for other values of λ, multiple instances of $\mathcal{R}(\lambda)$ may appear. In this paragraph, we take up the question of uniqueness of the resolvent operator; the question whether a solution $\mathcal{R}(\lambda)$ exists at all for a given value of λ will be deferred to

the next section. For our purposes, the following five theorems form a sufficient basis for the theory of resolvents presented in this work. We start out with:

■ COROLLARY XL
Assume that the operator equation:

$$\mathcal{B}(\lambda)(\mathcal{A}-\lambda\,\mathcal{E}) \;=\; (\mathcal{A}-\lambda\,\mathcal{E})\mathcal{B}(\lambda) \;=\; \mathcal{S}(\lambda) \tag{A.159}$$

for a given right-hand side operator $\mathcal{S}(\lambda)$ has two solutions $\mathcal{B}_1(\lambda)$, $\mathcal{B}_2(\lambda)$ which are bounded: $\|\mathcal{B}_{1,2}(\lambda)\,|\Psi\rangle\|^2 < \infty$ for all states $|\Psi\rangle \in \mathbb{H}$. Then, the difference of these operators is an eigenoperator to the projector $\mathcal{P}(\lambda)$ (Definition XV) onto the eigenstates of $\mathcal{A}$ with eigenvalue λ:

$$\mathcal{P}(\lambda)[\mathcal{B}_1(\lambda)-\mathcal{B}_2(\lambda)] \;=\; [\mathcal{B}_1(\lambda)-\mathcal{B}_2(\lambda)]\mathcal{P}(\lambda) \;=\; \mathcal{B}_1(\lambda)-\mathcal{B}_2(\lambda) \tag{A.160}$$

Proof. By subtracting the operator equation (A.159) for $k = 1, 2$, we find $\mathcal{A}[\mathcal{B}_1(\lambda) - \mathcal{B}_2(\lambda)] = \lambda[\mathcal{B}_1(\lambda) - \mathcal{B}_2(\lambda)]$. So, if $[\mathcal{B}_1(\lambda) - \mathcal{B}_2(\lambda)]\,|\Psi\rangle$ exists, this state is an eigenstate of $\mathcal{A}$ with eigenvalue λ. This is indeed the case for all $|\Psi\rangle \in \mathbb{H}$ because with $\mathcal{B}_1(\lambda)$, $\mathcal{B}_2(\lambda)$, also the difference operator $\mathcal{B}_1(\lambda) - \mathcal{B}_2(\lambda)$ is bounded, as the triangulum inequality of the norm immediately shows: $\|\mathcal{B}_1(\lambda) - \mathcal{B}_2(\lambda)\| \leq \|\mathcal{B}_1(\lambda)\| + \|\mathcal{B}_2(\lambda)\| < \infty$. Hence, $[\mathcal{B}_1(\lambda) - \mathcal{B}_2(\lambda)]\,|\Psi\rangle$ belongs to the eigenspace $\mathbb{M}_0(\lambda)$ of $\mathcal{A}$ for all $|\Psi\rangle \in \mathbb{H}$. This means $\mathcal{P}(\lambda)[\mathcal{B}_1(\lambda)-\mathcal{B}_2(\lambda)]\,|\Psi\rangle = [\mathcal{B}_1(\lambda)-\mathcal{B}_2(\lambda)]\,|\Psi\rangle$ for all $|\Psi\rangle \in \mathbb{H}$, or $\mathcal{P}(\lambda)[\mathcal{B}_1(\lambda) - \mathcal{B}_2(\lambda)] = [\mathcal{B}_1(\lambda) - \mathcal{B}_2(\lambda)]$. As $\mathcal{A}$ commutes with the bounded operator $\mathcal{B}_1(\lambda) - \mathcal{B}_2(\lambda)$ according to (A.159), Theorem VIII, part (vi) tells us that the difference operator also commutes with the polar decomposition operator $\mathcal{U}(\lambda)$ assigned to $\mathcal{A} - \lambda\mathcal{E}$, and therefore with the projector operator $\mathcal{P}(\lambda) = \mathcal{E} - \mathcal{U}(\lambda)^2$ [Theorem IX, part (ii)]. This completes the proof of (A.160). ■

If λ is not a member of the point spectrum of $\mathcal{A}$, in particular, if $\Im(\lambda) \neq 0$, then $\mathcal{P}(\lambda) = 0$ (Theorem XVI). Therefore, we find as an immediate consequence of Corollary XL:

■ THEOREM XLI
The operator equation $(\mathcal{A} - \lambda\mathcal{E})\mathcal{B}(\lambda) = \mathcal{S}(\lambda)$ has at most one bounded solution $\mathcal{B}(\lambda)$, if λ is not an element of the point spectrum of $\mathcal{A}$.

The other group of theorems classify unbounded solutions to the same equation (A.159) if $\mathcal{A}$ is an operator with non-degenerate spectrum, the continuous part of which is differentiable:

■ THEOREM XLII
If the spectrum of the self-adjoint operator $\mathcal{A}$ is differentiable and non-degenerate, then the set of solutions $\{\mathcal{B}(\lambda)\}$ to the operator equation:

$$\mathcal{B}(\lambda)(\mathcal{A}-\lambda\,\mathcal{E}) \;=\; (\mathcal{A}-\lambda\,\mathcal{E})\mathcal{B}(\lambda) \;=\; \mathcal{S}(\lambda) \tag{A.161}$$

is either empty or forms a one-dimensional continuous set:

$$\mathcal{B}_\mu(\lambda) \;=\; \mathcal{B}_0(\lambda) + \mu\,\mathcal{C}(\lambda) \tag{A.162}$$

Here, μ denotes an arbitrary complex number, and $\mathcal{C}(\lambda)$ presents the orthonormal family of operators associated to $\mathcal{A}$.

Proof. Let $\delta\mathcal{B}(\lambda)$ denote the difference of two solutions $\mathcal{B}(\lambda)$, given that a solution $\mathcal{B}_0(\lambda)$ actually exists. Then, by subtraction we find from (A.161) that $\mathcal{A}\delta\mathcal{B}(\lambda) = \delta\mathcal{B}(\lambda)\mathcal{A} = \lambda\delta\mathcal{B}(\lambda)$. Thus, $\delta\mathcal{B}(\lambda)$ is eigenoperator of $\mathcal{A}$. By the uniqueness theorem for non-degenerate spectra (Theorem XXXIII), we conclude that $\delta\mathcal{B}(\lambda) = \mu\,\mathcal{C}(\lambda)$ with some complex number μ. On the other hand, with $\mathcal{B}_0(\lambda)$ also $\mathcal{B}_0(\lambda) + \mu\,\mathcal{C}(\lambda)$ presents a solution to the operator equation (A.161), as is easily shown by insertion. ■

Note: If λ is in the resolvent set of $\mathcal{A}$, Theorem XLII asserts that there exists at most one (bounded or unbounded) solution $\mathcal{B}_0(\lambda)$ to (A.161), as $\mathcal{C}(\lambda) = 0$ in the resolvent set. Thus, Theorem XLII formally extends Theorem XLI for operators with non-degenerate spectra. However, it will turn out that the solution to the resolvent problem $[\mathcal{S}(\lambda) = \mathcal{E}]$ is always bounded in this case (see Theorems XLV and XLVII).

As usual, the content of this theorem may be extended to sets of commuting operators $\{\mathcal{A}_1, \ldots, \mathcal{A}_n\}$ with non-degenerate spectrum $\{\lambda_1, \ldots, \lambda_n\}$. Obviously, the solution operators $\mathcal{B}(\lambda_1, \ldots, \lambda_n)$ are separable in this set (Definition XXXVII):

■ THEOREM XLIII
If $\mathcal{B}_{1,2}(\lambda_1, \ldots, \lambda_n)$ present two solutions to the set of operator equations ($k = 1, \ldots, n$):

$$\mathcal{B}_j(\lambda_1, \ldots, \lambda_n)(\mathcal{A}_k - \lambda_k\mathcal{E}) \;=\; (\mathcal{A}_k - \lambda_k\mathcal{E})\mathcal{B}_j(\lambda_1, \ldots, \lambda_n) \;=\; \mathcal{S}(\lambda_1, \ldots, \lambda_n) \tag{A.163}$$

then their difference is a multiple of the orthonormal family $\mathcal{C}(\lambda_1, \ldots, \lambda_n)$ belonging to the set $\{\mathcal{A}_1, \ldots, \mathcal{A}_n\}$:

$$\mathcal{B}_1(\lambda_1, \ldots, \lambda_n) - \mathcal{B}_2(\lambda_1, \ldots, \lambda_n) \;=\; \mu\,\mathcal{C}(\lambda_1, \ldots, \lambda_n) \tag{A.164}$$

It is well worth noting that even if the right-hand side operator $\mathcal{S}(\lambda)$ is self-adjoint, $\mathcal{S}(\lambda)^+ = \mathcal{S}(\lambda)$, the solution $\mathcal{B}(\lambda)$ of Corollary XL need not be self-adjoint for real λ. However, then with $\mathcal{B}(\lambda)$ also $\mathcal{B}(\lambda)^+$ forms a solution to the operator equation (A.159) as may be inferred immediately by forming the adjoint equation. Thus, for operators $\mathcal{A}$ with non-degenerate spectrum, Theorem XLII asserts that $\mathcal{B}(\lambda) - \mathcal{B}(\lambda)^+ = \mu\,\mathcal{C}(\lambda)$ is a multiple of the orthonormal family, and it follows with $\mathcal{C}(\lambda)^+ = \mathcal{C}(\lambda)$ [Theorem XXVI, part (i)]:

■ THEOREM XLIV
Let $\mathcal{A}$ be a self-adjoint operator with non-degenerate spectrum, and $\mathcal{B}(\lambda)$ a solution of $\mathcal{B}(\lambda)(\mathcal{A}-\lambda\,\mathcal{E}) = (\mathcal{A}-\lambda\,\mathcal{E})\mathcal{B}(\lambda) = \mathcal{S}(\lambda)$ with real parameter λ and given self-adjoint operator $\mathcal{S}(\lambda) = \mathcal{S}(\lambda)^+$. Then, for the antisymmetric part of $\mathcal{B}(\lambda)$ holds:

$$\frac{1}{2i}\left\{\mathcal{B}(\lambda)-\mathcal{B}(\lambda)^+\right\} = \alpha\,\mathcal{C}(\lambda) \tag{A.165}$$

where α is some real number.

Again, an analogous statement holds for sets of commuting operators $\{\mathcal{A}_1,\ldots,\mathcal{A}_n\}$ with non-degenerate spectrum.

Existence theorems for the resolvent. In this section, we examine whether any solutions $\mathcal{R}(\lambda)$ to the resolvent problem (Definition XXXIX) exist at all. First, it is easy to show that for $\Im(\lambda)\neq 0$, the resolvent $\mathcal{R}(\lambda)$ is bounded and unique:

■ THEOREM XLV
If $\Im(\lambda)\neq 0$, then the resolvent problem:

$$\mathcal{R}(\lambda)(\mathcal{A}-\lambda\,\mathcal{E}) = (\mathcal{A}-\lambda\,\mathcal{E})\mathcal{R}(\lambda) = \mathcal{E} \tag{A.166}$$

for some self-adjoint operator $\mathcal{A}$ has a bounded unique solution in form of an operator Stieltjes integral:

$$\mathcal{R}(\lambda) = \int \frac{\mathrm{d}\Pi(\mu)}{\mu-\lambda} \tag{A.167}$$

Proof. As the spectral family $\Pi(\mu)$ commutes with the generating operator $\mathcal{A}$ and itself [Theorem XIII, part (i)], $\mathcal{A}-\lambda\mathcal{E}$ commutes with $\mathcal{R}(\lambda)$. Furthermore, we have according to the spectral theorem (Theorem XXI):

$$(\mathcal{A}-\lambda\,\mathcal{E})\mathcal{R}(\lambda) = \lim_{\mu_{j+1}-\mu_j\to 0^+}\sum_j(\mu_j-\lambda)\,\mathcal{I}(\mu_j,\mu_{j+1})\lim_{\mu'_{k+1}-\mu'_k\to 0^+}\sum_k\frac{\mathcal{I}(\mu'_k,\mu'_{k+1})}{\mu'_k-\lambda} \tag{A.168}$$

for arbitrary dense partitionings $\{\mu_j\}$, $\{\mu'_k\}$ of the real axis. Hence, we may set $\mu_k=\mu'_k$ and find from the orthonormality of the interval projectors $\mathcal{I}(\mu_k,\mu_{k+1})$ [Theorem XIV, parts (ii) and (iv)] using the resolution of the identity (A.64):

$$(\mathcal{A}-\lambda\,\mathcal{E})\mathcal{R}(\lambda) = \lim_{\mu_{k+1}-\mu_k\to 0^+}\sum_k\mathcal{I}(\mu_k,\mu_{k+1}) = \mathcal{E} \tag{A.169}$$

This solution is unique because $\mathcal{R}(\lambda)$ is bounded (Theorem XLI). Let $\delta=\Im(\lambda)$; then, we obtain for every state $|\Phi\rangle\in\mathbb{H}$:

$$\|(\mathcal{A}-\lambda\mathcal{E})\,|\Phi\rangle\|^2 = \langle\Phi\,|(\mathcal{A}-\lambda^*\mathcal{E})(\mathcal{A}-\lambda\mathcal{E})|\,\Phi\rangle = \left\langle\Phi\,\middle|(\mathcal{A}-\Re(\lambda)\mathcal{E})^2+\delta^2\mathcal{E}\middle|\,\Phi\right\rangle \geq \delta^2\,\langle\Phi|\Phi\rangle \tag{A.170}$$

Now, if we set $|\Phi\rangle = \mathcal{R}(\lambda)\,|\Psi\rangle$ for an arbitrarily chosen state $|\Psi\rangle \in \mathbb{H}$, we find:

$$\langle\Psi|\Psi\rangle \;=\; \|(\mathcal{A}-\lambda\mathcal{E})\mathcal{R}(\lambda)\,|\Psi\rangle\|^2 \;=\; \|(\mathcal{A}-\lambda\mathcal{E})\,|\Phi\rangle\|^2 \;\geq\; \delta^2\,\|\mathcal{R}(\lambda)\,|\Psi\rangle\|^2 \tag{A.171}$$

Thus, for all $|\Psi\rangle \in \mathbb{H}$, we have $\|\mathcal{R}(\lambda)\,|\Psi\rangle\|^2 \leq \delta^{-2}\,\langle\Psi|\Psi\rangle$, so $\mathcal{R}(\lambda)$ is bounded. ■

This theorem may be extended to the case of real λ outside the spectrum of $\mathcal{A}$, i. e., for λ in the resolvent set of $\mathcal{A}$. For the following developments, it is useful to introduce first an auxiliary operator $\mathcal{R}_\eta(\lambda)$:

■ DEFINITION XLVI
Let $\Pi(\mu)$ be the spectral family generated by the self-adjoint operator $\mathcal{A}$. For $\eta > 0$ and real λ, we define an operator $\mathcal{R}_\eta(\lambda)$ via:

$$\mathcal{R}_\eta(\lambda) \;=\; \left\{\int_{-\infty}^{\lambda-\eta} + \int_{\lambda+\eta}^{\infty}\right\} \frac{\mathrm{d}\Pi(\mu)}{\mu-\lambda} \tag{A.172}$$

Obviously, $\mathcal{R}_\eta(\lambda)$ is hermitian, commutes with $\mathcal{A}$ and is bounded. For a given state $|\Psi\rangle \in \mathbb{H}$, we have:

$$\begin{aligned}\|\mathcal{R}_\eta(\lambda)\,|\Psi\rangle\|^2 \;&=\; \left\{\int_{-\infty}^{\lambda-\eta} + \int_{\lambda+\eta}^{\infty}\right\} \frac{\mathrm{d}\,\langle\Psi\,|\Pi(\mu)|\,\Psi\rangle}{(\mu-\lambda)^2} \\ &\leq\; \left\{\int_{-\infty}^{\lambda-\eta} + \int_{\lambda+\eta}^{\infty}\right\} \frac{1}{\eta^2}\,\langle\Psi\,|\Pi(\mu)|\,\Psi\rangle \;\leq\; \frac{1}{\eta^2}\,\langle\Psi|\Psi\rangle\end{aligned} \tag{A.173}$$

Let us apply $\mathcal{R}_\eta(\lambda)$ onto $\mathcal{A}$. From the foregoing proof to Theorem XLV we immediately confirm the relation:

$$\mathcal{R}_\eta(\lambda)(\mathcal{A}-\lambda\mathcal{E}) \;=\; (\mathcal{A}-\lambda\mathcal{E})\mathcal{R}_\eta(\lambda) \;=\; \mathcal{E} - \mathcal{I}(\lambda-\eta,\lambda+\eta) \tag{A.174}$$

We now may state that:

■ THEOREM XLVII
If λ is real and a member of the resolvent set of $\mathcal{A}$, then the resolvent problem $\mathcal{R}(\lambda)(\mathcal{A}-\lambda\,\mathcal{E}) \;=\; (\mathcal{A}-\lambda\,\mathcal{E})\mathcal{R}(\lambda) \;=\; \mathcal{E}$ has a unique bounded solution:

$$\mathcal{R}(\lambda) \;=\; \int \frac{\mathrm{d}\Pi(\mu)}{\mu-\lambda} \tag{A.175}$$

Proof. If λ is real and in the resolvent set, then there exists an open interval $\mu_- < \mu < \mu_+$ in the resolvent set containing λ (Definition XVIII). We choose $\eta = \min\{\lambda-\mu_-, \mu_+-\lambda\}$; then, obviously, $\mathcal{I}(\lambda-\eta,\lambda+\eta) = 0$ and thus according to (A.174) $\mathcal{R}_\eta(\lambda)(\mathcal{A}-\lambda\mathcal{E}) = \mathcal{E}$, so we find $\mathcal{R}(\lambda) = \mathcal{R}_\eta(\lambda)$. Since $\mathcal{R}_\eta(\lambda)$ is bounded (A.173), Theorem XLI states that $\mathcal{R}(\lambda)$ (A.175) is the unique solution to the resolvent problem. ■

Next, we proceed to the point spectrum of $\mathcal{A}$.

■ THEOREM XLVIII
If λ is an eigenvalue of $\mathcal{A}$, then the resolvent problem has no solution.

Proof. Assume that $\mathcal{R}(\lambda)$ exists in this case. Let $|\Phi\rangle$ be a non-vanishing eigenstate of $\mathcal{A}$ with eigenvalue λ, i. e., $(\mathcal{A}-\lambda\mathcal{E})\,|\Phi\rangle = 0$ with $\langle\Phi|\Phi\rangle > 0$. But on the other hand, $|\Phi\rangle = \mathcal{R}(\lambda)(\mathcal{A}-\lambda\mathcal{E})\,|\Phi\rangle = \mathcal{R}(\lambda)\cdot 0 = 0$, in contradiction. Thus, $\mathcal{R}(\lambda)$ cannot exist. ■

We may, however, present a restricted solution to the resolvent problem if λ is a member of the point spectrum. Assume that λ is an isolated eigenvalue of $\mathcal{A}$, i. e., there is a finite distance $\delta > 0$ to the closest neighbour in the (point or continuous) spectrum of $\mathcal{A}$. Then, we find from Definition XV $\mathcal{I}(\lambda-\eta,\lambda+\eta) = \mathcal{P}(\lambda)$ for $0 < \eta < \delta$. Consequently, we obtain from (A.174):

$$\mathcal{R}_\eta(\lambda)(\mathcal{A}-\lambda\mathcal{E}) \;=\; (\mathcal{A}-\lambda\mathcal{E})\mathcal{R}_\eta(\lambda) \;=\; \mathcal{E}-\mathcal{P}(\lambda) \tag{A.176}$$

for $0 < \eta < \delta$. It is seen that $\mathcal{R}_\eta(\lambda)$ is a bounded inverse to the operator $\mathcal{A}-\lambda\mathcal{E}$ for all states $|\Psi\rangle$ in the image space $\mathbb{M}_+(\lambda)\oplus\mathbb{M}_-(\lambda)$ of $\mathcal{A}-\lambda\mathcal{E}$ (Theorem XI), i. e., for all states $|\Psi\rangle$ with $\mathcal{P}(\lambda)\,|\Psi\rangle = 0$. By Corollary XL and Theorem XLII, we obtain the following statement known as the Fredholm alternative:

■ THEOREM XLIX
Let λ be an isolated eigenvalue of the self-adjoint operator $\mathcal{A}$. Then the equation:

$$\mathcal{R}(\lambda)(\mathcal{A}-\lambda\,\mathcal{E})\,|\Psi\rangle \;=\; (\mathcal{A}-\lambda\,\mathcal{E})\mathcal{R}(\lambda)\,|\Psi\rangle \;=\; |\Psi\rangle \tag{A.177}$$

has solutions only for $\langle\Psi\,|\mathcal{P}(\lambda)|\,\Psi\rangle = 0$, where $\mathcal{P}(\lambda)$ denotes the projector onto the eigenspace of $\mathcal{A}$ with eigenvalue λ. In this case, a special solution $\mathcal{R}_{\mathrm{PV}}(\lambda)$ is given by the Cauchy principal value integral:

$$\mathcal{R}_{\mathrm{PV}}(\lambda) \;=\; \fint \frac{\mathrm{d}\Pi(\mu)}{\mu-\lambda} \tag{A.178}$$

and the general solution by $\mathcal{R}(\lambda) = \mathcal{R}_{\mathrm{PV}}(\lambda) + \mathcal{P}(\lambda)\mathcal{B}\mathcal{P}(\lambda)$. Here, $\mathcal{B}$ stands for an arbitrary operator. If $\mathcal{A}$ has non-degenerate spectrum, then this result simplifies to $\mathcal{R}(\lambda) = \mathcal{R}_{\mathrm{PV}}(\lambda) + \mu\,\mathcal{P}(\lambda)$, where μ presents some complex number.

Now, only the continuous spectrum remains to be discussed. We have already seen that no normalizable eigenstates of $\mathcal{A}$ exist within the continuous spectrum (Definition XVIII), i. e., there is no $|\Psi\rangle \in \mathbb{H}$ so that $(\mathcal{A}-\lambda\mathcal{E})\,|\Psi\rangle = 0$. On the other hand, we know that since $\mathcal{A}$ has been assumed densely defined (see the text following Definition VI), the product $|\chi\rangle = (\mathcal{A}-\lambda\mathcal{E})\,|\Psi\rangle$ exists on a subset of states $|\Psi\rangle$ dense in $\mathbb{H}$. Also, there is an infinite-dimensional space of states $|\Psi\rangle$ that populate the invariant subspace $\mathbb{M}(\lambda-\eta,\lambda+\eta)$ projected upon by the interval operator $\mathcal{I}(\lambda-\eta,\lambda+\eta)$ for any $\eta > 0$

[Theorem XVII, part (ii)]: $|\Psi\rangle = \mathcal{I}(\lambda-\eta,\lambda+\eta)\,|\Psi\rangle$. For such states, we clearly obtain the bound (Theorem XXII):

$$\left\langle \Psi \left| (\mathcal{A}-\lambda\mathcal{E})^2 \right| \Psi \right\rangle \;=\; \int_{\lambda-\eta}^{\lambda+\eta} (\mu-\lambda)^2 \,\mathrm{d}\,\langle \Psi\,|\Pi(\mu)|\,\Psi\rangle \;\leq\; \eta^2\;\langle\Psi|\Psi\rangle \tag{A.179}$$

Now we consider the inversion of this process. Introducing we note that the space $\mathbb{R}(\lambda)\subseteq\mathbb{H}$ of image states $|\chi\rangle = (\mathcal{A}-\lambda\mathcal{E})\,|\Psi\rangle$ covers the Hilbert space $\mathbb{H}$ again densely. (For otherwise, there would a state $\left|\chi^{\perp}\right\rangle$ orthogonal to all states $|\chi\rangle\in\mathbb{R}$, i. e., for all states $|\Psi\rangle$ in the domain $\mathbb{D}$ of $\mathcal{A}$, we would find $\left\langle\chi^{\perp}\,|\mathcal{A}-\lambda\mathcal{E}|\,\Psi\right\rangle = \left\langle\Psi\,|\mathcal{A}-\lambda\mathcal{E}|\,\chi^{\perp}\right\rangle^{*} = 0$, which implies that $\left|\chi^{\perp}\right\rangle$ is an eigenstate of $\mathcal{A}$ with eigenvalue λ. But we excluded this option by our Definition XVIII of the continuous spectrum of $\mathcal{A}$.)

Therefore, for a subset of states $|\chi\rangle$ dense in $\mathbb{H}$, the inverse linear transformation $|\Psi\rangle = \mathcal{R}(\lambda)\,|\chi\rangle$ is well-defined. This means that $\mathcal{R}(\lambda)$ is densely defined, and as $(\mathcal{A}-\lambda\mathcal{E})\mathcal{R}(\lambda)\,|\chi\rangle = (\mathcal{A}-\lambda\mathcal{E})\,|\Psi\rangle = |\chi\rangle$ for a dense subset of states $|\chi\rangle$ in the Hilbert space $\mathbb{H}$, we see that a resolvent operator $\mathcal{R}(\lambda)$ exists in the continuous spectrum of $\mathcal{A}$.

But $\mathcal{R}(\lambda)$ cannot be bounded. Choose again a state $|\Psi\rangle$ from the interval subspace $\mathbb{M}(\lambda-\eta,\lambda+\eta)$. Then, with $|\chi\rangle = (\mathcal{A}-\lambda\mathcal{E})\,|\Psi\rangle$ and $|\Psi\rangle = \mathcal{R}(\lambda)\,|\chi\rangle$ we obtain from (A.179):

$$\|\mathcal{R}(\lambda)\,|\chi\rangle\|^2 \;=\; \langle\Psi|\Psi\rangle \;\geq\; \frac{1}{\eta^2}\;\langle\chi|\chi\rangle \tag{A.180}$$

As $\eta\to 0^{+}$, $\|\mathcal{R}(\lambda)\,|\chi\rangle\|$ grows without bound.

Finally, we note that in the continuous spectrum, the Cauchy principal value integral $\mathcal{R}_{\mathrm{PV}}(\lambda)$ (A.178):

$$\mathcal{R}_{\mathrm{PV}}(\lambda) \;=\; \fint \frac{\mathrm{d}\Pi(\mu)}{\mu-\lambda} \;=\; \lim_{\eta\to 0^{+}} \left\{ \int_{-\infty}^{\lambda-\eta} + \int_{\lambda+\eta}^{\infty} \right\} \frac{\mathrm{d}\Pi(\mu)}{\mu-\lambda} \tag{A.181}$$

presents a possible choice for the resolvent operator $\mathcal{R}(\lambda)$, since according to (A.174) we have:

$$\mathcal{R}_{\mathrm{PV}}(\lambda)(\mathcal{A}-\lambda\mathcal{E}) \;=\; \lim_{\eta\to 0^{+}} \{\mathcal{E}-\mathcal{I}(\lambda-\eta,\lambda+\eta)\} \;=\; \mathcal{E} \tag{A.182}$$

as $\Pi(\lambda)$ is a continuous function. We may summarize these insights into the following theorem:

■ THEOREM L

If λ is a member of the continuous spectrum of the self-adjoint operator $\mathcal{A}$, then for the resolvent problem:

$$\mathcal{R}(\lambda)(\mathcal{A}-\lambda\,\mathcal{E}) \;=\; (\mathcal{A}-\lambda\,\mathcal{E})\mathcal{R}(\lambda) \;=\; \mathcal{E} \tag{A.183}$$

we find that a special hermitian solution is given by the Cauchy principal value integral:

$$\mathcal{R}_{\mathrm{PV}}(\lambda) \;=\; \fint \frac{\mathrm{d}\Pi(\mu)}{\mu - \lambda} \tag{A.184}$$

No solution $\mathcal{R}(\lambda)$ is bounded. If furthermore $\mathcal{A}$ possesses a differentiable non-degenerate spectrum, we additionally conclude that the set of all solutions $\mathcal{R}_\mu(\lambda)$ is given by:

$$\mathcal{R}_\mu(\lambda) \;=\; \mathcal{R}_{\mathrm{PV}}(\lambda) + \mu\,\mathcal{C}(\lambda) \tag{A.185}$$

where μ is an arbitrary complex number, and $\mathcal{C}(\lambda)$ denotes the orthonormal family of operators belonging to $\mathcal{A}$. The antisymmetric part of any solution $\mathcal{R}(\lambda)$ is a real multiple of $\mathcal{C}(\lambda)$:

$$\frac{1}{2i}\,\big\{\mathcal{R}(\lambda) - \mathcal{R}(\lambda)^+\big\} \;=\; \alpha\,\mathcal{C}(\lambda) \quad , \qquad \alpha \in \mathbb{R} \tag{A.186}$$

Proof. The statements (A.185) and (A.186) follow directly from Theorem XLII and Theorem XLIV, respectively. ∎

Advanced and retarded solutions. In the heuristic derivation presented in Section 2.3, we have explained how the propagator of the time-dependent Schrödinger equation $K_F(\mathbf{r}, t; \mathbf{r}', t')$ (2.8) may be employed to derive the Green function $G(\mathbf{r}, \mathbf{r}'; E)$ (2.12) for the corresponding time-independent problem. We now give a formal presentation of this subject in terms of operators.

For the moment, we return to the time-dependent inhomogeneous Schrödinger equation in its coordinate-independent form (A.16) for stationary Hamiltonian $\mathcal{H}$:

$$(i\hbar\partial_t - \mathcal{H})\,\mathcal{G}(t, t') \;=\; \mathcal{E}\,\delta(t - t') \tag{A.187}$$

Now it is easy to see that any Green function $\mathcal{G}(t, t')$ of the time-dependent problem (A.17) that solves (A.187) in turn generates a solution $\mathcal{R}(E)$ of the resolvent problem $(E\mathcal{E} - \mathcal{H})\mathcal{R}(E) = \mathcal{E}$ (note the customary change of sign in the eigenvalue problem) via the Fourier transform:

$$\mathcal{R}(E) \;=\; \int dt\, e^{iE(t-t')/\hbar}\,\mathcal{G}(t, t') \tag{A.188}$$

In Section A.2.2, we singled out two particularly simple members of the class of Green function operators, the advanced and retarded Green functions $\mathcal{G}_{\mathrm{adv}}(t, t')$, $\mathcal{G}_{\mathrm{ret}}(t, t')$

(A.21), (A.22) that vanish for $t > t'$ and $t < t'$, respectively. We now study the special resolvents $\mathcal{R}_{\rm adv}(E)$ and $\mathcal{R}_{\rm ret}(E)$ that are assigned to them by expression (A.188). It suffices to consider in detail $\mathcal{R}_{\rm ret}(E)$, the operator whose spatial representation yields the standard Green function $G(\mathbf{r},\mathbf{r}';E)$ (2.13) first introduced in Section 2.3. Using the spectral representation of the Green function operator $\mathcal{G}_{\rm ret}(t,t')$ (A.20), (A.77),

$$\mathcal{G}_{\rm ret}(t,t') \;=\; -\frac{i}{\hbar}\,\Theta(t-t')\int e^{-\,i\mu(t-t')/\hbar}\,{\rm d}\Pi(\mu) \tag{A.189}$$

we find from (A.188) introducing a small parameter $\eta \to 0^+$ in order to ensure convergence of the integration with respect to time $\tau = t - t'$ for the spectral representation of $\mathcal{R}_{\rm ret}(E)$:

$$\mathcal{R}_{\rm ret}(E) \;=\; -\frac{i}{\hbar}\int {\rm d}\Pi(\mu)\lim_{\eta\to 0^+}\left\{\int_0^\infty d\tau\, e^{i(E+i\eta)\tau/\hbar}\,e^{-\,i\mu\tau/\hbar}\right\} \;=\; \lim_{\eta\to 0^+}\int \frac{{\rm d}\Pi(\mu)}{E-\mu+i\eta} \tag{A.190}$$

In the same way, the relations (A.19) and (A.21) lead to the advanced solution of the resolvent problem:

$$\mathcal{R}_{\rm adv}(E) \;=\; \mathcal{R}_{\rm ret}(E)^+ \;=\; \lim_{\eta\to 0^+}\int \frac{{\rm d}\Pi(\mu)}{E-\mu-i\eta} \tag{A.191}$$

Employing the distribution relation [215] for any analytic test function $\phi(\mu)$:

$$\int \frac{\phi(\mu)\,d\mu}{E-\mu\pm i\eta} \;=\; \fint \frac{\phi(\mu)\,d\mu}{E-\mu} \;\mp\; i\pi\phi(E) \tag{A.192}$$

that is easily confirmed by shifting the paths of integration into the complex plane and using the theory of residues, one obtains for the resolvent operators $\mathcal{R}_{\rm ret}(E)$ and $\mathcal{R}_{\rm adv}(E)$:

$$\mathcal{R}_{\rm ret/adv}(E) \;=\; \fint \frac{{\rm d}\Pi(\mu)}{E-\mu} \;\mp\; i\pi\int \delta(E-\mu)\,{\rm d}\Pi(\mu) \tag{A.193}$$

If E belongs to the resolvent set of $\mathcal{H}$ (Definition XVIII), the imaginary term in (A.193) automatically vanishes, and one is led back to the unique bounded solution presented in Theorem XLVII. However, if E is a member of the continuous spectrum of $\mathcal{H}$ that we assume to be analytic (i. e., $\langle\Psi\,|\Pi(\mu)|\,\Psi\rangle$ is an analytic function for a subset of states $|\Psi\rangle$ dense in the Hilbert space $\mathbb{H}$) in a neighborhood of $\mu = E$, we may employ the density of states "operator" $\partial\Pi(E)/\partial E$ of Definition XXIII and find from (A.193) that the antisymmetric part of $\mathcal{R}_{\rm ret}(E)$ is given by $-\pi\,\partial\Pi(E)/\partial E$. If the spectrum of $\mathcal{H}$ is

non-degenerate, the resolvent operators $\mathcal{R}_{\mathrm{ret/adv}}(E)$ may be displayed as a function of the orthonormal family of operators $\mathcal{C}(E)$ associated with $\mathcal{H}$ (Theorem XXIX):

$$\mathcal{R}_{\mathrm{ret/adv}}(E) \;=\; \left\{ \sum_{\mathrm{p.s.}} + \fint_{\mathrm{c.s.}} d\mu \right\} \frac{\mathcal{C}(\mu)}{E-\mu} \;\mp\; i\pi\, \mathcal{C}(E) \tag{A.194}$$

The antisymmetric part of $\mathcal{R}_{\mathrm{ret/adv}}(E)$ is a multiple of the operator $\mathcal{C}(E)$, thus confirming the statement of Theorem XLIV. Summarizing, we find:

■ THEOREM LI
A particular solution $\mathcal{R}_{\mathrm{ret}}(E)$ to the resolvent problem:

$$(E\mathcal{E}-\mathcal{H})\mathcal{R}(E) \;=\; \mathcal{R}(E)(E\mathcal{E}-\mathcal{H}) \;=\; \mathcal{E} \tag{A.195}$$

for some self-adjoint operator $\mathcal{H}$ is obtained via the Laplace transform of the time evolution operator $\mathcal{U}(t-t')$. This retarded resolvent operator is given by:

$$\mathcal{R}_{\mathrm{ret}}(E) \;=\; -\frac{i}{\hbar} \lim_{\eta\to 0^+} \int_0^\infty d\tau\, e^{i(E+i\eta)\tau/\hbar}\, \mathcal{U}(\tau) \tag{A.196}$$

and its spectral decomposition reads:

$$\mathcal{R}_{\mathrm{ret}}(E) \;=\; \lim_{\eta\to 0^+} \int \frac{\mathrm{d}\Pi(\mu)}{E-\mu+i\eta} \tag{A.197}$$

If E is a member of the continuous spectrum of $\mathcal{H}$ which is furthermore analytic in a neighborhood of $\mu = E$, then $\mathcal{R}_{\mathrm{ret}}(E)$ may be displayed by the special solution (A.184) of Theorem L and the density of states operator:

$$\mathcal{R}_{\mathrm{ret}}(E) \;=\; \mathcal{R}_{\mathrm{PV}}(E) \;-\; i\pi\, \frac{\partial \Pi(E)}{\partial E} \tag{A.198}$$

Perturbations of the resolvent. Like in the case of time-dependent perturbations (Section A.2.3) we will deliver a brief exposition of the behavior of the resolvent operator $\mathcal{R}(E)$ when its inverse $E\mathcal{E}-\mathcal{H}_0$ is perturbed by introduction of an additional operator (the "potential") $\mathcal{V}$ of adjustable strength, $\mathcal{H}(\lambda) = \mathcal{H}_0 + \lambda\mathcal{V}$.

Obviously, the "correct" resolvent $\mathcal{R}_\lambda(E)$ of the perturbed operator $\mathcal{H}(\lambda)$ fulfils $\mathcal{R}_\lambda(E)[E\mathcal{E}-\mathcal{H}(\lambda)] = [E\mathcal{E}-\mathcal{H}(\lambda)]\mathcal{R}_\lambda(E) = \mathcal{E}$, i. e.,

$$(E\mathcal{E}-\mathcal{H}_0)\mathcal{R}_\lambda(E) \;=\; \mathcal{E} + \lambda\,\mathcal{V}\mathcal{R}_\lambda(E) \tag{A.199}$$

But the inverse operator to $E\mathcal{E} - \mathcal{H}_0$ is $\mathcal{R}_0(E)$, so by multiplying (A.199) by $\mathcal{R}_0(E)$ from the left, we obtain the expression:

$$\mathcal{R}_\lambda(E) \;=\; \mathcal{R}_0(E) + \lambda\,\mathcal{R}_0(E)\mathcal{V}\mathcal{R}_\lambda(E) \tag{A.200}$$

which resembles the integral equation (A.27) in the time-dependent case. Again, by repeatedly replacing $\mathcal{R}_\lambda(E)$ on the right-hand side in (A.200) by the entire expression we may formally expand $\mathcal{R}_\lambda(E)$ into a power series with respect to the perturbation strength λ:

$$\mathcal{R}_\lambda(E) \;=\; \mathcal{R}_0(E)\left\{\mathcal{E} + \lambda\,\mathcal{V}\mathcal{R}_0(E) + \lambda^2\left[\mathcal{V}\mathcal{R}_0(E)\right]^2 + \ldots\right\} \;=\; \mathcal{R}_0(E)\,\frac{\mathcal{E}}{\mathcal{E} - \lambda\,\mathcal{V}\mathcal{R}_0(E)} \tag{A.201}$$

Our knowledge of the properties of resolvent operators permits us to inquire into the convergence behavior of this series. Assume that the perturbation operator $\mathcal{V}$ is bounded, $\|\mathcal{V}\| < \infty$. If E is in the resolvent set of $\mathcal{H}_0$, then also $\mathcal{R}_0(E)$ is bounded (Theorem XLVII), and the series (A.201) converges within a finite circle $|\lambda| < 1/\,\|\mathcal{V}\mathcal{R}_0(E)\|$. If, however, E belongs to the continuous spectrum of $\mathcal{H}_0$, then $\|\mathcal{R}_0(E)\| = \infty$ (Theorem L), and the convergence radius of the formal series (A.201) is strictly zero. Still, (A.201) may be useful as an asymptotic series expression, and we will generally be content with the linear or Born approximation to $\mathcal{R}_\lambda(E)$:

$$\mathcal{R}_\lambda(E) \;\approx\; \mathcal{R}_0(E) + \lambda\,\mathcal{R}_0(E)\mathcal{V}\mathcal{R}_0(E) \tag{A.202}$$

For an extensive study of formal perturbation theory, see the monograph by Kato [228].

A.4 Remarks on Green Functions in One Dimension

Evidently, we developed the operator formalism presented in the preceding section with a very specific application in mind. Our interest obviously is directed onto the solutions $\psi_E(\mathbf{r})$ of the time-independent Schrödinger equation $[E - H(\mathbf{r},\mathbf{p})]\,\psi_E(\mathbf{r}) = 0$, where the Hamiltonian is given by a second-order linear partial differential operator $H(\mathbf{r},\mathbf{p} = -i\hbar\boldsymbol{\nabla}) = p^2/2M + U(\mathbf{r})$ [83]. As it is quite difficult to state properties of this partial differential equation which are generally valid, in particular if the potential $U(\mathbf{r})$ is anisotropic and does not settle down for large distances $r \to \infty$ (as it does in the case of field emission, $U(\mathbf{r}) = -\mathbf{r}\cdot\mathbf{F}$, that this treatise centers upon), we step down and consider the much simpler corresponding one-dimensional stationary

Schrödinger equation (which is sufficient for our purpose):

$$\left\{E + \frac{\hbar^2}{2M}\frac{\partial^2}{\partial x^2} - U(x)\right\}\psi_E(x) = 0 \tag{A.203}$$

The properties of the bounded solutions $\psi_E(x)$ of this second-order ordinary linear differential equation have been studied extensively in particular for potentials $U(x)$ which for large values of x quickly settle down to some limiting values: $U(x) \to U_\pm$ as $x \to \pm\infty$. The corresponding theory is nicely displayed in the textbook by Messiah [83]. Less known, at least to physicists, is the behavior of the solutions $\psi_E(x)$ in the case of potentials $U(x)$ which are asymptotically not bounded: $U(x) \to \pm\infty$ as $|x| \to \infty$. Clearly, the quantum mechanics of uniformly accelerated particles in one dimension is based upon a potential of this class: $U(x) = -Fx$. Therefore, this section is devoted to a study of the equation (A.203), its solutions $\psi_E(x)$, and the corresponding Green functions $G(x, x'; E)$ with particular attention directed to unbounded potentials $U(x)$. It will be seen that the results depend critically on the specific asymptotic properties of the potential function $U(x)$.

A.4.1 The Liouville-Green Approximation

Before we enter a detailed discussion of the characteristics of linear second-order ordinary differential equations, their connection to operator theory (Section A.3) and the corresponding Green functions $G(x, x'; E)$, we first need some knowledge of the properties of the eigenfunctions $\psi_E(x)$ of (A.203) in the asymptotic limits $x \to \pm\infty$. We naively expect that $\psi_E(x)$ drops off exponentially in tunneling regions with $E < U(x)$ and describes a particle traveling with classical velocity $v_{\rm cl}(x) = \sqrt{2[E - U(x)]/M}$ in sectors with $E > U(x)$. Indeed, this assertion holds for a wide class of potentials $U(x)$ and is advantageously applied in the Liouville-Green (LG) approximation to $\psi_E(x)$ (that in physics is better known as WKB approximation). It is based on the following theorem that we present in the form given by Olver in his monograph [235], p. 190–228:

■ THEOREM LII (LG APPROXIMATION)
Let $y_E(x)$ denote the set of solutions to the Schrödinger-type equation with real energy E:

$$\left\{\frac{\partial^2}{\partial x^2} + \frac{2M}{\hbar^2}[E - U(x)]\right\}y_E(x) = \left\{\frac{\partial^2}{\partial x^2} \pm k_E(x)^2\right\}y_E(x) = 0 \tag{A.204}$$

Let $a < x < \infty$ be an interval that contains no turning points of $y_E(x)$, i. e., no zeros of

the wave number $k_E(x)$. If the auxiliary function $F(x)$:

$$F(x) \;=\; \int_x^\infty \frac{d\xi}{k_E(\xi)^{1/2}} \left(\frac{\partial^2}{\partial \xi^2} \frac{1}{k_E(\xi)^{1/2}} \right) \tag{A.205}$$

is of bounded variation in $a < x < \infty$,

$$V(a) \;=\; \underset{a<x<\infty}{\mathrm{Var}}\; F(x) \;=\; \int_a^\infty d\xi \, |F'(\xi)| \;<\; \infty \tag{A.206}$$

then for $E < U(x)$ in $a < x < \infty$ there exists a pair of solutions $y_E^{(r)}(x)$, $y_E^{(i)}(x)$,

$$y_E^{(r,i)}(x) \;=\; \frac{1}{k_E(x)^{1/2}} \exp\left\{ \pm \int_a^x d\xi \, k_E(\xi) \right\} \cdot \left[1 + \epsilon_{r,i}(x) \right] \tag{A.207}$$

and for $E > U(x)$ in $a < x < \infty$ there exists a pair of solutions $y_E^{(+)}(x)$, $y_E^{(-)}(x)$,

$$y_E^{(\pm)}(x) \;=\; \frac{1}{k_E(x)^{1/2}} \exp\left\{ \pm i \int_a^x d\xi \, k_E(\xi) \right\} \cdot \left[1 + \epsilon_{\pm}(x) \right] \tag{A.208}$$

so that in any of these functions,

$$|\epsilon(x)| \;\leq\; \exp\left\{ V(a) \right\} - 1 \tag{A.209}$$

presents an error bound to the correction term $\epsilon(x)$ in $a < x < \infty$.

This theorem asserts that in asymptotic regions where $U(x)$ uniformly rises towards infinity, up to scaling exactly one bounded solution $y_E^{(r)}(x)$ of (A.203) exists which decays exponentially whereas all other solutions diverge. Since (A.203) obviously possesses just two linearly independent solutions, for $U(x) \to -\infty$ as $x \to \infty$ the existence of $y_E^{(\pm)}(x)$ implies that all solutions $y_E(x)$ are bounded in the sector $a < x < \infty$ and asymptotically vanish as $x \to \infty$. (In passing we note that for certain classes of potentials $U(x)$, Theorem LII fails as the error bound diverges for all a, $V(a) \to \infty$. For example, this failure occurs for all periodic potentials.)

A.4.2 When is a Simple Hamiltonian Self-Adjoint?

As usual, we now interpret the eigenvalue equation (A.203) as the spatial representation (A.105) of the eigenoperator equation $(E\mathcal{E} - \mathcal{H})\mathcal{C}_\Psi(E) = 0$ [Theorem XXVI, part (x)], where the eigenfunctions $\psi_E(x)$ are generated by a state $|\Psi\rangle$ in the Hilbert space $\mathbb{H}$ defined below via the orthonormal family of operators $\mathcal{C}_\Psi(E)$ assigned to $|\Psi\rangle$ (Definition XXV): $\psi_E(x)\psi_E(x')^* = \langle x \,|\mathcal{C}_\Psi(E)|\, x' \rangle$ (A.102), and the Hamiltonian $\mathcal{H}$ is

represented by the expression $\langle x\,|\mathcal{H}|\,x'\rangle = \delta(x-x')H(x,p)$ which is diagonal in configuration space. (We base our approach onto the orthonormal families $\mathcal{C}_\Psi(E)$ rather than directly on eigenstates of $\mathcal{H}$ as we want to include the continuous spectrum of $\mathcal{H}$ into the following discussion. For details, refer to Section A.3.4.) In quantum mechanics, particles correspond to normalizable wave packets $\phi(x,t)$ with $\int dx\,|\phi(x,t)|^2 < \infty$, hence physically sensible states are represented by square-integrable functions $\phi(x,t)$ which form the Hilbert space $\mathbb{H}$ of the problem. As $H(x,p)$ is obviously unbounded, not all square-integrable functions $\chi(x) = \langle x|\chi\rangle$ may serve as a "substrate" for the Hamiltonian $\mathcal{H}$ (for example, discontinuous functions or functions which drop off too slowly as $x \to \pm\infty$ are ruled out); however, there are arbitrary close "neighbour" functions $\tilde{\chi}(x)$ with $\|\chi - \tilde{\chi}\|^2 \to 0$ for which $(\partial_x^2 \pm k_E(x)^2)\,\tilde{\chi}(x)$ (A.204) represents itself a square-integrable function. Thus, $\mathcal{H}$ is indeed densely defined in the Hilbert space $\mathbb{H}$ of square-integrable functions. (See also the text following Definition VI.)

Often, the assumption is tacitly made that the operator kernel $H(x,p) = \partial_x^2 \pm k_E(x)^2$ is furthermore self-adjoint and consequently allows for an expansion of any square-integrable function $\chi(x)$ into the eigenfunctions of $H(x,p)$ (Theorem XXX). In the framework of the theory presented in Section A.3, completeness of the set of eigenfunctions requires that the spectrum of $\mathcal{H}$ either be non-degenerate, or $\mathcal{H}$ must be separable within a set of commuting operators with non-degenerate spectra. Both conditions are not self-evident and first must be verified for a given potential $U(x)$ in (A.203). In particular, there are quite simple potentials for which $H(x,p)$ is not self-adjoint, as we shall see now.

Non-degeneracy of the spectrum. Introducing, let us examine the question under which condition the spectrum of $\mathcal{H}$ is non-degenerate. The heuristic idea we pursue is that the irregular solution $y_E^{(i)}(x)$ (A.207) in the tunneling sector $E > U(x)$ of the Schrödinger equation (A.204) as an exponentially growing function cannot represent the eigenfunction $\psi_E(x)$ assigned to any orthonormal family $\mathcal{C}_\Psi(E)$ of $\mathcal{H}$. Indeed, we know that the matrix element $\langle\Phi\,|\mathcal{C}_\Psi(E)|\,\Phi\rangle = |\int dx\,\phi(x)^*\psi_E(x)|^2$ where $\phi(x) = \langle x|\Phi\rangle$ is some square-normalizable function is bounded by the corresponding matrix element of the density of states operator $\langle\Phi|\,\partial\Pi(E)/\partial E\,|\Phi\rangle$ [Theorem XXVI, part (ii)] which in turn is bounded for all E in the continuous spectrum of the operator $\mathcal{H}$ (Definition XXIII). But there are numerous wave functions $\phi(x)$ for which $\int dx\,\phi(x)^* y_E^{(i)}(x)$ diverges, but $\int dx\,|\phi(x)|^2$ exists (for example, divergence of the former integral is ensured whenever the wave function $\phi(x)$ drops off polynomially for large $|x|$, $\phi(x) \sim |x|^{-(1+\alpha)}$ as $|x| \to \infty$). Therefore, the wave function $y_E^{(i)}(x)$ (A.207) and thus all divergent solutions $y_E(x)$ of (A.204) do not represent proper eigenfunctions $\psi_E(x)$ of the Hamiltonian $\mathcal{H}$, but rather are spurious solutions for finite parts of the real axis and must be discarded. In other words: All eigenfunctions $\psi_E(x)$ of the operator $\mathcal{H}$ for both the point and continuous spectra are bounded.

Together with the properties of the LG approximation (Theorem LII) this clearly implies that the spectrum of $\mathcal{H}$ is non-degenerate if and only if $U(x) \to \infty$ in at least one of the asymptotic sectors $|x| \to \infty$. For the following, let us assume that $U(x) \to \infty$ as $x \to -\infty$; then, the spectrum is non-degenerate, and the eigenfunctions $\psi_E(x)$ of the Schrödinger equation (A.204), if they exist at all, are uniquely given as multiples of the regular function $y_E^{(r)}(x)$ (A.207) in $-\infty < x < a$ (where they vanish exponentially) and its continuation towards $x \to \infty$.

Self-adjointness of the Hamiltonian. It is a common assertion that the second-order linear differential operator $\partial_x^2 \pm k_E(x)^2$ (A.204) we are considering is hermitian for real energies E, which means that for any two states $|\Phi\rangle$, $|\Psi\rangle$ in the domain of the Hamiltonian $\mathcal{H}$ the symmetry relation $\langle\Phi|\mathcal{H}\Psi\rangle = \langle\mathcal{H}\Phi|\Psi\rangle$ must hold. In the spatial representation, by partial integration we find that this condition is equivalent to the requirement that the Wronskian determinant asymptotically vanishes for all "proper" wave functions $\phi(x) = \langle x|\Phi\rangle$, $\psi(x) = \langle x|\Psi\rangle$:

$$\lim_{\substack{b\to+\infty \\ a\to-\infty}} \int_a^b dx \, \left\{\phi(x)^* \left[\partial_x^2 \pm k_E(x)^2\right] \psi(x) - \psi(x) \left[\partial_x^2 \pm k_E(x)^2\right] \phi(x)^*\right\} = \\ = \lim_{\substack{b\to+\infty \\ a\to-\infty}} \left[\phi(x)^* \partial_x \psi(x) - \psi(x) \partial_x \phi(x)^*\right]_{x=a}^{x=b} = 0 \qquad \text{(A.210)}$$

Now it is an easy task to construct tentative "wave functions" $f(x)$, $g(x)$ whose Wronskian determinant does not vanish as $x \to \pm\infty$. Clearly, self-adjointness of $\mathcal{H}$ implies that such functions $f(x)$, $g(x)$ do not belong to the domain of $\mathcal{H}$, which means that either $f(x)$ or $[\partial_x^2 \pm k_E(x)^2]\, f(x)$ or the corresponding expressions for $g(x)$ are not normalizable. We will reverse the argument and examine under which conditions for the potential $U(x)$ normalizability of $f(x)$ and $[\partial_x^2 \pm k_E(x)^2]\, f(x)$ enforces the vanishing of the Wronskian in (A.210).

Let us note in advance that the Wronskian of $f(x)$, $g(x)$ may be expressed as a linear combination of "diagonal" elements $u_k(x)^* \partial_x u_k(x)$, where $u_{1,2}(x) = f(x) \pm g(x)$, and $u_{3,4}(x) = f(x) \pm i g(x)$. Thus, it suffices to work with diagonal expressions $u(x)^* \partial_x u(x)$. We therefore assume that there is a normalizable wave function $u(x)$ with $|u(x)^* \partial_x u(x)| > \epsilon > 0$ for all $a < x < \infty$, so that $v(x) = [\partial_x^2 \pm k_E(x)^2]\, u(x)$ is equally normalizable. If such a solution actually exists, then $\mathcal{H}$ cannot be self-adjoint. In the following, we will present a criterion for self-adjointness of $\mathcal{H}$ and sketch its derivation; a more careful account is given in the monograph by Titchmarsh [236], p. 107–128.

We remark that $u(x)^* \partial_x u(x) < \infty$ must be bounded in the asymptotic regimes $x \to \pm\infty$ since otherwise the difference of matrix elements calculated in (A.210) does not exist, and $u(x)$ is not an element of the Hilbert space, contrary to our assumption. Let

us now determine the following integral which must be finite since the constituting functions $u(x)$, $v(x) = [\partial_x^2 \pm k_E(x)^2]\, u(x)$ are assumed square integrable:

$$\lim_{b\to\infty} \int_a^b dx\, u(x)^* \left[\partial_x^2 \pm k_E(x)^2\right] u(x) \;=\; \lim_{b\to\infty} \left\{u(b)^* \partial_x u(b) - u(a)^* \partial_x u(a)\right\} \;- \int_a^\infty dx\; |u'(x)|^2 \;\pm\; \int_a^\infty dx\, k_E(x)^2\, |u(x)|^2 \;<\; \infty \quad \text{(A.211)}$$

As $|u(b)^* \partial_x u(b)| > 0$, but $u(b) \to 0$ (as $u(x)$ is assumed normalizable), $\partial_x u(b)$ tends towards infinity. Simultaneously, as the boundary terms in (A.211) are of finite size, the integral appearing in (A.211) must also be finite:

$$\left| \int_a^\infty dx\; \left\{ |\partial_x u(x)|^2 \;\mp\; k_E(x)^2\, |u(x)|^2 \right\} \right| \;<\; \infty \quad \text{(A.212)}$$

In the case of tunneling ($E < U(x)$), the positive sign applies in (A.212), and the integrand is non-negative. This however means that $\partial_x u(x)$ must vanish in the limit $x \to \infty$, which in turn implies $u(x)\partial_x u(x) \to 0$ as $x \to \infty$. This shows that the assertion (A.210) indeed holds for any pair of square-integrable functions $\phi(x)$, $\psi(x)$: If $U(x) \to \infty$ for $x \to \pm\infty$, then the Hamiltonian operator $H(x,p) = -\hbar^2 \partial_x^2 / 2M + U(x)$ is self-adjoint. The harmonic oscillator potential $U(x) = m\omega^2 x^2/2$ presents a well-known example.

The situation is slightly more complicated in the case of classically allowed motion, i. e., $E > U(x)$. Then, from (A.212) we may just infer that the integrand itself must vanish as $x \to \infty$. Assuming that $\partial_x u(x)$ indeed diverges for large x, this means that the contributions of the sum in (A.212) must nearly cancel: $|\partial_x u(x)| = k_E(x)|u(x)| + \mathcal{O}[u(x)]$. But then we find in the limit $x \to \infty$:

$$|u(x)|^2 \;\sim\; \frac{|u(x)\partial_x u(x)|}{k_E(x)} \;>\; \frac{\epsilon}{k_E(x)} \quad \text{(A.213)}$$

as we assumed that the modulus of the mixed product is bounded from below. Yet from the normalizability of $u(x)$, we have on the other hand the estimate:

$$\epsilon \int_a^\infty \frac{dx}{k_E(x)} \;<\; \int_a^\infty dx\; |u(x)|^2 \;<\; \infty \quad \text{(A.214)}$$

Clearly, this is only possible if the integral on the left-hand side exists, i. e., if the wave number $k_E(x)$ rises sufficiently quickly. If the integral is infinite, the product $u(x)\partial_x u(x)$ must again vanish as $x \to \infty$, which implies via (A.210) that the Hamiltonian $\mathcal{H}$ is self-adjoint. In the case that the condition (A.214) holds, (A.210) need not be fulfilled for every pair of square-integrable functions, and $\mathcal{H}$ indeed fails to be

self-adjoint. (We will give a physical explanation for this strange behavior later on.) Summarizing, we find:

■ THEOREM LIII
The Hamiltonian operator in one dimension $H(x,p) = -\hbar^2\partial_x^2/2M + U(x)$ is self-adjoint in the space of square-integrable functions $\psi(x)$ if the potential $U(x)$ fulfils the conditions of the LG approximation (Theorem LII) and belongs to one of the following classes:

(i). $U(x)$ is bounded from below, or

(ii). $U(x)$ fulfils the Weyl criterion: If $U(x) \to -\infty$ in one or both asymptotic sectors, then in the respective regions the condition:

$$\int_a^\infty \frac{dx}{\sqrt{E-U(x)}} \to \infty \quad , \qquad \int_{-\infty}^a \frac{dx}{\sqrt{E-U(x)}} \to \infty \tag{A.215}$$

must hold for all values of E.

As an example, the Hamiltonian $\mathcal{H}$ of the uniform field problem with $U(x) = -Fx$ is self-adjoint (see also Appendix D.2.3), whereas the Hamiltonian for the structurally similar potential $U(x) = -\beta x^3$ is not.

Properties of the spectrum. We now inquire into the nature of the spectrum of the Hamiltonian operator $\mathcal{H}$. In order to ensure non-degeneracy (see above), we restrict ourselves to the analysis of potentials $U(x)$ that diverge as x takes on large negative values: $U(x) \to \infty$ for $x \to -\infty$. Then, the spectral properties of $\mathcal{H}$ depend on the behavior of the potential $U(x)$ for large positive values of x. For our discussion, we turn our attention to the asymptotic properties of the eigenfunctions $\psi_E(x)$ as displayed in the LG approximation (Theorem LII).

We have already seen that all eigenfunctions $y_E(x)$ (A.204) of the Schrödinger equation that are not bounded are meaningless artifacts within the functional analysis approach to second-order linear differential equations. We used this restriction in order to show that the spectrum of $\mathcal{H}$ is non-degenerate if $U(x) \to \infty$ in one of the asymptotic sectors. Now, if $U(x) > E$ also in the region $x \to \infty$, the eigenfunction must be bounded for $x \to \pm\infty$. This is only possible if $\psi_E(x)$ is simultaneously a multiple of the regular solution $y^{(r)}_{E,-}(x)$ for $x \to -\infty$ and of the regular solution $y^{(r)}_{E,+}(x)$ for $x \to +\infty$ (A.207). Clearly, this means that an eigenfunction $\psi_E(x)$ of $\mathcal{H}$ only exists if the left-hand and right-hand regular solutions $y^{(r)}_{E,-}(x)$, $y^{(r)}_{E,+}(x)$ are linearly dependent. In this case, however, $\psi_E(x)$ drops exponentially for $x \to \pm\infty$, and is therefore normalizable: The function $\psi_E(x) = \langle x|\Psi\rangle$ is the spatial representation of an eigenstate $|\Psi\rangle$ of $\mathcal{H}$, and E is a member of the point spectrum of $\mathcal{H}$. As a criterion for the appearance of

an actual eigenstate of $\mathcal{H}$, we may conveniently use the Wronskian determinant of the left-hand and right-hand regular solutions [83]:

$$\mathcal{W}\left[y^{(r)}_{E,-}, y^{(r)}_{E,+}\right] \;=\; y^{(r)}_{E,-}(x)\partial_x y^{(r)}_{E,+}(x) - y^{(r)}_{E,+}(x)\partial_x y^{(r)}_{E,-}(x) \tag{A.216}$$

which is independent of x and vanishes only if both solutions are linearly dependent. $\mathcal{W}[y^{(r)}_{E,-}, y^{(r)}_{E,+}]/y^{(r)}_{E,-}(x)y^{(r)}_{E,+}(x)$ is for fixed argument x a continuous function of the energy E [83]; thus, the zeros of $\mathcal{W}[y^{(r)}_{E,-}, y^{(r)}_{E,+}]$ which correspond to the eigenvalues of $\mathcal{H}$ are discrete. Finally, we note that the point spectrum of $\mathcal{H}$ is bounded from below; if $E \leq \min U(x)$, then we obtain for the expectation value of $\mathcal{H}$ for any square-normalizable wave function $u(x)$:

$$\int dx\, u(x)\,[H(x,p) - E]\,u(x) \;=\; \int dx\, \left\{\frac{\hbar^2}{2M}\,|\partial_x u(x)|^2 + [U(x) - E]\,|u(x)|^2\right\} \;>\; 0 \tag{A.217}$$

This means that $u(x)$ cannot be an eigenfunction of $\mathcal{H}$ with energy E, so the point spectrum of the Hamiltonian is confined to the region $E > \min U(x)$.

Now we turn to the opposite case and assume that $\mathcal{H}$ is self-adjoint (Theorem LIII), but $E > U(x)$ as $x \to \infty$. Then, all solutions $y_E(x)$ of the Schrödinger equation (A.204) are bounded in the positive asymptotic region (A.208). This obviously implies that under these conditions an eigenfunction $\psi_E(x)$ of $\mathcal{H}$ always exists. Thus, we expect a continuous spectrum of non-normalizable eigenfunctions for classically allowed motion. To prove this assertion, we note that from the preceding paragraph we know that in the case of self-adjoint Hamiltonian $\mathcal{H}$, for all normalizable wave functions $u(x)$ the condition $u(x)\partial_x u(x) \to 0$ as $x \to \infty$ must hold. But for the eigenfunction $\psi_E(x)$ as a real combination of the asymptotic solutions $y^{(\pm)}_E(x)$ (A.208), we find in the asymptotic limit:

$$\begin{aligned}\psi_E(x)\partial_x\psi_E(x) \;&=\; \left[\alpha y^{(+)}_E(x) + \alpha^* y^{(-)}_E(x)\right]\, ik_E(x)\left[\alpha y^{(+)}_E(x) - \alpha^* y^{(-)}_E(x)\right] \\ &\sim\; -\,2\,|\alpha|^2\,\sin\left\{\int_a^x d\xi\, k_E(\xi) \,+\, 2\delta(E)\right\}\end{aligned} \tag{A.218}$$

where $\delta(E)$ denotes some real scattering phase. As $|\alpha|^2 > 0$, the eigenfunction $\psi_E(x)$ cannot be normalizable in the strict sense, and rather represents the spatial representation (A.102) of the orthonormal family $\mathcal{C}(E)$ of $\mathcal{H}$ in the continuous spectrum of the Hamiltonian. (See Section A.3.4.) We may summarize:

■ THEOREM LIV

Let $\mathcal{H}$ be the Hamiltonian operator in one dimension assigned to the potential $U(x)$ which shall be amenable to a treatment in terms of the LG approximation (Theorem

LII). Let also $U(x) \to \infty$ as $x \to -\infty$. Then, we find for the spectrum of the Hamiltonian operator $\mathcal{H}$:

(i). If $U(x)$ is bounded by U_0 from below, then $\mathcal{H}$ is self-adjoint and bounded by U_0 from below. The spectrum of $\mathcal{H}$ is non-degenerate. If the potential settles down to a finite value $U(x) \to U_1$ as $x \to \infty$, then a point spectrum of $\mathcal{H}$ may exist which is confined to the interval $U_0 < E \leq U_1$. The continuous spectrum of $\mathcal{H}$ covers the interval $U_1 < E < \infty$. If $U(x) \to \infty$ is unbounded as $x \to \infty$, then only a pure point spectrum exists (oscillator case).

(ii). If $U(x) \to -\infty$ as $x \to \infty$ and the Weyl criterion (A.215) holds, then $\mathcal{H}$ is self-adjoint, its spectrum is non-degenerate and continuous in $-\infty < E < \infty$. No point spectrum exists.

(iii). If $U(x) \to -\infty$ as $x \to \infty$ and the Weyl criterion (A.215) fails, then $\mathcal{H}$ is not self-adjoint. All eigenfunctions $\psi_E(x)$ of $\mathcal{H}$ are bounded, and the point spectrum of $\mathcal{H}$ covers the entire complex E plane.

Proof. Only part (iii) remains to be proven. We refer to Titchmarsh [236], p. 125. See also (A.239) and the following text in Section A.4.3. ■

Physical interpretation. We have seen that the properties of the Hamiltonian $\mathcal{H}$ critically depend upon the convergence of the integral (A.215). Clearly, this mathematical feature should find some counterpart in the physical picture of quantum theory. A rather intellegible approach rests upon the temporal evolution of states $|\Psi(t)\rangle$.

Evidently, for motion in common potentials $U(x)$, the particle number $\langle\Psi(t)|\Psi(t)\rangle$ in the system presents a conserved quantity. Since the state $|\Psi(t)\rangle$ is propagated in time by the time evolution operator $\mathcal{U}(t,t')$, conservation of probability $\langle\Psi(t)|\Psi(t)\rangle = \langle\Psi\,|\mathcal{U}(t,0)^{+}\mathcal{U}(t,0)|\,\Psi\rangle = \langle\Psi|\Psi\rangle$ implies that $\mathcal{U}(t,t')$ is a unitary operator. As $\mathcal{U}(t,t') = \exp[-i\mathcal{H}(t-t')/\hbar]$ (A.15), unitarity of the evolution of states is linked to the self-adjointness of the generating operator $\mathcal{H}$, $\mathcal{H}^{+} = \mathcal{H}$.

Now, what happens if $U(x) \to -\infty$ as $x \to \infty$, and the Weyl criterion (A.215) does not hold? For this case, we note that the classical time of flight $\tau_{\rm cl}(a,b)$ between the positions a and b:

$$\tau_{\rm cl}(a,b) \;=\; \int_a^b \frac{dx}{v_{\rm cl}(x)} \;=\; \frac{m}{\hbar}\int_a^b \frac{dx}{k_E(x)} \tag{A.219}$$

remains finite even as $b \to \infty$ (A.214): In such potentials, classical particles are accelerated that strongly that they cover infinite distances in finite time $\tau_{\rm cl}(a,\infty) < \infty$. Via the Ehrenfest theorem [83], one may show that the same property is valid for quantum wave packets $\chi(x,t)$ which leave any finite spatial interval, so $\langle\chi(t)|\chi(t)\rangle$ is a function

of time t. For such a system, $\mathcal{U}(t,t')$ cannot present a unitary operator which confirms our mathematical result that $\mathcal{H}$ is not self-adjoint (Theorem LIII).

Nevertheless, there are arbitrarily many eigenfunctions $\psi_E(x)$ for such a Hamiltonian operator [Theorem LIV, part (iii)] which all represent stationary states. But every physical state $\chi(x,t)$ of this system decays in time, so the set of mathematical eigenfunctions $\psi_E(x)$ does not represent any physical state of the system! This example shows that one has to be careful in transferring results of "conventional" scattering theory to systems with unbounded potentials $U(x)$. But within this section, we have also shown that the ordinary technique of eigenstate expansions holds for the linear potential $U(x) = -Fx$ that is of central importance to the main part of this work.

A.4.3 Basic Properties of the Green Function

In the preceding section, we established quite general conditions for the potential function $U(x)$ that lead to a self-adjoint Hamiltonian operator $\mathcal{H}$ with non-degenerate spectrum, which we further characterized above. Following the general course displayed in Section A.3, we now turn our attention to the inverse operator to the Hamiltonian, the resolvent operator $\mathcal{R}(E)$ which is defined via $(E\mathcal{E}-\mathcal{H})\mathcal{R}(E) = \mathcal{R}(E)(E\mathcal{E}-\mathcal{H}) = \mathcal{E}$ (A.157). The Green function $G(x,x';E)$ is simply the spatial representation of the resolvent operator $\mathcal{R}(E)$, $G(x,x';E) = \langle x\,|\mathcal{R}(E)|\,x'\rangle$. Therefore, the Green function solves the inhomogeneous one-dimensional Schrödinger equation (A.156):

$$\{E - H(x,p)\}\; G(x,x';E) \;=\; \delta(x-x') \tag{A.220}$$

We already discussed general properties of the resolvent $\mathcal{R}(E)$ in Section A.3.6; in particular, we have proven that this operator exists for all values of E except those in the point spectrum of $\mathcal{H}$ (Theorems XLV, XLVII and L). Furthermore, $\mathcal{R}(E)$ is bounded and unique if E is a member of the resolvent set (Theorems XLV and XLVII), whereas all operators $\mathcal{R}(E)$ are unbounded and densely defined in $\mathbb{H}$ if E is in the continuous spectrum of $\mathcal{H}$ (Theorem L). Assuming that the Hamiltonian $\mathcal{H}$ shows a non-degenerate spectrum, we conclude from Theorem L that any two solutions $\mathcal{R}_{1,2}(E)$ differ only by a multiple of the orthonormal family $\mathcal{C}(E)$ associated to $\mathcal{H}$. We now will use these properties in order to establish a representation of the Green function $G(x,x';E)$ in terms of the eigenfunctions $y_E(x)$ (A.204) of the Hamiltonian $H(x,p)$.

The fundamental Green function. Since the spatial representation of the operator $\langle x\,|\mathcal{C}(E)|\,x'\rangle = \psi_E(x)\psi_E(x')^*$ (A.102) just involves the normalized eigenfunctions $\psi_E(x)$ of the continuous spectrum of $\mathcal{H}$, we may concentrate onto a special solution of the Green function problem. From Section A.3.6, we infer that such a solution for all E

outside the point spectrum of $\mathcal{H}$ is given by the Cauchy principal value integral (A.184) (see Theorems XLV, XLVII and L):

$$G_f(x,x';E) \;=\; \langle x\,|\mathcal{R}_{\mathrm{PV}}(E)|\,x'\rangle \;=\; \fint \frac{\mathrm{d}\,\langle x\,|\Pi(\mu)|\,x'\rangle}{E-\mu} \tag{A.221}$$

which we call the fundamental Green function of the problem (A.204). (If E is in the resolvent set of $\mathcal{H}$, (A.221) is indeed the only solution to the resolvent problem.) Assuming that the spectrum of the Hamiltonian is non-degenerate, we may expand $\mathcal{R}_{\mathrm{PV}}(E)$ into the orthonormal family $\mathcal{C}(E)$ (Theorem XXIX) and thus $G_f(x,x';E)$ into the set of normalized eigenfunctions of $\mathcal{H}$:

$$G_f(x,x';E) \;=\; \left\{\sum_{\text{p.s.}} + \fint_{\text{c.s.}} d\mu\right\} \frac{\langle x\,|\mathcal{C}(\mu)|\,x'\rangle}{E-\mu} \;=\; \left\{\sum_{\text{p.s.}} + \fint_{\text{c.s.}} d\mu\right\} \frac{\psi_\mu(x)\psi_\mu(x')}{E-\mu} \tag{A.222}$$

In (A.222), we used the fact that the normalized eigenfunctions $\psi_E(x)$ of $\mathcal{H}$ are defined only up to a phase factor in order to choose real solutions of the Schrödinger equation (A.203), a differential equation with real coefficients.

Basic properties. From (A.220)–(A.222), a number of important properties of the fundamental Green function $G_f(x,x';E)$ for Hamiltonians with non-degenerate spectra may be inferred fairly easily. We gather them into the following theorem:

■ THEOREM LV

Let $\mathcal{H}$ denote a self-adjoint Hamiltonian operator in a single dimension, $H(x,p) = -\hbar^2\partial_x^2/2M + U(x)$ with a potential function $U(x)$ that allows treatment in the framework of the LG approximation (Theorem LII) and diverges in the left-hand asymptotic sector: $U(x) \to \infty$ as $x \to -\infty$, thus ensuring non-degeneracy of the spectrum (Theorem LIV). Then, the fundamental Green function $G_f(x,x';E)$ shows the following features:

(i). $G_f(x,x';E)$ is real, symmetric and continuous at $x = x'$:

$$G_f(x,x';E) \;=\; G_f(x',x;E) \;=\; G_f(x,x';E)^* \tag{A.223}$$

(ii). $G_f(x,x';E)$ is everywhere bounded

(iii). There exist two solutions $y_{E,-}(x)$ and $y_{E,+}(x)$ of the Schrödinger equation (A.204) that are bounded as $x \to -\infty$ and $x \to \infty$, respectively, so that:

$$G_f(x,x';E) \;=\; \begin{cases} y_{E,-}(x)\,y_{E,+}(x') & (x < x') \\ y_{E,-}(x')\,y_{E,+}(x) & (x > x') \end{cases} \tag{A.224}$$

(iv). The Wronskian determinant of the solutions $y_{E,-}(x)$, $y_{E,+}(x)$ is fixed:

$$\mathcal{W}\left[y_{E,-}, y_{E,+}\right] \;=\; y_{E,-}(x)\partial_x y_{E,+}(x) - y_{E,+}(x)\partial_x y_{E,-}(x) \;=\; \frac{2M}{\hbar^2} \tag{A.225}$$

(v). If E is contained in the continuous spectrum, then we may set $y_{E,-}(x) = \psi_E(x)$ in parts (iii), (iv). Furthermore, one has the "orthogonality condition":

$$\int_{-\infty}^{\infty} dx\, \psi_E(x)\, G_f(x, x'; E) \;=\; 0. \tag{A.226}$$

Proof. Part (i) immediately follows from expression (A.222). For the following parts, let us note that the inhomogeneous Schrödinger equation (A.220) implies that $G_f(x, x'; E)$ is itself a solution of the standard Schrödinger equation (A.203) in the sectors $x < x'$ and $x > x'$. The form (A.224) stated in part (iii) automatically incorporates continuity of $G_f(x, x'; E)$ at $x = x'$.

To prove part (ii), we remark that $G_f(x, x'; E)$ may only be unbounded if the irregular, exponentially growing solutions $y_E^{(i)}(x)$ (A.207) of the Schrödinger equation (A.204) are involved in the representation (A.224). Let us consider the case that E is in the resolvent set of $\mathcal{H}$; then $\mathcal{R}_{\rm PV}(E)$ is a bounded operator (Theorem XLVII), and $\mathcal{R}_{\rm PV}(E)\,|\Phi\rangle$ must be bounded for all states in $\mathbb{H}$ representing square-integrable functions $\phi(x) = \langle x|\Phi\rangle$. Thus, $|\int dx\, \phi(x)^* y_{E,\pm}(x)|^2 < \infty$ must hold for all square-integrable functions, which is not true if one of the functions $y_{E,\pm}(x)$ is exponentially growing in an asymptotic sector (see Section A.4.2). But all other solutions $y_E(x)$ of (A.204) are bounded. This proof equally holds for the continuous spectrum, where $\mathcal{R}_{\rm PV}(E)$ becomes unbounded. (Note that the issue of boundedness of $G_f(x, x'; E)$ only arises in tunneling sectors with $U(x) > E$; in asymptotic regions of classically allowed motion, all solutions $y_E(x)$ of the Schrödinger equation (A.204) are bounded anyway (A.208), thus also $G_f(x, x'; E)$ (A.224) is bounded there.)

Proposition (iv) follows if we integrate by parts the inhomogeneous equation (A.220) with respect to x over an infinitesimal interval $x' - \eta < x < x' + \eta$, where $\eta \to 0^+$. Using the representation (A.224), this procedure yields:

$$\frac{\hbar^2}{2M} \lim_{\eta\to 0^+} \frac{\partial}{\partial x} \left\{G_f(x = x' + \eta, x'; E) - G_f(x = x' - \eta, x'; E)\right\} \;=\; \frac{\hbar^2}{2M}\, \mathcal{W}\left[y_{E,-}, y_{E,+}\right] \;=\; 1 \tag{A.227}$$

Finally, to show part (v) we note that $\psi_E(x)$ apart from scaling presents the only bounded solution of (A.204) as $x \to -\infty$, which implies $y_{E,-}(x) = \mu\psi_E(x)$ (A.207). A peek on (A.224) reveals that we may even fix $\mu = 1$. The second statement relies on the orthonormality property of the (real) eigenfunctions $\psi_E(x)$. From (A.106) and (A.222), we obtain:

$$\begin{aligned} \int dx\, \psi_E(x)\, G_f(x, x'; E) \;&=\; \lim_{\eta\to 0^+} \left\{\int_{-\infty}^{E-\eta} + \int_{E+\eta}^{\infty}\right\} \frac{d\mu\, \psi_\mu(x')}{E - \mu} \int_{-\infty}^{\infty} dx\, \psi_\mu(x)\psi_E(x) \\ &=\; \lim_{\eta\to 0^+} \left\{\int_{-\infty}^{E-\eta} + \int_{E+\eta}^{\infty}\right\} \frac{d\mu\, \psi_\mu(x')}{E - \mu}\, \delta(E - \mu) \;=\; 0 \end{aligned} \tag{A.228}$$

uniformly as $\eta \to 0^+$. ∎

A.4.4 The Green Function in the Resolvent Set

We are now going to determine the Green function $G_f(x,x';E)$ (A.222) in terms of the eigenfunctions $y_E(x)$ of (A.204) for self-adjoint Hamiltonians with non-degenerate spectrum. Let us first suppose that E is a member of the resolvent set, i. e., the spectral family $\Pi(\mu)$ shall be constant in a neighborhood of E (Definition XVIII). Then, the resolvent operator $\mathcal{R}(\mathcal{E})$ is bounded and unique (Theorem XLVII), and the same properties hold for $G(x,x';E)$ [Theorem LV, part (ii)].

An explicit construction rests upon the representation (iii) of Theorem LV. Theorem LIV, part (i) tells us that the resolvent set of $\mathcal{H}$ is limited to energies E with $E < U(x)$ as $U(x) \to \pm\infty$; thus, apart from scaling, bounded regular solutions $y_{E,\pm}(x)$ in the asymptotic regimes $x \to \pm\infty$ according to the LG approximation (Theorem LII) are given uniquely by the functions $\psi^{(r)}_{E,\pm}(x)$ (A.207). Finally, the Wronskian condition [Theorem LIV, part (iv)] completely fixes the Green function:

$$G(x,x';E) \;=\; \frac{2M}{\hbar^2}\,\frac{\psi^{(r)}_{E,-}(x_<)\,\psi^{(r)}_{E,+}(x_>)}{\mathcal{W}\left[y^{(r)}_{E,-}, y^{(r)}_{E,+}\right]} \tag{A.229}$$

where we introduced the abbreviations $x_< = \min(x,x')$, $x_> = \max(x,x')$. Note that $G(x,x';E)$ diverges whenever the Wronskian of the left-hand side and right-hand side regular solutions $\psi^{(r)}_{E,-}(x)$, $\psi^{(r)}_{E,+}(x)$ vanishes. But then, both functions are multiples of a normalizable and globally regular eigenfunction $\psi_E(x)$ of the Hamiltonian, so E is a member of the point spectrum of $\mathcal{H}$, and $\mathcal{R}(E)$ fails to exist (Theorem XLVIII). See also the text following (A.216).

A.4.5 Results for the Continuous Spectrum

Next, we consider the case where E is in the continuous spectrum of the self-adjoint Hamiltonian $\mathcal{H}$, which we again enforce to be non-degenerate by setting $U(x) \to \infty$ as $x \to -\infty$ (Theorem LV). We know that in this case the Green function $G(x,x';E)$ is no longer unique; however, for non-degenerate spectrum, any two solutions to (A.220) differ only by a multiple of the orthonormal family (Theorem L), the spatial representation of which is a product of eigenfunctions of $\mathcal{H}$: $\langle x\,|\mu\,\mathcal{C}(E)|\,x'\rangle \;=\; \mu\,\psi_E(x)\psi_E(x')$ (A.102). Thus, knowledge of the fundamental Green function $G_f(x,x';E)$ (A.221) is sufficient for the construction of all possible Green functions of the problem, including the retarded Green function $G(x,x';E) = \langle x\,|\mathcal{R}_{\rm ret}(E)|\,x'\rangle$ (A.198) of Theorem LI upon which source theory is based.

The irregular solution. Let us now construct $G_f(x,x';E)$ for the continuous case. From Theorem LV, parts (i), (iii), and (v), we infer that $G_f(x,x';E)$ may be displayed

as a product of the (real) normalized eigenfunction $\psi_E(x)$ of $\mathcal{H}$ with some special real solution $\varphi_E(x)$ of the corresponding Schrödinger equation (A.203):

$$G_f(x,x';E) \;=\; \psi_E(x_<)\,\varphi_E(x_>) \tag{A.230}$$

Here, we set again $x_< = \min(x,x')$, $x_> = \max(x,x')$. The particular solution $\varphi_E(x)$ is known as the solution of the second kind or irregular solution of (A.203), since under the conditions of Theorem LV, it must grow without bound in the tunneling sector $x \to -\infty$. (For $x \to \infty$, it is bounded like all other solutions $y_E(x)$ of (A.204).)

We shall see that the asymptotic character of the eigenfunction $\psi_E(x)$ as $x \to \infty$ completely fixes the behavior of the irregular solution $\varphi_E(x)$ in this sector. Indeed, the asymptotics of $\psi_E(x)$, $\varphi_E(x)$ as $x \to \infty$ are characterized by a single real parameter, the scattering phase $\delta(E)$ of the system, as we shall elaborate now.

For $x \to \infty$, the LG approximation (Theorem LII) states that any solution to the Schrödinger equation may be expressed by a linear combination of ingoing and outgoing waves $y_E^{(\pm)}(x)$ (A.208):

$$y_E^{(\pm)}(x) \;\sim\; \frac{1}{k_E(x)^{1/2}}\,\exp\left\{\pm i\int_a^x d\xi\, k_E(\xi)\right\} \tag{A.231}$$

Since both the regular and irregular solutions $\psi_E(x)$, $\varphi_E(x)$ in (A.230) are real, within the asymptotic sector $x \to \infty$ they are special linear combinations of the functions $y_E^{(\pm)}(x)$ (A.231):

$$\begin{aligned}\psi_E(x) \;&=\; \sqrt{\frac{M}{2\hbar^2}}\,\left\{\alpha y_E^{(+)}(x) + \alpha^* y_E^{(-)}(x)\right\}\\ \varphi_E(x) \;&=\; \sqrt{\frac{M}{2\hbar^2}}\,\left\{\beta y_E^{(+)}(x) + \beta^* y_E^{(-)}(x)\right\}\end{aligned} \tag{A.232}$$

Here, α and β are complex parameters that depend on the energy E as well as the cut-off a chosen in (A.231). We now aim to express these coefficients in terms of the scattering phase $\delta(E)$ using general properties of the functions $\psi_E(x)$ and $\varphi_E(x)$.

The Wronskian relation. First, let us examine the Wronskian relation of these functions. It is easy to check that the Wronskian determinant of the complex "waves" $y_E^{(\pm)}(x)$ (A.231) is independent of x: $\mathcal{W}[y_E^{(+)}, y_E^{(-)}] = -2i$. Thus, from (A.232) one finds for the (spatially constant) Wronskian of the regular and irregular solutions in the limit $x \to \infty$:

$$\mathcal{W}\left[\psi_E, \varphi_E\right] \;=\; \frac{M}{2\hbar^2}\,(\alpha\beta^* - \alpha^*\beta)\,\mathcal{W}\left[y_E^{(+)}, y_E^{(-)}\right] \;=\; -\frac{iM}{\hbar^2}\,(\alpha\beta^* - \alpha^*\beta) \tag{A.233}$$

By comparison with Theorem LV, part (iv) we conclude that $\alpha\beta^* - \alpha^*\beta = 2i$ must hold.

Orthonormality of the eigenfunction. In the second step, we employ the orthonormality relation for the regular wave functions $\psi_E(x)$ (A.106). In the continuous spectrum, for real $\psi_E(x)$ we have:

$$\int_{-\infty}^{\infty} dx\, \psi_E(x)\psi_{E'}(x) \;=\; \delta(E-E') \tag{A.234}$$

Clearly, this implies a restriction on the parameter α in (A.232). To find it, we note that the integrand in (A.234) may be expressed as the derivative of the Wronskian of both eigenfunctions [83], as is easily verified employing the Schrödinger equation (A.203):

$$\frac{\partial}{\partial x}\,\mathcal{W}\left[\psi_E(x),\psi_{E'}(x)\right] \;=\; \frac{2M}{\hbar^2}\,(E-E')\,\psi_E(x)\psi_{E'}(x) \tag{A.235}$$

Because both $\psi_E(x)$, $\psi_{E'}(x)$ exponentially vanish as $x \to -\infty$ (Section A.4.2), so does the Wronskian there, and we find for any b,

$$\int_{-\infty}^{b} dx\, \psi_E(x)\psi_{E'}(x) \;=\; \frac{\hbar^2}{2M}\,\frac{\mathcal{W}\left[\psi_E(b),\psi_{E'}(b)\right]}{E-E'} \tag{A.236}$$

For large $b \to \infty$, we obviously may evaluate this integral using the asymptotic expression (A.232) for the eigenfunction $\psi_E(x)$ in the limit $x \to \infty$. This is particularly simple if $U(x) \to -\infty$ as $x \to \infty$, like in the case of field emission. (The following results hold, however, equally for potentials $U(x)$ bounded from below.)

The calculation involves Wronskians of the type $\mathcal{W}[y_E^{(+)}(b), y_{E'}^{(\pm)}(b)]$ (A.231) for large values of b near the transition $E = E'$. Using the relation $\partial_E k_E(x) = M/\hbar^2 k_E(x)$, one obtains after a short calculation that the contribution for equally oriented waves is approximately given by:

$$\mathcal{W}[y_E^{(+)}(b), y_{E'}^{(+)}(b)] \;\sim\; \frac{i}{2}\,\frac{E'-E}{E-U(b)}\,\exp\left\{2i\int_a^b d\xi\, k_E(\xi)\right\} \tag{A.237}$$

which vanishes for $E \to E'$ as it must be, and approaches zero as $b \to \infty$. Of greater interest are the mixed Wronskians that yield for sufficiently small difference in energy $E - E'$:

$$\mathcal{W}[y_E^{(+)}(b), y_{E'}^{(-)}(b)] \;\sim\; -2i\,\exp\left\{i\,(E-E')\,\frac{M}{\hbar^2}\int_a^b \frac{d\xi}{k_E(\xi)}\right\} \tag{A.238}$$

Now we may employ these auxiliary results in order to obtain from the representation (A.232) of $\psi_E(x)$ the asymptotical behavior of the overlap integral (A.236) as $E \to E'$ and $b \to \infty$:

$$\int_{-\infty}^{b} dx\, \psi_E(x)\psi_{E'}(x) \;\sim\; \frac{|\alpha|^2}{E-E'}\,\sin\left\{(E-E')\,\frac{M}{\hbar^2}\int_a^b \frac{d\xi}{k_E(\xi)}\right\} \tag{A.239}$$

From this expression, we infer that for $b \to \infty$, the overlap integral does not vanish for $E \to E'$ and remains bounded for $E = E'$ if the Weyl condition (A.215) is violated, i. e., the integral:

$$\gamma(b) \;=\; \frac{M}{\hbar^2} \int_a^b \frac{d\xi}{k_E(\xi)} \tag{A.240}$$

appearing in (A.239) remains finite even for $b \to \infty$. In this case, the eigenfunctions $\psi_E(x)$ of $\mathcal{H}$ are square-integrable, but not orthogonal, and E is a member of the point spectrum of the Hamiltonian $\mathcal{H}$ which cannot be self-adjoint, in agreement with the assertions of Theorems LIII and LIV.

Thus, we find that $\gamma(b)$ is unbounded as $b \to \infty$, and the sine term oscillates ever more rapidly. In order to see what expression (A.239) means in this case, we employ a regular test function $\chi(E)$ and estimate as $\gamma(b) \to \infty$:

$$\begin{aligned}\int_{-\infty}^{\infty} dE\, \chi(E) \int_{-\infty}^{b} dx\, \psi_E(x)\psi_{E'}(x) \;&\sim\; |\alpha|^2 \int_{-\infty}^{\infty} dE\, \chi(E)\, \frac{\sin\{\gamma(b)(E-E')\}}{E-E'} \\ &=\; |\alpha|^2 \int_{-\infty}^{\infty} \frac{du}{u} \sin u\; \chi\left(E' + \frac{u}{\gamma(b)}\right) \;\sim\; |\alpha|^2\, \chi(E') \int_{-\infty}^{\infty} \frac{du}{u} \sin u \;=\; \pi\, |\alpha|^2\, \chi(E')\end{aligned} \tag{A.241}$$

Here, we used Dirichlet's integral formula $\int \sin u\, du/u = \pi$ [188]. On the other hand, we infer from the orthonormality condition for eigenfunctions (A.234) that the integral (A.241) must yield $\chi(E')$. By comparison, we obtain a condition on the modulus of α: $|\alpha|^2 = 1/\pi$.

The orthogonality condition. Finally, to gain a second relation between α and β, we may exploit the orthogonality condition stated in Theorem LV, part (v) which requires that as $b \to \infty$, for the regular and irregular solutions $\psi_E(x)$ and $\varphi_E(x)$ (A.230) the relation:

$$\begin{aligned}\int_{-\infty}^{b} dx\, \psi_E(x)\, \psi_E(x_<)\, \varphi_E(x_>) \;=\; \varphi_E(x') \int_{-\infty}^{x'} dx'\, \psi_E(x)^2 \;+ \\ \psi_E(x') \int_{x'}^{b} dx\, \psi_E(x)\, \varphi_E(x) \;\to\; 0\end{aligned} \tag{A.242}$$

must hold for all x'. Since the first integral in (A.242) is manifestly finite, this condition implies that for any b, c in the asymptotic sector $x \to \infty$, according to (A.236) the integral:

$$\int_c^b dx\, \psi_E(x)\, \varphi_E(x) \;=\; \frac{\hbar^2}{2M} \frac{\partial}{\partial E} \Big[\mathcal{W}\left[\psi_E(b), \varphi_{E'}(b)\right] - \mathcal{W}\left[\psi_E(c), \varphi_{E'}(c)\right]\Big]_{E=E'} \tag{A.243}$$

must be bounded. (Here, we took advantage of the fact that $\varphi_E(x)$ is a solution of the Schrödinger equation (A.203).) Inserting the asymptotic expressions (A.232) for $\psi_E(x)$ and $\varphi_E(x)$, and using the auxiliary results (A.237) and (A.238), we find for the Wronskian of the regular and irregular functions $\mathcal{W}[\psi_E(b), \varphi_{E'}(b)]$ for large values of b in the limit $E \to E'$:

$$\mathcal{W}[\psi_E(b), \varphi_{E'}(b)] \sim \frac{M}{\hbar^2} \{(\alpha\beta^* + \alpha^*\beta) \sin[\gamma(b)(E - E')] - i(\alpha\beta^* - \alpha^*\beta) \cos[\gamma(b)(E - E')]\} \quad \text{(A.244)}$$

which is in agreement with our former result (A.233). (Here, $\gamma(b)$ again denotes the integral (A.240) which diverges as $b \to \infty$.) From this expression, we immediately may calculate the overlap integral (A.243) and obtain in the asymptotic sector:

$$\int_c^b dx\, \psi_E(x)\, \varphi_E(x) \sim \frac{1}{2} (\alpha\beta^* + \alpha^*\beta) [\gamma(b) - \gamma(c)] \quad \text{(A.245)}$$

Since $\gamma(b) - \gamma(c) \to \infty$ as $b - c \to \infty$, finiteness of the integral (A.245) in the limit $b \to \infty$ requires that the first factor vanishes. Hence, the orthogonality condition [Theorem LV, part (v)] enforces the relation $\alpha\beta^* + \alpha^*\beta = 0$.

Scattering phase representation. We now may combine the three conditions we found for the coefficients α and β in (A.232). Clearly, we have $\alpha^*\beta = -i$, and consequently $\beta/\alpha = -i/|\alpha|^2 = -i\pi$: The coefficients α and β of the regular and irregular solutions of the Schrödinger equation (A.203) in the asymptotic sector are in constant proportion and of fixed modulus: $|\alpha|^2 = 1/\pi$, $|\beta|^2 = \pi$.

These properties become clearer in a modulus-phase representation of α, β. Let $\alpha = \exp[i\delta(E)]/i\sqrt{\pi}$; then, we obtain from (A.231) and (A.232):

■ THEOREM LVI
In the sector of validity of the LG approximation, the regular and irregular solutions $\psi_E(x)$, $\varphi_E(x)$ of the Schrödinger equation have the following asymptotic form as $x \to \infty$:

$$\psi_E(x) \sim \sqrt{\frac{2M}{\pi\hbar^2}} \frac{1}{k_E(x)^{1/2}} \sin\left\{\int_a^x d\xi\, k_E(\xi) + \delta(E)\right\}$$
$$\varphi_E(x) \sim -\sqrt{\frac{2\pi M}{\hbar^2}} \frac{1}{k_E(x)^{1/2}} \cos\left\{\int_a^x d\xi\, k_E(\xi) + \delta(E)\right\} \quad \text{(A.246)}$$

Here, $\delta(E)$ represents a generalized scattering phase which depends on the potential $U(x)$ (and on the cut-off a, of course).

Since $\sin(z - \pi/2) = -\cos z$, (A.246) implies that the phase of the irregular solution $\varphi_E(x)$ in the asymptotic regime $x \to \infty$ lags by $\pi/2$ behind the phase of the regular solution $\psi_E(x)$.

A.4.6 Hankel Solutions and the Retarded Green Function

From the results of the preceding section one easily may rebuild the wave functions (A.231) we started from—solutions which ultimately behave as an outgoing (ingoing) wave in the asymptotic limit $x \to \infty$. Adopting the custom in the related theory of Bessel functions [81,188], we denote these functions as the Hankel solutions $h_E^{(\pm)}(x)$ of the Schrödinger equation (A.203). From the asymptotic forms of $\psi_E(x)$ and $\varphi_E(x)$ (Theorem LVI), we conclude that outgoing-wave solutions are given by:

$$h_E^{(\pm)}(x) \;=\; \varphi_E(x) \mp i\pi\, \psi_E(x) \tag{A.247}$$

They are proportional to the LG solutions $y_E^{(\pm)}(x)$ (A.208) of the differential equation (A.204), and we find for their asymptotic behavior:

$$h_E^{(\pm)}(x) \;=\; -\sqrt{\frac{2\pi M}{\hbar^2}}\, y_E^{(\pm)}(x) \;\sim\; -\sqrt{\frac{2\pi M}{\hbar^2}}\, \frac{1}{k_E(x)^{1/2}}\, \exp\left\{ \pm i \left[\int_a^x d\xi\, k_E(\xi) \,+\, \delta(E) \right] \right\} \tag{A.248}$$

Obviously, we may in turn express the regular and irregular solutions $\psi_E(x)$, $\varphi_E(x)$ of the Schrödinger equation by the Hankel solutions (A.247):

$$\begin{aligned} \varphi_E(x) \;&=\; \frac{1}{2} \left[h_E^{(+)}(x) + h_E^{(-)}(x) \right] \\ \psi_E(x) \;&=\; \frac{i}{2\pi} \left[h_E^{(+)}(x) - h_E^{(-)}(x) \right] \end{aligned} \tag{A.249}$$

The Hankel solutions come in handy when determining the retarded and advanced Green functions assigned to the Schrödinger equation (A.203). For the corresponding resolvent operators, we found in Section A.3.6 that $\mathcal{R}_{\text{ret/adv}}(E) = \mathcal{R}_{\text{PV}}(E) \mp i\pi\, \mathcal{C}(E)$ (A.194) where $\mathcal{C}(E)$ denotes the orthonormal family assigned to the Hamiltonian $\mathcal{H}$. The Green functions are just the spatial representations of these operators, so we obtain from (A.102), (A.221) and (A.230):

$$\begin{aligned} G_{\text{ret/adv}}(x, x'; E) \;&=\; \langle x \,|\mathcal{R}_{\text{PV}}(E)|\, x' \rangle \;\mp\; i\pi\, \langle x \,|\mathcal{C}(E)|\, x' \rangle \\ &=\; \psi_E(x_<)\, \varphi_E(x_>) \;\mp\; i\pi\, \psi_E(x)\, \psi_E(x') \end{aligned} \tag{A.250}$$

Obviously, this expression may be rewritten in terms of the Hankel functions $h_E^{(\pm)}(x)$ (A.247):

■ THEOREM LVII

The retarded/advanced Green functions $G_{\rm ret}(x,x';E)$ $[G_{\rm adv}(x,x';E)]$ possess the following representation in terms of the Hankel functions (outgoing/ingoing wave solutions) $h_E^{(\pm)}(x)$:

$$G_{\rm ret/adv}(x,x';E) \;=\; \psi_E(x_<)\, h_E^{(\pm)}(x_>) \tag{A.251}$$

where $x_< = \min(x,x')$ and $x_> = \max(x,x')$.

A.5 Properties of Multipole Green Functions

In this section, we turn our attention to a mathematical justification of the multipole source approach introduced in Section 2.4. There, we noticed that solutions of Laplace's differential equation with definite angular momentum, the multipole potentials $\Phi_{lm}(\mathbf{r}-\mathbf{r}')$ with $\Phi_{lm}(\mathbf{R}) = R^{-(l+1)}Y_{lm}(\hat{R})$ (2.19) well known from electrostatics [84], are generated by special pointlike sources with implicit angular orientation, the multipole sources $\delta_{lm}(\mathbf{r}-\mathbf{r}') = K_{lm}[\partial/\partial\mathbf{r}']\delta(\mathbf{r}-\mathbf{r}')$ (2.23) obtainable from the conventional delta function singularity $\delta(\mathbf{r}-\mathbf{r}')$ by means of differentiation with respect to the source location $\mathbf{r}'$ (2.20)–(2.23):

$$\begin{aligned} \Delta\,\Phi_{lm}(\mathbf{r},\mathbf{r}') \;&=\; -\,\frac{4\pi}{(2l-1)!!}\,\delta_{lm}(\mathbf{r}-\mathbf{r}') \\ \Phi_{lm}(\mathbf{r},\mathbf{r}') \;&=\; -\,\frac{4\pi}{(2l-1)!!}\,K_{lm}\left(\frac{\partial}{\partial\mathbf{r}'}\right) G(\mathbf{r},\mathbf{r}') \end{aligned} \tag{A.252}$$

Here, $G(\mathbf{r},\mathbf{r}') = -1/4\pi|\mathbf{r}-\mathbf{r}'|$ denotes the Green function of potential theory. By analogy, we introduced multipole solutions of the inhomogeneous Schrödinger equation (2.24), the multipole Green functions $G_{lm}(\mathbf{r},\mathbf{r}';E)$ (2.25):

$$\begin{aligned} \left\{E + \frac{\hbar^2}{2M}\Delta \;-\; U(\mathbf{r})\right\} G_{lm}(\mathbf{r},\mathbf{r}';E) \;&=\; \delta_{lm}(\mathbf{r}-\mathbf{r}') \\ G_{lm}(\mathbf{r},\mathbf{r}';E) \;&=\; K_{lm}\left(\frac{\partial}{\partial\mathbf{r}'}\right) G(\mathbf{r},\mathbf{r}';E) \end{aligned} \tag{A.253}$$

By definition, the multipole Green function $G_{lm}(\mathbf{r},\mathbf{r}';E)$ is a spherical tensor gradient of the ordinary stationary Schrödinger Green function $G(\mathbf{r},\mathbf{r}';E)$ (2.12). Appealing to common sense, we claimed that the multipole Green function $G_{lm}(\mathbf{r},\mathbf{r}';E)$ which we defined in a purely mathematical manner in (A.253) indeed shows the desired physical behavior of (lm) spherical symmetry in the vicinity of the source $\mathbf{r} \to \mathbf{r}'$, even if the potential $U(\mathbf{r})$ explicitly breaks rotational symmetry. (This manifestly has been the case for the uniform field problem $U(\mathbf{r}) = -Fz$ which we considered in Chapter 5.) So far, the multipole character of $G_{lm}(\mathbf{r},\mathbf{r}';E)$ has only been proven for

the simple problem of free quantum motion, where $G_{lm}^{(\mathrm{free})}(\mathbf{r},\mathbf{r}';E)$ reduces to the (lm) partial wave of the scattering problem [see formula (C.17) in Appendix C.1]. In fact, the original multipole potential $\Phi_{lm}(\mathbf{r},\mathbf{r}')$ in (A.252) may be viewed as a special case of the free-particle source problem (Appendix C.1.2).

The purpose of this section is to extend the proof of the multipole character of $G_{lm}(\mathbf{r},\mathbf{r}';E)$ to a wide class of potentials which comprises all functions $U(\mathbf{r})$ that are analytic in a neighborhood of the source position $\mathbf{r}'$. (Note that there are important examples of the Schrödinger equation where this assumption fails, including the Coulomb problem $U(\mathbf{r}) = \alpha/|\mathbf{r}-\mathbf{r}'|$.) For such potentials $U(\mathbf{r})$, we may exploit general analycity properties of differential equations like the potential and Schrödinger equations (A.252), (A.253) which state that all solutions to these equations may be expanded into a power series except at the singularity $\mathbf{r} = \mathbf{r}'$ (Section A.5.1). The major part of the current section is devoted to an extension of this theory to the neighborhood of this singularity. In a quite technical proof, we establish that for all locally regular potentials $U(\mathbf{r})$, the corresponding ordinary Green functions $G(\mathbf{r},\mathbf{r}';E)$ share a common underlying structure, and we even provide a formal series expansion for these functions (Section A.5.2). Using these intermediary results, it is but a simple task to verify the multipole character of the derived Green functions $G_{lm}(\mathbf{r},\mathbf{r}';E)$ (A.253). This is done in Section A.5.3. Some conclusions that follow for the assigned partial multipole currents $J_{lml'm'}(\mathbf{r}';E)$ defined in Section 2.4 are stated in the final section of this chapter.

A.5.1 Notes on Elliptic Differential Equations

Unlike the far-field properties of scattering wave functions [230], the local behavior of the wave function solutions $\psi(\mathbf{r})$ to the homogeneous Schrödinger equation apparently has found little attention in the physics community. Our considerations, however, require specific knowledge of the characteristics of $\psi(\mathbf{r})$ in the vicinity of sources. Fortunately, some general properties of the wave function have been established in the course of mathematical studies of linear partial differential equations, and we will cite the relevant statement (Theorem LIX) below. (For its proof, we refer to the monograph by Hörmander [237], p. 177.) Let us start out with the notion of an elliptic differential operator.

■ DEFINITION LVIII

Let $D(r_k,\partial/\partial r_k)f(\mathbf{r}) = \sigma(\mathbf{r})$ be a linear partial differential equation with the differential operator $D(r_k,\partial/\partial r_k)$ which is assumed to be a polynomial of ν.th order in the derivatives $\partial_{r_1},\ldots,\partial_{r_D}$:

$$D(r_k,\partial/\partial r_k) = \sum_{\mu=0}^{\nu} \sum_{\alpha_1+\ldots+\alpha_D=\mu} P^{(\mu)}_{\alpha_1,\ldots,\alpha_D}(\mathbf{r}) \frac{\partial^\mu}{\partial r_1^{\alpha_1}\cdot\ldots\cdot\partial r_D^{\alpha_D}} \tag{A.254}$$

If its homogeneous part $D_\nu(r_k, \partial/\partial r_k)$ of maximum order ν in the derivatives:

$$D_\nu(r_k, \partial/\partial r_k) \;=\; \sum_{\alpha_1+\ldots+\alpha_D\,=\,\nu} P^{(\nu)}_{\alpha_1,\ldots,\alpha_D}(\mathbf{r})\,\frac{\partial^\nu}{\partial r_1^{\alpha_1}\cdot\ldots\cdot\partial r_D^{\alpha_D}} \tag{A.255}$$

fulfils with the replacement $\xi_k = \partial/\partial r_k$ the following relation for all $\mathbf{r} \in \mathbb{S}$, where $\mathbb{S}$ denotes a sector of the D–dimensional configuration space,

$$D_\nu(r_k, \xi_k) \;=\; 0 \qquad \Longrightarrow \qquad \xi^2 \;=\; \sum_{k\,=\,1}^{D} \xi_k^2 \;=\; 0 \tag{A.256}$$

then the differential operator $D(r_k, \partial/\partial r_k)$ is called elliptic in $\mathbb{S}$.

As an example, we note that for both the Lagrangian and Hamiltonian operators Δ, $H(\mathbf{r}, \mathbf{p})$ in (A.252) and (A.253), $\nu = 2$, and apart from prefactors, $D_2(r_k, \partial/\partial r_k) = \Delta$. Therefore, $D_\nu(r_k, \xi_k) = \xi^2$, and both differential operators are elliptic everywhere. The situation is somewhat different for the equation:

$$\left\{R^2\Delta_{\mathbf{R}} - 2\,\mathbf{R}\cdot\boldsymbol{\nabla}_{\mathbf{R}} + R^2 w(\mathbf{R})\right\} f(\mathbf{R}) \;=\; 0 \tag{A.257}$$

whose close relation to the inhomogeneous Schrödinger equation (2.12) we will soon reveal. For the differential equation (A.257), obviously $D_2(R_k, \xi_k) = R^2\xi^2$, so the condition (A.256) holds everywhere except at the origin $\mathbf{R} = \mathbf{o}$: The equation (A.257) is elliptic for all $\mathbf{R} \neq \mathbf{o}$. Ellipticity of a differential operator brings about a strong restriction of the solution set of the corresponding linear equation, as the following theorem shows:

■ THEOREM LIX
Let $D(r_k, \partial/\partial r_k)$ be an elliptic differential operator in the sector $\mathbb{S} \subseteq \mathbb{R}^D$ with coefficient functions $P^{(\mu)}_{\alpha_1,\ldots,\alpha_D}(\mathbf{r})$ which are analytic in $\mathbb{S}$. If $f(\mathbf{r})$ is a solution of the inhomogeneous linear equation:

$$D(r_k, \partial/\partial r_k) f(\mathbf{r}) \;=\; \sigma(\mathbf{r}) \tag{A.258}$$

where $\sigma(\mathbf{r})$ is also analytic in $\mathbb{S}$, then $f(\mathbf{r})$ is analytic in $\mathbb{S}$.

Essentially, this theorem states that if all coefficent functions $P^{(\mu)}_{\alpha_1,\ldots,\alpha_D}(\mathbf{r})$, $\sigma(\mathbf{r})$ involved in (A.258) are locally regular, then every solution $f(\mathbf{r})$ may be expanded in a convergent power series in $r_1, \ldots, r_D$. From the foregoing examples, we see that all solutions to the inhomogeneous Schrödinger equation (2.11):

$$\left\{E + \frac{\hbar^2}{2M}\,\Delta - U(\mathbf{r})\right\} \psi_\sigma(\mathbf{r}; E) \;=\; \sigma(\mathbf{r}) \tag{A.259}$$

are globally (locally) analytic, if the potential $U(\mathbf{r})$ and the source term $\sigma(\mathbf{r})$ have this property. Setting $\sigma(\mathbf{r}) \equiv 0$, we find in particular that for analytic $U(\mathbf{r})$, all solutions $\psi_E(\mathbf{r})$ of the homogeneous stationary Schrödinger equation are analytic. If we are willing to exclude the singularity at $\mathbf{r} = \mathbf{r}'$ from the sector $\mathbb{S}$, the same property holds for the multipole Green functions $G_{lm}(\mathbf{r}, \mathbf{r}'; E)$ (A.253). In the same vein, all solutions $f(\mathbf{R})$ of equation (A.257) are at least locally analytic for $R > 0$, provided $w(\mathbf{R})$ is an analytic function in a neighborhood of $\mathbf{R} = \mathbf{o}$. Thus, the question arises how these solutions may be continued in the singular points $\mathbf{r} = \mathbf{r}'$ and $\mathbf{R} = \mathbf{o}$, respectively. This is the topic of the following section.

A.5.2 Analycity Properties of the Green Function

Let us now study the local behavior of the conventional Green function $G(\mathbf{r}, \mathbf{r}'; E)$ assigned to the stationary Schrödinger equation, which is a special solution to the differential equation:

$$\left\{ E + \frac{\hbar^2}{2M} \Delta - U(\mathbf{r}) \right\} g(\mathbf{r}, \mathbf{r}'; E) \;=\; \delta(\mathbf{r} - \mathbf{r}') \tag{A.260}$$

In the following, we shall show that the set of solutions $g(\mathbf{r}, \mathbf{r}'; E)$, which also includes the Green functions $G(\mathbf{r}, \mathbf{r}'; E)$, bears a consistent structure in the vicinity of the point-like singularity at $\mathbf{r} = \mathbf{r}'$, provided only that $U(\mathbf{r})$ may be expanded into a convergent power series in the neighborhood of $\mathbf{r}'$. This development requires rather involved calculations, so we will adopt a step-by-step approach.

Motivation. In order to recognize a joint pattern in the solutions of (A.260), it is advisable to examine the Green functions of those few model potentials $U(\mathbf{r})$ that allow for a closed-form solution $G(\mathbf{r}, \mathbf{r}'; E)$. For this purpose, we use the Green function of the free-particle problem $G^{(\mathrm{free})}(\mathbf{r}, \mathbf{r}'; E)$ (C.5) of Appendix C [which, as a special case, also contains the Green function of potential theory, $G(\mathbf{r}, \mathbf{r}') = -1/4\pi|\mathbf{r} - \mathbf{r}'|$ if we set $E = 0$ and $\hbar^2 = 2M$ in (A.260)], and the Green function of the uniform field problem $U(\mathbf{r}) = -Fz$ (5.18) which we derived in Section 5.2. (This selection probably exhausts the class of potentials $U(\mathbf{r})$ in three spatial dimensions which permit to construct $G(\mathbf{r}, \mathbf{r}'; E)$ in explicit form for all values of $\mathbf{r}$, $\mathbf{r}'$, and E.) Let us now expand these functions into a power series in $\mathbf{r}$ and $\mathbf{r}'$. For the retarded Green function of free particle motion ($U \equiv 0$), we easily find from (C.5):

$$G^{(\mathrm{free})}(\mathbf{r}, \mathbf{r}'; E) \;=\; -\frac{M}{2\pi\hbar^2} \frac{e^{ik|\mathbf{r}-\mathbf{r}'|}}{|\mathbf{r} - \mathbf{r}'|} \;=\; -\frac{M}{2\pi\hbar^2} \frac{\cos(k|\mathbf{r} - \mathbf{r}'|)}{|\mathbf{r} - \mathbf{r}'|} \;-\; \frac{iMk}{2\pi\hbar^2} \frac{\sin(k|\mathbf{r} - \mathbf{r}'|)}{k|\mathbf{r} - \mathbf{r}'|}$$

$$= -\frac{M}{2\pi\hbar^2}\frac{1}{|\mathbf{r}-\mathbf{r}'|}\left\{1-\frac{1}{2}k^2(\mathbf{r}-\mathbf{r}')^2+\frac{1}{24}k^4(\mathbf{r}-\mathbf{r}')^4-\ldots\right\}- \frac{iMk}{2\pi\hbar^2}\left\{1-\frac{1}{6}k^2(\mathbf{r}-\mathbf{r}')^2+\frac{1}{120}k^4(\mathbf{r}-\mathbf{r}')^4-\ldots\right\} \tag{A.261}$$

Here, $k^2 = 2ME/\hbar^2$, and $\Im[k] > 0$ is required to obtain a bounded solution for $E < 0$. In the case of ballistic motion in a homogeneous force field environment, a fairly cumbersome calculation starting from the expression (5.18) yields:

$$\begin{aligned}
G(\mathbf{r},\mathbf{r}';E) &= \frac{M}{2\hbar^2}\frac{1}{|\mathbf{r}-\mathbf{r}'|}\left[\mathrm{Ci}(\alpha_+)\,\mathrm{Ai}'(\alpha_-)-\mathrm{Ci}'(\alpha_+)\,\mathrm{Ai}(\alpha_-)\right] \\
&= -\frac{M}{2\pi\hbar^2}\frac{1}{|\mathbf{r}-\mathbf{r}'|}\left\{1-2\beta^3F^2\left[2E+F(z+z')\right](\mathbf{r}-\mathbf{r}')^2+\right. \\
&\qquad \left.\frac{2}{3}\beta^6F^4\left[2E+F(z+z')\right]^2(\mathbf{r}-\mathbf{r}')^4-\ldots\right\}- \\
&\quad \frac{M\beta F}{\hbar^2}\left\{\left[\mathrm{Ai}'(\epsilon)\,\mathrm{Ci}'(\epsilon)+\beta\left[2E+F(z+z')\right]\mathrm{Ai}(\epsilon)\,\mathrm{Ci}(\epsilon)\right]\times\right. \\
&\qquad \left[1-\frac{2}{3}\beta^3F^2\left[2E+F(z+z')\right](\mathbf{r}-\mathbf{r}')^2\right]- \\
&\qquad \frac{1}{6}\beta^2F^2\left[\mathrm{Ai}(\epsilon)\,\mathrm{Ci}'(\epsilon)+\mathrm{Ai}'(\epsilon)\,\mathrm{Ci}(\epsilon)\right]\left[3(z+z')^2-(\mathbf{r}-\mathbf{r}')^2\right]+ \\
&\qquad \frac{1}{3}\beta^3F^3\left[\mathrm{Ai}'(\epsilon)\,\mathrm{Ci}'(\epsilon)-\beta\left[2E+F(z+z')\right]\mathrm{Ai}(\epsilon)\,\mathrm{Ci}(\epsilon)\right]\times \\
&\qquad \left.(z+z')\left[(z+z')^2-(\mathbf{r}-\mathbf{r}')^2\right]+\mathcal{O}(r_k^4)\right\}
\end{aligned} \tag{A.262}$$

Here, $\alpha_\pm = -\beta[2E+F(z+z')\pm F|\mathbf{r}-\mathbf{r}'|]$ (5.19), and as usual, we employed the inverse energy parameter β defined via $\beta^3 = M/4\hbar^2F^2$ (5.16), and the dimensionless energy parameter $\epsilon = -2\beta E$ (5.22).

The conjecture. Let us now emphasize some properties common to the expansions (A.261) and (A.262). We note that neither expansion represents an analytic function; rather, it seems that $G(\mathbf{r},\mathbf{r}';E)$ may be split into two parts that allow for a resolution into power series in the form:

$$G(\mathbf{r},\mathbf{r}';E) = -\frac{M}{2\pi\hbar^2}\frac{f(\mathbf{r},\mathbf{r}';E)}{|\mathbf{r}-\mathbf{r}'|}+h(\mathbf{r},\mathbf{r}';E) \tag{A.263}$$

Here, $h(\mathbf{r},\mathbf{r}';E) = h(\mathbf{r}',\mathbf{r};E)$ represents an analytic function in $\mathbf{r}$ which is invariant under exchange of the positions $\mathbf{r}$ and $\mathbf{r}'$ (and thus is also analytic in $\mathbf{r}'$). As (A.262) tells us, $h(\mathbf{r},\mathbf{r}';E)$ may be vastly complicated even for a simple linear potential $U(\mathbf{r}) = -Fz$. The structure of the second function $f(\mathbf{r},\mathbf{r}';E)$ in (A.263) is even more restricted; besides being symmetric and analytic in $\mathbf{r}$ (and $\mathbf{r}'$), $f(\mathbf{r},\mathbf{r}';E)$ appears to be real, and the leading terms of its power series expansion are fixed:

$$f(\mathbf{r},\mathbf{r}';E) \;=\; f(\mathbf{r},\mathbf{r}';E)^* \;=\; f(\mathbf{r}',\mathbf{r};E) \;=\; 1 - \frac{M[E-U(\mathbf{o})]}{\hbar^2}\,(\mathbf{r}-\mathbf{r}')^2 + \mathcal{O}(r_k^3) \quad \text{(A.264)}$$

In comparison to the expansion of $h(\mathbf{r},\mathbf{r}';E)$ in (A.262), the complexity of the Taylor series coefficients of $f(\mathbf{r},\mathbf{r}';E)$ appears notably reduced.

The decisive step in the proof of the conjecture stated in (A.263) and (A.264) consists in showing that a solution of the differential equation (A.260) in the form (A.263) actually exists. For this purpose, we will further simplify this ansatz and verify that for a locally analytic potential $U(\mathbf{r})$, a special solution $g_{\mathrm{sp}}(\mathbf{r},\mathbf{r}';E)$ of (A.260) is available that may be represented by:

$$g_{\mathrm{sp}}(\mathbf{r},\mathbf{r}';E) \;=\; -\frac{M}{2\pi\hbar^2}\,\frac{f(\mathbf{r},\mathbf{r}';E)}{|\mathbf{r}-\mathbf{r}'|} \quad \text{(A.265)}$$

where $f(\mathbf{r},\mathbf{r}';E)$ is locally analytic in $\mathbf{r}$. As $f(\mathbf{r},\mathbf{r}';E)$ turns out to be unique, the connection to (A.263) is rather straightforward. In order to prove (A.265), however, we first have to provide some statements of mathematical nature. These technical preliminaries are given below.

Mathematical preparations. We first present several useful mathematical relations which are neither widely known nor easily extracted from tables [81]. The first two deal with factorials, whereas the third one provides an estimate for sums over harmonic polynomials $Y_{lm}(\Omega)$ and is easily proven using the methods of Appendix B.2.

■ COROLLARY LX

For all integer $k \geq 0$, the inequality holds:

$$\frac{1}{2}\sqrt{\frac{\pi}{k+1}} \;<\; \frac{2^k k!}{(2k+1)!!} \;<\; \frac{1}{2}\sqrt{\frac{\pi}{k+1/2}} \quad \text{(A.266)}$$

Proof. Let us first replace the factorials in (A.266) by Gamma functions [81]. Obviously, we have $(2n-1)!!/2^n(n-1)! = \Gamma(2n)/2^{2n-1}\Gamma(n)^2$. In the next step, we apply a truncated series expansion of the logarithm $\ln\Gamma(n)$ of the Gamma function (for its proof, see the monograph by Olver [235], p. 293):

$$\ln\Gamma(z) \;=\; \left(z-\frac{1}{2}\right)\ln z - z + \ln\sqrt{2\pi} + \frac{1}{12\,z} - \frac{\vartheta(z)}{360\,z^3} \quad \text{(A.267)}$$

Here, z denotes a positive real variable, and in the remainder term, $0 < \vartheta(z) < 1$ holds. This implies an estimate for the desired product. Upon simplification, we find:

$$\ln\left(\frac{(2n-1)!!}{2^n(n-1)!}\right) = \ln\sqrt{\frac{n}{\pi}} - \frac{1}{8n} + \frac{\tilde{\vartheta}(n)}{180\,n^3} \tag{A.268}$$

Here, we obtain for the remainder term the bound $-1/16 < \tilde{\vartheta}(n) < 1$. Clearly, for $n \geq 1$ the asymptotic series in (A.268) delivers a negative contribution. For the second inequality, we replace $\sqrt{n}$ by $\sqrt{n-1/2}$ and note that $\ln(1-z) < -z$ holds for $0 < z < 1$ as the logarithm is a convex function. Thus, we find successively from (A.268) for $n \geq 1$:

$$\begin{aligned}\ln\left(\frac{(2n-1)!!}{2^n(n-1)!}\right) &= \ln\sqrt{\frac{n-1/2}{\pi}} - \frac{1}{2}\ln\left(1-\frac{1}{2n}\right) - \frac{1}{8n} + \frac{\tilde{\vartheta}(n)}{180\,n^3} \\ &> \ln\sqrt{\frac{n-1/2}{\pi}} + \frac{1}{8n} - \frac{1}{16\cdot 180\,n^3}\end{aligned} \tag{A.269}$$

From (A.268) and (A.269) we infer that for all $n \geq 1$, the inequalities $\ln\sqrt{(n-1/2)/\pi} < \ln[(2n-1)!!/2^n(n-1)!] < \ln\sqrt{n/\pi}$ hold. Noting that the exponential function is monotonic, we may remove the logarithms from this chain of inequalities. Upon inverting and replacing n by $k = n-1$, we finally end up with the inequalities (A.266). ■

■ COROLLARY LXI

For all integer $j, k, p \geq 0$, the Vandermonde identity holds:

$$\sum_{\mu+\lambda=p} \binom{j}{\mu}\binom{k-j}{\lambda} = \binom{k}{p} \tag{A.270}$$

Proof. This identity is easily proven by comparison of simple power series. On the one hand, we have for the binomial expansion of $(1+z)^k$:

$$(1+z)^k = \sum_{p=0}^{k}\binom{k}{p} z^p \tag{A.271}$$

On the other hand, this must be equal to:

$$(1+z)^j(1+z)^{k-j} = \sum_{\mu=0}^{j}\sum_{\lambda=0}^{k-j}\binom{j}{\mu}\binom{k-j}{\lambda} z^{\lambda+\mu} = \sum_{p=0}^{k} z^p \sum_{\mu+\lambda=p}\binom{j}{\mu}\binom{k-j}{\lambda} \tag{A.272}$$

By comparison of equal powers of z in (A.271) and (A.272), (A.270) follows. ■

■ COROLLARY LXII

Consider a linear combination of spherical harmonic functions $Y_{lm}(\Omega)$ where the quantum number l is fixed. Then,

$$\left|\sum_{m=-l}^{l} \alpha_m\, Y_{lm}(\Omega)\right| \leq \frac{2l+1}{\sqrt{4\pi}}\,\alpha_{\max} \tag{A.273}$$

where $\alpha_{\max} = \max\limits_m |\alpha_m|$.

Proof. Applying the Cauchy-Schwarz inequality to the left-hand side of (A.273), we find:

$$\left| \sum_{m=-l}^{l} \alpha_m \, Y_{lm}(\Omega) \right|^2 \leq \left(\sum_{m=-l}^{l} |\alpha_m|^2 \right) \left(\sum_{m=-l}^{l} |Y_{lm}(\Omega)|^2 \right) \tag{A.274}$$

Since the sum comprises $2l+1$ terms, the first factor on the right-hand side of (A.274) does not exceed $(2l+1)\alpha_{\max}^2$. Regarding the second factor, we take advantage of the addition theorem (B.9) for spherical harmonics; since for the Legendre polynomials, $P_l(1) = 1$ holds for all integer l, we find that this factor equals $(2l+1)/4\pi$, which completes the proof of (A.273). ■

Spherical power series. By their very definition, every analytic function in three dimensions $\varphi(\mathbf{a})$ may be expanded into a power series:

$$\begin{aligned} \varphi(\mathbf{a}) \;=\; \exp(\mathbf{a}\cdot\boldsymbol{\nabla})\,\varphi(\mathbf{o}) \;&=\; \sum_{k=0}^{\infty} \frac{1}{k!}\,(\mathbf{a}\cdot\boldsymbol{\nabla})^k\,\varphi(\mathbf{o}) \\ &=\; \sum_{k=0}^{\infty} \sum_{n_x+n_y+n_z=k} \frac{a_x^{n_x} a_y^{n_y} a_z^{n_z}}{n_x!\,n_y!\,n_z!}\,\frac{\partial^k}{\partial x^{n_x}\partial y^{n_y}\partial z^{n_z}}\,\varphi(\mathbf{r})\Big|_{\mathbf{r}=\mathbf{o}} \end{aligned} \tag{A.275}$$

The expansion (A.275) must converge at least in a neighborhood of $\mathbf{a} = \mathbf{o}$. For our purpose, a modified variant of (A.275) that is based on spherical rather than cartesian coordinates will prove much more convenient. We achieve this objective by expanding the shift operator $\exp(\mathbf{a}\cdot\boldsymbol{\nabla})$ into a multipole series instead of a Taylor series as in (A.275). This versatile technique which we utilized repeatedly in this volume is documented in Appendix B.3. Employing harmonic polynomials $K_{lm}(\mathbf{r}) = r^l Y_{lm}(\hat{r})$, from (B.15) and (B.16) we infer that $\varphi(\mathbf{a})$ may be expanded into an alternative yet equivalent series:

$$\varphi(\mathbf{a}) \;=\; \exp(\mathbf{a}\cdot\boldsymbol{\nabla})\,\varphi(\mathbf{o}) \;=\; 4\pi \sum_{l=0}^{\infty} \sum_{\nu=0}^{\infty} \frac{(-1)^\nu a^{2\nu} \Delta^\nu}{2^\nu \nu!(2l+2\nu+1)!!} \sum_{m=-l}^{l} K_{lm}(\mathbf{a})\, K_{lm}^*(\boldsymbol{\nabla})\,\varphi(\mathbf{o}) \tag{A.276}$$

(As usual, Δ stands for the Laplacian operator.) Obviously, we may reorder this series and collect terms of equal power in $\mathbf{a}$. Then, we obtain the spherical power expansion of the function $\varphi(\mathbf{a})$ that is stated in the following theorem:

■ THEOREM LXIII

Every function $\varphi(\mathbf{a})$ which is analytic in a ball around $\mathbf{a} = \mathbf{o}$ may there be expanded into a convergent spherical power series:

$$\varphi(\mathbf{a}) \;=\; 4\pi \sum_{k=0}^{\infty} a^k \sum_{\nu=0}^{[k/2]} \frac{(-1)^\nu}{2^\nu \nu!(2k-2\nu+1)!!} \sum_{m_\nu=2\nu-k}^{k-2\nu} \alpha_{\nu m_\nu}^{(k)}\, Y_{k-2\nu,m_\nu}(\hat{a}) \tag{A.277}$$

(The symbol $[z]$ denotes the largest integer not exceeding z.) Here, the expansion coefficients $\alpha^{(k)}_{\nu m_\nu}$ are given by the spherical tensor gradient $K_{lm}(\boldsymbol{\nabla})$ of $\varphi(\mathbf{r})$ and its derivatives:

$$\alpha^{(k)}_{\nu m_\nu} \;=\; \Delta^\nu \, K^*_{k-2\nu,m_\nu}(\boldsymbol{\nabla}) \, \varphi(\mathbf{r}) \Big|_{\mathbf{r}\,=\,\mathbf{o}} \tag{A.278}$$

Next, we explore the properties of the spherical power expansion. In particular, we deliver a necessary and sufficient condition for the convergence of this expansion (and consequently, for the analycity property of $\varphi(\mathbf{a})$ at the origin $\mathbf{a} = \mathbf{o}$) in terms of the coefficients $\alpha^{(k)}_{\nu m_\nu}$ (A.278). Furthermore, we establish a bound for the function $\varphi(\mathbf{a})$:

■ THEOREM LXIV
If, and only if, there exist two constants A, β so that:

$$\left|\alpha^{(k)}_{\nu m_\nu}\right| \;\leq\; A\,\beta^k\,k! \tag{A.279}$$

holds for all permitted triples of indices (k, ν, m_ν), then the spherical power expansion of $\varphi(\mathbf{a})$ (Theorem LXIII) converges absolutely in a neighborhood of $\mathbf{a} = \mathbf{o}$. In this case, its radius of convergence does not fall below $1/\beta$, and the function $\varphi(\mathbf{a})$ is bounded by:

$$|\varphi(\mathbf{a})| \;\leq\; \frac{\sqrt{4\pi}\,A}{(1-a\beta)^2} \qquad\qquad (0 \;\leq\; a\beta \;<\; 1) \tag{A.280}$$

Proof. We first show that (A.279) presents a necessary condition for absolute convergence of the series (A.277). Let us assume that (A.279) does not hold; then, for every choice of the parameters A and β, there exists an index triple (k, ν, m_ν) for which $|\alpha^{(k)}_{\nu m_\nu}| > A\,\beta^k\,k!$. We now estimate the contribution of this coefficient to the series (A.279). Absolute convergence of this series clearly implies that the series:

$$\tilde{\varphi}(\mathbf{a}) \;=\; 4\pi \sum_{k\,=\,0}^{\infty} a^k \sum_{\nu\,=\,0}^{[k/2]} \frac{1}{2^\nu \nu!(2k-2\nu+1)!!} \sum_{m_\nu\,=\,2\nu-k}^{k-2\nu} |\alpha^{(k)}_{\nu m_\nu}|\,|Y_{k-2\nu,m_\nu}(\hat{a})| \tag{A.281}$$

converges to a function $\tilde{\varphi}(\mathbf{a})$ in the vicinity of $\mathbf{a} = \mathbf{o}$. Noting that there exists a direction $\hat{a}$ for which $|Y_{k-2\nu,m_\nu}(\hat{a})| \geq 1/\sqrt{4\pi}$ (this statement immediately follows from the orthonormality relation (B.5) of the spherical harmonic functions $\int d\Omega\,|Y_{lm}(\Omega)|^2 = 1$, and the surface area of the unit sphere, $\int d\Omega = 4\pi$), and employing the estimate of Corollary LX, we find that along some direction $\hat{a}$, the inequality holds:

$$\begin{aligned}
\tilde{\varphi}(\mathbf{a}) \;&\geq\; \frac{4\pi a^k}{2^\nu \nu!(2k-2\nu+1)!!}\,|\alpha^{(k)}_{\nu m_\nu}|\,|Y_{k-2\nu,m_\nu}(\hat{a})| \\
&>\; 4\pi A(a\beta)^k\,\frac{1}{\sqrt{4\pi}}\sqrt{\frac{\pi}{k-\nu+1}}\,\frac{k!}{2^{k+1}\,\nu!(k-\nu)!} \;\geq\; \frac{\pi A}{\sqrt{k+1}}\left(\frac{a\beta}{2}\right)^k
\end{aligned} \tag{A.282}$$

(The last inequality follows from the fact that the second line takes on its minimum value for $\nu = 0$.) It is seen that for fixed $a \neq 0$, A and β may be selected in such a way that $\tilde{\varphi}(\mathbf{a})$ exceeds any arbitrarily given bound. Consequently, the series (A.281) converges at most in the point $\mathbf{a} = \mathbf{o}$, and $\varphi(\mathbf{a})$ is not analytic in $\mathbf{a} = \mathbf{o}$.

That the condition (A.279) is also sufficient already follows from the bound (A.280) which we are going to verify now. Introducing we note that obviously $|\varphi(\mathbf{a})| \leq \tilde{\varphi}(\mathbf{a})$ holds, so we will start our estimate from expression (A.281). To get rid of the sum over spherical harmonics $Y_{k-2\nu,m_\nu}(\hat{a})$, we apply Corollary LXII; furthermore, we replace the double factorial by a single one via the inequality $(2k-2\nu+1)!! \geq (2k-2\nu)!! = 2^{k-\nu}(k-\nu)!$. Then, we obtain with $|\alpha^{(k)}_{\nu m_\nu}| \leq A\,\beta^k\,k!$ (A.279):

$$\begin{aligned} |\varphi(\mathbf{a})| \;&\leq\; 4\pi \sum_{k=0}^{\infty} a^k \sum_{\nu=0}^{[k/2]} \frac{A\beta^k k!}{2^k \nu!\,(k-\nu)!}\,\frac{2k-4\nu+1}{\sqrt{4\pi}} \\ &\leq\; \sqrt{4\pi}\,A \sum_{k=0}^{\infty} \left(\frac{a\beta}{2}\right)^k \sum_{\nu=0}^{[k/2]} (2k-4\nu+1)\binom{k}{\nu} \end{aligned} \tag{A.283}$$

Next, we provide an estimate for the ν summation. One may easily check that the inequality holds for all integer $k \geq 0$:

$$\sum_{\nu=0}^{[k/2]} (2k-4\nu+1)\binom{k}{\nu} \;\leq\; (k+1)\sum_{\nu=0}^{k}\binom{k}{\nu} \;=\; 2^k(k+1) \tag{A.284}$$

[The binomial sum already has been evaluated—set $z = 1$ in (A.271).] Hence we end up with the estimate for $|\varphi(\mathbf{a})|$:

$$|\varphi(\mathbf{a})| \;\leq\; \sqrt{4\pi}\,A \sum_{k=0}^{\infty} (k+1)\,(a\beta)^k \tag{A.285}$$

Equation (A.285) is in fact equivalent to (A.280), since $\sum_0^\infty (k+1)z^k = \partial_z(1-z)^{-1} = (1-z)^{-2}$ for $|z| < 1$. ■

Let us note that for a locally analytic function $\varphi(\mathbf{a})$ that does not vanish at $\mathbf{a} = \mathbf{o}$, we always may fix $A = |\alpha^{(0)}_{00}| = |\varphi(\mathbf{o})|/\sqrt{4\pi}$ (A.278) in the estimate (A.279). Then, Theorem LXIV states that there exists some constant β so that $|\varphi(\mathbf{a})| \leq (1-a\beta)^{-2}|\varphi(\mathbf{o})|$ for $0 \leq a\beta < 1$.

Constructing a series solution. After these preliminaries, we turn our attention back to the proposed solution $g_{\rm sp}(\mathbf{r},\mathbf{r}';E)$ (A.265) of the Schrödinger equation (A.260), and show that such a solution for locally analytic potentials $U(\mathbf{r})$ always uniquely exists. Since the proof turns out to be quite extensive in length, we will proceed in several steps and first show that the solution (A.265) is real and unique if it exists at all. Next, we will provide a recurrence relation for the spherical power series of the denominator

function $f(\mathbf{r},\mathbf{r}';E)$ in the tentative solution (A.265). In the final step, we verify that this series actually converges in a neighborhood of $\mathbf{r}=\mathbf{r}'$.

Let us start out and prove the uniqueness of $f(\mathbf{r},\mathbf{r}';E)$. Thanks to Theorem LIX, this is a simple task: Assume that there exist two different locally analytic functions $f_1(\mathbf{r},\mathbf{r}';E)$ and $f_2(\mathbf{r},\mathbf{r}';E)$ so that (A.260), (A.265):

$$\left\{E+\frac{\hbar^2}{2M}\Delta-U(\mathbf{r})\right\}\frac{f_{1,2}(\mathbf{r},\mathbf{r}';E)}{|\mathbf{r}-\mathbf{r}'|} \;=\; -\frac{2\pi\hbar^2}{M}\,\delta(\mathbf{r}-\mathbf{r}') \tag{A.286}$$

This clearly implies that the difference of both functions $[f_1(\mathbf{r},\mathbf{r}';E)-f_2(\mathbf{r},\mathbf{r}';E)]/|\mathbf{r}-\mathbf{r}'|$ is a solution to the corresponding homogeneous Schrödinger equation, and thus, according to Theorem LIX, is an analytic function in $\mathbf{r}$. On the other hand, its numerator $[f_1(\mathbf{r},\mathbf{r}';E)-f_2(\mathbf{r},\mathbf{r}';E)]$ is also an analytic function in $\mathbf{r}$ by assumption. Obviously, both requirements are mutually exclusive except for the trivial solution $f_1(\mathbf{r},\mathbf{r}';E)=f_2(\mathbf{r},\mathbf{r}';E)$: The function $f(\mathbf{r},\mathbf{r}';E)$ is unique. We note that this also implies that $f(\mathbf{r},\mathbf{r}';E)$ must be real, since for real E and $U(\mathbf{r})$ both $f(\mathbf{r},\mathbf{r}';E)$ and $f(\mathbf{r},\mathbf{r}';E)^*$ are solutions of (A.286), and hence must be equal.

It remains to be shown that an analytic function $f(\mathbf{r},\mathbf{r}';E)$ that meets the requirements of (A.286) actually exists for well-behaved potentials $U(\mathbf{r})$. This turns out to be a more challenging problem. As a natural starting point, we examine which conditions the function $f(\mathbf{r},\mathbf{r}';E)$ in (A.265) must obey. Since $\Delta[1/|\mathbf{r}-\mathbf{r}'|]=-4\pi\delta(\mathbf{r}-\mathbf{r}')$ (C.18), we find upon differentiation in (A.265):

$$\left\{E+\frac{\hbar^2}{2M}\Delta-U(\mathbf{r})\right\}g_{\mathrm{sp}}(\mathbf{r},\mathbf{r}';E) \;=\; f(\mathbf{r},\mathbf{r}';E)\delta(\mathbf{r}-\mathbf{r}') \;- \frac{[\Delta+w(\mathbf{r})]f(\mathbf{r},\mathbf{r}';E)}{4\pi|\mathbf{r}-\mathbf{r}'|} + \frac{[(\mathbf{r}-\mathbf{r}')\cdot\boldsymbol{\nabla}]f(\mathbf{r},\mathbf{r}';E)}{2\pi|\mathbf{r}-\mathbf{r}'|^3} \tag{A.287}$$

Here, we set $w(\mathbf{r})=2M[E-U(\mathbf{r})]/\hbar^2$. From (A.287), we immediately infer that $g_{\mathrm{sp}}(\mathbf{r},\mathbf{r}';E)$ will be a solution of the inhomogeneous problem (A.260) if $f(\mathbf{r},\mathbf{r}';E)$ is a solution of the modified differential equation:

$$\left\{(\mathbf{r}-\mathbf{r}')^2[\Delta+w(\mathbf{r})]-2(\mathbf{r}-\mathbf{r}')\cdot\boldsymbol{\nabla}\right\}f(\mathbf{r},\mathbf{r}';E) \;=\; 0 \tag{A.288}$$

which additionally obeys $f(\mathbf{r}',\mathbf{r}';E)=1$. Introducing the relative distance $\mathbf{R}=\mathbf{r}-\mathbf{r}'$ besides $\mathbf{r}'$ as a new variable, we find that (A.288) is equivalent to the differential equation (A.257) presented in Section A.5.1:

$$\left\{R^2\Delta_{\mathbf{R}}-2\,\mathbf{R}\cdot\boldsymbol{\nabla}_{\mathbf{R}}+R^2w(\mathbf{R})\right\}f(\mathbf{R}) \;=\; 0 \tag{A.289}$$

Here, $w(\mathbf{R})$ and $f(\mathbf{R})$ implicitly depend on $\mathbf{r}'$. We have already seen that $\mathbf{R}=\mathbf{o}$ is a special point of equation (A.289), and solutions $f(\mathbf{R})$ might depart there from the

ordinary regularity properties of elliptic differential equations (Theorem LIX). On the other hand, the form of (A.289) strongly resembles ordinary second-order equations (e. g., the Bessel differential equation) whose singular points are characterized by the fact that a part of the solution set nevertheless allows for a series expansion. Indeed, the concept of weak (or regular) singular points [89] is usefully applied to the point $\mathbf{R} = \mathbf{o}$ in the partial differential equation (A.289).

As announced before, the representation in spherical coordinates is especially apt for the solution of (A.289). Obviously, the source location $\mathbf{r}'$ presents a natural choice for the coordinate origin. Expressing the Laplacian in spherical coordinates [83], with $\mathbf{R} \cdot \boldsymbol{\nabla}_{\mathbf{R}} = R\partial_R$ we obtain from (A.289):

$$\left\{ R^2 \frac{\partial^2}{\partial R^2} - L^2 \right\} f(\mathbf{R}) = -R^2 w(\mathbf{R}) f(\mathbf{R}) \tag{A.290}$$

As usual, L^2 denotes the square of the angular momentum operator. Since we are interested in a regular solution $f(\mathbf{R})$ with $f(\mathbf{o}) = 1$, we expand both $f(\mathbf{R})$ and the potential function $w(\mathbf{R})$ into spherical power series (Theorem LXIII):

$$\begin{aligned} f(\mathbf{R}) &= 4\pi \sum_{k=0}^{\infty} R^k \sum_{\nu=0}^{[k/2]} \frac{(-1)^\nu}{2^\nu \nu! (2k-2\nu+1)!!} \sum_{m_\nu} \alpha^{(k)}_{\nu m_\nu} Y_{k-2\nu,m_\nu}(\hat{R}) \\ w(\mathbf{R}) &= 4\pi \sum_{j=0}^{\infty} R^j \sum_{\mu=0}^{[j/2]} \frac{(-1)^\mu}{2^\mu \mu! (2j-2\mu+1)!!} \sum_{m_\mu} \omega^{(j)}_{\mu m_\mu} Y_{j-2\mu,m_\mu}(\hat{R}) \end{aligned} \tag{A.291}$$

As $U(\mathbf{r})$ is assumed analytic, the coefficients (A.278):

$$\omega^{(j)}_{\mu m_\mu} = \Delta^\mu_{\mathbf{R}} K^*_{j-2\mu,m_\mu}(\boldsymbol{\nabla}_{\mathbf{R}}) \left[\frac{2M}{\hbar^2} [E - U(\mathbf{R})] \right]_{\mathbf{R}=\mathbf{o}} \tag{A.292}$$

of the second power series in (A.291) must be bounded by $|\omega^{(j)}_{\mu m_\mu}| \leq W \kappa^j j!$, where W and κ are two constants (Theorem LXIV). We now insert the series (A.291) into (A.290). Noting that $R^k Y_{k-2\nu,m_\nu}(\hat{R})$ is an eigenfunction of the differential operator in (A.290):

$$\left\{ R^2 \frac{\partial^2}{\partial R^2} - L^2 \right\} R^k Y_{k-2\nu,m_\nu}(\hat{R}) = 2(k-\nu)(2\nu-1) R^k Y_{k-2\nu,m_\nu}(\hat{R}) \tag{A.293}$$

we thus obtain the equality:

$$8\pi \sum_{k=0}^{\infty} R^k \sum_{\nu=0}^{[k/2]} \frac{(-1)^\nu (k-\nu)(2\nu-1)}{2^\nu \nu! (2k-2\nu+1)!!} \sum_{m_\nu} \alpha^{(k)}_{\nu m_\nu} Y_{k-2\nu,m_\nu}(\hat{R}) =$$

$$= -16\pi^2 R^2 \sum_{j=0}^{\infty}\sum_{l=0}^{\infty} R^{j+l} \sum_{\mu=0}^{[j/2]} \frac{(-1)^\mu}{2^\mu \mu!(2j-2\mu+1)!!} \sum_{\lambda=0}^{[l/2]} \frac{(-1)^\lambda}{2^\lambda \lambda!(2l-2\lambda+1)!!} \times \sum_{m_\mu} \omega^{(j)}_{\mu m_\mu} Y_{j-2\mu,m_\mu}(\hat{R}) \sum_{m_\lambda} \alpha^{(l)}_{\lambda m_\lambda} Y_{l-2\lambda,m_\lambda}(\hat{R}) \quad \text{(A.294)}$$

For $k > 0$, the expansion coefficients $\alpha^{(k)}_{\nu m_\nu}$ of the desired function $f(\mathbf{R})$ may be singled out. For this purpose, we compare equal powers in R in (A.294), and project upon a specific coefficient $\alpha^{(k)}_{\nu m_\nu}$ by integrating over the unit sphere Ω using $Y_{k-2\nu,m_\nu}(\hat{R})^*$ as a weight function. Taking advantage of the orthonormality relation (B.5) of the spherical harmonic functions, and replacing the conjugate complex function by means of the identity $Y_{k-2\nu,m_\nu}(\hat{R})^* = (-1)^{m_\nu} Y_{k-2\nu,-m_\nu}(\hat{R})$ (see Edmonds [128], p. 21), this procedure yields:

$$\alpha^{(k)}_{\nu m_\nu} = \frac{(-1)^{\nu+m_\nu+1}\, 2^{\nu+1}\pi\, \nu!(2k-2\nu+1)!!}{(2\nu-1)(k-\nu)} \sum_{j=0}^{k-2}\sum_{\mu=0}^{[j/2]} \frac{(-1)^\mu}{2^\mu \mu!(2j-2\mu+1)!!} \times \sum_{\lambda=0}^{[(k-j)/2-1]} \frac{(-1)^\lambda}{2^\lambda \lambda!(2k-2j-2\lambda-3)!!} \sum_{m_\mu}\sum_{m_\lambda} \omega^{(j)}_{\mu m_\mu}\, \alpha^{(k-j-2)}_{\lambda m_\lambda} \times \int d\Omega\, Y_{k-2\nu,-m_\nu}(\Omega)\, Y_{j-2\mu,m_\mu}(\Omega)\, Y_{k-j-2\lambda-2,m_\lambda}(\Omega) \quad \text{(A.295)}$$

This rather involved recurrence relation expresses the expansion coefficient $\alpha^{(k)}_{\nu m_\nu}$ ($k \geq 1$) in terms of the lower-order coefficients $\alpha^{(0)}_{00}$, $\alpha^{(1)}_{\lambda m_\lambda}$, ..., $\alpha^{(k-2)}_{\lambda m_\lambda}$. The integral containing a product of three spherical harmonics is discussed in Appendix B.7; it is also known as the Gaunt coefficient $I^{k-2\nu,j-2\mu,k-j-2\lambda-2}_{-m_\nu,\,m_\mu,\,m_\lambda}$ (B.61) and may be expressed as a product of two Wigner $3j$–symbols (B.62), (B.63) (see Edmonds [128], p. 63). Of greater relevance to our considerations is the fact that the Gaunt coefficent vanishes unless its indices obey a set of selection rules (B.64). Manifestly, the coefficients $\alpha^{(k)}_{\nu m_\nu}$ [and thus $f(\mathbf{R})$] are fixed once a value for $\alpha^{(0)}_{00}$ is chosen. This particular coefficient is not restricted by (A.294) and (A.295) [as readily may be inferred from the fact that $f(\mathbf{R})$ is a solution of the homogeneous linear differential equation (A.289)], yet the original problem (A.287) enforces $f(\mathbf{o}) = 4\pi Y_{00}(\Omega)\alpha^{(0)}_{00} = 1$, i. e., $\alpha^{(0)}_{00} = 1/\sqrt{4\pi}$. Therefore, the recurrence relation (A.295) confirms the verdict of Theorem LIX that at most one regular solution $f(\mathbf{r},\mathbf{r}';E)$ in (A.265) exists. However, it furthermore provides additional information about the leading-order behavior of this tentative solution: Clearly, the right-hand side of (A.295) vanishes for $k = 1$, so linear terms are absent in the expansion of $f(\mathbf{R})$. In a similar fashion, one easily shows using the selection rules (B.64) for the Gaunt coefficient that of the $k = 2$ series contributions, only the coefficient $\alpha^{(2)}_{10}$ survives. (Indeed, all series coefficients $\alpha^{(k)}_{0m_0}$ for which $\nu = 0$ with the exception of $\alpha^{(0)}_{00}$

vanish; see below.) One obtains $\alpha_{10}^{(2)} = 3\,\omega_{00}^{(0)}$ and therefore:

$$f(\mathbf{R}) \;=\; 4\pi \left\{ \alpha_{00}^{(0)} Y_{00}(\Omega) - \frac{R^2}{6}\, \alpha_{10}^{(2)} Y_{00}(\Omega) + \ldots \right\} \;=\; 1 - \frac{1}{2}\, k(\mathbf{r}')^2 R^2 + \ldots \qquad \text{(A.296)}$$

where $k(\mathbf{r}')^2 = 2M[E - U(\mathbf{r}')]/\hbar^2$ denotes the local wave number at the source location $\mathbf{r}'$. Obviously, this expansion is compatible to our earlier observation (A.264).

Proof of series convergence. It remains to be shown that the recursive series solution (A.295) actually corresponds to a locally analytic function $f(\mathbf{R})$, i. e., we must prove that the coefficients $\alpha_{\nu m_\nu}^{(k)}$ in (A.295) lead to a convergent spherical power series (Theorem LXIII) for some $\mathbf{R} \neq \mathbf{o}$. In view of Theorem LXIV, this means that there exists some constant β so that for all expansion coefficients, $|\alpha_{\nu m_\nu}^{(k)}| \leq \beta^k k!/\sqrt{4\pi}$ holds. [For convenience, we set $A = \alpha_{00}^{(0)} = 1/\sqrt{4\pi}$ in (A.279).] We note in advance that analycity of $f(\mathbf{R})$ in a neighborhood of $\mathbf{R} = \mathbf{o}$ implies analycity of $f(\mathbf{r}, \mathbf{r}'; E)$ throughout the sector of analycity of the potential $U(\mathbf{r})$, since $f(\mathbf{r}, \mathbf{r}'; E)$ is a solution of a differential equation which is elliptic for $\mathbf{r} \neq \mathbf{r}'$ (A.288), so Theorem LIX applies.

The appearance of the recurrence relation suggests an inductive proof of the crucial inequality $|\alpha_{\nu m_\nu}^{(k)}| \leq \beta^k k!/\sqrt{4\pi}$. With $\alpha_{00}^{0} = 1/\sqrt{4\pi}$ and $\alpha_{\nu m_\nu}^{(1)} \equiv 0$ (A.296), it clearly holds for $k = 0$ and $k = 1$. We now assume that is valid for all $\alpha_{\lambda m_\lambda}^{(j)}$ with $j = 0, 1, \ldots, k-2$; then, we have to prove that this inequality also holds for $\alpha_{\nu m_\nu}^{(k)}$. Obviously this requires a proper estimate of the right-hand side in the recurrence relation (A.295). Having all necessary tools at hand, we now show how to get rid of the multiple sums in (A.295).

In advance, we note that the potential $U(\mathbf{r})$ is locally analytic, so the spherical power expansion coefficients $\omega_{\mu m_\mu}^{(j)}$ of the auxiliary function $w(\mathbf{R})$ (A.291) are bounded by $|\omega_{\mu m_\mu}^{(j)}| \leq W \kappa^j j!$, where W and κ are some constants (Theorem LXIV). In the first important step, we recognize that the selection rules (B.64) for the Gaunt coefficient $I_{-m_\nu,\, m_\mu,\, m_\lambda}^{k-2\nu,\, j-2\mu,\, k-j-2\lambda-2}$, i. e., the integral over spherical harmonic functions in (A.295), implicitly limit the range of the summation indices μ and λ. Here, from the "triangulum relation" $l_2 + l_3 \geq l_1$, we obtain the condition $\mu + \lambda \leq \nu - 1$. (In particular, this means that $\alpha_{0 m_0}^{(k)} \equiv 0$.) Keeping this restriction in mind, we may take care of the Gaunt coefficient and indeed the "magnetic" sums over m_μ and m_λ by means of an inequality (B.70) derived in Appendix B.7. For $\mu + \lambda < \nu$, we find in (A.295):

$$\left| \sum_{m_\mu} \sum_{m_\lambda} \omega_{\mu m_\mu}^{(j)}\, \alpha_{\lambda m_\lambda}^{(k-j-2)} \int d\Omega\, Y_{k-2\nu,\,-m_\nu}(\Omega)\, Y_{j-2\mu,\,m_\mu}(\Omega)\, Y_{k-j-2\lambda-2,\,m_\lambda}(\Omega) \right| \leq$$

$$\leq \left(\max_{m_\mu} \left|\omega^{(j)}_{\mu m_\mu}\right|\right) \left(\max_{m_\lambda} \left|\alpha^{(k-j-2)}_{\lambda m_\lambda}\right|\right) \sum_{m_\mu} \sum_{m_\lambda} \left|I^{k-2\nu, j-2\mu, k-j-2\lambda-2}_{-m_\nu, m_\mu, m_\lambda}\right|$$

$$\leq \frac{W}{4\pi} \kappa^j \beta^{k-j-2} \, j! \, (k-j-2)! \, \sqrt{(2j-4\mu+1)(2k-2j-4\lambda-3)} \tag{A.297}$$

In the case $\mu+\lambda \geq \nu$, the sum identically vanishes. Furthermore, we replace the double factorials in (A.295) with the estimates provided by Corollary LX. We then obtain from (A.295) and (A.297):

$$\begin{aligned}
\left|\alpha^{(k)}_{\nu m_\nu}\right| \;\leq\; & \frac{W}{4\pi} \frac{2^{\nu+1} \, \pi \, \nu!}{(2\nu-1)(k-\nu)} \, 2^{k-\nu+1} (k-\nu)! \, \sqrt{\frac{k-\nu+1}{\pi}} \sum_{j=0}^{k-2} \kappa^j \beta^{k-j-2} \;\times \\
& \sum_{\mu=0}^{\infty} \frac{\Theta_{\mu,[j/2]} \, j!}{2^{j+1} \, \mu! \, (j-\mu)!} \sum_{\lambda=0}^{\infty} \frac{\Theta_{\lambda,[(k-j)/2-1]} \, (k-j-2)!}{2^{k-j-1} \, \lambda! \, (k-j-\lambda-2)!} \;\times \\
& 2\pi \, \Theta_{\mu+\lambda,\nu-1} \sqrt{\frac{(j-2\mu+1/2)(k-j-2\lambda-3/2)}{(j-\mu+1/2)(k-j-\lambda-3/2)}} \\
\leq \quad & 2\sqrt{\pi} \, W \, \frac{\nu! \, (k-\nu-1)! \, \sqrt{k-\nu+1}}{2\nu-1} \sum_{j=0}^{k-2} \kappa^j \beta^{k-j-2} \;\times \\
& \sum_{\mu=0}^{\infty} \sum_{\lambda=0}^{\infty} \Theta_{\mu+\lambda,\nu-1} \binom{j}{\mu} \binom{k-j-2}{\lambda}
\end{aligned} \tag{A.298}$$

Here, we used the step symbol $\Theta_{\mu,\nu}$ which is defined by $\Theta_{\mu,\nu} = 1$ for $\mu \leq \nu$ and $\Theta_{\mu,\nu} = 0$ for $\mu > \nu$. The latter inequality in (A.298) follows from $\Theta_{\mu,\nu} \leq 1$ and the fact that the radicand in (A.298) never exceeds one in value. To get rid of the remaining sums in (A.298), we note that we may rewrite the double binomial sum in a way as to take advantage of the Vandermonde identity of Corollary LXI:

$$\sum_{\sigma=0}^{\nu-1} \sum_{\mu+\lambda=\sigma} \binom{j}{\mu} \binom{k-j-2}{\lambda} \;=\; \sum_{\sigma=0}^{\nu-1} \binom{k-2}{\sigma} \;\leq\; \nu \binom{k-2}{\nu-1} \tag{A.299}$$

In the last, occasionally rather crude approximation we replace $\binom{k-2}{\sigma}$ with its maximum value in $0 \leq \sigma < \nu \leq [k/2]$ which it takes on for $\sigma = \nu - 1$. We see that (A.299) leaves an isolated geometric series for the j summation in (A.298) which is easily evaluated to yield:

$$\left|\alpha^{(k)}_{\nu m_\nu}\right| \;\leq\; 2\sqrt{\pi} \, W \, \frac{\beta^{k-1} - \kappa^{k-1}}{\beta - \kappa} \, \frac{\nu^2 \, (k-2)! \, \sqrt{k-\nu+1}}{2\nu-1} \tag{A.300}$$

Since for $1 \leq \nu \leq [k/2]$ and $k \geq 2$ we may easily show that:

$$\frac{\nu^2\,(k-2)!\,\sqrt{k-\nu+1}}{2\nu-1} \;\leq\; \frac{(\nu+1)\,\sqrt{k-\nu+1}}{2k(k-1)}\,k! \;\leq\; \frac{k+2}{4(k-1)\,\sqrt{k}}\,k! \;\leq\; \frac{1}{\sqrt{2}}\,k! \quad \text{(A.301)}$$

(where equality holds for $k=2$, $\nu=1$), we thus end up with the following inequality for the expansion coefficient $\alpha^{(k)}_{\nu m_\nu}$ (A.295):

$$\left|\alpha^{(k)}_{\nu m_\nu}\right| \;\leq\; \frac{2\sqrt{2}\,\pi W}{\kappa^2}\,\frac{\kappa}{\beta}\,\frac{1-(\kappa/\beta)^{k-1}}{\beta/\kappa-1}\;\cdot\;\frac{1}{\sqrt{4\pi}}\,\beta^k k! \quad \text{(A.302)}$$

Obviously, the induction step is established if we are able to find some value of β so that the prefactor in (A.302) is smaller than unity. In (A.302) we have employed a suggestive notation from which we may easily infer that a possible choice for the constant β is given implicitly by the relation:

$$\frac{\beta}{\kappa}\left(\frac{\beta}{\kappa}-1\right) \;=\; \frac{2\sqrt{2}\,\pi W}{\kappa^2} \quad \text{(A.303)}$$

because for the positive solution of this quadratic equation, the prefactor in (A.302) is then given by $1-(\kappa/\beta)^{k-1} \leq 1$. Solving for β, we find from (A.303):

$$\beta \;=\; \frac{\kappa}{2}\left(1+\sqrt{1+\frac{8\sqrt{2}\,\pi W}{\kappa^2}}\right) \quad \text{(A.304)}$$

Thus, the analycity of the function $f(\mathbf{r},\mathbf{r}';E)$ in the solution (A.265) of the differential equation (A.260) is verified. By means of Theorem LXIV, (A.304) furthermore delivers a bound for this particular solution.

Analycity properties of local solutions. Let us now gather our insights into a concise statement. We remark that we were able to show that a special solution to the differential equation (A.260) in the form (A.265) exists where $f(\mathbf{r},\mathbf{r}';E)$ has the desired property of local analycity. To generate the complete solution set of (A.260), we have to add solutions $h(\mathbf{r},\mathbf{r}';E)$ of the corresponding homogeneous Schrödinger equation. Since this equation is based on an elliptic differential operator, Theorem LIX tells us that $h(\mathbf{r},\mathbf{r}';E)$ also must be a function analytic in $\mathbf{r}$, and its sector of analycity coincides with the range of analycity of the potential function $U(\mathbf{r})$ in (A.260). Therefore, we have:

■ THEOREM LXV

Let $\mathbb{S} \subseteq \mathbb{R}^3$ the sector of analycity of the potential $U(\mathbf{r})$ in the inhomogeneous Schrödinger equation:

$$\left\{E + \frac{\hbar^2}{2M}\,\Delta - U(\mathbf{r})\right\} g(\mathbf{r},\mathbf{r}';E) \;=\; \delta(\mathbf{r}-\mathbf{r}') \tag{A.305}$$

Then, every solution $g(\mathbf{r},\mathbf{r}';E)$ with $\mathbf{r}' \in \mathbb{S}$ may be written in the form:

$$g(\mathbf{r},\mathbf{r}';E) \;=\; -\,\frac{M}{2\pi\hbar^2}\,\frac{f(\mathbf{r},\mathbf{r}';E)}{|\mathbf{r}-\mathbf{r}'|} \;+ h(\mathbf{r},\mathbf{r}';E) \tag{A.306}$$

where $f(\mathbf{r},\mathbf{r}';E)$ is a uniquely determined, real function whose expansion in leading order is given by:

$$f(\mathbf{r},\mathbf{r}';E) \;=\; 1 - \frac{M[E-U(\mathbf{r}')]}{\hbar^2}\,(\mathbf{r}-\mathbf{r}')^2 + \mathcal{O}(r_k^3) \tag{A.307}$$

The function $h(\mathbf{r},\mathbf{r}';E)$ is a solution of the homogeneous Schrödinger equation corresponding to (A.305). In the sector $\mathbb{S}$, both functions $f(\mathbf{r},\mathbf{r}';E)$ and $h(\mathbf{r},\mathbf{r}';E)$ are analytic in $\mathbf{r}$.

Furthermore, there exist two constants κ and W so that the spherical derivatives of the potential function $U(\mathbf{r})$ are bounded by:

$$\left|\Delta^{\mu}\, K_{j-2\mu,m_\mu}(\boldsymbol{\nabla})\,[E-U(\mathbf{r})]\right|_{\mathbf{r}\,=\,\mathbf{r}'} \;\leq\; \frac{\hbar^2 W}{2M}\,\kappa^j\; j! \tag{A.308}$$

With these constants, a local bound for the special solution $g_{\mathrm{sp}}(\mathbf{r},\mathbf{r}';E)$ (A.265) of (A.305) with $h(\mathbf{r},\mathbf{r}';E) \equiv 0$ is given by:

$$|g_{\mathrm{sp}}(\mathbf{r},\mathbf{r}';E)| \;\leq\; \frac{M}{2\pi\hbar^2}\,\frac{1}{|\mathbf{r}-\mathbf{r}'|\,(1-\beta|\mathbf{r}-\mathbf{r}'|)^2} \tag{A.309}$$

Here, the parameter β reads:

$$\beta \;=\; \frac{\kappa}{2}\left(1+\sqrt{1+\frac{8\sqrt{2}\,\pi W}{\kappa^2}}\right) \tag{A.310}$$

Note: That local analycity of the potential $U(\mathbf{r})$ indeed presents a nontrivial assumption guaranteeing the local analycity of the solutions $g(\mathbf{r},\mathbf{r}';E)$ in (A.305) may be seen from the non-analytic Coulomb interaction with $U(\mathbf{r}) = \alpha/r$ ($\alpha \neq 0$). The Green function $G_{\mathrm{Coul}}(\mathbf{r},\mathbf{o};E)$ of this problem which is proportional to the $l = 0$ Coulomb scattering wave $[G_0 + iF_0](\eta,\rho)$ (for further information, we refer to the handbook

by Abramowitz and Stegun [81], p. 538) contains logarithmic terms in its $r \to 0$ expansion which render it manifestly non-analytic at $\mathbf{r} = \mathbf{o}$. (See also the textbook by Messiah [83], p. 487.)

Symmetry properties of the Green functions. We have seen that analycity of the potential $U(\mathbf{r})$ in the Schrödinger equation (A.305) enforces the analycity of the functions $f(\mathbf{r}, \mathbf{r}'; E)$ and $h(\mathbf{r}, \mathbf{r}'; E)$ in the representation (A.306) of the solution set $g(\mathbf{r}, \mathbf{r}'; E)$ (Theorem LXV). In its present form, this statement only holds for power expansions of these functions with respect to the first coordinate $\mathbf{r}$. The theory of multipole sources $\delta_{lm}(\mathbf{r} - \mathbf{r}')$ (2.23) in Section 2.4 is however based on multipole Green functions $G_{lm}(\mathbf{r}, \mathbf{r}'; E)$ (2.25) which are derivatives of the Green function $G(\mathbf{r}, \mathbf{r}'; E)$ with respect to the coordinate $\mathbf{r}'$ rather than $\mathbf{r}$. Therefore, we have to extend our studies on the analycity of the Green function onto the second position parameter $\mathbf{r}'$. For this purpose, we employ the symmetry properties of the Green function.

We remind the reader that the Green function $G(\mathbf{r}, \mathbf{r}'; E)$ assigned to a self-adjoint Hamiltonian operator $H(\mathbf{r}, \mathbf{p})\delta(\mathbf{r} - \mathbf{r}') = \langle \mathbf{r} \,|\mathcal{H}|\, \mathbf{r}' \rangle$ is just the spatial representation of the resolvent operator $\mathcal{R}(E)$ with $(E\mathcal{E} - \mathcal{H})\mathcal{R}(E) = \mathcal{R}(E)(E\mathcal{E} - \mathcal{H}) = \mathcal{E}$ (Definition XXXIX). In the course of our discussion of resolvents in Appendix A.3.6, we established that $\mathcal{R}(E)$ exists for all values of E except those in the point spectrum of $\mathcal{H}$ (Theorem XLVIII), that $\mathcal{R}(E)$ is bounded and unique in the resolvent set of $\mathcal{H}$ (Theorem XLVII) whereas multiple instances of an unbounded solution $\mathcal{R}(E)$ may exist in the continuous spectrum of $\mathcal{H}$ (Theorem L). For all real values of E outside the point spectrum of $\mathcal{H}$, a self-adjoint solution $\mathcal{R}_{\mathrm{PV}}(E)$ is given by the Cauchy principal value integral (A.184):

$$G_f(\mathbf{r}, \mathbf{r}'; E) \;=\; \langle \mathbf{r} \,|\mathcal{R}_{\mathrm{PV}}(E)|\, \mathbf{r}' \rangle \;=\; \fint \frac{\mathrm{d}\, \langle \mathbf{r} \,|\Pi(\mu)|\, \mathbf{r}' \rangle}{E - \mu} \tag{A.311}$$

In Section A.4.3, we denoted this solution the fundamental Green function of the problem (A.221), and its basic features in the one-dimensional case are stated in Theorem LV. Obviously, this special Green function is hermitian: $G_f(\mathbf{r}, \mathbf{r}'; E) = G_f(\mathbf{r}', \mathbf{r}; E)^*$. In the continuous spectrum of $\mathcal{H}$, however, another set of Green functions forms the foundation of quantum source theory (Section 2.3). These are the advanced and retarded solutions of the resolvent problem whose Stieltjes integral representations are given in Theorem LI:

$$G_{\mathrm{ret/adv}}(\mathbf{r}, \mathbf{r}'; E) \;=\; \left\langle \mathbf{r} \,\middle|\mathcal{R}_{\mathrm{ret/adv}}(E)\middle|\, \mathbf{r}' \right\rangle \;=\; \lim_{\eta \to 0^+} \int \frac{\mathrm{d}\, \langle \mathbf{r} \,|\Pi(\mu)|\, \mathbf{r}' \rangle}{E - \mu \pm i\eta} \tag{A.312}$$

Not being self-adjoint, these solutions nevertheless are interrelated through the exchange of positions: $G_{\mathrm{ret}}(\mathbf{r}, \mathbf{r}'; E) = G_{\mathrm{adv}}(\mathbf{r}', \mathbf{r}; E)^*$. We remark that all these Green

functions become symmetric if the spatial matrix element $\langle \mathbf{r} \,|\Pi(\mu)|\, \mathbf{r}' \rangle$ of the spectral family $\Pi(\mu)$ assigned to $\mathcal{H}$ is purely real. Obviously, then $G(\mathbf{r}, \mathbf{r}'; E) = G(\mathbf{r}', \mathbf{r}; E)$ holds in (A.311) and (A.312).

Let us study the consequences of this symmetry relation. From Theorem LXV, the Green function $G_f(\mathbf{r}, \mathbf{r}'; E)$ (A.311) may be displayed in the form,

$$G_f(\mathbf{r}, \mathbf{r}'; E) \;=\; -\frac{M}{2\pi\hbar^2}\,\frac{f(\mathbf{r}, \mathbf{r}'; E)}{|\mathbf{r} - \mathbf{r}'|} \;+ h_f(\mathbf{r}, \mathbf{r}'; E) \tag{A.313}$$

where $f(\mathbf{r}, \mathbf{r}'; E)$ is a real function and $h_f(\mathbf{r}, \mathbf{r}'; E)$ is a local solution of the homogeneous Schrödinger equation (which need not be bounded as $r \to \infty$). Since the differential operator in (A.305) is real, with $G_f(\mathbf{r}, \mathbf{r}'; E)$ also $G_f(\mathbf{r}, \mathbf{r}'; E)^*$ is a valid solution to (A.305); on the other hand, $\mathcal{R}_{\mathrm{PV}}(E)$ is a self-adjoint operator, so $G_f(\mathbf{r}, \mathbf{r}'; E)^* = G_f(\mathbf{r}', \mathbf{r}; E)$ holds. From (A.306) and (A.313), we thus obtain:

$$G_f(\mathbf{r}', \mathbf{r}; E) \;=\; -\frac{M}{2\pi\hbar^2}\,\frac{f(\mathbf{r}', \mathbf{r}; E)}{|\mathbf{r} - \mathbf{r}'|} \;+ h_f(\mathbf{r}', \mathbf{r}; E) \;=\; -\frac{M}{2\pi\hbar^2}\,\frac{f(\mathbf{r}, \mathbf{r}'; E)}{|\mathbf{r} - \mathbf{r}'|} \;+ h_f(\mathbf{r}, \mathbf{r}'; E)^* \tag{A.314}$$

Clearly, this implies that the function $f(\mathbf{r}, \mathbf{r}'; E)$ is symmetric in its arguments, and $h_f(\mathbf{r}, \mathbf{r}'; E) = h_f(\mathbf{r}', \mathbf{r}; E)^*$ is a hermitian function. If, in particular, E is a member of the resolvent set of $\mathcal{H}$, then the Green function is uniquely given by (A.313), so by comparison with (A.314) we find that $h_f(\mathbf{r}, \mathbf{r}'; E) = h_f(\mathbf{r}', \mathbf{r}; E)$ is a unique real symmetric function, too.

By the same chain of arguments, in the continuous spectrum of $\mathcal{H}$ we obtain for the representations (A.306) of the advanced and retarded solutions $G_{\mathrm{ret/adv}}(\mathbf{r}, \mathbf{r}'; E)$ (A.312) the symmetry relation $h_{\mathrm{ret}}(\mathbf{r}, \mathbf{r}'; E) = h_{\mathrm{adv}}(\mathbf{r}', \mathbf{r}; E)^*$. We note that these relations are less restrictive than our former conjecture $G(\mathbf{r}, \mathbf{r}'; E) = G(\mathbf{r}', \mathbf{r}; E)$ which was suggested by the two examples (A.261) and (A.262) we worked out; however, for these simple potentials the Hamiltonian $\mathcal{H}$ is separable within a set of self-adjoint operators with non-degenerate spectrum (Definition XXXVII) whose eigenfunctions furthermore may be chosen entirely real; by expansion into these eigenfunctions, it may be shown that the matrix element of the spectral family $\Pi(E)$ of $\mathcal{H}$, $\langle \mathbf{r} \,|\Pi(E)|\, \mathbf{r}' \rangle$, takes on only real values. Hence, symmetry of the Green functions (A.311), (A.312) with respect to the exchange of the variables $\mathbf{r}$ and $\mathbf{r}'$ follows. (In exactly this manner we established the corresponding symmetry property of their one-dimensional counterpart $G_f(x, x'; E)$ [Theorem LV, part (i)] in Section A.4.3.) It appears, however, that an extension of this proof to the common case of nonseparable Hamiltonians $\mathcal{H}$ poses difficult problems.

Nevertheless, the symmetry relation $f(\mathbf{r}, \mathbf{r}'; E) = f(\mathbf{r}', \mathbf{r}; E)$ and its weaker cousins $h_f(\mathbf{r}', \mathbf{r}; E) = h_f(\mathbf{r}, \mathbf{r}'; E)^*$ and $h_{\mathrm{ret}}(\mathbf{r}', \mathbf{r}; E) = h_{\mathrm{adv}}(\mathbf{r}, \mathbf{r}'; E)^*$, together with the analycity

of these functions in the first variable (Theorem LXV) obviously enforce analycity of the functions $f(\mathbf{r},\mathbf{r}';E)$ and $h(\mathbf{r},\mathbf{r}';E)$ in the expression (A.306) for the Green function $G(\mathbf{r},\mathbf{r}';E)$ with respect to both positions $\mathbf{r}$ and $\mathbf{r}'$. Hence, we may state:

■ THEOREM LXVI
Let $H(\mathbf{r},\mathbf{p}) = p^2/2M + U(\mathbf{r})$ be a self-adjoint Hamiltonian in three spatial dimensions with a potential $U(\mathbf{r})$ that is analytic in a sector $\mathbb{S} \subseteq \mathbb{R}^3$. Then, the retarded Green function $G(\mathbf{r},\mathbf{r}';E)$ exists if $H(\mathbf{r},\mathbf{p})$ does not support a bound state with energy E. For real E, it may be displayed in the form:

$$G(\mathbf{r},\mathbf{r}';E) \;=\; -\,\frac{M}{2\pi\hbar^2}\,\frac{f(\mathbf{r},\mathbf{r}';E)}{|\mathbf{r}-\mathbf{r}'|} \;+ h(\mathbf{r},\mathbf{r}';E) \tag{A.315}$$

where $f(\mathbf{r},\mathbf{r}';E) = f(\mathbf{r}',\mathbf{r};E)$ is a real symmetric function which is analytic for $\mathbf{r},\mathbf{r}' \in \mathbb{S}$; its leading-order expansion reads:

$$f(\mathbf{r},\mathbf{r}';E) \;=\; 1 - \;\frac{M[E-U(\mathbf{o})]}{\hbar^2}\,(\mathbf{r}-\mathbf{r}')^2 + \mathcal{O}(r_k^3, r_k'^3) \tag{A.316}$$

whereas $h(\mathbf{r},\mathbf{r}';E)$ is a solution of the homogeneous Schrödinger equation analytic in $\mathbf{r},\mathbf{r}' \in \mathbb{S}$. If E is not an eigenvalue of $H(\mathbf{r},\mathbf{p})$, then $h(\mathbf{r},\mathbf{r}';E)$ is also a real and symmetric function.

A.5.3 Near-Field Approximations for Multipole Sources

Using the results on the analycity properties of the stationary Schrödinger Green function that we established in the previous section, it is now a fairly straightforward task to deliver an approximation describing the behavior of the multipole Green functions $G_{lm}(\mathbf{r},\mathbf{r}';E)$ in the vicinity of the source $\mathbf{r} \approx \mathbf{r}'$. We remind the reader that these functions are defined as the spherical tensor gradients $K_{lm}[\partial/\partial\mathbf{r}']$ of the ordinary Green function $G(\mathbf{r},\mathbf{r}';E)$ with respect to the source position $\mathbf{r}'$ (A.253). Following Theorem LXVI, this means that for a locally analytic potential $U(\mathbf{r})$, we have to analyze an expression of the form:

$$G_{lm}(\mathbf{r},\mathbf{r}';E) \;=\; -\,\frac{M}{2\pi\hbar^2}\,K_{lm}\left(\frac{\partial}{\partial\mathbf{r}'}\right)\left\{\frac{f(\mathbf{r},\mathbf{r}';E)}{|\mathbf{r}-\mathbf{r}'|}\right\} + K_{lm}\left(\frac{\partial}{\partial\mathbf{r}'}\right)h(\mathbf{r},\mathbf{r}';E) \tag{A.317}$$

where the leading terms of the expansion of the analytic function $f(\mathbf{r},\mathbf{r}';E)$ are given by (A.316). The basic idea behind (A.317) is that sufficiently close to the point source $\delta(\mathbf{r}-\mathbf{r}')$ at $\mathbf{r}'$, the Green function $G(\mathbf{r},\mathbf{r}';E)$ adopts a universal behavior that is determined by the structure of the source rather than the potential function $U(\mathbf{r})$. In fact, in the vicinity of the source the function $G(\mathbf{r},\mathbf{r}';E)$ is adequately described by the (isotropic) Green function of potential theory ($E = 0$, $U(\mathbf{r}) \equiv 0$) which reads

$G(\mathbf{r},\mathbf{r}') = -M/2\pi\hbar^2|\mathbf{r}-\mathbf{r}'|$ (C.18). In this section, we now examine how this universality property translates to the case of oriented multipole Green functions $G_{lm}(\mathbf{r},\mathbf{r}';E)$.

Let us beforehand deal with the solution $h(\mathbf{r},\mathbf{r}';E)$ of the homogeneous Schrödinger equation in (A.315). According to Theorem LXVI, for analytic potentials $U(\mathbf{r})$ this is an analytic function in $\mathbf{r}$ and $\mathbf{r}'$ which is unique if E is outside the spectrum of the Hamiltonian $\mathcal{H}$. Clearly, this implies that:

$$h_{lm}(\mathbf{r},\mathbf{r}';E) \;=\; K_{lm}\left(\frac{\partial}{\partial\mathbf{r}'}\right) h(\mathbf{r},\mathbf{r}';E) \tag{A.318}$$

also presents an analytic function in $\mathbf{r}$ and $\mathbf{r}'$ which is unique if E is in the resolvent set of $\mathcal{H}$. We note that a more restrictive replacement for (A.318) is available for spherically symmetric potentials $U(R)$ like the free-particle propagation problem $[U(\mathbf{r}) \equiv 0]$ considered in Appendix C: In this case, $h(\mathbf{r},\mathbf{r}';E) = h(R^2;E)$ is an isotropic function only depending on the relative distance $R = |\mathbf{r}-\mathbf{r}'|$ [see (A.261)]. Then, we may exploit the fact that the spherical tensor gradient $K_{lm}[\partial/\partial\mathbf{r}']$ in (A.318) is a tensor operator of (lm) angular momentum acting on a spherical scalar which must result according to the addition rules of angular momenta in a function $h_{lm}(\mathbf{r},\mathbf{r}';E)$ of pure (lm) spherical symmetry. This function furthermore may be expanded into a Taylor series. From our considerations on spherical power series (Theorem LXIII) we conclude that $h_{lm}(\mathbf{r},\mathbf{r}';E)$ may be represented in the form:

$$h_{lm}(\mathbf{r},\mathbf{r}';E) \;=\; K_{lm}(\mathbf{r}-\mathbf{r}')\, h_l(R^2;E) \tag{A.319}$$

Here, $h_l(R^2;E)$ is an analytic and isotropic function independent of the magnetic quantum number m. The latter statement follows from the Wigner-Eckart theorem in its application to spherical scalars (see Edmonds [128], p. 75, and also Appendix B.4). As an example, we consider the free-particle multipole Green function $G_{lm}^{(\mathrm{free})}(\mathbf{r},\mathbf{r}';E)$ (Appendix C.1) with $E \geq 0$. According to (A.261), here we have $h^{(\mathrm{free})}(R^2;E) = -iM\sin(kR)/2\pi\hbar^2 R$, and following (C.17):

$$h_{lm}^{(\mathrm{free})}(\mathbf{r},\mathbf{r}';E) \;=\; -\frac{iMk^{2l+1}}{2\pi\hbar^2}\, K_{lm}(\mathbf{r}-\mathbf{r}')\, \frac{j_l(kR)}{(kR)^l} \tag{A.320}$$

Here, $j_l(kR)$ denotes the spherical Bessel function [81], and $(kR)^{-l}j_l(kR)$ is an analytic function of the argument k^2R^2 with limiting value $[(2l+1)!!]^{-1}$ (B.13). We again emphasize that the usage of expression (A.319) depends on the presence of an isotropic potential function $U(R)$; otherwise, we have to content ourselves with the less stringent form (A.318). Notably, the uniform field Green function $G(\mathbf{r},\mathbf{r}';E)$ (A.262) based on the potential $U(\mathbf{r}) = -Fz$ does not fit into the scheme (A.319).

The treatment of the derivative of the special solution involving the unique, real, symmetric and analytic function $f(\mathbf{r},\mathbf{r}';E)$ in (A.317) turns out to be only slightly more

involved. Since the spherical tensor gradient $K_{lm}[\partial/\partial\mathbf{r}']$ decomposes into a sum of products of l partial derivatives $\partial/\partial x', \partial/\partial y', \partial/\partial z'$, we clearly may emulate the action of this operator by a sequence of single differentiation operations applied to the structure in (A.317). In general, we find that for any analytic function $f_j(\mathbf{r},\mathbf{r}';E)$, we may write:

$$\frac{\partial}{\partial \mathbf{r}_i'}\left\{\frac{f_j(\mathbf{r},\mathbf{r}';E)}{|\mathbf{r}-\mathbf{r}'|^{2j+1}}\right\} = \frac{(\mathbf{r}-\mathbf{r}')^2\,\partial_i' f_j(\mathbf{r},\mathbf{r}';E) + (2j+1)(r_i-r_i')f_j(\mathbf{r},\mathbf{r}';E)}{|\mathbf{r}-\mathbf{r}'|^{2(j+1)+1}}$$
$$= \frac{f_{j+1}(\mathbf{r},\mathbf{r}';E)}{|\mathbf{r}-\mathbf{r}'|^{2(j+1)+1}} \tag{A.321}$$

where $f_{j+1}(\mathbf{r},\mathbf{r}';E)$ again presents an analytic function in $\mathbf{r}$, $\mathbf{r}'$. We furthermore note that if the leading terms in the Taylor series of $f_j(\mathbf{r},\mathbf{r}';E)$ expanded around $\mathbf{r}=\mathbf{r}'$ are of order $|\mathbf{r}-\mathbf{r}'|^p$ [$k = p, p+1, \ldots$ in (A.275)], then the order of $f_{j+1}(\mathbf{r},\mathbf{r}';E)$ at $\mathbf{r}=\mathbf{r}'$ will be incremented to $|\mathbf{r}-\mathbf{r}'|^{p+1}$. Thus, we obtain:

$$K_{lm}\left(\frac{\partial}{\partial\mathbf{r}'}\right)\left\{\frac{f(\mathbf{r},\mathbf{r}';E)}{|\mathbf{r}-\mathbf{r}'|}\right\} = \frac{f_{lm}(\mathbf{r},\mathbf{r}';E)}{|\mathbf{r}-\mathbf{r}'|^{2l+1}} \tag{A.322}$$

with some analytic function $f_{lm}(\mathbf{r},\mathbf{r}';E)$ which vanishes like $|\mathbf{r}-\mathbf{r}'|^l$ as $\mathbf{r}\to\mathbf{r}'$. Our particular interest now obviously is directed to the behavior of (A.322) near the source, i. e., for $\mathbf{r}\approx\mathbf{r}'$. Clearly, we expect a universal asymptotic form not affected from the details of the potential $U(\mathbf{r})$ which then must resemble the multipole structure of the multipole Green function $\Phi_{lm}(\mathbf{r},\mathbf{r}')$ (2.19) of potential theory ($E=0, U(\mathbf{r})\equiv 0$). Thus, from (A.252) and (C.20) we conclude that in the vicinity of the source, $f_{lm}(\mathbf{r},\mathbf{r}';E)\sim (2l-1)!!\,K_{lm}(\mathbf{r}-\mathbf{r}')$ should hold asymptotically, independent of $U(\mathbf{r})$.

Let us now prove this assertion. To this end, we take advantage of the fact that the function $f(\mathbf{r},\mathbf{r}';E)$ in leading order may be written in the form (A.316):

$$f(\mathbf{r},\mathbf{r}';E) = \cos(k|\mathbf{r}-\mathbf{r}'|) + (\mathbf{r}-\mathbf{r}')^2\tilde{f}(\mathbf{r},\mathbf{r}';E) \tag{A.323}$$

where $k^2 = 2M[E-U(\mathbf{o})]/\hbar^2$ and $\tilde{f}(\mathbf{r},\mathbf{r}';E)$ is also analytic with $\tilde{f}(\mathbf{r}',\mathbf{r}';E)=0$. [For a mathematically exact justification of (A.323), we note that the coefficients $\alpha^{(k)}_{\nu m_\nu}$ (A.295) of the spherical power expansion (Theorem LXIII) of $f(\mathbf{r},\mathbf{r}';E)$ vanish for $\nu=0$ with the single exception of $\alpha^{(0)}_{00} = 1/\sqrt{4\pi}$, which means that the factor $(\mathbf{r}-\mathbf{r}')^2$ may be extracted from the function $f(\mathbf{r},\mathbf{r}';E)-1$. See also (A.261), (A.262).] Hence, we may rewrite (A.322):

$$\frac{f_{lm}(\mathbf{r},\mathbf{r}';E)}{|\mathbf{r}-\mathbf{r}'|^{2l+1}} = K_{lm}\left(\frac{\partial}{\partial\mathbf{r}'}\right)\left\{\frac{\cos k|\mathbf{r}-\mathbf{r}'|}{|\mathbf{r}-\mathbf{r}'|}\right\} + K_{lm}\left(\frac{\partial}{\partial\mathbf{r}'}\right)\left\{|\mathbf{r}-\mathbf{r}'|\,\tilde{f}(\mathbf{r},\mathbf{r}';E)\right\} \tag{A.324}$$

The first term in (A.322) incidentally represents the free-particle Green function part $f^{(\mathrm{free})}_{lm}(\mathbf{r},\mathbf{r}';E)$ which is explicitly evaluated in Appendix C.1 of this treatise. Indeed,

subtracting from the free-particle Green function $G_{lm}^{(\mathrm{free})}(\mathbf{r},\mathbf{r}';E)$ (C.17) the homogeneous contribution $h_{lm}^{(\mathrm{free})}(\mathbf{r},\mathbf{r}';E)$ (A.320), we obtain:

$$\begin{aligned} K_{lm}\left(\frac{\partial}{\partial\mathbf{r}'}\right)\left\{\frac{\cos k|\mathbf{r}-\mathbf{r}'|}{|\mathbf{r}-\mathbf{r}'|}\right\} &= \frac{K_{lm}(\mathbf{r}-\mathbf{r}')}{|\mathbf{r}-\mathbf{r}'|^{2l+1}}\,(k|\mathbf{r}-\mathbf{r}'|)^{l+1}\,n_l(k|\mathbf{r}-\mathbf{r}'|) \\ &= (2l-1)!!\,\frac{K_{lm}(\mathbf{r}-\mathbf{r}')}{|\mathbf{r}-\mathbf{r}'|^{2l+1}}\left(1+\frac{k^2(\mathbf{r}-\mathbf{r}')^2}{2(2l-1)}+\mathcal{O}[(\mathbf{r}-\mathbf{r}')^4]\right) \end{aligned} \tag{A.325}$$

Here, we denoted the irregular spherical Bessel function by $n_l(kR)$ ($R=|\mathbf{r}-\mathbf{r}'|$), using the sign convention employed by Messiah [83], p. 488. (See also the handbook by Abramowitz and Stegun [81], p. 437.) The important point is that $(kR)^{l+1}n_l(kR)$ is again an analytic and isotropic function that approaches the value $(2l-1)!!$ as $\mathbf{r}\to\mathbf{r}'$. The second term in (A.324) may be evaluated by repeated application of (A.321). We immediately find:

$$K_{lm}\left(\frac{\partial}{\partial\mathbf{r}'}\right)\left\{|\mathbf{r}-\mathbf{r}'|\,\tilde{f}(\mathbf{r},\mathbf{r}';E)\right\} = \frac{\tilde{f}_{lm}(\mathbf{r},\mathbf{r}';E)}{|\mathbf{r}-\mathbf{r}'|^{2l-1}} \tag{A.326}$$

Here, $\tilde{f}_{lm}(\mathbf{r},\mathbf{r}';E)$ is an analytic function of $\mathbf{r}$ and $\mathbf{r}'$ which is at least of order $|\mathbf{r}-\mathbf{r}'|^{l+1}$ at the pole $\mathbf{r}=\mathbf{r}'$. Again, a simpler representation is available for spherically symmetric potentials $U(R)$. By the same reasoning as above (A.319), we may show that in this case, the function $f_{lm}(\mathbf{r},\mathbf{r}';E)$ decomposes into a product of a solid harmonic $K_{lm}(\mathbf{r}-\mathbf{r}')$ with an analytic and isotropic function $f_l(R^2;E)$ which fulfils $f_l(0;E)=(2l-1)!!$:

$$f_{lm}(\mathbf{r},\mathbf{r}';E) = K_{lm}(\mathbf{r}-\mathbf{r}')\,f_l(R^2;E) \tag{A.327}$$

The free-particle solution $f_{lm}^{(\mathrm{free})}(\mathbf{r},\mathbf{r}';E)$ in (A.325) just presents an example. Let us now finally gather these results into a concise statement:

■ THEOREM LXVII

Let $H(\mathbf{r},\mathbf{p})=p^2/2M+U(\mathbf{r})$ be a self-adjoint Hamiltonian with a potential $U(\mathbf{r})$ which is analytic in a sector $\mathbb{S}\subseteq\mathbb{R}^3$. Then, the retarded multipole Green function $G_{lm}(\mathbf{r},\mathbf{r}';E)$ exists if E is not a member of the point spectrum of the Hamiltonian $H(\mathbf{r},\mathbf{p})$; it may be displayed in the form:

$$G_{lm}(\mathbf{r},\mathbf{r}';E) = -\frac{M}{2\pi\hbar^2}\,\frac{f_{lm}(\mathbf{r},\mathbf{r}';E)}{|\mathbf{r}-\mathbf{r}'|^{2l+1}} + h_{lm}(\mathbf{r},\mathbf{r}';E) \tag{A.328}$$

where $f_{lm}(\mathbf{r},\mathbf{r}';E)$ and $h_{lm}(\mathbf{r},\mathbf{r}';E)$ are analytic functions for $\mathbf{r},\,\mathbf{r}'\in\mathbb{S}$. The leading-order expansion for the function $f_{lm}(\mathbf{r},\mathbf{r}';E)$ reads:

$$f_{lm}(\mathbf{r},\mathbf{r}';E) = (2l-1)!!\,K_{lm}(\mathbf{r}-\mathbf{r}')\left(1+\frac{k^2(\mathbf{r}-\mathbf{r}')^2}{2(2l-1)}\right)+\mathcal{O}(r_k^{l+3},r_k'^{l+3}) \tag{A.329}$$

where $k^2 = 2M[E - U(\mathbf{o})]/\hbar^2$ is the local wave number at the origin. If the potential $U(\mathbf{r})$ is isotropic with respect to $\mathbf{r}'$, then these functions may be factorized:

$$\begin{aligned} f_{lm}(\mathbf{r}, \mathbf{r}'; E) &= K_{lm}(\mathbf{r} - \mathbf{r}')\, f_l[(\mathbf{r} - \mathbf{r}')^2; E] \\ h_{lm}(\mathbf{r}, \mathbf{r}'; E) &= K_{lm}(\mathbf{r} - \mathbf{r}')\, h_l[(\mathbf{r} - \mathbf{r}')^2; E] \end{aligned} \tag{A.330}$$

Here, $f_l[(\mathbf{r}-\mathbf{r}')^2; E]$ and $h_l[(\mathbf{r}-\mathbf{r}')^2; E]$ are analytic and isotropic functions independent of the magnetic quantum number m.

A.5.4 Multipole Current Matrix Elements

Finally, we may use the knowledge about multipole Green functions $G_{lm}(\mathbf{r}, \mathbf{r}'; E)$ that we have gained in the preceding section in order to infer some fundamental properties of the associated multipole current matrix elements $J_{lml'm'}(\mathbf{r}'; E)$ (2.30) that we introduced in Section 2.4. These matrix elements are required for the calculation of the total current $J_D(\mathbf{r}'; E)$ (2.29) emitted by a generalized point source $D(\mathbf{r} - \mathbf{r}')$ (2.26) and are given by:

$$J_{lml'm'}(\mathbf{r}'; E) = \frac{i}{\hbar} \lim_{\mathbf{r} \to \mathbf{r}'} \{A_{lml'm'}(\mathbf{r}, \mathbf{r}'; E) - A_{l'm'lm}(\mathbf{r}', \mathbf{r}; E)^*\} \tag{A.331}$$

where $A_{lml'm'}(\mathbf{r}, \mathbf{r}'; E)$ denotes the differential expression (2.28):

$$A_{lml'm'}(\mathbf{r}, \mathbf{r}'; E) = K^*_{lm}\left(\frac{\partial}{\partial \mathbf{r}}\right) K_{l'm'}\left(\frac{\partial}{\partial \mathbf{r}'}\right) G(\mathbf{r}, \mathbf{r}'; E) \tag{A.332}$$

Note that we chose to swap the arguments $\mathbf{r}$ and $\mathbf{r}'$ in the second matrix element in (A.331). Let us assume that $G(\mathbf{r}, \mathbf{r}'; E)$ represents the retarded Green function of the problem; then, we may use the symmetry property $G_{\mathrm{adv}}(\mathbf{r}, \mathbf{r}'; E) = G_{\mathrm{ret}}(\mathbf{r}', \mathbf{r}; E)^*$ (Section A.5.2) to restate the total current matrix element (A.331) in the form:

$$J_{lml'm'}(\mathbf{r}'; E) = \frac{i}{\hbar} \lim_{\mathbf{r} \to \mathbf{r}'} K^*_{lm}\left(\frac{\partial}{\partial \mathbf{r}}\right) K_{l'm'}\left(\frac{\partial}{\partial \mathbf{r}'}\right) \{G_{\mathrm{ret}}(\mathbf{r}, \mathbf{r}'; E) - G_{\mathrm{adv}}(\mathbf{r}, \mathbf{r}'; E)\} \tag{A.333}$$

This is the expression listed in Section 2.4.3. With the help of Theorem LXVI, we may even simplify it further: Since both Green functions $G_{\mathrm{ret/adv}}(\mathbf{r}, \mathbf{r}'; E)$ show identical singular parts $f(\mathbf{r}, \mathbf{r}'; E)$, we may replace them by their regular parts $h_{\mathrm{ret/adv}}(\mathbf{r}, \mathbf{r}'; E)$ (A.315) and obtain:

$$J_{lml'm'}(\mathbf{r}'; E) = \frac{i}{\hbar} \lim_{\mathbf{r} \to \mathbf{r}'} K^*_{lm}\left(\frac{\partial}{\partial \mathbf{r}}\right) K_{l'm'}\left(\frac{\partial}{\partial \mathbf{r}'}\right) \tilde{h}(\mathbf{r}, \mathbf{r}'; E) \tag{A.334}$$

where $\tilde{h}(\mathbf{r}, \mathbf{r}'; E) = h_{\mathrm{ret}}(\mathbf{r}, \mathbf{r}'; E) - h_{\mathrm{adv}}(\mathbf{r}, \mathbf{r}'; E)$ is a locally analytic function. Thus, the same property holds for the total current matrix elements $J_{lml'm'}(\mathbf{r}'; E)$.

Symmetries and the Green function. Let us now examine how rotational symmetries of the Hamiltonian $H(\mathbf{r},\mathbf{p})$ manifest themselves in the total current matrix elements $J_{lml'm'}(\mathbf{r}';E)$. Assume that the Hamiltonian operator $\mathcal{H}$ is invariant with respect to some (unitary) symmetry operation $\mathcal{S}$ with $\mathcal{S}^{-1}=\mathcal{S}^{+}$; then, $\mathcal{HS}=\mathcal{SH}$ must hold. Now consider the corresponding resolvent operator $\mathcal{R}(E)=(E\mathcal{E}-\mathcal{H})^{-1}$ (Definition XXXIX): We obviously have $\mathcal{S}=\mathcal{R}(E)(E\mathcal{E}-\mathcal{H})\mathcal{S}=\mathcal{R}(E)\mathcal{S}(E\mathcal{E}-\mathcal{H})$, so by applying the operator $\mathcal{R}(E)$ from the right, we obtain $\mathcal{SR}(E)=\mathcal{R}(E)\mathcal{S}$. This shows that the resolvent operator $\mathcal{R}(E)$ shares the symmetries of the Hamiltonian $\mathcal{H}$. At this point, we remark that the Green function $G(\mathbf{r},\mathbf{r}';E)$ denotes just the spatial representation of $\mathcal{R}(E)$. Hence, the symmetry $\mathcal{S}$ translates to $G(\mathbf{r},\mathbf{r}';E)$:

$$G(\mathbf{r},\mathbf{r}';E)=\langle\mathbf{r}\,|\mathcal{R}(E)|\,\mathbf{r}'\rangle=\left\langle\mathbf{r}\,\middle|\mathcal{S}^{+}\mathcal{R}(E)\mathcal{S}\middle|\,\mathbf{r}'\right\rangle=\langle\mathcal{S}\,\mathbf{r}\,|\mathcal{R}(E)|\,\mathcal{S}\,\mathbf{r}'\rangle=G(\mathcal{S}\,\mathbf{r},\mathcal{S}\,\mathbf{r}';E) \tag{A.335}$$

Our interest is directed in particular to rotational symmetries $\mathcal{S}(\Omega)$. Obviously, the Hamiltonian $H(\mathbf{r},\mathbf{p})$ will be invariant under a given rotation if the potential $U(\mathbf{r})$ is: $U[\mathcal{S}(\Omega)\,\mathbf{r}]=U(\mathbf{r})$. Now, let $\mathbf{r}'$ be a fixed point of this rotation: $\mathcal{S}(\Omega)\,\mathbf{r}'=\mathbf{r}'$. Then, the Green function $G(\mathbf{r},\mathbf{r}';E)$ will also show the rotational symmetry: $G[\mathcal{S}(\Omega)\,\mathbf{r},\mathbf{r}';E]=G(\mathbf{r},\mathbf{r}';E)$. We used this property implicitly already in our proof of Theorem LXVII.

Spherical symmetry. We first consider potentials which are spherically symmetric with respect to some origin $\mathbf{r}'$: $U(\mathbf{r})=U(|\mathbf{r}-\mathbf{r}'|)$. This case obviously covers all central potentials $U(r)$ (where $\mathbf{r}'=\mathbf{o}$), but also sources in a simple field-free environment (see Section 3.2 and Appendix C). Here, with $G(\mathbf{r},\mathbf{r}';E)$ also the locally analytic function $\tilde{h}(\mathbf{r},\mathbf{r}';E)$ in (A.334) is a spherical scalar: $\tilde{h}(\mathbf{r},\mathbf{r}';E)=\tilde{h}[(\mathbf{r}-\mathbf{r}')^2;E]$. Consequently, the object $K_{l'm'}[\partial/\partial\mathbf{r}']\,\tilde{h}(\mathbf{r},\mathbf{r}';E)$ is a spherical tensor of rank (l,m), and by the addition rules for angular momenta [238], we find that according to Theorem LXIII we may expand the argument of the limiting operation in (A.334) into a multipole series:

$$K^{*}_{lm}\left(\frac{\partial}{\partial\mathbf{r}}\right)K_{l'm'}\left(\frac{\partial}{\partial\mathbf{r}'}\right)\tilde{h}\left[(\mathbf{r}-\mathbf{r}')^2;E\right]=\sum_{j=0}^{\infty}\sum_{\mu=-j}^{j}(-1)^m\begin{pmatrix}l & l' & j\\ -m & m' & -\mu\end{pmatrix}\tilde{h}_{ll'j}\left[(\mathbf{r}-\mathbf{r}')^2;E\right]K_{j\mu}(\mathbf{r}-\mathbf{r}') \tag{A.336}$$

Here, a Wigner $3j$–symbol appears, and the scalar functions $\tilde{h}_{ll'j}\left[(\mathbf{r}-\mathbf{r}')^2;E\right]$ represent reduced matrix elements independent of the magnetic quantum numbers m, m', and μ. (This property of spherical tensors is known as the Wigner-Eckart theorem [238]. Expansions related to (A.336) are covered in greater detail in Appendix B.4.) Now, we note that the limit $\mathbf{r}\to\mathbf{r}'$ in (A.334) singles out the scalar term of the series (A.336) with $j=\mu=0$ as $K_{j\mu}(\mathbf{r}-\mathbf{r}')$ is a homogeneous polynomial of order j in

the variables $R_k = (\mathbf{r} - \mathbf{r}')_k$. But for $j = \mu = 0$, the $3j$–symbol contained in (A.336) delivers a zero result unless the selection rules $l = l'$ and $m = m'$ hold simultaneously, which means that all off-diagonal total current matrix elements $J_{lml'm'}(\mathbf{r}'; E)$ in (A.331) vanish. Furthermore, for $l = l'$ and $m = m'$ the $3j$–symbol adopts the value $(-1)^{l+m}/(2l+1)$ [238] which shows that for fixed l, the diagonal total current matrix element $J_{lm}(\mathbf{r}'; E) = J_{lmlm}(\mathbf{r}'; E)$ (2.33) does not depend on the choice of m, as one would naively expect anyway. In this treatise, the behavior detailed above is encountered in the Wigner law (3.27) describing the emission of sources in a field-free environment.

Cylindrical symmetry. Finally, let us analyze the case of potentials $U(z)$ that are merely symmetric with respect to rotations around a set of parallel axes, one of which we fix as the z axis. (An important example for this class of potentials, the uniform field potential $U(z) = -Fz$, is examined in Chapter 5 of this volume.) Clearly, for any axis containing $\mathbf{r}'$ parallel to the z axis, the Green function $G(\mathbf{r}, \mathbf{r}'; E)$ then possesses cylindrical symmetry and hence must present an eigenstate of the corresponding angular momentum operator $\mathcal{L}_z$ with eigenvalue $m = 0$. However, the total angular momentum of this function is no longer restricted. Thus, according to Theorem LXIII in Section A.5.2, we may expand the analytic auxiliary function $\tilde{h}(\mathbf{r}, \mathbf{r}'; E)$ (A.334) (which shares its symmetry properties with $G(\mathbf{r}, \mathbf{r}'; E)$) into a spherical power series:

$$\tilde{h}(\mathbf{r}, \mathbf{r}'; E) \;=\; \sum_{J=0}^{\infty} \tilde{h}_J \left[(\mathbf{r} - \mathbf{r}')^2; E\right] \; K_{J0}(\mathbf{r} - \mathbf{r}') \tag{A.337}$$

Proceeding in a manner analogous to (A.336), we may exploit the rules for the addition of angular momenta in order to evaluate the spherical tensor gradients appearing in (A.334):

$$\begin{aligned} K^*_{lm}\left(\frac{\partial}{\partial \mathbf{r}}\right) K_{l'm'}\left(\frac{\partial}{\partial \mathbf{r}'}\right) \tilde{h}(\mathbf{r}, \mathbf{r}'; E) \;=\; & \sum_{j=0}^{\infty} \sum_{\mu=-j}^{j} \sum_{j'=0}^{\infty} \sum_{\mu'=-j'}^{j'} \sum_{J=0}^{\infty} (-1)^m \;\times \\ & \begin{pmatrix} l & j' & j \\ -m & \mu' & -\mu \end{pmatrix} \begin{pmatrix} l' & J & j' \\ m' & 0 & -\mu' \end{pmatrix} \tilde{h}_{ll'jj'J}\left[(\mathbf{r} - \mathbf{r}')^2; E\right] K_{j\mu}(\mathbf{r} - \mathbf{r}') \end{aligned} \tag{A.338}$$

In this fairly complicated formula, again Wigner $3j$–symbols and reduced matrix elements $\tilde{h}_{ll'jj'J}[(\mathbf{r} - \mathbf{r}')^2; E]$ occur. It is easy to show that for potentials $U(\mathbf{r})$ with total spherical symmetry, i. e., $J \equiv 0$ in the sum (A.337), (A.338) reduces to the less intricate expression (A.336). In the general case, however, under the condition $j = \mu = 0$ enforced by the limiting operation in (A.334), from the properties of the $3j$–symbols we find that the total current matrix element will vanish unless the conditions $j' = l$ and $\mu' = m = m'$ hold. Thus, only the elements $J_{lml'm}(\mathbf{r}'; E)$ (A.331) with $m = m'$ need to

be considered in the case of cylindrical symmetry. This insight forms the foundation of the notation introduced in (2.31)–(2.33) in Section 2.4.

A.6 Conventional Perturbation Theory

In this final section, we want to show that the non-standard quantum source formalism of Chapter 2 delivers results equivalent to a number of well-known approaches to quantum scattering and perturbation theory even though the mathematical apparatus behind them is fairly different. (It may seem that the necessary agreement of the results from those various techniques renders the development of even another method like the source approach a superfluous exercise in mathematics. However, different methods suit different problems and needs, as may be illustrated by the fact that multipole source theory opens a simple path to the treatment of sources with angular orientation (Chapter 5), a task where the approaches noted in the following either fail or become extremely tedious.)

A.6.1 Eigenfunction Expansions of the Current

Let us first study the relation of the current $J(E)$ generated by a source $\sigma(\mathbf{r})$, i. e., an inhomogeneity in the Schrödinger equation (2.11), to the eigenfunctions $\psi_E(\mathbf{r})$ of the corresponding Hamiltonian $H(\mathbf{r},\mathbf{p})$. It is occasionally asserted that the Green function $G(\mathbf{r},\mathbf{r}';E)$ generally allows for an expansion into these eigenstates [82], but under closer scrutiny it appears that an eigenfunction expansion of the resolvent operator (Section A.3.6) requires certain properties of the Hamiltonian operator $\mathcal{H}$ it is based upon: The spectral family $\Pi(E)$ of $\mathcal{H}$ must be differentiable in the continuous spectrum of the Hamiltonian (Definition XXIII), and the spectrum of $\mathcal{H}$ must be either non-degenerate (Theorem XXIX), or the operator $\mathcal{H}$ should be separable within a set of one (Theorem XXXIV) or several commuting self-adjoint operators $\{\mathcal{A}_1,\ldots,\mathcal{A}_n\}$ (Theorem XXXVIII) with non-degenerate spectrum. (A full account of the theory is presented in Section A.3.) Only in these cases the spatial representations of the resolvent operators $\mathcal{R}(E)$ (Definition XXXIX) and the density of states operator $\partial\Pi(E)/\partial E$ (Definition XXIII) have well-defined expansions in terms of eigenfunctions, see e. g. (A.102), (A.124) and (A.152). Fortunately, under these premises, most analytically solvable problems in quantum theory allow for the resolution into eigenfunctions as they are based on separable Hamiltonians (see the text following Definition XXXVII for some examples). Now we are going to establish these expansions.

Operator representation of the current. In Section 2.3.2 we found that the current $J(E)$ generated by a source term $\sigma(\mathbf{r})$ may be displayed as a sesquilinear form con-

taining the retarded Green function $G(\mathbf{r},\mathbf{r}';E)$ as an integral kernel (2.17):

$$J(E) \;=\; -\frac{2}{\hbar}\,\Im\left[\int d^3r \int d^3r'\,\sigma(\mathbf{r})^*\,G(\mathbf{r},\mathbf{r}';E)\,\sigma(\mathbf{r}')\right] \tag{A.339}$$

The shape of this expression suggests that it just displays the spatial representation of a diagonal matrix element that involves an source state $|\sigma\rangle \in \mathbb{H}$ (where $\sigma(\mathbf{r}) = \langle\mathbf{r}|\sigma\rangle$ represents the source term assumed square-integrable in $\mathbb{R}^3$), and the resolvent operators $\mathcal{R}(E)$ of Section A.3.6, in particular the retarded resolvent operator $\mathcal{R}_{\rm ret}(E)$ (Theorem LI) that source theory is based upon. Indeed, we find from (A.339):

$$J(E) \;=\; -\frac{2}{\hbar}\,\Im\left[\langle\sigma\,|\mathcal{R}_{\rm ret}(E)|\,\sigma\rangle\right] \;=\; -\frac{2}{\hbar}\,\Im\left[\langle\sigma\,|\mathcal{R}_{\rm PV}(E)|\,\sigma\rangle \;-\; i\pi\;\langle\sigma\,|\partial\Pi(E)/\partial E|\,\sigma\rangle\right] \tag{A.340}$$

Here, we used (A.198). Remarking that $\mathcal{R}_{\rm PV}(E)$ is self-adjoint (Definition XLVI) and that the sesquilinear forms generated by the density of states "operator" $\partial\Pi(E)/\partial E$ are hermitian and non-negative [as the parent spectral family $\Pi(E)$ is self-adjoint and monotonic, see Theorem XIII, part (ii)], we find that the matrix elements appearing in (A.340) are real, thus $J(E)$ is a non-negative function of the energy E given by:

$$J(E) \;=\; \frac{2\pi}{\hbar}\,\left\langle\sigma\left|\frac{\partial\Pi(E)}{\partial E}\right|\sigma\right\rangle \tag{A.341}$$

Equation (A.341) gives the current $J(E)$ in terms of Dirac representation theory (Section A.2.1). We see that $J(E)$ is proportional to the expectation value of the density of states operator. In particular, this means that $J(E) = 0$ outside the continuous spectrum of $\mathcal{H}$ (Definition XVIII). Furthermore $J(E)$ is not defined at all if E is in the point spectrum of $\mathcal{H}$.

The fact that the current never becomes negative may be assigned to the "retarded" behavior of the time-dependent Green function operator $\mathcal{G}_{\rm ret}(t,t')$ (Section A.2.2) from which the resolvent $\mathcal{R}_{\rm ret}(E)$ is derived (A.190). The causality of $\mathcal{G}_{\rm ret}(t,t')$ is reflected in the fact that the current flows from the source into the continuum. Indeed, it is easy to show that the current $J(E)$ in (A.341) changes its sign if we replace $G(\mathbf{r},\mathbf{r}';E)$ in (A.339) by the advanced Green function $G_{\rm adv}(\mathbf{r},\mathbf{r}';E)$ (A.193) which amounts to a time reversal operation.

Eigenfunction representation. Let us now assume that $\mathcal{H}$ that is separable within a set of self-adjoint operators $\{\mathcal{A}_1,\ldots,\mathcal{A}_n\}$ (Definition XXXVII). Then, the density of states operator may be expanded into the eigenfunctions $\psi_{\mu_1,\ldots,\mu_n}(\mathbf{r})$ of the non-degenerate spectrum of this set (A.152), and we obtain from (A.341) the eigenfunction

representation of the current $J(E)$:

$$J(E) \;=\; \frac{2\pi}{\hbar} \prod_{k=1}^{n} \left\{ \sum_{\text{p.s.}} + \int_{\text{c.s.}} d\mu_k \right\} \delta[E - E(\mu_1, \ldots, \mu_n)] \left| \int d^3 r \, \sigma(\mathbf{r})^* \, \psi_{\mu_1,\ldots,\mu_n}(\mathbf{r}) \right|^2 \tag{A.342}$$

This result is especially useful for the determination of the multipole current $J_{lm}(\mathbf{r}'; E)$ (2.33) generated by the multipole sources $\sigma(\mathbf{r}) = \delta_{lm}(\mathbf{r} - \mathbf{r}') = K_{lm}[\partial/\partial\mathbf{r}']\,\delta(\mathbf{r} - \mathbf{r}')$ (2.23), the idealized normalized pointlike sources of multipole angular orientation introduced in Section 2.4. Performing the integration and differentiation procedure in (A.342), we are led to the representation of the multipole current $J_{lm}(\mathbf{r}'; E)$ in terms of the spherical tensor gradients [88–90] of the eigenfunctions $\psi_{\mu_1,\ldots,\mu_n}(\mathbf{r})$:

$$J_{lm}(\mathbf{r}'; E) \;=\; \frac{2\pi}{\hbar} \prod_{k=1}^{n} \left\{ \sum_{\text{p.s.}} + \int_{\text{c.s.}} d\mu_k \right\} \delta[E - E(\mu_1, \ldots, \mu_n)] \left| K_{lm}\left(\frac{\partial}{\partial \mathbf{r}'}\right) \psi_{\mu_1,\ldots,\mu_n}(\mathbf{r}') \right|^2 \tag{A.343}$$

Like the current $J(E)$ in the general case (A.341), also the multipole currents $J_{lm}(\mathbf{r}'; E)$ are manifestly non-negative.

The Tersoff-Hamann rule. As a special case, the expression (A.343) contains the common pointlike isotropic source $\sigma(\mathbf{r}) = \delta(\mathbf{r} - \mathbf{r}') = 4\pi\,\delta_{00}(\mathbf{r} - \mathbf{r}')$. For the corresponding s–wave current $J_{00}(\mathbf{r}'; E)$ (2.34), from (A.341) we directly obtain for this pointlike source with $|\sigma\rangle = |\mathbf{r}'\rangle$ [see (A.7)]:

$$J_{00}(\mathbf{r}'; E) \;=\; \frac{1}{2\hbar} \left\langle \mathbf{r}' \left| \frac{\partial \Pi(E)}{\partial E} \right| \mathbf{r}' \right\rangle \;=\; \frac{1}{2\hbar}\, n(\mathbf{r}'; E) \tag{A.344}$$

where $n(\mathbf{r}'; E) = \langle \mathbf{r}' \,|\partial\Pi(E)/\partial E|\, \mathbf{r}' \rangle$ (A.152) denotes the local density of states (LDOS) of the system for energy E and position $\mathbf{r}'$. This connection between current and LDOS has been pointed out in particular by Tersoff and Hamann [77,78] in their STM model (see Chapter 8).

As an example, we calculate the current $J_{00}(\mathbf{o}; E)$ generated by a normalized s–wave source $\sigma(\mathbf{r}) = \delta_{00}(\mathbf{r})$ located in the origin of a three-dimensional homogeneous field environment ($U(\mathbf{r}) = -Fz$). As the local density of states $n(\mathbf{o}; E)$ for this system has already been determined in Section A.3.5, according to (A.155) and (A.344) we immediately find:

$$J_{00}(\mathbf{o}; E) \;=\; \frac{M\beta F}{2\pi\hbar^3} \left\{ \mathrm{Ai}'(-2\beta E)^2 + 2\beta E\, \mathrm{Ai}(-2\beta E)^2 \right\} \tag{A.345}$$

(As usual, β denotes the inverse energy parameter as defined in (5.16), $\beta^3 = M/4\hbar^2 F^2$.) This result, which is obviously available in a very different manner from the direct Green function approach (5.48) that is pursued in Chapter 5, is also tabulated in Appendix E.3, entry (E.11).

A.6.2 The Fermi Golden Rule

In this section, we want to show how the quantum source approach presented in Chapter 2 reconciles with the arguably most popular method in perturbative quantum scattering calculations, Fermi's Golden Rule [114]. As is generally known, the rule asserts that the transition rate $\rho_{0\to f}$ from the initial state $|\Psi_0\rangle$ which is an "eigenstate" in the continuous spectrum of some unperturbed Hamiltonian $\mathcal{H}_0$ with energy E_0 into some different normalized final "eigenstate" $|\Phi_f\rangle$ of $\mathcal{H}_0$ with eigenvalue E_f in first-order perturbation theory is given by:

$$\rho_{0\to f} \;=\; \frac{2\pi}{\hbar}\,\left|\langle\Phi_f\,|\lambda\,\mathcal{W}|\,\Psi_0\rangle\right|^2\,\delta(E_f - E_0 - \hbar\omega) \tag{A.346}$$

Here, $\lambda\,\mathcal{V}(t) = \lambda\,\mathcal{W}\,e^{-i\omega t}$ is a perturbation operator of adjustable strength λ periodic in time, i. e., the complete Hamiltonian is given by $\mathcal{H}_\lambda(t) = \mathcal{H}_0 + \lambda\,\mathcal{W}\,e^{-i\omega t}$. Note that (A.346) only comprises contributions at most quadratic in the strength parameter λ.

Formal representation. In (A.346) we used the Dirac notation for eigenstates of the continuous spectrum which is not fortunate since the corresponding eigenfunctions $\psi_0(\mathbf{r}) = \langle\mathbf{r}|\Psi_0\rangle$ are not normalizable in the strict sense, and thus $|\Psi_0\rangle$ is not a true member of the Hilbert space (see Section A.3.2). Rather, these states are properly defined via the orthonormal family $\mathcal{C}(\mu_1,\ldots,\mu_n)$ of a set of self-adjoint operators $\{\mathcal{A}_1,\ldots,\mathcal{A}_n\}$ in which the unperturbed Hamiltonian $\mathcal{H}_0$ is separable (A.102). For convenience, we will nevertheless keep the bra-ket notation of (A.346) in the case of the initial "state" $|\Psi_0\rangle$; we remark, however, that the final "state" $|\Phi_f\rangle$ is represented by some member of the orthonormal family: $|\Phi_f\rangle\langle\Phi_f| = \mathcal{C}(\mu_1,\ldots,\mu_n)$. Using this notation, we replace (A.346) by the equivalent expression for the decay rate of $|\Psi_0\rangle$ into some eigenstate $(\mu_1,\ldots,\mu_n)$ in the spectrum of $\mathcal{H}_0$:

$$\rho_{0\to(\mu_1,\ldots,\mu_n)} \;=\; \frac{2\pi|\lambda|^2}{\hbar}\,\left\langle\Psi_0\left|\mathcal{W}^+\mathcal{C}(\mu_1,\ldots,\mu_n)\mathcal{W}\right|\Psi_0\right\rangle\,\delta\left[E(\mu_1,\ldots,\mu_n) - E_0 - \hbar\omega\right] \tag{A.347}$$

Clearly, in the source-theoretical approach our interest is directed towards the total decay rate of the initial state $|\Psi_0\rangle$ rather than to the specific transition rates $\rho_{0\to(\mu_1,\ldots,\mu_n)}$ (A.347) into single channels. Indeed, we may monitor the temporal decay of the corresponding time-dependent wave function $|\Psi_0(t)\rangle \;=\; e^{-iE_0t/\hbar}\,|\Psi_0\rangle$ by observing the

formation of a scattered part of the wave function $|\Psi_\lambda(t)\rangle = |\Psi(t)\rangle - |\Psi_0(t)\rangle$ caused by the perturbation operator $\lambda\mathcal{V}(t)$, where $|\Psi(t)\rangle$ and $|\Psi_0(t)\rangle$ denote the evolution of the wave functions under the action of the perturbed and unperturbed Hamiltonian operators $\mathcal{H}_\lambda(t)$ and $\mathcal{H}_0$, respectively. In the framework of quantum source theory, the rate of formation for $|\Psi_\lambda(t)\rangle$ should be accessible in form of a current $J[\Psi_0]$ (Section 2.3).

We therefore add up the decay rates $\rho_{0\to(\mu_1,\dots,\mu_n)}$ (A.347) for a complete set of final states $(\mu_1,\dots,\mu_n)$ in order to obtain the current $J[\Psi_0]$ predicted by Fermi's Golden Rule. Comparing with the resolution of the spectral density operator $\partial\Pi_0(E)/\partial E$ (Definition XXIII) assigned to the unperturbed Hamiltonian $\mathcal{H}_0$ into the orthonormal family $\mathcal{C}(\mu_1,\dots,\mu_n)$ (A.137), (A.152), we finally find that the current may be expressed as a matrix element involving the density of states of $\mathcal{H}_0$ at the energy $E = E_0 + \hbar\omega$:

$$\begin{aligned} J[\Psi_0] &= \frac{2\pi|\lambda|^2}{\hbar} \prod_{k=1}^{n} \left\{ \sum_{\text{p.s.}} + \int_{\text{c.s.}} d\mu_k \right\} \left\langle \Psi_0 \left| \mathcal{W}^+ \mathcal{C}(\mu_1,\dots,\mu_n) \mathcal{W} \right| \Psi_0 \right\rangle \times \\ &\qquad\qquad \delta\left[E(\mu_1,\dots,\mu_n) - E_0 - \hbar\omega\right] \\ &= \frac{2\pi|\lambda|^2}{\hbar} \left\langle \Psi_0 \left| \mathcal{W}^+ \frac{\partial\Pi_0(E)}{\partial E} \mathcal{W} \right| \Psi_0 \right\rangle \Big|_{E=E_0+\hbar\omega} \end{aligned} \tag{A.348}$$

We will show now how this result emerges in the quantum source approach.

Current due to a time-dependent localized source. Like in the preceding Section A.6.1, it is useful to put forward a formal version of the modified equation of continuity (2.15) for the inhomogeneous Schrödinger equation (2.7). Integrating over a volume Ω which completely contains the source $\sigma_\lambda(\mathbf{r},t)$ (where λ denotes the strength of the perturbation), by the divergence theorem we immediately obtain the relation:

$$\frac{\partial}{\partial t} \langle\Psi_\lambda(t)|\Psi_\lambda(t)\rangle_\Omega + \int_{\partial\Omega} \mathbf{j}_\lambda(\mathbf{r},t) \cdot d\mathbf{n}(\mathbf{r}) = -\frac{2}{\hbar} \Im\left[\langle\sigma_\lambda(t)|\Psi_\lambda(t)\rangle\right] \tag{A.349}$$

which is analogous to (A.341). Here, $\partial\Omega$ denotes the surface of the volume Ω, and the notation $\langle\Psi_\lambda(t)|\Psi_\lambda(t)\rangle_\Omega$ is used to indicate that the implicit spatial integration is to be performed only in Ω.

Source-theoretical derivation. Clearly, Fermi's Golden Rule in form of the expression (A.348) should arise in the linear approximation of time-dependent perturbation theory for the wave function $|\Psi_\lambda(t)\rangle$ (Section A.2.3). Considering only terms at most linear in the perturbative parameter λ, we thus obtain for the modified Schrödinger equation (A.25):

$$\left[i\hbar\partial_t - \mathcal{H}_0\right] \left\{|\Psi(t)\rangle - |\Psi_0(t)\rangle\right\} = \lambda\,\mathcal{V}(t)\,|\Psi_0(t)\rangle \tag{A.350}$$

(Here, we conveniently used the fact that $|\Psi_0(t)\rangle$ is a solution of the unperturbed problem.) Our first task is to solve this equation for $|\Psi_\lambda(t)\rangle = |\Psi(t)\rangle - |\Psi_0(t)\rangle$ including only terms linear in λ.

Even this simple task requires some discussion. Obviously, we are interested in a solution that primordially stems from the unperturbed eigenstate $|\Psi_0(t)\rangle$. On the other hand, imprinting a simple periodic time dependence on the perturbation $\mathcal{V}(t) = \mathcal{W}e^{-i\omega t}$ does not distinguish between "past" and "future" of the system, as the strength of the interaction potential remains constant in time. A simple solution to this problem is achieved by adding a converging factor to $\mathcal{V}(t)$: $\mathcal{V}(t) = \mathcal{W}e^{-i\omega t}\, e^{\eta t/\hbar}$. As $\eta \to 0^+$, the additional factor will exert arbitrary small influence on $\mathcal{V}(t)$ for any finite interval of time t, but it will enforce the vanishing of $\mathcal{V}(t)$ in the asymptotic limit $t \to -\infty$. Clearly, this also means $|\Psi_\lambda(t)\rangle \to 0$ as $t \to -\infty$, so the solution of (A.350) for $\eta \to 0^+$ will be causal and correspond to the retarded choice of the Green function, as the source $|\sigma(t)\rangle = \lambda\, \mathcal{V}(t)\, |\Psi_0(t)\rangle$ precedes the effect, i. e., the scattered wave function $|\Psi_\lambda(t)\rangle$. Copying the procedure of Section (A.2.3), the linear approximation to the scattered wave function we desire is simply given by the Born approximation (A.28) to (A.350), where we have to set $t' \to -\infty$ and employ the converging factor introduced above:

$$|\Psi_\lambda(t)\rangle \;\approx\; -\frac{i\lambda}{\hbar} \int_{-\infty}^{t} d\tau\, \mathcal{U}_0(t,\tau)\, \mathcal{V}(\tau)\; |\Psi_0(\tau)\rangle \tag{A.351}$$

Now, as an eigenstate of $\mathcal{H}_0$ (A.105), the time dependence of the unperturbed solution $|\Psi_0(t)\rangle$ in this equation is clearly given by $|\Psi_0(t)\rangle = e^{-i\Omega t}\, |\Psi_0\rangle$, where $E_0 = \hbar\Omega$. Furthermore, we may expand the time evolution operator $\mathcal{U}_0(t,\tau) = \exp(-i\mathcal{H}_0(t-\tau)/\hbar)$ (A.15) assigned to $\mathcal{H}_0$ into the spectral family $\Pi_0(E)$ of $\mathcal{H}_0$. According to (A.77) and (A.82), we find:

$$\mathcal{U}_0(t,\tau) \;=\; \int e^{-iE(t-\tau)/\hbar}\, \mathrm{d}\Pi_0(E) \;=\; \sum_{\text{p.s.}} e^{-iE_k(t-\tau)/\hbar}\, \mathcal{P}_0(E_k) + \int_{\text{c.s.}} dE\, e^{-iE(t-\tau)/\hbar}\, \frac{\partial \Pi_0(E)}{\partial E} \tag{A.352}$$

Inserting all these ingredients into the Born approximation (A.351), we obtain:

$$\begin{aligned} |\Psi_\lambda(t)\rangle \;&\approx\; -\frac{i\lambda}{\hbar} \int \mathrm{d}\Pi_0(E)\, \mathcal{W}\, |\Psi_0\rangle \left\{ \int_{-\infty}^{t} d\tau\, e^{\eta\tau/\hbar}\, e^{-iE(t-\tau)/\hbar}\, e^{-i(\Omega+\omega)\tau} \right\} \\ &\approx\; \lambda\, e^{\eta t/\hbar}\, e^{-i(\Omega+\omega)t} \left\{ \sum_{\text{p.s.}} \mathcal{P}_0(E) \;+\; \int_{\text{c.s.}} dE\, \frac{\partial \Pi_0(E)}{\partial E} \right\} \frac{\mathcal{W}\, |\Psi_0\rangle}{\hbar(\Omega+\omega) - E + i\eta} \end{aligned} \tag{A.353}$$

where the limit $\eta \to 0^+$ is implied. A notable feat of (A.353) is the harmonic behavior of the scattered wave function $|\Psi_\lambda(t)\rangle$: Ignoring the arbitrarily slowly varying con-

verging factor $e^{\eta t/\hbar}$, the scattered wave oscillates with a single frequency: $|\Psi_\lambda(t)\rangle = e^{-i(\Omega+\omega)t}\,|\Psi_\lambda\rangle$, which implies that its square modulus in any given volume Ω $\langle\Psi_\lambda|\Psi_\lambda\rangle_\Omega$ is constant within finite intervals of time t. (In this respect, the system resembles classical oscillators driven by a periodic perturbation.) Furthermore, we note that (A.353) diverges whenever $\hbar(\Omega+\omega)$ matches the energy E_k of a bound state of $\mathcal{H}_0$. The failure of the approximation (A.353) in these cases may be traced back to the fact that true eigenstates of $\mathcal{H}_0$ are always normalizable, whereas the "norm" of the "eigenstate" $|\Psi_0\rangle$ in the continuous spectrum of $\mathcal{H}_0$ is necessarily infinite (A.80). Thus, the range of validity of (A.353) is limited to those values of $\hbar(\Omega+\omega)$ that correspond to the continuous spectrum and resolvent set of $\mathcal{H}_0$.

Now we may insert the approximate solution (A.353) into the equation of continuity (A.349). Ignoring the additional term $e^{\eta t/\hbar}$ which yields unity for all finite times t, we immediately infer from (A.353) that the scattering solution $|\Psi_\lambda(t)\rangle$ supports a constant number of particles inside the volume Ω. Thus, the source term $|\sigma_\lambda(t)\rangle = \lambda e^{-i(\Omega+\omega)t}\mathcal{W}\,|\Psi_0\rangle$ of (A.350) causes a stationary current of scattered particles, and we obtain the following Stieltjes integral representation [231] for the current $J[\Psi_0]$:

$$\begin{aligned} J[\Psi_0] &= -\frac{2}{\hbar}\,\Im\left[\,\langle\sigma_\lambda(t)|\Psi_\lambda(t)\rangle\right] = \lim_{\eta\to 0^+} -\frac{2|\lambda|^2}{\hbar}\,\Im\left[\int \frac{\mathrm{d}\,\langle\Psi_0\,|\mathcal{W}^+\,\Pi_0(E)\,\mathcal{W}|\,\Psi_0\rangle}{\hbar(\Omega+\omega)-E+i\eta}\right] \\ &= \frac{2\pi|\lambda|^2}{\hbar}\,\left\langle\Psi_0\,\middle|\,\mathcal{W}^+\,\frac{\partial\Pi_0(E)}{\partial E}\,\mathcal{W}\,\middle|\,\Psi_0\right\rangle\Big|_{E=E_0+\hbar\omega} \end{aligned} \tag{A.354}$$

The last line follows from the fact that apart from the energy denominator, the integrand as the diagonal matrix element of a hermitian operator is real. By application of the distribution formula [215]:

$$\int \frac{\phi(E)\,dE}{\hbar(\Omega+\omega)-E+i\eta} = \fint \frac{\phi(E)\,dE}{\hbar(\Omega+\omega)-E} - i\pi\phi[\hbar(\Omega+\omega)] \tag{A.355}$$

that we repeatedly used before (A.192), we are led to the representation (A.81) for the density of states operator $\partial\Pi_0(E)/\partial E$, and finally arrive at (A.354).

Comparison of (A.348) and (A.354) shows that Fermi's Golden Rule and the quantum source approach of Section 2.3 indeed deliver identical results for the total transition rate within the continuous spectrum of the Hamiltonian $\mathcal{H}_0$ caused by a periodic perturbative potential $\lambda\,\mathcal{V}(t)$, as it must be. We should also note that we already employed a less formal variant of this derivation in order to illustrate how an electron source emerges within the photodetachment setup (3.11). There, the perturbation was caused by the interaction of negatively charged ions with the periodic electric field of a laser beam, thus generating a stationary current of monoenergetic electrons moving under the influence of an external uniform force field representing the unperturbed Hamiltonian (Section 3.1).

A.6.3 The Transfer Hamiltonian Method

Finally, in this subsection we want to apply the quantum source formalism in order to justify the perturbative approach that has been traditionally used to calculate tunneling currents in the STM setup (Chapter 8), the transfer Hamiltonian theory involving matrix elements of the current density operator which was originally developed by Bardeen [193] for the description of layered metal-insulator-superconductor (MIS) diodes of planar structure [194]. Shortly following the first experimental reports of scanning tunneling microscopy [72], the transfer Hamiltonian technique was employed by Tersoff and Hamann [77, 78, 181] for a basic theoretical description of STM. They found the simple result that the tunneling current $J(\mathbf{R})$ in the STM junction is principially determined by the local density of states (LDOS) $n(\mathbf{R}; E_F)$ of the sample at the apex $\mathbf{R}$ of the STM tip, evaluated at the Fermi level E_F. Notwithstanding its simplicity, this standard theoretical description of the STM imaging process still represents the benchmark for more sophisticated and computationally demanding approaches to the STM problem. As an important refinement, later on the transfer Hamiltonian technique was extended to tips supporting non-spherical states by Chen [182, 183].

We have seen that the notion of the local density of states $n(\mathbf{r}'; E)$ arises quite naturally in the source approach (A.152) and is connected to the imaginary part of the retarded Green function $\Im[G(\mathbf{r}', \mathbf{r}'; E)]$ of the quantum system under consideration (Theorem LI). Therefore, we may expect that quantum source theory, in particular in its multipole form of Section 2.4, not only is apt for a description of STM as demonstrated in Chapter 8, but also that we are indeed able to establish equivalence to the practical and successful transfer Hamiltonian approach. This is done in the following.

The Bardeen approach. Let us quickly review the expression for the tunneling current $J(\mathbf{R})$ obtained in the transfer Hamiltonian method. For simplicity, we first examine only the current contribution $\rho_{0\to f}$ that is generated by a specific "eigenstate" $\psi_E^0(\mathbf{r}) = \langle \mathbf{r}|\Psi_E^0\rangle$ of the tip placed at $\mathbf{R}$ and flows through the junction towards the sample, where it populates some selected normalized sample eigenstate $\phi_E^f(\mathbf{r}) = \langle \mathbf{r}|\Phi_E^f\rangle$ of the same energy. In general, both "eigenstates" are in the continuous spectrum of the tip-sample Hamiltonian $\mathcal{H}$ and thus are not normalizable in the ordinary sense; for convenience, we nevertheless keep the Dirac notation. (Let us first ignore the reverse process and thermodynamic weighing factors which will be easily included later.) Then, Tersoff-Hamann theory asserts that this partial current is given by:

$$\rho_{0\to f} \;=\; \frac{2\pi}{\hbar}\,\left|\left\langle \Phi_E^f\,|\mathcal{M}|\,\Psi_E^0\right\rangle\right|^2\,\delta(E_0 - E_f) \tag{A.356}$$

We chose our notation in a manner that emphasizes the close relation of the transfer Hamiltonian approach to Fermi's Golden Rule (A.346).

The quantity $\langle \Phi_E^f \,|\mathcal{M}|\, \Psi_E^0 \rangle$, the so-called transfer Hamiltonian matrix element, was first derived by Bardeen [193] to describe tunneling through a layered MIS structure as noted above, and contains an expression reminiscent of the current integral that involves the normalized wave functions $\psi_E^0(\mathbf{r})$ and $\phi_E^f(\mathbf{r})$ of the unperturbed semi-systems: The wave function $\phi_E^f(\mathbf{r})$ oscillates in the metal part and decays exponentially within the barrier region whereas $\psi_E^0(\mathbf{r})$ is contained in the superconductor region and leaks into the barrier from the other side. Using these notations, Bardeen obtained for the matrix element $\langle \Phi_E^f \,|\mathcal{M}|\, \Psi_E^0 \rangle$:

$$\left\langle \Phi_E^f \,|\mathcal{M}|\, \Psi_E^0 \right\rangle \;=\; -\frac{i\hbar^2}{2M} \int_{\partial\Omega} \left[\phi_E^f(\mathbf{r})^* \boldsymbol{\nabla} \psi_E^0(\mathbf{r}) - \psi_E^0(\mathbf{r}) \boldsymbol{\nabla} \phi_E^f(\mathbf{r})^* \right] \cdot d\mathbf{n}(\mathbf{r}) \qquad \text{(A.357)}$$

Here, $\partial\Omega$ denotes a surface within the insulator layer that separates both conducting regions, and $d\mathbf{n}(\mathbf{r})$ its surface normal. Obviously, in principle the current matrix element $\langle \Phi_E^f \,|\mathcal{M}|\, \Psi_E^0 \rangle$ should not depend on the exact choice of $\partial\Omega$, a requirement that is only approximately fulfilled by (A.357).

Source view of Tersoff-Hamann theory. This expression was taken over by Tersoff and Hamann [77,78] to describe tunneling in the tip-sample system of STM. It is tempting to identify $\phi_E^f(\mathbf{r})$ with the wave functions of the sample that are ideally represented by the normalized eigenstates $\psi_E(\mathbf{r})$ of the complete tip-sample potential $U(\mathbf{r}, \mathbf{R})$, including the applied voltage V, i. e., solutions of the customary stationary Schrödinger equation:

$$\left[E + \frac{\hbar^2}{2M} \Delta - U(\mathbf{r}, \mathbf{R}) \right] \psi_E(\mathbf{r}) \;=\; 0 \qquad \text{(A.358)}$$

Since the wave functions $\psi_E(\mathbf{r})$ decay exponentially in the tunneling sector outside the sample, the potential of the tip region hardly influences their structure. (It should be noted, however, that this is not true in the rare case that E represents an eigenenergy of the isolated tip, in which case $\psi_E(\mathbf{r})$ will grow exponentially in the tunnel region, and the tunneling current $J(\mathbf{R}; E)$ is strongly enhanced. This is exactly the condition of resonant tunneling.)

Unlike the sample states, the tip state $\psi_E^0(\mathbf{r})$ is not as easily obtained as in Bardeen's original problem of stacked layers. This is because the tip side in the STM setup represents a finite-size potential structure that does not support eigenstates (except for isolated bound states that are responsible for resonant tunneling). There is, however, a workaround to that problem that has implicitly been used by Tersoff and Hamann,

and it again relies on the introduction of an electronic source term $\sigma(\mathbf{r}-\mathbf{R})$ as presented in Section 2.3 of this work. Let us state the main properties required of the function $\psi_E^0(\mathbf{r})$: It should be concentrated within the tip region $\mathbf{r} \approx \mathbf{R}$, and decay exponentially in the tunneling region, towards the sample surface. Furthermore, in the vicinity of the integration surface $\partial\Omega$, it is required to be a solution of the stationary Schrödinger equation (A.358) of the system. A natural candidate for the wave function $\psi_E^0(\mathbf{r})$ is therefore given by a solution of the modified Schrödinger equation (2.11):

$$\left[E + \frac{\hbar^2}{2M}\Delta - U(\mathbf{r},\mathbf{R})\right] \psi_E^0(\mathbf{r}) \;=\; \sigma(\mathbf{r}-\mathbf{R}) \tag{A.359}$$

In fact, the s–wave originally used by Tersoff and Hamann [77,78] for the tip side in (A.357):

$$\psi_E^0(\mathbf{r}) \;=\; -\,C\,\frac{M}{2\pi\hbar^2}\,\frac{\exp\left(-\,\kappa\,|\mathbf{r}-\mathbf{R}|\right)}{|\mathbf{r}-\mathbf{R}|} \tag{A.360}$$

where the evanescent wave vector κ is connected to the work function Φ of the surface via $\hbar\kappa = (2m\Phi)^{1/2}$, is just the free-particle solution to a pointlike source $\sigma(\mathbf{r}) = C\delta(\mathbf{r}-\mathbf{R})$ for an energy $E = -\Phi$, and therefore proportional to the free-particle Green function $G^{(\mathrm{free})}(\mathbf{r},\mathbf{R};-\Phi)$ (3.25). In the general case, following (2.14) the tip-side wave function $\psi_E^0(\mathbf{r})$ will be given by the convolution of the tip source term $\sigma(\mathbf{r}-\mathbf{R})$ with the Green function $G(\mathbf{r},\mathbf{r}';E)$ of the system (the choice of boundary condition proves irrelevant here):

$$\psi_E^0(\mathbf{r}) \;=\; \int d^3r'\, G(\mathbf{r},\mathbf{r}';E)\,\sigma(\mathbf{r}'-\mathbf{R}) \tag{A.361}$$

(Note that the Green function $G(\mathbf{r},\mathbf{r}';E)$ implicitly depends on the location of the tip $\mathbf{R}$, as the potential $U(\mathbf{r},\mathbf{R})$ in (A.359) is a function of the tip position.)

It is now easily proven that with this choice of wave functions $\phi_E^f(\mathbf{r}) = \psi_E(\mathbf{r})$ and $\psi_E^0(\mathbf{r})$, both the source method and the conventional theory lead to equivalent results. To this end, we note that in the case of STM, the integration surface $\partial\Omega$ in Bardeen's integral (A.357) may be closed around the tip. By virtue of the divergence theorem, and using (A.358) and (A.359), we obtain:

$$\begin{aligned}\left\langle \Phi_E^f \left|\mathcal{M}\right| \Psi_E^0 \right\rangle \;&=\; -\,\frac{i\hbar^2}{2M}\int_\Omega d^3r\;\left[\psi_E(\mathbf{r})^*\,\Delta\,\psi_E^0(\mathbf{r}) - \psi_E^0(\mathbf{r})\,\Delta\,\psi_E(\mathbf{r})^*\right] \\ &=\; -\,i\int_\Omega d^3r\,\sigma(\mathbf{r}-\mathbf{R})\,\psi_E(\mathbf{r})^* \;=\; -\,i\,\langle\Phi_E^f|\sigma(\mathbf{R})\rangle\end{aligned} \tag{A.362}$$

Here, Ω denotes the volume enclosed by $\partial\Omega$. Notably, identification of the tip state $\psi_E^0(\mathbf{r})$ with the solution of the inhomogeneous equation (A.359) ensures that the transfer Hamiltonian matrix element $\langle \Phi_E^f \left|\mathcal{M}\right| \Psi_E^0\rangle$ (A.357) is independent of the choice of

the separating surface $\partial\Omega$ as long as the source $\sigma(\mathbf{r}-\mathbf{R})$ is completely contained in the volume Ω, as it must be.

Like in the preceding section, we now may sum up all current contributions $\rho_{0\to f}$ (A.356) that belong to the specific energy $E = E_f = E_0$ in order to find the current $J(\mathbf{R};E)$ of electrons with energy E tunneling from tip to sample. We again assume that the Hamiltonian $\mathcal{H}$ of the tip-sample system is separable into a set of n self-adjoint operators $\{\mathcal{A}_1,\ldots,\mathcal{A}_n\}$ with non-degenerate spectrum (Definition XXXVII in Section A.3.5). Then, the normalized sample states $|\Phi_E^f\rangle$ may be represented through the orthonormal family of operators $\mathcal{C}(\mu_1,\ldots,\mu_n)$ of that set: $|\Phi_E^f\rangle\langle\Phi_E^f| = \mathcal{C}(\mu_1,\ldots,\mu_n)$ for some member $(\mu_1,\ldots,\mu_n)$ of the combined spectrum. Summing over all "final" states $|\Phi_E^f\rangle$ in (A.356), we obtain for $J(\mathbf{R};E)$ using (A.362) and the representation (A.152) of the density of states operator $\partial\Pi(E)/\partial E$ assigned to the Hamiltonian $\mathcal{H}$ in terms of the orthonormal family $\mathcal{C}(\mu_1,\ldots,\mu_n)$:

$$\begin{aligned} J(\mathbf{R};E) &= \frac{2\pi}{\hbar}\prod_{k=1}^{n}\left\{\sum_{\text{p.s.}}+\int_{\text{c.s.}}d\mu_k\right\}\langle\sigma(\mathbf{R})\,|\mathcal{C}(\mu_1,\ldots,\mu_n)|\,\sigma(\mathbf{R})\rangle\;\delta\left[E(\mu_1,\ldots,\mu_n)-E\right] \\ &= \frac{2\pi}{\hbar}\left\langle\sigma(\mathbf{R})\left|\frac{\partial\Pi(E)}{\partial E}\right|\sigma(\mathbf{R})\right\rangle \end{aligned} \tag{A.363}$$

Comparing with (A.341), we find that the current $J(\mathbf{R};E)$ obtained in the transfer Hamiltonian approach equals the stationary current generated by the formal electron source $\sigma(\mathbf{r}-\mathbf{R})$ for the same energy E. If this source is approximated through a pointlike structure $\sigma(\mathbf{r}-\mathbf{R}) = C\delta(\mathbf{r}-\mathbf{R})$, then according to (A.344) source theory verifies the famous result of Tersoff and Hamann that $J(\mathbf{R};E)$ is proportional to the local density of states $n(\mathbf{R};E)$ at the tip apex $\mathbf{R}$ [77,78].

Source representation of the STM current. From the current contributions $J(\mathbf{R};E)$ (A.363), it is now but a simple task to find a formal representation for the total current $J(\mathbf{R})$ passed through an STM junction at finite temperature T. Let $\mathcal{H}$ denote the Hamiltonian of the tip-sample system, where the source properties of the tip are represented by the source term $\sigma(\mathbf{r}-\mathbf{R}) = \langle\mathbf{r}|\sigma(\mathbf{R})\rangle$. Bearing in mind that the applied voltage V causes a relative shift of the Fermi levels E_F in the tip and sample region by eV and correspondingly different occupation factors $f(E) = \{\exp[(E-E_F)/kT]+1\}^{-1}$ in these regions (see Chapter 8), the total current $J(\mathbf{R})$ is obtained from $J(\mathbf{R};E)$ by integration as the difference between the partial currents directed from tip to sample and vice versa:

$$J(\mathbf{R}) = \frac{2\pi}{\hbar}\int\left[f(E)-f(E+eV)\right]\,\mathrm{d}\,\langle\sigma(\mathbf{R})\,|\Pi(E)|\,\sigma(\mathbf{R})\rangle \tag{A.364}$$

This Stieltjes integral representation of $J(\mathbf{R})$ involves the spectral family $\Pi(E)$ (Definition XII) assigned to the Hamiltonian $\mathcal{H}$ of the tip-sample system in the STM setup.

Appendix B

Developments on Solid Harmonics

AMONG THE SPECIAL FUNCTIONS of mathematical physics, the spherical harmonics $Y_{lm}(\hat{r})$ ($\hat{r} = \mathbf{r}/r$) occupy a prominent position due to their widespread use and versatility. This appendix deals with a class of closely related functions, so-called solid harmonics, which cover harmonic functions that are simultaneously eigenstates of angular momentum. From the results of Section 2.4 we may infer that the term solid harmonics refers to harmonic polynomials $K_{lm}(\mathbf{r}) = r^l Y_{lm}(\hat{r})$ (regular solid harmonics) as well as multipole potentials $\Phi_{lm}(\mathbf{r}) = r^{-(l+1)} Y_{lm}(\hat{r})$ (irregular solid harmonics) (2.19). Both sets of functions are interesting in their own right: The harmonic polynomials $K_{lm}(\mathbf{r})$ present simple homogeneous polynomials of order l in the coordinates x, y and z carrying the angular orientation of the underlying spherical harmonic $Y_{lm}(\hat{r})$, whereas the class of multipole potentials $\Phi_{lm}(\mathbf{r})$ forms the base of the developments in potential theory.

Owing to their popularity, over the years a vast amount of articles and reviews [88–90, 128, 239, 240] concerning the mathematical properties of these functions has been published. Surprisingly, some quite useful expansions are missing in the generally available literature on the subject. This includes two important theorems that describe the behavior of solid harmonics with respect to differentiation and spatial translation operations, which are fundamental to our mathematical presentation of the theory of uniform field multipole Green functions (Chapter 5). Hence, in this appendix it is our policy to provide detailed proofs for those expansions not included in the works cited above. We will however state without proof some widely known formulae connected to spherical harmonics whose derivation is readily accessible from the literature.

B.1 Harmonic Polynomials in Cylindrical Coordinates

We start out with the representation of harmonic polynomials $K_{lm}(\mathbf{r})$ in terms of cylindrical coordinates (ρ, z, ϕ) where $x + iy = \rho \exp(i\phi)$. (For a proof of the following formula, we cite the table of Varshalovich, Moskalev, and Khersonskii [240], p. 133,

which presents a comprehensive source for information of this kind.)

$$K_{lm}(x,\,y,\,z) \;=\; \sum_{j\,=\,|m|}^{l\;\prime} U_{jlm}\,\rho^{j} e^{im\phi} z^{l-j} \tag{B.1}$$

In this expression, the prime indicates that the sum index j should be incremented by two ($j = |m|,\, |m|+2,\, \ldots$). The expansion coefficient U_{jlm} appearing in (B.1) reads in explicit form:

$$U_{jlm} \;=\; \frac{i^{j+m}}{2^{j}\,(l-j)!}\,\sqrt{\frac{2l+1}{4\pi}}\,\frac{\sqrt{(l+m)!\,(l-m)!}}{\left(\frac{j-m}{2}\right)!\,\left(\frac{j+m}{2}\right)!} \tag{B.2}$$

For a vector $\mathbf{a} = a\hat{e}_z$ pointing in the direction of the quantization axis, the expansion (B.1) drastically simplifies. We immediately obtain for this special case:

$$K_{lm}(a\hat{e}_z) \;=\; \sqrt{\frac{2l+1}{4\pi}}\;a^{l}\,\delta_{m0} \tag{B.3}$$

Note that apart from the $m = 0$ (longitudinal) contribution, all harmonic polynomials vanish along the axis of quantization.

B.2 The Addition Theorem

The special value of $K_{lm}(a\hat{e}_z)$ stated in (B.3) may also be obtained from the standard representation of $Y_{lm}(\hat{r})$ in terms of spherical coordinates. The longitudinal harmonic polynomial $K_{l0}(r,\theta,\phi)$ then reads (see the monograph by Edmonds [128], p. 24):

$$K_{l0}(r,\theta) \;=\; \sqrt{\frac{2l+1}{4\pi}}\;r^{l}\,P_{l}(\cos\theta) \tag{B.4}$$

Here, $P_l(\cos\theta)$ denotes the Legendre polynomial of the l.th order [81]. We note that $P_l(1) = 1$ holds for all integer l, thus proving again the formula for the special value given in (B.3).

As eigenfunctions of the hermitian operators for the angular momentum $L^2(\theta,\phi)$ and $L_z(\phi)$, the spherical harmonics $Y_{lm}(\theta,\phi)$ form a complete base of orthonormal functions on the surface Ω of the unit sphere:

$$\int d\Omega\, Y^{*}_{lm}(\Omega)\, Y_{LM}(\Omega) \;=\; \delta_{lL}\,\delta_{mM} \tag{B.5}$$

(See also Appendix A.3, in particular the notes following Definition XXXVII.) It is mainly this orthonormality relation that the application of spherical harmonics and related functions in series expansions is founded upon.

In the course of rotations $\mathcal{R}$ of the unit sphere, the total angular momentum l remains conserved, yet the same property generally does not hold true for the magnetic quantum number m. Rather, the set of functions $Y_{lm}(\Omega)$, $m = -l, -l+1, \ldots, l-1, l$, forms a $(2l+1)$–dimensional representation of the rotation group. Consequently, the expansion of spherical harmonics in a rotated frame is performed by some rotation matrix $\mathcal{D}^{(l)}(\mathcal{R}) = \mathcal{D}^{(l)}(\Phi_E, \Theta_E, \Psi_E)$ of rank $2l+1$:

$$Y_{lM}(\mathcal{R}\hat{r}) \;=\; \sum_{m=-l}^{l} \mathcal{D}^{(l)}_{Mm}(\Phi_E, \Theta_E, \Psi_E)\, Y_{lm}(\hat{r}) \tag{B.6}$$

Here, $(\Phi_E, \Theta_E, \Psi_E)$ represent the Euler angles of the rotation $\mathcal{R}$ [142]. The elements of the rotation matrix $\mathcal{D}^{(l)}_{Mm}(\mathcal{R})$ are given e. g. in the book of Edmonds [128], p. 58.

Since the orthonormality property (B.5) is preserved under arbitrary rotations $\mathcal{R}$, $\mathcal{D}^{(l)}(\mathcal{R})$ must be a unitary matrix [128]. This immediately follows from (B.6) by integration:

$$\begin{aligned}\int d\Omega\, Y^*_{lM}(\mathcal{R}\hat{r})\, Y_{lM'}(\mathcal{R}\hat{r}) &= \sum_{m,\mu=-l}^{l} \mathcal{D}^{(l)}_{Mm}(\mathcal{R})^*\, \mathcal{D}^{(l)}_{M'\mu}(\mathcal{R}) \int d\Omega\, Y^*_{lm}(\hat{r})\, Y_{l\mu}(\hat{r}) \\ &= \sum_{m=-l}^{l} \mathcal{D}^{(l)}_{Mm}(\mathcal{R})^*\, \mathcal{D}^{(l)}_{M'm}(\mathcal{R}) \;=\; \delta_{MM'}\end{aligned} \tag{B.7}$$

Hence, we find that the unitarity condition $\mathcal{D}^{(l)}(\mathcal{R})\, \mathcal{D}^{(l)}(\mathcal{R})^+ = \mathcal{E}$ is fulfilled.

We may exploit the unitary of the $\mathcal{D}^{(l)}(\Phi_E, \Theta_E, \Psi_E)$ in order to show that the "scalar product" of sets of spherical harmonics $Y_{lm}(\hat{r}')$, $Y_{lm}(\hat{r})$ is indeed a scalar, i. e., remains unchanged in the course of rotations $\mathcal{R}$:

$$\begin{aligned}\sum_{M=-l}^{l} Y^*_{lM}(\mathcal{R}\hat{r}')\, Y_{lM}(\mathcal{R}\hat{r}) &= \sum_{m,\mu=-l}^{l} \left(\sum_{M=-l}^{l} \mathcal{D}^{(l)}_{Mm}(\mathcal{R})^*\, \mathcal{D}^{(l)}_{M\mu}(\mathcal{R}) \right) Y^*_{lm}(\hat{r}')\, Y_{l\mu}(\hat{r}) \\ &= \sum_{m=-l}^{l} Y^*_{lm}(\hat{r}')\, Y_{lm}(\hat{r})\end{aligned} \tag{B.8}$$

Equation (B.8) assumes an especially compact form when the rotation $\mathcal{R}$ is chosen in such a way that $\mathcal{R}\hat{r}' = \hat{e}_z$ points in the direction of the quantization axis. According to (B.3), in this case only the term with $M = 0$ will contribute to the sum in (B.8). In combination with (B.4), we obtain the following formula:

$$\sum_{m=-l}^{l} Y^*_{lm}(\hat{r}')\, Y_{lm}(\hat{r}) \;=\; \frac{2l+1}{4\pi}\, P_l(\cos\alpha) \tag{B.9}$$

Here, α denotes the invariant angle between the unit vectors $\hat{r}$ and $\hat{r}'$. The relation (B.9) is known as the addition theorem for spherical harmonics [83, 128].

B.3 Multipole Expansion of Plane Waves

In this treatise, generally two kinds of series expansion are repeatedly used: Often, we consider angular distributions of certain fields where the decomposition into multipoles, i. e., eigenfunctions of angular momentum is appropriate. The other important expansion technique considers translations leading to Taylor series. The eigenfunctions are given here by plane waves $\exp(i\mathbf{a}\cdot\mathbf{p})$. To connect both methods, the multipole expansion of a plane wave is required, which we will state below.

B.3.1 The Plane Wave Expansion

This endeavour starts out with an ubiquitous expansion formula for the plane wave $\exp(iap\cos\alpha)$ in terms of Legendre polynomials (see the handbook by Abramowitz and Stegun [81], p. 440):

$$e^{iap\cos\alpha} = \sum_{l=0}^{\infty} (2l+1)\, i^l\, j_l(ap)\, P_l(\cos\alpha) \tag{B.10}$$

In this expression, $j_l(ap)$ denotes the regular spherical Bessel function of order l [81, 83]. We may restate this expansion in a more fruitful fashion by introducing spherical harmonics $Y_{lm}(\hat{a})$, $Y_{lm}(\hat{p})$ in favor of the Legendre polynomial. Using the addition theorem (B.9) for spherical harmonics, and interpreting α as the angle between two vectors $\mathbf{a}$, $\mathbf{p}$ of modulus a and p, respectively, we obtain from (B.10) the expansion of a plane wave in terms of multipoles:

$$e^{i\mathbf{a}\cdot\mathbf{p}} = 4\pi \sum_{l=0}^{\infty} i^l\, j_l(ap) \sum_{m=-l}^{l} Y^*_{lm}(\hat{a})\, Y_{lm}(\hat{p}) \tag{B.11}$$

This expression may be further rewritten in terms of harmonic polynomials $K_{lm}(\mathbf{r}) = r^l\, Y_{lm}(\hat{r})$:

$$e^{i\mathbf{a}\cdot\mathbf{p}} = 4\pi \sum_{l=0}^{\infty} Z_l(ap) \sum_{m=-l}^{l} K^*_{lm}(\mathbf{a})\, K_{lm}(i\mathbf{p}) \tag{B.12}$$

Here, $Z_l(z) = z^{-l} j_l(z)$ is an even entire function of the argument z. Since we require its expansion into a power series in Appendix A.5.2, we state here its Taylor expansion

(see Abramowitz and Stegun [81], p. 437):

$$Z_l(z) \;=\; \frac{j_l(z)}{z^l} \;=\; \sum_{\nu=0}^{\infty} \frac{(-1)^\nu z^{2\nu}}{2^\nu\,\nu!(2l+2\nu+1)!!} \;=\; \frac{1}{(2l+1)!!}\left(1 - \frac{z^2}{2(2l+3)} + \mathcal{O}(z^4)\right) \tag{B.13}$$

B.3.2 Multipole Expansion of the Translation Operator

Nothing prevents us to interpret the multipole series (B.12) not as an expansion of an ordinary function but of a functional operator. It is a natural choice to substitute the vector $\mathbf{p}$ by the momentum operator $\mathbf{p} = -i\boldsymbol{\nabla}$. Then, we obtain the expansion of the displacement operator $\mathcal{T}(\mathbf{a}) = \exp(\mathbf{a}\cdot\boldsymbol{\nabla})$ which shifts the argument of analytic functions $f(\mathbf{r})$ by a fixed vector $\mathbf{a}$:

$$\mathcal{T}(\mathbf{a})\, f(\mathbf{r}) \;=\; e^{\mathbf{a}\cdot\boldsymbol{\nabla}}\, f(\mathbf{r}) \;=\; f(\mathbf{r}+\mathbf{a}) \tag{B.14}$$

in terms of the multipole differentiation operator $K_{lm}(\boldsymbol{\nabla})$, the spherical tensor gradient [85–87] which presents a homogeneous polynomial of the partial derivatives $\partial/\partial x$, $\partial/\partial y$, and $\partial/\partial z$. From (B.12) we immediately find the expansion of $\mathcal{T}(a)$:

$$\mathcal{T}(\mathbf{a}) \;=\; e^{\mathbf{a}\cdot\boldsymbol{\nabla}} \;=\; 4\pi \sum_{l=0}^{\infty} Z_l\left(\sqrt{a^2\boldsymbol{\nabla}^2}\right) \sum_{m=-l}^{l} K^*_{lm}(\mathbf{a})\, K_{lm}(\boldsymbol{\nabla}) \tag{B.15}$$

Here, the operator $Z_l(\sqrt{a^2\boldsymbol{\nabla}^2})$ should be interpreted as a series in the Laplacian Δ:

$$Z_l\left(\sqrt{a^2\boldsymbol{\nabla}^2}\right) \;=\; \sum_{\nu=0}^{\infty} \frac{(-1)^\nu a^{2\nu}\Delta^\nu}{2^\nu\,\nu!(2l+2\nu+1)!!} \;=\; \frac{1}{(2l+1)!!}\left(1 - \frac{a^2\Delta}{2(2l+3)} + \mathcal{O}(a^4\Delta^2)\right) \tag{B.16}$$

Obviously, the general expansion (B.15), (B.16) will simplify if we intend to apply the translation operator $\mathcal{T}(\mathbf{a})$ to a harmonic function $W(\mathbf{r})$. Since $\Delta\, W(\mathbf{r}) = 0$, we obtain from (B.14)–(B.16) the following multipole series for the shifted harmonic function $W(\mathbf{r}+\mathbf{a})$:

$$W(\mathbf{r}+\mathbf{a}) \;=\; e^{\mathbf{a}\cdot\boldsymbol{\nabla}}\, W(\mathbf{r}) \;=\; \sum_{l=0}^{\infty} \frac{4\pi}{(2l+1)!!} \sum_{m=-l}^{l} K^*_{lm}(\mathbf{a})\, K_{lm}(\boldsymbol{\nabla})\, W(\mathbf{r}) \tag{B.17}$$

This formula forms the foundation for the translation theorem for harmonic polynomials presented in Section B.5.

B.4 The Differentiation Rule for Solid Harmonics

In potential theory, it is common knowledge that the potential $W(\mathbf{r})$ generated by some distribution of sources as a harmonic function in a source-free region may be expanded into a series of harmonic polynomials $K_{lm}(\mathbf{r}-\mathbf{r}')$ with respect to some origin $\mathbf{r}'$. A very similar development holds for $r' \to \infty$; then, $W(\mathbf{r})$ may be represented as a series of multipole potentials $\Phi_{lm}(\mathbf{r})$ [84]. Hence, it is natural to examine harmonic polynomials $K_{lm}(\mathbf{r})$ and multipole potentials $\Phi_{lm}(\mathbf{r})$ as special harmonic functions in the general translation formula (B.17). As a result, we will obtain the important translation theorems for both classes of functions in the course of the following section. But first we have to evaluate the action of a spherical gradient operator $K_{lm}(\boldsymbol{\nabla})$ on solid harmonics $K_{LM}(\mathbf{r})$ and $\Phi_{LM}(\mathbf{r})$, respectively. We will denote the results of this operations, which are mathematically interesting in their own right, as the differentiation rule for solid harmonics that to our best knowledge does not appear in the generally available literature on the subject.

B.4.1 Differentiation Rule For Harmonic Polynomials

We first examine the effects of a harmonic polynomial $K_{lm}(\boldsymbol{\nabla})$ in momentum space that acts on a L.th-order harmonic polynomial $K_{LM}(\mathbf{r})$ in physical space. Let us note that the Laplace operator $\Delta = -\boldsymbol{\nabla}^2$ commutes with the momentum-space polynomial $K_{lm}(\boldsymbol{\nabla})$. Hence, the resulting homogeneous polynomial of order $L-l$ will again belong to the class of harmonic functions. Since $K_{lm}(\boldsymbol{\nabla})$ obviously represents a spherical tensor operator of rank l, i. e., behaves under rotations $\mathcal{R}$ like the spherical harmonic function $Y_{lm}(\hat{r})$, due to the rules for the addition of angular momenta [128, 238] the magnetic quantum number of this polynomial is also uniquely fixed to $M+m$. Therefore, we find:

$$K_{lm}(\boldsymbol{\nabla})\, K_{LM}(\mathbf{r}) \;=\; C_{LM}^{lm}\, K_{L-l,M+m}(\mathbf{r}) \tag{B.18}$$

with a coefficient C_{LM}^{lm} that still has to be determined. Equation (B.18) possibly presents the simplest case of the Wigner-Eckart theorem [238], leading to "selection rules" $0 \leq l \leq L$ and $|M+m| \leq L-l$. (Otherwise, we obtain a vanishing result.)

To isolate the coefficient C_{LM}^{lm}, we project the component of $K_{L-l,M+m}(\mathbf{r})$ from the left-hand side, exploiting the orthonormality relation of spherical harmonics (B.5). This immediately leads to an integral representation for C_{LM}^{lm}:

$$\int d\Omega\, K_{L-l,M+m}^{*}(\mathbf{r})\, K_{lm}(\boldsymbol{\nabla})\, K_{LM}(\mathbf{r}) \;=\; r^{2(L-l)}\, C_{LM}^{lm} \tag{B.19}$$

On the other hand, from the Wigner-Eckart theorem, which, in short, states that matrix elements of spherical tensor operators, like those of $K_{lm}(\boldsymbol{\nabla})$ in (B.19), show a universal

dependence on the magnetic quantum numbers involved, we find that this integral can be expressed in terms of the Wigner $3j-$symbol [238,241]:

$$\int d\Omega\, K^*_{L-l,M+m}(\mathbf{r})\, K_{lm}(\boldsymbol{\nabla})\, K_{LM}(\mathbf{r}) \;=\; (-1)^{L-l+M+m}\, r^{2(L-l)}\, D_{Ll} \begin{pmatrix} (L-l) & l & L \\ -(M+m) & m & M \end{pmatrix} \tag{B.20}$$

which in turn has been evaluated by Racah [242]:

$$\begin{pmatrix} (L-l) & l & L \\ -(M+m) & m & M \end{pmatrix} \;=\; (-1)^{L-M} \;\times \\ \sqrt{\frac{(2l)!\,(2L-2l)!\,(L+M)!\,(L-M)!}{(2L+1)!\,(l+m)!\,(l-m)!\,(L-l+M+m)!\,(L-l-M-m)!}} \tag{B.21}$$

By comparison of (B.19) and (B.20) we find that the desired coefficient C^{lm}_{LM} is connected to the Wigner $3j-$symbol by the relation:

$$C^{lm}_{LM} \;=\; (-1)^{L-l+M+m}\, D_{Ll} \begin{pmatrix} (L-l) & l & L \\ -(M+m) & m & M \end{pmatrix} \tag{B.22}$$

Here, D_{Ll} denotes the reduced matrix element which is characteristic of (B.20) but independent of M and m. In order to determine D_{Ll}, we explicitly calculate the integral (B.20) for $M = L$, $m = -l$. With the coordinate representation [128]:

$$K_{L,\pm L}(\mathbf{r}) \;=\; \frac{(\mp 1)^L}{2^L\, L!} \sqrt{\frac{(2L+1)!}{4\pi}}\, (x \pm iy)^L \tag{B.23}$$

and the obvious differentiation property:

$$(\partial_x - i\partial_y)^l\, (x+iy)^L \;=\; \frac{2^l\, L!}{(L-l)!}\, (x+iy)^{L-l} \tag{B.24}$$

we obtain after a simple calculation the coefficient $C^{l,-l}_{LL}$ (B.18):

$$K_{l,-l}(\boldsymbol{\nabla})\, K_{LL}(\mathbf{r}) \;=\; \frac{(-1)^l}{2^l\, l!} \sqrt{\frac{(2l+1)!\,(2L+1)!}{4\pi\,(2L-2l+1)!}}\, K_{L-l,L-l}(\mathbf{r}) \tag{B.25}$$

Using (B.22) we now may evaluate the reduced matrix element D_{Ll}. From (B.21) we find that the $3j-$symbol for $M = L$, $m = -l$ yields $(2L+1)^{-1/2}$. Hence,

$$D_{Ll} \;=\; \sqrt{2L+1}\, C^{l,-l}_{LL} \;=\; \frac{(-1)^l}{2^l\, l!} \sqrt{\frac{(2L+1)\,(2L+1)!\,(2l+1)!}{4\pi\,(2L-2l+1)!}} \tag{B.26}$$

Following these preliminaries, from (B.22) we are finally able to express the coefficients C_{LM}^{lm} in terms of factorials:

$$K_{lm}(\boldsymbol{\nabla})\, K_{LM}(\mathbf{r}) \;=\; \frac{(-1)^m\,(2l)!}{2^l\,l!\,\sqrt{4\pi}} \;\times \\ \sqrt{\frac{(2L+1)\,(2l+1)\,(L+M)!\,(L-M)!}{(2L-2l+1)\,(l+m)!\,(l-m)!\,(L-l+M+m)!\,(L-l-M-m)!}}\; K_{L-l,M+m}(\mathbf{r}) \tag{B.27}$$

This formula constitutes the differentiation rule for harmonic polynomials $K_{LM}(\mathbf{r})$. A related theorem has been stated by Hobson [88] as the result of a rather tedious direct calculation.

B.4.2 Differentiation Rule For Multipole Potentials

The corresponding rule for multipole potentials $\Phi_{LM}(\mathbf{r})$ is obtained by similar considerations. We first note that the action of a momentum-space harmonic polynomial $K_{lm}(\boldsymbol{\nabla})$ on the multipole potential $\Phi_{LM}(\mathbf{r})$ results in another multipole potential of rank $L+l$ [cf. equation (B.18)]:

$$K_{lm}(\boldsymbol{\nabla})\, \Phi_{LM}(\mathbf{r}) \;=\; \tilde{C}_{LM}^{lm}\; \Phi_{L+l,M+m}(\mathbf{r}) \tag{B.28}$$

This can be inferred from the fact that $K_{lm}(\boldsymbol{\nabla})$ is a spherical tensor operator of rank l, and that any single spatial differentiation operation acting on $\Phi_{LM}(\mathbf{r}) = K_{LM}(\mathbf{r})/r^{2L+1}$ leads to a harmonic function of increased rank $L+1$. Hence, the angular momentum quantum number of the resulting multipole potential takes its maximum value $L+l$.

The determination of $\tilde{C}_{LM}^{lm}$ proceeds analogously to (B.19)–(B.22). By orthonormality and the Wigner-Eckart theorem, we find:

$$\begin{aligned} \tilde{C}_{LM}^{lm} \;&=\; r \int d\Omega\, K_{L+l,M+m}^{*}(\mathbf{r})\, K_{lm}(\boldsymbol{\nabla})\, \Phi_{LM}(\mathbf{r}) \\ &=\; (-1)^{L+l+M+m}\, \tilde{D}_{Ll} \begin{pmatrix} (L+l) & l & L \\ -(M+m) & m & M \end{pmatrix} \end{aligned} \tag{B.29}$$

Here, the $3j$–symbol reads in explicit form [242] (in comparison to (B.21), note the change of sign in the upper left entry):

$$\begin{pmatrix} (L+l) & l & L \\ -(M+m) & m & M \end{pmatrix} \;=\; (-1)^{l-L-M-m} \;\times \\ \sqrt{\frac{(2L)!\,(2l)!\,(L+l+M+m)!\,(L+l-M-m)!}{(2L+2l+1)!\,(L+M)!\,(L-M)!\,(l+m)!\,(l-m)!}} \tag{B.30}$$

Again, the reduced matrix element $\tilde{D}_{Ll}$ may be evaluated once a single coefficient $\tilde{C}^{lm}_{LM}$ is known. For convenience, we set $M = L$, $m = l$. By application of an easily confirmed algebraical relation,

$$(\partial_x + i\partial_y)^l \, \frac{(x+iy)^L}{r^{2L+1}} \;=\; (-1)^l \, \frac{(2L+2l-1)!!}{(2L-1)!!} \, \frac{(x+iy)^{L+l}}{r^{2L+2l+1}} \;, \tag{B.31}$$

we now may employ the explicit coordinate representation of the multipole potential $\Phi_{LL}(\mathbf{r}) = K_{LL}(\mathbf{r})/r^{2L+1}$ (B.23) to show that

$$K_{ll}(\boldsymbol{\nabla}) \, \Phi_{LL}(\mathbf{r}) \;=\; \frac{(-1)^l \, (2L+1) \, (2l+1)!!}{\sqrt{4\pi \, (2L+2l+1)}} \, \sqrt{\frac{(2L+2l)!}{(2L+1)! \, (2l+1)!}} \; \Phi_{L+l,L+l}(\mathbf{r}) \tag{B.32}$$

For $M = L$, $m = l$ the $3j$–symbol acquires the value $(2L+2l+1)^{-1/2}$. Hence, from (B.29) and (B.32) we obtain the reduced matrix element $\tilde{D}_{Ll}$:

$$\tilde{D}_{Ll} \;=\; \sqrt{2L+2l+1} \; \tilde{C}^{ll}_{LL} \;=\; \frac{(-1)^l \, (2L+1) \, (2l+1)!!}{\sqrt{4\pi}} \, \sqrt{\frac{(2L+2l)!}{(2L+1)! \, (2l+1)!}} \tag{B.33}$$

Combining the results (B.28)–(B.33) we may represent the coefficients $\tilde{C}^{lm}_{LM}$ in closed form:

$$\begin{aligned} K_{lm}(\boldsymbol{\nabla}) \, \Phi_{LM}(\mathbf{r}) \;=\; & \frac{(-1)^l \, (2l)!}{2^l \, l! \, \sqrt{4\pi}} \;\times \\ & \sqrt{\frac{(2L+1) \, (2l+1) \, (L+l+M+m)! \, (L+l-M-m)!}{(2L+2l+1) \, (L+M)! \, (L-M)! \, (l+m)! \, (l-m)!}} \; \Phi_{L+l,M+m}(\mathbf{r}) \end{aligned} \tag{B.34}$$

Equation (B.34), which superficially resembles (B.27), presents the most general form of the differentiation rule for multipole potentials $\Phi_{lm}(\mathbf{r})$. It includes the important special case $L = M = 0$; then, we obtain a variant of Maxwell's theorem [88–90, 239]:

$$K_{lm}(\boldsymbol{\nabla}) \; [1/r] \;=\; (-1)^l \, (2l-1)!! \, \Phi_{lm}(\mathbf{r}) \tag{B.35}$$

Hence, the momentum-space harmonic polynomials $K_{lm}(\boldsymbol{\nabla})$ may be used to generate the associated multipole potentials $\Phi_{lm}(\mathbf{r})$ by differentiation. It is exactly this property (2.20) that motivated our introduction of multipole delta functions $\delta_{lm}(\mathbf{r}-\mathbf{r}')$ (2.23) as orientated pointlike sources and the corresponding multipole Green functions $G_{lm}(\mathbf{r},\mathbf{r}';E)$ (2.25) in Section 2.4. An alternative proof of the identities (2.20) and (B.35) is presented in Appendix C.1, see formula (C.20).

We finally note that both expansions (B.27) and (B.34) may be interpreted as special cases of a general differentiation rule for quite arbitrary functions $f(r) \, Y_{LM}(\hat{r})$ of

definite angular momentum (L, M). From the Wigner-Eckart theorem [238], we obtain the formal expansion:

$$K_{lm}(\boldsymbol{\nabla})\,[f(r)\,Y_{LM}(\hat{r})] \;=\; \sum_{\lambda=\,|L-l|}^{L+l} \mathcal{C}_{lL}^{\lambda}[f(r)]\,Y_{\lambda,M+m}(\hat{r}) \tag{B.36}$$

A number of involved closed-form expressions for the appearing coefficient functions $\mathcal{C}_{lL}^{\lambda}[f(r)]$ have been derived by different authors [85–87, 243, 244]. In the case of solid harmonics, they all reduce to the substantially simpler expressions (B.27) and (B.34) that to our best knowledge so far did not appear in literature.

B.5 The Translation Theorem for Solid Harmonics

Now we are in the position to state the translation theorems that expand a solid harmonic function, e. g., $K_{LM}(\mathbf{r}+\mathbf{a})$, in a series of shifted harmonic polynomials $K_{lm}(\mathbf{r})$. We will also derive an analogous expansion for the corresponding irregular functions, the multipole potentials $\Phi_{lm}(\mathbf{r})$.

B.5.1 Translation Theorem For Harmonic Polynomials

From (B.17), we immediately obtain the following formal multipole expansion of the shifted harmonic polynomial $K_{LM}(\mathbf{r}+\mathbf{a})$:

$$K_{LM}(\mathbf{r}+\mathbf{a}) \;=\; \sum_{l=\,0}^{\infty} \frac{4\pi}{(2l+1)!!} \sum_{m=\,-l}^{l} K_{lm}^{*}(\mathbf{a})\,K_{lm}(\boldsymbol{\nabla})\,K_{LM}(\mathbf{r}) \tag{B.37}$$

To establish an explicit expression for the multipole series, we eliminate the spherical tensor gradient $K_{lm}(\boldsymbol{\nabla})$ by means of the differentiation rule (B.27) derived above. The selection rules discussed in the context of (B.18) guarantee that the l sum in (B.37) is in fact finite, and we find:

$$\begin{aligned} K_{LM}(\mathbf{r}+\mathbf{a}) \;=\; \sum_{l=\,0}^{L} \sqrt{\frac{4\pi\,(2L+1)}{(2l+1)\,(2L-2l+1)}} \sum_{m=\,-l}^{l} \sqrt{\frac{(L+M)!\,(L-M)!}{(l+m)!\,(l-m)!}} \;\times \\ \frac{(-1)^m}{\sqrt{(L-l+M+m)!\,(L-l-M-m)!}}\,K_{lm}^{*}(\mathbf{a})\,K_{L-l,M+m}(\mathbf{r}) \end{aligned} \tag{B.38}$$

In the second sum over m, terms that lead to negative factorials in the expansion should be left out. Equation (B.38) presents the translation theorem for harmonic polynomials $K_{LM}(\mathbf{r}+\mathbf{a})$ in its general form. Similar "addition theorems" that expand shifted harmonic polynomials $K_{lm}(\mathbf{r}-\mathbf{r}')$ into products of harmonic polynomials

$K_{j\mu}(\mathbf{r})$ and $K_{JM}(\mathbf{r}')$ centered around $\mathbf{r}$ and $\mathbf{r}'$, respectively, have also been established by several authors [245, 246].

The translation expansion (B.38) considerably simplifies if the translation vector $\mathbf{a}$ is aligned to the direction of the quantization axis, i. e., $\mathbf{a} = a\hat{e}_z$. In this case, the generator $\partial/\partial z$ of the translation commutes with the z component of the angular momentum operator $\mathbf{L} = -i\mathbf{r} \times \boldsymbol{\nabla}$ which means that the magnetic quantum number M of the original solid harmonic will not be affected by the shift operation. Hence, in the translation theorem (B.38) the m sum will disappear. Of course, this property may also be inferred directly from the special value of the harmonic polynomial $K_{lm}(a\hat{e}_z)$ (B.4) that we already established in Section B.1. Introducing it into the general series (B.38), we are left with the simpler expansion:

$$K_{lm}(\mathbf{r} + a\hat{e}_z) \;=\; \sum_{j=|m|}^{l} T_{jlm}\, a^{l-j} K_{jm}(\mathbf{r}) \tag{B.39}$$

Here, for convenience we introduced the translation parameters T_{jlm} that take the symmetric form (B.38):

$$T_{jlm} \;=\; \frac{1}{(l-j)!}\sqrt{\frac{(2l+1)\,(l+m)!\,(l-m)!}{(2j+1)\,(j+m)!\,(j-m)!}} \tag{B.40}$$

As a special case, $T_{jjm} = 1$. This immediately follows from the observation that (B.39) may be interpreted as a Taylor expansion of the harmonic polynomial $K_{lm}(\mathbf{r})$. In a different fashion, expansions equivalent to (B.39) were also derived by Hobson [88] and Morse and Feshbach [89]. The formulae (B.39) and (B.40) are massively utilized in the derivations of Chapter 5.

B.5.2 Translation Theorem For Multipole Potentials

Again, corresponding expansions can be given for the multipole potentials $\Phi_{LM}(\mathbf{r})$. To this end, we express the shifted multipole potential $\Phi_{LM}(\mathbf{r} + \mathbf{a})$ by the displacement operator $\exp(\mathbf{a} \cdot \boldsymbol{\nabla})$ (B.15) and obtain using (B.17):

$$\Phi_{LM}(\mathbf{r} + \mathbf{a}) \;=\; \sum_{l=0}^{\infty} \frac{4\pi}{(2l+1)!!} \sum_{m=-l}^{l} K^*_{lm}(\mathbf{a})\, K_{lm}(\boldsymbol{\nabla})\, \Phi_{LM}(\mathbf{r}) \tag{B.41}$$

Application of the differentiation rule for multipole potentials (B.34) in (B.41) instantaneously yields the most general form of the translation theorem for multipole po-

tentials $\Phi_{LM}(\mathbf{r}+\mathbf{a})$:

$$\Phi_{LM}(\mathbf{r}+\mathbf{a}) \;=\; \sum_{l\,=\,0}^{\infty} (-1)^l \sqrt{\frac{4\pi\,(2L+1)}{(2l+1)\,(2L+2l+1)}} \;\times \\ \sum_{m\,=\,-l}^{l} \sqrt{\frac{(L+l+M+m)!\,(L+l-M-m)!}{(L+M)!\,(L-M)!\,(l+m)!\,(l-m)!}}\; K^{*}_{lm}(\mathbf{a})\,\Phi_{L+l,M+m}(\mathbf{r}) \quad \text{(B.42)}$$

Unlike the series for shifted harmonic polynomials $K_{LM}(\mathbf{r}+\mathbf{a})$ (B.38), the multipole expansion series of a shifted multipole function $\Phi_{LM}(\mathbf{r}+\mathbf{a})$ (B.42) is infinite and converges only within the circle $a < r$. This property follows from the fact that the shifted multipole function will diverge at the origin, i. e., for the special shift $\mathbf{a} = -\mathbf{r}$. The range of the expansion (B.42) is however easily extended by analytical continuation; to obtain a convergent series for $a > r$, $\mathbf{r}$ and $\mathbf{a}$ should be simply exchanged on the right-hand side of the translation theorem (B.42).

Like its regular relative (B.38), the translation expansion (B.42) will simplify if the displacement proceeds along the quantization axis, i. e., $\mathbf{a} = a\hat{e}_z$. Inserting (B.3) into (B.42), we find that for $a < r$,

$$\Phi_{lm}(\mathbf{r}+a\hat{e}_z) \;=\; \sum_{j\,=\,l}^{\infty} \tilde{T}_{jlm}\, a^{j-l}\, \Phi_{jm}(\mathbf{r}) \quad \text{(B.43)}$$

where the multipole translation parameters $\tilde{T}_{jlm}$ are given by:

$$\tilde{T}_{jlm} \;=\; \frac{(-1)^{j-l}}{(j-l)!} \sqrt{\frac{(2l+1)\,(j+m)!\,(j-m)!}{(2j+1)\,(l+m)!\,(l-m)!}} \quad \text{(B.44)}$$

Equations (B.42) and (B.43) present the counterpart to the polynomial expansion (B.39) and (B.40). We note that $\tilde{T}_{jjm} = 1$; hence, the multipole contribution of lowest order is invariant with respect to translations. Again, similar expansions have been stated by Hobson, and Morse and Feshbach [88,89].

Finally, let us conclude our mathematical developments on the theory of solid harmonics with the observation that another interesting simplification occurs if we let $L = M = 0$ in equation (B.42). Let $a < r$; then, the result of (B.42) in terms of harmonic polynomials $K_{lm}(\mathbf{r})$ reads:

$$\Phi_{00}(\mathbf{r}-\mathbf{a}) \;=\; \sum_{l\,=\,0}^{\infty} \frac{1}{r^{2l+1}}\, \frac{\sqrt{4\pi}}{2l+1} \sum_{m\,=\,-l}^{l} K^{*}_{lm}(\mathbf{a})\, K_{lm}(\mathbf{r}) \quad \text{(B.45)}$$

(Here, we employed the obvious parity properties of $K_{lm}(\mathbf{a})$ as a homogeneous polynomial of order l.) Using the addition theorem for harmonic polynomials (B.9) we

proved earlier in Section B.2, this expression may be rewritten in terms of the invariant angle α between the vectors $\mathbf{r}$ and $\mathbf{a}$. With $K_{00} = \sqrt{1/4\pi}$ (B.5), we find:

$$\frac{1}{|\mathbf{r}-\mathbf{a}|} = \sum_{l=0}^{\infty} \frac{a^l}{r^{l+1}} P_l(\cos\alpha) \tag{B.46}$$

Hence, we see that the general translation theorem (B.42) for the monopol case $L = M = 0$ reduces to the well-known generating function expansion of $|\mathbf{r}-\mathbf{a}|^{-1}$ into Legendre polynomials $P_l(\cos\alpha)$ [81].

B.5.3 Miscellaneous Formulae

We conclude this section with two formulae that are related to the translation theorems for solid harmonics and are easily derived from them. These expressions are required in the formal manipulation of the multipole scattering waves $G_{lm}(\mathbf{r}, \mathbf{o}; E)$ in the uniform field environment (Chapter 5); here, we state them for reference.

First, we note that the translation expansion of harmonic polynomials $K_{lm}(\mathbf{r} + a\hat{e}_z)$ (B.39) may as well be interpreted as a Taylor series of $K_{lm}(\mathbf{r})$ with respect to shifts in the z direction. Hence, we immediately find for the derivative of the harmonic polynomial $K_{lm}(\mathbf{r})$ with respect to z:

$$\frac{\partial}{\partial z} K_{lm}(\mathbf{r}) = T_{l-1,lm}\, K_{l-1,m}(\mathbf{r}) \tag{B.47}$$

Finally, we give a rule for products of the coefficients T_{jlm} that is most easily proved by using the explicit form (B.40) of these numbers:

$$T_{jlm} T_{j-1,jm} = (l-j+1) T_{j-1,lm} \tag{B.48}$$

B.6 Example: Evaluation of Some Integrals

As an application of the preceding paragraphs, we show how to evaluate two integrals appearing in the course of the calculation of the multipole Green functions $G_{lm}(\mathbf{r}, \mathbf{o}; E)$ in a uniform field environment (Section 5.3). In equation (5.25), we are faced with the problem of finding an explicit expression for the integral $I^{(1)}_{lm}$:

$$I^{(1)}_{lm} = \int d^3q\, e^{-i\mathbf{q}\cdot\boldsymbol{\rho}}\, K_{lm}(\mathbf{q} + \tau\hat{e}_z)\, e^{-i\tau q^2/4} \tag{B.49}$$

To perform the integration in spherical coordinates it is necessary to expand the factors $e^{-i\mathbf{q}\cdot\boldsymbol{\rho}}$ and $K_{lm}(\mathbf{q} + \tau\hat{e}_z)$ in the integrand of (B.49) into a series of spherical harmonics

$Y_{lm}(\hat{q})$. From (B.39) and (B.11), we find:

$$e^{-i\mathbf{q}\cdot\boldsymbol{\rho}}\, K_{lm}(\mathbf{q}+\tau\hat{e}_z) \;=\; 4\pi \sum_{j=|m|}^{l} T_{jlm}\, q^j\, \tau^{l-j} \;\times \\ \sum_{\lambda=0}^{\infty} (-i)^\lambda j_\lambda(\rho q) \sum_{\mu=-\lambda}^{\lambda} Y_{\lambda\mu}(\hat{\rho})\, Y^*_{\lambda\mu}(\hat{q})\, Y_{jm}(\hat{q}) \quad \text{(B.50)}$$

The spherical harmonics $Y_{lm}(\hat{q})$ form an orthonormal base of functions on the unit sphere. Therefore, integration with respect to $\hat{q}$ in (B.49) will project the terms with $\lambda = j$ and $\mu = m$ from the triple sum (B.50), and we are left with a finite sum of radial integrals (strictly spoken, a distribution):

$$I^{(1)}_{lm} \;=\; 4\pi \sum_{j=|m|}^{l} (-i)^j\, T_{jlm}\, \tau^{l-j}\, Y_{jm}(\hat{\rho}) \int_0^\infty dq\, q^{j+2}\, j_j(\rho q)\, e^{-i\tau q^2/4} \quad \text{(B.51)}$$

The evaluation of the remaining integral requires some knowledge about the properties of spherical Bessel functions. We employ a differentiation representation of $j_j(\rho q)$ known as Rayleigh's formula (Abramowitz and Stegun [81], p. 439):

$$j_j(\rho q) \;=\; \left(\frac{\rho}{q}\right)^j \left(-\frac{1}{\rho}\frac{\partial}{\partial\rho}\right)^j \frac{\sin(\rho q)}{\rho q} \;=\; \frac{\rho^j}{q^{j+2}} \left(-\frac{1}{\rho}\frac{\partial}{\partial\rho}\right)^{j+1} \cos(\rho q) \quad \text{(B.52)}$$

Inserting (B.52) into the radial integral of (B.51) leads to a simple Gaussian integral. We immediately find:

$$\int_0^\infty dq\, \cos(\rho q)\, e^{-i\tau q^2/4} \;=\; \sqrt{\frac{\pi}{i\tau}}\, e^{i\rho^2/\tau} \quad \text{(B.53)}$$

This expression, however, is an eigenfunction of the differential operator appearing in (B.52), and we obtain:

$$\int_0^\infty dq\, q^{j+2}\, j_j(\rho q)\, e^{-i\tau q^2/4} = \rho^j \left(-\frac{1}{\rho}\frac{\partial}{\partial\rho}\right)^{j+1} \left\{\sqrt{\frac{\pi}{i\tau}}\, e^{i\rho^2/\tau}\right\} = \sqrt{\frac{\pi}{i\tau}} \left(\frac{2}{i\tau}\right)^{j+1} \rho^j\, e^{i\rho^2/\tau} \quad \text{(B.54)}$$

Inserting (B.54) into (B.51) finally yields the desired result for the integral (B.49):

$$I^{(1)}_{lm} \;=\; \left(\frac{4\pi}{i\tau}\right)^{3/2} e^{i\rho^2/\tau} \sum_{j=|m|}^{l} (-2)^j\, T_{jlm}\, \tau^{l-2j}\, K_{jm}(\boldsymbol{\rho}) \quad \text{(B.55)}$$

Next, we evaluate an integral closely related to (B.55) that appears in the calculation of the total multipole currents (Section 5.5):

$$I_{lm}^{(2)} \;=\; \int d^3q\, K_{lm}^*(\mathbf{q}-\tau\hat{e}_z)\, K_{lm}(\mathbf{q}+\tau\hat{e}_z)\, e^{-i\tau q^2/4} \tag{B.56}$$

We will perform the integration using spherical coordinates. To this end, we again remove the undesirable shifts $\pm\tau\hat{e}_z$ in the arguments of the harmonic polynomials $K_{lm}(\mathbf{q})$ by application of the translation theorem (B.39) stated in Appendix B.5:

$$K_{lm}^*(\mathbf{q}-\tau\hat{e}_z)\, K_{lm}(\mathbf{q}+\tau\hat{e}_z) \;=\; \sum_{j=|m|}^{l} (-1)^{l-j}\, T_{jlm} \;\times \sum_{J=|m|}^{l} T_{Jlm}\, \tau^{2l-j-J}\, q^{j+J}\, Y_{jm}^*(\hat{q})\, Y_{Jm}(\hat{q}) \tag{B.57}$$

The angular part of the integration is now trivial, and we find:

$$I_{lm}^{(2)} \;=\; \sum_{j=|m|}^{l} T_{jlm}^2\, (i\tau)^{2(l-j)} \int_0^\infty dq\, q^{2(j+1)}\, e^{-i\tau q^2/4} \tag{B.58}$$

Formally, the radial integral in (B.58) may be reduced to a simple Gaussian integral by means of differentiation with respect to τ:

$$\int_0^\infty dq\, q^{2(j+1)}\, e^{-i\tau q^2/4} \;=\; \left(4i\,\frac{\partial}{\partial\tau}\right)^{j+1} \sqrt{\frac{\pi}{i\tau}} \;=\; \frac{2^{j+1}(2j+1)!!\sqrt{\pi}}{(i\tau)^{j+3/2}} \tag{B.59}$$

Hence, the desired integral (B.56) may be written as a finite series in the parameter $1/\sqrt{i\tau}$:

$$I_{lm}^{(2)} \;=\; \sqrt{\pi} \sum_{j=|m|}^{l} T_{jlm}^2\, \frac{2^{j+1}(2j+1)!!}{(i\tau)^{3j-2l+3/2}} \tag{B.60}$$

B.7 Integrals Involving Products of Three Spherical Harmonics

In the final section of this appendix, we examine integrals that contain a product of three spherical harmonic functions $Y_{lm}(\Omega)$ in the form:

$$I_{m_1 m_2 m_3}^{l_1 l_2 l_3} \;=\; \int d\Omega\, Y_{l_1 m_1}(\Omega)\, Y_{l_2 m_2}(\Omega)\, Y_{l_3 m_3}(\Omega) \tag{B.61}$$

Integrals of this type are common in atomic physics [247] and have been extensively studied. Honoring the pioneering work on these expressions, the symbol $I^{l_1 l_2 l_3}_{m_1 m_2 m_3}$ is also known as the Gaunt coefficient [248]. In the following, we will establish an explicit formula for the Gaunt coefficients, study selection rules for them, and provide an estimate for these symbols that comes in handy in the mathematical considerations of Appendix A.5.

B.7.1 Explicit Representation

Let us first give a closed-form expression for the Gaunt coefficient $I^{l_1 l_2 l_3}_{m_1 m_2 m_3}$. Clearly, equation (B.61) may be interpreted as the $(l_1, m_1), (l_3, m_3)$ matrix element of the spherical tensor operator $Y_{l_2 m_2}(\Omega)$. To evaluate it, we take advantage of the Wigner-Eckart theorem [128] which states that the dependence of $I^{l_1 l_2 l_3}_{m_1 m_2 m_3}$ on the magnetic quantum numbers m_1, m_2, m_3 may be split off into a Wigner $3j$–symbol (see the textbook by Messiah [238], p. 1076):

$$I^{l_1 l_2 l_3}_{m_1 m_2 m_3} \;=\; D_{l_1 l_2 l_3} \begin{pmatrix} l_1 & l_2 & l_3 \\ m_1 & m_2 & m_3 \end{pmatrix} \tag{B.62}$$

Here, $D_{l_1 l_2 l_3}$ denotes the reduced matrix element of the operator $Y_{l_2 m_2}(\Omega)$ which is independent of the magnetic quantum numbers. [We already used the same strategy in (B.20) and (B.29).] For the spherical harmonic function, the reduced matrix element $D_{l_1 l_2 l_3}$ reads (see Edmonds [128], p. 63):

$$D_{l_1 l_2 l_3} \;=\; \sqrt{\frac{(2l_1+1)(2l_2+1)(2l_3+1)}{4\pi}} \begin{pmatrix} l_1 & l_2 & l_3 \\ 0 & 0 & 0 \end{pmatrix} \tag{B.63}$$

It is seen that the Gaunt coefficient (B.61) allows for a representation as a product of two Wigner $3j$–symbols.

B.7.2 Selection Rules

From the integral expression (B.61), a number of conditions may be read off that necessarily hold unless $I^{l_1 l_2 l_3}_{m_1 m_2 m_3}$ vanishes. The left-hand side of equation (B.61) obviously represents a scalar quantity which remains invariant under rotations and inversions. Therefore, the integrand must be of positive parity and contain a spherically scalar contribution proportional to $Y_{00}(\Omega) = (4\pi)^{-1/2}$. Since $r^l Y_{lm}(\hat{r}) = K_{lm}(\mathbf{r}) = (-1)^l K_{lm}(-\mathbf{r}) = (-1)^l r^l Y_{lm}(-\hat{r})$, the spherical harmonic $Y_{lm}(\Omega)$ is a function of parity $(-1)^l$, and the coefficient $I^{l_1 l_2 l_3}_{m_1 m_2 m_3}$ must vanish if the sum of all total angular momenta $l_1 + l_2 + l_3$ is an odd integer. For the second condition, we note that the magnetic quantum numbers m_1, m_2, m_3 simply add up in the composition of angular momenta,

so the sum rule $m_1 + m_2 + m_3 = 0$ must be fulfilled. Furthermore, from the addition rules of angular momenta [238] we infer that $|l_2 - l_3| \leq l_1 \leq l_2 + l_3$ must hold: $I^{l_1 l_2 l_3}_{m_1 m_2 m_3}$ vanishes unless a triangle with sides of length l_1, l_2, l_3 may be formed. We summarize these rules:

$$I^{l_1 l_2 l_3}_{m_1 m_2 m_3} \neq 0 \qquad \Longrightarrow \qquad \begin{cases} l_1 + l_2 + l_3 = 2L \\ m_1 + m_2 + m_3 = 0 \\ |l_2 - l_3| \leq l_1 \leq l_2 + l_3 \end{cases} \tag{B.64}$$

B.7.3 An Estimate for the Gaunt Symbols

We now apply these conditions in order to obtain an estimate for the Gaunt coefficient $I^{l_1 l_2 l_3}_{m_1 m_2 m_3}$ that is employed in Appendix A.5.2, (A.297). We first construct a sum rule for these symbols. In advance, we note that the spherical harmonics $Y_{lm}(\Omega)$ form a complete set of functions on the unit sphere, because they present normalized simultaneous eigenstates of the self-adjoint angular momentum operators $\mathcal{L}^2$ and $\mathcal{L}_z$ which form a commuting set of operators with non-degenerate spectrum in the sense of Definition XXXVI (Appendix A.3.5). Thus, for any function $\chi(\Omega)$ which is square-normalizable with respect to the unit sphere, we find using the generalized Fourier expansion (A.143), (A.144) the following relation:

$$\begin{aligned} \int d\Omega \; |\chi(\Omega)|^2 \; &= \; \sum_{l=0}^{\infty} \sum_{m=-l}^{l} \int d\Omega \, \chi(\Omega)^* \, Y_{lm}(\Omega) \int d\Omega' \, Y_{lm}(\Omega')^* \chi(\Omega') \\ &= \; \sum_{l=0}^{\infty} \sum_{m=-l}^{l} \left| \int d\Omega \, Y_{lm}(\Omega)^* \chi(\Omega) \right|^2 \end{aligned} \tag{B.65}$$

This is Parseval's theorem for spherical harmonics. (An alternative proof of the completeness of the set of functions $Y_{lm}(\Omega)$ is presented in the monograph by Sansone [232], p. 270.)

For its application to Gaunt coefficients (B.61), we obviously have to set $\chi(\Omega) = Y_{l_2 m_2}(\Omega)^* Y_{l_3 m_3}(\Omega)^*$ in (B.65). In view of the conditions (B.64), we then obtain a representation of an integral involving the product of four spherical harmonics $Y_{lm}(\Omega)$ in terms of the symbols $I^{l_1 l_2 l_3}_{m_1 m_2 m_3}$:

$$\int d\Omega \; |Y_{l_2 m_2}(\Omega)|^2 \, |Y_{l_3 m_3}(\Omega)|^2 \; = \; \sum_{l_1 \, = \, |l_2 - l_3|}^{l_2 + l_3} \; \sum_{m_1 \, = \, -l_1}^{l_1} \left(I^{l_1 l_2 l_3}_{m_1 m_2 m_3} \right)^2 \tag{B.66}$$

To resolve the integral, we note that its sum over all possible values of m_2, ($m_2 = -l_2, -l_2 + 1, \ldots, l_2 - 1, l_2$), assumes a very simple form. From the addition theorem

(B.9) for spherical harmonics, the relation (B.3), and their orthonormality property (B.5), we successively find:

$$\sum_{m_2=-l_2}^{l_2} \int d\Omega \; |Y_{l_2 m_2}(\Omega)|^2 \, |Y_{l_3 m_3}(\Omega)|^2 \;=\; \frac{2l_2+1}{4\pi} \int d\Omega \; |Y_{l_3 m_3}(\Omega)|^2 \;=\; \frac{2l_2+1}{4\pi} \tag{B.67}$$

Together with (B.66), this relation yields a sum rule for Gaunt coefficients:

$$\sum_{l_1=|l_2-l_3|}^{l_2+l_3} \sum_{m_1=-l_1}^{l_1} \sum_{m_2=-l_2}^{l_2} \left(I^{l_1 l_2 l_3}_{m_1 m_2 m_3}\right)^2 \;=\; \frac{2l_2+1}{4\pi} \tag{B.68}$$

To obtain the estimate employed in Appendix A.5, we now examine a partial sum over absolute values of Gaunt coefficients. First, we state the inequality:

$$\left(\sum_{m_1=-l_1}^{l_1} \sum_{m_2=-l_2}^{l_2} \left| I^{l_1 l_2 l_3}_{m_1 m_2 m_3} \right| \right)^2 \;\leq\; (2l_1+1) \sum_{m_1=-l_1}^{l_1} \sum_{m_2=-l_2}^{l_2} \left(I^{l_1 l_2 l_3}_{m_1 m_2 m_3}\right)^2 \tag{B.69}$$

Here, we used the fact that at most $2l_1+1$ terms in these sums contribute since $m_2 = -(m_1+m_3)$ is fixed by the selection rule (B.64), and the sum over m_1 comprises $2l_1+1$ terms. Additionally, we employed once again the Cauchy-Schwarz inequality, here in the form $(\sum_{\nu=1}^{k} 1 \cdot a_\nu)^2 \leq (\sum_{\nu=1}^{k} 1)(\sum_{\nu=1}^{k} |a_\nu|^2)$, which is also known as the inequality of the arithmetic and quadratic means. On combination of (B.68) and (B.69), we finally arrive at the desired inequality for Gaunt coefficients $I^{l_1 l_2 l_3}_{m_1 m_2 m_3}$:

$$\sum_{m_1=-l_1}^{l_1} \sum_{m_2=-l_2}^{l_2} \left| I^{l_1 l_2 l_3}_{m_1 m_2 m_3} \right| \;\leq\; \sqrt{\frac{(2l_1+1)(2l_2+1)}{4\pi}} \tag{B.70}$$

Appendix C

Free-Particle Multipole Sources

EXACTLY SOLVABLE quantum mechanical problems in three dimensions are rare, yet one of the most thoroughly studied problems in quantum physics concerns the propagation of a free particle not subject to external forces [83,114]. Obviously, in spherical coordinates the multipole Green functions of a free particle $G_{lm}^{(\mathrm{free})}(\mathbf{r},\mathbf{r}';E)$ must coincide with the usual spherical partial waves, products of spherical harmonics $Y_{lm}(\hat{R})$ with spherical or half-integer Bessel functions of the third kind $h_l^{(\pm)}(kR)$ [81]. In the following sections, we will confirm mathematically that the multipole source formalism presented in Section 2.4 indeed is compatible to the well-known results of spherical partial wave theory [92]. This assertion has been made without proof in Section 3.2. Furthermore, the solution of the free-particle source problem presents the key to an understanding of the behavior of quantum multipole sources in quite general potential environments $U(\mathbf{r})$. This connection is illuminated in Appendix A.5 of this volume. In a somewhat detached portion of this appendix (Section C.3), we examine the position-momentum uncertainty relation for two-dimensional wave packets of definite angular momentum. We derive a generalized Heisenberg inequality for the uncertainty product and provide minimum uncertainty wave functions which are conveniently employed in Section 7.2 of this treatise.

C.1 Multipole Spherical Waves

For the purpose of demonstration we now will present a brief mathematical analysis of the free particle source problem in quantum mechanics. Clearly, from rotational symmetry the free multipole Green functions $G_{lm}^{(\mathrm{free})}(\mathbf{r},\mathbf{r}';E)$ should be given by the outgoing-wave or Hankel-type solutions of the wave equation [83]:

$$G_{lm}^{(\mathrm{free})}(\mathbf{r},\mathbf{r}';E) \;=\; C_{lm}(k)\,Y_{lm}(\hat{R})\,h_l^{(+)}(kR) \tag{C.1}$$

Here, $E = \hbar^2k^2/2M$, $\mathbf{R} = \mathbf{r} - \mathbf{r}'$ presents the relative distance vector between $\mathbf{r}$ and $\mathbf{r}'$, $R = |\mathbf{R}|$ denotes its length, and $\hat{R} = \mathbf{R}/R$ is the unit vector in the direction of $\mathbf{R}$.

$Y_{lm}(\hat{R})$ denotes a spherical harmonic function of angular momentum l and m, and the symbol $h_l^{(+)}(kR)$ represents a first-type spherical Hankel function of order l. $C_{lm}(k)$ is an energy-dependent normalization factor that will be established in the course of the subsequent calculation.

C.1.1 Spherical Waves as Multipole Green Functions

We start out from the defining differential equation (2.12) of the free-particle Green function $G^{(\text{free})}(\mathbf{r}, \mathbf{r}'; E)$:

$$\left\{\Delta + k^2\right\} G^{(\text{free})}(\mathbf{r}, \mathbf{r}'; E) \;=\; \frac{2M}{\hbar^2}\,\delta(\mathbf{r} - \mathbf{r}') \tag{C.2}$$

Since the problem is invariant under translation operations, a spatial Fourier transform, leading to the Green function in momentum space $G^{(\text{free})}(\mathbf{p}; k)$ will simplify the calculation ($\mathbf{R} = \mathbf{r} - \mathbf{r}'$):

$$G^{(\text{free})}(\mathbf{p}; k) \;=\; \int d^3R\, e^{-\,i\mathbf{p}\cdot\mathbf{R}}\, G^{(\text{free})}(\mathbf{r}, \mathbf{r}'; E) \tag{C.3}$$

From (C.2), one immediately finds:

$$G^{(\text{free})}(\mathbf{p}; k) \;=\; \frac{2M}{\hbar^2}\,\frac{1}{k^2 - p^2 + i\eta} \tag{C.4}$$

Here, $\eta \to 0^+$ denotes an infinitesimal positive parameter that is needed to enforce the retarded (outgoing wave) character of the Green function. [Formally, (C.4) displays the momentum representation of the retarded resolvent $\mathcal{R}_{\text{ret}}(E)$ to the free-particle Hamiltonian $\mathcal{H}_{(\text{free})}$ (Theorem LI in Appendix A.3.6). Note that the operator $\mathcal{H}_{(\text{free})}$ is separable in the set of momentum operators p_x, p_y, p_z (Definition XXXVII). Thus, the momentum space Green function is diagonal in $\mathbf{p}$: $G^{(\text{free})}(\mathbf{p}, \mathbf{p}'; E) = \delta(\mathbf{p} - \mathbf{p}')G^{(\text{free})}(\mathbf{p}; k)$.] In fact, by the inverse transformation to (C.3) we obtain from (C.4) the Green function $G^{(\text{free})}(\mathbf{r}, \mathbf{r}'; E)$ of a free particle in physical space:

$$G^{(\text{free})}(\mathbf{r}, \mathbf{r}'; E) \;=\; \frac{M}{4\pi^3\hbar^2}\int \frac{d^3p\, e^{i\mathbf{p}\cdot\mathbf{R}}}{k^2 - p^2 + i\eta} \;=\; -\,\frac{M}{2\pi\hbar^2}\,\frac{\exp ik|\mathbf{r} - \mathbf{r}'|}{|\mathbf{r} - \mathbf{r}'|} \tag{C.5}$$

We now generalize this result to multipole sources.

By definition (2.25), the set of multipole Green functions $G_{lm}(\mathbf{r}, \mathbf{r}'; E)$ is generated from the customary Green function $G(\mathbf{r}, \mathbf{r}'; E)$ by application of the spherical tensor gradient $K_{lm}(\partial/\partial\mathbf{r}')$:

$$G_{lm}^{(\text{free})}(\mathbf{r}, \mathbf{r}'; E) \;=\; K_{lm}\left(\frac{\partial}{\partial \mathbf{r}'}\right) G^{(\text{free})}(\mathbf{r}, \mathbf{r}'; E) \tag{C.6}$$

In the momentum representation (C.3), the differential operator of (C.6) translates into an ordinary harmonic polynomial. Hence, we obtain from (C.4) the following expression for the transform of the multipole Green function:

$$G_{lm}^{(\mathrm{free})}(\mathbf{p};k) \;=\; \frac{2M}{\hbar^2}\,\frac{(-ip)^l\,Y_{lm}(\hat{p})}{k^2-p^2+i\eta} \tag{C.7}$$

From (C.7), the multipole Green function in physical space (C.1) is available by the inverse Fourier transform to (C.3). This leads to an integral representation for $G_{lm}^{(\mathrm{free})}(\mathbf{r},\mathbf{r}';E)$:

$$G_{lm}^{(\mathrm{free})}(\mathbf{r},\mathbf{r}';E) \;=\; \frac{(-i)^l M}{4\pi^3\hbar^2}\int d^3p\, e^{i\mathbf{p}\cdot\mathbf{R}}\,\frac{p^l\,Y_{lm}(\hat{p})}{k^2-p^2+i\eta} \tag{C.8}$$

In order to perform the integration in spherical coordinates, we expand the plane wave $\exp(i\mathbf{p}\cdot\mathbf{R})$ into a multipole series (B.11) as demonstrated in Appendix B.3:

$$e^{i\mathbf{p}\cdot\mathbf{R}} \;=\; 4\pi\sum_{L=0}^{\infty} i^L\,j_L(pR)\sum_{M=-L}^{L} Y_{LM}^*(\hat{p})\,Y_{LM}(\hat{R}) \tag{C.9}$$

Here, the symbol $j_L(pR)$ denotes the regular spherical Bessel function of order L. Since the spherical harmonics $Y_{LM}(\hat{p})$ present a base of orthonormal functions on the unit sphere (B.5), only the (l,m)–term of the expansion (C.9) contributes to the integral (C.8). We obtain:

$$G_{lm}^{(\mathrm{free})}(\mathbf{r},\mathbf{r}';E) \;=\; \frac{M}{\pi^2\hbar^2}\,Y_{lm}(\hat{R})\int_0^\infty \frac{dp\,p^{l+2}\,j_l(pR)}{k^2-p^2+i\eta} \tag{C.10}$$

The remaining integral (that actually takes the character of a distribution) may be evaluated by the technique of complex residues. Let us first remark that the regular Bessel function may be replaced by a suitable combination of Hankel functions [83]:

$$j_l(z) \;=\; \frac{1}{2i}\,\Big\{h_l^{(+)}(z)-h_l^{(-)}(z)\Big\} \tag{C.11}$$

whose parity is given by the formula:

$$h_l^{(\pm)}(-z) \;=\; (-1)^{l+1}\,h_l^{(\mp)}(z) \tag{C.12}$$

(We note that the normalization convention used here deviates from our more general definition of Hankel functions in Appendix A.4.6, (A.249).) Therefore, the integrand in (C.10) is a even function of p, and we may rewrite this integral in the following

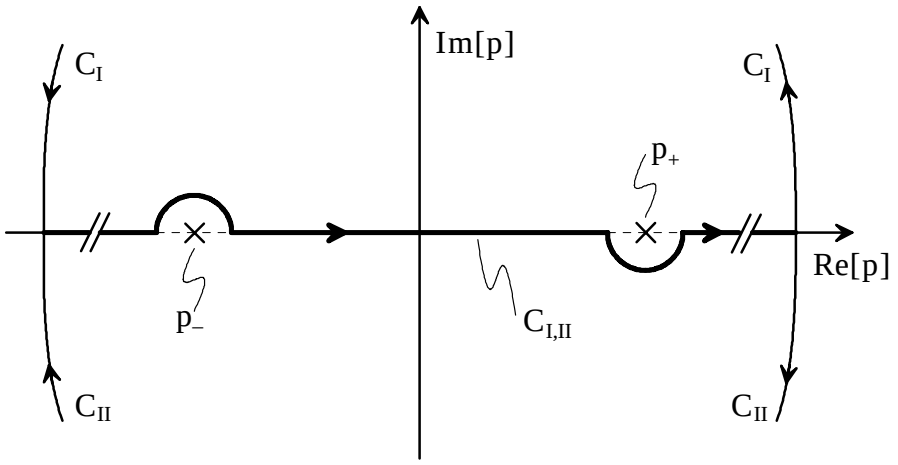

Figure 37: Evaluation of the integral (C.13) by complex contour integration. The integration paths avoid the poles of the integrand at $p_\pm = \pm(k + i\eta)$ and are closed in the upper (path $C_{\rm I}$) and lower (path $C_{\rm II}$) half of the complex p plane, respectively.

fashion:

$$\int_0^\infty \frac{dp\, p^{l+2}\, j_l(pR)}{k^2 - p^2 + i\eta} \;=\; \frac{1}{4i} \int_{-\infty}^{\infty} dp\, p^{l+2}\, \frac{h_l^{(+)}(pR) - h_l^{(-)}(pR)}{k^2 - p^2 + i\eta} \tag{C.13}$$

From the asymptotics (A.248) of the Hankel functions [83]:

$$h_l^{(\pm)}(z) \underset{|z|\to\infty}{\longrightarrow} \frac{1}{z}\, \exp\{\pm i(z - l\pi/2)\} \tag{C.14}$$

we immediately conclude that the integration contours $C_{\rm I}$ [$C_{\rm II}$] in (C.13) for the part containing $h_l^{(+)}(pR)$ [$h_l^{(-)}(pR)$] may be closed in the upper [lower] half of the complex p plane. (See Figure 37.) The poles of the integrand are located at $p_\pm = \pm(k + i\eta)$; their respective residues are (C.12):

$$\begin{aligned} \mathrm{res}(p_+) &= -\frac{1}{2}\, k^{l+1}\, h_l^{(+)}(kR) \\ \mathrm{res}(p_-) &= \frac{1}{2}\, (-k)^{l+1}\, h_l^{(-)}(-kR) \;=\; \frac{1}{2}\, k^{l+1}\, h_l^{(+)}(kR) \end{aligned} \tag{C.15}$$

(Note that these values depend on the sign of the infinitesimal parameter η.) Adding the contributions of both contours, we find for the integral (C.13):

$$\int_0^\infty \frac{dp\, p^{l+2}\, j_l(pR)}{k^2 - p^2 + i\eta} \;=\; -\frac{\pi}{2}\, k^{l+1}\, h_l^{(+)}(kR) \tag{C.16}$$

Inserting this result into (C.10), we finally obtain the desired explicit expression for the free-particle multipole Green function $G_{lm}^{(\mathrm{free})}(\mathbf{r},\,\mathbf{r}';\,E)$ we already anticipated in (C.1):

$$G_{lm}^{(\mathrm{free})}(\mathbf{r},\mathbf{r}';E) \;=\; -\,\frac{M}{2\pi\hbar^2}\,k^{l+1}\,Y_{lm}(\hat{R})\,h_l^{(+)}(kR) \tag{C.17}$$

C.1.2 A Differentiation Rule for Multipole Potentials

As an important consequence, this derivation also contains a differentiation rule for common (electrostatic) multipole potentials $\Phi_{lm}(\mathbf{R})$ (2.19) as a limiting case. It is well-known that the potential Green function is given by $G(\mathbf{r},\mathbf{r}') = -1/4\pi R$:

$$\Delta\left\{\frac{1}{|\mathbf{r}-\mathbf{r}'|}\right\} \;=\; -\,4\pi\,\delta(\mathbf{r}-\mathbf{r}') \tag{C.18}$$

However, this differential equation is covered by (C.2) in the limit $k \to 0$. Using the principal asymptotic form of the spherical Hankel functions [83],

$$h_l^{(+)}(z) \underset{|z|\to 0}{\longrightarrow} \frac{(2l-1)!!}{z^{l+1}} \tag{C.19}$$

one obtains from (C.6), (C.17) and (C.18) the following equality [88–90]:

$$K_{lm}\left(\frac{\partial}{\partial\mathbf{r}'}\right)\left\{\frac{1}{|\mathbf{r}-\mathbf{r}'|}\right\} \;=\; (2l-1)!!\,\frac{Y_{lm}(\hat{R})}{R^{l+1}} \tag{C.20}$$

This representation of electrostatic multipoles has been applied in Section 2.4.

C.2 The Wigner Law

In this concluding section, we aim at the calculation of the total current $J_{lm}^{(\mathrm{free})}(E)$ emitted by a multipole source in a field-free environment. Since the problem under consideration is spherically symmetric, the result will only depend on the angular momentum quantum number l, but not on m.

From Section 2.4, we infer that the total multipole current $J_{lm}^{(\mathrm{free})}(E)$ emitted from a multipole point source $\delta_{lm}(\mathbf{r}-\mathbf{r}')$ of unit strength is given by (2.33):

$$J_{lm}^{(\mathrm{free})}(E) \;=\; -\,\frac{2}{\hbar}\lim_{\mathbf{r}\to\mathbf{r}'}\Im\left[K_{lm}^{*}\left(\frac{\partial}{\partial\mathbf{r}}\right)K_{lm}\left(\frac{\partial}{\partial\mathbf{r}'}\right)G^{(\mathrm{free})}(\mathbf{r},\mathbf{r}';E)\right] \tag{C.21}$$

The calculation becomes particularly compact if one starts out with the time-dependent free particle propagator in momentum space $K_{(\mathrm{free})}(\mathbf{q},t;\mathbf{q}',t')$:

$$\left\{i\hbar\frac{\partial}{\partial t} - \frac{\hbar^2 q^2}{2M}\right\}K_{(\mathrm{free})}(\mathbf{q},t;\mathbf{q}',t') \;=\; i\hbar\,\delta(\mathbf{q}-\mathbf{q}')\,\delta(t-t') \tag{C.22}$$

One then immediately finds that the free retarded propagator for $t > t'$ is given by:

$$K_{(\mathrm{free})}(\mathbf{q},\mathbf{q}';T) \;=\; \delta(\mathbf{q}-\mathbf{q}')\,\exp\left(-\frac{i\hbar q^2 T}{2M}\right) \tag{C.23}$$

where we set $T = t - t'$. For $t < t'$, $K_{(\mathrm{free})}(\mathbf{q},\mathbf{q}';T)$ vanishes (see Appendix A.2.2). The momentum space propagator and the free Green function are connected by a spatio-temporal Fourier transform (2.13):

$$G^{(\mathrm{free})}(\mathbf{r},\mathbf{r}';E) \;=\; -\,\frac{i}{(2\pi)^3\hbar}\int_0^\infty dT\,e^{iET/\hbar}\int d^3q\,e^{i\mathbf{q}\cdot\mathbf{r}}\int d^3q'\,e^{-\,i\mathbf{q}'\cdot\mathbf{r}'}\,K_{(\mathrm{free})}(\mathbf{q},\mathbf{q}';T) \tag{C.24}$$

Here, we note that the plane waves occurring in this formula are eigenfunctions of the harmonic polynomial momentum operators of (C.21):

$$K_{lm}\left(\frac{\partial}{\partial\mathbf{r}'}\right)\,e^{-\,i\mathbf{q}'\cdot\mathbf{r}'} \;=\; (-i)^l\,K_{lm}(\mathbf{q}')\,e^{-\,i\mathbf{q}'\cdot\mathbf{r}'} \tag{C.25}$$

A similar relation holds for the second differential operator. Upon introduction of the explicit expression for the propagator $K_{(\mathrm{free})}(\mathbf{q},\mathbf{q}';T)$ (C.23), we find for the current $J^{(\mathrm{free})}_{lm}(E)$ (C.21):

$$J^{(\mathrm{free})}_{lm}(E) \;=\; \lim_{\mathbf{r}\to\mathbf{r}'}\Im\left[\frac{i}{4\pi^3\hbar^2}\int_0^\infty dT\,e^{iET/\hbar}\int d^3q\,e^{i\mathbf{q}\cdot(\mathbf{r}-\mathbf{r}')}\,q^{2l}\,Y^*_{lm}(\hat{q})\,Y_{lm}(\hat{q})\,e^{-\,i\hbar q^2T/2M}\right] \tag{C.26}$$

After performing the limiting procedure ($\mathbf{r}\to\mathbf{r}'$), the angular part of the $\mathbf{q}$–integration becomes trivial. To determine the result of the T–integration, we introduce an infinitesimal positive parameter $\eta \to 0^+$ in order to enforce convergence. This yields ($E = \hbar^2k^2/2M$):

$$\int_0^\infty dT\,e^{i\hbar(k^2-q^2+i\eta)T/2M} = \frac{2iM}{\hbar(k^2-q^2+i\eta)} = \frac{2iM}{\hbar}\left[\mathrm{PP}\left(\frac{1}{k^2-q^2}\right) - \frac{i\pi}{2q}\,\delta(k-q)\right] \tag{C.27}$$

Here, q has been assumed positive, and we once more used the well-known formal distribution relation [215]:

$$\lim_{\eta\to 0^+}\frac{1}{k^2-q^2+i\eta} \;=\; \mathrm{PP}\left(\frac{1}{k^2-q^2}\right) \;-\; i\pi\,\delta(k^2-q^2)\;, \tag{C.28}$$

where $\mathrm{PP}(\ldots)$ denotes the Cauchy principal value of the q integration. As can be seen from (C.26), the principal value integral is purely real and therefore does not

contribute to the total current $J_{lm}^{(\mathrm{free})}(E)$. Hence, the total multipole current is given by:

$$J_{lm}^{(\mathrm{free})}(E) \;=\; \Im\left[\frac{i}{4\pi^3\hbar^2}\int_0^\infty q^2\,dq\,\frac{\pi M}{\hbar q}\,\delta(k-q)\,q^{2l}\right] \tag{C.29}$$

Using (C.29), we finally obtain for the total multipole current emitted from a (l,m)–multipole source of unit strength in a field-free environment:

$$J_{lm}^{(\mathrm{free})}(E) \;=\; \frac{M}{4\pi^2\hbar^3}\,k^{2l+1} \tag{C.30}$$

In agreement with the source-theoretical result (C.30), it is generally observed that total reaction cross sections near threshold show a $E^{\,l+1/2}$ excess energy dependence. This well-established power law was first derived by Wigner [92] (Wigner's law).

C.3 Uncertainty Relations in Two Spatial Dimensions

One of the most widely known properties of quantum mechanical wave functions in a single dimension is the complementarity of their position and momentum information content: Due to the famous Heisenberg uncertainty relation, the product of the respective variations Δx and Δp_x never falls below the minimum value $\hbar/2$, where equality occurs only for special Gaussian "minimum uncertainty wave packets." The proof of this statement is usually based on formal properties of Hilbert space (see Appendix A.3) and may be looked up in virtually any textbook on quantum mechanics [83, 114]. Here, however, we are interested in a multidimensional variant of the uncertainty relation describing the dynamics of electrons in two dimensions. Angular momentum eigenstates of minimum position-momentum uncertainty play a decisive role in a heuristic model of multidimensional tunneling (see Section 7.2). These wave functions may be identified by means of a technique closely related to the canonical scheme used in the proof of the conventional Heisenberg uncertainty relation. Since this approach apparently has been nowhere published, we present an account of the technique below.

Here, we shall limit our considerations to two-dimensional eigenstates of the angular momentum operator L_z. In polar coordinates, these functions may be separated into a radial and an angular part characterized by the quantum number m: $\Psi(R,\phi) = \psi(R)\exp(im\phi)$. As an immediate consequence, the mean positions $\langle x\rangle$, $\langle y\rangle$ and the corresponding average momenta $\langle p_x\rangle$, $\langle p_y\rangle$ all vanish. Hence, the uncertainties of position and momentum are entirely governed by the variances $\langle R^2\rangle = \langle x^2+y^2\rangle$ and $\langle p^2\rangle = \langle p_x^2+p_y^2\rangle$. In order to introduce the formal apparatus required to determine these expectation values, let us first consider the normalization integral for the

wave function $\Psi(R,\phi)$:

$$\begin{aligned}\langle\Psi|\Psi\rangle &= \int\int dx\,dy\;|\Psi(x,y)|^2 \\ &= 2\pi\int_0^\infty dR\,R\;|\psi(R)|^2 \;=\; 2\pi\,\langle\psi\,|R|\,\psi\rangle_{R\phi} \;=\; 2\pi\left\|\sqrt{R}\;\psi\right\|_{R\phi}^2\end{aligned} \tag{C.31}$$

We have expanded this simple expression to some length to point out the connection between the conventional metric space $\mathbb{R}^2 = \mathbb{L}^2(-\infty,+\infty)\otimes\mathbb{L}^2(-\infty;+\infty)$ which is denoted here by the standard scalar product $\langle\Psi|\Psi\rangle$, and the diagonal element $\langle\psi\,|R|\,\psi\rangle_{R\phi}$ assigned to the simpler norm $\|\chi\|_{R\phi}^2 = \int_0^\infty dR\,|\chi(R)|^2$ in the Hilbert space of square-integrable radial functions $\mathbb{L}^2(0,\infty)$. Obviously, this reduction in complexity is linked to the cylindrical symmetry present in $\Psi(R,\phi)$.

Let us now rewrite the averages $\langle R^2\rangle$ and $\langle p^2\rangle$ we are looking for in terms of the metric $\|\chi\|_{R\phi}^2$. This is particularly simple for the square distance $\langle R^2\rangle$. By analogy with (C.31), one immediately arrives at:

$$\left\langle\Psi\left|R^2\right|\Psi\right\rangle \;=\; 2\pi\left\langle\psi\left|R^3\right|\psi\right\rangle_{R\phi} \;=\; 2\pi\left\|R^{3/2}\,\psi\right\|_{R\phi}^2 \tag{C.32}$$

For the mean square momentum $\langle p^2\rangle$, we first state the two-dimensional Laplacian operator Δ in polar coordinates [83]:

$$\Delta \;=\; \frac{1}{R}\frac{\partial}{\partial R}\left(R\,\frac{\partial}{\partial R}\right) + \frac{1}{R^2}\,\frac{\partial^2}{\partial\phi^2} \tag{C.33}$$

For a L_z eigenstate, the latter summand may be replaced by $-m^2/R^2$. Since $\mathbf{p} = -i\hbar\boldsymbol{\nabla}$, the average square momentum $\langle p^2\rangle$ assigned to $\Psi(R,\phi)$ is given by:

$$\begin{aligned}\left\langle\Psi\left|p^2\right|\Psi\right\rangle &= 2\pi\hbar^2\int_0^\infty dR\,R\,\psi(R)^*\left\{\frac{m^2}{R^2} \;-\; \frac{1}{R}\,\frac{\partial}{\partial R}\,R\,\frac{\partial}{\partial R}\right\}\psi(R) \\ &= 2\pi\hbar^2\left\langle\psi\left|\frac{m^2}{R} \;-\; \frac{\partial}{\partial R}\,R\,\frac{\partial}{\partial R}\right|\psi\right\rangle_{R\phi}\end{aligned} \tag{C.34}$$

It now proves convenient to transform (C.34) into a "norm style" expression resembling (C.31) and (C.32). For this purpose, we employ a decomposition of the operator in (C.34) that is somewhat akin to the notion of a "square root operator" introduced in Appendix A.3.3 and set $p^2 = \mathcal{P}^+\mathcal{P}$. (Note that for a proper root operator, $\mathcal{P}^+ = \mathcal{P}$ must additionally hold.) One easily verifies the product representation:

$$\frac{m^2}{R} \;-\; \frac{\partial}{\partial R}\,R\,\frac{\partial}{\partial R} \;=\; \left(-\,\frac{\partial}{\partial R}\,\sqrt{R} \;-\; \frac{|m|}{\sqrt{R}}\right)\left(\sqrt{R}\,\frac{\partial}{\partial R} \;-\; \frac{|m|}{\sqrt{R}}\right) \tag{C.35}$$

With the help of (C.35), (C.34) may be rewritten:

$$\left\langle \Psi \left| p^2 \right| \Psi \right\rangle \;=\; 2\pi\hbar^2 \left\| \left(\sqrt{R}\, \frac{\partial}{\partial R} \;-\; \frac{|m|}{\sqrt{R}} \right) \psi \right\|_{R\phi}^2 \tag{C.36}$$

For an estimate of the uncertainty product $\Delta R \cdot \Delta p$, we use the Cauchy-Schwarz inequality on the product of (C.32) and (C.36):

$$\begin{aligned} \left\langle \Psi \left| R^2 \right| \Psi \right\rangle \left\langle \Psi \left| p^2 \right| \Psi \right\rangle \;&\geq\; \left| \langle \Psi \left| R\,\mathcal{P} \right| \Psi \rangle \right|^2 \\ &\geq\; (2\pi\hbar)^2 \left| \left\langle \psi \left| R^{3/2} \left(R^{1/2}\, \frac{\partial}{\partial R} \;-\; \frac{|m|}{R^{1/2}} \right) \right| \psi \right\rangle_{R\phi} \right|^2 \end{aligned} \tag{C.37}$$

Here, equality holds if and only if the states $R\,|\Psi\rangle$ and $\mathcal{P}\;|\Psi\rangle$ are linearly dependent, i. e., there exists some (complex) constant $\tilde{\lambda}$ so that:

$$\left\{ R^{1/2}\, \frac{\partial}{\partial R} \;-\; \frac{|m|}{R^{1/2}} \;+ \tilde{\lambda} R^{3/2} \right\} \psi(R) \;=\; 0 \tag{C.38}$$

is fulfilled. This first-order differential equation is easily solved for $\psi(R)$; it is found that this special class of radial parts is comprised of modified Gaussian functions:

$$\psi(R) \;=\; \alpha\, R^{|m|}\, \exp(-\tilde{\lambda} R^2/2) \tag{C.39}$$

Here, α denotes a constant of proportionality, and $\Re[\tilde{\lambda}] > 0$ must hold for reasons of normalizability. We may interpret the functions (C.39) as the ground states of a two-dimensional harmonic oscillator in the subspaces of angular momentum eigenstates with quantum number m.

For our subsequent analysis, we split the operator occurring in the expectation value in (C.37) into a hermitian and an antihermitian contribution:

$$R^2\, \frac{\partial}{\partial R} \;- |m| R \;=\; -(|m|+1) R + R\, \frac{\partial}{\partial R}\, R \tag{C.40}$$

Since $\langle \psi \left| R \right| \psi \rangle_{R\phi}$ is real, but $\langle \psi \left| R \partial_R R \right| \psi \rangle_{R\phi}$ purely imaginary, the inequality (C.37) may be further rewritten:

$$\begin{aligned} \left\langle \Psi \left| R^2 \right| \Psi \right\rangle \left\langle \Psi \left| p^2 \right| \Psi \right\rangle \;&\geq\; (2\pi\hbar)^2 \left\{ (|m|+1)^2 \left\langle \psi \left| R \right| \psi \right\rangle_{R\phi}^2 + \left| \left\langle \psi \left| R \partial_R R \right| \psi \right\rangle_{R\phi} \right|^2 \right\} \\ &\geq\; \hbar^2 \left(|m|+1 \right)^2 \langle \Psi | \Psi \rangle^2 \end{aligned} \tag{C.41}$$

Here, we used the fact that according to (C.31), the norm of $\Psi(R,\phi)$ is given by $\langle \Psi | \Psi \rangle = 2\pi \left\langle \psi \left| R \right| \psi \right\rangle_{R\phi}$.

Reordering (C.41), we immediately obtain:

$$\left\langle R^2 \right\rangle \left\langle p^2 \right\rangle \;=\; \frac{\left\langle \Psi \left| R^2 \right| \Psi \right\rangle \left\langle \Psi \left| p^2 \right| \Psi \right\rangle}{\left\langle \Psi | \Psi \right\rangle \left\langle \Psi | \Psi \right\rangle} \;\geq\; \hbar^2 \left(|m| + 1 \right)^2 \tag{C.42}$$

This proves that the uncertainty product $\Delta R \cdot \Delta p$ for a two-dimensional angular momentum eigenstate with quantum number m is bounded from below by $\Delta R \cdot \Delta p \geq \hbar \left(|m| + 1 \right)$. (Obviously, this formula is in agreement with the standard Heisenberg uncertainty relation which demands $\Delta x \cdot \Delta p_x + \Delta y \cdot \Delta p_y \geq \hbar$.) For states of minimum uncertainty, equality must hold in the chain of inequalities in (C.41). We already identified those generalized Gaussian functions $\psi(R)$ (C.39) for which the first two expressions in (C.41) become equal. For the second comparison, we note that the left-hand and right-hand statements will coincide if the following expectation value vanishes:

$$\left\langle \psi \left| R \frac{\partial}{\partial R} R \right| \psi \right\rangle_{R\phi} \;=\; \int_0^\infty dR \, R \, \psi(R)^* \, \frac{\partial}{\partial R} \left[R \, \psi(R) \right] \;=\; 0 \tag{C.43}$$

Since $R \partial_R R$ is an antihermitian operator, this matrix element is purely imaginary, and thus must vanish for any choice of a real wave function $\psi(R)$ in (C.43). In view of (C.39), this means that for a minimum uncertainty wave function, the parameter $\tilde{\lambda}$ must be selected real and positive. We thus have proven that the angular momentum eigenstates of minimum position-momentum uncertainty with quantum number m are given by the Gaussian-type functions:

$$\Psi(R, \phi) \;=\; \alpha \, R^{|m|} \, \exp(-\lambda^2 R^2 / 2 + i m \phi) \tag{C.44}$$

where $\lambda^2 > 0$ is a positive real constant; for their uncertainty product, $\Delta R \cdot \Delta p = \hbar \left(|m| + 1 \right)$ holds. These functions play an important role in the description of the lateral profile of ballistic tunneling currents (Section 7.2).

Appendix D

The Airy Differential Equation

THIS MATHEMATICAL APPENDIX PROVIDES a brief introduction to the theory of the Airy differential equation and its solutions, the Airy functions. Notwithstanding the fact that apart from equations with constant coefficients, Airy's differential equation arguably presents the simplest linear ordinary differential equation of second order available, its solutions seemingly have not found widespread attention at least in the physics community. Because these functions prove indispensable in the mathematical treatment of the problem of ballistic motion in quantum mechanics [9, 114], as may be inferred from Chapter 5 of this treatise, we give a short presentation of their properties which is largely founded on the functional analytical framework provided in Appendix A.3 and A.4. For a table of the Airy functions and information on their use in uniform asymptotic analysis, we refer to p. 446 in the handbook by Abramowitz and Stegun [81], and the monograph by Olver [235]. As offspring of a considerably simple equation, numerous integrals involving the Airy functions may be solved in closed form, a fact that is surprisingly little known. For compilations of some of these integrals, see [151, 234].

D.1 Airy Functions

We first gather some information on the Airy differential equation and its solutions, the Airy functions. The following deliberations prepare the ground for the discussion of the quantum mechanical problem of uniformly accelerated motion in one dimension which we will tackle in Section D.2.

D.1.1 Airy's Differential Equation

We start out with Airy's differential equation, a linear ordinary differential equation of the second order [81]:

$$\left\{ \frac{\partial^2}{\partial x^2} - x \right\} y(x) = 0 \tag{D.1}$$

Here, x denotes a real variable as we are mainly interested in solutions (Airy functions) $y(x)$ with real argument. To obtain a set of solutions to (D.1), we employ the Laplacian method [114] and set $y(x) = \int dt\, Z(t)\, e^{xt}$ where t is a complex variable and the integration is performed along some complex contour C. Inserting this ansatz in (D.1), we find the condition that:

$$\int_C dt\, (t^2 - x)\, Z(t)\, e^{xt} \;=\; 0 \tag{D.2}$$

must hold independently from our choice for x. This may be achieved by setting $Z(t) = \exp(-t^3/3)$; then, by integration we find that the Laplace ansatz will yield a solution of (D.1) whenever the integrand $Z(t)e^{xt} = e^{-t^3/3+xt}$ vanishes at the endpoints of the contour C for all x. Clearly, this will only happen for $|t| \to \infty$ in those sectors I, II, III of the complex t plane where $\Re[t^3] > 0$. The situation is depicted in Figure 38. The drawing shows the three principal paths $C_{\mathrm{I-II}}$, $C_{\mathrm{II-III}}$, and $C_{\mathrm{III-I}}$ that may be chosen for the integration. (Evidently, the exact path of integration C may be arbitrarily shifted as long as the path does not leave its initial and final sectors for $|t| \to \infty$.) Of the corresponding solutions $y_{\mathrm{I-II}}(x)$, $y_{\mathrm{II-III}}(x)$, and $y_{\mathrm{III-I}}(x)$, at most two are linearly independent. This becomes obvious by closing the contour in Figure 38:

$$y_{\mathrm{I-II}}(x) + y_{\mathrm{II-III}}(x) + y_{\mathrm{III-I}}(x) \;=\; 0 \tag{D.3}$$

Furthermore, the paths $C_{\mathrm{I-II}}$ and $C_{\mathrm{III-I}}$ may be chosen symmetric with respect to the real t axis, so the relevant solutions form a complex conjugate pair:

$$y_{\mathrm{I-II}}(x) + y_{\mathrm{III-I}}(x)^* \;=\; 0 \tag{D.4}$$

which together with (D.3) shows that the special solution $y_{\mathrm{II-III}}(x)$ is purely imaginary:

$$y_{\mathrm{II-III}}(x) \;=\; y_{\mathrm{III-I}}(x)^* - y_{\mathrm{III-I}}(x) \tag{D.5}$$

Let us now examine this solution.

D.1.2 The Regular Solution

Here, we are interested in the asymptotic behavior of the particular solution $y_{\mathrm{II-III}}(x)$. We have seen in Section A.4 that the asymptotic character of the solutions $y(x)$ in (D.1) determines their use in spectral representations of their generating differential operators, here $D(x, \partial_x) = \partial_x^2 - x$. Moreover, we already can infer a considerable amount of information on the asymptotic nature of the solution set $y(x)$ by means of the Liouville-Green approximation (Theorem LII) which is here clearly applicable with

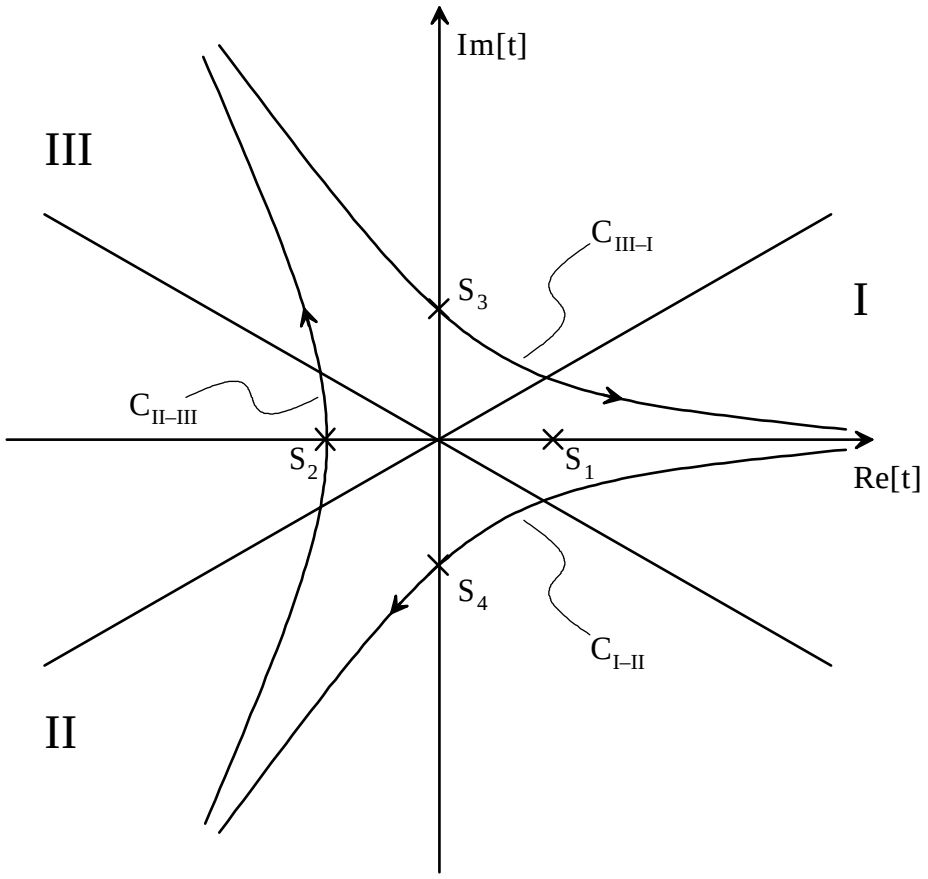

Figure 38: Integration paths in the complex t plane that yield Laplace-type solutions to Airy's differential equation (D.1). Saddle points $S_{1,2} = \pm\sqrt{x}$ (for positive x) and $S_{3,4} = \pm i\sqrt{|x|}$ (for negative x) of the integrand are indicated.

$k_E(x)^2 = x$. For the current problem, the LG theorem states that within the "tunneling sector" $x > 0$, a special pair $y_{r,i}(x)$ of solutions to (D.1) is given by (A.207):

$$y_{r,i}(x) \;=\; \frac{1}{x^{1/4}}\,\exp\left\{\pm\,\frac{2}{3}\,x^{3/2}\right\}\,\cdot\,[1+\epsilon(x)] \tag{D.6}$$

where the correction term $\epsilon(x)$ is bounded by (A.206), (A.209):

$$|\epsilon(x)| \;\leq\; \exp\left\{\int_x^\infty \frac{d\xi}{\xi^{1/4}}\,\frac{\partial^2}{\partial\xi^2}\,\frac{1}{\xi^{1/4}}\right\} - 1 \;=\; \exp\left\{\frac{5}{24}\,x^{-3/2}\right\} - 1 \tag{D.7}$$

which vanishes like $|\epsilon(x)| \sim 5/24\,x^{3/2}$ as $x \to \infty$. (For expansions of the Airy functions into asymptotic series, see [81].) We will now show that $y_{\mathrm{II-III}}(x)$ indeed presents a multiple of the regular LG solution $y_r(x)$. For this purpose we approximate $y_{\mathrm{II-III}}(x)$

for large positive arguments x by the method of steepest descents (saddle point approximation). For a thorough survey of this mathematical technique, we refer to the textbook by Bleistein and Handelsman [127].

The method depends on the presence of stationary points of the exponent in the integrand $e^{-t^3/3+xt}$. For positive x, these are here clearly given by $S_{1,2} = \pm\sqrt{x}$. Along the real axis, $S_1 = \sqrt{x}$ presents a maximum of the integrand, whereas $S_2 = -\sqrt{x}$ is connected to a minimum. Since any analytic function $f(t)$ will take its extremal values within a region Ω of the complex t plane on its boundary $\partial\Omega$ [sake for zeros of $f(t)$], the characterization of a stationary point as maximum cannot hold for all directions in the complex plane; rather, all stationary points present saddle points of $f(t)$. The saddle point technique now relies on the identification of the directions of steepest descent of $f(t)$ for the stationary points of the integrand, and subsequently approximating the integral by expanding the exponent into a series, thus producing a Gaussian integral easily evaluated.

Let us now apply this program to the function $y_{\mathrm{II-III}}(x)$. From the symmetry properties of the integrand, it is clear that the direction of steepest descent for $S_1 = \sqrt{x}$ is indeed along the real t axis, whereas for $S_2 = -\sqrt{x}$ it runs parallel to the imaginary axis, where the integrand drops exponentially to both sides of S_2. A peek on Figure 38 shows that the contour $C_{\mathrm{II-III}}$ may be chosen in a way as to pass through S_2 along the direction of steepest descent. The Gaussian approximation delivers for large positive x using the proper variable $iu = t + \sqrt{x}$:

$$\begin{aligned} y_{\mathrm{II-III}}(x) &= \int_{C_{\mathrm{II-III}}} dt\, e^{-t^3/3+xt} \\ &\sim i\int_{-\infty}^{\infty} du\, \exp\left(-\frac{2}{3}\,x^{3/2} - u^2 x^{1/2}\right) = \frac{i\sqrt{\pi}}{x^{1/4}}\,\exp\left(-\frac{2}{3}\,x^{3/2}\right) \end{aligned} \tag{D.8}$$

Thus, for large arguments, the solution $y_{\mathrm{II-III}}(x)$ drops exponentially. A comparison with the regular LG solution $y_r(x)$ D.6 reveals that $y_{\mathrm{II-III}}(x) = i\sqrt{\pi}\, y_r(x)$. For the common designation of this function, however, one shifts the path of integration $C_{\mathrm{II-III}}$ to the imaginary axis, sets $t = iu$ and finally divides by $2\pi i$. The resulting real function is known as the regular Airy function $\mathrm{Ai}(x)$ [81]:

$$\mathrm{Ai}(x) = \frac{1}{2\pi}\int_{-\infty}^{\infty} du\, e^{iu^3/3+iux} = \frac{1}{\pi}\int_0^{\infty} du\, \cos\left(\frac{u^3}{3} + ux\right) \tag{D.9}$$

Evidently, $y_{\mathrm{II-III}}(x) = 2\pi i\,\mathrm{Ai}(x)$.

The regular solution plays a dominant role in the functional analytical approach to second-order linear equations as it takes part in the eigenfunction expansion of the differential operator (see Section A.4.2). The normalization properties of these eigenfunctions, however, depend on their asymptotic behavior in the sector of classically

allowed motion $x \to -\infty$ (Theorem LVI) which we treat next. In this case, the saddle point approximation relies on the characteristics of $e^{-t^3/3+xt}$ in the neighborhood of the complex conjugate pair of stationary points $S_{3,4} = \pm i\sqrt{|x|}$. Instead of dealing with $y_{\mathrm{II-III}}(x)$, here we find it easier to perform this task for one of the remaining solutions, say $y_{\mathrm{III-I}}(x)$, which is one of the topics of the following subsection [see (D.13)], and calculate the asymptotic form of $\mathrm{Ai}(x)$ via the relation (D.5). This yields together with (D.8), (D.9) [81]:

$$\mathrm{Ai}(x) \sim \begin{cases} \frac{1}{2\sqrt{\pi}\, x^{1/4}} \exp\left(-\frac{2}{3}\, x^{3/2}\right) & (x \to \infty) \\ \frac{1}{\sqrt{\pi}\, |x|^{1/4}} \sin\left(\frac{2}{3}\, |x|^{3/2} + \frac{\pi}{4}\right) & (x \to -\infty) \end{cases} \tag{D.10}$$

By comparison with the outgoing-wave solutions $y_{\pm}(x)$ (A.208) of the LG approximation (Theorem LII) we infer that $\mathrm{Ai}(x) = (2\sqrt{\pi})^{-1} y_r(x) = (2i\sqrt{\pi})^{-1} [e^{i\pi/4} y_+(x) - e^{-i\pi/4} y_-(x)]$. This concludes our treatment of the regular Airy function $\mathrm{Ai}(x)$. A plot of this function illustrating the asymptotic behavior (D.10) is displayed in Figure 39.

D.1.3 The Irregular and Hankel Solutions

Notwithstanding the fact that the functional analytical theory of differential operators is built mainly upon their regular eigenfunctions, i. e., for the Airy differential equation (D.1) relies upon the Airy function $\mathrm{Ai}(x)$ (D.10), the outgoing-wave solutions $y_{\pm}(x)$ (A.208) of the LG approximation play a major role in the explicit determination of the fundamental and retarded Green functions $G_f(x, x'; E)$ and $G(x, x'; E)$ of the problem, see (A.222), (A.230), (A.251). Obviously, the corrresponding asymptotically divergent solutions of the Airy differential equation must be related to the Laplace solutions $y_{\mathrm{I-II}}(x)$ and $y_{\mathrm{III-I}}(x)$ (Figure 38), which essentially form a complex conjugate pair (D.4). Let us establish their asymptotic behavior now.

Again, the technique of our choice founds on the stationary values of the integrand $e^{-t^3/3+xt}$. For large positive values of x, the contour $C_{\mathrm{III-I}}$ may be placed along the positive real axis, where it crosses through the saddle point $S_1 = \sqrt{x}$ on the path of steepest descent, as discussed before (Figure 38). Expanding the exponent around S_1, we obtain from the Gaussian approximation with $u = t - \sqrt{x}$ for large positive arguments x:

$$y_{\mathrm{III-I}}(x) = \int_{C_{\mathrm{III-I}}} dt\, e^{-t^3/3+xt} \sim \int_{-\infty}^{\infty} du \, \exp\left(\frac{2}{3}\, x^{3/2} - u^2 x^{1/2}\right) = \frac{\sqrt{\pi}}{x^{1/4}} \exp\left(\frac{2}{3}\, x^{3/2}\right) \tag{D.11}$$

The same approximation clearly holds for $-y_{\mathrm{I-II}}(x)$. Unlike their difference $y_{\mathrm{II-III}}(x)$ (D.5), (D.8), the functions $y_{\mathrm{III-I}}(x)$ and $y_{\mathrm{I-II}}(x)$ are irregular solutions of (D.1) for $x \to$

∞ in the sense of the LG approximation (D.6), and they are obviously linearly independent to the regular solution $\mathrm{Ai}(x)$ (D.9).

Next, we tackle the asymptotic limit $x \to -\infty$ using the method of steepest descent once more. In this case, the stationary points of the integrand are given by the conjugate complex pair $S_{3,4} = \pm i\sqrt{|x|}$. Subsequently, we only consider the function $y_{\mathrm{III-I}}(x)$; the asymptotic behavior of $y_{\mathrm{I-II}}(x)$ follows from (D.4).

It may be inferred from Figure 38 that the integration contour $C_{\mathrm{III-I}}$ may be deformed to pass through the stationary point $S_3 = i\sqrt{|x|}$. Since the integrand $e^{-t^3/3+xt}$ drops exponentially both in sectors I and III of the complex t plane, we may approximate the integral $y_{\mathrm{III-I}}(x)$ by a Gaussian function near S_3 along a path of steepest descent which we have to determine first. As usual, we set $e^{i\theta}u = t - i\sqrt{|x|}$ and expand the exponent:

$$-\frac{t^3}{3} + xt = -\frac{2i}{3}|x|^{3/2} - ie^{2i\theta}u^2|x|^{1/2} + \mathcal{O}(u^3) \tag{D.12}$$

For a path of steepest descent, we set $e^{2i\theta} = -i$ or $\theta = -\pi/4$. We therefore have to integrate along a path $C_{\mathrm{III-I}}$ that cuts the imaginary axis under an angle of $45°$ (see Figure 38). Under these circumstances, we find for large negative x:

$$y_{\mathrm{III-I}}(x) \sim e^{i\theta}\int_{-\infty}^{\infty} du\, \exp\left(-\frac{2i}{3}|x|^{3/2} - u^2|x|^{1/2}\right) = \frac{\sqrt{\pi}}{|x|^{1/4}}\exp\left\{-i\left(\frac{2}{3}x^{3/2} + \frac{\pi}{4}\right)\right\} \tag{D.13}$$

and in the same way according to (D.4),

$$y_{\mathrm{I-II}}(x) \sim -\frac{\sqrt{\pi}}{|x|^{1/4}}\exp\left\{i\left(\frac{2}{3}x^{3/2} + \frac{\pi}{4}\right)\right\} \tag{D.14}$$

It is seen that $y_{\mathrm{III-I}}(x)$ and $y_{\mathrm{I-II}}(x)$ are ingoing and outgoing wave solutions for $x \to -\infty$ in the sense of the LG approximation (A.208): $y_{\mathrm{III-I}}(x) = \sqrt{\pi}\, e^{-i\pi/4}y_-(x)$, $y_{\mathrm{I-II}}(x) = -\sqrt{\pi}\, e^{i\pi/4}y_+(x)$. From (D.5), (D.13) and (D.14) we furthermore may infer the asymptotic form (D.10) of the regular solution $\mathrm{Ai}(x)$ as $x \to -\infty$.

Again, a slightly different notation for these functions is in standard use. We reverse the direction of the path of integration $C_{\mathrm{I-II}}$ in Figure 38 and shift it to the negative imaginary and real positive t axes, respectively. After division by π, we arrive at the outgoing Airy Hankel function $\mathrm{Ci}(x)$:

$$\mathrm{Ci}(x) = -\frac{1}{\pi}\int_{C_{\mathrm{I-II}}} dt\, e^{-t^3/3+xt} = \frac{1}{\pi}\int_0^{\infty} dt\, e^{-t^3/3+xt} + \frac{i}{\pi}\int_0^{\infty} dt\, e^{-it^3/3-ixt} \tag{D.15}$$

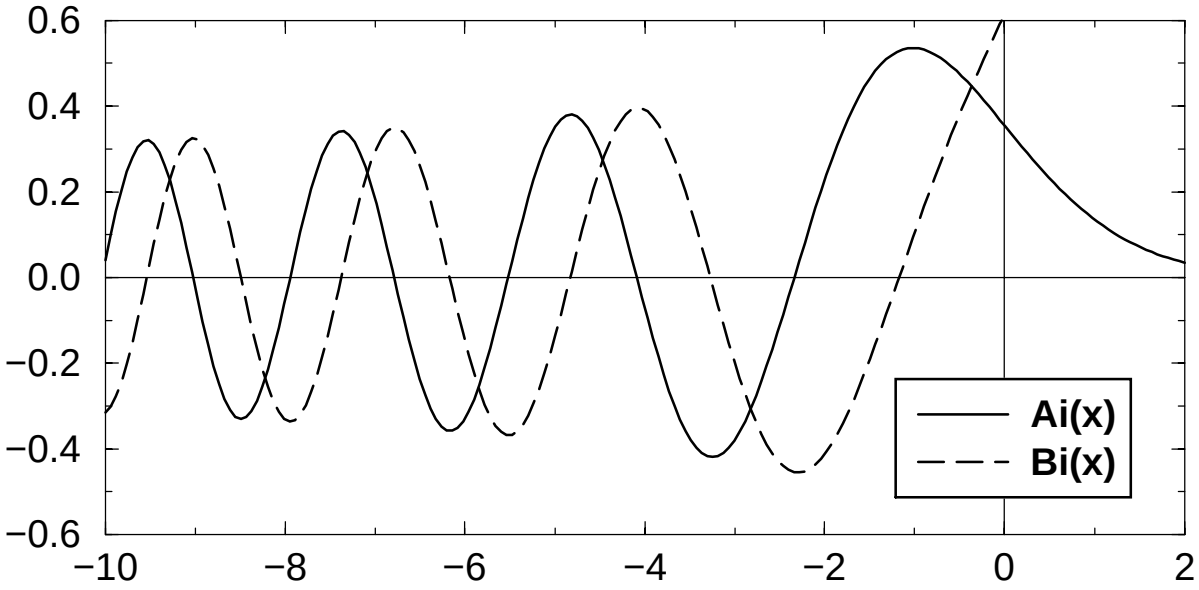

Figure 39: The Airy functions $\mathrm{Ai}(x)$ and $\mathrm{Bi}(x)$ in the real domain.

For large negative arguments x, the Airy Hankel function $\mathrm{Ci}(x)$ adopts the following asymptotic form:

$$\mathrm{Ci}(x) \sim \frac{1}{\sqrt{\pi}\,|x|^{1/4}} \exp\left\{ i \left(\frac{2}{3}\,|x|^{3/2} + \frac{\pi}{4} \right) \right\} \tag{D.16}$$

By comparison with (D.10), it is seen that the imaginary part of the complex solution $\mathrm{Ci}(x)$ is given by the regular Airy function $\mathrm{Ai}(x)$. The real part of $\mathrm{Ci}(x)$ presents a second real, linearly independent solution $\mathrm{Bi}(x)$ to the Airy differential equation (D.1) which is known as the irregular Airy function. From (D.11), (D.15), and (D.16), we obtain the integral representation [81]:

$$\mathrm{Bi}(x) = \frac{1}{\pi} \int_0^\infty dt\, \exp\left(-\frac{t^3}{3} + xt \right) + \frac{1}{\pi} \int_0^\infty dt\, \sin\left(\frac{t^3}{3} + xt \right) \tag{D.17}$$

and the leading asymptotic forms of $\mathrm{Bi}(x)$:

$$\mathrm{Bi}(x) \sim \begin{cases} \frac{1}{\sqrt{\pi}\,x^{1/4}} \exp\left(\frac{2}{3}\,x^{3/2} \right) & (x \to \infty) \\ \frac{1}{\sqrt{\pi}\,|x|^{1/4}} \cos\left(\frac{2}{3}\,|x|^{3/2} + \frac{\pi}{4} \right) & (x \to -\infty) \end{cases} \tag{D.18}$$

Note that for $x \to -\infty$, the functions $\mathrm{Ai}(x)$ and $\mathrm{Bi}(x)$ are shifted by $\pi/2$ in phase. A plot of both functions is displayed in Figure 39.

D.2 Quantum Mechanics of Freely Falling Bodies

Following these mathematical preliminaries, we want to determine the eigenfunctions $y_E(x)$ for the one-dimensional Schrödinger equation of uniformly accelerated motion which corresponds to the potential $U(x) = -Fx$:

$$\left\{ E + \frac{\hbar^2}{2M} \frac{\partial^2}{\partial x^2} + Fx \right\} y_E(x) \;=\; 0 \tag{D.19}$$

and express them in terms of the Airy functions $\mathrm{Ai}(u)$, $\mathrm{Bi}(u)$, $\mathrm{Ci}(u)$ (D.9), (D.15), (D.17). To get rid of the numerous constants in (D.19), it is a good idea to introduce dimensionless variables much as in the discussion of Chapter 5, see (5.22). Using the standard inverse energy parameter $\beta = (M/4\hbar^2F^2)^{1/3}$ (5.16), we define $\epsilon = -2\beta E$, $u = 2\beta Fx$ (note that the latter definition differs from the notation applied in Chapter 5 by a factor of two), which leads to a simplified version of (D.19):

$$\left\{ \frac{\partial^2}{\partial u^2} + u - \epsilon \right\} y_\epsilon(u) \;=\; 0 \tag{D.20}$$

By comparison with the Airy differential equation (D.1), we find that the complete set of solutions of (D.20) is given by a linear combination of the Airy functions $\mathrm{Ai}(\epsilon - u)$ and $\mathrm{Bi}(\epsilon - u)$:

$$y_\epsilon(u) \;=\; \lambda\,\mathrm{Ai}(\epsilon - u) + \mu\,\mathrm{Bi}(\epsilon - u) \tag{D.21}$$

Here, λ and μ denote arbitrary complex coefficients.

D.2.1 Normalized Solutions

Among its eigenfunctions $y_E(x)$, only those that are globally bounded are relevant in the functional analytical approach to the Schrödinger equation (D.19) and appear in eigenfunction expansions of normalizable wave packets $\psi(x) = \langle x|\Psi\rangle$, as has been explained in Section A.4.2. The asymptotic forms (D.10), (D.18) of the Airy functions obviously show that these solutions $y_E^{(r)}(x)$ which are regular in the sense of the LG approximation (Theorem LII) must be multiples of the regular Airy function $\mathrm{Ai}(\epsilon - u)$. Switching back to the original notation, we therefore find that regular solutions are given by:

$$y_E^{(r)}(x) \;=\; \lambda\,\mathrm{Ai}\left[-2\beta(E + Fx)\right] \tag{D.22}$$

From the structure of this equation we may infer that the regular eigenfunctions for different energy eigenvalues E, as are indeed all solutions (D.21), are interrelated

through a simple translation operation of the argument. For fixed λ, we find:

$$y_E^{(r)}(x) \;=\; y_{E=0}^{(r)}(x + E/F) \tag{D.23}$$

We already used this kind of symmetry transformation in our treatments of ballistic motion in classical and quantum physics, see (4.26) and (5.20).

It is evident that among the regular solutions $y_E^{(r)}(x)$ in (D.22), only one value of $|\lambda|$ leads to the normalized eigenfunction $\psi_E(x)$ for the continuous spectrum of the Hamiltonian $H(x,p) = p^2/2M - Fx$ in the sense of Appendix A.3.4, see (A.102), (A.106). We may fix the phase of the normalization coefficient λ in (D.22) by requiring that $\psi_E(x)$ be real and positive as $x \to -\infty$. Then, λ is determined by the asymptotic behavior of $y_E^{(r)}(x)$ as $x \to \infty$ (Theorem LVI). With the semiclassical wave number $k_E^2(x) = 2M(E+Fx)/\hbar^2$ (D.19), Theorem LVI states that the normalized eigenfunction $\psi_E(x)$ asymptotically vanishes like:

$$\psi_E(x) \;\sim\; \left(\frac{2M}{\pi^2\hbar^2(E+Fx)}\right)^{1/4} \sin\left\{\frac{1}{\hbar}\int_a^x d\xi\sqrt{2M(E+F\xi)} \;+\delta(E)\right\} \tag{D.24}$$

On the other hand, we already found the asymptotics of the Airy function (D.22) in the preceding section (D.10):

$$y_E^{(r)}(x) \;\sim\; \lambda\,\left(\frac{1}{2\pi^2\beta(E+Fx)}\right)^{1/4} \sin\left\{\frac{2}{3}\,[2\beta(E+Fx)]^{3/2} \;+\; \frac{\pi}{4}\right\} \tag{D.25}$$

Clearly, equality of both expressions requires $\lambda = (4\beta M/\hbar^2)^{1/4} = 2\beta\sqrt{F}$. Thus, the normalized eigenfunction $\psi_E(x)$ in the continuous spectrum of $H(x,p)$ is the special member in the set of regular solutions $y_E^{(r)}(x)$ (D.22):

$$\psi_E(x) \;=\; 2\beta\sqrt{F}\;\mathrm{Ai}\,[-2\beta(E+Fx)] \tag{D.26}$$

As expected [Theorem LIV, part (ii)], the continuous spectrum of $H(x,p)$ covers all values $-\infty < E < \infty$ and is non-degenerate. We already used the expression (D.26) for the determination of a complete set of orthonormal eigenfunctions $\psi_{p_x,p_y,E_\parallel}(\mathbf{r})$ for the problem of ballistic motion in three dimensions (A.148) and the calculation of the corresponding local density of states (LDOS) $n(\mathbf{o};E)$ in a uniform field environment (A.153).

D.2.2 Green Functions of Free Falling Motion

Finally we determine the Green functions of the ballistic motion problem in a single dimension along a very similar line. From Appendix A.3.6, Theorem L we infer that

the inhomogeneous Schrödinger equation corresponding to the Hamiltonian (D.19) with non-degenerate, entirely continuous spectrum:

$$\left\{E + \frac{\hbar^2}{2M}\frac{\partial^2}{\partial x^2} + Fx\right\} G(x,x';E) \;=\; \delta(x-x') \tag{D.27}$$

possesses a one-dimensional family of solutions $G(x,x';E)$ which differ only by a product of normalized eigenfunctions $\mu\,\langle x\,|\mathcal{C}(E)|\,x'\rangle \;=\; \mu\psi_E(x)\psi_E(x')$ (D.26). In Sections A.4.3 and A.4.6, we singled out two special solutions, the fundamental Green function $G_f(x,x';E)$ (A.221) whose properties are stated in Theorem LV, and the retarded Green function $G(x,x';E)$ (Theorem LI) which corresponds to a causal solution and forms the basis of quantum source theory.

We start with the fundamental Green function $G_f(x,x';E)$. According to (A.230), this real-valued Green function may be displayed as the product of the regular eigenfunction $\psi_E(x)$ with another real solution of (D.19), the "irregular" solution $\varphi_E(x)$: $G_f(x,x';E) = \psi_E(x_<)\varphi_E(x_>)$. The asymptotic properties of the function $\varphi_E(x)$ are laid down in Theorem LVI; to leading order, in the case of the uniform force field problem one obtains this limiting form for $x \to \infty$:

$$\varphi_E(x) \;\sim\; -\left(\frac{2\pi^2 M}{\hbar^2(E+Fx)}\right)^{1/4} \cos\left\{\frac{1}{\hbar}\int_a^x d\xi\sqrt{2M(E+F\xi)} + \delta(E)\right\} \tag{D.28}$$

It is seen that for large x, the phase of $\varphi_E(x)$ lags by $\pi/2$ behind the phase of the regular eigenfunction $\psi_E(x)$ (D.24). Therefore, in the set of solutions (D.21) we have to look for an Airy function that shows the same behavior with respect to the regular solution $\mathrm{Ai}\,[-2\beta(E+Fx)]$ whose asymptotic shape is stated in (D.25). Comparing with (D.18), we conclude that $\varphi_E(x)$ must be a multiple of the irregular Airy function: $\varphi_E(x) = \mu\,\mathrm{Bi}\,[-2\beta(E+Fx)]$. (See also Figure 39.) In the asymptotic sector $x \to \infty$, this function reads:

$$\varphi_E(x) \;\sim\; \mu\left(\frac{1}{2\pi^2\beta(E+Fx)}\right)^{1/4} \cos\left\{\frac{2}{3}\,[2\beta(E+Fx)]^{3/2} \;+\; \frac{\pi}{4}\right\} \tag{D.29}$$

By comparison of (D.28) and (D.29), we infer that the coefficient μ is given by $\mu = -2\pi\beta\sqrt{F}$. Thus, we obtain for the irregular solution $\varphi_E(x)$ of the problem (D.27) in the sense of Theorem LVI:

$$\varphi_E(x) \;=\; -\,2\pi\beta\sqrt{F}\;\mathrm{Bi}\,[-2\beta(E+Fx)] \tag{D.30}$$

From (D.26) and (D.30), we now may easily construct the fundamental Green function $G_f(x,x';E)$ (A.230) of the problem in terms of Airy functions:

$$G_f(x,x';E) \;=\; -\,4\pi\beta^2 F\,\mathrm{Ai}\,[-2\beta(E+Fx_<)]\,\mathrm{Bi}\,[-2\beta(E+Fx_>)] \tag{D.31}$$

Here, the abbreviations denote $x_< = \min(x, x')$ and $x_> = \max(x, x')$, respectively.

Our knowledge of $\psi_E(x)$ and $\varphi_E(x)$ enables us to write down immediately the normalized outgoing-wave or Hankel solution $h_E^{(+)}(x)$ of the uniform field Schrödinger equation (D.19). Following (A.247), this complex-valued wave function is given by:

$$h_E^{(+)}(x) \;=\; \varphi_E(x) - i\pi\psi_E(x) \;=\; -\,2\pi\beta\sqrt{F}\;\mathrm{Ci}\,[-2\beta(E+Fx)] \tag{D.32}$$

where $\mathrm{Ci}(u) = \mathrm{Bi}(u) + i\,\mathrm{Ai}(u)$ is the Airy Hankel function defined in (D.15). Finally, we arrive at the retarded Green function $G(x, x'; E)$ of ballistic motion [9] by matching the regular and Hankel solutions (D.26), (D.32) at $x = x'$ (Theorem LVII). Using the symbols $x_< = \min(x, x')$ and $x_> = \max(x, x')$ of (D.31), this procedure yields:

$$G(x, x'; E) \;=\; -\,4\pi\beta^2 F\,\mathrm{Ai}\,[-2\beta(E+Fx_<)]\,\mathrm{Ci}\,[-2\beta(E+Fx_>)] \tag{D.33}$$

D.2.3 Notes on Self-Adjointness

The simple structure of the Hamiltonian $\mathcal{H}$ of one-dimensional ballistic motion (D.19) allows us to verify in a direct manner some of the conclusions regarding the spectral properties of $\mathcal{H}$ we attained in Appendix A.4 using the abstract notions of functional analysis. We start out with the spectrum of $\mathcal{H}$. In Section A.4.2 we found that for the linear potential $U(x) = -Fx$, the spectrum should be non-degenerate and entirely continuous in $-\infty < E < \infty$, and the point spectrum of $\mathcal{H}$ should be empty [Theorem LIV, part (ii)]. Later on, we will show that the eigenfunctions $\psi_E(x)$ in the continuous spectrum of $\mathcal{H}$ form a complete set in the sense of Theorem XXX. Furthermore, the spectral theorem holds for $\mathcal{H}$ which also proves the self-adjointness of this operator [Theorem LIII, part (ii)].

We first examine the spectrum of (D.19). We have seen that for a given value of E, apart from scaling, the unique bounded eigenfunction $y_E^{(r)}(x)$ of (D.19) reads $y_E^{(r)}(x) = \mathrm{Ai}\,[-2\beta(E+Fx)]$ (D.22). Moreover, all these eigenfunctions possess the same shape and may be generated by a simple shift operation from the $E = 0$ wave function $y_r(x) = \mathrm{Ai}(-2\beta Fx)$ (D.23). In order to prove that the normalized solutions $\psi_E(x)$ (D.26) are eigenfunctions in the continuous spectrum of $\mathcal{H}$ in the sense of (A.102), we note that the normalization integral $\int dx\,\psi_E(x)^2$ must diverge, as otherwise $\psi_E(x) = \langle x|\Psi_E\rangle$ would be the spatial representation of a proper eigenstate $|\Psi_E\rangle$ of $\mathcal{H}$ in the Hilbert space $\mathbb{H}$ of square-integrable functions, and consequently E a member of the point spectrum of $\mathcal{H}$. Fortunately, the Airy function in (D.26) is of sufficiently simple structure as to allow for an explicit determination of this normalization integral for any finite interval $a < x < b$. One finds for the indefinite integral involving the square

of an Airy function [151,234]:

$$\int du\ \mathrm{Ai}(u)^2 \ = \ u\,\mathrm{Ai}(u)^2 - \mathrm{Ai}'(u)^2 + C \tag{D.34}$$

This formula may easily be verified by means of the Airy differential equation (D.1). Thus, we obtain for the corresponding eigenfunction integral, noting that the right-hand side of (D.34) drops exponentially as $u \to \infty$ (D.10):

$$\begin{aligned}\int_{-\infty}^{b} dx\,\psi_E(x)^2 \ &= \ 2\beta\left\{2\beta(E+Fb)\,\mathrm{Ai}\left[-2\beta(E+Fb)\right]^2 + \mathrm{Ai}'\left[-2\beta(E+Fb)\right]^2\right\} \\ &\sim \ \frac{2\beta}{\pi}\sqrt{2\beta(E+Fb)} \qquad\qquad [2\beta(E+Fb) \ \gg \ 1]\end{aligned} \tag{D.35}$$

For the asymptotic form of (D.35) in the limit $b \to \infty$, we refer to the LG approximation of the regular Airy function $\mathrm{Ai}(x)$ (D.10). Manifestly, $\int dx\,\psi_E(x)^2 \to \infty$ for all E. Thus, the point spectrum of $\mathcal{H}$ is empty, and the continuous spectrum covers the entire real axis.

Next, we have to check that the eigenfunctions $\psi_E(x)$ (D.26) indeed form a complete set that allows for an expansion of any square-integrable wave function $\phi(x) = \langle x|\Phi\rangle$ in the sense of Theorem XXX. This means we have to show that:

$$\int dx\,\left|\phi(x) - \int dE\,\psi_E(x)\int d\xi\,\psi_E(\xi)\phi(\xi)\right|^2 \ = \ 0 \tag{D.36}$$

In terms of distribution theory [215], the condition (D.36) implies that the eigenfunctions $\psi_E(x)$ must fulfil the completeness relation:

$$\int dE\,\psi_E(x)\psi_E(\xi) \ = \ \delta(x-\xi) \tag{D.37}$$

which we are going to prove now. Inserting the explicit form (D.26) for $\psi_E(x)$ and introducing dimensionless variables $\epsilon = -2\beta E$, $\lambda = -2\beta F x$, and $\mu = -2\beta F\xi$ (5.22), where $\beta^3 = M/4\hbar^2F^2$ (5.16), we find successively using the integral representation of the regular Airy function $\mathrm{Ai}(x)$ (D.9):

$$\begin{aligned}\int dE\,\psi_E(x)\psi_E(\xi) \ &= \ 2\beta F\int d\epsilon\ \mathrm{Ai}(\epsilon+\lambda)\,\mathrm{Ai}(\epsilon+\mu) \\ &= \ \frac{\beta F}{\pi}\int du\int dv\,e^{i(u^3-v^3)/3}\,e^{i\lambda u - i\mu v}\ \cdot\ \frac{1}{2\pi}\int d\epsilon\,e^{i\epsilon(u-v)} \\ &= \ \frac{\beta F}{\pi}\int du\,e^{iu(\lambda-\mu)} \ = \ 2\beta F\,\delta(\lambda-\mu) \ = \ \delta(x-\xi)\end{aligned} \tag{D.38}$$

In the course of the calculation, we used twice the completeness relation for plane waves $\int dx\, e^{ipx} e^{-iqx} = 2\pi\delta(p-q)$ that we already stated in (A.145)–(A.147), as well as the formula $|\alpha|\,\delta(x) = \delta(x/\alpha)$ [215]. Thus, it is seen that the completeness of the set of plane waves $(2\pi)^{-1/2} e^{ipx}$ (as originally stated by the Fourier theorem) implies the completeness of the set of eigenfunctions $\psi_E(x)$ (D.26) of the one-dimensional uniform field problem.

Finally, we may show in a very similar manner that the spectral theorem (Theorem XXIX) holds, which in its spatial representation claims that the Hamiltonian in (D.19) may be expanded into products of eigenfunctions (D.26):

$$\langle x\,|\mathcal{H}|\,\xi\rangle \;=\; \int dE\, E\, \psi_E(x)\psi_E(\xi) \tag{D.39}$$

Using the notation of expression (D.38), we successively transform the right-hand side in equation (D.39):

$$\begin{aligned}
\int dE\, E\, \psi_E(x)\psi_E(\xi) \;&=\; -F \int d\epsilon\; \epsilon\; \mathrm{Ai}(\epsilon+\lambda)\,\mathrm{Ai}(\epsilon+\mu) \\
&=\; -\frac{F}{2\pi} \int du \int dv\, e^{i(u^3-v^3)/3}\, e^{i\lambda u - i\mu v} \;\cdot\; \frac{1}{2\pi i}\frac{\partial}{\partial u}\left\{\int d\epsilon\, e^{i\epsilon(u-v)}\right\} \\
&=\; \frac{F}{2\pi} \int du\, (u^2+\lambda)\, e^{iu(\lambda-\mu)} \\
&=\; F\left\{\lambda - \frac{\partial^2}{\partial\lambda^2}\right\}\delta(\lambda-\mu) \;=\; \left\{-\frac{\hbar^2}{2M}\frac{\partial^2}{\partial x^2} - Fx\right\}\delta(x-\xi)
\end{aligned} \tag{D.40}$$

(The second step involves a partial integration; in the third step, differentiation with respect to the parameter λ is employed.) By comparison with the (diagonal) field emission Hamiltonian $H(x,p)$ in (D.19), we realize that the spectral theorem (D.39) indeed holds. As the left-hand side of this equation presents the spatial representation of a self-adjoint operator, namely $\int dE\, E\, \mathcal{C}(E) = \int E\, \mathrm{d}\Pi(E)$, according to Theorem XXIX the Hamiltonian $\mathcal{H}$ of one-dimensional uniform acceleration itself must be self-adjoint.

D.3 Integral Representation of Airy Products

Finally, we want to gather a number of formulae regarding the retarded propagator $K_D(\mathbf{r},\mathbf{r}';T)$ (5.9) and the corresponding Green function $G_D(\mathbf{r},\mathbf{r}';E)$ for the ballistic problem in D spatial dimensions. These additional results supplement the discussion in Sections 5.1 and 5.2 in the main body of this volume. Throughout this section, we will use the dimensionless set of variables for the energy ϵ, time τ, position vectors

$\boldsymbol{\rho} = (\xi, \upsilon, \zeta)$ and momentum vectors $\boldsymbol{\kappa}$ that we already introduced in (5.22). For convenience, we list the definitions of these parameters once more. With the abbreviation $\beta^3 = M/4\hbar^2F^2$ (5.16), we have:

$$\begin{aligned} \epsilon &= -2\beta E \qquad & \tau &= T/2\hbar\beta \\ \boldsymbol{\rho} &= \beta F \mathbf{r} \qquad & \boldsymbol{\kappa} &= \mathbf{k}/\beta F \end{aligned} \tag{D.41}$$

D.3.1 The Propagator of Accelerated Motion

Let us first restate the retarded propagator $K_D(\mathbf{r}, \mathbf{r}'; T)$ of a particle moving in D dimensions subject to a uniform force field $\mathbf{F}$. Employing the new set of variables (D.41), the propagator (5.9) reads:

$$K_D(\boldsymbol{\rho}, \boldsymbol{\rho}'; \tau) \;=\; \Theta(\tau) \left(\frac{\beta F}{\sqrt{i\pi\tau}}\right)^D \exp\left\{ i \left[\frac{1}{\tau} (\boldsymbol{\rho} - \boldsymbol{\rho}')^2 + \tau(\zeta + \zeta') - \frac{\tau^3}{12} \right] \right\} \tag{D.42}$$

Here, $\Theta(\tau)$ denotes the Heaviside step function, as usual.

We will also require a Fourier representation of the propagator (D.42). To perform the transformation, we first calculate the auxiliary D–dimensional integral:

$$F_D \;=\; \int d^D\rho \int d^D\rho'\, e^{i\boldsymbol{\kappa}\cdot\boldsymbol{\rho} + i\boldsymbol{\kappa}'\cdot\boldsymbol{\rho}'}\, e^{i(\boldsymbol{\rho}-\boldsymbol{\rho}')^2/\tau \,+\, i\tau(\zeta+\zeta')} \tag{D.43}$$

To evaluate this Gaussian integral, we introduce new variables $\mathbf{u}$, $\mathbf{v}$, $\mathbf{p}$ and $\mathbf{q}$ directed along the principal axes of the quadratic form in the exponential:

$$\begin{aligned} \mathbf{u} &= \boldsymbol{\rho} + \boldsymbol{\rho}' \qquad & \mathbf{p} &= (\boldsymbol{\kappa} + \boldsymbol{\kappa}')/2 \\ \mathbf{v} &= \boldsymbol{\rho} - \boldsymbol{\rho}' \qquad & \mathbf{q} &= (\boldsymbol{\kappa} - \boldsymbol{\kappa}')/2 \end{aligned} \tag{D.44}$$

These variables have been chosen to preserve the scalar product: $\boldsymbol{\kappa}\cdot\boldsymbol{\rho} + \boldsymbol{\kappa}'\cdot\boldsymbol{\rho}' = \mathbf{p}\cdot\mathbf{u} + \mathbf{q}\cdot\mathbf{v}$. We then obtain instead of (D.43) a form that is easily integrated:

$$F_D \;=\; \frac{1}{2^D} \int d^D u\, e^{i\mathbf{p}\cdot\mathbf{u} + i\tau u_z} \int d^D v\, e^{i\mathbf{q}\cdot\mathbf{v} - v^2/i\tau} \;=\; \pi^D\, (i\pi\tau)^{D/2}\, \delta(\mathbf{p} + \tau\hat{e}_z)\, e^{-i\tau q^2/4} \tag{D.45}$$

Here, $\hat{e}_z$ denotes an unit vector in the direction of force. Replacing the original variables and performing the inverse transformation, we find:

$$\begin{aligned} K_D(\boldsymbol{\rho}, \boldsymbol{\rho}'; \tau) \;=\; \Theta(\tau) \left(\frac{\beta F}{2\pi}\right)^D \int d^D\kappa \int d^D\kappa'\; \delta(\boldsymbol{\kappa} + \boldsymbol{\kappa}' + 2\tau\hat{e}_z) \;\times \\ \exp\left\{ -i \left[\boldsymbol{\kappa}\cdot\boldsymbol{\rho} + \boldsymbol{\kappa}'\cdot\boldsymbol{\rho}' + \frac{\tau}{16} (\boldsymbol{\kappa} - \boldsymbol{\kappa}')^2 + \frac{\tau^3}{12} \right] \right\} \end{aligned} \tag{D.46}$$

This alternative to (D.42) proves useful throughout Chapter 5. In practice, we will be interested in physical space ($D = 3$).

D.3.2 The Green Function in $2D + 1$ Dimensions

The connection between the ballistic propagator $K_D(\mathbf{r}, \mathbf{r}'; T)$ (5.9) and the corresponding energy Green function $G_D(\mathbf{r}, \mathbf{r}'; E)$ (5.10) has been put forward in Section 5.2. Without losing generality, we may set $\mathbf{r}' = 0$ [see (5.20)]. For the D–dimensional ballistic problem, we then obtain from (2.13) and (D.42), using the set of dimensionless variables (D.41):

$$G_D(\boldsymbol{\rho}, \mathbf{o}; \epsilon) \;=\; -2i\beta\,(\beta F)^D \int_0^\infty \frac{d\tau}{(i\pi\tau)^{D/2}}\, \exp\left\{ i\left[\frac{\rho^2}{\tau} + \tau(\zeta - \epsilon) - \frac{\tau^3}{12}\right]\right\} \tag{D.47}$$

We now want to establish an explicit expression for $G_D(\boldsymbol{\rho}, \mathbf{o}; \epsilon)$ for spaces of odd dimension, $D = 2k+1$. As indicated in Section 5.2, all these Green functions are available from the one-dimensional Green function $G(\zeta, 0; \epsilon)$ by means of an unusual differentiation technique (5.12). In the reduced set of variables (D.41), this retarded Green function which we evaluated earlier (D.33) reads:

$$G(\zeta, 0; \epsilon) \;=\; -4\pi\beta^2 F\ \mathrm{Ci}(\epsilon - \zeta - |\zeta|)\,\mathrm{Ai}(\epsilon - \zeta + |\zeta|) \tag{D.48}$$

To perform the integration in (D.47), we first introduce some useful abbreviations for expressions containing products of Airy functions and their derivatives that will frequently appear in Chapter 5. We start from an obvious integral representation of such products that is immediately available from (D.47) and (D.48):

$$\int_0^\infty \frac{d\tau}{\sqrt{i\tau}}\, e^{i\left[\rho^2/\tau + \tau(\zeta-\epsilon) - \tau^3/12\right]} \;=\; -2i\pi\sqrt{\pi}\ \mathrm{Ci}(\epsilon - \zeta - \rho)\,\mathrm{Ai}(\epsilon - \zeta + \rho) \tag{D.49}$$

By comparison with (D.47) it appears reasonable to introduce an auxiliary function $Q_k(\rho, \zeta; \epsilon)$ (k denotes an integer index which may also be negative) that covers a whole family of integrals related to (D.49):

$$Q_k(\rho, \zeta; \epsilon) \;=\; \frac{i}{2\pi\sqrt{\pi}} \int_0^\infty \frac{d\tau}{(i\tau)^{k+1/2}}\, e^{i\left[\rho^2/\tau + \tau(\zeta-\epsilon) - \tau^3/12\right]} \tag{D.50}$$

In the traditional sense, this integral converges only in the index range $-5/2 < k < 3/2$. Otherwise, $Q_k(\rho, \zeta; \epsilon)$ should be interpreted as a distribution rather than a conventional function. Clearly, comparison with (D.49) yields its value for $k = 0$:

$$Q_0(\rho, \zeta; \epsilon) \;=\; \mathrm{Ci}(\epsilon - \zeta - \rho)\,\mathrm{Ai}(\epsilon - \zeta + \rho) \tag{D.51}$$

The functions $Q_k(\rho,\zeta;\epsilon)$ with nonzero index k may be reduced to (D.49). For $k>0$, we use the differentiation rule (5.12) to obtain the recurrence formula:

$$Q_{k+1}(\rho,\zeta;\epsilon) \;=\; -\,\frac{1}{2\rho}\,\frac{\partial}{\partial\rho}\,Q_k(\rho,\zeta;\epsilon) \tag{D.52}$$

Similarly, a recurrence formula for decreasing values of k may be read off the definition (D.50) of these auxiliary functions:

$$Q_{k-1}(\rho,\zeta;\epsilon) \;=\; \frac{\partial}{\partial\zeta}\,Q_k(\rho,\zeta;\epsilon) \tag{D.53}$$

Employing (D.51)–(D.53), we evaluate the integrals (D.50) in explicit form ($k\geq 0$):

$$\begin{aligned} Q_k(\rho,\zeta;\epsilon) &= \left(-\,\frac{1}{2\rho}\,\frac{\partial}{\partial\rho}\right)^k \,\mathrm{Ci}(\epsilon-\zeta-\rho)\,\mathrm{Ai}(\epsilon-\zeta+\rho) \\ Q_{-k}(\rho,\zeta;\epsilon) &= \frac{\partial^k}{\partial\zeta^k}\,\mathrm{Ci}(\epsilon-\zeta-\rho)\,\mathrm{Ai}(\epsilon-\zeta+\rho) \end{aligned} \tag{D.54}$$

Following these preliminaries, we may use the auxiliary functions $Q_k(\rho,\zeta;\epsilon)$ to express the uniform field Green function $G_D(\mathbf{r},\mathbf{r}';E)$ (D.47) in an odd-dimensional space ($D=2k+1$). Allowing for an arbitrary choice of the source location $\boldsymbol{\rho}'$ by virtue of the symmetry relation (5.20), we finally find:

$$G_D(\boldsymbol{\rho},\boldsymbol{\rho}';\epsilon) \;=\; -\,4\pi\beta^2 F\left(\frac{\beta^2F^2}{\pi}\right)^k Q_k(|\boldsymbol{\rho}-\boldsymbol{\rho}'|,\zeta+\zeta';\epsilon) \tag{D.55}$$

D.3.3 Asymptotic Evaluation of the Current

In the course of Section 5.5, we established a general formula for the total current $J_{lm}(E)$ carried by the multipole Green function of (l,m) angular symmetry $G_{lm}(\mathbf{r},\mathbf{o};E)$ in the homogeneous field environment (5.48). For an asymptotic evaluation which holds good for large positive or negative values of the particle energy parameter $\epsilon=-2\beta E$, however, the integral representation of the current $J_{lm}(E)$ (5.46) proves much more convenient (see Section 5.5.3). The calculation relies on asymptotic estimates for the integral:

$$I_{jl}(\epsilon) \;=\; \Im\left[\int_0^\infty \frac{i\,d\tau}{(i\tau)^{3j-2l+3/2}}\,e^{-i(\epsilon\tau+\tau^3/12)}\right] \tag{D.56}$$

which we are going to establish now. We note that the integrand in (D.56) bears close resemblance to the simpler, purely exponential expressions occurring in our analysis of Airy's differential equation (Section D.1), so the techniques applied there are also

relevant to our treatment of (D.56) that we shall pursue shortly. However, this calculation turns out to be more involved due to the fact that the integrand in (D.56) shows an additional singularity at the origin and is furthermore double-valued in the complex τ plane. In the following, we discuss how to deal with these complications.

In the first step, let us introduce $u = i\tau$ as new integration variable. Employing a vanishingly small positive parameter $\eta \to 0^+$, we then may rewrite the imaginary part in (D.56) into a complex path integral:

$$I_{jl}(\epsilon) \;=\; \frac{1}{2i} \lim_{\eta \to 0+} \int_C \frac{du}{u^{3j-2l+3/2}}\, e^{-\eta/\sqrt{u}}\, e^{-\epsilon u + u^3/12} \tag{D.57}$$

Here, the path C leads along the imaginary u axis, but avoids the singularity at the origin $u = 0$ by circling it in the anticlockwise sense. Likewise, it is not affected by the cut in the complex u plane which we place along the negative real u axis. (This choice is obviously enforced by the behavior of the converging factor $\exp(-\eta/\sqrt{u})$ near the singularity $u = 0$.) This original integration path, together with the cut, is depicted in Figure 40.

In order to gain asymptotic estimates for (D.57), we employ the saddle point approximation method which involves shifts of the path of integration. Clearly, these are restrained by several conditions: First, the integration limits, here $u = \pm i\infty$, must not be shifted into regions where the integrand in (D.57) asymptotically diverges. Since the large-scale behavior of this function is given by the factor $\exp(u^3/12)$, this means that the endpoints of the integration cannot leave any of three parent sectors of the u plane (shaded areas in Figure 40). We already encountered this situation in Section D.1. But now, additionally we have to circumvent the cut and pass the real axis to the right of the singularity at $u = 0$, which complicates the evaluation of the integral.

Let us now determine the stationary points of the exponent in the integrand of (D.57). Clearly, these fulfil the relation $u^2 = 4\epsilon$. For $\epsilon > 0$, i. e., in the case of a tunneling source, we find $u = \pm 2\sqrt{\epsilon}$. Like in the case of the regular Airy function $\mathrm{Ai}(x)$ for positive arguments (Section D.1.2), only the saddle point which presents a minimum of the integrand along the real u axis is relevant for the evaluation of (D.57). Here, the contribution is due to the stationary point $S_- = 2\sqrt{\epsilon}$. Therefore, we deform the path of integration into the new contour C_- which passes through S_- on the path of steepest descent which is perpendicular to the real u axis. The situation resembles that of Section D.1.2, thus we may follow the procedure outlined there and find that the saddle point approximation to (D.57) yields for $\epsilon > 0$:

$$\begin{aligned} I_{jl}(\epsilon) \;&\sim\; \frac{1}{2}\,(2\sqrt{\epsilon}\,)^{2l-3j-3/2}\, \exp\left\{-\frac{4}{3}\,\epsilon^{3/2}\right\} \int_{-\infty}^{\infty} dv\, e^{-\epsilon^{1/2} v^2/2} \left[1 + \mathcal{O}\left(\frac{v^2}{\epsilon}\right)\right] \\ &\sim\; \sqrt{\pi}\,(4\epsilon)^{l-1-3j/2}\, \exp\left\{-\frac{4}{3}\,\epsilon^{3/2}\right\} \left[1 + \mathcal{O}(\epsilon^{-3/2})\right] \end{aligned} \tag{D.58}$$

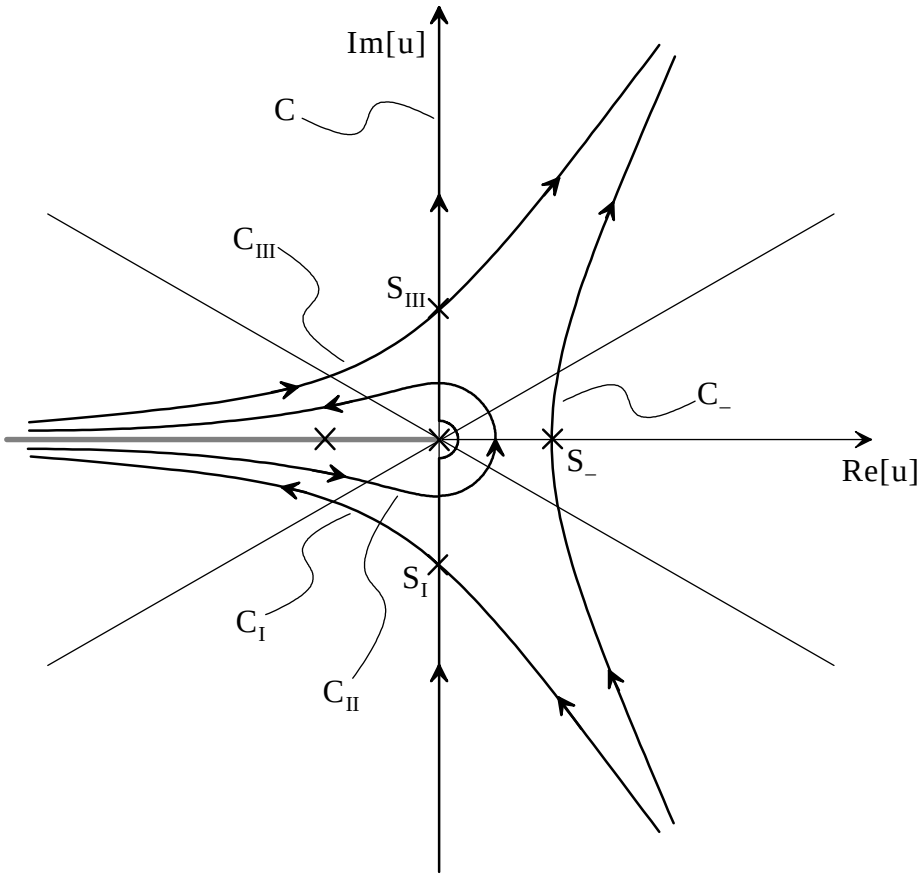

Figure 40: Integration paths for the evaluation of the integral (D.57). The figure displays the original contour C and its shifted counterparts for large values of $\epsilon = -2\beta E$. For $\epsilon > 0$, the contour is deformed to C_- and runs through the saddle point $S_- = 2\sqrt{\epsilon}$. In the case $\epsilon < 0$, the contour is split into three parts $C_{\rm I}$, $C_{\rm II}$, $C_{\rm III}$ traversing the saddle points $S_{\rm I}$, $S_{\rm III}$ at $\pm 2i\sqrt{|\epsilon|}$, yet avoiding the cut in the complex u plane (dark grey line) by circling the singularity at $u = 0$.

As expected, $I_{jl}(\epsilon)$ drops exponentially with increasing energy parameter ϵ.

We face a more complicated situation when we turn to the asymptotic limit of classically allowed motion, i. e., we now consider the case $\epsilon < 0$. Then, the stationary points of the exponent in (D.57) form a complex conjugate pair $S_{\rm I} = -2i\sqrt{\epsilon}$, $S_{\rm III} = 2i\sqrt{\epsilon}$, both of which will equally contribute to the approximation of (D.57). Clearly, this state of affairs resembles the circumstances we found in evaluating the exponential representation of the solutions of the Airy differential equation (D.1) for large negative arguments x. Thus, we will take over the prescription of Section D.1.3 and introduce contours of steepest descent $C_{\rm I}$, $C_{\rm III}$ which lead through the respective saddle points $S_{\rm I}$, $S_{\rm III}$, intersecting the imaginary u axis under an angle $\pi/4$, and terminate on the negative real u axis at $u \to -\infty \mp i\eta$, $\eta \to 0^+$. Due to the presence of the additional

singularity at $u = 0$ and the cut along the negative real axis, we cannot simply link the contours $C_{\rm I}$ and $C_{\rm III}$ at $u \to -\infty$ as we did in the Airy case (Section D.1.3). Rather, we have to loop back around the singularity along an additional contour $C_{\rm II}$. (See Figure 40.) Not surprisingly, the contour $C_{\rm II}$ delivers contributions to the integral (D.57) of an entirely different nature compared to the more familiar contributions of the outer paths $C_{\rm I}$ and $C_{\rm III}$, which we expect to be of oscillatory character according to the results of Section D.1.3. Let us first study the asymptotic structure of the loop integral along $C_{\rm II}$, the contribution $I_{jl}^{({\rm II})}(\epsilon)$ of which we will denote the secular part of (D.57), as opposed to the oscillatory part delivered by $C_{\rm I}$ and $C_{\rm III}$.

For large negative values of ϵ, the factor $e^{-\epsilon u}$ in the integrand of (D.57) will quickly decay as $\Re[u] \to -\infty$. Therefore, most of the secular contribution to (D.57) will originate from the part of the contour $C_{\rm II}$ located near the singularity at $u = 0$. In this region, however, the asymptotically dominant term $e^{u^3/12}$ varies very little. Thus, we may approximate for the integral $I_{jl}^{({\rm II})}(\epsilon)$:

$$I_{jl}^{({\rm II})}(\epsilon) \;\sim\; \frac{1}{2i} \int_{C_{\rm II}} \frac{e^{-\epsilon u}\, du}{u^{3j-2l+3/2}} \left[1 + \mathcal{O}(u^3)\right] \tag{D.59}$$

Remarkably, this integral may be evaluated exactly in terms of the Gamma function, since a famous representation of $\Gamma(z)$ in terms of a complex contour integral reads:

$$\frac{1}{\Gamma(z)} \;=\; \frac{1}{2\pi i} \int_{C_{\rm II}} e^t t^{-z}\, dt \tag{D.60}$$

(A proof of this formula which is due to Hankel (1864) may be found in the monograph by Olver [235], p. 37.) Replacing the Gamma function for the half-integer argument in (D.59) by a double factorial, we finally obtain for the secular part of the integral (D.57) for $\epsilon < 0$:

$$I_{jl}^{({\rm II})}(\epsilon) \;\sim\; \frac{\pi |\epsilon|^{3j-2l+1/2}}{\Gamma(3j-2l+3/2)} \left[1 + \mathcal{O}(|\epsilon|^{-3})\right] \;\sim\; \frac{\sqrt{2\pi}\,(2|\epsilon|)^{3j-2l+1/2}}{(6j-4l+1)!!} \left[1 + \mathcal{O}(|\epsilon|^{-3})\right] \tag{D.61}$$

The secular term (D.59), which grows for fixed l with increasing j, provides the dominant current contribution for $\epsilon < 0$ and is related to the Wigner law (C.30) describing the total current emitted from a multipole source in a field-free environment (Appendix C.2).

As noted above, the remaining contributions from the paths $C_{\rm I}$ and $C_{\rm III}$ are fairly different in character. Clearly, they arise mainly from the neighborhood of the saddle points $S_{\rm I}$ and $S_{\rm III}$ at $u = \pm 2i\sqrt{|\epsilon|}$, respectively. We have already discussed in Section D.1.3 how to estimate the contributions $I_{jl}^{({\rm I})}(\epsilon)$ and $I_{jl}^{({\rm III})}(\epsilon)$ of these paths by

the method of steepest descents, and we recall that the corresponding shifted contours must cross the imaginary u axis at an angle of $\pi/4$ (Figure 40). In this context, it suffices to consider the contribution $I_{jl}^{(\mathrm{III})}(\epsilon)$ due to the contour C_{III}; by a symmetry argument, one may easily infer that $I_{jl}^{(\mathrm{I})}(\epsilon)$ delivers just the conjugate complex value to $I_{jl}^{(\mathrm{III})}(\epsilon)$. Introducing a new variable of integration $v = e^{-i\pi/4}(u - 2i\sqrt{|\epsilon|})$ similar to the procedure in (D.12) and (D.13), we find that in Gaussian approximation, $I_{jl}^{(\mathrm{III})}(\epsilon)$ takes on the form ($\epsilon < 0$):

$$\begin{aligned} I_{jl}^{(\mathrm{III})}(\epsilon) \;&\sim\; \frac{1}{2i}\left(2i\sqrt{|\epsilon|}\right)^{2l-3j-3/2} \exp\left(\frac{4i}{3}\,|\epsilon|^{3/2} + \frac{i\pi}{4}\right) \int_{-\infty}^{\infty} dv\, e^{-\,|\epsilon|^{1/2}v^2/2} \left[1 + \mathcal{O}\left(\frac{v^2}{|\epsilon|}\right)\right] \\ &\sim\; \frac{\sqrt{\pi}}{(2i\sqrt{|\epsilon|})^{3j-2l+2}} \exp\left(\frac{4i}{3}\,|\epsilon|^{3/2}\right) \left[1 + \mathcal{O}(|\epsilon|^{-\,3/2})\right] \end{aligned} \tag{D.62}$$

Now, it is straightforward to determine the complete oscillatory contribution to the integral (D.57) by forming the real part of (D.62):

$$I_{jl}^{(\mathrm{I})}(\epsilon) + I_{jl}^{(\mathrm{III})}(\epsilon) \;\sim\; \frac{(-1)^{l+1}\sqrt{\pi}}{2^{3j-2l+1}}\,|\epsilon|^{l-1-3j/2} \cos\left(\frac{4}{3}\,|\epsilon|^{3/2} + \frac{j\pi}{2}\right) \left[1 + \mathcal{O}(|\epsilon|^{-\,3/2})\right] \tag{D.63}$$

We note that unlike its secular counterpart (D.61), the oscillatory contribution (D.63) in the asymptotic expansion of $I_{jl}(\epsilon)$ (D.57) becomes particularly conspicuous for small index j.

Finally, we may combine both partial expressions (D.61) and (D.63) in order to obtain the complete asymptotic form for the integral (D.56) in the limit of large negative energy parameter ϵ, i. e., for classically allowed motion:

$$\begin{aligned} I_{jl}(\epsilon) \;\sim\; &\frac{\sqrt{2\pi}\,(2|\epsilon|)^{3j-2l+1/2}}{(6j-4l+1)!!} \left[1 + \mathcal{O}(|\epsilon|^{-\,3})\right] \;+ \\ &\frac{(-1)^{l+1}\sqrt{\pi}}{2^{3j-2l+1}}\,|\epsilon|^{l-1-3j/2} \cos\left(\frac{4}{3}\,|\epsilon|^{3/2} + \frac{j\pi}{2}\right) \left[1 + \mathcal{O}(|\epsilon|^{-\,3/2})\right] \end{aligned} \tag{D.64}$$

This formula, which is dominated by the secular term (D.61) for $3j > 2l - 1$, has been applied in the evaluation of the total current in uniform field photodetachment in Section 5.5.3. (See also Section 6.3.)

Appendix E

Table of Uniform Field Green Functions

FOR REFERENCE PURPOSES, this appendix lists explicit expressions for the most important scattering partial waves in the homogeneous force field environment $U(\mathbf{r}) = -Fz$, where the direction of the force field $\mathbf{F}$ has been assumed aligned to the z axis. They have been obtained from the general formulae derived in Chapter 5. To keep the notation concise, we use the following abbreviations originally introduced in Section 5.2. The outgoing Airy wave $\mathrm{Ci}(z)$ is defined by (5.15) [see also Appendix D.1]:

$$\mathrm{Ci}(z) \;=\; \mathrm{Bi}(z) + i\,\mathrm{Ai}(z) \tag{E.1}$$

Arguments of the Airy functions $\mathrm{Ai}(z)$ and $\mathrm{Ci}(z)$ generally will contain the expressions $\alpha_\pm$ (5.19) involving parabolic coordinates $\eta = r - z$, $\xi = r + z$:

$$\alpha_\pm \;=\; -\,\beta\,[2E + F(z \pm r)] \tag{E.2}$$

Also, the inverse energy parameter β appears abundantly (5.16):

$$\beta \;=\; \left(\frac{M}{4\hbar^2 F^2}\right)^{1/3} \tag{E.3}$$

In the following paragraphs, for the sake of simplicity all quantities have been tabulated under the premise that the source is located at the origin $\mathbf{r}' = \mathbf{o}$ (Section 5.2). Generalized expressions for arbitrarily located sources $\mathbf{r}'$ can be gained from them by the parameter replacements (5.20):

$$\mathbf{r} \longrightarrow \mathbf{r} - \mathbf{r}'\,, \qquad\qquad E \longrightarrow E + Fz' \tag{E.4}$$

E.1 Multipole Green Functions

First, we present exact expressions for the partial s– and p–waves in the linear potential $U(\mathbf{r}) = -Fz$ ($l = 0, 1$). They follow directly from the functional form (5.28) established

in Section 5.3. For simplicity, the quantization axis of angular momentum has been aligned to the direction of force, i. e., the z axis. Note that the s–wave is proportional to the conventional uniform field Green function $G(\mathbf{r},\mathbf{o};E)$ (5.18).
Isotropic emission ($l=0,\ m=0$):

$$G_{00}(\mathbf{r},\mathbf{o};E) \;=\; \frac{\beta^3F^2}{\sqrt{\pi}\,r}\left[\mathrm{Ci}(\alpha_+)\,\mathrm{Ai}'(\alpha_-)-\mathrm{Ci}'(\alpha_+)\,\mathrm{Ai}(\alpha_-)\right] \tag{E.5}$$

Emission as p-wave, longitudinal polarization ($l=1,\ m=0$):

$$\begin{aligned}G_{10}(\mathbf{r},\mathbf{o};E) \;=\; \sqrt{\frac{3}{\pi}}\,\frac{\beta^3F^2}{r^3}\,\{z\,\left[\mathrm{Ci}(\alpha_+)\,\mathrm{Ai}'(\alpha_-)-\mathrm{Ci}'(\alpha_+)\,\mathrm{Ai}(\alpha_-)\right]\;+\\ 2\beta Fr\left[\beta\left[z(2E+Fz)-Fr^2\right]\,\mathrm{Ci}(\alpha_+)\,\mathrm{Ai}(\alpha_-)+z\,\mathrm{Ci}'(\alpha_+)\,\mathrm{Ai}'(\alpha_-)\right]\}\end{aligned} \tag{E.6}$$

Emission as p-wave, circular polarization ($l=1,\ m=\pm1$):

$$\begin{aligned}G_{1,\pm1}(\mathbf{r},\mathbf{o};E)=\sqrt{\frac{3}{2\pi}}\,\beta^3F^2\,\frac{x\pm iy}{r^3}\,\{\left[\mathrm{Ci}'(\alpha_+)\,\mathrm{Ai}(\alpha_-)-\mathrm{Ci}(\alpha_+)\,\mathrm{Ai}'(\alpha_-)\right]\;-\\ 2\beta Fr\left[\mathrm{Ci}'(\alpha_+)\,\mathrm{Ai}'(\alpha_-)+\beta\left[2E+Fz\right]\mathrm{Ci}(\alpha_+)\,\mathrm{Ai}(\alpha_-)\right]\}\end{aligned} \tag{E.7}$$

E.2 Current Density Distributions

In this section, we present the exact current density distributions $j_{lmm}(\mathbf{r},\mathbf{o};E)$ (5.42) as generated by the scattering partial waves $G_{00}(\mathbf{r},\mathbf{o};E)$, $G_{10}(\mathbf{r},\mathbf{o};E)$ and $G_{1,\pm1}(\mathbf{r},\mathbf{o};E)$ (E.5)–(E.7) that we stated in the preceding paragraph. These functions are always composed of products of the regular Airy function $\mathrm{Ai}(\alpha_-)$ and its derivative, weighed by polynomial prefactors. Note that in the case of p–waves, only the diagonal elements of the current density matrix are presented; the off-diagonal entries are available from the general formula (5.42) in Section 5.4.
Isotropic emission ($l=0,\ m=0$):

$$j_{000}(\mathbf{r},\mathbf{o};E) \;=\; \frac{M\beta F}{8\pi^2\hbar^3r^3}\left\{z\;\mathrm{Ai}'(\alpha_-)^2+\beta\left[z(2E+Fz)+Fr^2\right]\mathrm{Ai}(\alpha_-)^2\right\} \tag{E.8}$$

Emission as p-wave, longitudinal polarization ($l=1,\ m=0$):

$$\begin{aligned}j_{100}(\mathbf{r},\mathbf{o};E) \;=\; \frac{3M(\beta F)^2}{8\pi^2\hbar^3r^5}\,\left\{2\beta^2Fz\left[Fr(r^2+z^2)+2z^2(2E+Fz)\right]\mathrm{Ai}'(\alpha_-)^2\;-\right.\\ 2\beta F\,(r+z)\,(z^2+2rz-r^2)\;\mathrm{Ai}(\alpha_-)\,\mathrm{Ai}'(\alpha_-)+\left\{(3z^2-r^2)\;+\right.\\ \left.\left.2\beta^3F\left[Fr^2-z(2E+Fz)\right]\left[Fr(r^2+z^2)-2z^2(2E+Fz)\right]\right\}\mathrm{Ai}(\alpha_-)^2\right\}\end{aligned} \tag{E.9}$$

Emission as p-wave, circular polarization ($l = 1,\ m = \pm 1$):

$$j_{111}(\mathbf{r}, \mathbf{o}; E) \;=\; \frac{3M(\beta F)^3}{8\pi^2\hbar^3}\,\frac{x^2+y^2}{r^5}\,\Big\{\,[2z(2E+Fz)+Fr(r+z)]\,\mathrm{Ai}'(\alpha_-)^2\;-\\ z\;\mathrm{Ai}(\alpha_-)\,\mathrm{Ai}'(\alpha_-)+(2E+Fz)\,[2z(2E+Fz)+Fr(r-z)]\,\mathrm{Ai}(\alpha_-)^2\,\Big\} \tag{E.10}$$

E.3 Total Multipole Currents

In Section 5.5, we calculated a general expression for the total multipole current $J_{lm}(E)$ (5.48) carried by a scattering partial wave $G_{lm}(\mathbf{r}, \mathbf{o}; E)$ (5.28) in the homogeneous field environment. Here, we put explicit formulae for these currents on display ($l = 0, 1, 2$). Resembling their current density counterparts $j_{lmm}(\mathbf{r}, \mathbf{o}; E)$ (E.8)–(E.10) shown in the preceding section, they are composed of squares of regular Airy functions $\mathrm{Ai}(-2\beta E)$. As usual, the source is placed at the origin, $\mathbf{r}' = \mathbf{o}$. For ease of notation, in the arguments of the Airy functions the abbreviation $\epsilon = -2\beta E$ (5.22) has been kept.

Isotropic emission ($l = 0,\ m = 0$):

$$J_{00}(E) \;=\; \frac{M\beta F}{2\pi\hbar^3}\,\left\{\mathrm{Ai}'(\epsilon)^2+2\beta E\;\mathrm{Ai}(\epsilon)^2\right\} \tag{E.11}$$

Emission as p-wave, longitudinal polarization ($l = 1,\ m = 0$):

$$J_{10}(E) \;=\; \frac{M}{2\pi\hbar^3}\,(2\beta F)^3\,\left\{2\beta^2E^2\;\mathrm{Ai}(\epsilon)^2-\mathrm{Ai}(\epsilon)\,\mathrm{Ai}'(\epsilon)+\beta E\;\mathrm{Ai}'(\epsilon)^2\right\} \tag{E.12}$$

Emission as p-wave, circular polarization ($l = 1,\ m = \pm 1$):

$$J_{11}(E) \;=\; \frac{M}{2\pi\hbar^3}\,(2\beta F)^3\,\left\{2\beta^2E^2\;\mathrm{Ai}(\epsilon)^2-\frac{1}{4}\;\mathrm{Ai}(\epsilon)\,\mathrm{Ai}'(\epsilon)+\beta E\;\mathrm{Ai}'(\epsilon)^2\right\} \tag{E.13}$$

Emission as d-wave, longitudinal polarization ($l = 2,\ m = 0$):

$$J_{20}(E) \;=\; \frac{M}{\pi\hbar^3}\,(2\beta F)^5\,\left\{\left(2\beta^3E^3+\frac{9}{16}\right)\;\mathrm{Ai}(\epsilon)^2+\beta E\;\mathrm{Ai}(\epsilon)\,\mathrm{Ai}'(\epsilon)+\beta^2E^2\;\mathrm{Ai}'(\epsilon)^2\right\} \tag{E.14}$$

Emission as d-wave, tesseral polarization ($l = 2,\ m = \pm 1$):

$$J_{21}(E) \;=\; \frac{M}{\pi\hbar^3}\,(2\beta F)^5\,\left\{\left(2\beta^3E^3+\frac{9}{16}\right)\;\mathrm{Ai}(\epsilon)^2-\frac{1}{4}\,\beta E\;\mathrm{Ai}(\epsilon)\,\mathrm{Ai}'(\epsilon)+\beta^2E^2\;\mathrm{Ai}'(\epsilon)^2\right\} \tag{E.15}$$

Emission as d-wave, circular polarization ($l = 2,\ m = \pm 2$):

$$J_{22}(E) \;=\; \frac{M}{\pi\hbar^3}\,(2\beta F)^5\,\left\{\left(2\beta^3E^3+\frac{3}{32}\right)\,\mathrm{Ai}(\epsilon)^2-\frac{1}{4}\,\beta E\;\mathrm{Ai}(\epsilon)\,\mathrm{Ai}'(\epsilon)+\beta^2E^2\;\mathrm{Ai}'(\epsilon)^2\right\} \tag{E.16}$$

E.4 Momentum-Space Green Functions

Here, we tabulate explicit expressions for the uniform field multipole Green functions $G_{lm}(\mathbf{k}_\perp, z; E)$ (5.70) in the mixed momentum space representation introduced in Section 5.6. The source has again been placed at $\mathbf{r}' = \mathbf{o}$. The formulae presented here are valid for the sector of space $z \geq 0$ only; for $z \leq 0$, the arguments of the Airy functions $\mathrm{Ai}(\epsilon_\parallel)$ and $\mathrm{Ci}(\epsilon_\parallel - 2\beta F z)$ should be exchanged. For the sake of brevity, in the following we will employ the dimensionless "longitudinal energy" parameter $\epsilon_\parallel$ (see Section 5.6) defined as:

$$\epsilon_\parallel \;=\; -2\beta\left[E-\frac{\hbar^2k_\perp^2}{2M}\right] \tag{E.17}$$

The polar angle of the lateral momentum $\mathbf{k}_\perp$ is denoted by ϕ.
Isotropic emission ($l = 0,\ m = 0$):

$$G_{00}(\mathbf{k}_\perp, z; E) \;=\; -\frac{\beta^2F}{\sqrt{\pi}}\;\mathrm{Ci}(\epsilon_\parallel - 2\beta F z)\,\mathrm{Ai}(\epsilon_\parallel) \tag{E.18}$$

Emission as p-wave, longitudinal polarization ($l = 1,\ m = 0$):

$$G_{10}(\mathbf{k}_\perp, z; E) \;=\; 2\sqrt{\frac{3}{\pi}}\,\beta^3F^2\;\mathrm{Ci}(\epsilon_\parallel - 2\beta F z)\,\mathrm{Ai}'(\epsilon_\parallel) \tag{E.19}$$

Emission as p-wave, circular polarization ($l = 1,\ m = 1$):

$$G_{11}(\mathbf{k}_\perp, z; E) \;=\; -\,i\sqrt{\frac{3}{2\pi}}\,\beta^3F^2k_\perp\,e^{i\phi}\;\mathrm{Ci}(\epsilon_\parallel - 2\beta F z)\,\mathrm{Ai}(\epsilon_\parallel) \tag{E.20}$$

Emission as d-wave, longitudinal polarization ($l = 2,\ m = 0$):

$$G_{20}(\mathbf{k}_\perp, z; E) \;=\; 8\sqrt{\frac{5}{\pi}}\,\beta^4F^3\;\left(E-\frac{3}{4}\,\frac{\hbar^2k_\perp^2}{M}\right)\;\mathrm{Ci}(\epsilon_\parallel - 2\beta F z)\,\mathrm{Ai}(\epsilon_\parallel) \tag{E.21}$$

Emission as d-wave, tesseral polarization ($l = 2,\ m = 1$):

$$G_{21}(\mathbf{k}_\perp, z; E) \;=\; i\sqrt{\frac{30}{\pi}}\,\beta^4F^3k_\perp\,e^{i\phi}\;\mathrm{Ci}(\epsilon_\parallel - 2\beta F z)\,\mathrm{Ai}'(\epsilon_\parallel) \tag{E.22}$$

Emission as d-wave, circular polarization ($l = 2,\ m = 2$):

$$G_{22}(\mathbf{k}_\perp, z; E) \;=\; \frac{1}{2}\sqrt{\frac{15}{2\pi}}\,\beta^4 F^3 k_\perp^2\, e^{2i\phi}\;\mathrm{Ci}(\epsilon_\parallel - 2\beta F z)\,\mathrm{Ai}(\epsilon_\parallel) \tag{E.23}$$

E.5 Far-Field Approximations

In this concluding section, we present simplified expressions for the uniform field multipole waves $G_{lm}^{(\mathrm{as})}(\mathbf{r}, \mathbf{o}; E)$ (5.82) and the corresponding current density distributions $j_{lmm'}^{(\mathrm{as})}(\mathbf{r}, \mathbf{o}; E)$ (5.95) which hold asymptotically in the far-field limit $\beta F z \gg 1$. For a derivation of these quantities, see Sections 5.7 and 5.8.

In the following table, we use a notation that clearly emphasizes the connection of the quantum mechanical Green function to the classical picture. In the far field, the classical radius of the particle distribution $R_{\mathrm{cl}}(E)$ is given by (6.1):

$$R_{\mathrm{cl}}(E)^2 \;=\; 4Ez/F \tag{E.24}$$

Furthermore, we introduce the lateral distance from the source $R^2 = r^2 - z^2$ and denote the relative lateral position $R/R_{\mathrm{cl}}(E)$ with the symbol Ω. It is easy to show that in the far-field limit the replacements:

$$\begin{aligned} \alpha_+ &= -\beta\,[2E + F(r+z)] \;\sim\; -\beta^2 F^2 R_{\mathrm{cl}}(E)^2/\epsilon \\ \alpha_- &= -\beta\,[2E - F(r-z)] \;\sim\; \epsilon(1-\Omega^2) \end{aligned} \tag{E.25}$$

are permissible. As usual, $\epsilon = -2\beta E$, and the auxiliary parameters $\alpha_\pm$ have been defined in (E.2).

E.5.1 Far-Field Green Functions

In the following table, we list the explicit asymptotic formulae derived from (5.82) for s–, p– and d–multipole waves in a homogeneous force field environment. The position of the source again coincides with the origin. For a comparison with the corresponding more involved exact expressions, see Appendix E.1.
Isotropic emission ($l = 0,\ m = 0$):

$$G_{00}^{(\mathrm{as})}(\mathbf{r}, \mathbf{o}; E) \;=\; \frac{2i\beta^3 F^2\sqrt{-\epsilon}}{\sqrt{\pi}\,R_{\mathrm{cl}}(E)}\;\mathrm{Ci}(\alpha_+)\,\mathrm{Ai}\left[\epsilon(1-\Omega^2)\right] \tag{E.26}$$

Emission as p-wave, longitudinal polarization ($l = 1,\ m = 0$):

$$G_{10}^{(\mathrm{as})}(\mathbf{r}, \mathbf{o}; E) \;=\; -4i\sqrt{\frac{3}{\pi}}\,\frac{\beta^4 F^3\sqrt{-\epsilon}}{R_{\mathrm{cl}}(E)}\;\mathrm{Ci}(\alpha_+)\,\mathrm{Ai}'\left[\epsilon(1-\Omega^2)\right] \tag{E.27}$$

Emission as p-wave, circular polarization ($l = 1,\ m = 1$):

$$G_{11}^{(\mathrm{as})}(\mathbf{r},\mathbf{o};E) \;=\; 2\sqrt{\frac{6}{\pi}}\,\frac{\beta^4F^3\epsilon}{R_{\mathrm{cl}}(E)}\,\Omega\,e^{i\phi}\;\mathrm{Ci}(\alpha_+)\,\mathrm{Ai}\left[\epsilon(1-\Omega^2)\right] \tag{E.28}$$

Emission as d-wave, longitudinal polarization ($l = 2,\ m = 0$):

$$G_{20}^{(\mathrm{as})}(\mathbf{r},\mathbf{o};E) \;=\; 4i\sqrt{\frac{5}{\pi}}\,\frac{\beta^5F^4(-\epsilon)^{3/2}}{R_{\mathrm{cl}}(E)}\,(3\Omega^2-2)\;\mathrm{Ci}(\alpha_+)\,\mathrm{Ai}\left[\epsilon(1-\Omega^2)\right] \tag{E.29}$$

Emission as d-wave, tesseral polarization ($l = 2,\ m = 1$):

$$G_{21}^{(\mathrm{as})}(\mathbf{r},\mathbf{o};E) \;=\; -4\sqrt{\frac{30}{\pi}}\,\frac{\beta^5F^4\epsilon}{R_{\mathrm{cl}}(E)}\,\Omega\,e^{i\phi}\;\mathrm{Ci}(\alpha_+)\,\mathrm{Ai}'\left[\epsilon(1-\Omega^2)\right] \tag{E.30}$$

Emission as d-wave, circular polarization ($l = 2,\ m = 2$):

$$G_{22}^{(\mathrm{as})}(\mathbf{r},\mathbf{o};E) \;=\; -2i\sqrt{\frac{30}{\pi}}\,\frac{\beta^5F^4(-\epsilon)^{3/2}}{R_{\mathrm{cl}}(E)}\,\Omega^2\,e^{2i\phi}\;\mathrm{Ci}(\alpha_+)\,\mathrm{Ai}\left[\epsilon(1-\Omega^2)\right] \tag{E.31}$$

E.5.2 Far-Field Current Distributions

For this final table, we compile the far-field asymptotic current density matrix elements $j_{lmm'}^{(\mathrm{as})}(\mathbf{r},\mathbf{o};E)$ (5.95) for $l = 0, 1$ and $l = 2$ (diagonal elements only). The symbol k denotes the initial electronic wave number. Missing entries in the table are available through the following symmetry relations:

$$j_{lmm'}^{(\mathrm{as})}(\mathbf{r},\mathbf{o};E) \;=\; j_{l,-m',-m}^{(\mathrm{as})}(\mathbf{r},\mathbf{o};E) \;=\; j_{lm'm}^{(\mathrm{as})}(\mathbf{r},\mathbf{o};E)^* \tag{E.32}$$

For $l = 0, 1$, the corresponding exact expressions are listed in Appendix E.2.
Isotropic emission ($l = 0,\ m = m' = 0$):

$$j_{000}^{(\mathrm{as})}(\mathbf{r},\mathbf{o};E) \;=\; \frac{Mk^2}{8\pi^2\hbar^3\beta F\,R_{\mathrm{cl}}(E)^2}\;\mathrm{Ai}\left[\epsilon(1-\Omega^2)\right]^2 \tag{E.33}$$

Emission as p-wave, longitudinal polarization ($l = 1,\ m = m' = 0$):

$$j_{100}^{(\mathrm{as})}(\mathbf{r},\mathbf{o};E) \;=\; \frac{3Mk^2\beta F}{2\pi^2\hbar^3R_{\mathrm{cl}}(E)^2}\;\mathrm{Ai}'\left[\epsilon(1-\Omega^2)\right]^2 \tag{E.34}$$

Emission as p-wave, circular polarization ($l = 1,\ m = m' = 1$):

$$j_{111}^{(\mathrm{as})}(\mathbf{r},\mathbf{o};E) \;=\; \frac{3Mk^4}{16\pi^2\hbar^3\beta F\,R_{\mathrm{cl}}(E)^2}\,\Omega^2\;\mathrm{Ai}\left[\epsilon(1-\Omega^2)\right]^2 \tag{E.35}$$

Emission as p-wave, mixed polarization ($l = 1$, $m = 1$, $m' = 0$):

$$j^{(\mathrm{as})}_{110}(\mathbf{r}, \mathbf{o}; E) \;=\; i\, e^{-i\phi}\, \frac{3Mk^3}{4\sqrt{2}\,\pi^2\hbar^3 R_{\mathrm{cl}}(E)^2}\, \Omega\ \mathrm{Ai}\left[\epsilon(1-\Omega^2)\right] \mathrm{Ai}'\left[\epsilon(1-\Omega^2)\right] \tag{E.36}$$

Emission as p-wave, mixed polarization ($l = 1$, $m = 1$, $m' = -1$):

$$j^{(\mathrm{as})}_{11,-1}(\mathbf{r}, \mathbf{o}; E) \;=\; -\, e^{-2i\phi}\, \frac{3Mk^4}{16\pi^2\hbar^3\beta F\, R_{\mathrm{cl}}(E)^2}\, \Omega^2\ \mathrm{Ai}\left[\epsilon(1-\Omega^2)\right]^2 \tag{E.37}$$

Emission as d-wave, longitudinal polarization ($l = 2$, $m = m' = 0$):

$$j^{(\mathrm{as})}_{200}(\mathbf{r}, \mathbf{o}; E) \;=\; \frac{5Mk^6}{32\pi^2\hbar^3\beta F\, R_{\mathrm{cl}}(E)^2}\, (2-3\Omega^2)^2\ \mathrm{Ai}\left[\epsilon(1-\Omega^2)\right]^2 \tag{E.38}$$

Emission as d-wave, tesseral polarization ($l = 2$, $m = m' = 1$):

$$j^{(\mathrm{as})}_{211}(\mathbf{r}, \mathbf{o}; E) \;=\; \frac{15Mk^4\beta F}{4\pi^2\hbar^3 R_{\mathrm{cl}}(E)^2}\, \Omega^2\ \mathrm{Ai}'\left[\epsilon(1-\Omega^2)\right]^2 \tag{E.39}$$

Emission as d-wave, circular polarization ($l = 2$, $m = m' = 2$):

$$j^{(\mathrm{as})}_{222}(\mathbf{r}, \mathbf{o}; E) \;=\; \frac{15Mk^6}{64\pi^2\hbar^3\beta F\, R_{\mathrm{cl}}(E)^2}\, \Omega^4\ \mathrm{Ai}\left[\epsilon(1-\Omega^2)\right]^2 \tag{E.40}$$

Bibliography

[1] *Atoms in Intense Fields*, edited by M. Gavrila, *Advances in Atomic, Molecular and Optical Physics, Supplement*, (Academic Press, London, 1992).

[2] U. Hefter, R. D. Mead, P. A. Schulz, W. C. Lineberger, Phys. Rev. A **28**, 1429 (1983).

[3] C. Blondel, P. Cacciani, C. Delsart, R. Trainham, Phys. Rev. A **40**, 3698 (1989).

[4] C. Blondel, C. Delsart, F. Dulieu, Phys. Rev. Lett. **77**, 3755 (1996).

[5] H. C. Bryant, in *Atomic Spectra and Collisions in External Fields*, edited by K. T. Taylor, M. H. Nayfeh, C. W. Clark, (Plenum, New York, 1988).

[6] F. I. Dalidchik, V. Z. Slonim, Zh. Eksp. Teor. Fiz. **70**, 47 (1976)
[English translation: Sov. Phys. JETP **43**, 25 (1976)].

[7] V. Z. Slonim, F. I. Dalidchik, Zh. Eksp. Teor. Fiz. **71**, 2057 (1976)
[English translation: Sov. Phys. JETP **44**, 1081 (1977)].

[8] B. Gottlieb, M. Kleber, J. Krause, Z. Phys. A **339**, 201 (1991).

[9] C. Bracher, W. Becker, S. A. Gurvitz, M. Kleber, M. S. Marinov, Am. J. Phys. **66**, 38 (1998).

[10] I. I. Fabrikant, Zh. Eksp. Teor. Fiz. **79**, 2070 (1980)
[English translation: Sov. Phys. JETP **52**, 1045 (1980)].

[11] I. I. Fabrikant, Zh. Eksp. Teor. Fiz. **83**, 1675 (1982)
[English translation: Sov. Phys. JETP **56**, 967 (1982)].

[12] I. I. Fabrikant, Phys. Rev. A **40**, 2373 (1989).

[13] I. I. Fabrikant, J. Phys. B **23**, 1139 (1990).

[14] I. I. Fabrikant, J. Phys. B **26**, 2533 (1993).

[15] I. I. Fabrikant, J. Phys. B **27**, 4545 (1994).

[16] Yu. N. Demkov, V. D. Kondratovich, V. N. Ostrovsky, Pis'ma Zh. Eksp. Teor. Fiz. **34**, 425 (1981) [English translation: Sov. Phys. JETP Lett. **34**, 403 (1981)].

[17] V. D. Kondratovich, V. N. Ostrovsky, J. Phys. B **23**, 21 (1990).

[18] V. D. Kondratovich, V. N. Ostrovsky, J. Phys. B **23**, 3785 (1990).

[19] V. N. Ostrovsky, D. A. Telnov, J. Phys. B **26**, 415 (1993).

[20] P. Golovinskii, Zh. Eksp. Teor. Fiz. **112**, 1574 (1997)
[English translation: Sov. Phys. JETP **85**, 857 (1997)].

[21] T. Mercouris, C. A. Nicolaides, J. Phys. B **23**, 2037 (1990).

[22] B. Gao, A. F. Starace, Phys. Rev. A **42**, 5580 (1990).

[23] N. Y. Du, I. I. Fabrikant, A. F. Starace, Phys. Rev. A **48**, 2968 (1993).

[24] M. Q. Bao, I. I. Fabrikant, A. F. Starace, Phys. Rev. A **58**, 411 (1998).

[25] A. R. P. Rau, H.-Y. Wong, Phys. Rev. A **37**, 632 (1988).

[26] A. R. P. Rau, H.-Y. Wong, Phys. Rev. A **38**, 1660 (1988).

[27] H.-Y. Wong, A. R. P. Rau, C. H. Greene, Phys. Rev. A **37**, 2393 (1988).

[28] C. H. Greene, N. Rouze, Z. Phys. D **9**, 219 (1988).

[29] V. Z. Slonim, C. H. Greene, Rad. Eff. Def. Solids **122**, 679 (1991).

[30] W. P. Reinhardt, in *Atomic Excitations and Recombination in External Fields*, edited by M. H. Nayfeh, C. W. Clark (Gordon and Breach, New York, 1985).

[31] M. L. Du, J. B. Delos, Phys. Rev. A **38**, 5609 (1988).

[32] M. L. Du, J. B. Delos, Phys. Lett. A **134**, 476 (1989).

[33] M. L. Du, Phys. Rev. A **40**, 4983 (1989).

[34] W. A. M. Blumberg, R. M. Jopson, D. J. Larson, Phys. Rev. Lett. **40**, 1320 (1978).

[35] W. A. M. Blumberg, W. M. Itano, D. J. Larson, Phys. Rev. D **19**, 139 (1979).

[36] D. J. Larson, R. Stoneman, Phys. Rev. A **31**, 2210 (1985).

[37] J. D. Rudmin, L. P. Ratliff, J. N. Yukich, D. J. Larson, J. Phys. B **29**, L881 (1996).

[38] C. H. Greene, Phys. Rev. A **36**, 4236 (1987).

[39] I. I. Fabrikant, Phys. Rev. A **43**, 258 (1991).

[40] Q. Wang, A. F. Starace, Phys. Rev. A **51**, 1260 (1995).

[41] Q. Wang, A. F. Starace, Phys. Rev. A **55**, 815 (1997).

[42] M. L. Du, J. B. Delos, Phys. Rev. Lett. A **58**, 1731 (1987).

[43] M. L. Du, Phys. Rev. A **40**, 1330 (1989).

[44] A. D. Peters, J. B. Delos, Phys. Rev. A **47**, 3020 (1993).

[45] A. D. Peters, J. B. Delos, Phys. Rev. A **47**, 3036 (1993).

[46] G. C. Yang, M. L. Du, Chin. Phys. Lett. **13**, 817 (1996).

[47] A. D. Peters, C. Jaffe, J. B. Delos, Phys. Rev. A **56**, 331 (1997).

[48] A. D. Peters, C. Jaffe, J. Gao, J. B. Delos, Phys. Rev. A **56**, 345 (1997).

[49] Z. Y. Liu, D. H. Wang, S. L. Lin, W. Z. Shi, Phys. Rev. A **54**, 4078 (1996).

[50] Z. Y. Liu, D. H. Wang, Phys. Rev. A **55**, 4605 (1997).

[51] Z. Y. Liu, D. H. Wang, Phys. Rev. A **56**, 2670 (1997).

[52] Z. Y. Liu, D. H. Wang, Phys. Lett. A **233**, 401 (1997).

[53] T. P. Grozdanov, Phys. Rev. A **51**, 607 (1995).

[54] S. Bivona, R. Burlon, G. Ferrante, C. Leone, Phys. Rev. A **51**, 3096 (1995).

[55] Q. Wang, A. F. Starace, Phys. Rev. A **48**, R1741 (1993).

[56] M. C. Baruch, T. F. Gallagher, D. J. Larson, Phys. Rev. Lett. **65**, 1336 (1990).

[57] M. C. Baruch, W. G. Sturrus, N. D. Gibson, D. J. Larson, Phys. Rev. A **45**, 2825 (1992).

[58] N. D. Gibson, B. J. Davies, D. J. Larson, Phys. Rev. A **47**, 1946 (1993).

[59] N. D. Gibson, B. J. Davies, D. J. Larson, Phys. Rev. A **48**, 310 (1993).

[60] H. C. Bryant, A. Mohagheghi, J. E. Stewart, J. B. Donahue, C. R. Quick, R. A. Reeder, V. Yuan, C. R. Hummer, W. W. Smith, S. Cohen, W. P. Reinhardt, L. Overman, Phys. Rev. Lett. **58**, 2412 (1987).

[61] J. E. Stewart, H. C. Bryant, P. G. Harris, A. H. Mohagheghi, J. B. Donahue, C. R. Quick, R. A. Reeder, V. Yuan, C. R. Hummer, W. W. Smith, S. Cohen, Phys. Rev. A **38**, 5628 (1988).

[62] P. G. Harris, H. C. Bryant, A. H. Mohagheghi, C. Tang, J. B. Donahue, C. R. Quick, R. A. Reeder, S. Cohen, W. W. Smith, J. E. Stewart, C. Johnstone, Phys. Rev. A **41**, 5968 (1990).

[63] C. Blondel, C. Delsart, F. Dulieu, C. Valli, Eur. Phys. J. D **5**, 207 (1999).

[64] C. Valli, C. Blondel, C. Delsart, Phys. Rev. A **59**, 3809 (1999).

[65] R. P. Feynman, A. R. Hibbs, *Quantum Mechanics and Path Integrals*, (Mc Graw-Hill, New York, 1965).

[66] G. Möllenstedt, C. Jönsson, Z. Phys. **155**, 472 (1959).

[67] C. Bracher, M. Kleber, W. Becker, in *Tunneling and its Implications (Proceedings of the Adriatico Research Conference)*, edited by D. Mugnai, A. Ranfagni, L. S. Schulman, (World Scientific, Singapore, 1997), p. 191.

[68] H.-W. Fink, Phys. Scr. **38**, 260 (1988).

[69] H.-W. Fink, W. Stocker, H. Schmid, J. Vac. Sci. Technol. B **8**, 1323 (1990).

[70] H.-W. Fink, W. Stocker, H. Schmid, Phys. Rev. Lett. **65**, 1204 (1990).

[71] H.-W. Fink, H. Schmid, H. J. Kreuzer, A. Wierzbicki, Phys. Rev. Lett. **67**, 1543 (1991).

[72] G. Binnig, H. Rohrer, C. Gerber, E. Weibel, Phys. Rev. Lett. **49**, 57 (1982).

[73] V. M. Hallmark, S. Chiang, J. F. Rabolt, J. D. Swalen, R. J. Wilson, Phys. Rev. Lett. **59**, 2879 (1987).

[74] J. Wintterlin, J. Wiechers, H. Brune, T. Gritsch, H. Höfer, R. J. Behm, Phys. Rev. Lett. **62**, 59 (1989).

[75] C. Bracher, M. Riza, M. Kleber, Phys. Rev. B **56**, 7704 (1997).

[76] C. Bracher, M. Riza, M. Kleber, Appl. Phys. A **66**, S901 (1998).

[77] J. Tersoff, D. R. Hamann, Phys. Rev. Lett. **50**, 1998 (1983).

[78] J. Tersoff, D. R. Hamann, Phys. Rev. B **31**, 805 (1985).

[79] S. Datta, *Electronic Transport in Mesoscopic Systems*, (Cambridge University Press, Cambridge, 1995).

[80] Y. Imry, *Introduction to Mesoscopic Physics*, (Oxford University Press, New York, 1997).

[81] M. Abramowitz, I. A. Stegun, *Handbook of Mathematical Functions*, (Dover, New York, 1965).

[82] E. N. Economou, *Green's Functions in Quantum Physics*, *Solid–State Sciences 7*, 2nd edn. (Springer-Verlag, Berlin, 1983).

[83] A. Messiah, *Quantum Mechanics (Vol. I)*, (North-Holland, Amsterdam, 1964).

[84] J. D. Jackson, *Classical Electrodynamics*, (Wiley, New York, 1962).

[85] B. F. Bayman, J. Math. Phys. **19**, 2558 (1978).

[86] E. G. P. Rowe, J. Math. Phys. **19**, 1962 (1978).

[87] E. J. Weniger, E. O. Steinborn, J. Math. Phys. **24**, 2553 (1983).

[88] E. W. Hobson, *The Theory of Spherical and Ellipsoidal Harmonics*, (Cambridge University Press, Cambridge, 1931).

[89] P. M. Morse, H. Feshbach, *Methods of Theoretical Physics (Vol. II)*, (McGraw-Hill, New York, 1953).

[90] C. Müller, *Spherical Harmonics (Lecture Notes in Mathematics Vol. 17)*, (Springer, Berlin, 1966).

[91] C. Blondel, Phys. Scr. T**58**, 31 (1995).

[92] E. P. Wigner, Phys. Rev. **73**, 1002 (1948).

[93] J. W. Farley, Phys. Rev. A **40**, 6286 (1989).

[94] L. Mandel, E. Wolf, *Optical Coherence and Quantum Optics*, (Cambridge University Press, Cambridge, 1995).

[95] K. R. Lykke, K. K. Murray, W. C. Lineberger, Phys. Rev. A **43**, 6104 (1991).

[96] M. Scheer, R. C. Bilodeau, J. Thøgersen, H. K. Haugen, Phys. Rev. A **57**, R1493 (1998).

[97] M. Scheer, C. A. Brodie, R. C. Bilodeau, H. K. Haugen, Phys. Rev. A **58**, 2051 (1998).

[98] M. Scheer, R. C. Bilodeau, C. A. Brodie, H. K. Haugen, Phys. Rev. A **58**, 2844 (1998).

[99] V. B. Beretstetskii, E. M. Lifshitz, L. P. Pitaevskii, *Quantum Electrodynamics (Course of Theoretical Physics Vol. IV)*, 2nd edn. (Pergamon, Oxford, 1982).

[100] J. H. Van Vleck, Proc. Natl. Acad. Sci. (U. S.) **14**, 178 (1928).

[101] P. L. Kapur, R. Peierls, Proc. Roy. Soc. A **163**, 606 (1937).

[102] H. M. Van Horn, E. E. Salpeter, Phys. Rev. **157**, 751 (1967).

[103] T. Banks, C. Bender, T. Wu, Phys. Rev. D **8**, 3346 (1973).

[104] T. Banks, C. Bender, Phys. Rev. D **8**, 3366 (1973).

[105] W. H. Miller, in *Advances in Chemical Physics Vol. 25*, edited by I. Prigogine, S. A. Rice, (Wiley, New York, 1974), p. 69.

[106] D. M. Brink, *Semi-Classical Methods in Nucleus-Nucleus Scattering*, (Cambridge University Press, Cambridge, 1985).

[107] M. Razavy, A. Pimpale, Phys. Rep. **168**, 305 (1988).

[108] Z. H. Huang, T. E. Feuchtwang, P. H. Cutler, E. Kazes, Phys. Rev. A **41**, 32 (1990).

[109] P. Bowcock, R. Gregory, Phys. Rev. D **44**, 1774 (1991).

[110] L. S. Schulman, *Techniques and Applications of Path Integration*, (Wiley, New York, 1981).

[111] E. Schrödinger, Ann. Phys. (Leipzig) **79**, 361 (1926).

[112] L. S. Brown, Y. Zhang, Am. J. Phys. **62**, 806 (1994).

[113] H. Goldstein, *Classical Mechanics*, 2nd edn. (Addison-Wesley, Reading, Mass., 1980).

[114] L. D. Landau, E. M. Lifshitz, *Quantum Mechanics (Course of Theoretical Physics Vol. III)* (Pergamon, London, 1959).

[115] A. J. Leggett, Prog. Theor. Phys. Suppl. **69**, 80 (1980).

[116] D. W. McLaughlin, J. Math. Phys. **13**, 1099 (1972).

[117] R. D. Carlitz, D. A. Nicole, Ann. Phys. (New York) **164**, 411 (1985).

[118] E. M. Ilgenfritz, H. Perlt, J. Phys. A **25**, 5729 (1992).

[119] R. R. Schlicher, W. Becker, J. Bergou, M. O. Scully, in *Quantum Electrodynamics and Quantum Optics, Proceedings of the NATO Advanced Study Institute, Boulder, CO, USA, 27 May—8 June 1983*, edited by A. O. Barut, (Plenum, New York, 1984), p. 405.

[120] E. H. Kennard, Z. Phys. **44**, 326 (1927).

[121] M. Kleber, Phys. Rep. **236**, 331 (1994).

[122] J. Schwinger, Phys. Rev. **82**, 664 (1951).

[123] R. W. Robinett, Am. J. Phys. **64**, 803 (1996).

[124] G. P. Arrighini, N. L. Durante, C. Guidotti, Am. J. Phys. **64**, 1036 (1996).

[125] Y. L. Li, C. H. Liu, S. J. Franke, J. Acoust. Soc. Am. **87**, 2285 (1990).

[126] B. Gottlieb, M. Kleber, Ann. Phys. (Leipzig) **1**, 369 (1992).

[127] N. Bleistein, R. A. Handelsman, *Asymptotic Expansions of Integrals*, (Dover, New York, 1986).

[128] A. R. Edmonds, *Angular Momentum in Quantum Mechanics*, (Princeton University Press, Princeton, 1957).

[129] F. Shimizu, K. Shimizu, H. Takuma, Phys. Rev. A **46**, R17 (1992).

[130] R. R. Freeman, N. P. Economou, G. C. Bjorklund, K. T. Lu, Phys. Rev. Lett. **41**, 1463 (1978).

[131] C. Blondel, R.-J. Champeau, C. Delsart, J. Phys. B **18**, 2403 (1985).

[132] A. R. P. Rau, J. Phys. B **12**, L193 (1979).

[133] E. Luc-Koenig, A. Bachelier, Phys. Rev. Lett. **43**, 921 (1979).

[134] E. Luc-Koenig, A. Bachelier, J. Phys. B **13**, 1769 (1980).

[135] J. Gao, J. B. Delos, Phys. Rev. A **56**, 356 (1997).

[136] G. Yang, J.-M. Mao, M. Du, Phys. Rev. A **59**, 2053 (1999).

[137] C. Bordas, Phys. Rev. A **58**, 400 (1998).

[138] G. H. Fuller, J. Phys. Chem. Ref. Data **5**, 835 (1976).

[139] H. Helm, N. Bjerre, M. J. Dyer, D. L. Huestis, M. Saeed, Phys. Rev. Lett. **70**, 3221 (1993).

[140] C. Bordas, M. J. Dyer, T. Fairfield, H. Helm, K. C. Kulander, Phys. Rev. A **51**, 3726 (1995).

[141] C. Bordas, F. Paulig, H. Helm, D. L. Huestis, Rev. Sci. Instrum. **67**, 2257 (1996).

[142] K. N. Srinivasa Rao, *The Rotation and Lorentz Groups and their Representations for Physicists*, (Wiley, New York, 1988).

[143] R. Morin, A. Gargani, Phys. Rev. B **48**, 6643 (1993).

[144] S. Horch, R. Morin, J. Appl. Phys. **74**, 3652 (1993).

[145] R. Morin, H.-W. Fink, Appl. Phys. Lett. **65**, 2362 (1994).

[146] A. A. Lucas, H. Morawitz, G. R. Henry, J.-P. Vigneron, P. Lambin, P. H. Cutler, T. E. Feuchtwang, J. Vac. Sci. Technol. A **6**, 296 (1988).

[147] N. García, J. J. Sáenz, H. De Raedt, J. Phys.: Condens. Matter **1**, 9931 (1989).

[148] N. D. Lang, A. Yacoby, Y. Imry, Phys. Rev. Lett. **63**, 1499 (1989).

[149] H. De Raedt, N. García, J. J. Sáenz, Phys. Rev. Lett. **63**, 2260 (1989).

[150] E. Tekman, S. Ciraci, A. Baratoff, Phys. Rev. B **42**, 9221 (1990).

[151] C. Bracher, *Betrachtungen zum Begriff der Verweildauer in der Quantenmechanik*, (Diploma thesis, Technische Universität München, 1995) (unpublished).

[152] J. Summhammer, J. Schmiedmayer, Phys. Scr. **42**, 124 (1990).

[153] R. Gomer, *Field Emission and Field Ionization*, (Harvard University Press, Cambridge, Mass., 1961).

[154] E. H. Hauge, J. A. Støvneng, Rev. Mod. Phys. **61**, 917 (1989).

[155] R. Landauer, Th. Martin, Rev. Mod. Phys. **66**, 217 (1994).

[156] *Tunneling and its Implications (Proceedings of the Adriatico Research Conference)*, edited by D. Mugnai, A. Ranfagni, L. S. Schulman, (World Scientific, Singapore, 1997).

[157] *Proceedings of the Workshop on Superluminal(?) Velocities*, (Cologne, 1998), edited by P. Mittelstaedt, G. Nimtz, Ann. Phys. (Leipzig) **7**, 585 (1998).

[158] G. Nimtz, A. Enders, J. Physique I **2**, 1693 (1992).

[159] A. M. Steinberg, P. G. Kwiat, R. Y. Chiao, Phys. Rev. Lett. **71**, 708 (1993).

[160] C. Bracher, M. Kleber, Ann. Phys. (Leipzig) **4**, 696 (1995).

[161] C. Bracher, J. Phys. B **30**, 2717 (1997).

[162] C. Bracher, M. Kleber, Ann. Phys. (Leipzig) **7**, 687 (1998).

[163] A. I. Baz', Yad. Fiz. **4**, 252 (1966) [English translation: Sov. J. Nucl. Phys. **4**, 182 (1967)].

[164] A. I. Baz', Yad. Fiz. **5**, 229 (1967) [English translation: Sov. J. Nucl. Phys. **5**, 161 (1967)].

[165] M. Büttiker, R. Landauer, Phys. Rev. Lett. **49**, 1739 (1982).

[166] N. W. Ashcroft, N. D. Mermin, *Solid State Physics*, (Saunders, Philadelphia, 1976).

[167] N. D. Lang, W. Kohn, Phys. Rev. B **3**, 1215 (1971).

[168] B. Gottlieb, *Propagatormethoden für mesoskopisches Tunneln am Beispiel des Rastertunnelmikroskops*, (Dissertation, Technische Universität München, 1995) (unpublished).

[169] G. Binnig, C. F. Quate, Ch. Gerber, Phys. Rev. Lett. **56**, 930 (1986).

[170] D. W. Pohl, W. Denk, M. Lanz, Appl. Phys. Lett. **44**, 651 (1984).

[171] U. Ch. Fischer, D. W. Pohl, Phys. Rev. Lett. **62**, 458 (1989).

[172] *Proceedings of the 9th International Conference on Scanning Tunneling Microscopy/Spectroscopy and Related Techniques (STM'97), Hamburg, 1997*, Appl. Phys. A **66** (Supplement), p. S3–S1288 (1998).

[173] G. Binnig, H. Rohrer, Sci. Am. **253**, 40 (1985).

[174] H. K. Wickramasinghe, Sci. Am. **261**, 74 (1989).

[175] P. K. Hansma, J. Tersoff, J. Appl. Phys. **61**, R1 (1987).

[176] C. J. Chen, *Introduction to Scanning Tunneling Microscopy*, (Oxford University Press, New York, 1993).

[177] *Scanning Tunneling Microscopy I*, edited by H.-J. Güntherodt, R. Wiesendanger, 2nd edn. (Springer, Berlin, 1994).

[178] *Scanning Tunneling Microscopy II*, edited by R. Wiesendanger, H.-J. Güntherodt, 2nd edn. (Springer, Berlin, 1995).

[179] *Scanning Tunneling Microscopy III*, edited by R. Wiesendanger, H.-J. Güntherodt, 2nd edn. (Springer, Berlin, 1996).

[180] M. Riza, *Streutheoretische Beschreibung des Rastertunnelmikroskops*, (Diploma thesis, Technische Universität München, 1996) (unpublished).

[181] T. E. Feuchtwang, P. H. Cutler, Phys. Scr. **35**, 132 (1987).

[182] C. J. Chen, J. Vac. Sci. Technol. A **6**, 319 (1988).

[183] C. J. Chen, Phys. Rev. B **42**, 8841 (1990).

[184] C. J. Chen, Phys. Rev. Lett. **65**, 448 (1990).

[185] R. Landauer, IBM J. Res. Dev. **1**, 223 (1957).

[186] R. Landauer, Z. Phys. B **68**, 217 (1987).

[187] M. Tsukada, K. Kobayashi, N. Isshiki, H. Kageshima, Surf. Sci. Rep. **13**, 265 (1991).

[188] I. S. Gradshteyn, I. M. Ryzhik, *Table of Integrals, Series and Products (Corrected and Enlarged Edition)*, (Academic Press, San Diego, 1980).

[189] N. García, C. Ocal, F. Flores, Phys. Rev. Lett. **50**, 2002 (1983).

[190] E. Stoll, A. Baratoff, A. Selloni, P. Carnevali, J. Phys. C **17**, 3073 (1984).

[191] Z. H. Huang, T. E. Feuchtwang, P. H. Cutler, E. Kazes, J. Vac. Sci. Technol. A **8**, 177 (1989).

[192] C. Noguera, Phys. Rev. B **42**, 1629 (1990).

[193] J. Bardeen, Phys. Rev. Lett. **6**, 57 (1961).

[194] I. Giaever, Phys. Rev. Lett. **5**, 147 (1960).

[195] C. B. Duke, *Tunneling in Solids*, in *Solid State Physics Supplement 10*, edited by F. Seitz, D. Turnbull, (Academic, New York, 1969), p. 207.

[196] W. Sacks, S. Gauthier, S. Rousset, J. Klein, M. A. Esrick, Phys. Rev. B **36**, 961 (1987).

[197] D. Lawunmi, M. C. Payne, J. Phys.: Condens. Matter **2**, 3811 (1990).

[198] D. M. Eigler, E. K. Schweizer, Nature **344**, 524 (1990).

[199] A. Zangwill, *Physics at Surfaces*, (Cambridge University Press, Cambridge, 1988).

[200] M. F. Crommie, C. P. Lutz, D. M. Eigler, Science **262**, 218 (1993).

[201] E. J. Heller, M. F. Crommie, C. P. Lutz, D. M. Eigler, Nature **369**, 464 (1994).

[202] M. F. Crommie, C. P. Lutz, D. M. Eigler, E. J. Heller, Physica D **83**, 98 (1995).

[203] M. F. Crommie, C. P. Lutz, D. M. Eigler, E. J. Heller, Surf. Sci. **361/362**, 864 (1996).

[204] W. Sacks, D. Roditchev, J. Klein, Phys. Rev. B **57**, 13118 (1998).

[205] N. D. Lang, Phys. Rev. Lett. **55**, 230 (1985).

[206] N. D. Lang, Phys. Rev. Lett. **56**, 1164 (1986).

[207] N. D. Lang, Comments Cond. Mat. Phys. **14**, 253 (1989).

[208] M. F. Crommie, C. P. Lutz, D. M. Eigler, Phys. Rev. B **48**, 2851 (1993).

[209] G. Doyen, E. Koetter, J. P. Vigneron, M. Scheffler, Appl. Phys. A **51**, 281 (1990).

[210] P. Sautet, C. Joachim, Chem. Phys. Lett. **185**, 23 (1991).

[211] C. Chavy, C. Joachim, A. Altibelli, Chem. Phys. Lett. **214**, 569 (1993).

[212] I. S. Tilinin, M. K. Rose, J. C. Dunphy, M. Salmeron, M. A. Van Hove, Surf. Sci. **418**, 511 (1998).

[213] W. Sacks, C. Noguera, Phys. Rev. B **43**, 11612 (1991).

[214] K. v. Klitzing, G. Dorda, M. Pepper, Phys. Rev. Lett. **45**, 494 (1980).

[215] I. Halperin, L. Schwartz, *Introduction to the Theory of Distributions*, (University of Toronto Press, Toronto, 1952).

[216] J. Ferrer, A. Martín-Rodero, F. Flores, Phys. Rev. B **38**, 10113 (1988).

[217] A. Yazdani, D. M. Eigler, N. D. Lang, Science **272**, 1921 (1996).

[218] *CRC Handbook of Chemistry and Physics*, edited by D. R. Lide, 78th edn. (CRC Press, Boca Raton, 1997).

[219] C. Kittel, *Introduction to Solid State Physics*, 2nd edn. (Wiley, New York, 1956).

[220] Yu. N. Demkov, V. N. Ostrovskii, *Zero-Range Potentials and Their Application in Atomic Physics*, (Plenum, New York, 1988).

[221] K. Wódkiewicz, Phys. Rev. A **43**, 68 (1991).

[222] Y. S. Chan, E. J. Heller, Phys. Rev. Lett. **78**, 2570 (1997).

[223] J. Rauch, *Partial Differential Equations*, (Springer, New York, 1991).

[224] G. F. Roach, *Green's Functions: Introductory Theory with Applications*, (Van Nostrand Reinhold, London, 1970).

[225] G. Strang, *Linear Algebra and its Applications*, 3rd edn. (Harcourt Brace Jovanovich, Orlando, 1988).

[226] P. A. M. Dirac, *The Principles of Quantum Mechanics*, 4th edn. (Clarendon Press, Oxford, 1958).

[227] R. P. Feynman, Phys. Rev. **76**, 749 (1949).

[228] T. Kato, *Perturbation Theory for Linear Operators*, (Springer, Berlin, 1966).

[229] M. Reed, B. Simon, *Methods of Modern Mathematical Physics Vol. I: Functional Analysis*, (Academic Press, New York, 1972).

[230] R. G. Newton, *Scattering Theory of Waves and Particles*, 2nd edn. (Springer, New York, 1982).

[231] A. E. Taylor, *General Theory of Functions and Integration*, (Blaisdell, New York, 1965).

[232] G. Sansone, *Orthogonal Functions*, (Dover, New York, 1991).

[233] F. Riesz, B. Sz.–Nagy, *Leçons d'analyse fonctionelle*, (Akadémiai Kiadó, Budapest, 1953).

[234] D. E. Aspnes, Phys. Rev. **147**, 554 (1966).

[235] F. W. J. Olver, *Asymptotics and Special Functions*, (Academic Press, New York, 1974).

[236] E. C. Titchmarsh, *Eigenfunction Expansions Associated with Second-Order Differential Equations (Part I)*, 2nd edn. (Clarendon Press, Oxford, 1962).

[237] L. Hörmander, *Linear Partial Differential Operators*, (Springer, Berlin, 1963).

[238] A. Messiah, *Quantum Mechanics (Vol. II)*, (North-Holland, Amsterdam, 1962).

[239] A. Erdélyi, W. Magnus, F. Oberhettinger, F. G. Tricomi, *Higher Transcendental Functions (Vol. II)*, (McGraw-Hill, New York, 1953).

[240] D. A. Varshalovich, A. N. Moskalev, V. K. Khersonskii, *Quantum Theory of Angular Momentum: Irreducible Tensors, Spherical Harmonics, Vector Coupling Coefficients, 3nj–Symbols*, (World Scientific, Singapore, 1988).

[241] U. Fano, G. Racah, *Irreducible Tensorial Sets*, (Academic Press, New York, 1959).

[242] G. Racah, Phys. Rev. **62**, 438 (1942).

[243] F. D. Santos, Nucl. Phys. **A212**, 341 (1973).

[244] M. A. Rashid, J. Math. Phys. **27**, 549 (1986).

[245] M. J. Caola, J. Phys. A **11**, L23 (1978).

[246] S. Chakrabarti, D. P. Dewangan, J. Phys. B **28**, L769 (1995).

[247] D. R. Hartree, *The Calculation of Atomic Structures*, (Wiley, New York, 1953).

[248] J. A. Gaunt, Trans. Roy. Soc. (London) A **228**, 195 (1928).